BAINITE IN STEELS

BAINITE IN STEELS

Transformations, Microstructure and Properties

SECOND EDITION

H. K. D. H. BHADESHIA
Professor of Physical Metallurgy
University of Cambridge
Fellow of Darwin College, Cambridge

Book 0735
Second edition first published in 2001 by
IOM Communications Ltd
1 Carlton House Terrace
London SW1Y 3DB

ISBN 1-86125-112-2

IOM Communicataions Ltd
is a wholly-owned subsidiary of
The Institute of Materials

First edition published in 1992 by
The Institute of Materials

Typeset in the UK by
Keyset Composition, Colchester

Printed and bound in the UK at
The University Press, Cambridge

Preface

Computational metallurgy has grown rapidly over the last twenty years and the subject has been embraced by industry with remarkable enthusiasm, resulting in close collaborations and long term partnerships between industry and academic research laboratories. No longer are alloys designed from experience alone but calculations are used to reduce the task and to introduce creativity. There are now numerous examples of profitable commercial products resulting from the application of this type of research.

The fact that bainitic steels have featured prominently in this kind of metallurgy is a testimony to the depth of understanding that has been achieved. The highest ever combinations of strength and toughness (1600 MPa, 130 MPa $m^{\frac{1}{2}}$) have been obtained in bainitic steels invented using theory alone. Optically visible bainite has been obtained under conditions where the diffusion distance of an iron atom is just 10^{-17} m. Automobiles have become safer because of the incorporation of bainite–containing strong steels to protect against sideways collisions. Gigantic magnetic fields have been used to stimulate bainite. New tungsten–containing creep–resistant bainitic steels, which can be used without post–weld heat treatment have now been in service for more than four years. Experimental techniques invented to characterise the nucleation of bainite on ceramic particles have been emulated in other fields of metallurgy.

Atomic resolution has shown that like ordinary bainite, substitutional solutes simply do not diffuse during the growth of acicular ferrite. The mechanism of carbide precipitation in bainite is better understood; but wouldn't it be nice if the displacements due to precipitation could be characterised?

The focus has shifted from stress to strain–affected transformation. Indeed, it has been proposed that 'there is no mechanism by which plastic strain can retard reconstructive transformation. Likewise, only displacive transformations can be mechanically stabilised.' This provides a simple way of establishing the atomic mechanism of transformation. The proposal has not yet been contradicted.

Bainite is thriving as a material. Most of the new products based on bainite are manufactured by large steel industries. There are in addition, university spin–offs. In one case, a large company has been created to manufacture and market only bainitic steels; the company concerned is possibly unique in

having the word 'bainite' in its title. In another case a fledgling 'dot-com' has been created to market the software useful in modelling the microstructure and properties of bainitic and other steels. A short monograph on bainite is now available in seven different languages on the world wide web.

Much has changed since the first edition of this book. There is a new clarity in the concepts associated with solid–state transformations. There is even transparency in the definition of problems which are not yet understood. To summarise, I sense real progress. It was useful therefore to write a second edition rather than just reprint the first. As with the first edition, this book is meant for all who are interested in transformations in steels or who are curious about phase changes in general.

Acknowledgements

This book has developed out of a long standing interest in the subject of bainite and I am grateful to many friends for their help and advice. In particular, I have benefited enormously from the support of Professor J. W. Christian, Professor M. Cohen, Dr. S. A. David, Professor D. V. Edmonds, Dr. H. Harada, Professor Sir Robert Honeycombe, Professor D. Hull, Professor C. J. Humphreys, Professor J. F. Knott, Professor G. B. Olson and Professor C. M. Wayman.

I have over the years enjoyed the privilege of working with many colleagues who have contributed to my understanding of bainite; J. R. Yang, M. Strangwood, A. Sugden, A. Ali, Shahid A. Khan, S. Mujahid, M. Takahashi, G. Rees and S. Babu, J. M. Gregg, S. V. Parker, N. Chester, S. B. Singh, S. J. Jones, M. Lord, E. Swallow, P. Shipway, P. Jacques and F. G. Caballero, T. Sourmail, H. S. Lalam and M. A. Yescas–Gonzalez, deserve a special mention in this respect.

I should also like to express my gratitude to John Garnham for being so generous with his knowledge on bainitic rail steels, to David Gooch for discussions on creep resistant bainitic steels, to Lars–Erik Svensson for introducing me to the acicular ferrite, and to Greg Olson for so many inspiring discussions on bainite. In addition, I would like to thank H.–O. Andren, S. S. Babu, G. Barritte, P. Clayton, D. V. Edmonds, M. Farooque, G. Fourlaris, I. Gutierrez, P. Jacques, B. Josefsson, T. Maki, Y. Ohmori, H. Ohtsuka, M. Oka, J. Race, G. Rees, J. M. Rodriguez–Ibabe, M. Takahashi, H. Tamehiro, R. Thomson, B. J. P. Sandvik, M. Umemoto and the late Javier J. Urcola for providing micrographs, as acknowledged in the text. Fig. 1.1 is reprinted with permission from E. C. Bain, *The Alloying Elements in Steel*, American Society for Metals, 1939.

I would like to express my gratitude to Peter Danckwerts of the Institute of Materials for the care with which he has produced this book and for his patience throughout the venture.

I dedicate this book to Anika, Maya, Narmada and Dharamshi.

Contents

Nomenclature

a	Length of an edge crack
Δa_m	Minimum detectable increase in austenite layer thickness
$\overline{A}$	Mean areal intercept in stereology
Ac_3	Temperature at which a sample becomes fully austenitic during heating
Ae_3	Temperature separating the $\alpha + \gamma$ and γ phase fields for a specific alloy
Ar_3	Temperature at which an austenitic sample begins to transform to ferrite during cooling
A_f	Temperature at which the transformation to austenite is complete
A_i	Atomic weight of element i
A_s	Temperature at which the transformation to austenite begins
$\underline{A}_s$	Mean free slip area in statistical theory for plasticity (Kocks, 1966)
$\overline{B}$	Matrix representing the Bain deformation
B_d	Highest temperature at which bainite forms under the influence of anexternally applied stress
B_S	Bainite-start temperature
B_σ	A temperature below which bainitic transformation is considered to be stress-assisted and above which it is considered to be strain-induced, during transformation under the influence of an externally applied stress
c	Length of an edge crack, or length of a microcrack nucleus
c_d	Diameter of a penny–shaped crack in a spheroidal particle
$c_i^{\alpha\theta}$	Concentration of element i in phase α which is in equilibrium with phase θ
c_o	Carbide thickness
C_i	Constants, with $i = 1, 2, 3 \ldots$
d	Interatomic spacing along a specific crystallographic direction
$\underline{d}$	Vector describing the shear component of an IPS
D_α	Diffusivity of carbon in ferrite
D or D_γ	Diffusivity of carbon in austenite
D_i^α	Diffusivity of element i phase α
$\underline{D}_{eff}$	Effective diffusion coefficient
$\overline{D}$	Weighted average diffusivity of carbon in austenite

E	Young's Modulus
f_1	Normalised supersaturation
f_C	Activity coefficient for carbon in austenite
f^*	Attempt frequency for atomic jumps across an interface
G	Growth rate
ΔG_m	Molar Gibbs free energy
G_N	Function specifying the free energy change needed in order to obtain a detectable rate of nucleation for Widmanstätten and bainite
G_N^α	Function specifying the critical value of $\Delta G^{\gamma\rightarrow\alpha}$ at the M_S temperature
G^*	Activation free energy for nucleation, or for interfacial motion
G_O^*	Activation free energy to overcome the resistance to dislocation motion without the aid of a chemical driving force
G_1^*	Activation free energy for the growth of an embryo into a nucleus
G_2^*	Activation free energy for the transfer of atoms across the nucleus/matrix interface
G_{dd}	Free energy dissipated in the process of solute diffusion ahead of an interface
G_F	Free energy per unit area of fault plane
G_i^0	Molar Gibbs free energy of pure i
G_{id}	Free energy dissipated in the transfer of atoms across an interface
G'_{id}	Free energy term describing the maximum glide resistance of dislocations
G_s	Strain energy per mole
G_{SB}	Stored energy of
G_{SW}	Stored energy of bainite
ΔG	General term representing driving force
ΔG_{CHEM}	Chemical driving force
ΔG_m	Molar Gibbs free energy change on transformation; alternatively, the maximum molar Gibbs free energy change accompanying nucleation
ΔG_{MECH}	Mechanical driving force
ΔG_{STRAIN}	Coherency strain energy during nucleation
$\Delta G\gamma \rightarrow \alpha$	Free energy change for transformation without composition change
h_α	Ledge height at the interface between α and the parent phase
H	Hardness of martensite
H_F	Hardness of tempered martensite when all excess carbon has precipitated
H_0	Hardness of virgin martensite
H_1	A function in the theory of diffusion–controlled growth

$\Delta H^{\gamma\alpha}$	Enthalpy change during the $\gamma \rightarrow \alpha$ transformation
${}^{v}I$	Nucleation rate per unit volume
J	Diffusion flux
k	Boltzmann constant
k_A	Constant in the Avrami equation
k_e	Equilibrium solute partitioning coefficient
k_g	Constant relating lath size to strength
k_i	Partitioning coefficient for alloying element i
k_p	Coefficient representing the strengthening effect of cementite particles; alternatively, a solute partitioning coefficient
k_ϵ	Coefficient in an equation for the strength of tempered martensite
K_I	Stress intensification factor in fracture mechanics
K_{IC}	Critical value of K_I, a measure of the toughness of a material
K_{ISCC}	Threshold value of the stress intensity below which stress corrosion cracks do not grow at a perceptible rate
ΔK	Stress intensity range during fatigue testing
ΔK_O	Threshold value of the stress intensity range during fatigue crack growth studies
Δl_m	Maximum relative length contraction due to isothermal reaustenitisation
$\overline{L}$	Mean intercept length in stereology, grain size
L_S	Lower bainite start temperature
m	Paris constant in fracture mechanics
m_i	Mass fraction of element i
M	Mobility of an interface
M_d	Highest temperature at which martensite forms under the influence of an externally applied stress
M_S	Martensite start temperature
n	Time exponent in the Avrami equation
n_A	Number of atoms in an embryo involved in nucleation
n_{Fe}	Number of iron atoms per unit volume of α
n_p	Number of close–packed planes involved in the faulting process during displacive nucleation
N	Number of cycles in fatigue loading
N_v	Number of particles per unit volume
p	Péclet number (a dimensionless velocity) or autocatalytic factor
P	Pressure
$\underline{P}$	Matrix representing a homogeneous invariant–plane strain deformation
q	Half the increase in the thickness of austenite during one-dimensional growth
Q	Activation energy

[13:43 3/9/01 C:/3B2 Templates/keith/3750 BAINITE.605/3750-prelims.3d] Ref: 0000 Auth: Title: Chapter 00 Page: 19 1-24

$\underline{Q}$	Matrix representing an inhomogeneous lattice–invariant deformation
r	Radius of a disc; alternatively, the distance ahead of a crack tip; alternatively the tip radius of a growing plate
r_1	Proof stress to ultimate tensile stress ratio
r_2	Ratio of σ_a to σ_s
r_C	Critical distance in fracture mechanics, related to K_{IC}; alternatively, critical tip radius at which the growth of a plate ceases
r_e	Value of r_2 at the endurance limit in fatigue
$\overline{r}$	Mean particle radius at time t
$\overline{r}_o$	Mean particle radius at time zero
R	Universal gas constant; alternatively, the semi–axis of an oblate ellipsoid
R_d	Rate at which growing austenite dilutes
s	Shear component of the IPS shape deformation
$\underline{S}$	Deformation matrix in the crystallographic theory of martensite
S_1, S_2	Functions in the Trivedi model for the growth of parabolic cylinders
S_V	Interfacial area per unit volume
t	Time; alternatively, the thickness of a disc
t_1	Time for isothermal transformation to bainite during austempering of cast iron
t_2	Time to the beginning of carbide precipitation from austenite during austempering
t_a	Time required to reach a given fraction ξ of isothermal transformation
t_c	Time required for a sub–unit to reach a limiting size
t_d	Time required to decarburise a plate of bainite
t_i	Time interval for step i in a series of isothermal heat treatments
t_θ	Time for the precipitation of cementite from ferrite
Δt	Time interval between the nucleation of successive sub–unit during sheaf lengthening
T	Temperature
T_c	Critical Zener ordering temperature for carbon atoms in ferrite; alternatively, the temperature below which cementite can in principle precipitate in association with upper bainitic ferrite
T_h	The temperature below which the nucleation of displacive transformations first becomes possible at a detectable rate
T_i	Isothermal transformation temperature
T_F	Temperature at which accelerated cooling is stopped
T_0	Temperature at which γ and α of the same composition have the same free energy

T_{om}	As T_0, but forcing the Zener ordering of carbon atoms in the ferrite
T_0'	As T_0, but accounting for the stored energy of ferrite
T_M	Melting temperature
T_r	Temperature below which a midrib is found in lower bainite plates
T_R	Temperature at which rolling deformation is stopped
T_t	Transition temperature for impact toughness
T_γ	Isothermal reaustenitisation temperature
$T^{\gamma\alpha}$	Austenite to ferrite transformation temperature
v^*	Activation volume
V	Volume of a sample
V^α	Volume of phase α
V_e^α	Extended volume of phase α
V_d	Diffusion field velocity
V_i	Velocity of an interface calculated on the basis of its mobility
V_k	Velocity of an interface calculated using a solute trapping function
V_I	Volume fraction of inclusions
V_l	Plate lengthening rate
V_{max}	Maximum volume fraction
V_{max}^S	Maximum volume of a sheaf
ΔV_m	Change in molar volume on transformation
V_S	Sheaf lengthening rate
ΔV_v	Minimum detectable change in volume fraction
V_α^s	Velocity of steps in the α/parent phase interface
V_m^θ	Molar volume of phase θ
V_τ	Volume per particle
w	Thickness of a bainite sub–unit
w_i	Weight percent of element i
w_i^{sol}	Weight percent of element i, in solution
W	Width of a fracture toughness specimen for a K_{IC} test
$\overline{x}$	Average mole fraction of carbon in an alloy
x_m	Maximum carbon supersaturation permitted in ferrite, on thermodynamic grounds
x_α	Carbon in αat interface
x_γ	Carbon concentration in austenite
x_γ^I	Carbon concentration in austenite before the start of austenite growth
$x^{\alpha\gamma}$	Mole fraction of carbon in ferrite which is in equilibrium or paraequilibrium with austenite
$x^{\gamma\alpha}$	Mole fraction of carbon in austenite which is in equilibrium or paraequilibrium with ferrite
$x_{T_0'}$	Carbon concentration given by the T_0' curve

x_{Ae_3}	Carbon concentration given by the Ae_3 curve
x^{θ}	Thickness of cementite particle
x_X	Concentration of X in cementite
$\overline{x}_X$	Average concentration of X in cementite
$x_X^{\alpha\theta}$	Concentration of X in ferrite which is in equilibrium with cementite
y	Semi–axis of an oblate ellipsoid
Y	Compliance function in fracture mechanics; alternatively, a constant in the theory of thermally activated dislocation motion
z	Coordinate normal to the interface plane; alternatively, a constant in the theory of thermally activated dislocation motion
z_d	Effective diffusion distance
Z	Position of the interface along coordinate z.
α	Allotriomorphic or idiomorphic ferrite which forms by reconstructive transformation
α_1	One–dimensional parabolic thickening rate constant
β	Constant in weld metal inclusion formation theory; alternatively, an autocatalytic factor
γ	Austenite
Γ	Capillarity constant
δ_b	Boundary thickness
Δ	Uniform dilatation accompanying transformation; alternatively, the average distance between neighbouring particles in tempered martensite
θ	Cementite
ϵ_1	Average transverse thickness of dislocation cell structure in martensite
κ	Mean % planar misfit between inclusion and ferrite
λ	Interledge spacing; alternatively an intersite jump distance during diffusion
μ	Shear modulus
μ_i	Chemical potential of element i
ν	Poisson's ratio
ρ	Density
ρ_A	Spacing of close–packed planes
ρ_d	Dislocation density
τ	Incubation time before the growth of an individual particle begins during isothermal transformation, or before a detectable degree of overall transformation. Alternatively, the shear stress resolved along the shear direction
τ_o	Resistance to dislocation motion
τ_μ	Athermal resistance to dislocation motion

κ	Percent planar matching during epitaxial nucleation
ψ	Constant in weld metal inclusion formation theory
σ	Applied stress
σ_a	Cyclic stress amplitude in a fatigue test
σ_C	Critical stress in fracture mechanics, related to K_{IC}; alternatively, solid solution strengthening due to carbon
σ_F	Stress necessary for the propagation of cleavage fracture
$\sigma_F e$	Strength of pure annealed iron
σ_g	Strengthening due to grain boundaries
σ_N	Normal stress on the habit plane
σ_p	Work of fracture, per unit area of crack surface
σ_r	Stress as a function of the distance r ahead of the crack tip
σ_s	Saturation value of σ_{iy} in a fatigue test
σ_{SS}	Solid solution strengthening due to substitutional solutes
σ_{iy}	Instantaneous flow stress at any particular stage of a test
σ_y	Yield stress or proof stress in monotonic loading tests
$\sigma_{\theta\alpha}$	θ/α interface free energy per unit area
σ_0	Intrinsic strength of martensite, not including microstructural strengthening
Ω	Volume per atom
Ω_{Fe}	Volume of an atom of Fe in α
Ω_c	Volume of a molecule of Fe_3C less $3\Omega Fe$
ξ	Volume fraction, or volume fraction divided by the equilibrium or some other limiting volume fraction
ξ_a	A specific value of ξ
ζ	Uniaxial dilatation normal to the habit plane
ASM	American Society for Metals
ASTM	American Society for Testing Materials
BCC	Body-centred cubic
BCT	Body-centred tetragonal
CE	Carbon equivalent
FATT	Fracture assessed ductile-brittle transition temperature
FCC	Face-centred cubic
HAZ	Heat-affected zone of welded joints
HREM	High-resolution transmission electron microscopy
HSLA	High-strength low-alloy (steels)
HV	Vickers Hardness
IIW	International Institute for Welding
IPS	Invariant-Plane Strain shape change
KS	Kurdjumov-Sachs
LEFM	Linear-Elastic-Fracture-Mechanics
NW	Nishiyama-Wasermann

p.p.m.	Parts per million by weight
SCR	Stress corrosion cracking resistance
SSAW	Self-Shielded Arc Weld
TRIP	Transformation–Induced Plasticity
TTT	Time-Temperature-Transformation diagram
ULCB	Ultra–low carbon bainitic steel
UTS	Ultimate tensile strength

Note: The term *residual austenite* refers to the austenite that exists at the reaction temperature during transformation to bainite, whereas the term *retained austenite* refers to the austenite which remains untransformed after cooling the specimen to ambient temperature.

1 *Introduction*

We begin with a historical survey of the exciting early days of metallurgical research during which bainite was discovered, covering the period up to about 1960, with occasional excursions into more modern literature. The early research was usually well conceived and was carried out with enthusiasm. Many of the original concepts survive to this day and others have been confirmed using the advanced experimental techniques now available. The thirty years or so prior to the discovery of bainite were in many respects formative as far as the whole subject of metallurgy is concerned. The details of that period are documented in the several textbooks and articles covering the history of metallurgy,[†] but a few facts deserve special mention, if only as an indication of the state-of-the-art for the period between 1920–1930.

The idea that martensite was an intermediate stage in the formation of pearlite was no longer accepted, although it continued to be taught until well after 1920. The β-iron controversy, in which the property changes caused by the paramagnetic to ferromagnetic transition in ferrite were attributed to the existence of another allotropic modification (β) of iron, was also in its dying days. The first evidence that a solid solution is an intimate mixture of solvent and solute atoms in a single phase was beginning to emerge (Bain, 1921) and it soon became clear that martensite consists of carbon dispersed atomically as an interstitial solid solution in a tetragonal ferrite crystal. Austenite was established to have a face-centred cubic crystal structure, which could sometimes be retained to ambient temperature by quenching. Bain had already proposed the homogeneous deformation which could relate the face-centred cubic and body-centred cubic or body-centred tetragonal lattices during martensitic transformation. It had been established using X-ray crystallography that the tempering of martensite led to the precipitation of cementite, or to alloy carbides if the tempering temperature was high enough. Although the surface relief associated with martensitic transformation had been observed, its impor-

[†]Notable historical works include: *The Sorby Centennial Symposium on the History of Metallurgy*, published by the A.I.M.E. in 1965 (includes an article by Bain himself), the commentary by H. W. Paxton, *Metallurgical Transactions* **1** (1970) 3479–3500, and by H. W. Paxton and J. B. Austin, *Metallurgical Transactions* **3** (1972) 1035–1042. Paxton's 1970 article is published along with a reproduction of the classic 1930 paper on the discovery of bainite by Davenport and Bain, and is based on first hand historical knowledge obtained directly from Davenport and Bain.

tance to the mechanism of transformation was not fully appreciated. Widmanstätten ferrite had been identified and was believed to precipitate on the octahedral planes of the parent austenite; some notions of the orientation relationship between the ferrite and austenite were also being discussed.

It was an era of major discoveries and great enterprise in the metallurgy of steels. The time was therefore ripe for the discovery of bainite. The term 'discovery' implies something new. In fact, microstructures containing bainite must have been encountered prior to the now acknowledged discovery date, but the phase was never clearly identified because of the confused microstructures that followed from the continuous cooling heat treatment procedures common in those days. A number of coincidental circumstances inspired Bain and others to attempt isothermal transformation experiments. That austenite could be retained to ambient temperature was clear from studies of Hadfield's steel which had been used by Bain to show that austenite has a face-centred cubic structure. It was accepted that increasing the cooling rate could lead to a greater amount of austenite being retained. Indeed, it had been demonstrated using magnetic techniques that austenite in low-alloy steels could exist at low temperatures for minutes prior to completing transformation. The concept of isothermal transformation was already exploited in industry for the manufacture of patented steel wire, and Bain was aware of this through his contacts at the American Steel and Wire Company. He began to wonder 'whether exceedingly small heated specimens rendered wholly austenitic might successfully be brought unchanged to any intermediate temperature at which, then their transformation could be followed' and he 'enticed' E. C. Davenport to join him in putting this idea into action.

1.1 The Discovery of Bainite

During the late 1920s, in the course of these pioneering studies on the *isothermal* transformation of austenite at temperatures above that at which martensite first forms, but below that at which fine pearlite is found, Davenport and Bain (1930) discovered a new microstructure consisting of an 'acicular, dark etching aggregate' which was quite unlike the pearlite or martensite observed in the same steel (Fig. 1.1). They originally called this microstructure 'martensite–troostite' since they believed that it 'forms much in the manner of martensite but is subsequently more and less tempered and succeeds in precipitating carbon'.

The structure was found to etch more rapidly than martensite but less so than troostite (fine pearlite). The appearance of 'low-range' martensite–troostite (formed at temperatures just above the martensite-start temperature M_S) was found to be somewhat different from the 'high-range' martensite–troostite formed at higher temperatures. The microstructure exhibited unusual

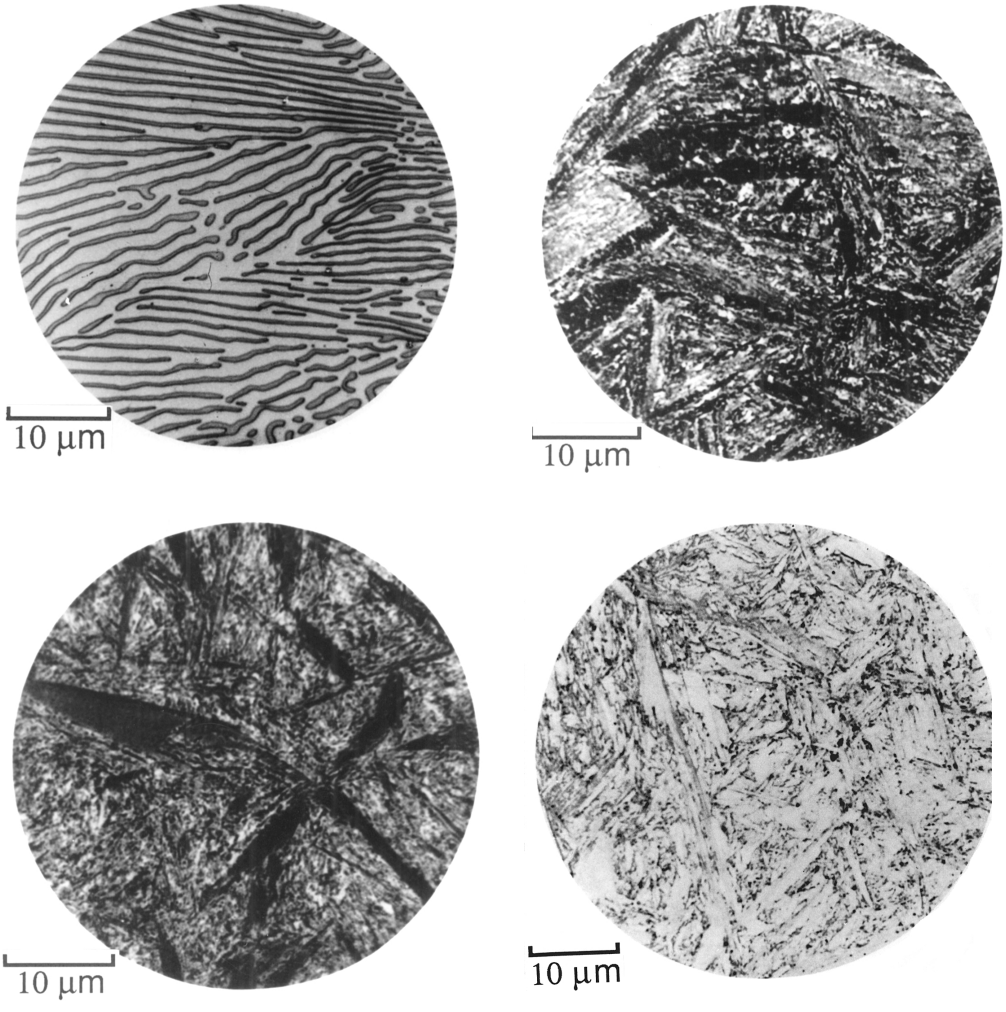

Fig. 1.1 Microstructures in a eutectoid steel: (a) Pearlite formed at 720 °C; (b) bainite obtained by isothermal transformation at 290 °C; (c) bainite obtained by isothermal transformation at 180 °C; (d) martensite. The micrographs were taken by Vilella and were published in the book *The Alloying Elements in Steel* (Bain, 1939). Notice how the bainite etches much darker than martensite, because its microstructure contains many fine carbides.

and promising properties; it was found to be 'tougher for the same hardness than tempered martensite' (Bain, 1939), and was the cause of much excitement at the newly established United States Steel Corporation Laboratory in New Jersey. It is relevant to note here the contributions of Lewis (1929) and Robertson (1929), who were the first to publish the results of isothermal

transformation experiments on eutectoid steel wires, probably because of their relevance to patented steel. But the Davenport and Bain experiments were unique in showing the progressive nature of the isothermal transformation of austenite, using both metallography and dilatometry. Their experiments were successful because they utilised very thin samples. Their method of representing the kinetic data in the form of time-temperature-transformation curves turned out to be so simple and elegant, that it would be inconceivable to find any contemporary materials scientist who has not been trained in the use or construction of 'TTT' diagrams.

In 1934, the research staff of the laboratory named the microstructure 'Bainite' in honour of their colleague E. C. Bain who had inspired the studies, and presented him with the first ever photomicrograph of bainite, taken at a magnification of $\times 1000$ (Smith, 1960; Bain, 1963).

The name 'bainite' did not immediately catch on. It was used rather modestly even by Bain and his co-workers. In a paper on the nomenclature of transformation products in steels, Vilella, Guellich and Bain (1936) mentioned an 'unnamed, dark etching, acicular aggregate somewhat similar to martensite' when referring to bainite. Hoyt, in his discussion to this paper appealed to the authors to name the structure, since it had first been produced and observed in their laboratory. Davenport (1939) ambiguously referred to the structure, sometimes calling it 'a rapid etching acicular structure', at other times calling it bainite. In 1940, Greninger and Troiano used the term 'Austempering Structures' instead of bainite. The 1942 edition of the book *The Structure of Steel* (and its reprinted version of 1947) by Gregory and Simmons contains no mention of bainite.

The high-range and low-range variants of bainite were later called 'upper bainite' and 'lower bainite' respectively (Mehl, 1939) and this terminology remains useful to this day. Smith and Mehl (1942) coined the term 'feathery bainite' for upper bainite which forms largely, if not exclusively, at the austenite grain boundaries in the form of bundles of plates, and only at high reaction temperatures, but this description has not found frequent use. Both upper and lower bainite were found to consist of aggregates of parallel plates, aggregates which were later designated sheaves of bainite (Aaronson and Wells, 1956).

1.2 The Early Research

Early work into the nature of bainite continued to emphasise its similarity with martensite. Bainite was believed to form with a supersaturation of carbon (Wever, 1932; Wever and Jellinghaus, 1932; Portevin and Jolivet, 1937,1938; Portevin and Chevenard, 1937). It had been postulated that the transformation involves the abrupt formation of flat plates of supersaturated ferrite along

certain crystallographic planes of the austenite grain (Vilella *et al*., 1936). The ferrite was then supposed to decarburise by rejecting carbon at a rate depending on temperature, leading to the formation of carbide particles which were quite unlike the lamellar cementite phase associated with pearlite. The transformation was believed to be in essence martensitic, 'even though the temperature be such as to limit the actual life of the quasi-martensite to millionths of a second'. Bain (1939) reiterated this view in his book *The Alloying Elements in Steel*. Isothermal transformation studies were by then becoming very popular and led to a steady accumulation of data on the bainite reaction, still variously referred to as the 'intermediate transformation', 'dark etching acicular constituent', 'acicular ferrite', etc.

In many respects, isothermal transformation experiments led to the clarification of microstructures, since individual phases could be studied in isolation. There was, however, room for difficulties even after the technique became well established. For alloys of appropriate composition, the upper ranges of bainite formation were found to overlap with those of pearlite, preceded in some cases by the growth of proeutectoid ferrite. The nomenclature thus became confused since the ferrite which formed first was variously described as massive ferrite, grain boundary ferrite, acicular ferrite, Widmanstätten ferrite, etc. On a later view, some of these microconstituents are formed by a 'displacive' or 'military' transfer of the iron and substitutional solute atoms from austenite to ferrite, and are thus similar to carbon-free bainitic ferrite, whereas others form by a 'reconstructive' or 'civilian' transformation which is a quite different kinetic process (Buerger, 1951; Christian, 1965a).

1.2.1 Crystallography

By measuring the crystallographic orientation of austenite using twin vestiges and light microscopy, Greninger and Troiano (1940) were able to show that the habit plane of martensite in steels is irrational. These results were consistent with earlier work on non-ferrous martensites and put paid to the contemporary view that martensite in steels forms on the octahedral planes of austenite. They also found that with one exception, the habit plane of bainite is irrational, and different from that of martensite in the same steel (Fig. 1.2). The habit plane indices varied with the transformation temperature and the average carbon concentration of the steel. The results implied a fundamental difference between bainite and martensite. Because the habit plane of bainite approached that of Widmanstätten ferrite at high temperatures, but the proeutectoid cementite habit at low temperatures, and because it always differed from that of martensite, Greninger and Troiano proposed that bainite from the very beginning grows as an aggregate of ferrite and cementite. A competition between the ferrite and cementite was supposed to cause the changes in the

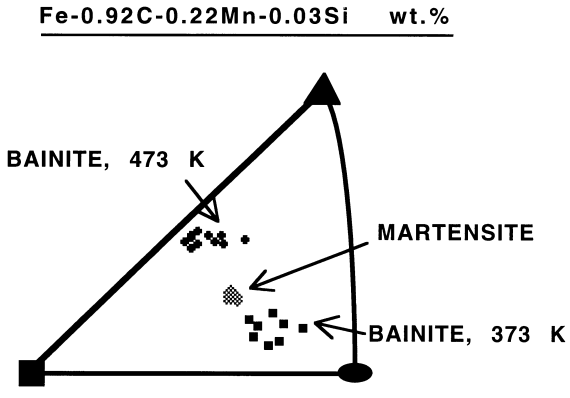

Fig. 1.2 An example of the results obtained by Greninger and Troiano (1940), showing the irrational habit of bainite, which changed as a function of the transformation temperature. Notice also that the habit plane of bainite is different from that of martensite in the same steel.

bainite habit, the ferrite controlling at high temperatures and the cementite at low temperatures. The competition between the ferrite and cementite was thus proposed to explain the observed variation of bainite habit plane. The crystallographic results were later confirmed using an indirect and less accurate method (Smith and Mehl, 1942). These authors also showed that the orientation relationship between bainitic ferrite and austenite does not change very rapidly with transformation temperature and carbon content and is within a few degrees of the orientations found for martensite and Widmanstätten ferrite, but differs considerably from that of pearlitic ferrite/austenite. Since the orientation relationship of bainite with austenite was not found to change, Smith and Mehl considered Greninger and Troianos' explanation for habit plane variation to be inadequate, implying that the habit plane cannot vary independently of the orientation relationship.

1.2.2 The Incomplete Reaction Phenomenon

It was known as long ago as 1939 that in certain alloy steels 'in which the pearlite change is very slow', the extent of transformation to bainite decreases, ultimately to zero, as the transformation temperature is increased (Allen *et al.*, 1939). For example, the bainite transformation in a Fe–2.98Cr–0.2Mn–0.38C wt% alloy was found to begin rapidly but cease shortly afterwards, with the maximum volume fraction of bainite obtained increasing with decreasing transformation temperature (Klier and Lyman, 1944). At no temperature investigated did the complete transformation of austenite occur solely by decomposition to

bainite. The residual austenite remaining untransformed after the cessation of the bainite reaction, reacted by another mechanism (pearlite) only after a further long delay. Cottrell (1945) in his experiments on a low-alloy steel, found that the amount of bainite that formed at 525 °C ($\ll Ae_3$) was negligible, and although the degree of transformation increased as the isothermal reaction temperature was decreased, the formation of bainite appeared to stop before reaching completion. Other experiments on chromium-containing steels revealed that the dilatometric expansion due to bainite became larger as the transformation temperature was reduced (Fig. 1.3, Lyman and Troiano, 1946). Oddly enough, the bainite transformation did not seem to reach completion on isothermal heat treatment, even though all of the austenite could readily transform to pearlite at a *higher* transformation temperature (Klier and Lyman, 1944). Often, the transformation of austenite at lower temperatures occurred in two stages, beginning with the bainite reaction which stopped prematurely, to be followed by the formation of pearlite at a slower rate. It is significant that the two reac-

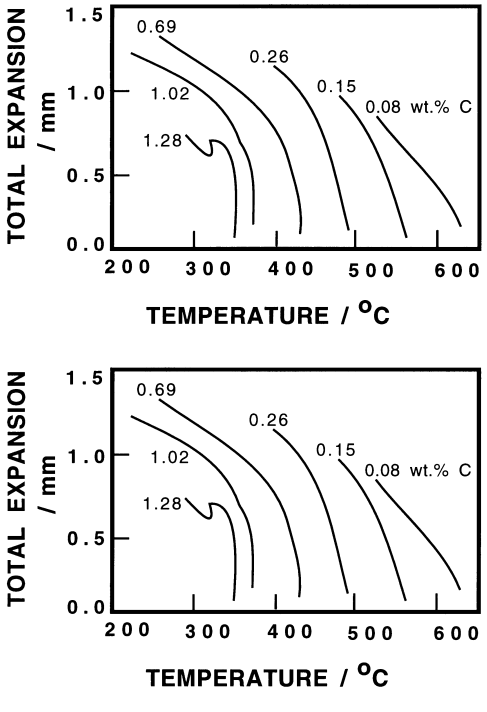

Fig. 1.3 Temperature dependence of the total dilatometric expansion due to the formation of bainite (Lyman and Troiano, 1946). Transformation to bainite does not begin until a critical temperature B_S, which is well below the equilibrium Ae_3 temperature. The amount of bainite that can form at any temperature increases with the undercooling below B_S.

tions may only be separated by a long delay in well-alloyed steels; in plain carbon steels 'the second reaction sets in within a few seconds after the beginning of the bainite reaction' (Klier and Lyman, 1944).

1.2.3 Carbon Redistribution

X-ray and other experiments indicated that the formation of bainite enriches the residual austenite in carbon. Klier and Lyman (1944) took this to mean that the austenite, prior to its transformation to bainite, becomes compositionally unstable and separates into carbon-rich and carbon-depleted volumes; in modern terminology, this would require uphill diffusion. The low carbon regions were then supposed to transform into supersaturated bainite of the same composition, by a 'martensite-like' lattice rearrangement, to be followed soon after by the precipitation of iron carbides. A similar suggestion had been made earlier by Kurdjumov (1933) in the context of Widmanstätten ferrite: 'regions of low carbon concentration in the γ crystal result from diffusion within the γ phase, and these regions can at this time transform into the α phase ...' Entin (1962) seemed to rediscover this idea, leading Aaronson (1966a) to prove using thermodynamics that an austenitic Fe–C solid solution cannot spontaneously undergo separation into carbon-rich and carbon-poor regions. There is no tendency for the austenitic solid solution to undergo spinodal decomposition. The concept nonetheless seems to crop up with notorious regularity even in modern literature (e.g. Prado, 1986; Prado *et al*., 1990).

The proof by Aaronson *et al*. does not of course rule out random fluctuations of composition, of the type associated with any solid solution in dynamic equilibrium. It has therefore been argued that the nucleation of bainite is favoured in regions of austenite where the carbon concentration is relatively low as a consequence of fluctuations (Degang *et al*., 1989). Indeed, carbon-free regions of several thousand iron atoms can exist at all temperatures in austenite of eutectoid composition (Russell, 1971). The difficulty arises when it is claimed that these carbon-depleted regions lead to an enhancement of the nucleation rate. For every such region there must also exist a carbon-enriched region where the probability of ferrite nucleation is presumably reduced, thereby balancing the effects of the depleted regions. Consequently, there is no advantage in adopting this microscopic approach. The usual macroscopic thermodynamic model in which the driving forces are calculated for uniform composition should suffice.

1.2.4 Thermodynamics

In a far-reaching paper, Zener (1946) attempted to give a rational thermodynamic description of the phase transformations that occur in steels. He

assumed that bainite growth is diffusionless, any carbon supersaturation in bainitic ferrite being relieved subsequent to growth, by partitioning into the residual austenite. The atomic mechanism of bainite growth was not discussed in detail, but he believed that unlike martensite, there is no strain energy associated with the growth of bainite. Thus bainite should form at a temperature just below T_0, where the austenite and ferrite of the same composition have identical free energies (Fig. 1.4).

However, T_0 is frequently used in martensite theory for the temperature at which austenite and martensite (i.e. supersaturated tetragonal 'ferrite') have the same free energy; for clarity, we follow Christian and Edmonds (1984) and call this temperature T_{om}. The Bain strain applied to a random interstitial solution of carbon in austenite automatically produces the ordered tetragonal form of ferrite if the carbon atoms are trapped in their original sites, but Zener

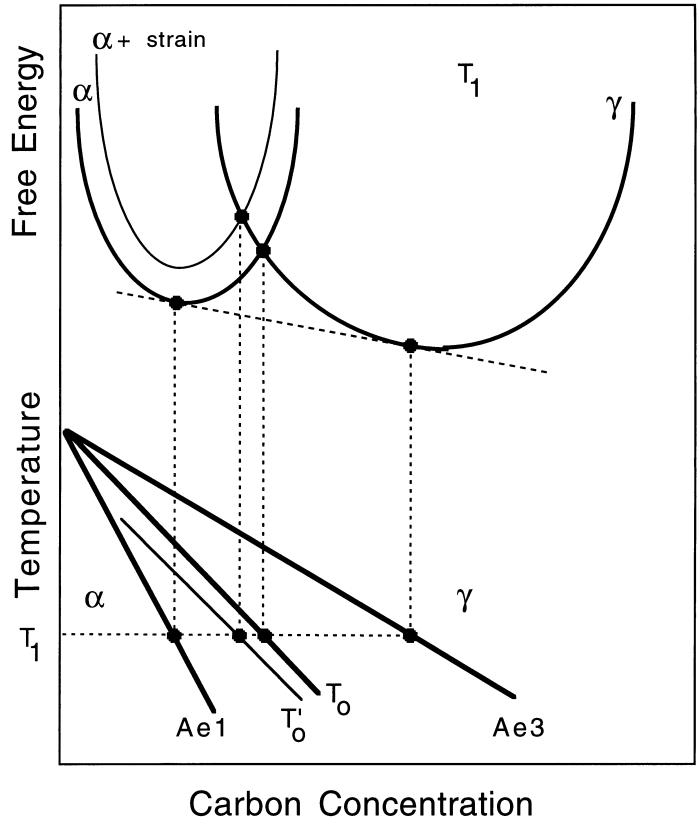

Fig. 1.4 Schematic illustration of the origin of the T_0 curve on the phase diagram. The T_0' curve incorporates a strain energy term for the ferrite, illustrated on the diagram by raising the free energy curve for ferrite by an appropriate quantity.

also supposed that the tetragonal form may be regarded as a result of an ordering of the interstitial atoms into one set of sites of the cubic structure. He derived an equation for the critical temperature T_c at which the cubic and tetragonal forms of ferrite have the same free energy. T_c rises with interstitial solute content, and thus intersects the M_S temperature and also has a joint intersection with the T_0 and T_{om} temperatures. Clearly T_{om} lies below T_0 at low carbon contents and above T_0 at high carbon contents. According to one interpretation (Owen, Wilson and Bell, 1964), martensite formed above room temperature is cubic at carbon contents below the intersection of M_S and T_c (above 2.5 at% carbon in plain iron–carbon alloys) and tetragonal above it. As Zener pointed out, martensite cannot form until the driving force obtained by supercooling below the T_0 or T_{om} temperature is large enough to provide the necessary strain energy.

It is usually assumed that bainite forming first as fully supersaturated ferrite nevertheless has a cubic structure, but it would seem more logical to assume a tetragonal structure unless the temperature of formation is above T_c.

The Zener model failed to provide an explanation of why the strain energy should exist for martensite and not for bainite. On the other hand, it explained the data showing that the degree of transformation to bainite increases with supercooling from zero at an upper limit, which is generally known as the bainite-start or B_S temperature. The carbon that partitions into the austenite *after* the formation of bainite changes its composition, until it eventually becomes thermodynamically impossible for the austenite to transform and the reaction stops. For a given alloy, a larger undercooling below T_0 would allow more bainite to form before diffusionless growth becomes impossible. Consistent with experimental data, the model also requires the bainite C curve of the TTT diagram to tend asymptotically to infinite time (Fig. 1.5) at a temperature corresponding to the T_0 or T_{om} temperature whichever is higher, since the transformation of austenite without a composition change cannot occur above this limit.

The initial plates of bainite, unlike those of many martensites, often grow to a limited size less than that of the parent austenite grain. Zener suggested that a layer of cementite around the plate stifles its subsequent growth.

1.2.5 Paraequilibrium

By 1947, it was evident that the cementite associated with bainite is different from that found in pearlite. The latter was always found to have a different substitutional solute concentration when compared with the average value, whereas the cementite in bainite had about the same substitutional content as the matrix from which it grew. Hultgren (1947), has cited several references

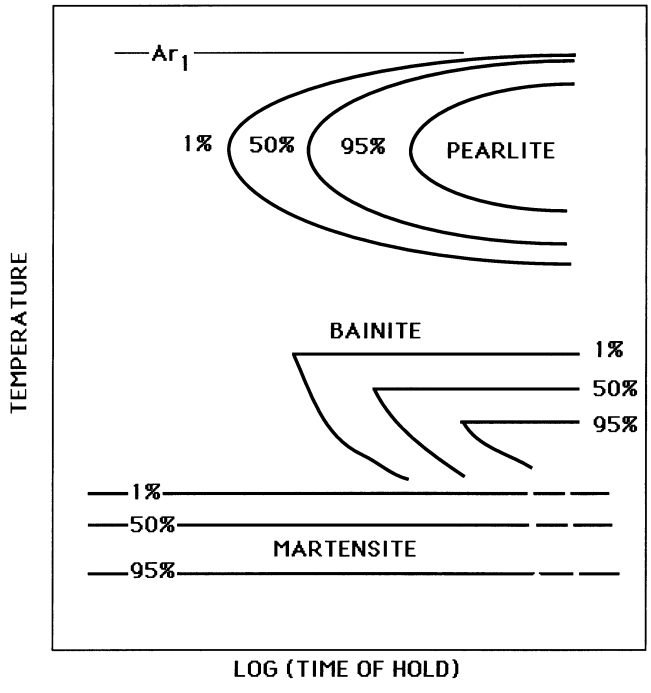

Fig. 1.5 Schematic TTT diagram illustrating the flat tops on the bainite C-curves (after Zener, 1946).

which report magnetic, chemical and X-ray data on extracted carbides which confirm this difference between the two kinds of cementite.

Hultgren was at the time proposing a model for the role of substitutional alloying elements in steels; at high temperatures where diffusion rates are reasonable, these elements can redistribute during transformation in a way consistent with equilibrium. The transformation was then said to occur under 'orthoequilibrium' conditions. This contrasts with 'paraequilibrium' in which the substitutional alloying elements are unable to partition, although carbon, which is a fast diffusing interstitial element, redistributes between the phases until its chemical potential is uniform throughout.

The mechanism of pearlite growth was not clear in those days, but the transformation was believed to be initiated by the nucleation of cementite. This led to the contrasting suggestion that bainite is initiated by the nucleation of ferrite (Mehl, 1939; Smith and Mehl, 1942; Mehl, 1948). Hultgren put these ideas together and proposed that upper bainite begins with the nucleation and growth of ferrite with a paraequilibrium carbon concentration, causing the residual austenite to become enriched in carbon. This bainitic ferrite, unlike the ferrite associated with pearlite, was believed to have a rational Kurdjumov–

Sachs or Nishiyama–Wasserman orientation relationship with the parent austenite in which it grows. This was considered to explain the observed difference in ferrite morphologies in bainite and pearlite. Bainitic ferrite was always found to consist of individual plates or sheaves whereas the ferrite in pearlite apparently formed alternating plates of a regularly spaced two-phase lamellar aggregate. The enrichment of austenite with carbon should eventually cause the paraequilibrium precipitation of cementite from austenite in a region adjacent to the bainitic ferrite. At the time, pearlitic cementite was thought to bear a rational orientation relation to the austenite grain into which the pearlite colony grows, and Hultgren proposed, without any evidence, that bainitic cementite should be randomly orientated to the austenite in which it precipitated. This process of ferrite and subsequent cementite precipitation then repeated, giving rise to the sheaf of bainite. Hultgren therefore considered upper bainite to be similar to pearlite but growing under paraequilibrium conditions and different in the orientation relations with austenite.

No explanation was offered for the occurrence of paraequilibrium with bainite, nor for the existence of the various orientation relationships. He admitted the possibility that bainite formed at lower temperatures (later known as *lower* bainite) 'forms directly', implying that the bainitic ferrite formed with a supersaturation of carbon, although the mechanism was not discussed.

The model of pearlite formation involving the repeated formation of ferrite and cementite was abandoned when Hillert (1962) demonstrated that a pearlite colony really consists of two interwoven crystals, one of ferrite and the other of cementite. Hillert (1957, 1962) also pointed out an important distinction between pearlite and upper bainite; in the former case, the ferrite and cementite phases grow cooperatively, whereas in the latter case, the plates of bainitic ferrite form first with the precipitation of cementite being a subsequent reaction.

1.2.6 Kinetics

Experiments by Wiester (1932), Hannemann *et al*. (1932–1933) and Forster and Scheil (1936, 1937) indicated that martensite can grow very rapidly in steels, a plate taking a few microseconds to grow right across an austenite grain. Bunshah and Mehl (1953) later measured the growth rate to be as high as $1\,\mathrm{km\,s^{-1}}$, i.e. about one-third of the velocity of sound in iron. This gave rise to the incorrect impression that martensitic transformation does not involve a 'nucleation and growth process'. Thus, Smith and Mehl (1942), wondered whether bainitic structures form by a process of nucleation and growth or whether the plates spring full-formed from the matrix lattice 'as they do in the transformation to martensite'. A nucleation and growth model was

favoured since the sizes of the reacted regions apparently increased with time at the reaction temperature. This was consistent with the work of Wever and his co-workers (1932), who found that in the bainite transformation range, the austenite decomposes relatively slowly. Furthermore, the progress of the bainite transformation could be represented by means of a C-curve on a TTT diagram (Davenport and Bain, 1930), with a well defined incubation period before the beginning of isothermal transformation. Martensitic transformation, on the other hand could not be suppressed by the fastest available quench rates (Troiano and Greninger, 1946); it seemed to form athermally and was represented on the TTT diagram by a family of lines parallel to the time axis (Cohen, 1946). The bainite reaction was found to follow C-curve kinetics even below the M_S temperature (Howard and Cohen, 1948).

It is in this context that Ko and Cottrell (1952) attempted to investigate whether bainite is 'a nucleation and growth reaction, or like martensite, forms in a fraction of a second'. They also wanted to establish whether the transformation leads to surface relief effects similar to those associated with martensitic transformations. Ko and Cottrell were able to demonstrate, through hot-stage light microscopy, that bainite grows relatively slowly and that its formation causes the shape of the transformed region to change, the shape change being characterised qualitatively as an invariant-plane strain (Fig. 1.6). They also noted that unlike pearlite which is not hindered by austenite grain boundaries (Mehl, 1948), bainite growth terminated at austenite twin or grain boundaries. The transformation was therefore similar to martensite, and Ko and Cottrell attempted to identify any clear differences that may exist between martensite and bainite.

It was known already that martensite first forms at a large undercooling below the T_0 temperature, at which ferrite and austenite of identical composition have equal free energy (Zener, 1946; Cohen *et al*., 1950). Since diffusionless transformation is *thermodynamically* feasible below T_0, the extra undercooling was believed necessary to account for the strain and to a lesser extent, the interface energy associated with the formation of the martensite plate. Bainite, which forms at higher temperatures, must have a different mechanism consistent with the smaller driving force available at elevated temperatures. Ko and Cottrell argued that a 'coherent nucleus' can develop either into martensite or into bainite depending on the driving force available for transformation, the nucleus developing into martensite below M_S. At the higher temperatures where bainite occurs, 'coherent growth' can only 'take place when the strain due to the density change is relieved'. This could happen if the amount of carbon dissolved in bainite is reduced, either by diffusion from bainite or by precipitation within bainite, or by a combination of these processes, depending on the transformation temperature. It is not clear from their description whether they envisaged initially diffusionless growth, followed by carbon dif-

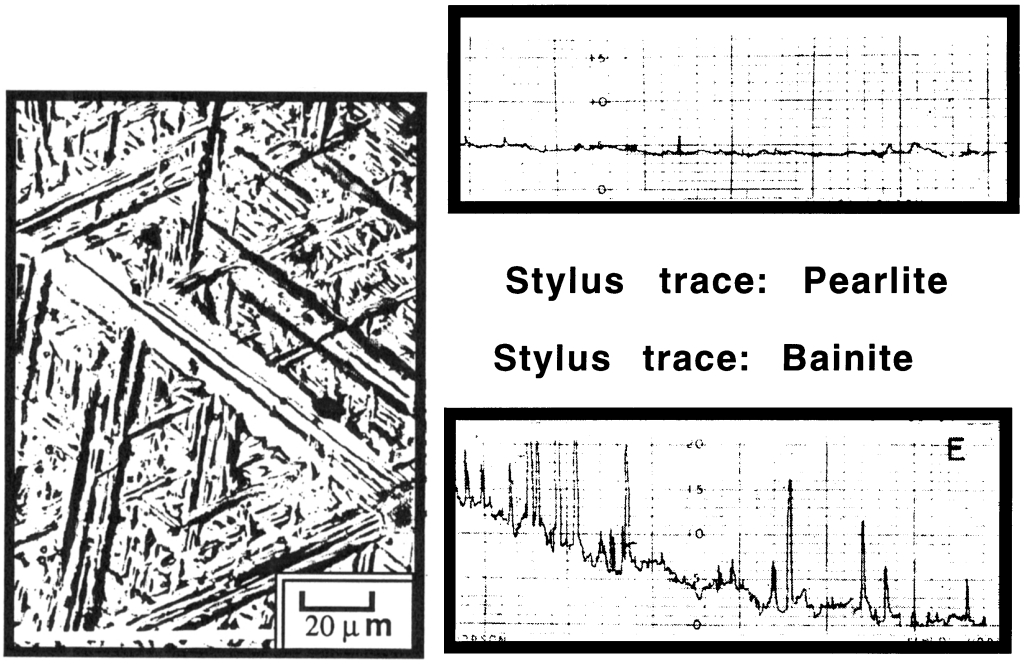

Fig. 1.6 Surface effects observed during the transformation of pre-polished samples of austenite (Ko and Cottrell, 1952): (a) Surface relief due to the formation of bainite; (b) Line traces obtained by traversing a stylus across the surface of a pearlitic and a bainitic sample. Notice the severe upheavals caused by bainite, which contrast with the negligible relief due to pearlite.

fusion to provide the driving force for further growth, or whether the diffusion and interface migration are coupled so that precipitation within the ferrite (for lower bainite) or carbon rejection to the austenite (for upper bainite) takes place at the moving interface. The former mechanism is illogical since the extra driving force is only available after a stage of initial growth to martensite which should not be possible (according to their growth condition) above M_S. Provided there is some way of circumventing the difficulty of forming the initial coherent nucleus (of whatever composition), the second type of growth model would allow bainite to form above M_S, and indeed above T_0. In some later work, Ko (1953) distinguished between incoherent ferrite and 'acicular ferrite' which he proposed should be regarded as carbon-free bainitic ferrite.

Kriesement and Wever (1956) pointed out that the appearance of bainite changes continuously between upper and lower bainite, and postulated that the microstructure evolves by the repeated and alternating nucleation and growth of lamellae of cementite and ferrite, from austenite. Unlike pearlite,

the growth direction of the macroscopic plate of bainite was supposed to be normal to the plane of the lamellae. Although this particular mechanism has since been shown to be incorrect, they identified clearly the condition necessary for cementite precipitation to occur from residual austenite during the bainite transformation. Cementite precipitates from austenite if the carbon concentration of the latter exceeds that given by the extrapolated $\gamma/\gamma + \theta$ phase boundary.

Although many of the characteristics of bainite, especially the morphology and the shape deformation, had been found to be similar to those of martensite, a different microstructural approach was developed by Aaronson (1962). He used the Dubé morphological classification (Dubé *et al*., 1958; Heckel and Paxton, 1961) for all non-pearlitic forms of ferrite and attributed the morphological variations to the dependence on the growth kinetics of an interface and to the nature of the site from which a precipitate crystal develops. In particular, plate morphologies were regarded as the result of the formation of immobile, partly coherent, planar interfaces which can grow normal to themselves only by the lateral migration of 'ledges'. In a later discussion of bainite, Aaronson (1969) developed the 'microstructural' definition in which bainite is regarded simply as a non-lamellar two-phase aggregate of ferrite and carbides in which the phases form consecutively, as distinct from pearlite where they form cooperatively. Aaronson stated that according to this definition, the upper limiting temperature of bainite formation should be that of the eutectoid reaction (Ae_1), and he denied that the kinetic B_S temperature has any fundamental significance. In those alloy systems where there seems clear evidence for a separate C-curve for bainite, the bainitic 'bay' and the apparent upper limit of bainite formation (B_S) were attributed to a special effect of certain alloying elements on the growth kinetics. Aaronson equally dismissed the observation of surface relief as a basis for classifying the various forms of ferrite.

1.3 Bainitic Steels: Industrial Practice

In spite of the early optimism about the potential of bainitic steels, commercial exploitation took many years to become established. The steels were not better than quenched and tempered martensitic steels, partly because of the coarse cementite particles associated with bainite and because the continuous cooling heat treatments which were popular in industry, could not in practice produce fully bainitic steels. The use of lean alloys gave mixed microstructures whereas intense alloying led to intolerable quantities of martensite. It was not until low-alloy, low-carbon steels containing boron and molybdenum were introduced by Irvine and Pickering (1958) that fully bainitic steels could be produced in commercial quantities using continuous cooling heat treatments. Nonetheless, martensitic steels dominated the high-strength steel market, with their better

overall mechanical properties and well understood physical metallurgy principles.

Even lower carbon concentrations than conceived by Irvine and Pickering could have led to better bainitic steels, with strength and toughness due to the submicron size grain structure of bainite. However, technology was not in those days sufficiently advanced to cope with the necessarily higher cooling rates required to produce bainite in very low-carbon steels, as the steel left the hot-rolling mill. The first system designed to accelerate cooling of hot sheet steel as it leaves the mill, was at the United Steel Company (UK), probably as a means to reduce the length of the run-out table which allows the strip to cool to a specified temperature before coiling. The faster cooling was achieved using a laminar water jet system (Adcock, 1962). The first papers discussing the metallurgical benefits of accelerated cooling were presented in 1965 (Morgan *et al*.). The technology of accelerated cooling designed to produce partially or wholly bainitic microstructures in very low-carbon, microalloyed steels has been perfected within the last fifteen years or so, with the new class of steels being the cause of much excitement (DeArdo, 1988).

An area of major success for bainite was in sector of creep resistant steels, where the so-called $2\frac{1}{4}$Cr–1Mo steel was known to be one of the best alloys for creep strength and microstructural stability in large components (Miller *et al*., 1940). The microstructural aspects of the steel may not have been appreciated in those days, but on continuous cooling it transforms into carbide-free upper bainite. In most applications, the microstructure is then heavily tempered at 700°C for several hours in order to relieve any residual stress. The tempering treatment and service at elevated temperatures causes the precipitation of a series of metastable alloy carbides, which together with solid solution strengthening by molybdenum, greatly enhance the creep strength. This particular alloy even now sustains the energy generation industry (Lundin *et al*., 1982).

1.4 Summary of the Early Research

By the beginning of the sixties, bainite was regarded as a transformation product differing significantly from various forms of proeutectoid ferrite as well as from pearlite and martensite. The results of the early research can be summarised as follows (Fig. 1.7).

Bainite can be obtained by isothermal transformation at all temperatures where the formation of pearlite and proeutectoid ferrite is sluggish, and also at temperatures below the martensite-start temperature. Upper bainite, which forms at high temperatures, was found to consist of sheaves of ferrite plates with cementite particles located between the plates. By contrast, lower bainite was characterised by fine cementite particles within the bainitic ferrite plates in addition to those between the plates.

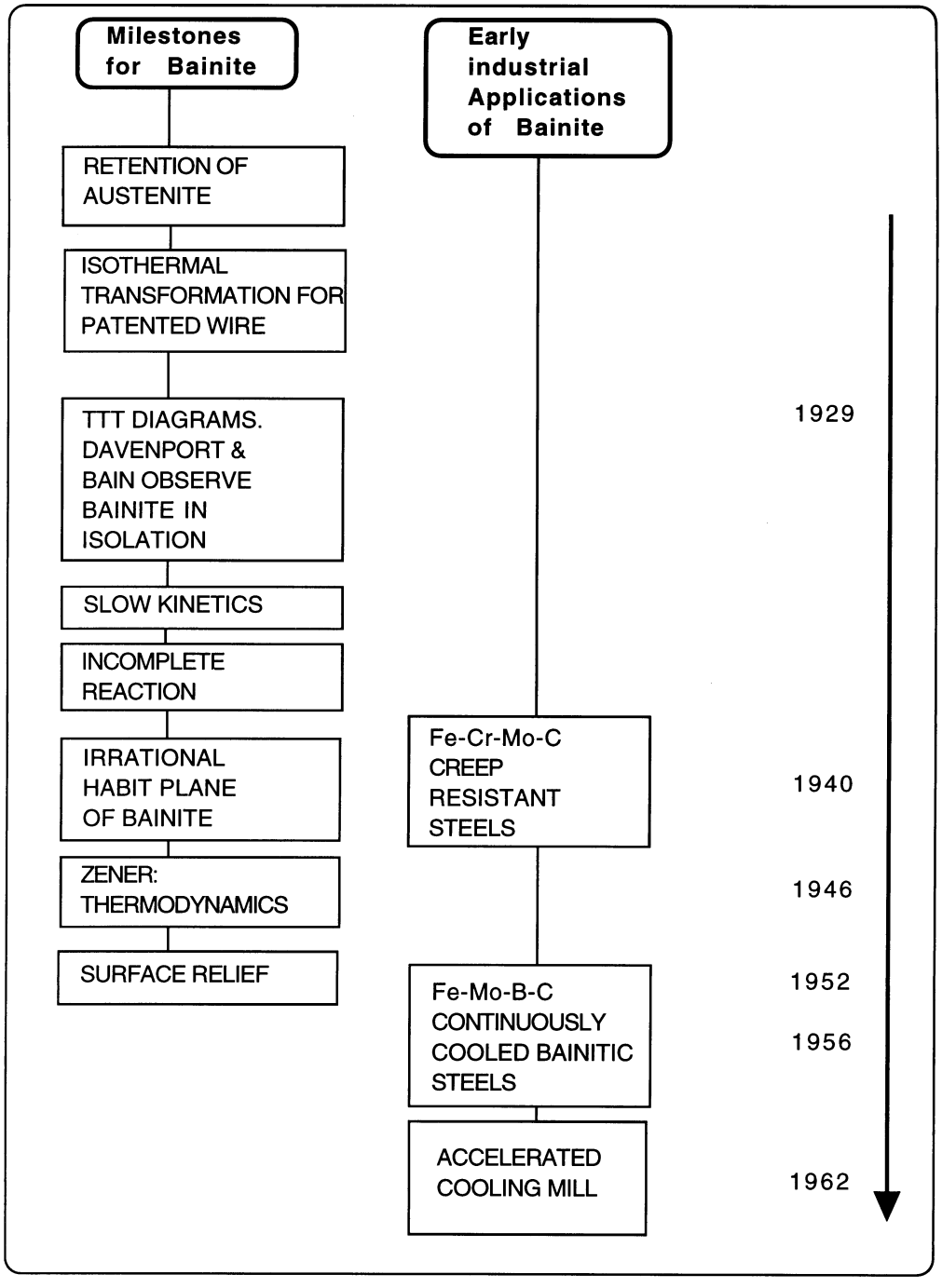

Fig. 1.7 Flow chart illustrating some of the important milestones in the history of bainite

Observations using light microscopy indicated that bainite sheaves lengthen at a rate much slower than martensite plates. Bainite sheaves were found to have irrational habit planes, the indices of which differed from those of martensite in the same alloy. The orientation relationship between bainitic ferrite and austenite was on the other hand similar to that between martensite and austenite. Bainite plates were never found to cross austenite grain boundaries and the formation of bainite was, like martensite, observed to cause the shape of the parent crystal to change. This shape deformation is in present day terminology better described as an invariant-plane strain.

In steels where transformation to bainite could be carried out without interference from other reactions, experiments demonstrated that the degree of transformation to bainite decreases (ultimately to zero) and that the time taken to initiate the reaction increases rapidly with increasing isothermal transformation temperature. This led to the definition of a bainite-start temperature (B_S) above which there is no reaction. This temperature was always found to lie well within the (metastable) $\alpha + \gamma$ phase field. Other reactions could follow bainite, but in all cases, the rapid growth of bainite stopped prematurely before the austenite was fully transformed.

The prevailing, albeit rather ill-defined concept of the bainitic reaction as involving a martensitic type interface combined with carbon diffusion-controlled growth had already led to the suggestion of bainitic reactions in non-ferrous alloys. In particular, the observation of surface relief effects apparently combined with compositional changes in the decomposition of some β-phase copper–zinc alloys had been used in a pioneering paper by Garwood (1954–5) to identify this decomposition as bainitic, and the difficulties in accounting for such a reaction in purely substitutional alloys had been emphasised (Christian, 1962). This remains an interesting aspect of transformation theory (Christian, 1997).

The early emphasis on the similarities between bainitic and martensitic transformations still dominated the literature in the 1960s. The contrasting views of Aaronson and co-workers were only beginning to emerge. This led to controversy but also stimulated research. There is now a clear picture of the mechanism of transformation, the quantitative aspects of which have contributed significantly to the design of some remarkable steels.

.

2 *Bainitic Ferrite*

The growth of pearlite occurs at a common transformation front with the austenite. The growth of the ferrite and cementite phases is coupled and their compositions are complementary since the carbon which cannot be accommodated by the ferrite is incorporated into the cementite. This contrasts with bainite which occurs in separable stages, first the growth of ferrite, followed by the precipitation of carbides. This chapter deals with the ferritic component of bainite, focusing on its morphology, crystallography, constitution and kinetics.

2.1 Sheaves of Bainite

2.1.1 Morphology

Both upper and lower bainite consist of aggregates of plates of ferrite, separated by untransformed austenite, martensite or cementite (Fig. 2.1). The aggregates of plates are called *sheaves* (Aaronson and Wells, 1956) and the plates within each sheaf are the *sub-units*. The sub-units are not isolated from each other but are connected in three dimensions. It follows that they share a common crystallographic orientation.

Many observations, including two-surface analysis experiments, show that the shape of a sheaf is that of a wedge-shaped plate (Oblak *et al*., 1964; Srinivasan and Wayman, 1968b). The thicker end of the wedge begins at the nucleation site which is usually an austenite grain surface. The sub-units which make up the sheaf have a lenticular plate or lath morphology, whose form is most prominent near the edge or tip of a sheaf where impingement effects are minimal (Fig. 2.2).

The shape is best observed in partly transformed specimens. The dimensions of a sub-unit are uniform within a sheaf because each sub-unit grows to a limiting size. New sub-units are most frequently nucleated near the tips of existing sub-units rather than on their sides. The overall morphology of a sheaf is illustrated in Fig. 2.3.

When the sub-units are in the form of laths, they are longest along the close-packed direction of the ferrite which is most parallel to a corresponding close-packed direction of the austenite (Davenport, 1974). As with martensite, plates tend to form at low temperatures, large carbon concentrations or in strong

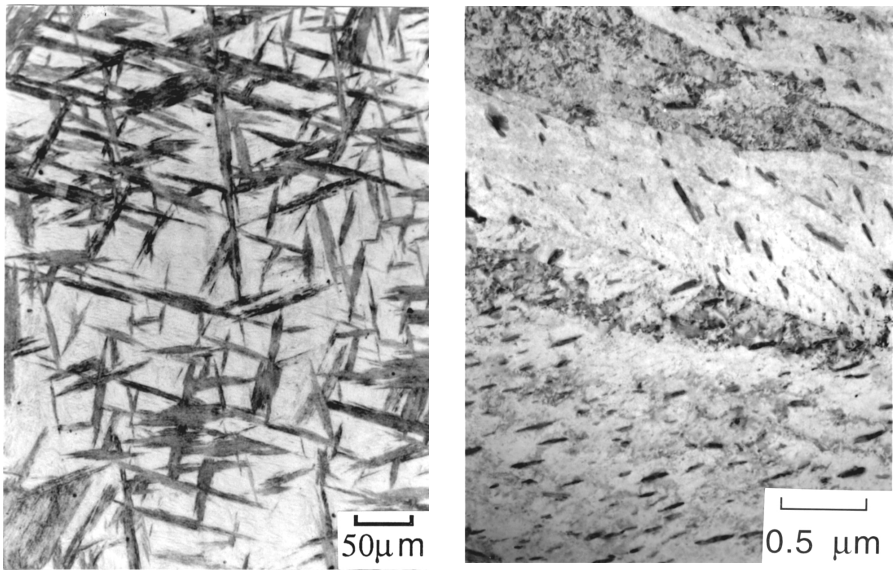

Fig. 2.1 (a) Light micrograph illustrating sheaves of lower bainite in a partially transformed (395 °C) Fe–0.3C–4Cr wt% alloy. The light etching matrix phase is martensite. (b) Corresponding transmission electron micrograph illustrating sub-units of lower bainite.

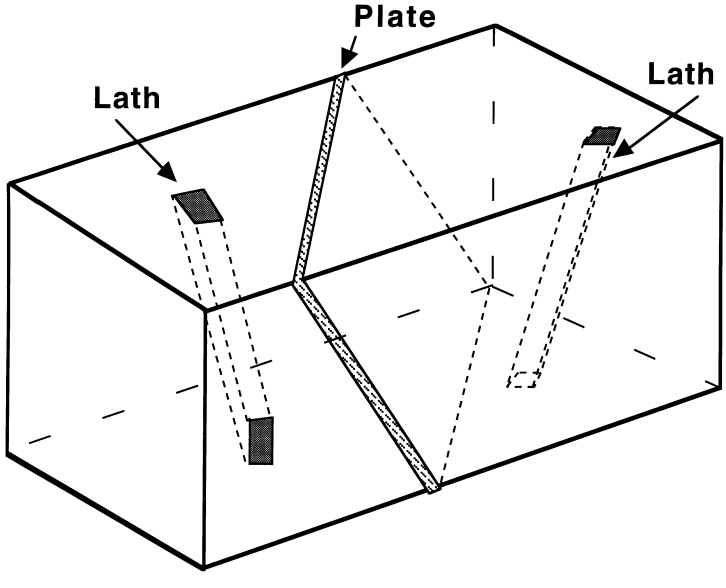

Fig. 2.2 The three-dimensional shape of a plate and of a lath.

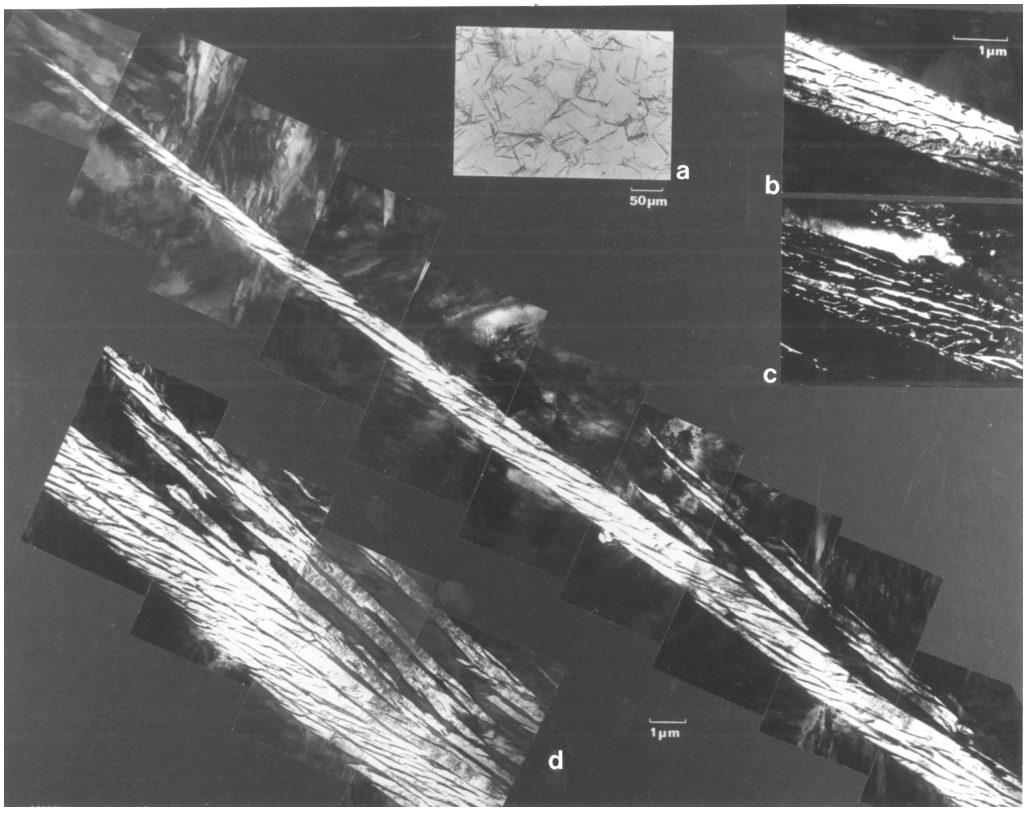

Fig. 2.3 Transmission electron micrograph of a sheaf of upper bainite in a partially transformed Fe–0.43C–2Si–3Mn wt% alloy: (a) light micrograph; (b, c) bright field and corresponding dark-field image of retained austenite between the sub-units; (d) montage showing the structure of the sheaf.

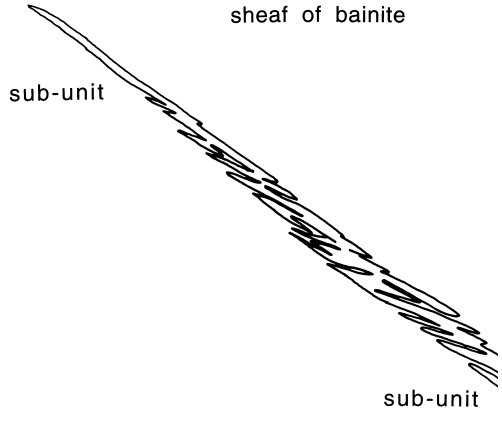

Fig. 2.3e Corresponding outline of the sub-units near the sheaf tip region.

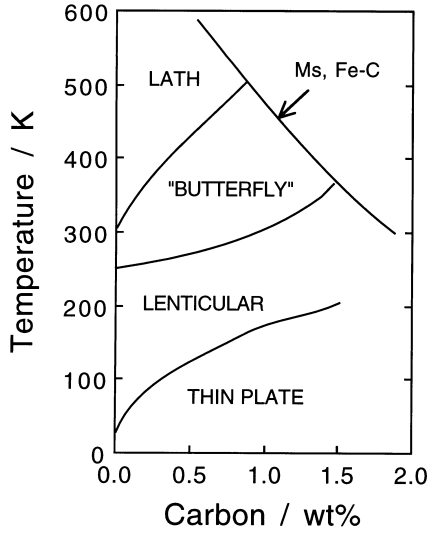

Fig. 2.4 The shape of martensite crystals as a function of the transformation temperature and carbon concentration of Fe–Ni–C alloys (after Maki and Tamura, 1986).

austenite, Fig. 2.4 (Kelly and Nutting, 1960; Davies and Magee, 1970a,b, 1971; Haezebrouck, 1987). Thus, a plate morphology can be induced by increasing the strength of the austenite even if the transformation temperature is increased at the same time (Laverrouz and Pineau, 1974). Similarly, the lath to plate transition can be induced using a magnetic field changing the driving force for transformation, without altering the transformation temperature (Korenko, 1973).

The physical basis for these correlations is not clear because the variables described are not independent. The strength of the austenite must play a role because it determines the extent to which the shape change is plastically accommodated. Lath martensite is associated with this plastic accommodation which ultimately stifles the growth of the lath.

This hypothesis has been developed in detail by Haezebrouck (1987) who proposed that a plate shape is promoted by rapid radial growth and a high yield stress in the parent phase. Both of these factors favour elastic growth. A high growth rate is equivalent to a high strain rate, which makes yielding more difficult. The radial growth must be elastic for small particles but whether this can be sustained as the particle grows depends on the flow behaviour of the austenite. The effect of plasticity is to cause the radial growth to arrest. If plasticity sets in at an early stage of growth, it is assumed that lath martensite is obtained. The model is consistent with experimental data, including the

Korenko experiment and the growth arrest. It does not, however, address the *shape* transition. A plate to lath transition depends on a change from isotropic to anisotropic radial growth.

The observed variations in microstructure as a function of temperature are summarised in Fig. 2.5.

Such changes in microstructure are illustrated vividly in Fig. 2.6, where the microstructure represents the effects of an abrupt change in the transformation temperature from 420°C to 290°C. This has resulted in a bimodal scale with a dramatic reduction in the plate size on lowering the temperature (Fig. 2.6).

2.1.2 *Thickness of bainite plates*

If the shape deformation is elastically accommodated then the plates can in principle maintain an elastic equilibrium with the matrix. They may continue to thicken isothermally until the strain energy balances the available free energy. It follows that if the plates are allowed to grow freely, they should be thicker at lower temperatures where the driving force is the greatest. This contradicts the experimental data because bainite is never elastically accommodated. Direct observations have shown that there is considerable plastic relaxation in the austenite adjacent to the bainite plates (Swallow and Bhadeshia, 1996). The dislocation debris generated in this process resists the

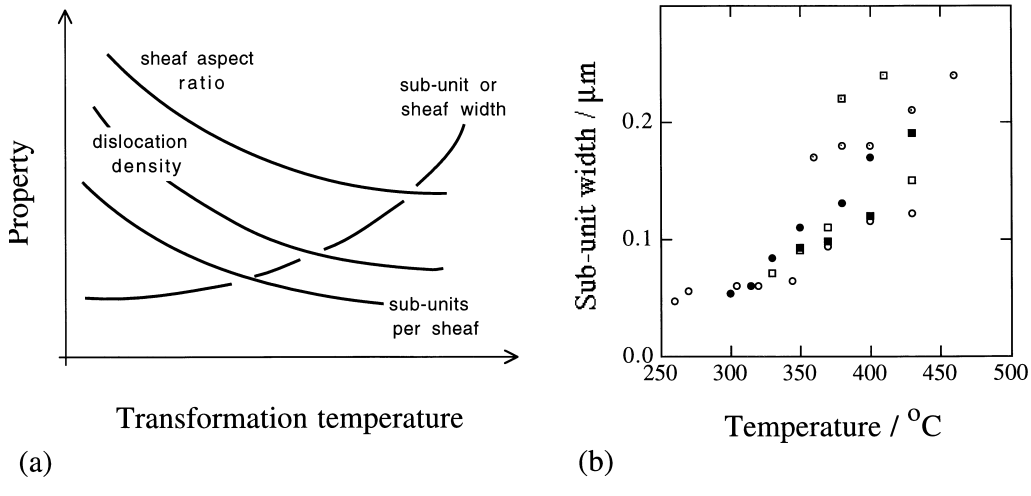

Fig. 2.5 (a) Qualitative trends in microstructure as a function of the transformation temperature. (b) Measurements of the bainite sub-unit thickness as a function of the transformation temperature for a variety of steels (Chang and Bhadeshia, 1995a; Singh and Bhadeshia, 1998.)

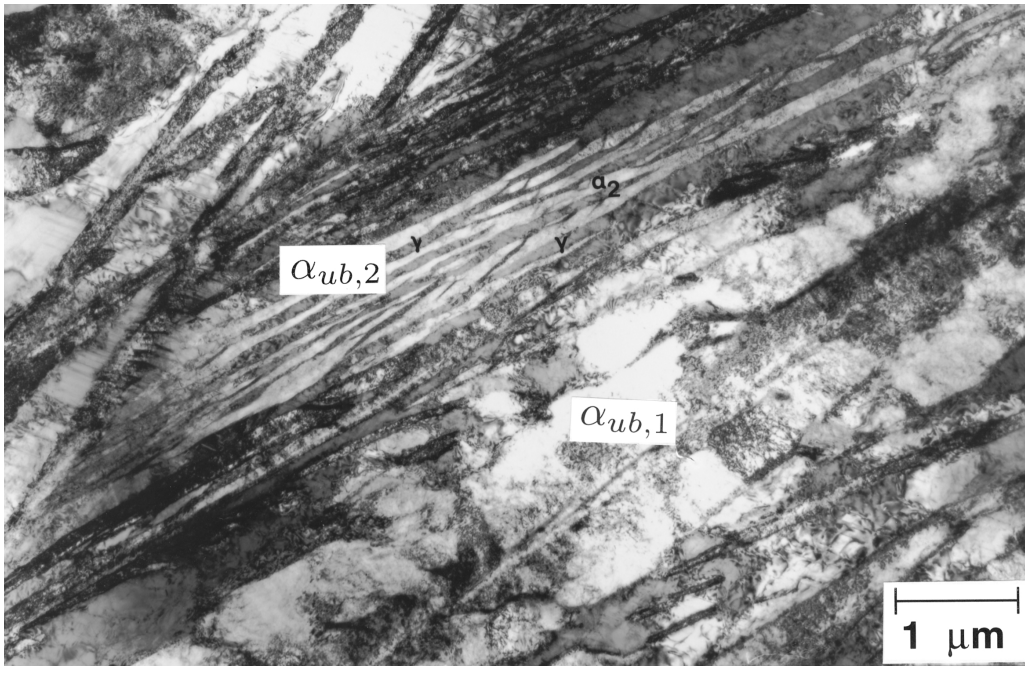

Fig. 2.6 A bimodal distribution of bainite plate thickness ($\alpha_{ub,1}$ and $\alpha_{ub,2}$, obtained by changing the isothermal transformation temperature from 420 °C to 290 °C. After Papadimitriou and Fourlaris (1997).

advance of the bainite/austenite interface, the resistance being greatest for strong austenite. The yield strength of the austenite must then feature in any assessment of plate size. In this scenario, the plates are expected to become thicker at high temperatures because the yield strength of the austenite will then be lower. Dynamic recovery at high temperatures may further weaken the austenite and lead to coarser plates. Indeed, high-temperature bainite often contains sub-grains which are finer for lower transformation temperatures (Pickering, 1958). These boundaries form by the recovery of the dislocation structure during transformation.

The thickness must also be influenced by impingement between adjacent plates; as in all transformations, a large nucleation rate corresponds to a finer microstructure.

The perceived effect of temperature could be indirect since both strength and the nucleation rate are strongly dependent on temperature. A quantitative analysis shows that temperature has only a small independent effect on the thickness of bainite plates (Fig. 2.7). The main conclusion is that strong austenite and high driving forces lead to a finer microstructure.

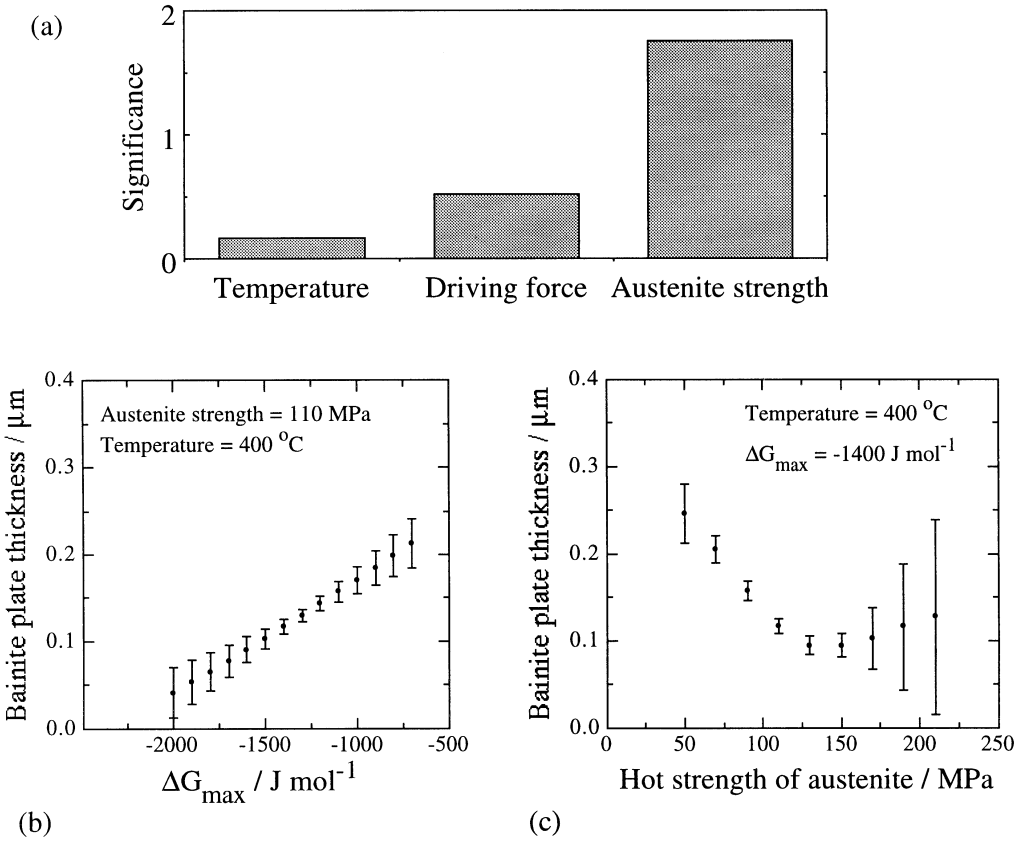

Fig. 2.7 (a) The model perceived significance of each of the variables plotted on the horizontal axis, in influencing the thickness of bainite plates. The vertical scale represents the ability of the variable to explain variations in plate thickness. (b) Variation in thickness with the chemical driving force. (c) Variation in thickness with the strength of the austenite. After Singh and Bhadeshia (1998).

2.1.3 Stereology

Crystals of bainite are anisotropic in shape. Their size is characterised by measuring the thickness on a random section in a direction normal to the long edges of the plates. The average value of many such measurements gives an apparent thickness which can be useful in correlations with mechanical properties. The true thickness requires stereological effects to be taken into account. If a plate is represented as a disc of radius r and thickness t with $r \gg t$, then the mean intercept length is given by $\overline{L}_3 = 2t$, and the mean intercept area is given by $\overline{A} = 2rt$ (Fullman, 1953). These intercepts must be taken at random.

The appropriate measure of the grain size is dependent on the application. For example, the strength will be a function of the dimensions of the slip planes within individual plates (Naylor, 1979; Daigne *et al.*, 1982). Assuming that there is a random distribution of slip plane orientations, the grain boundary strengthening term is of the form $\sigma_g = k_g M^{-1}$, where k_g is a constant and M is the mean value of the larger diameter of a slip plane. This differs from the Hall–Petch relation where it is the inverse square root of grain size which matters (Chapter 12).

2.2 Dislocation Density

Popular opinion is that bainite has a high dislocation density but there are few quantitative data to support this notion. Transmission electron microscopy has revealed a dislocation density ρ_d of about 4×10^{14} m^{-2} for an alloy with $B_S \simeq 650\,^{\circ}$C. This compares with allotriomorphic ferrite obtained at 800°C in the same steel with $\rho_d \simeq 0.5 \times 10^{14}$ m^{-2} (Smith, 1984). These data are similar to measurements on continuously cooled steel in which ρ_d {bainite} $\simeq 1.7 \times 10^{14}$ m^{-2} and ρ_d {allotriomorphic ferrite} $\simeq 0.37 \times 10^{14}$ m^{-2} (Graf *et al.*, 1985). It is significant that bainite contains more dislocations than allotriomorphic ferrite even when they form at similar temperatures.

The defect structure of bainite is often attributed to the shear transformation mechanism. However, such a mechanism need not lead to dislocations in the ferrite if the shape deformation is elastically accommodated. Thermoelasticity in martensites and shape memory alloys depends on the elastic accommodation of the shape deformation and the movement of any interfaces must occur without the creation of defects. It is only if the shape deformation is accompanied by plastic relaxation (Fig. 2.8), that the dislocations associated with this plastic strain are inherited by the product phase.

It is conceivable that the ferrite plate itself might relax. After all, the strength of both ferrite and austenite decreases at high temperatures. However, theory predicts that, for a plate shape, the strains are mostly accommodated in the austenite (Christian, 1965b, 1975). Hence, atomic-force microscope scans show that the displacements within the bainitic ferrite are much more regular than in the adjacent austenite (Fig. 2.8c). The plastic accommodation is more evident in Fig. 2.8d, where the strain is seen to extend into the austenite to a distance about equal to the width of the bainite.

Plastic relaxation has featured in many early observations. When polished samples of austenite are transformed to bainite, the adjacent austenite surface does not remain planar, but instead exhibits curvature which is characteristic of slip deformation (Srinivasan and Wayman, 1968b). Hot-stage transmission electron microscopy has shown that growth is accompanied by the formation of dislocations in and around the bainite (Nemoto, 1974). Direct observations

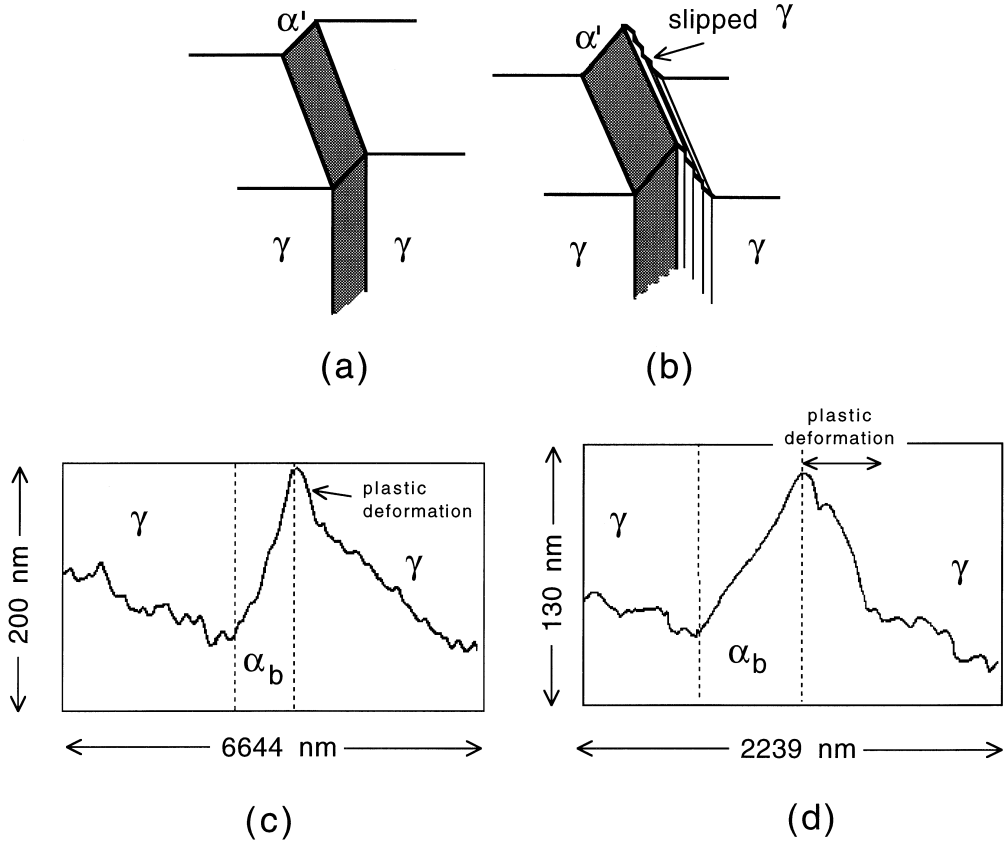

Fig. 2.8 (a) A perfect invariant-plane strain surface relief effect. (b) One where plastic relaxation of the shape change occurs in the adjacent matrix. (c,d) An actual atomic force microscope scan across the surface relief due to a bainite sub-unit (Swallow and Bhadeshia, 1996).

of the austenite/bainite interface show accommodation in both phases, Fig. 2.9. The austenite adjacent to the bainite can accommodate the shape deformation by mechanical twinning or faulting, with the density of defects increasing as the transformation temperature decreases (Bhadeshia and Edmonds, 1979a; Sandvik and Nevalainen, 1981; Sandvik, 1982a). These accommodation defects are common in martensitic transformations (Jana and Wayman, 1970).

The dislocation density of bainitic ferrite increases as the transformation temperature is reduced (Pickering, 1967). X-ray line profile measurements show an increase in the lattice strain due to dislocations as the transformation temperature is reduced. This can be used to estimate the dislocation density;

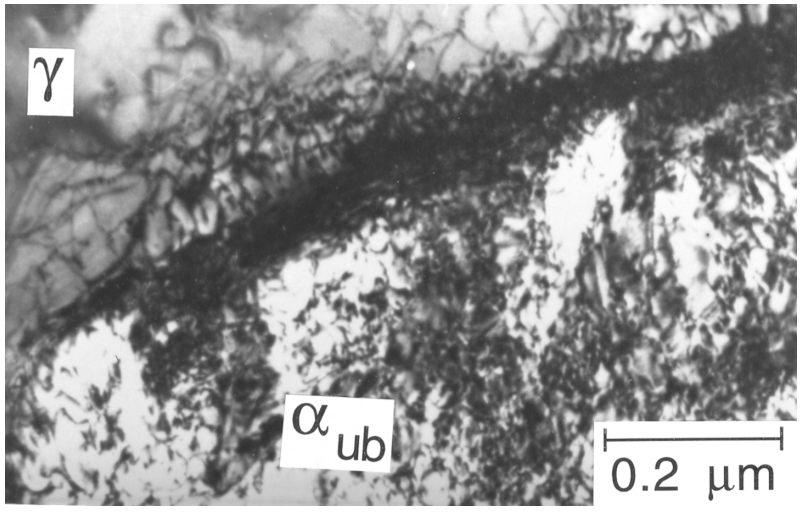

Fig. 2.9 Intense dislocation debris both at, and in the vicinity of the bainite/austenite transformation front (Bhadeshia and Edmonds, 1979a).

isothermal transformation to bainite at 300, 360 and 400 °C gave dislocation densities of 6.3×10^{15}, 4.7×10^{15} and $4.1 \times 10^{15}\,\mathrm{m}^{-2}$ respectively (Fondekar *et al*., 1970).

2.2.1 *Quantitative Estimation of Dislocation Density*

It might be assumed that for low-alloy steels the dislocation density depends mainly on transformation temperature via the influence of the latter on the strength of the parent and product phases. It should then be possible to treat all of the displacive transformations, martensite, bainite and Widmanstätten ferrite together. This leads to an empirical relationship which is valid over the range 570–920 K (Fig. 2.10):

$$\log \rho_d = 9.28480 + \frac{6880}{T} - \frac{1780360}{T^2} \tag{2.1}$$

where ρ_d is the dislocation density in m^{-2}, and T is the reaction temperature in Kelvin (Takahashi and Bhadeshia, 1990). For martensite the transformation temperature is taken to be the M_S temperature. Although the dislocation densities of martensite measured by Norström (1976) are also plotted in the Fig. 2.10, those data were not used in deriving the expression because of uncertainties in the method used to assess the thickness of the thin foil samples used.

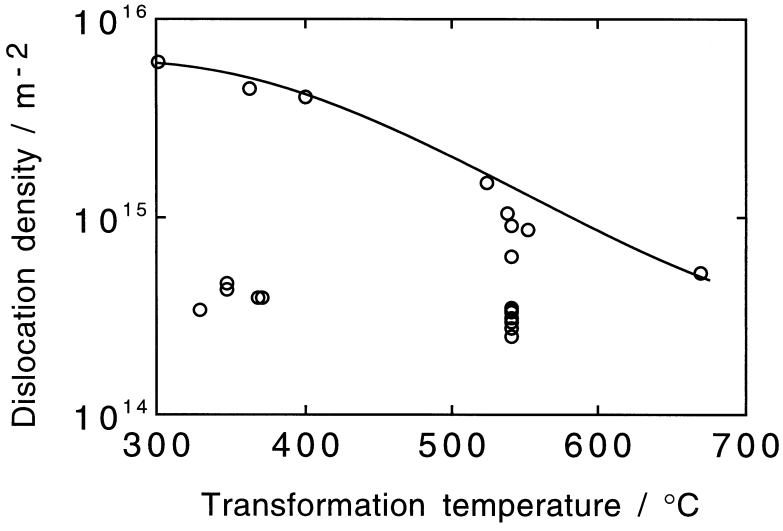

Fig. 2.10 Dislocation density of martensite, bainite, acicular ferrite and Widmanstätten ferrite as a function of the transformation temperature (Takahashi & Bhadeshia, 1990; Bhadeshia, 1997).

2.3 Chemical Composition

2.3.1 Substitutional Alloying Elements

There is no long-range redistribution of substitutional solutes during the growth of bainitic ferrite (e.g. Aaronson and Domain, 1966). High resolution experiments confirm this on the finest conceivable scale (Bhadeshia and Waugh, 1981, 1982; Stark *et al.*, 1988, 1990; Josefsson and Andren, 1988, 1989). The ratio of the iron to substitutional solute atoms remains constant everywhere during the formation of bainite. This is not surprising given the displacive character of the transformation and the low diffusivity of substitutional atoms at the temperatures where bainite forms. By contrast, all atoms, including iron must diffuse during a reconstructive transformation. Thus, it is possible to distinguish between a displacive and reconstructive mechanism even in pure iron.

A reconstructive transformation can be imagined to occur in two steps (Fig. 2.11): the change in crystal structure is achieved as in a displacive transformation; matter is then transferred in such a way that the shape deformation and strain energy associated with the first step is minimised. The matter must be transported over a distance about equal to the dimensions of the particle unless the interface is incoherent. This mass flow has been described as 'reconstructive diffusion' (Bhadeshia, 1985b).

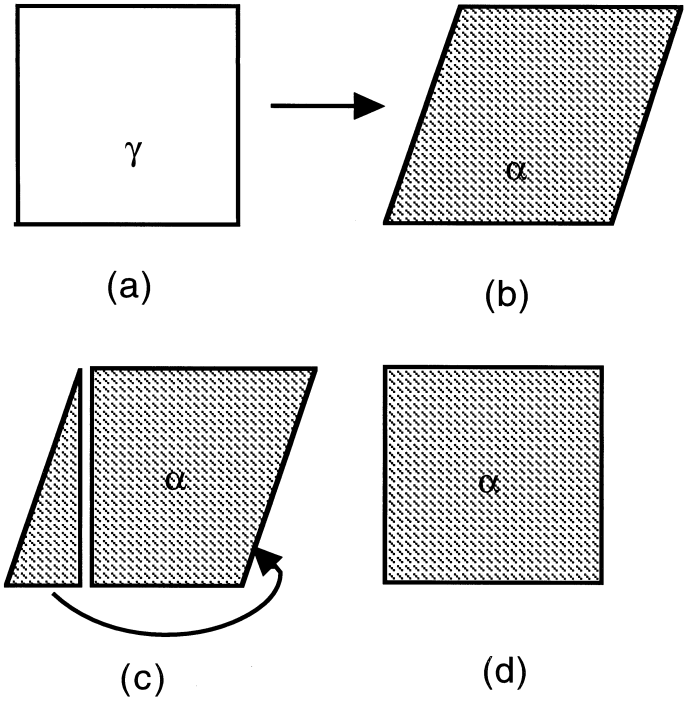

Fig. 2.11 Schematic illustration of the mass transport necessary to achieve reconstructive transformation, in both pure metals and alloys. Steps (a) to (b) represent displacive transformation, whereas (a) to (d) represent reconstructive transformation. The mass transport illustrated in (c) eliminates the shape change due to the shear.

The diffusion necessary for the lattice change provides an opportunity for the solvent and solute atoms to partition during transformation. In an alloy steel, the carbon atoms, which are in interstitial solution, can migrate at rates many orders of magnitude greater than the iron or substitutional solute atoms (Fig. 2.12). For diffusion-controlled growth the compositions at the transformation front are in local equilibrium, given by a tie-line of the phase diagram. However, the tie-line has to be chosen in such a way that both the carbon and the substitutional solute (X) can keep pace with the moving interface in spite of their vastly different diffusion coefficients. This can happen in two ways (Hillert, 1953; Kirkaldy, 1958; Purdy *et al.*, 1964; Coates, 1972, 1973a,b). First, the tie-line controlling the interface compositions is such that the gradient of carbon in the austenite is minimised (Fig. 2.13a). This is known as *partitioning, local equilibrium* or P–LE mode because there is the long-range partitioning of X. The P–LE mode of growth applies when the undercooling below the equilibrium transformation temperature is small.

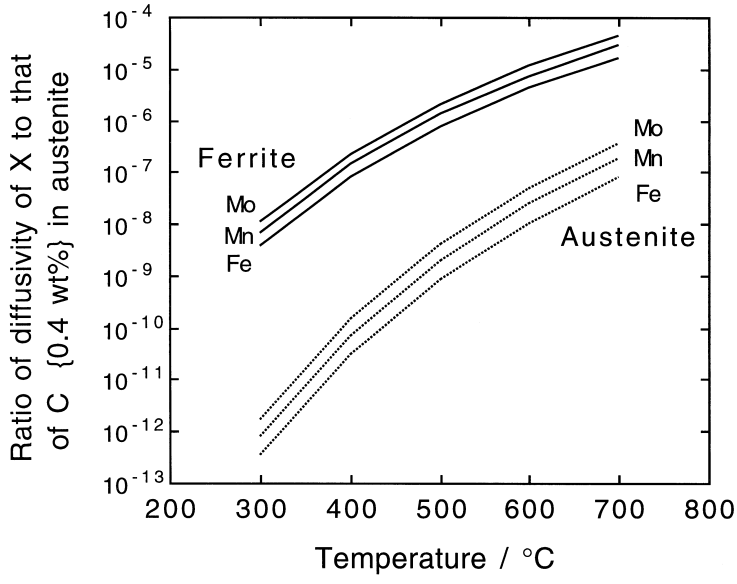

Fig. 2.12 A comparison of the diffusivities of iron and substitutional solutes relative to that of carbon (in austenite at a concentration of 0.4 wt%), in FCC and BCC iron, over the bainite transformation temperature range (data from Fridberg *et al.*,1969)

The second possibility is that a tie-line is selected so that the concentration gradient of X is large, thereby compensating for its small diffusivity (Fig. 2.13b). This is the *negligible partitioning local equilibrium* mode of transformation in which the ferrite has nearly the same X concentration as the austenite. This NP–LE mode occurs at large undercoolings below the equilibrium transformation temperature.

In the NP–LE mode, the concentration of X is uniform except for a small 'spike' in the parent phase adjacent to the interface. As the ratio of interstitial: substitutional diffusion rates increases, the width of this spike decreases, and when it becomes of the order of atomic dimensions, the concept of local equilibrium at the interface is invalid and has to be replaced (assuming the growth is nevertheless diffusion-controlled) by that of paraequilibrium (Hultgren, 1951; Rudberg, 1952; Aaronson *et al.*, 1966a,b). In conditions of paraequilibrium, there is no redistribution of Fe + X atoms between the phases, the Fe/X ratio remaining uniform right up to the interface. One interpretation of the paraequilibrium limit is that reconstructive transformation occurs with all displacements of the Fe + X atoms taking place in the incoherent interface; another interpretation might be that only displacive transformation can occur. In either case, to quote from Coates, 'the slow diffuser and the solvent

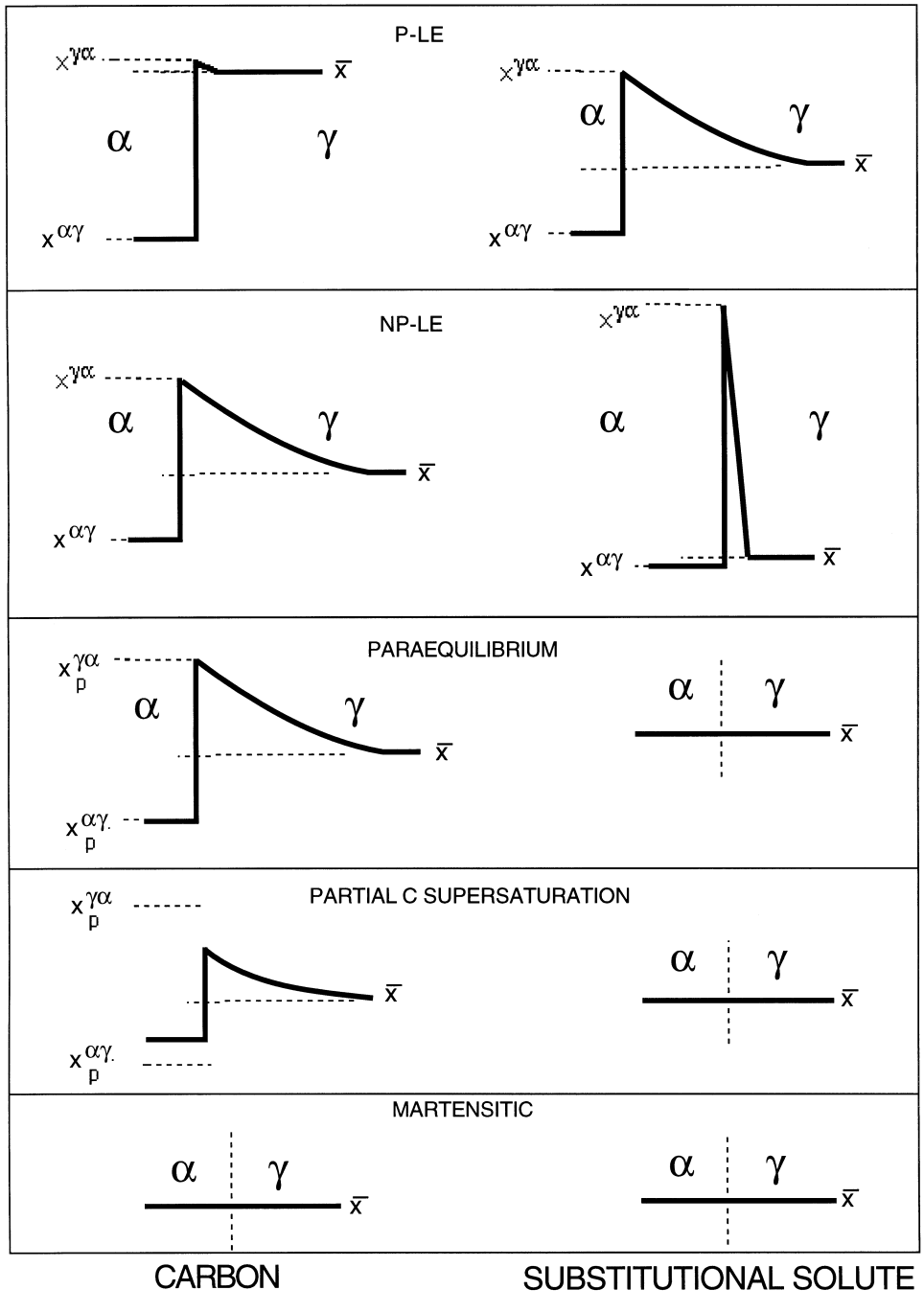

Fig. 2.13 The composition variations expected in the vicinity of the transformation interface, for a variety of growth mechanisms.

participate only in the change of crystal structure'. Paraequilibrium implies that a constant Fe:*X* ratio is maintained everywhere.

In conclusion, the experimental evidence that bainitic ferrite has the iron to substitutional atom ratio as its parent austenite is consistent with both reconstructive and displacive mechanisms for the change in crystal structure. However, reconstructive transformation with local equilibrium (or indeed any state between local and paraequilibrium) requires some perturbation of the substitutional solute content in the proximity of the interface. Experiments which have a chemical and spatial resolution on an atomic scale have all failed to show any evidence for the redistribution of alloying elements (Cr, Mn, Mo, Ni, Si) at the interface between bainitic ferrite and austenite, Fig. 2.14

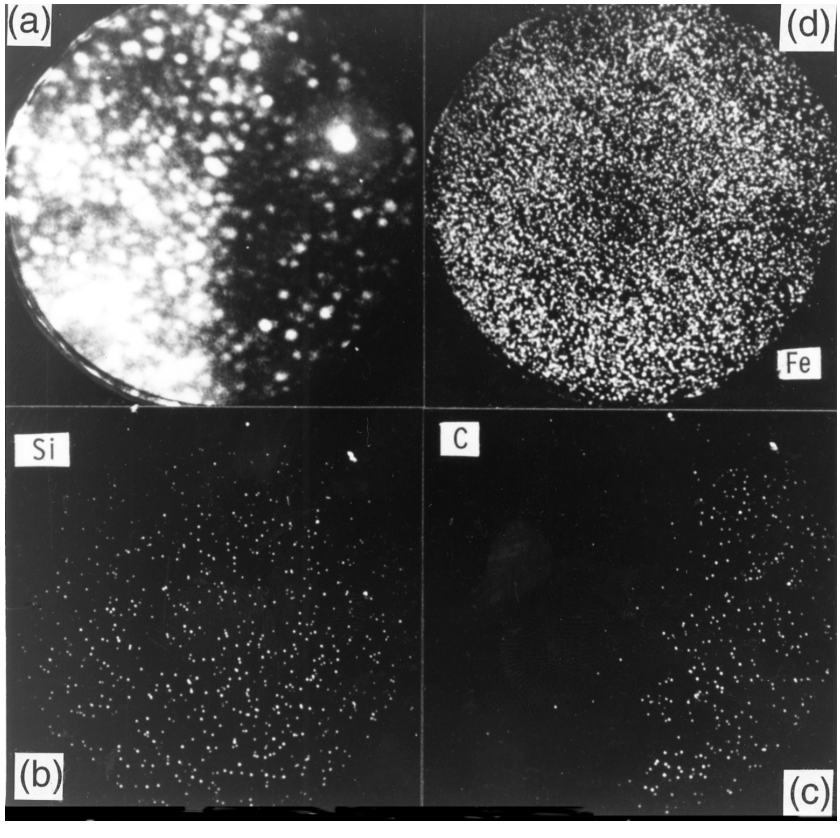

Fig. 2.14 Imaging atom-probe micrographs, taken across an austenite–bainitic ferrite interface in a Fe–C–Si–Mn alloy. The images confirm quantitative data (Bhadeshia and Waugh, 1982) showing the absence of any substitutional atom diffusion during transformation. (a) field-ion image; (b) corresponding silicon map; (c) corresponding carbon map; (d) corresponding iron map.

(Bhadeshia and Waugh, 1981, 1982; Stark *et al*., 1988, 1990; Josefsson and Andren, 1988, 1989). These experiments were all based on steels where other reactions, such as the precipitation of carbides, do not interfere with the formation of bainitic ferrite. Measurements of the growth rates of grain boundary allotriomorphs of ferrite from austenite in alloy steels under conditions where bulk segregation is not observed (e.g. Kinsman and Aaronson, 1973; Bradley *et al*., 1977) indicate calculated thicknesses of the spike of much less than 0.1 nm, and although these results are complicated by the effect of grain boundary diffusion, they are in general agreement with the concept that the lattice diffusion rate is inadequate to sustain local equilibrium at the growing interface. Only at temperatures above 600 °C, has the segregation of some (though by no means all) substitutional elements been obtained in grain boundary allotriomorphs (Aaronson and Domian, 1966b). Allotriomorphs are agreed to form by reconstructive mechanisms, but the absence of bulk segregation at moderately high transformation temperatures reinforces the belief, derived from the observed shape change, that bainitic ferrite forms at lower temperatures by a displacive rather than a reconstructive mechanism.

2.3.2 *Interstitial Alloying Elements*

A particular experimental difficulty with the bainite transformation is that in the case of upper bainite at least, it is almost impossible to say anything about the initial carbon content of the ferrite. This is because the time taken for any carbon to diffuse from the supersaturated ferrite into the austenite can be small. For the moment we refer to the interstitial content of bainitic ferrite *after* transformation. As will be seen later, the concentration *during* transformation is likely to be different.

Internal friction experiments indicate that the amount of carbon which associates with dislocations in bainitic ferrite increases as the transformation temperature decreases, but is independent of the average carbon concentration in the steel, at least in the range 0.1–0.4 wt%C (Pickering, 1967). This is consistent with the observation that the dislocation density of bainitic ferrite increases as the transformation temperature is reduced. The insensitivity to the carbon concentration is because most of the carbon ends up in the residual austenite. The results also show that at some stage during the evolution of bainitic ferrite, it must have contained a higher than equilibrium concentration of carbon.

These observations have been confirmed directly by using microanalysis on an imaging atom-probe, which has demonstrated quantitatively (Fig. 2.15) that the *post-transformation* carbon content of bainitic ferrite tends to be significantly higher than equilibrium (Bhadeshia and Waugh, 1982; Stark *et al*., 1988, 1990; Josefsson and Andren, 1988, 1989). Precise electron diffraction experiments

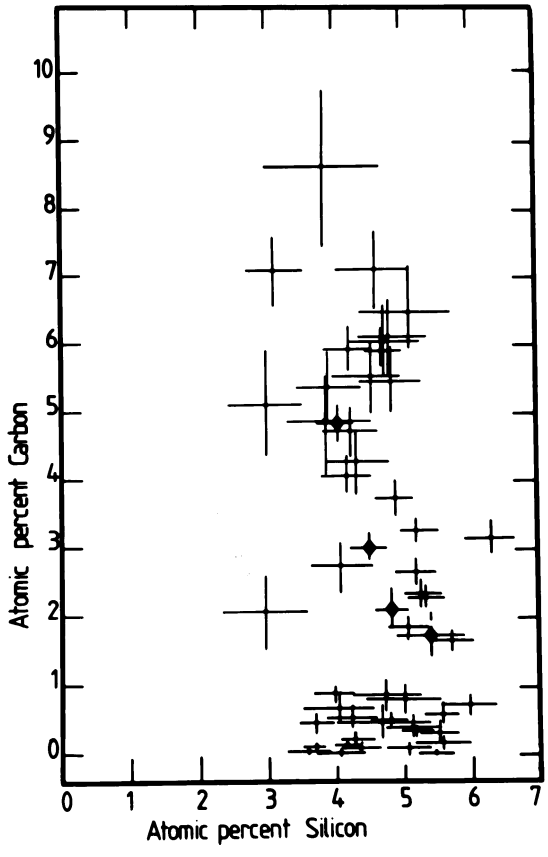

Fig. 2.15 Atom-probe determinations of the carbon and silicon concentrations of bainitic ferrite in an Fe–C–Mn–Si alloy transformed to upper bainite (Bhadeshia and Waugh, 1982). The average carbon concentration in the alloy is 1.93 at.%, so all concentrations below that level are measurements from bainitic ferrite.

using convergent beam Kikuchi lines to measure the lattice parameter of the bainitic ferrite also show that it contains a much larger concentration of carbon than expected from equilibrium (Zhang and Kelly, 1998a).

2.4 Crystallography

The properties of bainitic steels are believed to depend on the crystallographic texture that develops as a consequence of transformation from austenite. As an example, the ease with which slip deformation is transmitted across the adjacent plates of bainitic ferrite must be related to their relative orientation in space. Bainite grows in the form of clusters of plates called sheaves, with

little misorientation between the plates within any given sheaf. Where they touch, adjacent plates are separated by low-misorientation grain boundaries.

The relative orientations of the bainitic ferrite and its parent austenite are always close to the classic KS (Kurdjumov–Sachs, 1930) and NW (Nishiyama–Wasserman, 1934) relationships (Fig. 2.16), although as will become evident later, they can never be exactly KS or NW. These two rational relations differ only by a relative rotation of 5.26° about the normal to the parallel close-packed planes of the two structures. The exact relative orientation is found in martensites to be intermediate and irrational, as is predicted by the crystallographic theory. High accuracy is required to compare theory with experiment since the predicted orientation relation is insensitive to input parameters such as lattice spacings or lattice invariant deformation. In the case of bainite, as in that of lath martensite, such precision is difficult to achieve partly because of the experimental difficulties in retaining austenite and partly because of the high dislocation densities.

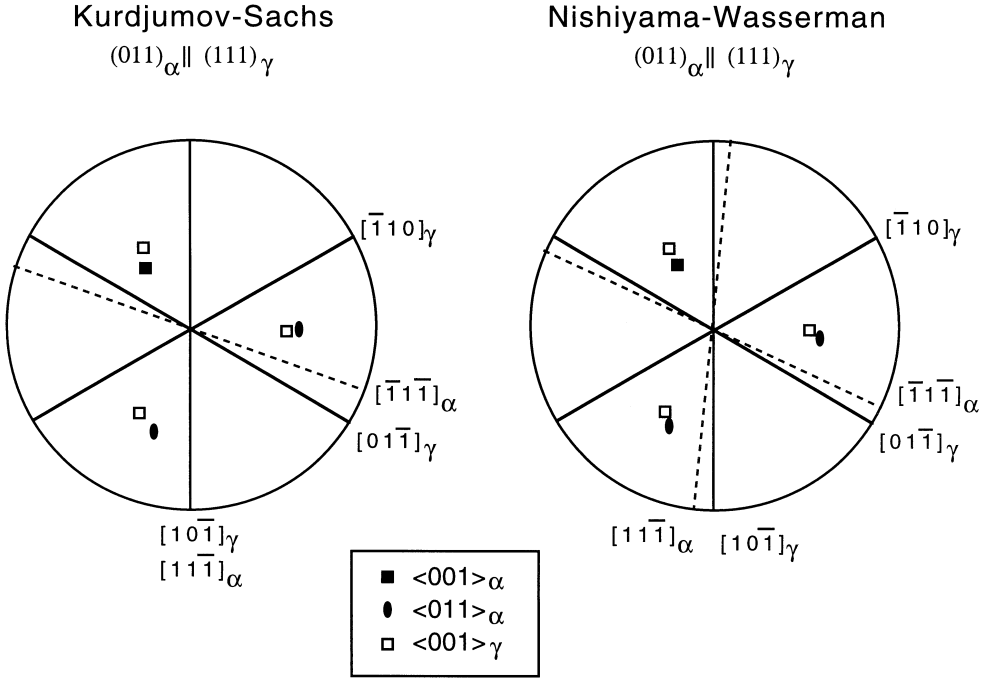

Fig. 2.16 Sterographic representation of the (a) Kurdjumov–Sachs and (b) Nishiyama–Wasserman orientation relationships. Note that NW can be generated from KS by a rotation of 5.26° about $[0\ 1\ 1]_\alpha$.

In spite of these difficulties, it is significant that the experimental data always lie well within the *Bain region* which encompasses the KS and NW relationships. The Bain strain is the pure part of the lattice deformation which for displacive transformations in steels converts austenite into ferrite or martensite (Fig 2.17, Bain, 1924). During the Bain strain, no plane or direction is rotated by more than 11° so that any pair of corresponding planes or directions may be made parallel by utilising a lattice deformation in which the Bain strain is combined with a rotation of not more than 11° (Crosky *et al.*, 1980). This

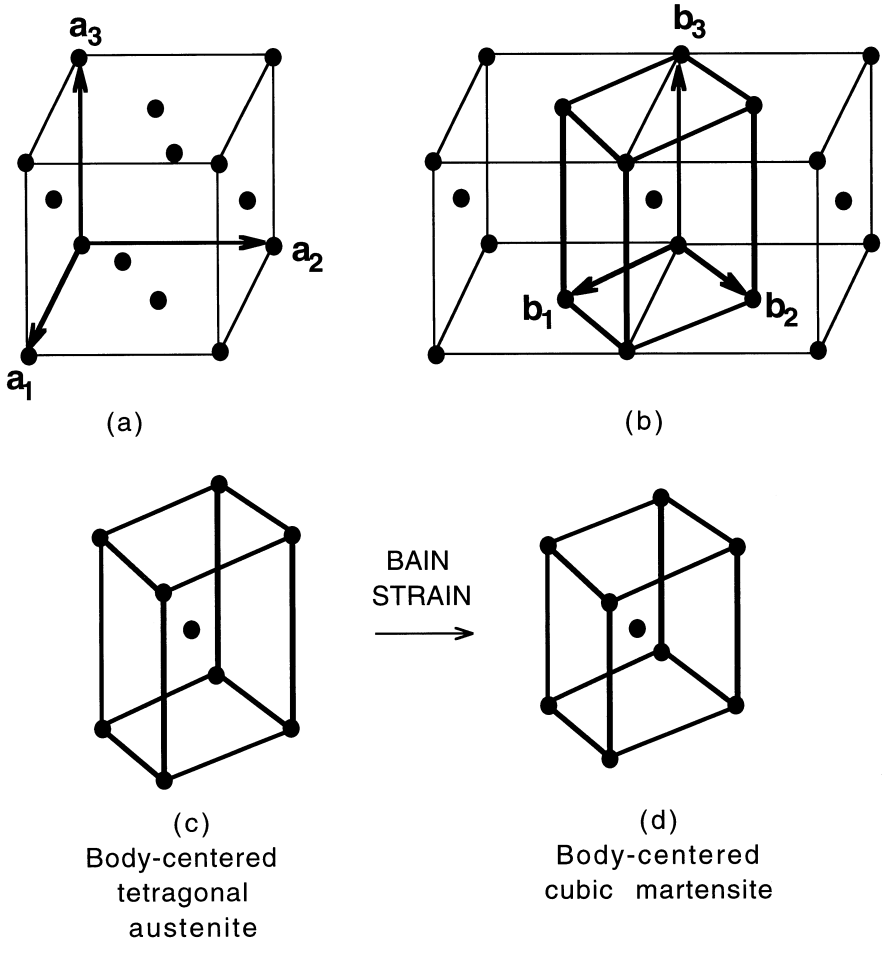

Fig. 2.17 (a) Conventional FCC unit cell of austenite, with basis vectors $\mathbf{a}_1, \mathbf{a}_2, \mathbf{a}_3$. (b) Relation between the FCC and body-centred tetragonal cell ($\mathbf{b}_1, \mathbf{b}_2, \mathbf{b}_3$) of austenite. (c,d) Bain Strain deforming the austenite lattice into a BCC martensite lattice.

defines the Bain region. The experimentally observed orientation relations are expected to lie within this region for displacive but not necessarily for reconstructive transformations. Thus, allotriomorphic ferrite is known to grow into austenite grains with which it has an orientation which is random or outside of the Bain region (King and Bell, 1975). It is therefore significant that bainitic ferrite always exhibits an orientation which is close to KS or NW and well within the Bain region.

There is an interesting consequence of the requirement that bainite must be within the Bain region of orientations. It is accepted that allotriomorphic ferrite, when it nucleates at an austenite grain surface, must also grow with an orientation relationship which is close to KS or NW in order to minimise the activation energy for nucleation. But allotriomorphic ferrite *grows* most rapidly along austenite grain boundaries with which it has a random orientation. Once nucleated, it therefore grows selectively, away from its original nucleation site. A grain of ferrite then has a large fraction of its interface with the austenite with which it has a random orientation. Bainite can only nucleate from allotriomorphic ferrite at the small fraction of interfaces where the orientation is in the Bain region (Fig. 2.18).

Pickering (1967) has suggested that the crystallography of bainite can be explained if the individual plates or laths adopt different variants of the NW or KS orientations, such that the ferrite orientations within a sheaf can be generated simply by rotation about the normal to a specific close-packed plane of the austenite. In this way, the bainite laths may nucleate side by side in rapid succession, the transformation strains determining the variant and hence the exact sequence. This early work was based on measurements of only ferrite–ferrite orientation relations, since the specimens may have contained only thin films of austenite which are observable only with high resolution microscopy. However, it must be admitted that results from more recent work in which measurements of the direct austenite–ferrite relations have been made are still contradictory. There is general agreement that adjacent plates or laths in bainite all have a $\{1\ 1\ 0\}_\alpha$ plane parallel (or almost parallel) to the same close-packed $\{1\ 1\ 1\}_\gamma$ and that the macroscopic habit plane is near to $\{1\ 1\ 1\}_\gamma$ in upper bainite but is irrational in lower bainite. Most investigators (e.g. Bhadeshia and Edmonds, 1980; Sandvik, 1982a) find all the plates within a sheath have a common orientation, but Sarikaya *et al*. (1986) claim that whilst some groups of adjacent laths have a common orientation, others have either different variants of the orientation relationship, or in lower bainite are twin-related. Similar discrepancies exist in crystallographic measurements on lath martensite where three types of orientation relation between adjacent laths of a packet are reported by some workers (Eterasivili *et al*., 1979; Sarikaya *et al*., 1986) and only one common orientation by others (Wakasa and Wayman, 1981; Sandvik and Wayman, 1983).

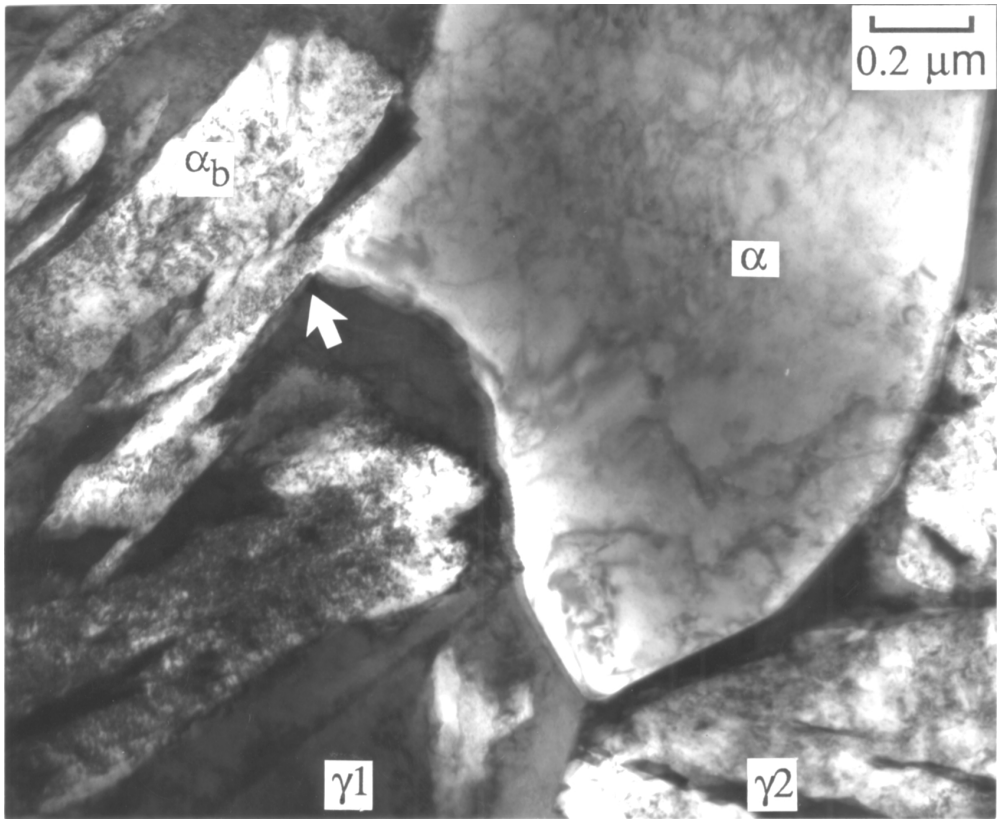

Fig. 2.18 Transmission electron micrograph showing an allotriomorph of ferrite at an austenite grain boundary. The allotriomorph is related to γ_1 by an orientation relationship which is close to KS, but is randomly orientated with respect to the lower grain. Consequently, a bainite plate has been able to nucleate from the allotriomorph only on the side where the orientation is suitable.

When there is a common orientation, the plates within a sheaf have small misorientations; there is also an appreciable spread of orientation within a single plate because of its high dislocation density. Direct crystallographic analysis indicates that all plates within a sheaf have an irrational orientation relation with the austenite which is closer to NW than to KS (Sandvik, 1982). Moreover, the shape deformations of all the plates are identical, Fig. 2.19, in agreement with earlier work (Srinivasan and Wayman, 1968b; Bhadeshia and Edmonds, 1980a). One further crystallographic observation made by Sandvik is of considerable interest. He found that twins formed in the austenite adjacent to the ferrite, and that the ferrite laths were able to grow through the twins, producing a reorientation of the lattice and also displacing the direction of the

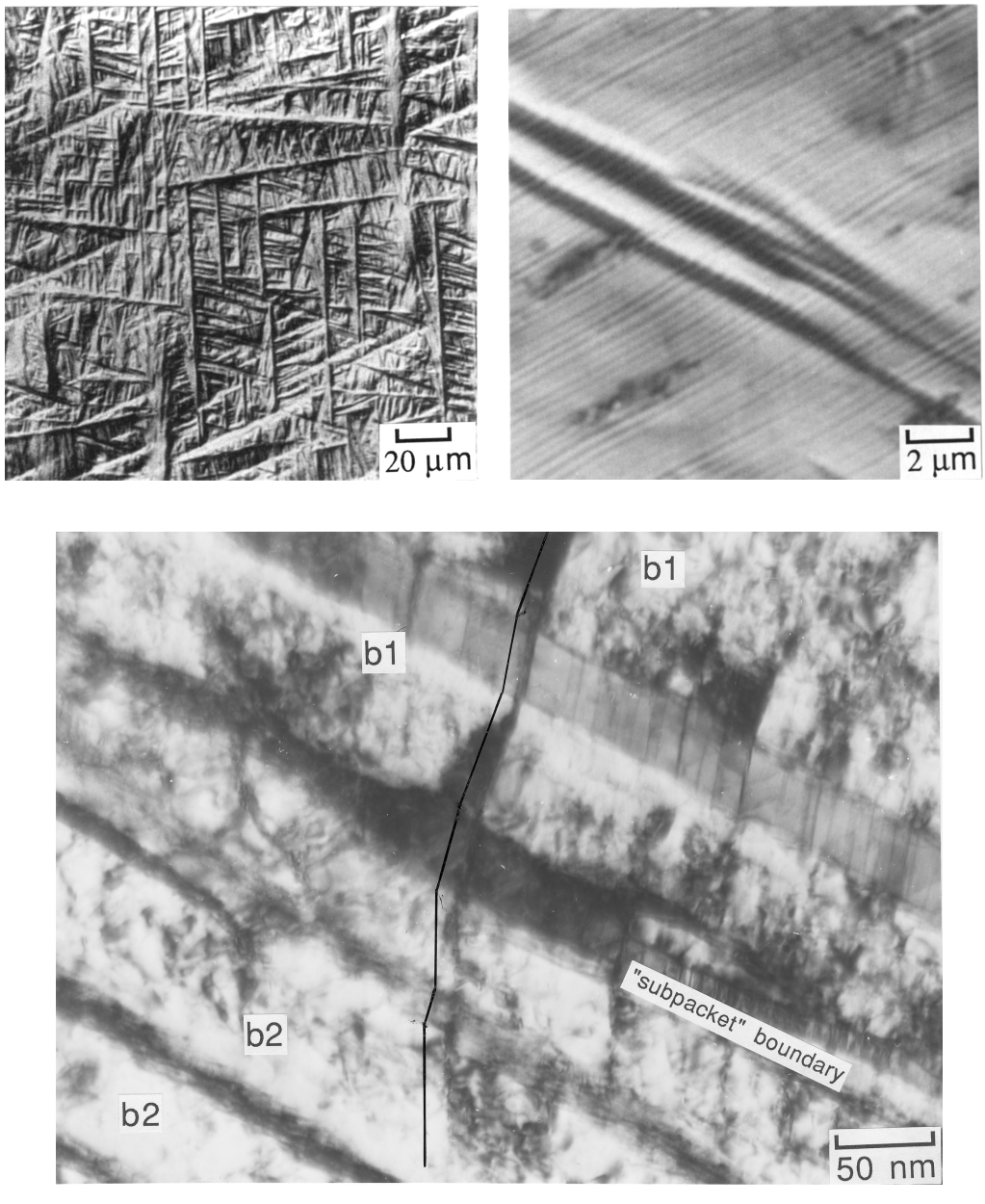

Fig. 2.19 (a) Nomarski differential interference contrast micrograph showing the general surface displacements due to upper bainite. (b) Higher magnification Nomarski image showing identical surface relief for all the sub-units within a given sheaf. (c) Sandvik's experiment showing the displacement of twin boundaries (parallel to the black line) caused by individual sub-units of bainite. The ferrite variants b1 and b2 belong to separate sheaves.

twin boundaries in the manner expected for a displacive (shear) transformation.

Similar results for the relative orientations of adjacent plates were obtained in a careful examination of lath martensite by Sandvik and Wayman, using an iron–nickel–manganese alloy which contained appreciable retained austenite (Sandvik and Wayman, 1983). They found that although the laths had slight relative misorientations of up to 2°, they all exhibited the same variant of the parent–matrix orientation relation, and thick layers of austenite between adjacent laths indicated that the laths did not form as a result of self accommodation of their shape strains. This form of lath martensite thus seems to be similar, in substructure at least, to the bainite investigated by Sandvik.

One possible reason for a common orientation might be that the individual plates of a sheaf are not separate crystals but are continuously connected portions of the growth front of one original nucleus. At the relatively high temperatures at which bainite (and lath martensite) form, the shape change may cause plastic deformation of the structure leading to copious generation of dislocations which stops the forward growth of a plate after it has attained a certain size. 'Nucleation' of a new plate would then simply be resumed growth caused by breakaway of a part of the original interface in a region near but not at the tip. In bainite, the growth would resume only after some carbon had been rejected from the ferrite into the austenite and would be most likely where pinning by dislocation debris is minimal and where the driving force is highest due to rapid dispersion of the carbon rejected to the austenite.

An alternative model is that the individual plates are completely separated from each other by thin layers of austenite, so that each is separately nucleated, but always in the same orientation. In general, the stress field at the tip will favour the same variant, whereas that at the side of the plate encourages an accommodating variant (Fig. 2.20).

Mutual accommodation of the shape deformation can occur between sheaves rather than between plates in each sheaf. Sandvik measured the misorientations between neighbouring sheaves and found that these correspond to different variants of his irrational orientation relation in which the same austenite {1 1 1} plane is parallel to a ferrite {1 1 0} plane. The six variants which satisfy this condition lead to four different relative orientations, one of which is only 3° from the original orientation and the others are respectively 8°, 11° and 14° away from a twin orientation. Sandvik comments that the first misorientation is difficult to detect, and that it is difficult to distinguish the remaining three from each other. He also comments that only the variant with orientation relation 14° from a twin relationship gives efficient self accommodation, and this was observed fairly infrequently. Adjacent sheaves are thus attributed to random association, although it is not clear why they should then all have the same pair of parallel close-packed planes. Sandvik and Nevalainen have also

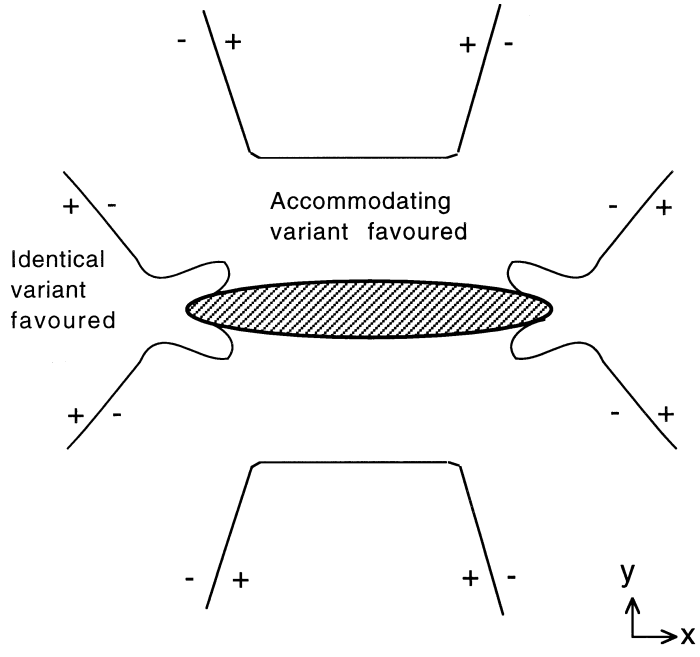

Fig. 2.20 Stress field contours of a martensitic particle lying in the xz plane with the transformation shear in the x direction. The positive signs represent regions where plates with the same shear direction are favoured, whereas the regions with the negative signs favour the formation of accommodating variants (Olson and Owen, 1976).

suggested that adjacent sheaves of bainitic ferrite are approximately twin related, and correspond to variants of a near NW orientation. Transmission electron microscopy by Josefsson (1989) has confirmed these observations in a Fe–Cr–Mo–C steel.

2.4.1 Autocatalytic Nucleation

Autocatalytic nucleation is a term commonly associated with martensitic transformations (Raghavan and Entwisle, 1965; Magee, 1970). The nucleation of martensite in steels is believed to begin at structural imperfections in the parent phase, such as arrays of dislocations. These are the preexisting defects which, on cooling below the M_S temperature dissociate into suitable partial dislocations in a way which leads to the nucleation of martensite (Olson and Cohen, 1976a–c). The defects are not all identical (they vary in potency) and are stimulated to grow into plates of martensite at different degrees of undercooling below the M_S temperature. This is the cause of the classical behaviour

observed for athermal martensitic reactions, in which the volume fraction of martensite varies only with the undercooling below M_S.

The initial number density of preexisting defects typically found in austenite is not large enough to explain the kinetics of martensitic transformation. The extra defects necessary to account for the faster than expected transformation rates are attributed to autocatalysis: when plates of martensite form, they induce new embryos which are then available for further transformation. Three mechanisms have been proposed for autocatalysis (Olson and Cohen, 1981). In stress-assisted nucleation, the activation of less potent defects at a given temperature is induced by the internally generated elastic stresses arising as a consequence of the shape change due to transformation. In strain-induced autocatalysis, the creation of new and more potent nucleating defects is induced by some plastic accommodation in the parent phase. Finally, *interfacial autocatalysis* refers to the nucleation of new martensitic units from the existing martensite/austenite interfaces. Autocatalysis is responsible for the *bursts* of transformation (Fig. 2.21) that occur in certain martensitic steels,

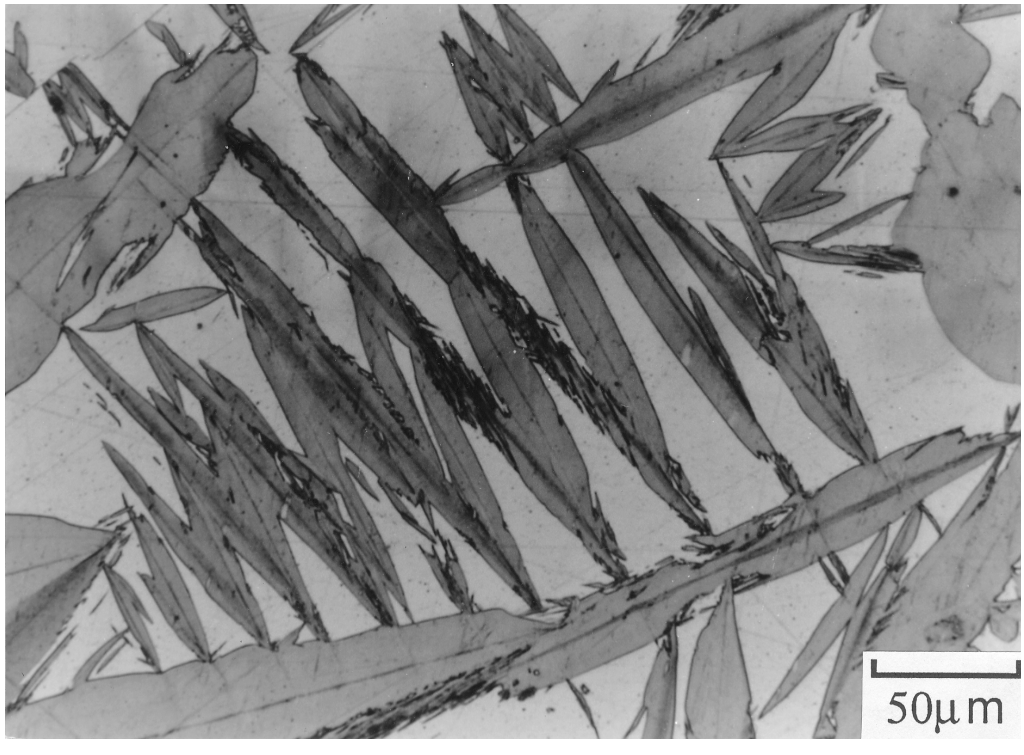

Fig. 2.21 A burst of autocatalytic martensitic transformation in a Fe–30Ni–0.31C wt% alloy. Such bursts are not observed during bainitic transformation.

whence the initial formation of a plate stimulates a disproportionately large degree of further transformation, sometimes causing the emission of audible clicks.

All of these effects arise as a consequence of the severe elastic and plastic disturbance of the austenite in the immediate vicinity of a plate of martensite. It is the shape change due to the martensitic transformation that is the cause of the disturbance. On this basis, autocatalysis should also feature prominently in bainitic transformations which are accompanied by similar shape deformations. There is, however, a significant difference in that bainite grows at relatively small driving forces, where defects induced by transformation do not seem to play as crucial a role in stimulating further nucleation. The initial nucleation event is almost always confined to the austenite grain surfaces, which presumably contain the most potent defects for nucleation. Intragranular nucleation of bainite can essentially be ignored except when nonmetallic particles may act as nucleation surfaces. The initial formation of a plate of bainite (or of a lath of martensite) must lead to appreciable elastic and plastic strains, but this does not seem to cause the nucleation of other plates in different orientations, as happens with plate martensite, and bursts of transformation are not observed. In the case of bainite, this may be because the driving force is only adequate for the formation of a carbon-free nucleus, and this may be impossible to form in the carbon-enriched region around an existing plate. Whatever the reason, it seems that strain-induced autocatalysis does not play an important role in bainite formation. As already discussed, there is some evidence for stress-assisted autocatalysis if it is indeed true that adjacent sheaves form in such a way as to help accommodate each other's shape deformation.

2.5 Crystallographic Theory

The deformation which converts the face-centred cubic structure of austenite to the body-centred cubic or body-centred tetragonal structure is known as the Bain Strain (Fig 2.17). Its principal deformation consists of a compression along the vertical axis $\mathbf{a}_3$ and a uniform expansion along $\mathbf{a}_1$ and $\mathbf{a}_2$. However, this deformation does not produce the experimentally observed orientation relationship; nor is it consistent with the observed invariant-plane strain shape deformation. An invariant-plane strain, on the other hand, cannot convert austenite into ferrite. The crystallographic theory, which resolves all of these difficulties, is now summarised (Wechsler *et al.*, 1953; Bowles and Mackenzie, 1954).

The Bain strain is a *pure* deformation because it leaves three mutually perpendicular directions unrotated, though distorted. The distortions η_i along these unrotated axes are defined as the ratios of the final to the initial lengths

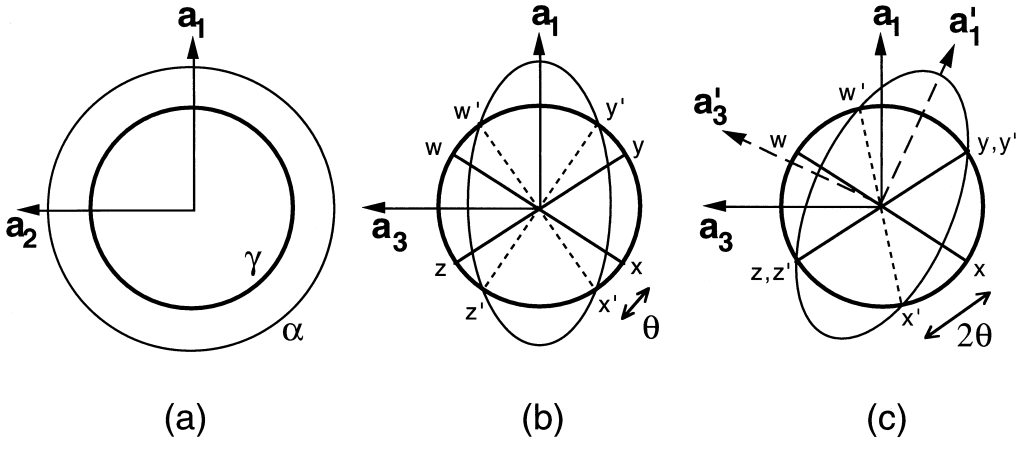

Fig. 2.22 (a) and (b) show the effect of the Bain strain on austenite, which when undeformed is represented as a sphere of diameter $wx = yz$ in three-dimensions. The strain transforms it to an ellipsoid of revolution. (c) shows the invariant-line strain obtained by combining the Bain strain with a rigid body rotation.

and are called the *principal distortions*. The Bain strain defines completely the lattice change so no further deformation is needed to complete the change in crystal structure.

Suppose that the austenite is represented by a sphere with its unit cell edges denoted by the vectors $\mathbf{a}_i$ with $i = 1, 2, 3$, as illustrated in Fig. 2.22a,b. The Bain strain changes the sphere into an ellipsoid of revolution about $\mathbf{a_1}$. There are no lines in the $(0\,0\,1)_\gamma$ plane which are undistorted. However, it is possible to find lines such as wx and yz which are undistorted by the deformation, but are rotated into the new positions $w'x'$ and $y'z'$. Since they are rotated by the Bain deformation they are not invariant-lines. In fact, the Bain strain does not produce an invariant-line strain (ILS). An invariant-line is necessary in the interface between the austenite and martensite in order to ensure a glissile interface.

The Bain strain can be converted into an invariant-line strain by adding a rigid body rotation as illustrated in Fig. 2.22c. The rotation reorients the α' lattice but has no effect on its crystal structure. The effect of the rotation is to make one of the original undistorted lines (in this case yz) invariant so that the total effect **RB** of the Bain strain **B** and the rotation **R** is indeed an invariant-line strain. This is the reason why the observed irrational orientation relationship (KS/NW type) differs from that implied by the Bain strain. The rotation required to convert **B** into an ILS precisely predicts the observed orientation from the Bain orientation.

It is apparent from Fig. 2.22c that there is no possible rotation which would convert **B** into an invariant-plane strain because there is no rotation capable of

making two of the non-parallel undistorted lines into invariant-lines. Thus, it is impossible to convert austenite into α' martensite by a strain which is an invariant-plane strain. A corollary to this statement is that the two crystals cannot ever be joined at an interface which is fully coherent and stress-free.

It remains to resolve the inconsistency that **BR** is an ILS whereas the observed shape deformation is an IPS. The operations needed to explain this are illustrated in Fig. 2.23. When combined with an appropriate rigid body rotation, the net homogeneous lattice deformation **RB** is an invariant-line strain

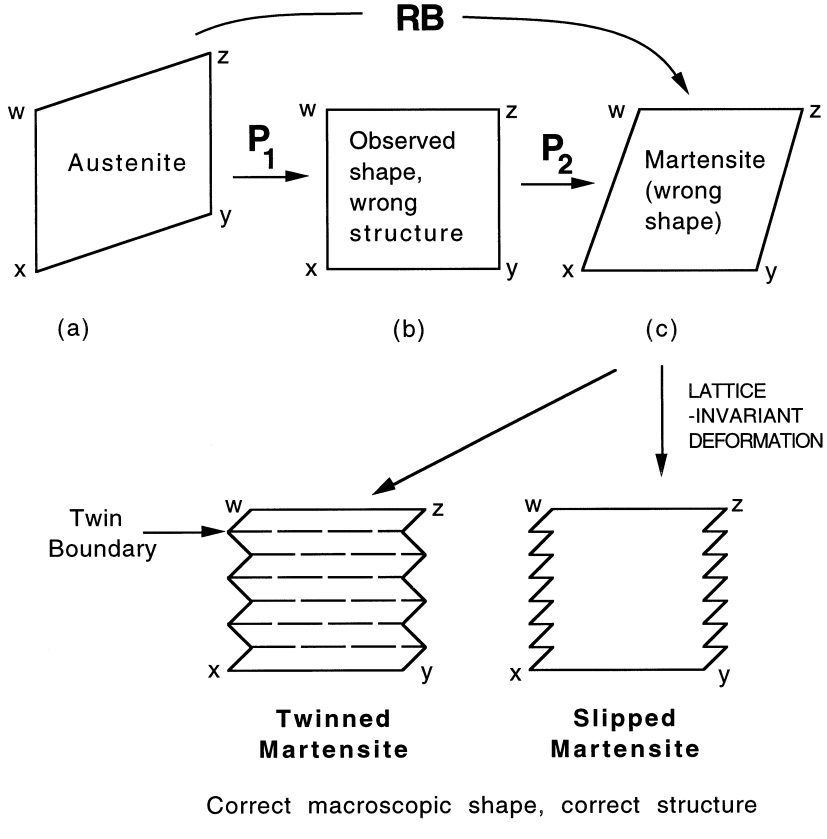

Fig. 2.23 The essential features of the phenomenological theory of martensite crystallography. (a) represents the austenite crystal and (c), (d) and (e) all have a body-centred cubic structure. (b) has an intermediate structure between FCC and BCC (or BCT). Although (c) has the BCC structure, its shape is inconsistent with the observed invariant-plane strain. The effect of the inhomogeneously applied lattice-invariant deformations is to correct the shape change to an IPS, without altering the structure.

(step *a* to *c*), the invariant-line being normal to the plane of the diagram and passing through the point *x*. Inconsistent with this, the observed shape deformation is an invariant-plane strain $\mathbf{P_1}$ (step *a* to *b*) but this gives the wrong crystal structure. The invariant-plane of the shape deformation is defined by *xw*. If, however, a second homogeneous shear $\mathbf{P_2}$ is combined with $\mathbf{P_1}$ (step *b* to *c*), then the correct structure is obtained but the wrong shape since[†]

$$\mathbf{P_1P_2} = \mathbf{RB}$$

The discrepancies are all resolved if the shape changing effect of $\mathbf{P_2}$ is cancelled macroscopically by an inhomogeneous lattice-invariant deformation, which may be slip or twinning as illustrated in Fig. 2.23. Notice that the habit plane in Fig. 2.23e,f is given by a fragmentation of the original plane *xw*, due to the inhomogeneous lattice-invariant shear. This is why the habit plane of martensite has peculiar indices. In the absence of a lattice-invariant deformation as in the $\gamma \rightarrow \epsilon$ transformation, the sequence stops at step *b* and therefore the habit plane has rational indices $\{1\,1\,1\}_\gamma$.

The theory neatly explains all the observed features of martensite crystallography. It is easy to predict the orientation relationship, by combining the Bain strain with a rigid body rotation which makes the net lattice deformation an invariant-line strain. The habit plane does not have rational indices because the amount of lattice-invariant deformation needed to recover the correct macroscopic shape is not usually rational. A substructure is predicted, consisting either of twins or slip steps, and this is observed experimentally. The transformation goes to all the trouble of ensuring that the shape deformation is macroscopically an invariant-plane strain because this reduces the strain energy when compared with the case where the shape deformation might be an invariant-line strain.

Finally, we note that the invariant-line lies at the intersection of the habit plane and the plane on which the lattice-invariant shear occurs. This is obvious since only the line common to the two invariant-planes can be invariant to their combined effect.

2.5.1 Application to Bainite

We have seen that the bainite transformation exhibits crystallographic features and surface relief effects identical to those associated with martensitic reactions. It is then natural to assume that the phenomenological theory of martensite crystallography should be applicable to bainite. The theory predicts

[†]Notice that a combination of two non-coplanar invariant-plane strains gives an invariant-line strain, the invariant-line lying at the intersection of the two invariant-planes.

a unique relationship between the habit plane, shape deformation, orientation relationship, lattice types and lattice-invariant deformation. It can be tested satisfactorily when all these variables are determined as a set. Much of the early data (reviewed by Bowles and Kenon, 1960) are incomplete in this sense, although consistent with the theory. The early measurements of habit planes must now be interpreted to refer to the habit planes of bainite sheaves, rather than of the individual plates.

A considerable difficulty in applying the theory to bainite is the lack of accurate structural information which is needed as input data. Thus if bainite grows with a full supersaturation but the carbon escapes in a short time, the measured lattice parameters of upper bainitic ferrite will not relate to the initially formed structure, which may even have been tetragonal. A problem exists for lower bainite if appreciable carbide precipitation has taken place before any measurements are possible.

Srinivasan and Wayman (1968b,c) reported the first detailed results on the crystallography of sheaves of lower bainite in a Fe–1.11C–7.9Cr wt% alloy ($B_S \simeq 300\,^{\circ}\mathrm{C}$, $M_S \simeq -34\,^{\circ}\mathrm{C}$) in which large quantities of austenite remained untransformed at ambient temperature. Each sheaf was found to have just one planar face when examined using light microscopy, and this was taken to be the habit plane. The irrational habit plane indices were found to exhibit a degree of scatter beyond experimental error, the mean indices being close to $(2\ 5\ 4)_\gamma$ relative to the orientation variant in which $(1\,1\,1)_\gamma$ is almost parallel to $(0\,1\,1)_\alpha$ and $[\bar{1}\,0\,1]_\gamma$ is at a small angle to $[\bar{1}\,\bar{1}\,1]_\alpha$; this is henceforth called the *standard variant*. The martensite habit plane in the same alloy is close to $(4\,9\,4)_\gamma$ and the difference in the two habits and in the exact orientation relations led Srinivasan and Wayman to the conclusion that the mode of displacive transformation is different in bainite and martensite. Their measured habit plane is only about 6° from that found for a different alloy by Sandvik, who pointed out that his result applied to an individual plate whereas that of Srinivasan and Wayman was for the average habit of a sheaf.

The shear component of the shape deformation, as averaged over the entire sheaf, was measured to be $\simeq 0.128$, the magnitude of the total shape strain being $\simeq 0.129$ (Table 2.1). This is consistent with the earlier data of Tsuya (1956) and Speich (1962). The actual shape strain for an individual sub-unit must of course be larger, and was estimated using crystallographic theory as being $\simeq 0.23$; this compares with the $\simeq 0.28$, 0.25 and 0.22 estimated for different alloys by Ohmori (1971a), Bhadeshia (1980a) and Sandvik (1982a) respectively. These values are in good agreement with a measurement of the shear component of the shape strain (0.22) of an individual sub-unit (Sandvik, 1982a) and with a value of 0.26 measured using atomic force microscopy (Swallow and Bhadeshia, 1996).

Table 2.1 Magnitude of the shape strain component parallel to the habit plane. The value of the shear is derived by measuring the tilts for each sheaf on two separate surfaces. After Wayman and Srinivasan (1969b).

Sheaf number	Tilt on surface 1	Tilt on surface 2	Angle of shape shear	Shear
1	5°48′	3°56′	7°9′	0.1254
2	5°24′	6°24′	8°27′	0.1486
3	5°17′	4°20′	7°0′	0.1228
4	6°45′	4°15′	7°55′	0.1393
5	6°9′	4°21′	8°20′	0.1466
6	3°43′	3°3′	5°13′	0.09156
7	4°15′	3°42′	8°24′	0.1474
8	4°0′	4°30′	6°	0.1035

Srinivasan and Wayman showed that their data on lower bainite are indeed consistent with solutions based on the phenomenological theory of martensite. The crystallography was, as expected, inconsistent with the lattice-invariant deformation being twinning since transformation twinning is not observed in bainitic ferrite.† It was found that the sheaf habit plane and orientation relationship could be predicted for an undistorted habit plane if it is assumed that the lattice invariant shear is irrational in both plane and direction. On the other hand, if the habit plane is permitted to undergo a small isotropic contraction, then the lattice-invariant shear (for the standard variant) consists of a double shear on the planes $(1\,\bar{1}\,1)_\gamma$ and $(1\,0\,1)_\gamma$ in the common direction $[\bar{1}\,0\,1]_\gamma$ (these correspond to $(1\,0\,1)_\alpha$, $(1\,1\,2)_\alpha$ and $[\bar{1}\,\bar{1}\,1]_\alpha$ respectively). This double system is equivalent to a single shear on an irrational plane, and is not associated with any of the difficulties encountered in theories which postulate more general combinations of lattice-invariant shears. The component planes on which the interface dislocations would glide are those most usually considered as candidates for single lattice-invariant shears in the martensite theory. However, at the time of the Srinivasan and Wayman work, it was not fully appreciated that the so-called habit plane of a sheaf which they measured, may differ from that of a plate within a sheaf which Sandvik measured, and it is not yet clear whether the phenomenological theory of martensite should be applied to the sheaf or the plate. It may be more important to minimise long-range distortions over the whole sheaf, in which case the invariant plane condition would apply to the apparent habit plane of the sheaf, but in cases where there are reasonably thick layers of austenite between the plates, it seems more logical to apply the theory to the individual plate.

2.5.2 High-Resolution Studies of the Shape Change

Of the transformation products listed in Table 2.2, both Widmanstätten ferrite and martensite can be obtained in the form of plates that are readily resolved using optical microscopy. Their shape deformations have been known for many decades, the measurements being made from the deflection of scratches or optical interference fringes on a surface polished flat prior to transformation.

Table 2.2 Approximate values of the shear strain s and dilatational strain δ for a variety of transformation products in steels.

Transformation	s	δ	Morphology	Reference
Widmanstätten ferrite	0.36	0.03	Thin plates	Watson & McDougall, 1973
Bainite	0.22	0.03	Thin plates	Sandvik, 1982a
	0.26		Thin plates	Swallow & Bhadeshia, 1996
Martensite	0.24	0.03	Thin plates	Dunne & Wayman, 1971
Allotriomorphic α	0	0.03	irregular	
Idiomorphic α	0	0.03	equiaxed	

However, the microstructure of bainite consists of fine plates of ferrite, each of which is only some 0.2 μm thick, which is below the limit of resolution in light microscopy. This has made it difficult to establish the surface relief introduced as bainite grows. Sandvik (1982a) first measured the shear strain of a single bainite plate using transmission electron microscopy to reveal the transformation-induced deflection of twins in austenite. He determined the shear strain s to be close to 0.22.

New methods have recently become available for the quantitative, high-resolution measurement of surface topography using scanning tunnelling or atomic force microscopy. The techniques have confirmed Sandvik's observations which revealed that the shear strain associated with an individual plate of bainite is about 0.26 ± 0.02 which is consistent with the magnitude expected from the phenomenological theory of martensite crystallography (Swallow and Bhadeshia, 1996). An example of an image of the surface displacements is presented in Fig. 2.24.

[†]A twinned interface is never thermodynamically favoured because of the creation of internal twin boundaries. But it can move more rapidly than when slip is the lattice-invariant deformation mode. Consequently, martensite which grows at high velocities will tend to contain transformation twins (Olson and Cohen, 1981b).

The atomic force microscopy has also shown that the low values of s measured in early work using light microscopy arise because the low resolution causes an averaging of the shape strain over the sheaf.

The plastic relaxation is of course, ultimately responsible for the arrest in the growth of the bainite plates, giving the sub-unit and sheaf hierarchies in the microstructure of bainite; as discussed in section 2.2.1, it also leads to an increase in the dislocation density of the bainite.

2.5.3 The Shape Change: Further Considerations

In talking about the application of the phenomenological theory of martensite to bainite, the classical view (Hull, 1954; Bilby and Christian, 1956; Christian, 1962) that the experimentally observed invariant-plane strain shape deformation implies a coordinated movement of at least the iron and substitutional atoms was implicitly accepted. Given that there has been some confusion in the literature about the interpretation of this shape change, it is worth presenting an assessment of the significance of the shape change (Christian and Edmonds, 1984; Christian, 1990a). The problem is important since the strain energy associated with the shape deformation when transformation occurs under constraint, cannot be ignored in the thermodynamic and kinetic descriptions of bainitic reactions, irrespective of the mechanism by which the shape change is proposed to arise.

The intersection of a plate of bainitic ferrite with a free surface causes that surface to tilt about the lines of intersection. This is the description of an invariant-plane strain, which is due to the combined effects of the lattice deformation and a lattice-invariant deformation. The tilting produced is homogeneous on a macroscopic scale, indicating that the net atomic displacements include common non-random components which accumulate during growth. This is an obvious conclusion, but the term *net atomic displacements* needs to be deconvoluted in order to assess the degree of diffusion which can be tolerated before the transformation must be regarded as a reconstructive reaction.

Focusing attention on equivalent lattice points which define unit cells (not necessarily primitive) of the two structures containing the same number of atoms, a change in shape will accompany transformation if the new set of lattice points can be related to the original set by a homogeneous deformation. It is then possible to specify (in a localised region at least) how particular vectors, planes and unit cells of one structure are derived from *corresponding* vectors, planes and unit cells of the other structure. This is termed a lattice correspondence and it defines the pure lattice deformation which carries the original lattice points, or some fraction of those points into points of the new lattice.

When interstitial atoms are present, they may move over large distances without affecting the correspondence; this is sometimes expressed by stating that there is an atomic correspondence for the solvent and substitutional solute atoms but not for the interstitials. A further relaxation of the condition is to allow the solvent and substitutional solute atoms to be displaced during transformation among the sites specified by the lattice correspondence, but not to create new sites or destroy any specified sites; in this way the lattice correspondence is preserved but there is no longer an atomic correspondence. Thus, a systematic shape change implies a lattice correspondence even if accompanied by some diffusion of atomic species. As will become evident later, the existence of this correspondence and the shape change requires an interface which is at least semi-coherent.

The detailed implications of the shape change on the mechanism of growth can be illustrated using the virtual operations illustrated in Fig. 2.25. A region of the matrix is first removed (leaving behind an equivalent hole) and then

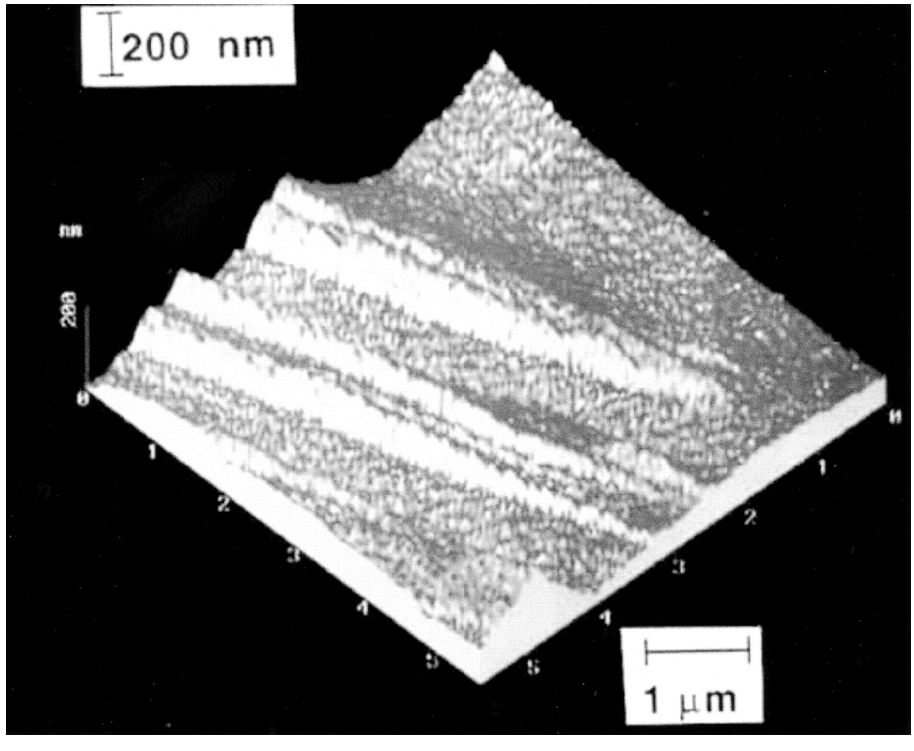

Fig. 2.24 High-resolution atomic-force microscope plot of the displacements caused by the formation of a single sub-unit of bainite. The surface was flat before transformation. Note the plastic deformation caused in the adjacent austenite (Swallow and Bhadeshia, 1996).

allowed to undergo unconstrained transformation with the help of a homogeneous lattice deformation which is not in general an invariant-plane strain (Fig. 2.25a,b). The particle is then allowed to have any required composition by transferring suitable numbers of solute atoms between interstitial sites in the particle and the matrix, and/or by interchanging atoms of substitutional species in the particle with atoms in the matrix (operation c, Fig. 2.25).

A number of further operations are now possible before the particle is reinserted into the hole in the matrix, in order to reduce the strain energy:

(i) The volume and shape of the particle may be made equal to that of the hole, by transferring atoms over long distances from the particle to sinks within the matrix or at its surface (operation d_1, Fig. 2.25). The strain energy then vanishes.

(ii) The total number of atoms in the particle may be conserved but its shape may nevertheless be adjusted by the creation and removal of atom sites. The strain energy is effectively that of a hole in the matrix filled with a compressible fluid of different natural volume. For a plate-shaped particle, the minimum in strain energy for this case corresponds to an IPS with a zero shear component, with the expansion or contraction being normal to the habit plane (operation d_2, Fig. 2.25). A plate-shaped particle will give the lowest strain energy if the volume change is appreciable, but there will only be a *preferred* habit plane if there is appreciable anisotropy of either the elastic properties or the interfacial energy.

(iii) The shape of the particle may be changed by conservative plastic deformation. The lowest strain energy for a plate-shaped particle then occurs if the plastic deformation converts the lattice deformation into a shape deformation which is an IPS on the habit plane, as in the theory of martensite crystallography (operation d_3, Fig. 2.25).

(iv) The shape of an epitaxially coherent particle (which has interfacial dislocations with Burger's vectors which have an edge character and which lie in the interface plane) may be changed by the removal or addition of particular planes of atoms, e.g. by dislocation climb from one surface to another, again giving lowest strain energy for an IPS on the habit plane of a plate precipitate. If there is no reconstruction of the atom sites, the shape change may retain an appreciable shear component (operation d_4, Fig. 2.25).

Particles of type d_1 and d_2 both require long range diffusion or mass transport, and there is no obvious reason why large scale redistributions of solute atoms cannot at the same time occur between the product and parent phases, if demanded by thermodynamic equilibrium. In d_1 there is no shape change,

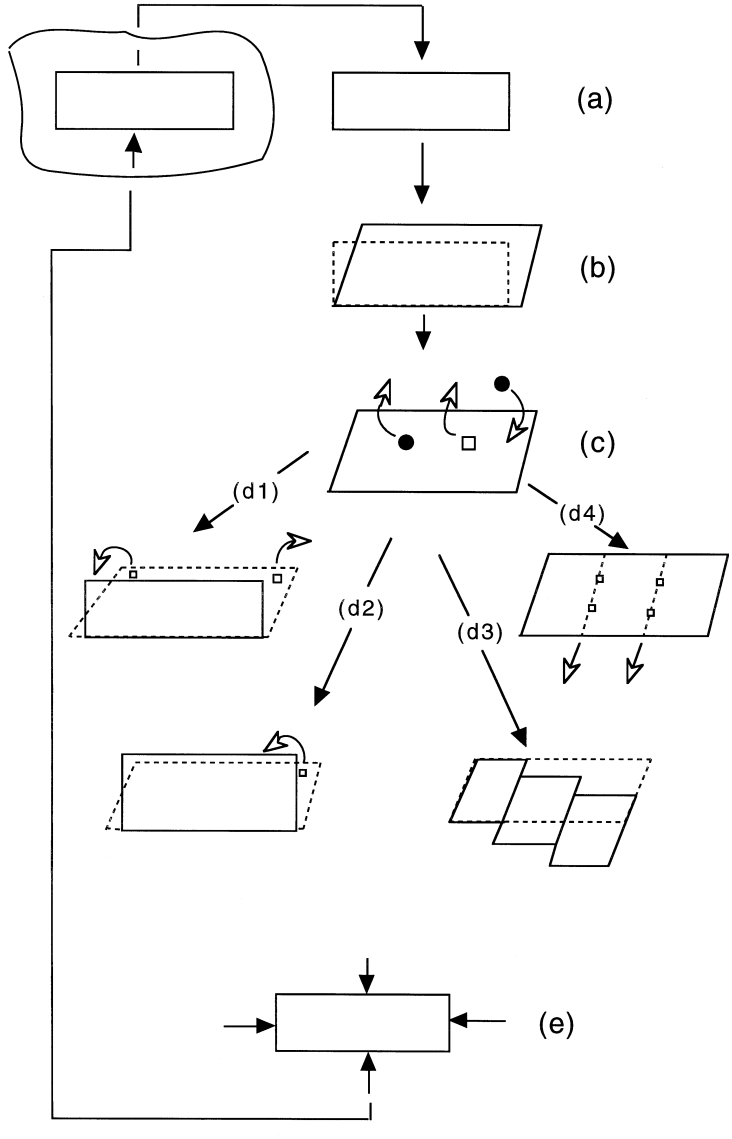

Fig. 2.25 Schematic diagram illustrating the virtual operations required to form a particle in a constraining matrix (after Christian and Edmonds, 1984).

whereas d_2 will lead to surface rumpling due to the volume change accompanying transformation; both of these kinds of transformation are therefore reconstructive. Shear stresses and strains are not transferred across the interface, which behaves in some respects as a liquid-like layer. Since there is no continuity of planes or vectors, the interface can be displaced only as a result of individual atomic migration and its velocity will depend on atomic mobility.

It could also be argued that in case (iv), the need to have sufficient atomic mobility for interfacial dislocations to climb means that in reality, other diffusion processes might also occur which remove the shear component of the shape deformation (Christian, 1962).

This leaves only the martensitic type change (iii) as a likely candidate for an IPS shape change, but step *c* (Fig. 2.25) ensures that the shape change cannot be taken to imply diffusionless transformation. It is easy to see how interstitial atoms can partition between the phases during growth without affecting the IPS shape change. There may also be an interchange of substitutional atoms (of the type necessary to induce ordering in equiatomic random alloys), but it is likely that the migration of these atoms can only occur over a few interatomic distances – otherwise, any longer range diffusion would destroy the shape change and its associated strain energy at the same time. It is therefore to be concluded that one implication of the observation of an invariant-plane strain shape change with a significant shear component is that any diffusion of solvent or substitutional atoms during transformation must be absent or minimal.

Suppose that there is an IPS deformation with a large shear and at the same time there is a composition change implying diffusion in the substitutional lattice. Such a transformation has been called diffusional–displacive transformation (Christian, 1994; 1997). This does not negate the consequences of the shape deformation, for example the strain energy, the plate shape, the requirement for a glissile interface etc. The existence of the shape deformation means that the diffusion flux is not adequate to eliminate the displacive character of the transformation, and furthermore, the fact that most of the atoms must move in a coordinated manner to produce the displacements in the first place. It is a mistake to imagine that the association of diffusion with a phase transformation means that it can be treated as a reconstructive reaction which is close to equilibrium. The IPS shape deformation with its shear therefore remains evidence for the displacive character of the transformation mechanism when the atomic mobility is clearly inadequate to permit the elimination of the shape deformation.

Further implications of the shape change become clear when its relationship with the interfacial structure is considered. The interface in cases (iii) and (iv) is semicoherent because for coherency $\mathbf{RB} = \mathbf{P}$, an equation which is rarely satisfied in general, and not satisfied for the FCC to BCC or BCT transformation in steels. For the epitaxial semicoherency illustrated in (iv), coherent patches on the invariant-plane are separated by interface dislocations whose motion with the interface requires climb and hence diffusion of atoms in substitutional sites. The semicoherent interface may alternatively be glissile; the interface dislocations then glide conservatively as the interface moves and growth does not require diffusion and hence has a high mobility even at low temperatures (case

iii). For ferrous bainites, the mobility of the solvent and substitutional atoms is negligible, and the experimental observation of a shape deformation with a significant shear component gives strong evidence that the bainitic–ferrite/austenite interface is semi-coherent and glissile.

2.5.4 The Shape Change and the Superledge Mechanism

The lattice correspondence that is implied by the IPS shape deformation is a relationship between the lattices of the parent and product phases, independent of the orientation of the actual interface between the enclosed particle and the matrix. It follows that all the interfaces surrounding an enclosed particle of bainitic ferrite must be semicoherent (Christian, 1990a). It is not tenable to consider some interface orientations to be incoherent ('disordered') while semi-coherency is maintained on other interface orientations, as is sometimes implied in the superledge mechanism of bainitic growth (Aaronson *et al.*, 1970). This mechanism considers that the growth of bainitic ferrite plates occurs by the propagation of macroscopic ledges on the habit plane. The model requires at least two differently oriented macroscopic interfaces around an enclosed bainitic ferrite particle, the invariant-plane and the superledge. Macroscopic interfaces like these can only exist if the distortion due to the coherency between the parent and product lattices is within an elastically tolerable range, i.e. if the shape deformation across the interface is a close approximation to an IPS. Thus, the presence of two different orientations of macroscopic interface means that there are two invariant-planes between the parent and product crystals, a situation only possible if the net shape deformation is zero, in contradiction with experimental evidence.

All interface orientations other than the invariant-plane of the observed IPS shape deformation (which is also the habit plane of the bainitic ferrite) must be small coherent steps in the semi-coherent habit plane interface. The small steps are in forced *coherency* with the matrix, and have the characteristics of transformation dislocations which can glide and climb conservatively (also called coherency dislocations, Olson and Cohen, 1979). Coherency implies that all the corresponding planes and lines are continuous across the step; thus, these transformation dislocations are not lattice discontinuities. There is therefore no difficulty in these transformation dislocations climbing and gliding conservatively even when the Burgers vector is not parallel to the line vector.[†] The strain energy associated with the small steps is tolerable only because of their

[†]The terms transformation dislocation and coherency dislocation are identical. They are distinct from the adjectives 'interface', 'intrinsic', 'misfit' and 'anticoherency', all of which are used to describe dislocations which form an intrinsic part of the boundary structure (Olson and Cohen, 1979; Christian, 1990a).

small size. It is therefore considered that large steps (or 'superledges') are most improbable because of their high strain energy (Christian, 1990a).

2.5.5 The Structure of the Interface

It has already been pointed out that any atomic height steps in the bainitic/austenite interface are transformation dislocations, with strain fields whose character can be specified by assigning a Burgers vector to each such dislocation. The motion of these steps (or coherency dislocations) which are in forced coherency, leads to phase change: there is continuity of planes and vectors across the steps so that regions of the parent lattice are homogeneously deformed into that of the product as the steps are displaced. Since the energy of the step varies with the square of the magnitude of its Burgers vector, the step is restricted to atomic height, which is another way of stating that superledges are impossible on a bainitic/austenite interface. The anticoherency or interface dislocations cause the lattice-invariant deformation as the interface is displaced.

There are no decisive observations of the structure of the bainitic ferrite/austenite interface, but general conclusions can nevertheless be deduced using other experimental data and theoretical considerations. The observation of an invariant-plane strain shape change accompanying the growth of bainitic ferrite, when combined with the negligible mobility of the solvent and substitutional solute atoms, provides strong evidence that the structure of the transformation interface must be glissile. The number of iron and substitutional solute atoms is conserved during growth. Since they are not required to diffuse during transformation, the interfacial mobility is expected to be high even at low temperatures.

A semi-coherent interface containing a single array of anticoherency dislocations is considered to be glissile when the dislocations are able to move conservatively as the interface migrates. The dislocations must therefore all be pure screw dislocations, or have Burger's vectors which do not lie in the interface plane. The interface plane is the irrational invariant-plane or habit plane of the bainite plate. A glissile interface also requires that the glide planes (of the anticoherency dislocations) associated with the ferrite lattice must meet the corresponding glide planes in the austenite lattice edge to edge in the interface along the dislocation lines (Christian and Crocker, 1980).

If more than one set of anticoherency dislocations exist, then these should either have the same line vector in the interface, or their respective Burger's vectors must be parallel (Christian and Crocker, 1980). This condition ensures that the interface can move as an integral unit. It also implies that the deformation caused by the anticoherency dislocations, when the interface moves can always be described as a simple shear (caused by a resultant anticoherency

dislocation which is a combination of all the anticoherency dislocations) on some plane which makes a finite angle with the interface plane, and intersects the latter along the line vector of the resultant anticoherency dislocation.

Obviously, if the anticoherency dislocation structure consists of just a single set of parallel dislocations, or of a set of different dislocations which can be summed to give a single glissile anticoherency dislocation, then it follows that there must exist in the interface, a line which is parallel to the resultant anticoherency dislocation line vector, along which there is zero distortion. Because this line exists in the interface, it is also unrotated. It is an *invariant-line* in the interface between the parent and product lattices. When full coherency is not possible between the two structures (as is the case for the FCC to BCC transformation), then for the interface to be glissile, the transformation strain relating the two lattices must be an invariant-line strain, with the invariant-line lying in the interface plane.

An interesting consequence of the restriction that the transformation strain must be an invariant-line strain is that models of the ferrite–austenite interface as a single array of anticoherency dislocations are not possible for any orientation between Nishiyama–Wasserman and Kurdjumov–Sachs if the most densely-packed planes of the two structures are regarded as exactly parallel (Knowles and Smith, 1982; Christian, 1990a). This is because for realistic values of the lattice parameters, it is not possible to obtain a transformation strain which is an invariant-line strain if the planes are exactly parallel. If it is assumed that the interface contains just one set of anticoherency dislocations then the predicted orientation relation always has the most densely-packed planes of the two structures at a small angle (about 0.5°) to each other – such a small deviation is unfortunately difficult to detect experimentally.

There have been a few recent high resolution studies of the interface between bainite and austenite (e.g. Kajiwara *et al.*, 1999). It has not, however, been recognised that it is necessary to characterise the strain fields of any defects in the interface in order to make deductions about the mechanism of transformation. False conclusions can be reached about atomic steps if work is not done to reveal whether these are pure steps or coherency dislocations whose motion accomplishes transformation.

2.5.6 *The Crystallography of a Lath of Bainite*

The sub-units of a bainite sheaf may adopt the morphology of a plate or of a lath, where the latter is idealised as a parallelepiped of dimensions a, b, and c, with $a > b > c$. The lath shape is adopted when the transformation occurs at high temperatures. The crystallography of such laths has been characterised in detail and to a high level of accuracy, by Davenport (1974), as follows:

Growth direction	$[\bar{1}\,0\,1]_\gamma \| [\bar{1}\,\bar{1}\,1]_\alpha$
Habit plane (area = *ab*)	$(2\,3\,2)_\gamma \simeq (\bar{1}\,5\,4)_\alpha$
Face of area = *ac*	$(1\,0\,1)_\gamma$
Orientation relationship (KS)	$[\bar{1}\,0\,1]_\gamma \| [\bar{1}\,\bar{1}\,1]_\alpha$
	$(111)_\gamma \| (011)_\alpha$

when the crystallography is, for consistency, stated in the standard variant described earlier. Hence, the major growth direction of each lath corresponds to the parallel close-packed directions from the α and γ lattices. This is consistent with less direct trace analysis results which indicated that the major growth direction of the laths lies along $< \bar{1}\,\bar{1}\,1 >_\alpha$ (Goodenow and Hehemann, 1965; Oblak and Hehemann, 1967; Ohmori and Honeycombe, 1971). The habit plane indices are significantly different from earlier data which indicated a $\{1\,1\,1\}_\gamma$ habit (Greninger and Troiano, 1940; Oblak and Hehemann, 1967; Ohmori, 1971b; Ohmori and Honeycombe, 1971) but those analysis were either of insufficient precision or were concerned with the apparent habit planes of sheaves (Davenport, 1974). Davenport also demonstrated that sets of two groups of laths with a common growth direction, but with virtually orthogonal habit planes, tended to form in close proximity. There is as yet, no detailed analysis available which can predict these results.

Sandvik (1982a) has measured, using single surface trace analysis, the habit planes of individual sub-units. The mean habit plane is close to $(0.373\ 0.663\ 0.649)_\gamma$ for an orientation relationship in which $(1\,1\,1)_\gamma \| (0\,1\,1)_\alpha$ and $[\bar{1}\,0\,1]_\gamma$ is approximately 4° from $[\bar{1}\,\bar{1}\,1]_\alpha$ (such an orientation is close to the Nishiyama–Wasserman orientation relationship). The habit plane was not found to vary significantly with transformation temperature. Using data from high-resolution observations of the displacements of austenite twins by the shape deformation due to transformation, he was able to show that the shear component of the shape strain of a sub-unit is about 0.22. Sandvik also showed that the observed shape strain direction and magnitude are close to the corresponding parameters for the classic $\{2\,2\,5\}_\gamma$ and $\{3\,10\,15\}_\gamma$ martensites in steels.

2.5 Microstructure of Bainite: The Midrib

High-carbon steels can sometimes transform to plates of lower bainite which do not have a homogeneous microstructure (Okamoto and Oka, 1986). When observed using light microscopy, a macroscopic plate of lower bainite is seen to have a black line running centrally along its axis (Fig. 2.26). Transmission electron microscopy reveals that this line corresponds to a centrally located, coplanar thin plate of martensite which is sandwiched between regions of lower bainite. The lower bainite containing the midrib is actually found to

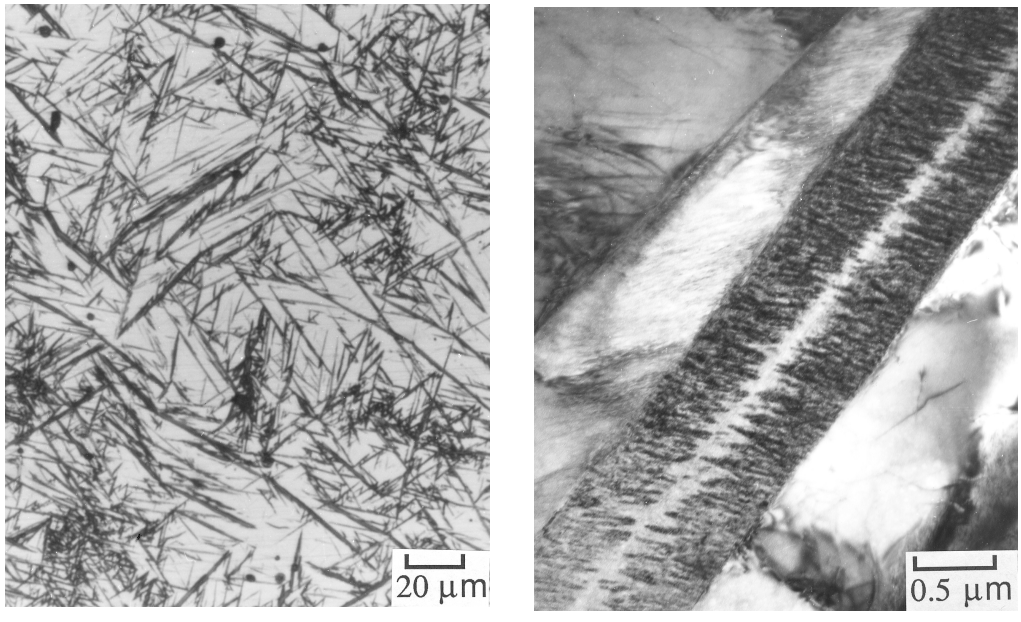

Fig. 2.26 Optical and transmission electron micrographs of the midrib associated with lower bainite in a plain carbon steel (after Okamoto and Oka, 1986).

evolve in two stages, from thin-plate martensite which forms first by the isothermal transformation of austenite, and which then stimulates the growth of the adjacent bainite regions.

Okamoto and Oka deduced that at relatively high transformation temperatures, the steels react to give lower bainite without a midrib, but as the transformation temperature is reduced to below a certain temperature T_r, this is replaced by the lower bainite with a thin-plate martensite midrib, which then gives way to just the thin-plate martensite; at a sufficiently low temperature (below the conventional M_S temperature), ordinary martensite with a lenticular plate morphology forms by the athermal transformation of austenite.

It was noted above that both the lower bainite containing the midrib, and thin-plate martensite isothermally form in the temperature range $T_r \rightarrow M_S$. Okamoto and Oka demonstrated that the difference between these two temperatures diminishes as the carbon concentration of the steel decreases, until at about 1wt% C, it becomes zero. Consequently, neither of these phases have been reported to occur in lower carbon steels.

The terminology *thin-plate martensite* has its origins in work done on nickel-rich Fe–Ni–C alloys, where the martensite transformation temperatures are

well below −100°C (Maki *et al.*, 1973, 1975). The martensite then tends to form as extremely thin, parallel-sided plates in preference to much thicker lenticular plates, especially as the carbon concentration is increased. Because of their large aspect ratios, the thin plates are elastically accommodated in the austenite matrix; their interfaces remain glissile. The plates can therefore thicken as the temperature is reduced, or indeed become thinner as the temperature is raised.

2.7 Summary

Bainite grows in the form of clusters of thin lenticular plates or laths, known as sheaves. The plates within a sheaf are known as sub-units. The growth of each sub-unit is accompanied by an invariant-plane strain shape change with a large shear component. The sub-units are to some extent separated from each other by films of residual phases such as austenite or cementite, so that the shape strain of the sheaf as a whole tends to be much smaller than that of an isolated sub-unit. The plates within any given sheaf tend to adopt almost the same crystallographic orientation and have identical shape deformations. Because of the relatively high temperatures at which bainite grows (where the yield stresses of ferrite and austenite are reduced), the shape strain causes plastic deformation which in turn leads to a relatively large dislocation density in both the parent and product phases; other kinds of defects, such as twinning and faulting are also found in the residual austenite. This plastic accommodation of the shape change explains why each sub-unit grows to a limited size which may be far less than the austenite grain size. The dislocation debris stifles the motion of the otherwise glissile interface. Consequently, the sheaf as a whole grows by the repeated 'nucleation' of new sub-units, mostly near the tips of those already existing.

The bainitic ferrite/austenite orientation relationship is always found to lie well within the Bain region; this and other features of the transformation are broadly consistent with the phenomenological theory of martensite crystallography. The growth of bainitic ferrite undoubtedly occurs without any redistribution of iron or substitutional solute atoms, even on the finest conceivable scale at the transformation interface. Although some excess carbon is retained in solution in the bainitic ferrite after transformation, most of it is partitioned into the residual austenite, and in the case of lower bainite, also precipitated as carbides within the ferrite. This redistribution of carbon could of course occur after the diffusionless growth of bainitic ferrite, and the subject is discussed in more detail in Chapters 5 and 6. All of the observed characteristics of bainitic ferrite prove that it grows by a displacive transformation mechanism.

3 *Carbide Precipitation*

Carbides are largely responsible for the commercial failure of many of the early bainitic steels. The alloys could not compete against the quenched and tempered martensitic steels with their finer dispersions of carbide particles. The details of mechanical properties are discussed in Chapter 10; the purpose here is to deal with the nature and extent of carbide precipitation reactions in the context of the mechanism of the bainite transformation.

3.1 Upper Bainite

In upper bainite the carbides precipitate from austenite which is enriched in carbon; upper bainitic ferrite itself is free from precipitates (Fig. 3.1a). The most common carbide is cementite but there are notable exceptions, particularly in

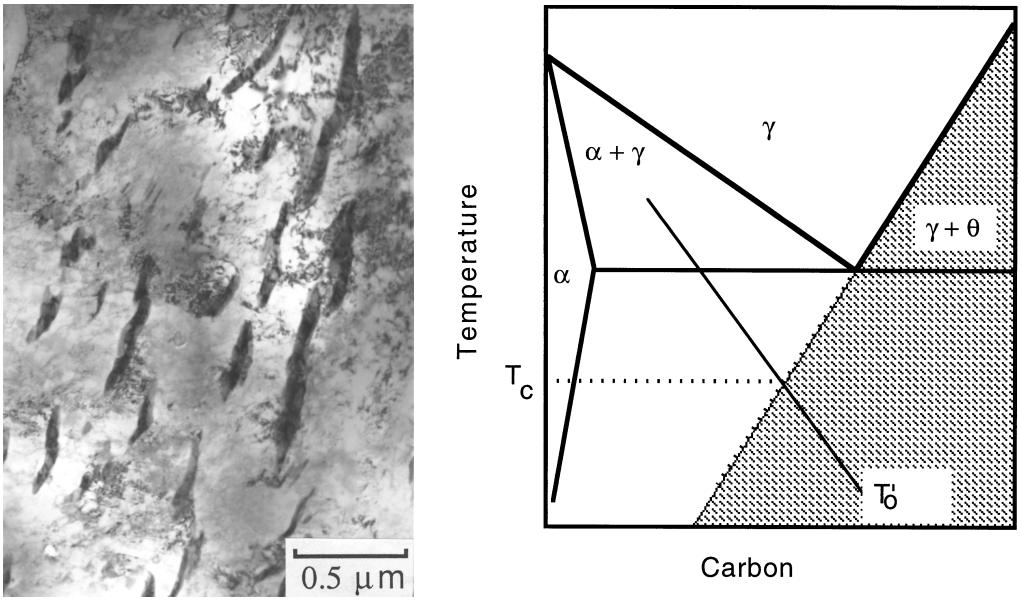

Fig. 3.1 (a) Distribution of cementite particles between the ferrite platelets in upper bainite (AISI 4340 steel). (b) Thermodynamic condition which must be satisfied before cementite can precipitate from austenite.

steels containing large concentrations of silicon. For example, the orthorhombic carbides reported by Schissler *et al*. (1975) and the *c*–carbide discovered by Sandvik (1982b), Table 3.1. Transition carbides, such as κ and the various orthorhombic forms listed in Table 3.1, only form because they are easier to nucleate, so they eventually transform into cementite.

Carbon is partitioned into the residual austenite during the bainite reaction. Cementite precipitation becomes possible when its carbon concentration x_γ exceeds the solubility limit given by the extrapolated $\gamma/(\gamma+\theta)$ phase boundary

Table 3.1 Carbides in bainite or in tempered bainite. Fe, M/C is the ratio of metal to carbon atoms. Actual lattice parameters are alloy dependent. See also a review by Yakel (1985).

Carbide	Crystal System	Fe, M/C	Reference
κ	Hexagonal $a = 6.9$ $c = 4.8$ Å	1.37	Deliry (1965) Pomey (1966)
ϵ	Hexagonal $a = 2.735$ $c - 4.339$ Å	2.4–3	Jack (1950, 1951) Hofer *et al*. (1949)
χ	Monoclinic $a = 11.563$ $b = 3.573$ Å $c = 5.058$ $\beta = 97.44^\circ$	2.2 or 2.5	Hägg (1934)
η	Orthorhombic $a = 4704$ $b = 4.318$ Å $c = 2.830$	2	Hirotsu and Nagakura (1972)
Fe_3C	Orthorthombic $a = 4.525$ $b = 5.087$ Å $c = 6.743$	3.0	
M_7C_3	Orthorhombic $a = 4.526$ $b = 7.010$ Å $c = 12.142$	7/3	Morniroli *et al*. (1983)
$(Fe, Si)C_X$	Orthorhombic $a = 8.8$ $b = 9.0$ $c = 14.4$ Å		Konoval *et al*. (1959)
$(Fe, Si)C_X$	Orthorhombic $a = 6.5$ $b = 7.7$ $c = 10.4$ Å		Schissler *et al*. (1975)
$(Fe, Si, Mn)C_X$	Orthorhombic $a = 14.8$ $b = 11.4$ $c = 8.5$ Å		Schissler *et al*. (1975)
$M_{23}C_6$	Cubic F $a = 10.621$ Å	23/6	
M_6C	Cubic F $a = 11.082$ Å	6	
c	Triclinic $a = 6.38$ $b = 5.05$ $c = 4.59$ Å $a = 90.0^\circ$ $\beta = 70.1^\circ$ $\gamma = 84.7^\circ$		Sandvik (1982b)

(Kriesement and Wever, 1956). This is illustrated in Fig. 3.1b, where the shaded area represents austenite which is unstable to the precipitation of cementite. It follows that if there are no kinetic hindrances, carbide precipitation will accompany the growth of upper bainite if the transformation temperature is below T_C (Fig. 3.1b).

The precipitation of carbides is peripheral to the formation of bainitic ferrite. On the other hand, their formation reduces the carbon concentration in the residual austenite, thus stimulating the formation of a further quantity of ferrite (designated α). Given the very small diffusion coefficients of iron and substitutional atoms at the temperatures involved (Fig. 3.2), and the absence of an incoherent interface or grain boundary to start the process, it is unlikely that this secondary ferrite forms by reconstructive transformation. Sandvik (1982b) has proposed that the decomposition of the residual austenite involves the displacive formation of a triclinic carbide, close to cementite in structure, and the subsequent formation of a small amount of *bainitic* ferrite. Nakamura and Nagakura (1986), in a study of the second stage of martensite tempering, suggested that cementite and ferrite form directly from austenite, the cementite nucleating on the ferrite/austenite boundaries and growing by rapid diffusion along this boundary. They also proposed that the secondary ferrite, which they called bainite, grows martensitically, from the carbon depleted austenite. Regions of secondary ferrite were observed to be twinned, and this was taken to indicate the formation of self–accommodating crystallographic variants of bainitic ferrite.

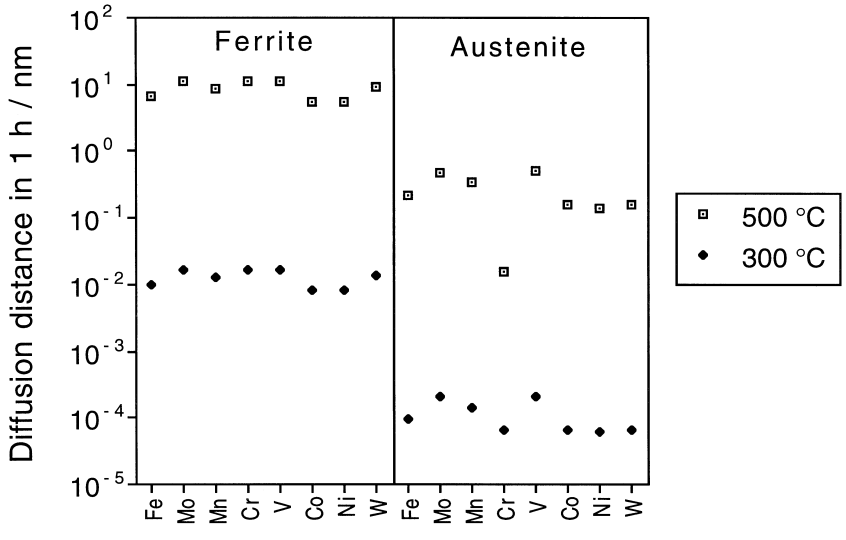

Fig. 3.2 $2(Dt)^{1/2}$ estimate of the diffusion distances for metal atoms in iron during one hour at temperature.

The sequence of reactions can be summarised as follows (α =secondary ferrite):

$$\begin{aligned} \gamma &\rightarrow \gamma + \alpha_{b,\text{supersaturated}} \\ &\rightarrow \alpha_{b,\text{unsaturated}} + \gamma_{\text{enriched}} \\ &\rightarrow \alpha_{b,\text{unsaturated}} + \alpha + \theta \end{aligned} \tag{3.1}$$

This contrasts with the cooperative growth of cementite and ferrite during the formation of pearlite in plain carbon steels:

$$\gamma \rightarrow \alpha + \theta \tag{3.2}$$

When pearlite grows in substitutionally alloyed steels, the austenite, ferrite and cementite may coexist in equilibrium over a range of temperatures, with the equilibrium compositions of all the phases changing with the temperature:

$$\gamma \rightarrow \alpha + \theta + \gamma' \tag{3.3}$$

The composition of the residual austenite (γ') is then expected to differ from that at the beginning of transformation. The reaction therefore stops before all the austenite is consumed.

In planar sections, the cementite particles in upper bainite are parallel to the habit planes of the bainitic ferrite plates. Using transmission electron microscopy, Fisher (1958) showed that these particles are in the form of irregular ribbons in three dimensions, particularly when bainite forms at high temperatures. Carbide precipitation also occurs at the austenite grain boundaries and this may influence mechanical properties, especially toughness in high strength steels (Pickering, 1958). The austenite grain boundaries are favoured heterogeneous nucleation sites so the carbides there can be expected to be coarse. When high carbon steels (> 0.45C wt%) are transformed in the bainite temperature range, there is a tendency for cementite to precipitate as thin films on the austenite grain surfaces (Stickels, 1974). These thin films are detrimental to toughness and their growth can be retarded by lowering the transformation temperature.

3.2 Lower Bainite

Lower bainite also consists of a non-lamellar aggregate of ferrite and two kinds of carbides. As in upper bainite, there is some precipitation from the enriched austenite. A finer dispersion of plate-like carbides is also found inside the ferrite plates. A common observation is that these latter carbides precipitate in a single crystallographic variant within a given ferrite plate, whereas the tempering of martensite leads to the precipitation of many variants of cementite (Fig. 3.3).

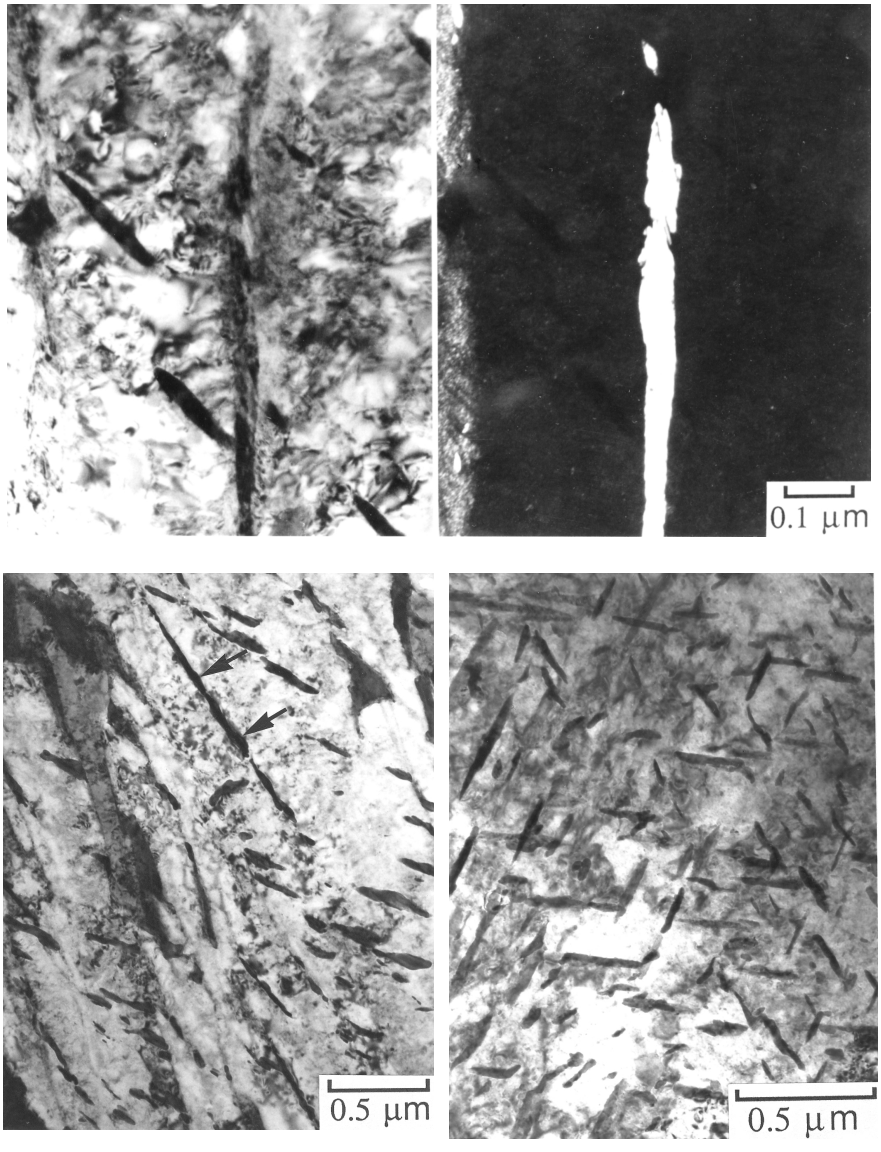

Fig. 3.3 (a–c) Fe–0.3C–4.08Cr wt%. (a) Lower bainite obtained by isothermal transformation for a short time period (435 °C, 10 min). Shows particles of cementite within the platelets but not between the platelets. (b) Corresponding dark field image showing the films of austenite between the bainitic ferrite platelets. (c) The same sample after prolonged heat treatment (435 °C, 30 min) at the isothermal transformation temperature, causing the precipitation of carbides between the ferrite platelets. (d) Typical multi-variant carbide precipitation in tempered martensite (415°C, 50 min, AISI 4340 steel). After Bhadeshia (1980a).

3.2.1 Precipitation within Lower Bainitic Ferrite

There are many observations that reveal the precipitation of carbides from supersaturated lower bainite in a process identical to the tempering of martensite. *In situ* hot-stage transmission electron microscopy has shown that the lower bainitic ferrite remains supersaturated with carbon some time after the completion of the ferrite growth (Kang *et al*., 1990).

Unlike the microstructure of tempered martensite, the carbides tend to adopt a single crystallographic variant in a given plate of lower bainite. They have their longest axes inclined at about 60° to the 'growth direction' of the ferrite platelets (ASTM, 1955; Irvine and Pickering, 1958; Speich, 1962; Shimizu and Nishiyama, 1963; Shimizu *et al*., 1964). The angle quoted must of course vary as a function of the plane of section; for lower bainitic ferrite with a habit plane $(0.761\ 0.169\ 0.626)_\gamma$, the cementite precipitates on $(1\,\bar{1}\,2)_\alpha$ giving an angle of 57° between the α and cementite habit plane normals (Bhadeshia, 1980a). Similar results have been obtained by Ohmori (1971a). In some cases, the carbides have been found to form on several different variants of the $\{1\,1\,2\}_\alpha$ plane, although a particular variant still tends to dominate (Srinivasan and Wayman, 1968b; Lai, 1975; Bhadeshia and Edmonds, 1979a). In fact, a re-examination of published micrographs sometimes reveals the presence of several variants which were not noticed in the original publication (see for example, Fig. 5, Degang *et al*., 1989).

Early experiments using Curie point measurements and dilatometry gave hints that the carbides are not always cementite (Wever and Lange, 1932; Allen *et al*., 1939; Antia *et al*., 1944). For example, the orthorhombic transition carbide discovered in high-silicon transformer steels by Konoval *et al*. (1959) has been reported to precipitate from lower bainitic ferrite in Fe–1.15C–3.9Si wt% alloy (Schissler *et al*., 1975). Nevertheless, the most common transition carbide in lower bainite is ϵ-carbide, first identified by Austin and Schwartz (1952) and subsequently confirmed by many others.

Matas and Hehemann interpreted these results to suggest that the initial carbide in hypoeutectoid bainitic-steels is ϵ, which is then replaced by cementite on holding at the isothermal transformation temperature. The rate at which the ϵ-carbide converts to cementite increases with temperature, but also depends on the steel composition. A high silicon concentration retards the reaction, as is commonly observed in the tempering of martensite (Owen, 1954; Gordine and Codd, 1969; Hobbs *et al*., 1972).

The detection of ϵ-carbide in lower bainite is important because it implies a large excess (≥ 0.25 wt%) of carbon trapped in bainitic ferrite when it first forms (Roberts *et al*., 1957). However, ϵ-carbide is not always found as a precursor to the precipitation of cementite in lower bainite. Bhadeshia and Edmonds (1979a) failed to detect ϵ-carbide in a high-silicon medium-carbon

steel (Fe–3.0Mn–2.02Si–0.43C wt%) even during the early stages of the lower bainite transformation. The steels in which ϵ-carbide has been observed during the formation of lower bainite are listed in Table 3.2.[†]

Table 3.2 Compositions of steels (wt%) in which ϵ-carbide has been found in lower bainite. The carbon concentration quoted for the alloy studied by Dubensky and Rundman represents an estimate of the concentration in the austenitic matrix of an austempered ductile cast iron.

C	Si	Mn	Ni	Cr	Mo	V	Reference
0.87	–	–	–	–	–	–	Austin and Schwartz, 1952, 1955
0.95	0.22	0.60	3.27	1.23	0.13	–	Matas and Hehemann, 1961
0.60	2.00	0.86	–	0.31	–	–	Matas and Hehemann, 1961
1.00	0.36	–	0.20	1.41	–	–	Matas and Hehemann, 1961
0.58	0.35	0.78	–	3.90	0.45	0.90	Matas and Hehemann, 1961
1.00	2.15	0.36	–	–	–	–	Deliry, 1965
0.60	2.00	0.86	–	0.31	–	–	Oblak and Hehemann, 1967
0.60	2.00	–	–	–	–	–	Hehemann, 1970
0.41	1.59	0.79	1.85	0.75	0.43	0.08	Lai, 1975
0.54	1.87	0.79	–	0.30	–	–	Huang and Thomas, 1977
0.85	2.55	0.3	–	–	–	–	Dorazil and Svejcar, 1979
0.74	2.40	0.51	–	0.52	–	–	Sandvik, 1982a
1.3	3.09	0.17	–	–	–	–	Dubensky and Rundman, 1985
0.40	2.01	–	4.15	–	–	–	Miihkinen and Edmonds, 1987a

These observations can be rationalised in terms of a theory of tempering due to Kalish and Cohen (1970), who showed that it is energetically favourable for carbon atoms to remain segregated at dislocations when compared with their presence in the ϵ-carbide lattice (Bhadeshia, 1980a). Carbon becomes trapped at dislocations and if the density of dislocations is sufficiently large, then the carbon is not available for the formation of ϵ-carbide. In such cases, precipitation of the more stable cementite occurs directly from supersaturated ferrite. Kalish and Cohen estimated that a dislocation density of $2 \times 10^{12}\,\mathrm{cm}^{-2}$ should prevent ϵ-carbide precipitation in steels containing up to 0.20 wt% carbon. This can be extrapolated to bainite bearing in mind that there are two competing reactions which help relieve the excess carbon in the ferrite: partitioning of carbon into the residual austenite and the precipitation of carbides in the

[†] ϵ-carbide has been reported in bainite produced by continuous cooling transformation, in a Fe–0.15C–0.94Mo–2.12Cr wt% steel (Baker and Nutting, 1959) and in a Fe–0.34C–1.25Mn–1.39Ni–0.34Mo wt% alloy isothermally transformed to bainite (Fondekar *et al.*, 1970). In both cases, the evidence quoted is uncertain. A study by Yu (1989) on similar steels has not revealed ϵ-carbide.

bainitic ferrite. The reactions interact since partitioning reduces the amount of carbon available for precipitation, and vice versa. Judging from available data (Table 3.2), the average carbon content of the steel must exceed about 0.55 wt% to permit the precipitation of ϵ-carbide. Otherwise, the partitioning of carbon into the austenite depletes the bainitic ferrite too rapidly to permit ϵ-carbide.

Nickel enhances the precipitation of ϵ-carbide which can therefore be obtained in bainite at lower carbon concentrations, $\simeq$0.4 wt% (Miihkinen and Edmonds, 1987a). Rao and Thomas (1980) have demonstrated a similar effect of nickel in martensitic steels; they found ϵ-carbides and cementite to be the dominant carbides during the tempering of martensite in Fe–0.27C–4Cr–5Ni and Fe–0.24C–2Mn–4Cr wt% steels respectively. Other substitutional solutes may also affect ϵ-carbide precipitation, but there are no systematic studies. As with martensite, when lower bainite is tempered, the metastable ϵ-carbide transforms to cementite and the reaction is accompanied by a volume contraction, which can be monitored accurately using dilatometry (Hehemann, 1970).

It is interesting that η-carbide (Fe_2C) has also been observed in lower bainitic ferrite obtained by transforming the austenitic matrix of a high-silicon cast iron (Franetovic *et al*., 1987a,b). This carbide has previously only been reported in tempered martensite (Hirotsu and Nagakura, 1972; Nagakura *et al*., 1983) and so reinforces the conclusion that the carbides precipitate from carbon-supersaturated lower bainitic ferrite. Like ϵ-carbide, the carbon concentration has to exceed some critical value before the η-carbide can be detected in lower bainite (Franetovic *et al*., 1987a,b).

3.2.2 *Precipitation between Lower Bainitic Ferrite Platelets*

There is no essential difference between upper and lower bainite when considering the precipitation of carbides from the carbon-enriched austenite. However, in lower bainite some of the excess carbon precipitates in the ferrite, thus reducing the quantity partitioned into the austenite (Hehemann, 1970). This in turn leads to a smaller fraction of inter-plate cementite when the austenite eventually decomposes. An important consequence is that lower bainite often has a higher toughness than upper bainite, even though it usually is stronger. The precipitation reactions for lower bainite can be summarised as follows:

Case 1: High dislocation density

$$\begin{aligned}\gamma &\rightarrow \gamma + \alpha_{b,\text{supersaturated}} \\ &\rightarrow \theta_{\text{in ferrite}} + \alpha_{b,\text{unsaturated}} + \gamma_{\text{enriched}} \\ &\rightarrow \alpha_{b,\text{unsaturated}} + \alpha + \theta_{\text{between ferrite plates}} + \theta_{\text{in ferrite}}\end{aligned} \tag{3.4}$$

Case 2: Low dislocation density

$$\begin{aligned}\gamma &\rightarrow \gamma + \alpha_{b,\text{supersaturated}} \\ &\rightarrow \epsilon_{\text{in ferrite}} + \alpha_{b,\text{unsaturated}} + \gamma_{\text{enriched}} \\ &\rightarrow \alpha_{b,\text{unsaturated}} + \epsilon_{\text{in ferrite}} + \alpha + \theta_{\text{between ferrite plates}} \\ &\rightarrow \alpha_{b,\text{unsaturated}} + \theta_{\text{in ferrite}} + \theta_{\text{between ferrite plates}} + \alpha\end{aligned} \tag{3.5}$$

κ-carbide was discovered in high-carbon steels transformed to lower bainite (Deliry, 1965; Pomey, 1966). It occurs as a transition carbide, precipitating at a late stage of the transformation, from the carbon-enriched residual austenite. The carbide has a high solubility for silicon and on continued holding at the isothermal transformation temperature, transforms to χ which in turn eventually gives way to the more stable cementite.

3.3 Kinetics of Carbide Precipitation

3.3.1 Partitioning and Distribution of Carbon

The carbon concentration of bainitic ferrite during transformation is of major importance in determining the kinetics of carbide precipitation. The transformation, however, occurs at high temperatures so excess carbon in the ferrite can be removed by precipitation or by partitioning into austenite. These two processes occur simultaneously, although one or the other may dominate depending on temperature. They can both be rapid because of the high mobility of carbon in iron.

The partitioning of excess carbon from ferrite into austenite was simulated experimentally by Matas and Hehemann (1960, 1961) who tempered mixtures of martensite and retained austenite. Single crystals of austenite were cooled below the M_S temperature (350 K) to obtain two microstructures, one containing 50% martensite and the other 90% martensite in a matrix of austenite. The crystals were then tempered at 405 K to allow the carbon to diffuse from martensite into austenite. The tempering induced the rapid precipitation of ϵ-carbide, thereby lowering the carbon concentration of the martensite to 0.22 wt%, a value consistent with that quoted by Roberts *et al*. (1957) for the equilibrium between martensite and ϵ-carbide. Continued tempering led to further reductions in the carbon concentration of the martensite as the carbon partitioned into the austenite. This partitioning occurred more rapidly for the sample containing less martensite, presumably because the larger amount of residual austenite provided a bigger sink for carbon.

The distribution of carbon in the residual austenite should not be assumed to be homogeneous after isothermal transformation to bainite (Fig. 3.4). The extent of enrichment is greater in the immediate vicinity of bainite platelets

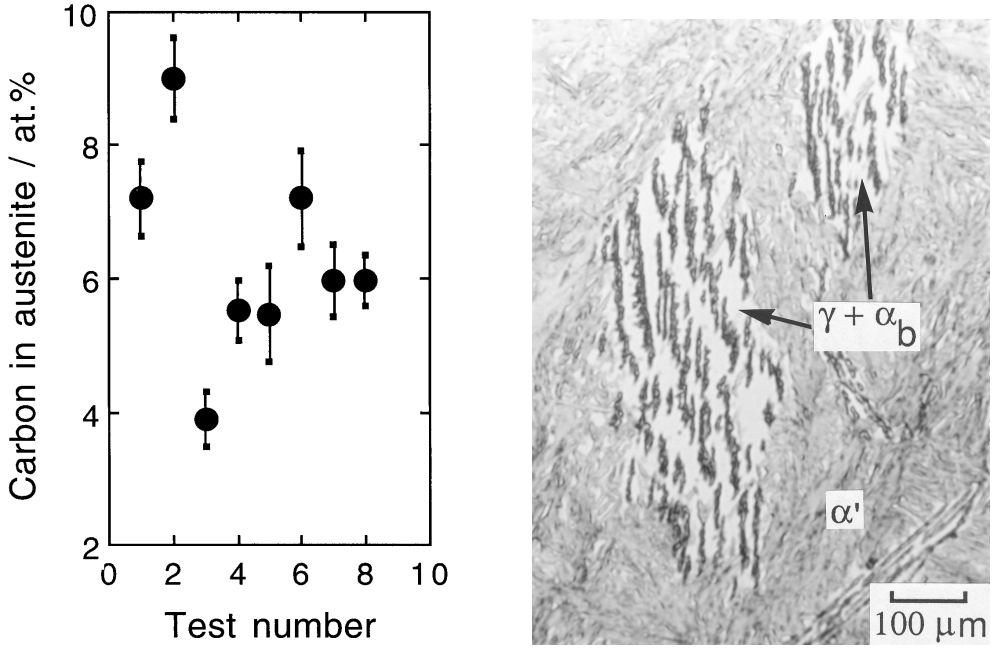

Fig. 3.4 The nonuniform distribution of carbon in the residual austenite associated with bainitic ferrite. (a) Direct measurements of the carbon concentration using an atom-probe; Fe–0.39C–2.05Si–4.08Ni wt%, isothermally transformed at 340°C for 10 h (Bhadeshia and Waugh, 1981). (b) Rim of austenite retained around a sheaf of bainite in Fe–0.81C–1.98Si–3Mn wt% steel, where the carbon concentration is expected to be largest.

or in the regions trapped between the platelets (Schrader and Wever, 1952; Matas and Hehemann, 1961). Carbon causes an expansion of the austenite so in some cases, two lattice parameters have been observed for the retained austenite, corresponding to different levels of carbon in the heterogeneous austenite within a single specimen (Matas and Hehemann, 1961). In many cases, the austenite which is relatively poor in carbon decomposes martensitically on cooling to ambient temperature. Any subsequent measurement of the carbon concentration of austenite (x_γ) using an X-ray method must then overestimate x_γ if it is assumed that the carbon was distributed uniformly in the residual austenite that existed at the isothermal transformation temperature. For example, for upper bainite in a high-silicon steel, X-ray measurements gave $x_\gamma = 1.7$ wt%, whereas volume fraction data gave an average concentration of 1.35 wt% (Houllier *et al.*, 1971).

3.3.2 *Kinetics of Precipitation from Residual Austenite*

Carbide formation lags behind that of bainitic ferrite, to an extent which depends both on the transformation temperature and on the alloy composition. In steels which transform rapidly, the delay may not be detectable. Using a chemical technique which separates precipitated carbon from that in solid solution, together with dilatometry, it has been shown that for high transformation temperatures, the amount of carbide formed is proportional to that of bainitic ferrite at any stage of the reaction (Vasudevan *et al.*, 1958). At lower temperatures, carbide precipitation follows significantly after the formation of bainitic ferrite.

With lower bainite, it is necessary to distinguish between the carbides within the bainitic ferrite which precipitate rapidly, and those which form by the slower decomposition of the carbon-enriched residual austenite (Fig. 3.3a,c). The slow rate of precipitation from austenite is due to the difference in the diffusion rates of carbon in ferrite and austenite, and because the supersaturation is larger for ferrite.

Striking evidence that the formation of carbides lags behind that of bainitic ferrite is found in silicon-rich steels. Thus, carbides do not form in upper bainite in Fe–0.31Cr–0.86Mn–2.00Si–0.60C wt% even after holding at the isothermal transformation temperature for several hours (Matas and Hehemann 1961). Similar results have been reported by Houllier *et al.*, (1971), Sandvik (1982b) and by many other researchers.

Silicon is usually present in steels as an aftermath of the deoxidation reactions involved in the steelmaking process. At large concentrations it retards the formation of cementite from austenite, making it possible to obtain a carbide-free microstructure of just bainitic ferrite and austenite (Entin, 1962; Deliry, 1965; Pomey, 1966; Hehemann, 1970; Houllier *et al.*, 1971; Bhadeshia and Edmonds, 1979a; Sandvik, 1982a,b). For the same reason, silicon favours the formation of gray cast iron with graphite instead of the cementite found in low-silicon white cast irons. It is well known that the precipitation of cementite during the tempering of martensite is significantly retarded by the presence of silicon (Bain, 1939; Allten and Payson, 1953; Owen, 1954; Keh and Leslie, 1963; Gordine and Codd, 1969; Hobbs *et al.*, 1972). This has been exploited in the design of one of the most successful ultrahigh-strength steels (commercial designation 300*M*, reviewed by Pickering, 1979).

Silicon has an incredibly low solubility in cementite. If it is forced, by the paraequilibrium transformation mechanism, to inherit the silicon as it grows then the driving force for precipitation is greatly reduced, thus retarding precipitation (Section 3.5). It was at one time thought that the retardation occurs because silicon stabilises transition carbides at the expense of

cementite (Reisdorf, 1963; Gordine and Codd, 1969) but experiments have shown that the transition carbides are not particularly enriched in silicon (Barnard *et al*., 1981).

Aluminium in solid solution also retards tempering reactions (Allten, 1954; Langer, 1968; Bhat, 1977). The effect is believed to be identical to that of silicon although detailed solubility data are not available.

Carbide-free bainitic microstructures can be obtained in steels containing little or no silicon or aluminium, for example in Fe–Cr–C alloys (Bhadeshia, 1980a), in low-carbon steels (Yang and Bhadeshia, 1987) and in copper-containing steels (Thompson *et al*., 1988). The classic '$2\frac{1}{4}$Cr1Mo' steel which is used in vast quantities in the electricity generation industry has a carbide-free bainitic microstructure. It is not yet possible to predict the effects of alloying elements on carbide precipitation reactions during the bainite transformation.

3.3.3 Kinetics of Precipitation within Bainitic Ferrite

It is particularly interesting that the precipitation of cementite from martensite or lower bainite can occur at temperatures below 400 K, in time periods too short to allow any substantial diffusion of iron atoms. The long-range diffusion of carbon atoms is of course necessary, but because carbon resides in interstitial solution, it can be very mobile at temperatures as low as 210 K (Winchell and Cohen, 1962).

The formation of cementite or other transition carbides of iron, in these circumstances of incredibly low atomic mobility, must differ from diffusional decomposition reactions. It has been believed for some time that the cementite lattice is generated by the homogeneous deformation of ferrite, combined with the necessary diffusion of carbon into the appropriate sites. In effect a displacive mechanism with paraequilibrium. The nature of the necessary displacements for generating cementite or ϵ-carbide structures have been considered phenomenologically by Andrews (1963), Hume-Rothery *et al*., (1942) and the subject has been reviewed by Yakel (1985). The models are not sufficiently developed to predict transformation kinetics except that they do no involve the diffusion of substitutional atoms and hence are consistent with rapid kinetics even at low temperatures.

The lack of atomic mobility over the temperature range where bainite grows has consequences also on the alloy carbides (such as Mo_2C) which require diffusion to grow. The size of such carbides is restricted by the distance through which the substitutional atoms can diffuse during the time scale of the experiment. This is illustrated by experiments in which the transformation of a Fe–Mo–C alloy was studied over a wide range of temperatures with the carbide type, size and composition being characterised at the highest spatial and chemical resolution possible (Stark and Smith, 1987). Fig. 3.5 shows that

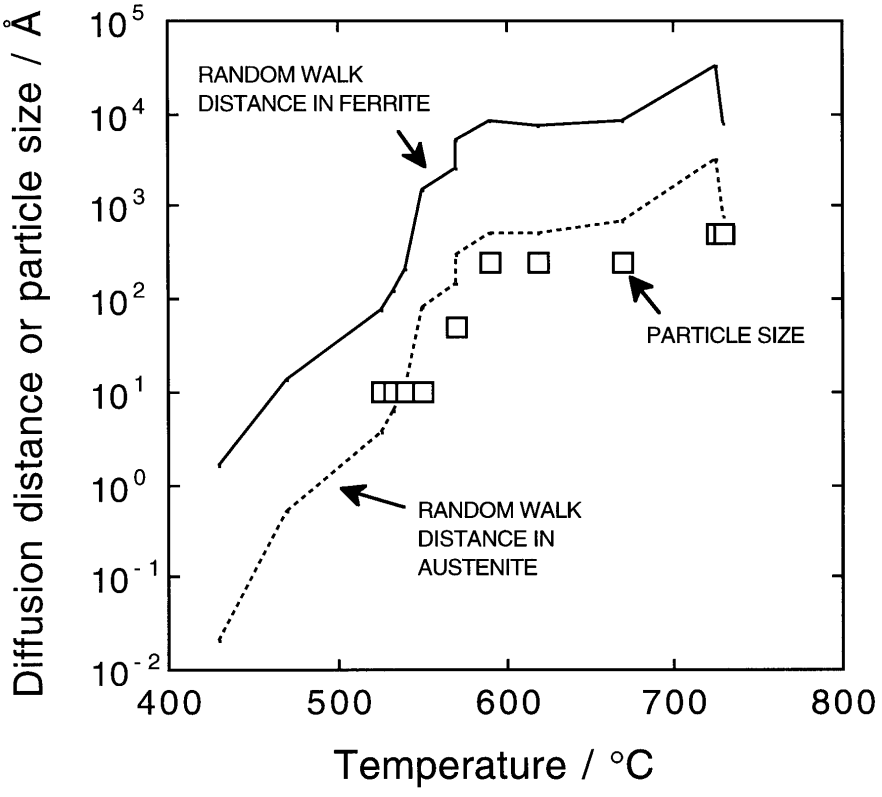

Fig. 3.5 Correlation of random walk distance for molybdenum atoms versus the measured molybdenum carbide carbide particle size (data due to Stark and Smith, 1987). The curves are the calculated $2(D_{Mo}t)^{0.5}$ values for specific heat-treatments. Molybdenum carbide was never found with bainite, only with ferrite which grew by reconstructive transformation.

the measured particle sizes correlate well with the random walk distance $2(D_{Mo}t)^{0.5}$, which is a measure of atomic mobility.

A second consequence is related to the mechanism by which the ferrite itself grows. The crystallographic change from $\gamma \rightarrow \alpha$ may occur without any diffusion. However, if the mechanism is reconstructive, then mass transport is essential during growth even when there is no change in composition (Bhadeshia, 1985b). The transformation can then only proceed at a rate consistent with this diffusion, in which case substitutional solutes like molybdenum have an opportunity to precipitate. It is noteworthy that Stark and Smith (1987) only found molybdenum carbides in ferrite which grew by a reconstructive transformation mechanism, and never in association with bainitic ferrite.

3.4 Crystallography of Carbide Precipitation in Bainite

During isothermal heat-treatments of the type used to generate bainite, the steel is not held at temperature for periods long enough to permit the long-range diffusion of substitutional atoms. Only iron carbides, such as ϵ, κ, η or cementite therefore precipitate. Other carbides which require the partitioning of substitutional solutes cannot form.

3.4.1 Cementite: Orientation Relationships

Shackleton and Kelly (1965) studied the orientation relationships between ferrite and cementite in bainite. The relationships were found to be identical to those known for cementite in tempered martensite. They most frequently observed the tempering or Bagaryatski (1950) orientation relationship:

$$\{0\,0\,1\}_\theta \| \{2\,1\,1\}_\alpha$$
$$< 1\,0\,0 >_\theta \| < 0\,\overline{1}\,1 >_\alpha$$

The next prominent α/θ orientation relationship, also found in tempered martensite, was:

$$\{0\,0\,1\}_\theta \| \{\overline{2}\,\overline{1}\,5\}_\alpha$$
$$< 1\,0\,0 >_\theta \quad \text{within } 2.6^\circ \text{ of } < 3\,\overline{1}\,1 >_\alpha$$
$$< 0\,1\,0 >_\theta \quad \text{within } 2.6^\circ \text{of } < 1\,3\,1 >_\alpha$$

In upper bainite, the large number of observed α_b/θ orientation relationships could all be derived assuming that the cementite precipitates from austenite with the Pitsch (1962) γ/θ relationship:

$$\{0\,0\,1\}_\theta \| \{\overline{2}\,2\,5\}_\gamma$$
$$< 1\,0\,0 >_\theta \quad \text{within } 2.6^\circ \text{of } < \overline{5}\,5\,\overline{4} >_\gamma$$
$$< 0\,1\,0 >_\theta \quad \text{within } 2.6^\circ \text{of } < \overline{1}\,\overline{1}\,0 >_\gamma$$

The α_b/θ relationships can be generated from the γ/θ relationship by allowing the ferrite to be a variant of the Kurdjumov and Sachs α/γ orientation relationship.

These results have been confirmed and are important in understanding the mechanism of the bainite transformation. They suggest that in lower bainite the carbides precipitate from ferrite which contains an excess of carbon. After all, precisely the same θ/α orientations are found during the tempering of martensite.

The θ/α orientation relationship found by Isaichev (1947) also occurs in lower bainite (Ohmori, 1971a; Huang and Thomas, 1977). Using rational indices, the Isaichev relationship can be expressed as follows:

$$< 0\,1\,0 >_\theta \| < 1\,\overline{1}\,\overline{1} >_\alpha$$
$$\{1\,0\,3\}_\theta \| \{1\,0\,1\}_\alpha$$

The Isaichev orientation relationship is close to that of Bagaryatskii making them difficult to distinguish using conventional electron diffraction. Accurate measurements on tempered martensite have repeatedly identified the Isaichev orientation relationship and this has led to the suggestion that the Bagaryatskii orientation does not exist (Zhang and Kelly, 1998b).

3.4.2 The Habit Plane of Cementite

Using single surface trace analysis, Shackleton and Kelly showed that for the tempering orientation relationship, the habit plane of cementite in lower bainitic ferrite is in the vicinity of the zone containing $\{1\,\overline{1}\,2\}_\alpha$ and $\{0\,\overline{1}\,1\}_\alpha$, corresponding to $\{1\,0\,1\}_\theta$ and $\{1\,0\,0\}_\theta$ respectively. The results are vague because of the irregular shape of the cementite particles and inaccuracies in the technique used. The long dimension of the cementite laths was found to be approximately $< 1\,\overline{1}\,\overline{1} >_\alpha$, corresponding to $< 0\,1\,0 >_\theta$. Note that for these data, the crystallographic indices have justifiably been quoted with respect to both the α and θ lattices since some of the trace analyses were carried out using diffraction information obtained simultaneously from both lattices. The results are consistent with the habit plane of cementite containing the direction of maximum coherency between the ferrite and cementite lattices, i.e. $< 0\,1\,0 >_\theta \parallel < 1\,\overline{1}\,\overline{1} >_\alpha$ (Andrews, 1963).

For some alloys, the observation of streaks in electron diffraction patterns has been interpreted to indicate a cementite habit of $\{0\,0\,1\}_\theta \| \{2\,1\,1\}_\alpha$ (Srinivasan and Wayman, 1968c). However, similar streaking has been observed for a cementite habit plane close to $\{2\,0\,1\}_\theta$. It is likely that the streaking is due to faulting on the $\{0\,0\,1\}_\theta$ planes (Ohmori, 1971a).

In upper bainite, the carbides precipitate from austenite and hence do not exhibit a consistent set of habit plane indices relative to ferrite. Relative to cementite the habit is close to $\{1\,0\,1\}_\theta$ with a long direction near $< 0\,1\,0 >_\theta$ (Shackleton and Kelly, 1965).

3.4.3 Three-Phase Crystallography

Crystallographic information can be interpreted in depth if the data are obtained *simultaneously* from austenite, ferrite and cementite. The first such

experiments were reported by Srinivasan and Wayman (1968b,c) and subsequent contradictory data were given by Bhadeshia (1980a). The two sets of data using *rational* indices as approximations to the measurements are as follows:

(Srinivasan and Wayman, 1968b,c)

$$[1\,1\,1]_\gamma \| [0\,1\,1]_\alpha \| [1\,0\,0]_\theta$$
$$[\bar{1}\,0\,1]_\gamma \| [\bar{1}\,\bar{1}\,1]_\alpha \| [0\,1\,0]_\theta$$
$$[1\,\bar{2}\,1]_\gamma \| [2\,\bar{1}\,1]_\alpha \| [0\,0\,1]_\theta$$

(Bhadeshia, 1980a)

$$[1\,1\,1]_\gamma \| [0\,1\,1]_\alpha$$
$$[0\,\bar{1}\,1]_\gamma \| [\bar{1}\,\bar{1}\,1]_\alpha$$

$$[0\,\bar{1}\,1]_\alpha \| [1\,0\,0]_\theta$$
$$[1\,\bar{1}\,\bar{1}]_\alpha \| [0\,1\,0]_\theta$$
$$[2\,1\,1]_\alpha \| [0\,0\,1]_\theta$$

For the first set of data, the habit plane of the cementite within the lower bainitic ferrite is found to be $(1\,1\,2)_\alpha$, corresponding to $(1\,0\,1)_\gamma$. Srinivasan and Wayman noted that this coincides with the presumed lattice-invariant deformation of lower bainite, implying that this somehow explains the single crystallographic variant of cementite in lower bainite, as compared with the many found when martensite is tempered. When the lattice-invariant deformation is slip, as is the case for bainite, it is incredibly difficult to establish any microstructural evidence in its support (although Ohmori, 1989, has claimed that the cementite traces in lower bainite can often be seen to be parallel to the traces of transformation twins in adjacent and approximately parallel plates of martensite). Srinivasan and Wayman interpreted the presence of the carbide on the appropriate planes to lend support to proposed mode of lattice invariant deformation in bainite. It was pointed out that the results may not be generally applicable, because they found that for a Fe–3.32Cr–0.66C wt% alloy the cementite habit plane seemed to be $\{0\,0\,1\}_\theta$ unlike the case for the richly alloyed sample.

Unfortunately, the second set of data above (Bhadeshia, 1980a) is not in agreement with the Srinivasan and Wayman hypothesis, and they noted themselves that the cementite habit plane in another Fe–Cr–C alloy containing less chromium and carbon was $(0\,0\,1)_\theta$ rather than $(0\,1\,0)_\theta$. Thus, although the lattice-invariant deformation may be linked to the nucleation of cementite under some circumstances, it does not provide a consistent explanation in

others. It also does not explain why multiple variants of carbides are observed in martensites.

3.4.4 Interphase Precipitation

An alternative view is that the cementite of lower bainite nucleates and grows at the austenite-ferrite interface, a process which is well established in the high temperature precipitation of carbides and is described as *interphase precipitation* (Honeycombe and Pickering, 1972). The carbon that is necessary to sustain the growth of cementite can be absorbed from the adjacent austenite and it is then not necessary for the ferrite to be supersaturated. It is argued that during nucleation, the cementite should adopt an orientation which provides good lattice matching with *both* α and γ. If it happens to be the case that there is only one orientation in space which allows good matching with both the adjacent phases, then the theory indicates that only one crystallographic variant of cementite should precipitate for a given variant of ferrite.

It seems intuitively reasonable that a particle at the transformation interface should attempt to lattice match simultaneously with both the adjacent phases. However, the experimental evidence quoted in support of the model (reviewed by Honeycombe, 1984) is inadequate. For example, during the interphase precipitation of $M_{23}C_6$ in chromium-rich steels, the carbide (which has a face-centred cubic lattice) adopts a cube-cube orientation with the austenite, and a Kurdjumov–Sachs orientation with the ferrite. However, $M_{23}C_6$ in austenite always precipitates in a cube–cube orientation with austenite, even in the absence of any ferrite. Suppose that the carbide precipitates in austenite, and that the austenite then transforms to ferrite, then it follows that the ferrite is likely to adopt a rational Kurdjumov–Sachs type orientation with the austenite, and *consequently* with the $M_{23}C_6$, the final three phase crystallography having nothing to do with simultaneous lattice matching between all three phases.

During interphase precipitation, the $M_{23}C_6$ could be completely oblivious of the ferrite, even though it may be in contact with the phase, but the good three phase crystallography would nevertheless follow simply because the $M_{23}C_6$ has a cube–cube orientation with the austenite. To test unambiguously, the theory requires a system where the particles which form at the interphase interface are able to adopt many different variants of an orientation relation with the austenite. It is suggested that interphase precipitation of Mo_2C is an example suitable for further work.

Given a Bagaryatskii orientation relationship between lower bainitic ferrite and its internal cementite particles, and a Kurdjumov–Sachs orientation relationship between the ferrite and austenite, it can be shown (Bhadeshia, 1980a) that the three phase crystallography expected on the basis of the lattice matching arguments is:

$$[1\,0\,0]_\theta \| [0\,\overline{1}\,1]_\alpha \| [1\,1\,1]_\gamma$$
$$[0\,1\,0]_\theta \| [1\,\overline{1}\,\overline{1}]_\alpha \| [\overline{1}\,0\,1]_\gamma$$

The experimental data for lower bainite are inconsistent with these orientation relations, the cementite failing to lattice match with the austenite. This conclusion remains if the α/γ orientation relationship is of the Nishiyama-Wasserman type.

There is another way of verifying this conclusion. Aaronson *et al*. (1978) have modelled the growth of cementite which nucleates at the α/γ interface. In this model, the penetration of the cementite into the adjacent ferrite or austenite is determined by the rate at which either of these phases transform into cementite. The growth of the cementite is treated in terms of a one-dimensional diffusion-controlled growth process. With the Zener approximation of a linear concentration gradient in the parent phase, the penetration of cementite in ferrite (G_α) and in austenite (G_γ) are given by:

$$G_\alpha \simeq \frac{1}{2}\left(\frac{D_\alpha}{t}\right)^{\frac{1}{2}} \frac{(\overline{c}^\alpha - c^{\alpha\theta})}{[2(c^{\theta\alpha} - c^{\alpha\theta})(c^{\theta\alpha} - \overline{c})]^{\frac{1}{2}}} \tag{3.6}$$

$$G_\gamma \simeq \frac{1}{2}\left(\frac{D_\gamma}{t}\right)^{\frac{1}{2}} \frac{(\overline{c}^\gamma - c^{\gamma\theta})}{[2(c^{\theta\gamma} - c^{\gamma\theta})(c^{\theta\gamma} - \overline{c})]^{\frac{1}{2}}} \tag{3.7}$$

where D_α is the diffusivity of carbon in ferrite, $\overline{c}$ is the average carbon concentration in the parent phase (α or γ), $c^{\gamma\theta}$ represents the concentration of carbon in the austenite which is in equilibrium with cementite and t represents the time after the nucleation event. If it is assumed that $c^{\theta\alpha}$ or $c^{\theta\gamma}$ are much greater than $\overline{c}$, $c^{\alpha\theta}$ or $c^{\gamma\theta}$, the ratio of growth rates is given by:

$$\frac{G^\alpha}{G^\gamma} = \frac{D_\alpha^{\frac{1}{2}}(\overline{c}^\alpha - c^{\alpha\theta})}{D_\gamma^{\frac{1}{2}}(\overline{c}^\gamma - c^{\gamma\theta})} \tag{3.8}$$

Note that the left hand side of this equation could be replaced by the corresponding ratio of particle dimensions in the two parent phases. Aaronson *et al*., made the further assumption that the carbon concentrations of the austenite and ferrite before the onset of cementite formation are given by $c^{\gamma\alpha}$ and $c^{\alpha\gamma}$ respectively. This in turn implies a number of further assumptions which are not consistent with experimental data: that carbide formation does not begin until the formation of all bainitic ferrite is complete, that there is no supersaturation of carbon in the bainitic ferrite and that the bainite transformation does not obey the incomplete-reaction phenomenon.

On the basis of these assumptions, the cementite in bainite essentially grows by drawing on the richer reservoir of carbon in the austenite, and should

therefore penetrate to a far greater extent into the austenite than into the ferrite. Contrary to this conclusion, direct observations prove that in the rare cases where a cementite particle in lower bainite happens to be in contact with the transformation interface, the cementite is confined to the ferrite (Bhadeshia, 1980a).

Aaronson *et al*. also concluded that since the model predicts that the interphase growth of cementite occurs into both bainitic ferrite and austenite, the debate about whether the carbides nucleate in α or γ is irrelevant. This is not justified because it assumes that the carbides nucleate at the interphase interface, whereas it is more likely that the carbides which precipitate within the lower bainitic ferrite nucleate and grow from the supersaturated bainitic ferrite.

3.4.5 Relief of Strain Energy

The evidence suggests that the occurrence of a single crystallographic variant of carbide in lower bainite cannot be explained in terms of either the interphase precipitation model or the lattice-invariant shear arguments. A possible alternative explanation is that the variant which forms is one that is best suited towards the relief of elastic strains associated with the austenite to lower bainite transformation (Bhadeshia, 1980a). The observation that carbide precipitation modifies the surface relief of lower bainite supports this conclusion, particularly since freshly formed plates, apparently without carbide precipitation, exhibit perfect invariant-plane strain relief (Clark and Wayman, 1970).

If this explanation is accepted, then it begs the question as to why multiple variants of carbides occur during the tempering of martensite. However, an examination of a large number of published micrographs in the literature indicates that even in tempered martensite, there is usually one dominant variant and in many cases, just one variant of carbide present. Examples can be found in standard textbooks such as that by Honeycombe (Fig. 8.3, 1981), or in research articles (Speich, Fig. 3, 1987).

3.4.6 Epsilon-Carbide

The orientation relationship between ϵ-carbide in tempered martensite was deduced by Jack (1950, 1951) as:

$$(1\,0\,1)_\alpha \| (1\,0\,\bar{1}\,1)_\epsilon$$
$$(2\,\bar{1}\,1)_\alpha \| (1\,0\,\bar{1}\,0)_\epsilon$$
$$(0\,1\,1)_\alpha \| (0\,0\,0\,1)_\epsilon$$
$$(\bar{1}\,\bar{1}\,1)_\alpha \| (1\,\bar{2}\,1\,0)_\epsilon$$

which also implies that:

$$(1\,0\,1)_\alpha \simeq 1.37^\circ \text{ from } (1\,0\,\bar{1}\,1)_\epsilon$$
$$[1\,0\,0]_\alpha \simeq 5^\circ \text{ from } [1\,1\,\bar{2}\,0]_\epsilon$$

The very same orientation relationship is also found for ϵ-carbide in lower bainite (Huang and Thomas, 1977). The carbide is in the form of plates which are approximately 6–20 nm thick and 70–400 nm long and possess a ragged interface with the matrix. Single-surface trace analysis suggests that on average the particles grow along $< 1\,0\,0 >_\alpha$ directions on $\{0\,0\,1\}_\alpha$ habit planes (Lai, 1975).

It has been suggested by Huang and Thomas that ϵ-carbides precipitates at the austenite/bainite interface, because its orientation with the ferrite can be generated by assuming a Kurdjumov–Sachs α/γ orientation, and an ϵ/γ relationship in which

$$\begin{aligned}(1\,1\,1)_\gamma &\| (0\,0\,0\,1)_\epsilon \\ (1\,\bar{1}\,0)_\gamma &\| (1\,\bar{2}\,1\,0)_\epsilon\end{aligned} \tag{3.9}$$

However, the three phase crystallography is not unique and hence does not explain the observed single variant of carbide in lower bainite.

During the prolonged ageing of bainite, Sandvik (1982a) found that small regions of austenite retained within bainite sheaves transform into ϵ carbide, with the three-phase crystallography described by Huang and Thomas. The observed ϵ-carbide habit plane, $(1\,0\,1)_\alpha \| (0\,0\,0\,1)_\epsilon$ is different from that claimed by Lai.

The orientation relationship expected between ϵ-carbide and austenite has until recently been a matter of speculation. The carbide has now been found to precipitate directly in austenite in high-carbon cast iron with the orientation relationship stated in equation 3.9 (Gutierrez *et al*., 1995). The precipitates are in the form of fine, coherent particles homogeneously distributed throughout the austenite and form in at least three variants of the orientation relationship (Fig. 3.6). When the austenite transforms to martensite, only two of these variants adopt the Jack orientation relationship with the martensite.

3.4.7 Eta-Carbide

η-carbide is a transition Fe_2C carbide in the orthorhombic crystal system. It is usually associated with the tempering of martensite (Hirotsu and Nagakura, 1972; Nagakura *et al*., 1983) where the martensite/carbide orientation relationship is found to be as follows:

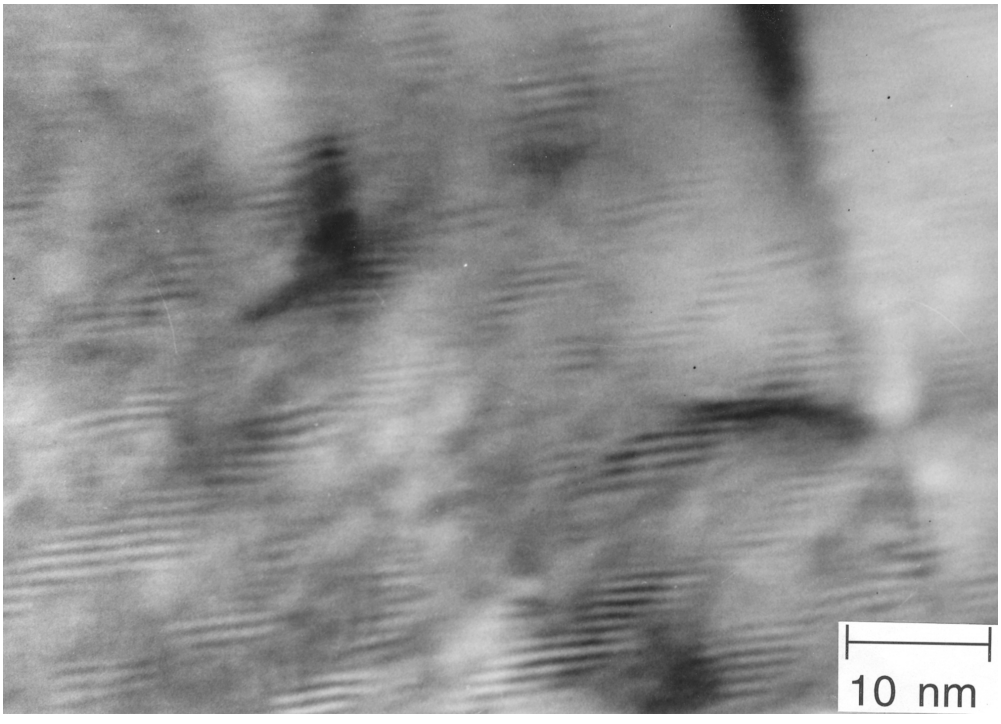

Fig. 3.6 The homogeneous precipitation of ϵ-carbide in austenite (Gutierrez *et al.*, 1995).

$$(1\,1\,0)_\eta \| \{0\,1\,0\}_\alpha$$
$$[0\,0\,1]_\eta \| < 1\,0\,0 >_\alpha$$

The carbide has been observed in lower bainite in grey cast iron, where electron diffraction confirms that (Franetovic *et al.*, 1987a,b):

$$[0\,0\,1]_\eta \| < 1\,0\,0 >_\alpha \| < 0\,\bar{1}\,1 >_\gamma$$

This information is consistent with the η-carbide/martensite orientation relationship stated earlier and lends further support to the hypothesis that the carbides within lower bainitic ferrite precipitate in a manner analogous to the tempering of martensite.

3.4.8 Chi-Carbide

χ-Carbide is another transition carbide which is metastable with respect to cementite. It is found during the tempering of martensite, where high-resolution electron microscopy has demonstrated that what at first sight appears to be faulted cementite in fact consists of interpenetrating layers of

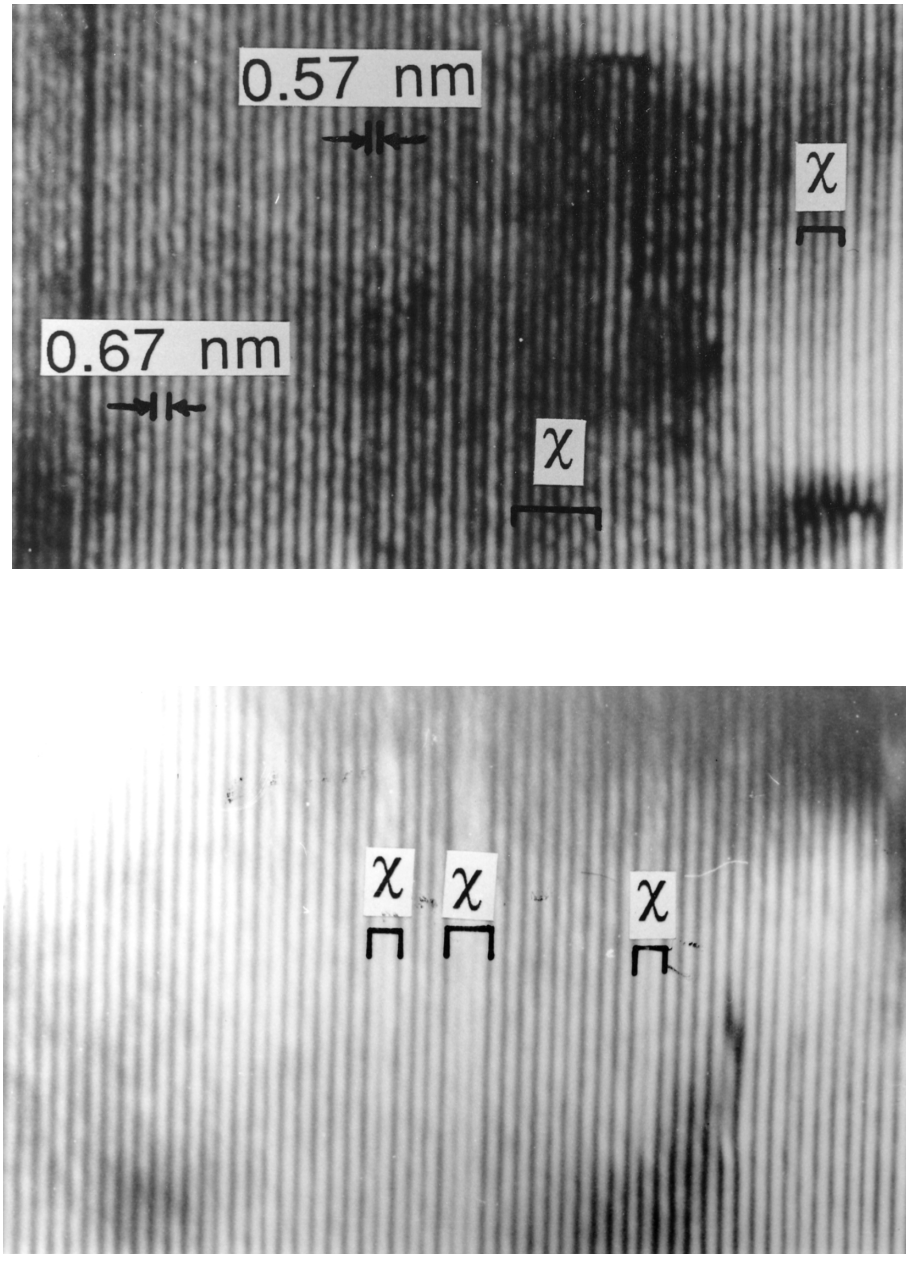

Fig. 3.7 Lattice resolution transmission electron micrographs showing the intergrowth of layers of cementite and χ-carbide (Ohmori, 1986). (a) Carbide particle which precipitated in lower bainitic ferrite; (b) carbide particle formed during the tempering of martensite.

cementite and χ, described as *microsyntactic intergrowth* (Nagakura *et al*., 1981; Nakamura *et al*., 1985). The $\{2\,0\,0\}_\chi$ planes are found to be parallel to the $\{0\,0\,1\}_\theta$ planes of different spacing (0.57 and 0.67 nm respectively). Thus, the faults in the cementite really correspond to regions of χ, each a few interplanar spacings thick, and this intimate mixture of cementite and χ consequently has a nonstoichiometric overall composition expressed by $Fe_{2n+1}C_n$, where $n \geq 3$.

Similar observations have been reported by Ohmori (1986), but for cementite in both tempered martensite and lower bainite, in a Fe–0.7C wt% steel (Fig. 3.7). In both cases, high-resolution electron microscopy (HREM) revealed that the cementite particles contained regions of χ-carbide, lending yet more support to the analogy between tempered martensite and lower bainite. This is consistent with Ohmori's observation that cementite in bainitic ferrite increases in size during transformation, as if growing from carbon supersaturated ferrite.

Ohmori (1986) has also claimed that the mechanism of precipitation in the lower bainite was different from that in tempered martensite, on the grounds that the cementite in the lower bainite contained a smaller amount of χ-carbide. A difficulty with this conclusion is that the amount of material examined in an HREM experiment is so small that it is unlikely to be representative. The heat-treatments utilised in producing lower bainite and martensite are also different making valid comparisons difficult.

Direct observations on martensite tempering, by Nakamura *et al*. (1985), indicate that the mechanism by which the mixed χ/cementite particles are replaced by cementite can be complicated and site dependent. One of the cementite layers in the mixed particle tends to grow into the surrounding matrix, at the expense of the mixed particle which dissolves. This dissolution is found to occur more rapidly for mixed particles which happen to be located at grain boundaries, presumably because such boundaries provide easy diffusion paths.

It is interesting that the mechanism involves the dissolution of both the cementite and χ in the mixed particles. This might be expected if it is assumed that the original particle forms by displacive transformation; the accompanying strain energy could then provide the driving force for its replacement by more globular cementite particles forming by reconstructive growth. Also, the boundaries between the χ and cementite layers are coherent and would not be expected to be very mobile, in which case, the cementite layers would be kinetically hindered from growing into the adjacent χ layers.

3.5 Chemical Composition of Bainitic Carbides

It has long been established, using magnetic, chemical and X-ray methods on extracted carbides, that the cementite associated with upper bainite has a substitutional solute content which is close to, or slightly higher than that of

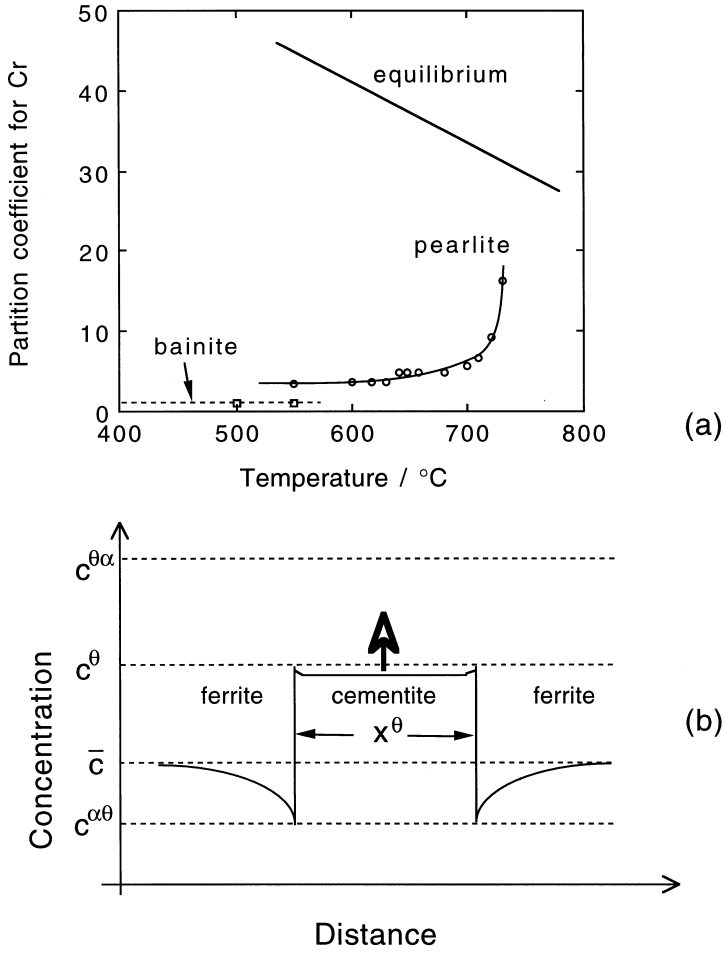

Fig. 3.8 (a) The partition coefficient for chromium in cementite, when the cementite is a part of bainite or pearlite, together with equilibrium data (Chance and Ridley, 1981). The partition coefficient is the ratio of the concentration in cementite to that in the ferrite. (b) The concentration profile that develops during the enrichment of a cementite particle.

the steel as a whole. This is not expected from considerations of chemical equilibrium (see for example, Hultgren, 1947, 1953).

Tsivinsky *et al*. (1959) reported that chromium and tungsten partitioned from austenite into cementite during the growth of pearlite, but not during that of bainite. Chance and Ridley (1981) found that for upper bainite in a Fe–0.81C–1.41Cr wt% alloy, the partition coefficient k_{Cr}, defined as (wt% Cr in θ)/(wt% Cr in α) could not be distinguished from unity (Fig. 3.8). Chance and Ridley

suggested that partitioning occurs during the pearlite reaction but at the same temperature does not occur with bainite because there is a fast diffusion path along the incoherent interface for pearlite.

These and other results provide compelling evidence that the carbides which form during the bainite reaction or indeed during the tempering of martensite grow by a displacive mechanism. Such a mechanism must naturally involve the diffusion of carbon, but not of substitutional solutes or iron atoms. It is particularly interesting that the precipitation of cementite from martensite or lower bainite can occur under conditions where the diffusion rates of iron and substitutional atoms are incredibly small compared with the rate of precipitation (Fig. 2.12). The long-range diffusion of carbon atoms is of course necessary, but because of its interstitial character, substantial diffusion of carbon remains possible even at temperatures as low as $-60\,^{\circ}\mathrm{C}$. The Fe:X ratio thus remains constant everywhere and subject to that constraint, the carbon achieves equality of chemical potential; the cementite is then said to grow by *paraequilibrium* transformation.

High-resolution evidence supporting the idea that the carbide particles grow by paraequilibrium displacive transformation has been published by Sandvik (1982b), Nakamura and Nagakura (1986) and Taylor *et al*. (1989a,b). In recent work it has been confirmed that the initial composition of the cementite precipitated during the tempering of martensite is not affected by the heterogeneous nucleation site, whether that is at plate boundaries or within the plates themselves (Thomson and Miller, 1995; Ghosh *et al*., 1999).

In a remarkable experiment, Babu *et al*. (1993) have shown using the atom-probe technique that the cementite obtained by tempering martensite is forced to inherit the silicon concentration of the martensite. They did not find any redistribution of substitutional solutes even on the finest conceivable scale; the atom-probe technique has single atom resolution for both chemical and spatial analysis (Fig. 3.9). The results rule out the possibility of local equilibrium at the interface and conclusively establish the paraequilibrium mode of cementite precipitation. The fact that silicon is trapped by cementite is important given that its equilibrium solubility in cementite is virtually zero. It follows from this that the trapped species such as Si must partition with prolonged heat treatment and this is precisely what is observed experimentally (Babu *et al*.).

To summarise, substitutional solute atoms are trapped in the cementite when the latter precipitates in bainite or martensite. That is, the cementite forms by a paraequilibrium transformation mechanism. In silicon-containing steels the free energy change associated with the paraequilibrium precipitation of cementite must be much smaller than when the cementite is free of silicon. It is probable that this is what leads to suppression of cementite in high-silicon bainitic or martensitic steels.

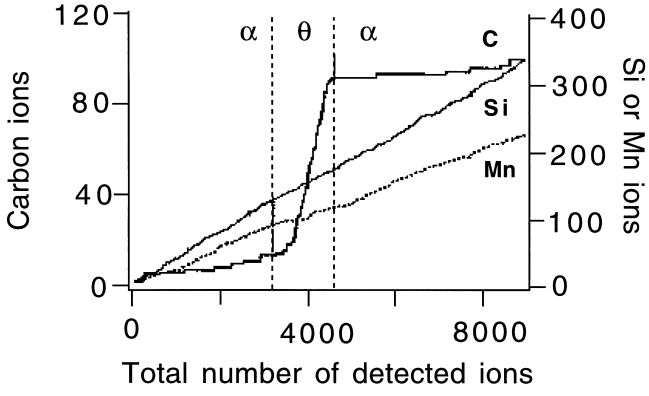

Fig. 3.9 The results of an atomic resolution chemical analysis experiment across a pair of ferrite/cementite (α/θ) interfaces. Any changes in composition are represented by a change in the slope. It is evident that there is no partitioning of silicon or manganese when cementite precipitates from martensite. The alloy used has the chemical composition Fe–1.84C–3.84Si–2.95Mn at%, and was tempered at 350 °C for 30 min (Babu *et al.*, 1993).

The response of carbides to a stress applied during the precipitation process can reveal further information about their mechanism of formation; this will be discussed in Chapter 8.

3.6 Summary

The growth of upper bainite leads to the partitioning of carbon into the residual austenite. If the transformation conditions render the austenite thermodynamically unstable with respect to carbide precipitation, then it eventually decomposes by the precipitation of cementite and more ferrite. In some alloys, cementite formation is preceded by that of transition iron-carbides such as κ or χ. In lower bainite, some of the carbon precipitates from supersaturated ferrite and the rest is partitioned into the remaining austenite. The quantity of carbides that precipitate from the austenite is therefore smaller when compared with upper bainite. Every carbide precipitation reaction that is found in tempered martensite has also been observed in lower bainite with exactly identical crystallographic and morphological characteristics. One difference is that the carbide particles in any given lower bainitic plate tend to precipitate in a single crystallographic orientation whereas the tempering of martensite usually leads to many crystallographic variants. This is because the self-stress of a lower bainite plate favours precipitation of a particular carbide variant, and this

effect is prominent in bainite where the driving force for carbide precipitation is smaller than that associated with the tempering of martensite.

The carbide precipitation reactions for both upper and lower bainite are secondary events which occur after the growth of bainitic ferrite. In some alloys, especially those containing large concentrations of silicon or aluminium, the carbide precipitation reaction can be so sluggish that for practical purposes, the bainite consists of a mixture of only bainitic ferrite and carbon-enriched residual austenite.

The mobility of atoms over the range of temperatures within which bainite grows is extraordinarily small. This and other observations suggest that the carbides grow by a displacive mechanism in which only the interstitial elements diffuse. This is consistent with the fact that there is no change in substitutional solute content when bainitic carbides precipitate, and with the crystallography of carbide precipitation.

4 *Tempering of Bainite*

4.1 Introduction

Tempering is a term historically associated with the heat treatment of martensite in steels. It describes how the microstructure and mechanical properties change as the metastable sample is held isothermally at a temperature where austenite cannot form. The changes during the tempering of martensite can be categorised into stages. During the first stage, excess carbon in solid solution segregates to defects or forms clusters within the solid solution. It then precipitates, either as cementite in low-carbon steels, or as transition iron-carbides in high-carbon alloys. The carbon concentration that remains in solid solution may be quite large if the precipitate is a transition carbide. Further annealing leads to stage 2, in which almost all of the excess carbon is precipitated, and the carbides all convert into more stable cementite. Any retained austenite may decompose during this stage. Continued tempering then leads to the spheroidisation of carbides, extensive recovery of the dislocation structure, and finally to the recrystallisation of the ferrite plates into equiaxed grains.

The description presented above is idealised. Many of the reactions ascribed to stage 1 can occur *during* the formation of the martensite when the martensite-start temperature is high, a phenomenon known as *autotempering*. Bainite forms at even higher temperatures so autotempering becomes an unavoidable part of the transformation. The redistribution of carbon from supersaturated ferrite into the residual austenite, and the precipitation of carbides during the bainite reaction, occur rapidly and are genuine autotempering effects (Fig. 4.1). The purpose of this Chapter is to deal primarily with the tempering effects which occur when a bainitic microstructure is reheated; the *in situ* tempering phenomena are described elsewhere in the text.

The rate of change of the microstructure and properties during tempering is expected to scale with the degree to which the virgin sample deviates from equilibrium. Bearing this in mind, there are a number of essential differences between the tempering behaviour of bainite and that of martensite.

Bainitic ferrite contains little carbon in solid solution since much of it is precipitated as cementite particles which are coarse when compared with tempered martensitic microstructures. Secondary hardening reactions in alloy

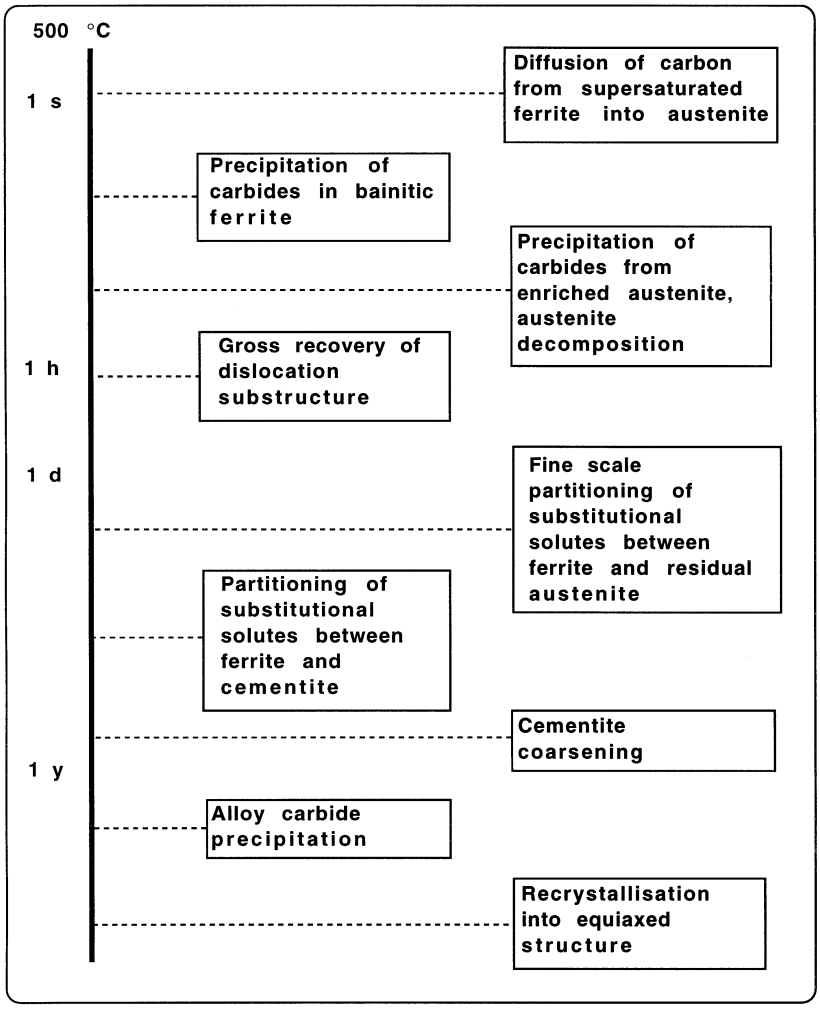

Fig. 4.1 The time scales associated with a variety of tempering phenomena for bainite.

steels with a bainitic microstructure are slower than with martensite, because the coarser cementite particles take longer to dissolve (Woodhead and Quarell, 1965). Secondary hardening involves the replacement of metastable cementite with substitutional-solute-rich alloy carbides.

When compared with martensite, bainite grows at relatively high temperatures where the microstructure undergoes recovery during transformation. The extent of this recovery is larger than would be associated with autotempered martensite. Consequently, when low-carbon steel bainitic microstructures are

annealed at temperatures as high as 700 °C (1 h), there is only a slight increase in recovery, and little change in the morphology of the ferrite platelets or the number density of the carbide particles (Irvine *et al*., 1957; Bush and Kelly, 1971).

Rapid softening occurs only when the plates of ferrite change into equiaxed ferrite. Whether this change is due simply to grain growth or to recrystallisation has not been investigated. In the former case it is the excess surface energy which constitutes the driving force, whereas during recrystallisation, it is the stored energy due to defects such as dislocations or due to elastic strains in the lattice which provides the major component of the driving force for the reaction. During the change to a more equiaxed microstructure, the cementite spherodises and coarsens considerably. Continued tempering then causes much smaller changes in hardness with time.

In marked contrast with martensitic steels, small variations in the carbon concentration (0.06–0.14 wt%) have little effect on the bainite tempering curve (Fig. 4.2). Carbon has a potent solid solution strengthening effect. Thus, the strength of martensite drops sharply as the carbon precipitates during tempering. For bainitic microstructures, the carbon is not in solid solution but is

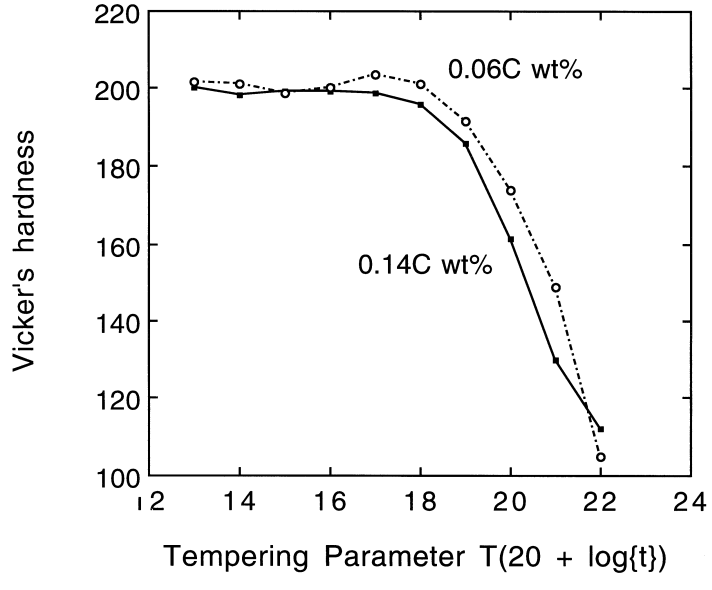

Fig. 4.2 Change in hardness for two bainitic steels containing different carbon concentrations, as a function of a time–temperature tempering parameter (after Irvine and Pickering, 1957). The tempering parameter is defined with the absolute temperature T and the time t in hours.

precipitated as coarse carbides which contribute little to strength (Irvine and Pickering, 1957; Irvine *et al*., 1957). It is expected therefore that the tempering response of bainite is insensitive to the average carbon concentration.

4.2 Tempering Kinetics

It is astonishing that there is as yet no quantitative model for the kinetics of tempering, certainly not of the kind that could be used in the design of alloys or heat-treatments. Figure 4.2 illustrates an empirical method of expressing tempering data using a time–temperature parameter, useful because it permits interpolation between experimental data and a method of estimating the effect of anisothermal heat treatments which are common in industrial practice.

The method has its origins in some pioneering work by Holloman and Jaffe (1945), who proposed that the effectiveness of an isothermal heat treatment should be related to the product:

$$t \exp\{-Q/RT\} \tag{4.1}$$

where Q is an effective activation energy and the other terms have their usual meanings. The product is the integral of the curve of $\exp\{-Q/RT\}$ versus time. To estimate the period required to achieve the same metallurgical effect at another temperature simply involves the assumption that the product $t \exp\{-Q/RT\}$, once evaluated, is constant irrespective of temperature. The product is often called the *kinetic strength* of the heat treatment and provides a rough method for combining the influence of time and temperature. The concept is difficult to justify, especially in circumstances where the driving force varies with temperature or where the mechanism of the metallurgical process alters with temperature. The parameter and many related parameters have nevertheless been useful in cases where rigorous solutions do not exist. Examples include the representation of creep data, weld microstructure calculations (Alberry *et al*., 1977, 1979, 1983; Ashby *et al*., 1982, 1984, 1987), and the rationalisation of martensite tempering data (Hollomon and Jaffe, 1945). Irvine and Pickering have demonstrated its usefulness in representing the hardness of tempered bainite.

4.3 Tempering of Steels Containing Austenite

The decomposition of retained austenite during the heat treatment of martensite in quenched steels occurs during the second stage of the tempering process. Appreciable quantities of retained austenite are usually only present in quenched steels which have carbon concentrations in excess of about 0.4 wt%. The conventional wisdom is that the austenite decomposes to bainite but it has

[12:16 3/9/01 C:/3B2 Templates/keith/3750 BAINITE.605/3750-004.3d] Ref: 0000 Auth: Title: Chapter 00 Page: 94 91-116

been demonstrated that the decomposition occurs by instead a reconstructive mechanism (Kennon and Burgess, 1978).

In many bainitic steels, the alloy composition is chosen to avoid the retention of austenite. However, large quantities of austenite can be retained in silicon-rich bainitic steels, in two forms: as thin films between the ferrite plates and as blocks between different sheaves of bainite. Both are enriched in carbon but the films more so because of their isolation between plates of ferrite.

4.3.1 Redistribution of Substitutional Solutes

There is no partitioning of substitutional solutes during the bainite reaction, in spite of the requirements of equilibrium. Given the opportunity, they should tend to redistribute in a manner which leads to a reduction in the overall free

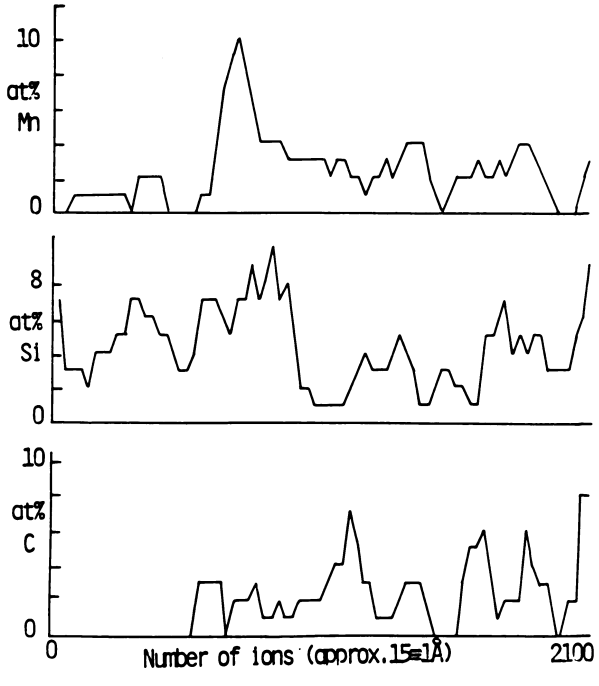

Fig. 4.3 A field ion microscope/atom-probe experiment on an alloy Fe–0.43C–2.24Si–2.82Mn wt%, heat treated at 328 °C for 11 days. This produces a mixture of bainitic ferrite and austenite with the reaction stopping after the first few minutes at temperature, the subsequent holding simply leading to an annealing of the microstructure. The diagram illustrates the composition profile obtained across the austenite/bainitic ferrite interface, which is identified by the point where significant levels of carbon begin to be detected. (Stark *et al*., 1990).

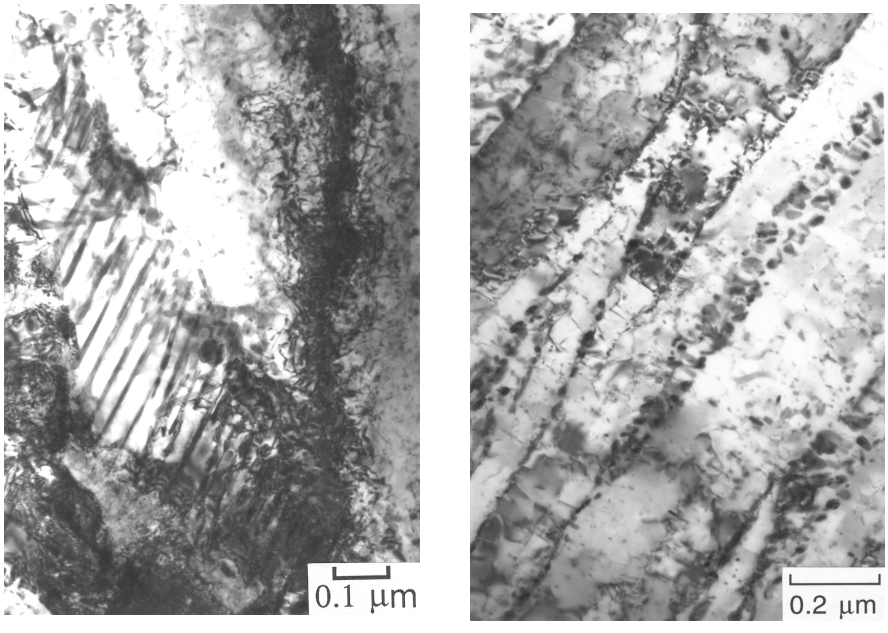

Fig. 4.4 Transmission electron micrographs illustrating the effect of tempering a mixture of bainitic ferrite and retained austenite, in a Fe–3Mn–2Si–0.4C wt% alloy, at 500 °C for 60 min. The austenite is supersaturated with respect to carbides. (a) The larger blocks of austenite tend to decompose into pearlite. (b) Arrays of discrete carbide particles form between the sub-units of bainitic ferrite when the films of austenite decompose. The microstructure prior to tempering consisted of just bainitic ferrite and residual carbon-enriched austenite.

energy. It is found that when a mixture of bainitic ferrite and austenite is tempered at low temperatures, the solutes partition before the austenite begins to decompose. The partitioning is on a fine scale and can only be detected using atomic resolution techniques. Figure 4.3 illustrates one such experiment, in which a mixture of bainitic ferrite and austenite was annealed at 328 °C for 11 days. There is clear evidence for the diffusion of manganese into the austenite at the interface, with a corresponding depletion zone in the adjacent ferrite.

4.3.2 Decomposition of Austenite

When the carbon concentration in all the regions of untransformed austenite is larger than or equal to that given by the T_0' curve, tempering can only induce further transformation by a mechanism involving the diffusion of carbon. The austenite may decompose into a mixture of ferrite and carbides if its carbon

concentration exceeds that given by the extrapolated $\gamma/(\gamma +$ carbide) phase boundary (Fig. 3.1b). The larger regions of austenite form colonies of pearlite with a fine interlamellar spacing, whereas the films of austenite decompose into discrete particles of cementite in a matrix of ferrite (Figure 4.4). The films are too thin to permit the onset of the cooperative growth needed to establish a pearlite colony. The T_c (Fig. 3.1b) condition for carbide formation may not be satisfied when tempering at high temperatures, in which case the austenite can transform to ferrite although, not by a bainitic mechanism.

Tempering need not involve a separate heat-treatment. Microstructural changes can occur when austenite is transformed isothermally to bainite, and then held at the transformation temperature for longer than is necessary to complete the bainite reaction. For example, any residual austenite may decompose slowly as the microstructure attempts to approach equilibrium. There is less bainite and more residual austenite at higher transformation temperatures; this combined with the greater atomic mobility at high temperatures leads to the formation of pearlite colonies following the bainite reaction. Bhadeshia and Edmonds (1979a) reported a case where transformation at a temperature close to B_S led to the formation of upper bainite within a matter of minutes, to be followed some 30 h later by pearlite. Figure 4.5 illustrates, in

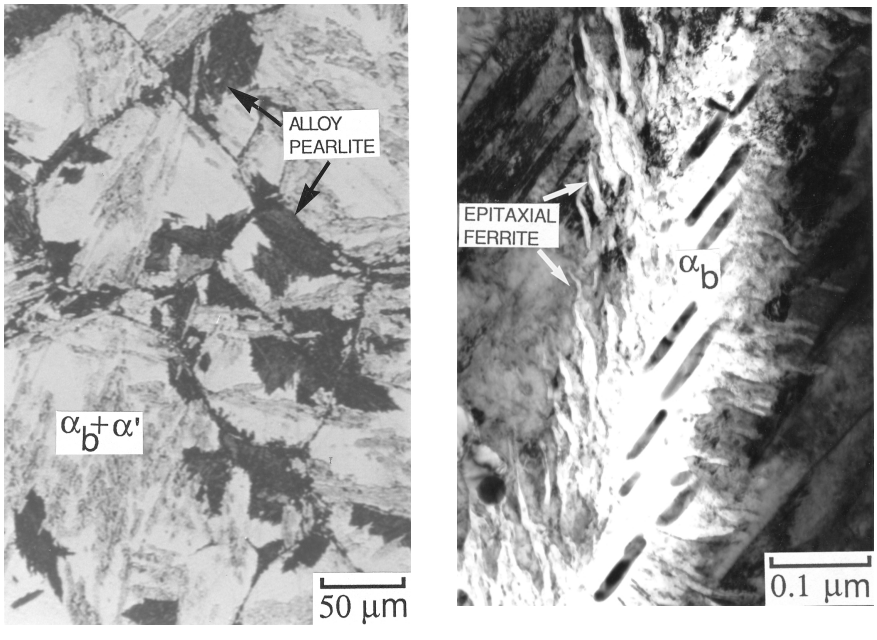

Fig. 4.5 The decomposition of residual austenite once the bainite reaction has stopped. (a) Pearlite colonies; (b) ferrite growing epitaxially from bainite plates.

another alloy, two different reconstructive reactions occurring after the bainite stopped following 30 min at temperature. Continued holding at the isothermal transformation temperature for 43 days led to the decomposition of residual austenite at an incredibly slow rate into two different products (Bhadeshia, 1981b, 1982b). The first of these is alloy pearlite which nucleates at the austenite grain boundaries and develops as a separate transformation. In the other, the original bainite/austenite interfaces move to produce epitaxial growth by a reconstructive mechanism (Fig. 4.5). The interfaces degenerate into a series of irregular perturbations. The ferrite in the perturbations has the same crystallographic orientation as the original bainite – it is in fact contiguous with the bainitic ferrite. It grows with the same substitutional solute content as the parent austenite but does not cause an IPS shape change. It is incredible that the perturbations took 43 days to grow to a length comparable to the thickness of the original bainite plates, which completed transformation in a matter of seconds. Reconstructive growth is bound to be much slower than displacive transformation at low homologous temperatures.

4.4 Coarsening of Cementite

Coarsening leads to a minimisation of the energy that is stored in a sample in the form of interfaces. The rate equation for a coarsening process controlled by the diffusion of solute through the matrix is given by (Greenwood, 1956; Lifshitz and Slyozov, 1961; Wagner, 1961):

$$\overline{r}^3 - \overline{r}_o^3 = (8\sigma^{\theta\alpha} c^{\alpha\theta} D_{eff} V_m^{\theta} t)/9RT \tag{4.2}$$

where V_m^{θ} is the molar volume of cementite, $c^{\alpha\theta}$ is the concentration of carbon in ferrite which is in equilibrium with cementite, $\overline{r}_3$ is the mean particle radius at time t and $\overline{r}_o^3$ is the mean particle radius at time zero, the moment when coarsening is defined to begin. $\sigma^{\theta\alpha}$ is the cementite–ferrite interface energy per unit area ($\simeq 690\,\mathrm{J\,m^2}$, Li *et al*., 1966) and D_{eff} is an effective diffusion coefficient for carbon in ferrite. Since there is little change in precipitate volume fraction during coarsening, the diffusion of carbon is coupled to that of iron in such a way that the total volume remains constant. D_{eff} is then given by (Li *et al*., 1966):

$$D_{eff} = \frac{n_{Fe} D_{Fe}^{\alpha} D_C^{\alpha} \Omega_{Fe} [\Omega_{Fe} + (n_C/n_{Fe})\Omega_C]}{(n_{Fe} D_{Fe}^{\alpha} \Omega_{Fe}^2) + (n_C D_C^{\alpha} \Omega_C^2)} \tag{4.3}$$

where n_{Fe} and n_C are the numbers of iron or carbon atoms per unit volume of ferrite respectively, D_{Fe}^{α} and D_C^{α} are the respective diffusivities of iron and carbon in ferrite, Ω_{Fe} is the volume per atom of ferrite and Ω_C is the volume of a molecule of Fe_3C less $3\Omega_{Fe}$. It has been shown that equation 4.3 describes to a fair accuracy, the coarsening kinetics of cementite during the tempering of

both upper and lower bainite in a Fe–0.67C–0.73Mn–0.27Si wt% commercial steel (Deep and Williams, 1975). The agreement with theory is best for the higher tempering temperatures, with an underestimation of the coarsening rate at lower temperatures. This discrepancy has been attributed to grain boundary diffusion contributing more to the net flux at low temperatures.

In fact, the microstructures of both tempered martensite and bainite contain two kinds of cementite particles, those located at the lath boundaries and a finer distribution within the laths. In upper bainite the cementite is located only at the lath boundaries. Figure 4.6 shows experimental data on the coarsening of cementite during the tempering of a medium carbon steel. The upper bound of each shaded region represents the lath-boundary cementite, the lower bound the intra-lath cementite. The bainitic microstructure is coarse to begin with because of the tempering inherent in the formation of bainite. With martensite the tempering induces the precipitation of cementite, with considerable intra–lath cementite and a larger overall number density of particles. Therefore, the coarsening rate is much larger for martensite; the bainitic microstructure shows greater stability to tempering. A consequence is that the matrix microstructure remains fine over a longer time period for bainite than for martensite.

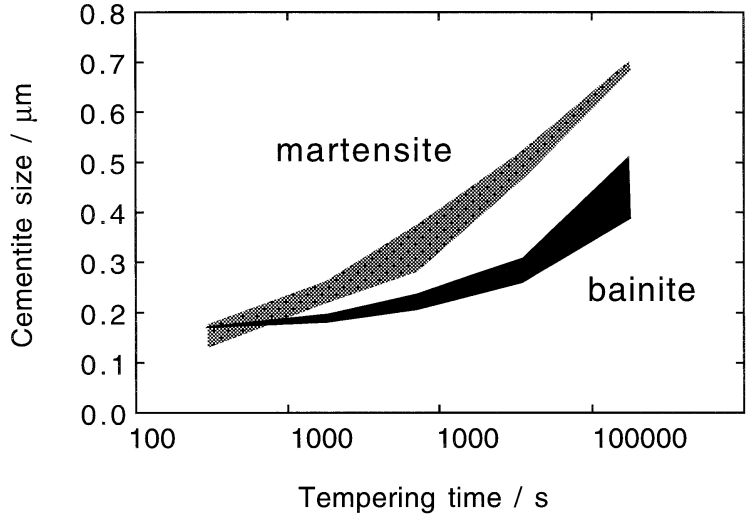

Fig. 4.6 Changes in the size of cementite particles as a function of the tempering time at 700 °C, with different starting microstructures. The upper bound of each shaded region represents the mean size of particles located at lath boundaries. The lower bound corresponds to particles within the laths. The data are for a Fe–0.45C–0.22Si–0.62Mn wt% steel; the bainite was produced by isothermal transformation at 380 °C. After Nam (1999).

A model which deals with the coarsening of cementite under conditions where both grain boundary and lattice diffusion are important has been presented by Venugopalan and Kirkaldy (1977). It takes account of the simultaneous coarsening of carbide particles and ferrite grains, allows for the multicomponent nature of alloys steels and works remarkably well in predicting the mean particle size, ferrite grain size and strength of tempered martensite; it has yet to be applied to bainite.

Elementary coarsening theory suggests that the time-independent particle size distribution, normalised relative to the mean particle radius, should be skewed towards large particles, with a sharp cut off at a normalised radius of 1.5. However, measured distributions for cementite in bainite do not fit this behaviour, the distributions instead being skewed towards smaller particle sizes. Deep and Williams point out that this behaviour is also found for cementite in tempered martensite.

4.5 Secondary Hardening and the Precipitation of Alloy Carbides

Secondary hardening is usually identified with the tempering of martensite in steels containing strong carbide forming elements like Cr, V, Mo and Nb. The formation of these alloy carbides necessitates the long-range diffusion of substitutional atoms and their precipitation is consequently sluggish. Carbides like cementite therefore have a kinetic advantage even though they may be metastable. Tempering at first causes a decrease in hardness as cementite precipitates at the expense of carbon in solid solution, but the hardness begins to increase again as the alloy carbides form. Hence the term *secondary hardening*. Coarsening eventually causes a decrease in hardness at long tempering times so that the net hardness versus time curve shows a secondary hardening peak.

There is no reason to suspect that the secondary hardening of bainite should be particularly different from that of martensite. Early work did not reveal any pronounced peaks in the tempering curves for bainite, perhaps because of the low molybdenum concentration in the steels used (Irvine *et al*., 1957). The peaks were subsequently found during the tempering of a vanadium containing bainitic steel but not for Cr or Mo containing bainitic steels (Fig. 4.7, Irvine and Pickering, 1957). An unexplained observation was that for the Mo containing steels, the carbide formed on tempering bainite is initially cementite, which then transforms to $(Fe, Mo)_{23}C_6$, whereas on tempering martensite in the same steels the ultimate carbides are found to be Mo_2C

Later work revealed clear evidence of secondary hardening in low carbon bainitic steels containing up to 2.95 wt% Mo, 2.12 wt% Cr and also in vanadium containing bainitic steels (Baker and Nutting, 1959; Irvine and Pickering,

[12:16 3/9/01 C:/3B2 Templates/keith/3750 BAINITE.605/3750-004.3d] Ref: 0000 Auth: Title: Chapter 00 Page: 100 91-116

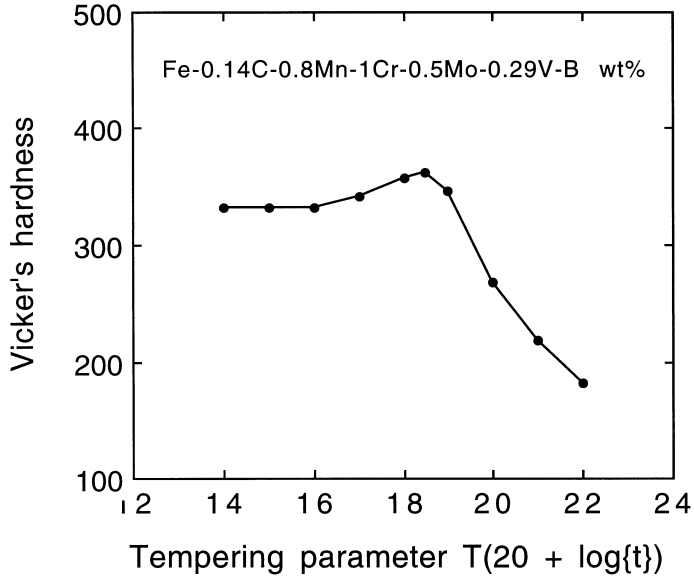

Fig. 4.7 Secondary hardening peak in a vanadium-containing bainitic steel (after Irvine and Pickering, 1957). The tempering parameter is defined with the absolute temperature T and the time t in hours.

1957). Whether or not *peaks* are observed in the tempering curves, the data are all consistent with secondary hardening because the tempering resistance is improved relative to plain carbon steels.

It would be interesting to see whether it is possible to design a steel in which the bainite secondary hardens as it forms. The B_S temperature would have to be around 650 °C and the alloy would have to be engineered to avoid interference from other transformation products.

4.6 Changes in the Composition of Cementite

The cementite that precipitates from austenite during the course of the bainite reaction has the same substitutional to iron atom ratio as the austenite, i.e. there is no partitioning of the substitutional solutes. Its composition is therefore far from equilibrium. Tempering helps the cementite to approach its equilibrium composition by the diffusion of solutes from the ferrite into the cementite.

Most of the chemical data on cementite composition changes during tempering have been obtained using either direct chemical analysis of extracted carbides, or energy dispersive X-ray analysis techniques associated with transmission electron microscopy. These techniques are not well suited for the analysis of carbon or nitrogen concentrations. These two elements can

mix to form carbonitrides. Thus, atom-probe field ion microscopy has shown that M_2C carbides found in tempered bainite have an average composition $[Cr_{0.41}Mo_{0.59}]_2[C_{0.96}N_{0.04}]$ (Josefsson *et al.*, 1987; Josefsson, 1989). In the discussion that follows, we shall neglect to consider the carbon and nitrogen, for which there are few data.

Some of the first results on the tempering of bainite were obtained by Baker and Nutting (1959) for a commercial steel with a chemical composition Fe–0.15C–2.12Cr–0.94Mo wt%. The cementite was found to become richer in Cr, Mo and Mn, the degree of enrichment being highest for Cr, with its concentration eventually reaching some 20 wt% (Fig. 4.8).

The enrichment of cementite decreases as alloy carbide formation begins, until the cementite eventually starts to dissolve (Fig. 4.9). This is expected since a dissolving particle of cementite will contain a chromium depleted zone in the cementite near the moving ferrite/austenite interface.

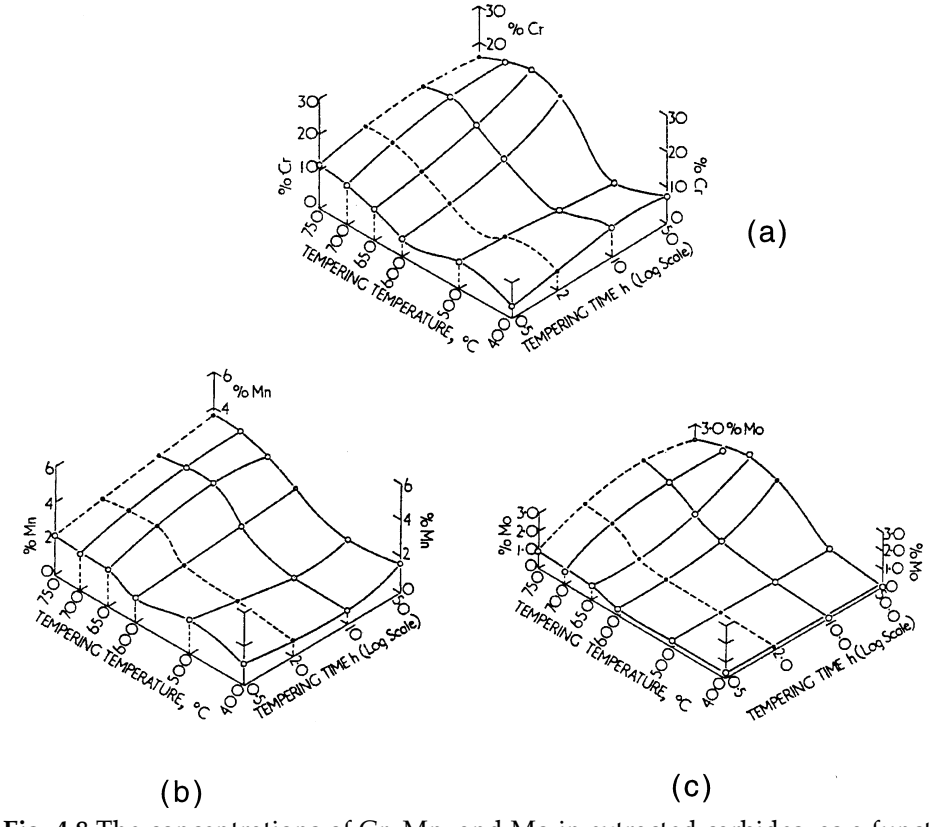

Fig. 4.8 The concentrations of Cr, Mn, and Mo in extracted carbides, as a function of the tempering time and temperature, for a steel with initial microstructure which is bainite (Baker and Nutting, 1959).

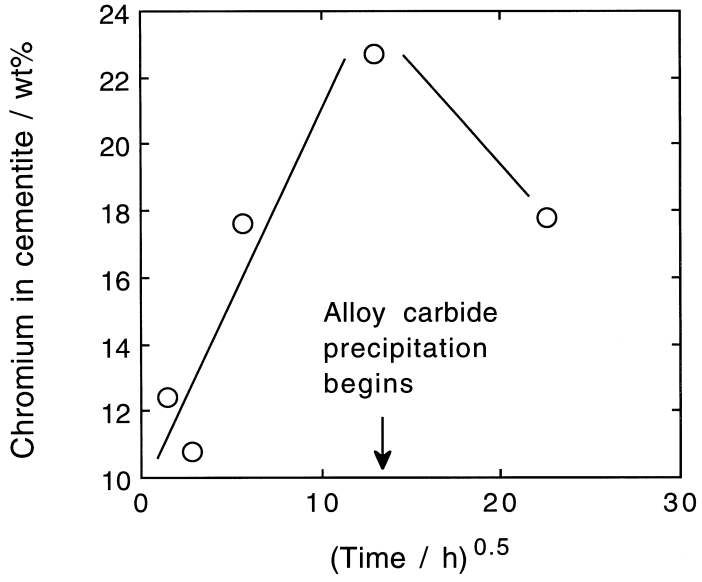

Fig. 4.9 Mean chromium concentration in cementite found in a tempered bainitic microstructure aged at 565 °C, in a '$2\frac{1}{4}$Cr1Mo' power plant steel (Thomson, 1990).

4.6.1 Remanent Life Prediction

The study of changes in the chemical composition of carbides during the tempering of bainite is of commercial importance. Where creep resistant bainitic steels are in service at elevated temperatures over long time periods (30 years), it is important for safety reasons to know accurately the time–temperature history of the steel at any stage during service. The thermal history of the steel can be related to the amount of creep life remaining in that steel, before the accumulated damage becomes intolerable. This remaining creep life is in the power generation industry called the *remanent life* (Bhadeshia *et al.*, 1998).

The accurate estimation of remanent life permits the safe use of existing power plant beyond their original design lives. The method can also help anticipate plant closures or it can facilitate the timely replacement of components. Power plant temperatures fluctuate and are difficult to record over long periods of time and for the large number of components involved (Fig. 4.10). Life assessment therefore has to be made on a conservative basis, which leads to expense due to premature closure of plant which has not exhausted its safe life. Any method which gives an accurate measure of the thermal history experienced by the steel during service can lead to savings by enabling more accurate assessments of the remaining creep life. At first sight, the obvious

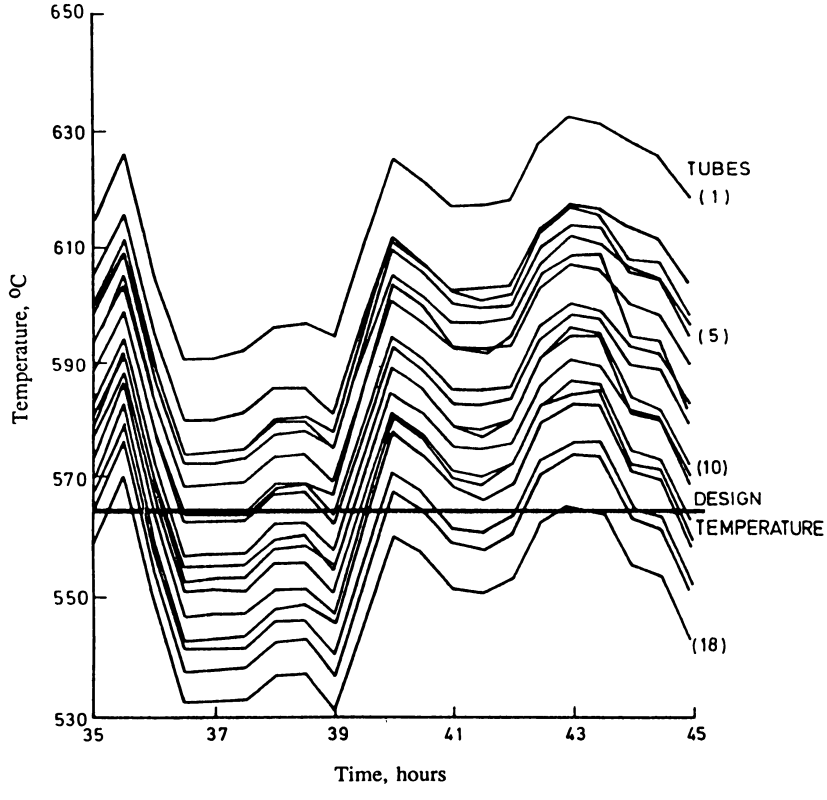

Fig. 4.10 Illustration of the variation in the temperature at different locations on a particular component ('reheater drum') of a 500 MW power station (Cane and Townsend, 1984).

thing to do would be to monitor the temperature everywhere using strategically located thermocouples, but this is impractical over the large time span involved and in the harsh environment of the power station.

The microstructure of the steel, and especially the chemical composition of the cementite, changes during service. These changes can be exploited to assess the effective thermal history experienced by the steel since its implementation. The microstructure is in this context, a recorder of time and temperature; for example, the cementite particles in the steel can be monitored by removing a few using extraction replicas. Their compositions can then be measured using a microanalysis technique to determine the extent of enrichment and hence an estimate of the effective service temperature. The interpretation and extrapolation of such data relies on the existence of theory capable of relating the

[12:16 3/9/01 C:/3B2 Templates/keith/3750 BAINITE.605/3750-004.3d] Ref: 0000 Auth: Title: Chapter 00 Page: 104 91-116

cementite composition to heat treatment. Such theory is discussed in a later section, after an introduction to the published work.

The use of cementite composition for thermal history assessment was first applied to the cementite in pearlite, where it was found empirically that the Cr and Mn concentrations varied with $t^{\frac{1}{3}}$, where t is the time at tempering temperature (Carruthers and Collins, 1981). We shall see later that a $t^{\frac{1}{2}}$ relationship can be justified theoretically.

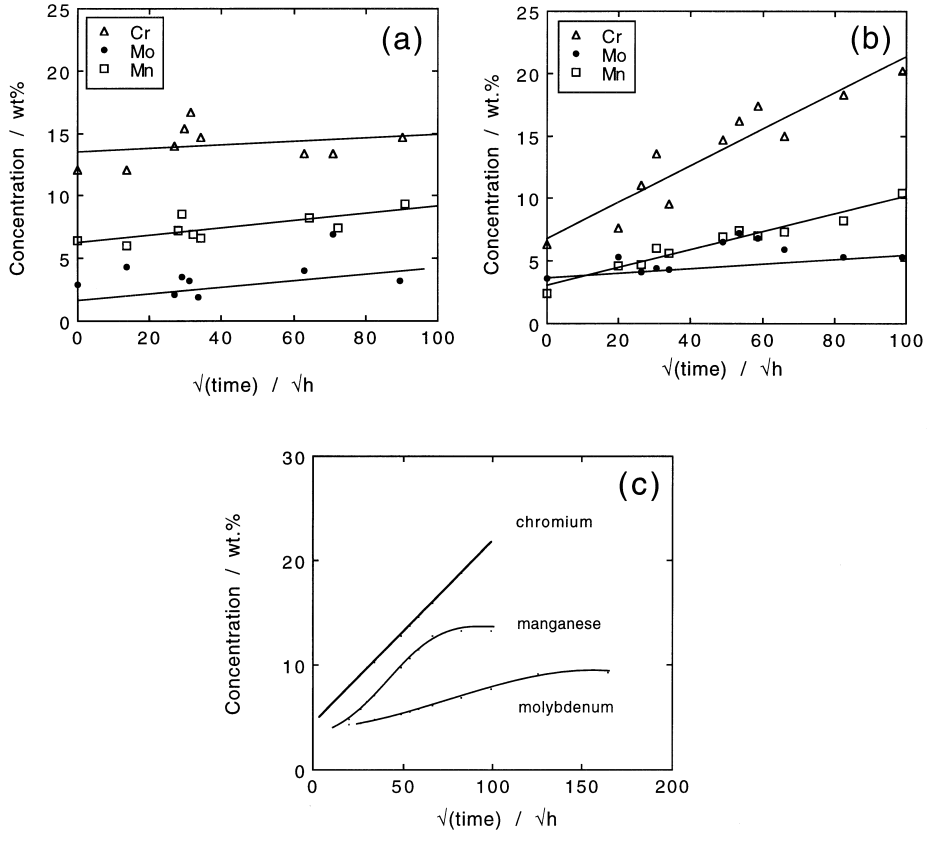

Fig. 4.11 Measured changes in the chemical composition of cementite particles as a function of the square root of time, during ageing at 550 °C. The steel composition is Fe–0.1C–0.24Si–0.48Mn–0.84Cr–0.48Mo wt%. The data have been replotted against $t^{\frac{1}{2}}$ instead of $t^{\frac{1}{3}}$ used in the original work. (a) Tempered at 550 °C following service at 565 °C for 70000 h. (b) Heat treated to give a fully bainitic microstructure, stress-relieved at 693 °C for one hour and then tempered at 550 °C for the periods illustrated. Data from Afrouz *et al*. (1983). (c) Finite difference calculations showing that the enrichment process will inevitably show deviations from the parabolic law at long ageing times (Bhadeshia, 1989).

Afrouz *et al*. (1983) reported similar results on a bainitic steel. The alloy was normalised to give a microstructure of allotriomorphic ferrite and 20% bainite, was then tempered in an unspecified way, and held at 565 °C for 70000 h at a stress of ≃17 MPa. This service-exposed material was then examined after further tempering at 550 °C for a range of time periods. As expected, the chromium and manganese concentrations of the cementite (M_3C) increased with time, the manganese possibly showing signs of saturation during the later stages of ageing, and the data for molybdenum exhibiting considerable scatter (Fig. 4.11).

Afrouz *et al*. also austenitised the service-exposed material so that after oil-quenching, a fresh fully bainitic microstructure was obtained; it is likely that both upper and lower bainite were present. This was then tempered at 693 °C for an hour to give coarse M_3C particles at the lath boundaries and within the bainite, and subsequently held at 550 °C for a variety of time periods. The change in M_3C composition was monitored during the latter tempering treatment (Fig. 4.11). The starting composition of the carbide is of course leaner than that of the service-exposed material and the rate of enrichment was found to be higher for the reheat-treated samples (Fig. 4.11).

4.6.2 *Theory for Carbide Enrichment*

The process by which carbide particles enrich during tempering has been analysed theoretically (Bhadeshia, 1989). The method is similar to the one employed in determining the time required to decarburise supersaturated plates of ferrite, as discussed in detail in Chapter 6. The kinetics of cementite composition change are given by:

$$t_c^{\frac{1}{2}} = \frac{c^{\theta}(\overline{c}_X - c_X)\pi^{\frac{1}{2}}}{4D^{\frac{1}{2}}(c_X^{\alpha\theta} - \overline{c}_X)} \tag{4.4}$$

where t_c is the time required for the carbide to reach a concentration c_X (the subscript represents a substitutional solute), and c_θ is the thickness of the cementite plate (Fig. 4.12a). D is the diffusion coefficient for the solute in the matrix (assumed to be identical to the corresponding diffusivity in the particle) and $c_X^{\alpha\theta}$ is the concentration of the substitutional solute in the ferrite which is in equilibrium with the cementite. A further outcome is that the carbide composition should depend on its size (Fig. 4.12b).

The time dependence of concentration is found to be $t^{\frac{1}{2}}$ rather than the $t^{\frac{1}{3}}$ which has been assumed in the past. The analysis neglects the overlap of the diffusion fields of different particles, an effect which is inevitable during long term heat treatment. This can be tackled using finite difference methods, which show that the time exponent must vary with time, since the boundary condi-

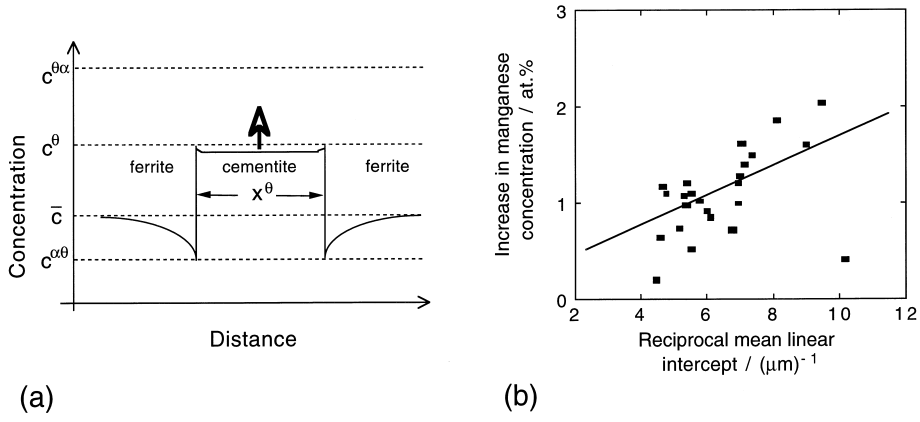

Fig. 4.12 (a) Solute concentration profile that develops during enrichment of cementite. $c^{\theta\alpha}$ is the concentration in cementite which is in equilibrium with ferrite. (b) Size dependence of the cementite chemical composition, for particles extracted from a bainitic microstructure aged for 4 weeks at 565 °C (Wilson, 1991). Detailed analysis shows that the scatter in the data is a consequence of the micro-analysis technique.

tions for the diffusion process change with the onset of soft impingement (Fig. 4.11c).

4.6.3 Effect of Carbon on Carbide Enrichment

There are two effects which depend on the carbon concentration of the steel. The ternary Fe–Cr–C phase diagram on the M_3C/α field shows that an increase in the carbon concentration is accompanied by a decrease in the equilibrium concentration of chromium in the carbide. Thus, the carbide enrichment rate is expected to decrease. A further effect is that the volume fraction of cementite increases, in general leading to an increase in particle thickness and volume fraction. The thickness increase retards the rate of enrichment (equation 4.4). If the carbide particles are closer to each other then soft-impingement occurs at an earlier stage, giving a slower enrichment at the later stages of annealing.

Local variations in carbon concentration may have a similar effect as changes in average concentration. Such variations can be present through solidification induced segregation, or because of microstructure variations caused by differences in cooling rates in thick sections. It is well known that the microstructure near the component surface can be fully bainitic with the core containing a

[12:16 3/9/01 C:/3B2 Templates/keith/3750 BAINITE.605/3750-004.3d] Ref: 0000 Auth: Title: Chapter 00 Page: 107 91-116

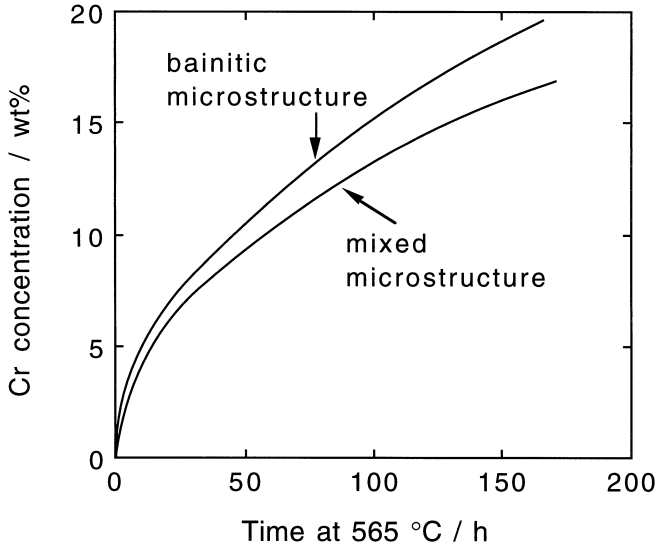

Fig. 4.13 $2\frac{1}{4}$Cr1Mo steel, cementite enrichment in a fully bainitic microstructure and one which is a mixture of allotriomorphic ferrite and bainite (Thomson and Bhadeshia, 1994).

large amount of allotriomorphic ferrite in addition to bainite. In the latter case, the bainite which grows after the allotriomorphic ferrite, transforms from high carbon austenite. The associated carbides are then found to enrich at a slower rate (Fig. 4.13). This discussion emphasises the role of carbon.

4.7 Sequence of Alloy Carbide Precipitation

Cementite is not the equilibrium carbide in many bainitic alloy steels, but it is nevertheless kinetically favoured because its growth mechanism does not require the long-range diffusion of substitutional solutes. The equilibrium combination of phases naturally depends on the steel composition. Alloy carbides become vital in steels where the resistance to creep deformation is of paramount importance; they obviously play a role in secondary hardened steels for use at ambient temperatures but such alloys tend to be martensitic rather than bainitic. Figure 4.14 shows the equilibrium phases to be found in creep-resistant steels. $M_{23}C_6$, M_2X and small fractions of carbonitrides are the equilibrium precipitates in the first two alloys which are generally used in the bainitic or partly bainitic microstructures. The other higher alloy steels are martensitic and are susceptible to the formation of Laves phases (intermetallic compounds). It is interesting that cementite is not an equilibrium phase in any of the alloys illustrated.

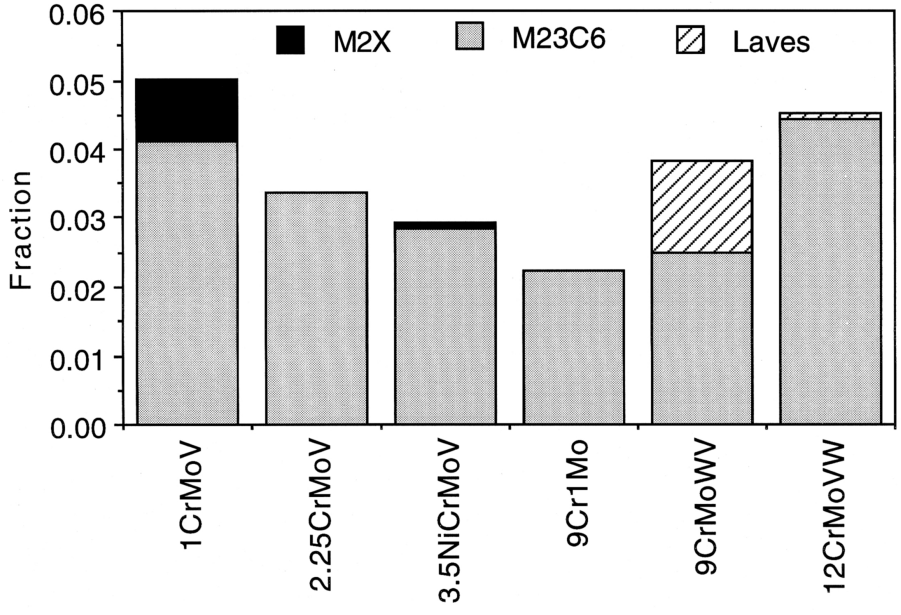

Fig. 4.14 Equilibrium fractions of carbides at 565 °C (838 K) in some common power plant steels, the first two of which frequently are bainitic. The remaining alloys are essentially martensitic. The detailed chemical compositions are given in Table 12.2. Small fractions of vanadium and niobium carbonitrides are present in some steels but are not shown. Thus, the modified 9Cr1Mo contains 0.0009 NbN and 0.003 VN, the 9CrMoWV steel contains 0.0008 NbN and 0.0032 VN.

The approach to equilibrium can be slow, especially when the tempering temperature is less than 600 °C. The change from cementite to the equilibrium carbide may occur via a number of other transition carbides. Baker and Nutting (1959) showed that during the tempering of bainite Fe–2.12Cr–0.94Mo–0.15C wt%, the first alloy carbide to form is M_2C, needles of which precipitate independently of the cementite (Fig. 4.15). Later work has shown that the M_2C contains substantial amounts of other elements; it is better represented as M_2C (Woodhead and Quarrel, 1965; Murphy and Branch, 1971). This applies to virtually all the alloy carbides in multicomponent steels.

M_7C_3 starts to form soon after the precipitation of M_2C, perhaps at the interface between the Cr-enriched cementite and ferrite. M_2C then begins to dissolve, giving way to $M_{23}C_6$. Both $M_{23}C_6$ and M_7C_3 are at high temperatures, completely or partly replaced by the equilibrium carbide M_6C.

With the exception of M_2C, new transition carbides seem to precipitate in association with preexisting carbides. The sequence of changes in Fe–2.12Cr–0.94Mo–0.15C wt% can be summarised as follows:

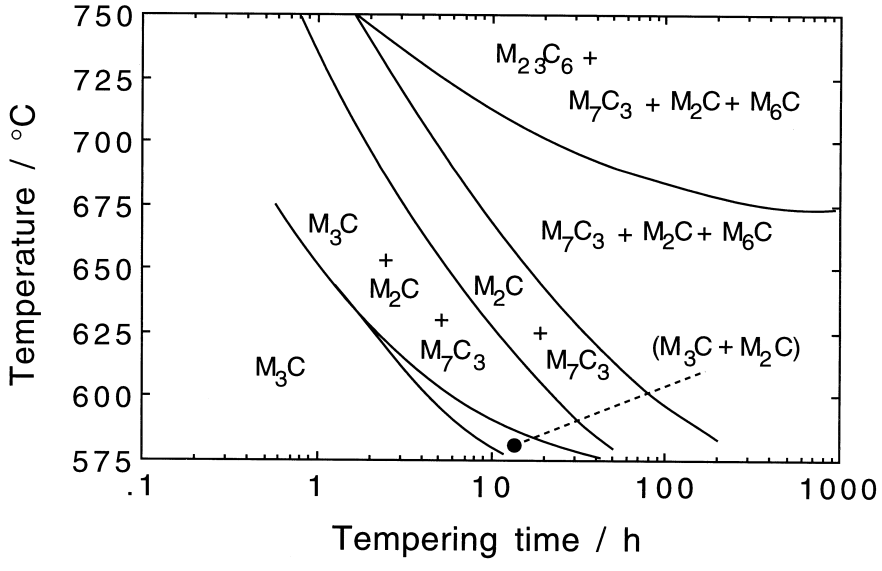

Fig. 4.15 An updated version of the classic Baker–Nutting carbide stability diagram for a $2\frac{1}{4}$Cr1Mo steel (after Nutting, 1998).

$$\begin{array}{l} \theta \rightarrow \theta + \mathrm{M_2C} \rightarrow \mathrm{M_{23}C_6} \rightarrow \mathrm{M_6C} \\ \quad\downarrow \\ \mathrm{M_7C_3} \rightarrow \qquad\quad \rightarrow \mathrm{M_6C} \end{array} \tag{4.5}$$

A different sequence has been reported by Pilling and Ridley (1982) for lower carbon Fe–Cr–Mo–C alloys containing lower carbon concentrations (0.018–0.09 wt%) which illustrates the sensitivity of the microstructure to the precise chemical composition:

$$\begin{array}{l} \theta \rightarrow \mathrm{M_2C} \rightarrow \mathrm{M_{23}C_6} \rightarrow \mathrm{M_6C} \\ \quad + \\ \mathrm{M_7C_3} \rightarrow \qquad\quad \rightarrow \mathrm{M_7C_3} \end{array} \tag{4.6}$$

Yu (1989) has shown that an increase in the silicon concentration to about 0.6 wt% stabilises (M_6C which is absent in silicon-free $2\frac{1}{4}$Cr1Mo steels) since silicon has a relatively high solubility in that carbide. It was also found to accelerate the precipitation of M_2C. An increase in the manganese concentration from 0 to 0.8 wt% was found to accelerate M_7C_3 precipitation. Enhanced chromium concentrations are known to accelerate the formation of $M_{23}C_6$ and

Table 4.1 Concentration (in wt%) of the major alloying elements in the steels used to demonstrate the model.

	C	N	Mn	Cr	Mo	Ni	V	Nb
$2\frac{1}{2}$Cr1Mo	0.15	–	0.50	2.12	0.9	0.17	–	–
3Cr1.5Mo	0.1	–	1.0	3.0	1.5	0.1	0.1	–
10CrMoV	0.11	0.056	0.50	10.22	1.42	0.55	0.20	0.50

this influences the sensitivity of the microstructure to severe hydrogen attack (Ritchie *et al.*, 1984; Spencer *et al.*, 1989).

Some of these detailed kinetic effects of the average composition of the steel on the precipitation processes can now be predicted theoretically (Robson and Bhadeshia, 1997). The compositions of three steels used for illustration are given in Table 4.1. These three alloys, whilst of quite different chemical compositions, show similar precipitation *sequences* but on vastly different time scales. For example, at 600 °C the time taken before $M_{23}C_6$ is observed is 1 h in the 10CrMoV steel, 10 h in the 3Cr1.5Mo alloy and in excess of 1000 h in the $2\frac{1}{4}$Cr1Mo steel.

A plot showing the predicted variation of volume fraction of each precipitate as a function of time at 600 °C is shown in Fig. 4.16. Consistent with experiments, the precipitation kinetics of $M_{23}C_6$ are predicted to be much slower in the $2\frac{1}{4}$Cr1Mo steel compared to the 10CrMoV and 3Cr1.5Mo alloys. One contributing factor is that in the $2\frac{1}{4}$Cr1Mo steel a relatively large volume fraction of M_2X and M_7C_3 form prior to $M_{23}C_6$. These deplete the matrix and therefore suppress $M_{23}C_6$ precipitation. The volume fraction of M_2X which forms in the 10CrMoV steel is relatively small, and there remains a considerable excess of solute in the matrix, allowing $M_{23}C_6$ to precipitate rapidly. Similarly, in the 3Cr1.5Mo steel the volume fractions of M_2X and M_7C_3 are insufficient to suppress $M_{23}C_6$ precipitation to the same extent as in the $2\frac{1}{4}$Cr1Mo steel.

Phase equilibrium is, of course, a function of temperature as well as the chemical composition. Precipitation sequences may therefore change with the temperature. In a Fe–1Cr–1Mo–0.75V–(B, Ti) wt% bainitic steel Collins (1989) showed that tempering led to the formation of TiC and V_4C_3, both of which also contained molybdenum. The V_4C_3 nucleates on TiC particles which form first. The TiC then converts *in situ* into molybdenum-rich M_2C precipitates. At 600 °C the stability of the carbides is in the following sequence

$$M_2C > V_4C_3 > TiC$$

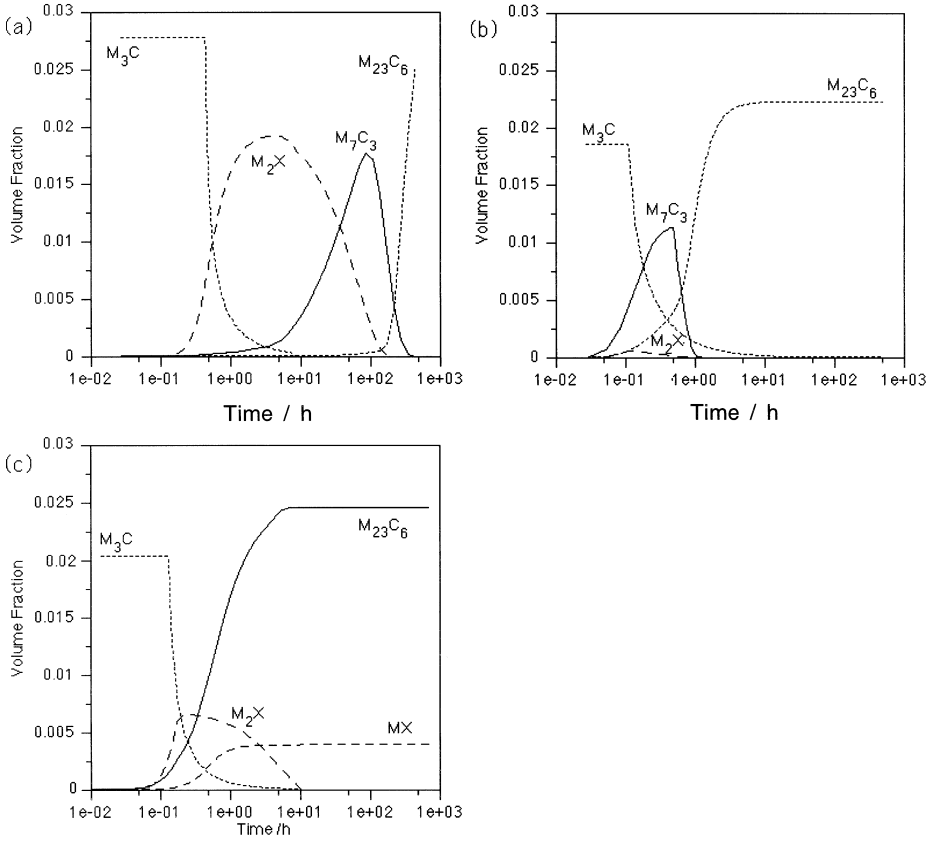

Fig. 4.16 The predicted evolution of precipitate volume fractions at 600 °C for three power plant materials (a) $2\frac{1}{4}$Cr1Mo (b) 3Cr1.5Mo and (c) 10CrMoV.

whereas at higher temperatures, the V_4C_3 is more stable than M_2C. The dependence on temperature is important because creep tests are often accelerated by raising the test temperature but the carbide structure at the higher temperature may be different, making the accelerated test unrepresentative.

4.7.1. Effect of Starting Microstructure on Tempering Reactions

There are no major differences in the alloy carbide precipitation reactions when the microstructure is changed from martensite to bainite (Baker and Nutting, 1959). If allotriomorphic ferrite is present in the microstructure then it may already contain alloy carbides which precipitate during the diffusional growth of the ferrite itself. In the $2\frac{1}{4}$Cr1Mo steel M_2C precipitates present in the ferrite

[12:16 3/9/01 C:/3B2 Templates/keith/3750 BAINITE.605/3750-004.3d] Ref: 0000 Auth: Title: Chapter 00 Page: 112 91-116

dissolve during tempering to be replaced by M_6C particles. By contrast, alloy carbides do not form during the growth of any of the displacive transformation products, including bainite and martensite.

The distribution and type of precipitates is also influenced by the microstructure (Lee, 1989). Thus, M_2C forms the main precipitate within a tempered bainite plate whereas mixtures of cementite, M_2C, M_7C_3 and $M_{23}C_6$ are found at the bainite plate boundaries. The boundaries are not only more effective heterogeneous nucleation sites but the cementite particles located there are sources of carbon for the precipitation of alloy carbides.

Any differences in the number density or distribution of nucleation sites will cause changes in the kinetics of precipitation reactions. The equilibrium carbide M_6C forms more rapidly in bainite than in pearlite or allotriomorphic ferrite (Lee, 1989).

4.8 Changes in the Composition of Alloy Carbides

Alloy carbides cannot form without the long-range diffusion of substitutional solutes. Given this *necessary* diffusion, it is not surprising that their compositions are at all times close to equilibrium. Small changes can be induced by one or more of the following phenomena:

1. The equilibrium chemical composition of particles with curved interfaces is dependent on the radius of curvature via the Gibbs–Thompson effect.
2. The phase rule allows greater degrees of freedom in steels containing one or more substitutional solutes. Thus, the tie-line controlling the equilibrium composition of the carbide may shift during the precipitation reaction, either as the solute content of the matrix is depleted or as other phases precipitate (Fujita and Bhadeshia, 1999).
3. Carbides adjust to a new equilibrium when the tempering temperature is changed (Strang *et al.*, 1999). It is common in industrial practice to use multiple tempering heat-treatments.

4.9 Precipitation Hardening with Copper

Unlike carbides or oxides, copper is regarded as a soft precipitate in iron; it strengthens the iron by about 40 MPa per wt% but does not cause a decrease in toughness.

Copper-bearing low-carbon steels with a mixed microstructure of ferrite and pearlite are used in heavy engineering applications which demand a combination of strength, toughness and weldability. These low carbon steels transform to carbide-free bainite, with thin films of retained austenite between the bainite

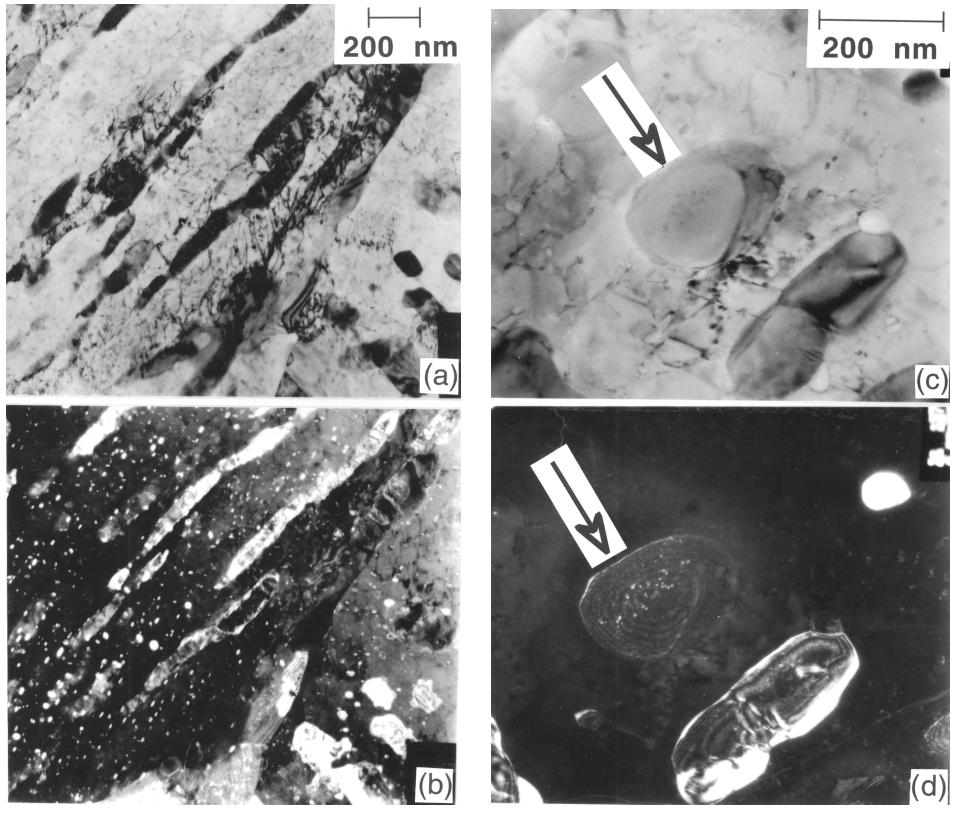

Fig. 4.17 Copper precipitation in bainite obtained by isothermal transformation at 350 °C for 65 minutes, followed by tempering at 550 °C for many hours (Fourlaris *et al.*, 1996). (a,b) Bright field transmission electron micrograph and corresponding dark field image showing copper precipitation in tempered bainitic ferrite. (c,d) Bright field and corresponding dark field image of copper precipitates in the cementite associated with bainite.

plates (Thompson *et al.*, 1988). Fine particles of copper in the bainitic ferrite contribute to the overall strength.

The precipitation of copper occurs from supersaturated bainite as a consequence either of autotempering or when the steel is deliberately tempered (Fourlaris *et al.*, 1996). Thus, no precipitation could be detected following the transformation of some experimental Cu-rich steels in the range 200–400 °C, either in the bainitic ferrite or in its associated cementite. Subsequent tempering at 550 °C resulted in fine copper precipitates in both the ferrite and cementite phases (Fig. 4.17). Copper, which is a substitutional solute, is not in this respect different from any secondary hardening element in steels.

[12:16 3/9/01 C:/3B2 Templates/keith/3750 BAINITE.605/3750-004.3d] Ref: 0000 Auth: Title: Chapter 00 Page: 114 91-116

A potential difficulty in quenched and tempered copper precipitation strengthened steels is their tendency to crack during stress-relief heat treatments following welding (Wilson *et al.*, 1988). Although the steels are immune to cold cracking, the copper particles are taken into solution in the heat-affected zone during welding. The stress-relief heat treatment then causes precipitation which hinders the annealing of residual stresses.

4.10 Summary

There are important differences in the tempering behaviour of bainite and martensite, because the former autotempers during transformation. Much of the carbon precipitates or partitions from the ferrite during the bainite reaction. Since $B_S > M_S$, the extent of autotempering is greatest for bainite, which consequently is less sensitive to additional tempering heat-treatments. The decrease in strength on tempering bainite is smaller because unlike martensite, there is hardly any carbon in solid solution. Major changes in strength occur only when the microstructure coarsens or with the onset of recrystallisation where equiaxed grains of ferrite replace the bainite plates. Minor changes in strength are due to cementite particle coarsening and a general recovery of the dislocation substructure. Bainitic steels containing strong carbide forming elements show secondary hardening similar to martensitic steels. In most cases, new carbides nucleate on existing metastable carbides, with the exception of M_2C which forms in isolation on dislocations.

5 *Thermodynamics*

5.1 Deviations from Equilibrium

Equilibrium is said to exist in a system when it reaches a state in which no further change is perceptible, no matter how long one waits (Pippard, 1981). This could happen if the system sinks into a very deep free energy minimum. Whether this represents the lowest free energy state, it is impossible to say, and a question more of philosophy than of practical consequence. It is more appropriate to refer to the state of metastable equilibrium, which represents a local minimum in free energy but does not exclude the existence of other deeper minima. The laws governing metastable equilibria are exactly identical to those dealing with equilibrium so this procedure has no obvious difficulties.

A bainitic microstructure is far from equilibrium. The free energy change accompanying the formation of bainite in an Fe–0.1C wt% alloy at 540 °C is $-580\,\mathrm{J\,mol^{-1}}$, whereas that for the formation of an equilibrium mixture of allotriomorphic ferrite and austenite at the same temperature is $-1050\,\mathrm{J\,mol^{-1}}$. Consequently, the excess energy of bainite is some $470\,\mathrm{J\,mol^{-1}}$ relative to allotriomorphic ferrite, equivalent to about 0.04 in units of RT_M, where R is the Gas Constant and T_M the absolute melting-temperature. This is about an order of magnitude larger than the stored energy of a severely deformed pure metal. It is small, however, when compared against highly metastable materials such as rapidly-quenched liquids which solidify as supersaturated solutions, or multilayered structures containing a large density of interfaces (Table 5.1). Thus, bainitic steels can be welded whereas all the other materials listed with higher stored energies would not survive the welding process.

The concepts of equilibrium, metastable equilibrium and indeed, constrained equilibrium, remain useful in spite of the large excess energies. For bainite, we shall apply them in the interpretation of the mechanism of transformation and obtain results which are of very great importance in the design of modern steels.

[12:16 3/9/01 C:/3B2 Templates/keith/3750 BAINITE.605/3750-005.3d] Ref: 0000 Auth: Title: Chapter 00 Page: 117 117-128

Table 5.1 Excess energies of metastable materials; adapted from Turnbull (1981)

Example	Excess energy RT_M
Highly supersaturated solution	1
Amorphous solid	0.5
Artificial multilayers	0.1
Bainite	0.04
Cold-deformed metal	0.003

5.2 Chemical Potential

Pure iron can exist in many allotropic forms including ferrite (α) and austenite (γ). These two phases can be said to be in equilibrium when their molar Gibbs free energies are identical;

$$G_m^{\alpha} = G_m^{\gamma} \tag{5.1}$$

There is then no net tendency for atoms to transfer from one allotrope to the other, because the free energy of the iron atom in α is precisely equal to that in γ.

Similarly, for an iron–carbon solid solution, equilibrium is when there is no net tendency for either iron or carbon atoms to transfer between ferrite and austenite, even though the two phases may differ in composition. That is, the free energy of a carbon (or iron) atom must be identical in ferrite and in austenite at equilibrium. It is no longer the case that the ferrite and austenite have identical free energies at equilibrium.

It therefore becomes useful when considering the thermodynamics of solid solutions to partition the free energy of phase into parts which are attributed to the individual components. This leads to the concept of a chemical potential. The molar Gibbs free energy of a binary solution can be written as a weighted average of its components A and B:

$$G_m = x_A\mu_A + x_B\mu_B \tag{5.2}$$

where μ_i is the chemical potential of element i in a solution where its concentration is x_i. This equation is represented graphically in Fig. 5.1, from which it can be seen that the chemical potential μ_A of A can be interpreted simply to represent the average free energy of a mole of A atoms *in a solution* of composition x_A.

Equilibrium is said to exist between homogeneous phases when the chemical potential μ_i of each component i is the same in all the phases present:

$$\mu_i^{\gamma} = \mu_i^{\alpha} \qquad \text{for all} \quad i. \tag{5.3}$$

[12:16 3/9/01 C:/3B2 Templates/keith/3750 BAINITE.605/3750-005.3d] Ref: 0000 Auth: Title: Chapter 00 Page: 118 117-128

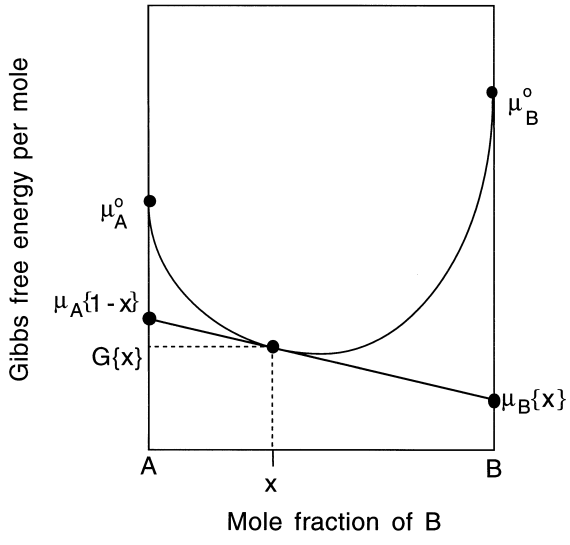

Fig. 5.1 The chemical potentials μ_A and μ_B for components A and B respectively, in a solution containing a mole fraction x of B and $1 - x$ of A. The potentials are given by the intercepts on the vertical axes of the tangent drawn at x to the curve representing the solution free energy. μ_A^0 and μ_B^0 are the molar Gibbs free energies of pure A and B respectively.

This is illustrated in Fig. 5.2, which shows that the equilibrium compositions $x^{\alpha\gamma}$ and $x^{\gamma\alpha}$ of ferrite and austenite respectively, can be determined by constructing a tangent which is common to both the free energy curves. The intercept of the tangent with the vertical axes gives the chemical potentials, which are identical for each species whatever the phase, by virtue of the fact that the tangent is common.

The concept of equilibrium in terms of phases which are *homogeneous* is rather restrictive. Instead, it is useful to consider equilibrium to exist locally. For example, it is a reasonable approximation that during diffusion-controlled growth, the compositions of the phases in contact at the interface are such as to allow equilibrium to exist locally even though there may be concentration gradients in the matrix ahead of the interface. As long as the phases are not too inhomogeneous, as with some artificial multilayered structures or during spinodal decomposition, classical equilibrium thermodynamics can be applied locally without raising any fundamental difficulties.

A form of constrained equilibrium which arises in substitutionally alloyed steels is *paraequilibrium*, in which the ratio of iron to substitutional solute atoms remains the same everywhere, but subject to that constraint, the carbon atoms achieve a uniform chemical potential at all locations (Fig. 2.11). Either the substitutional solute atoms, or the iron atoms are then trapped by the advan-

[12:16 3/9/01 C:/3B2 Templates/keith/3750 BAINITE.605/3750-005.3d] Ref: 0000 Auth: Title: Chapter 00 Page: 119 117-128

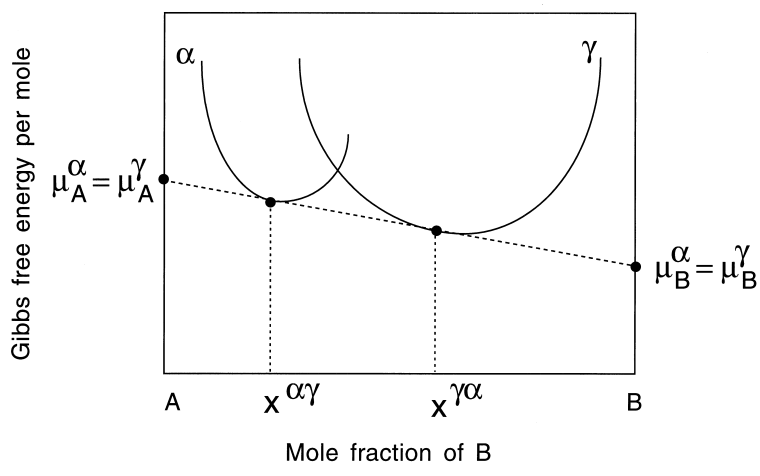

Fig. 5.2 The common tangent construction which defines the equilibrium chemical compositions of the the α and γ.

cing transformation interface. An atom is said to be trapped when its chemical potential increases on transfer across the interface.

Transformation can occur without any composition change at a temperature below T_0, where the parent and product phases of identical composition have equal free energy (Fig. 1.4).

The concepts of local equilibrium, paraequilibrium and transformation without any change in composition are easy to visualise and formulate. However, between the states of local and paraequilibrium, there can in principle exist an infinite number of alternatives in which the substitutional solutes partly partition between the phases. There may similarly be a gradation between paraequilibrium and composition-invariant transformation in which the extent to which carbon is partitioned may vary. Such intermediate states would have to be stabilised by some other rate-controlling factor such as interface kinetics. They would otherwise tend towards equilibrium, because any perturbation which leads to a reduction in free energy would be stable. We shall see in Chapter 6 that the stabilisation of such nonequilibrium states is in certain circumstances possible for solid-state transformations in steels.

5.3 Stored Energy due to Transformation

Much of the stored energy of bainite comes from the distortions due to the shape deformation accompanying transformation. For a plate in the form of an oblate ellipsoid of semi-axes R, R and y, with $R \gg y$, the strain energy per mole is given by (Christian, 1958):

[12:17 3/9/01 C:/3B2 Templates/keith/3750 BAINITE.605/3750-005.3d] Ref: 0000 Auth: Title: Chapter 00 Page: 120 117-128

$$G_s = \frac{\mu V_m}{1-\nu}\left[\frac{2}{9}(1+\nu)\Delta^2 + \frac{\pi y}{4R}\zeta^2 + \frac{(1-\nu)\pi y}{3R}\Delta\zeta\right] + \frac{1}{2}\mu V_m \frac{(2-\nu)\pi y}{4(1-\nu)R}s^2 \quad (5.4)$$

where μ and ν are the shear modulus and Poisson's ratio respectively of the surrounding matrix, V_m is the molar volume of the matrix, Δ is the uniform dilatation accompanying transformation, ζ is the additional uniaxial dilatation normal to the habit plane and s is the shear component of the shape change (Fig. 5.3).

The uniform dilatation Δ term has been used to interpret the crystallography of bainite but its existence has not been confirmed by measurements and so it is neglected in further discussions. The energy due to the shear and ζ strains comes to about $400\,\mathrm{J\,mol^{-1}}$ for bainite (Bhadeshia, 1981a). This is less than the corresponding term for martensite, which is about $600\ \mathrm{J\,mol^{-1}}$ because bainite plates usually have a smaller aspect ratio (y/R). The shear and dilatational components of the shape change are similar for martensite and bainite.

The stored energy of $400\,\mathrm{J\,mol^{-1}}$ applies strictly to an isolated plate of bainite which is elastically accommodated in the surrounding austenite. However, bainite grows as clusters of plates and it may be more appropriate to consider the sheaf as a whole, in which case the stored energy may be reduced by averaging the shear over the thickness of the sheaf in which the bainite plates are separated by intervening films of austenite or other phases.

The strain energy can be reduced by plastic relaxation. This is particularly relevant for bainite because the yield strength of austenite is reduced at high temperatures. The plastic deformation causes an increase in dislocation density, but since the deformation is driven by the shape change, the strain energy calculated on the basis of an elastically accommodated shape change should be an upper limit (Christian, 1979b). There may also be a reduction in the stored

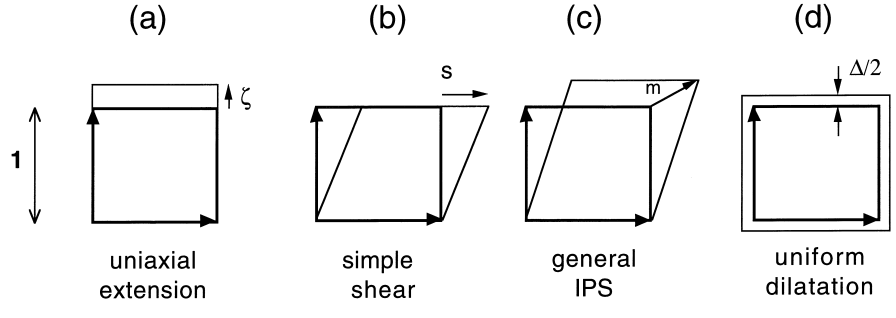

Fig. 5.3 The strains used in equation 5.4. (a) Uniaxial dilatation normal to the habit plane; (b) shear parallel to the habit plane; (c) a combination of shear and uniaxial dilatation which defines the invariant-plane strain (IPS) which is the shape deformation associated with bainite; (d) uniform dilatation.

[12:17 3/9/01 C:/3B2 Templates/keith/3750 BAINITE.605/3750-005.3d] Ref: 0000 Auth: Title: Chapter 00 Page: 121 117-128

energy per unit volume as transformation proceeds because of the tendency of adjacent sheaves to grow in mutually accommodating formations (Hehemann, 1970).

In martensitic reactions, transformation twinning can contribute about 100 $J\,mol^{-1}$ of stored energy; this is not applicable to bainite where the lattice-invariant shear is presumed to be slip.

5.4 Thermodynamics of Growth

5.4.1 Substitutional Solutes during Growth

The atom-probe experiments described in Chapter 2 have established that there is no redistribution of substitutional solutes during the bainite transformation. These experiments cover the finest conceivable scale for chemical analysis. They rule out any mechanism which requires the diffusion of substitutional solutes. This includes the local equilibrium modes of growth.

By contrast, all experimental data show that pearlite grows with the diffusion of substitutional solute atoms (Ridley, 1984, Al-Salman and Ridley, 1984). Chromium, molybdenum, silicon and cobalt have been shown to partition at the reaction front. The extent of partitioning is smaller for manganese and nickel, especially at large undercoolings, but there is localised diffusion (Hillert, 1982; Ridley, 1984). These observations are expected because pearlite is the classic example of a reconstructive transformation.

Solutes in iron affect the relative stabilities of austenite and ferrite. This thermodynamic effect is identical for all transformations. We have seen, however, that substitutional solutes do not diffuse at all during displacive transformations whereas they are required to do so during reconstructive transformation. It is for this reason that the observed effect of solutes, on the rate of transformation, is larger for reconstructive than for displacive transformations (Fig. 5.4).

5.4.2 Interstitial Solutes during Growth

It is simple to establish that martensitic transformation is diffusionless, by measuring the phase compositions before and after transformation. Bainite forms at somewhat higher temperatures where the carbon can escape out of the plate within a fraction of a second. Its original composition cannot therefore be measured directly.

There are three possibilities. The carbon may partition during growth so that the ferrite may never contain any excess carbon. The growth may on the other hand be diffusionless with carbon being trapped by the advancing interface.

[12:17 3/9/01 C:/3B2 Templates/keith/3750 BAINITE.605/3750-005.3d] Ref: 0000 Auth: Title: Chapter 00 Page: 122 117-128

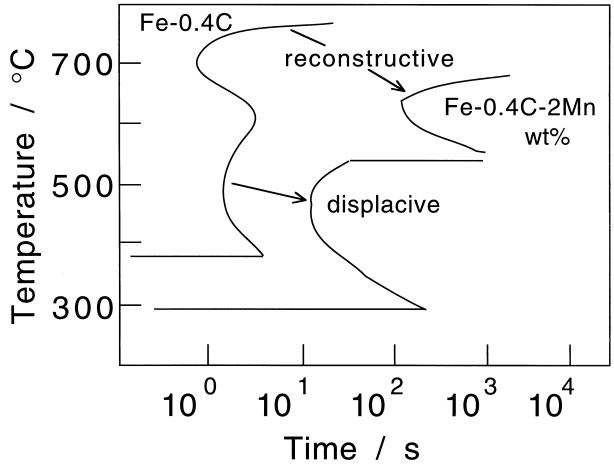

Fig. 5.4 Time-temperature-transformation diagrams showing the larger retarding effect that manganese has on a reconstructive transformation compared with its influence on a displacive transformation.

Finally, there is an intermediate case in which some carbon may diffuse with the remainder being trapped to leave the ferrite partially supersaturated.

Diffusionless growth requires that transformation occurs at a temperature below T_0, when the free energy of bainite becomes less than that of austenite of the same composition. Growth without diffusion can only occur if the carbon concentration of the austenite lies to the left of the T_0 curve (Fig. 1.4).

Suppose that the plate of bainite forms without diffusion, but that any excess carbon is soon afterwards rejected into the residual austenite. The next plate of bainite then has to grow from carbon-enriched austenite (Fig. 5.5a). This process must cease when the austenite carbon concentration reaches the T_0 curve. The reaction is said to be incomplete, since the austenite has not achieved its equilibrium composition given by the Ae_3 phase boundary. If on the other hand, the ferrite grows with an equilibrium carbon concentration then the transformation should cease when the austenite carbon concentration reaches the Ae_3 curve.

It is found experimentally that the transformation to bainite does indeed stop at the T_0 boundary (Fig. 5.5b). The balance of the evidence is that the growth of bainite below the B_S temperature involves the successive nucleation and martensitic growth of sub-units, followed in upper bainite by the diffusion of carbon into the surrounding austenite. The possibility that a small fraction of the carbon is nevertheless partitioned during growth cannot entirely be ruled out, but there is little doubt that the bainite is at first substantially supersaturated with carbon.

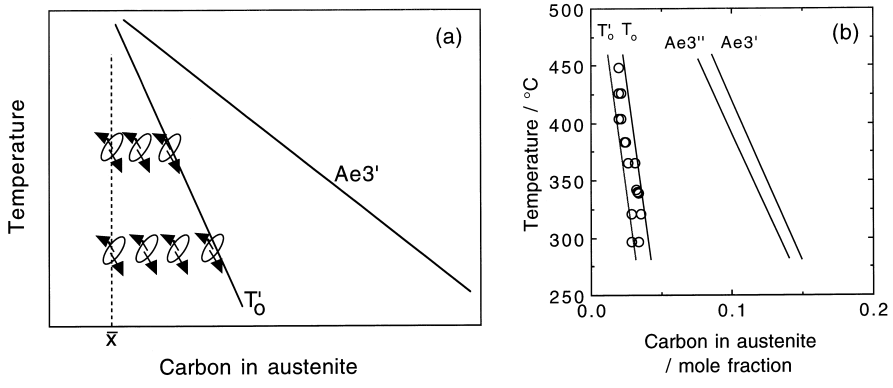

Fig. 5.5 The incomplete-reaction phenomenon. A plate of bainite grows without diffusion, then partitions its excess carbon into the residual austenite. The next plate thus grows from carbon-enriched austenite. This process can only continue until $x_\gamma = x'_{T_0}$. For paraequilibrium growth, the transformation should proceed until the carbon concentration reaches the Ae''_3 curve. (b) Experimental data on the incomplete reaction phenomenon for Fe–0.43C–3Mn–2.12Si wt% alloy (Bhadeshia and Edmonds, 1979a).

The chemical potentials are not uniform in the steel when the bainite reaction stops. The reaction remains incomplete in that the fraction of bainite is less than expected from a consideration of equilibrium between austenite and ferrite. The carbon concentration of the austenite at the point where the bainite reaction stops is far less than given by the Ae''_3 phase boundary.[†] This 'incomplete reaction phenomenon' explains why the degree of transformation to bainite is zero at the B_S temperature and increases with undercooling below B_S in steels where other reactions do not overlap with the formation of bainitic ferrite. The T'_0 curve has a negative slope on a temperature/carbon concentration plot, permitting the austenite to accommodate ever more carbon at lower temperatures.

The experimental evidence for the incomplete reaction phenomenon comes in many forms. The carbon concentration of the residual austenite at the point where the reaction stops has been measured using X-ray techniques, lattice imaging using high resolution transmission electron microscopy, field ion microscopy/atom probe methods, quantitative metallography and dilatometry. Real time neutron transmission experiments have also demonstrated the effect (Meggers *et al.*, 1994). It is always found that the concentration is far below that required by equilibrium or paraequilibrium, and is on the whole

[†]Ae3′ refers to the paraequilibrium $(\alpha + \gamma)/\gamma$ phase boundary. Ae''_3 is the corresponding boundary allowing for the stored energy of bainite.

[12:17 3/9/01 C:/3B2 Templates/keith/3750 BAINITE.605/3750-005.3d] Ref: 0000 Auth: Title: Chapter 00 Page: 124 117-128

consistent with that given by the T_0' curve of the phase diagram. The experimental evidence has been reviewed by Christian and Edmonds (1984). In dilatometric experiments, the length change due to transformation is zero above the B_S temperature, even though that temperature may be well within the $\gamma + \alpha$ phase field. The maximum length change then increases with undercooling below the B_S temperature. Numerous examples of the type illustrated in Fig. 5.6 can be found in the published literature.

The failure of the bainite reaction to reach completion reveals the role of carbon during transformation. An important consequence is that the T_0 curve can be used in the design of steels. In the context of bainite, the curve gives the limiting carbon concentration $x_{T_0'}$ of the austenite, a parameter of enormous importance in devising microstructures containing stable austenite. A discussion of the procedure is deferred to Chapters 12, 13, but Fig. 5.7 illustrates the remarkable predictive ability of the concept for a large variety of steels. By contrast, the Ae3′ phase boundary gives very poor estimates of the austenite composition in the context of bainite.

The incomplete transformation leaves films of austenite between bainite plates. These films improve the properties of steels. It has been found that the thickness of these austenite films can be estimated by assuming that the carbon diffusion field around an existing plate of ferrite prevents the close approach of another parallel plate. This is because the regions of austenite with the highest carbon concentration (i.e. $x_\gamma > x_{T_0'}$) are unable to transform

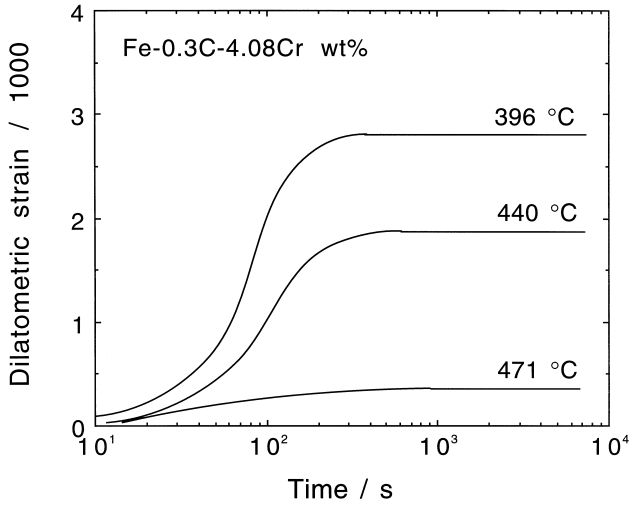

Fig. 5.6 Dilatometric length change data illustrating the incomplete reaction phenomenon for a Fe–0.3C–4.08Cr wt% alloy (Bhadeshia, 1981b).

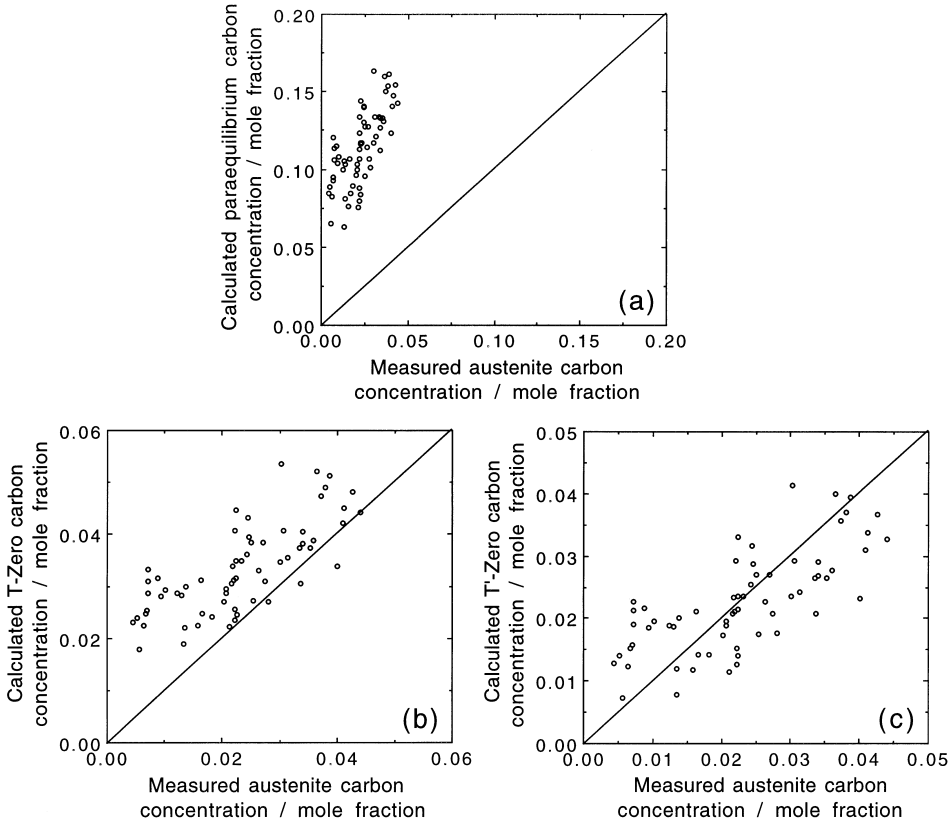

Fig. 5.7 A comparison of the measured carbon concentration of the austenite which remains untransformed when the bainite reaction stops, versus that calculated using the Ae3′, T_0 and T_0' criteria. After Chang and Bhadeshia (1995).

to bainite (Fig. 5.8). This simple theory predicts a dependence of film thickness on the bainite plate thickness since the net quantity of carbon partitioned into the austenite must increase with the thickness of the bainite plate. The correlation can be seen in Fig. 5.8c. Note that a better fit is seen in Fig. 5.8b because those calculations include both the plate thickness and the effects of alloying elements on the T_0' condition.

5.4.3 Approach to Equilibrium

Although the bainite reaction stops before equilibrium is reached, the remaining austenite can continue to decompose by reconstructive transformation, albeit at a greatly reduced rate. Pearlite often forms sluggishly after bainite. The delay between the cessation of bainite and the start of pearlite varies with

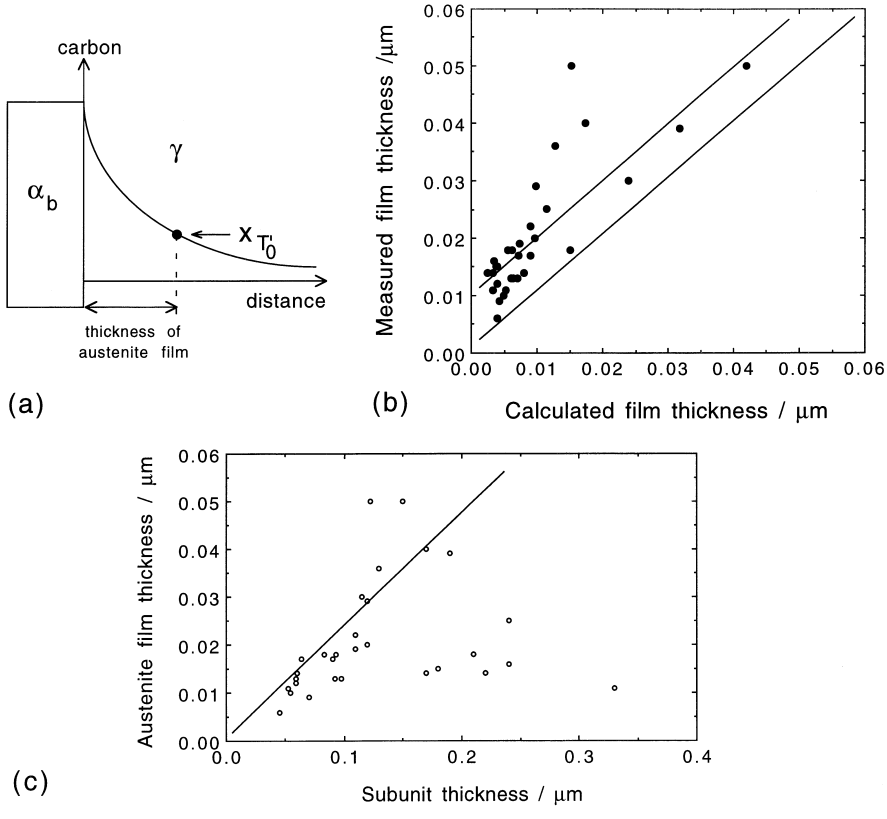

Fig. 5.8 (a) The thickness of the austenite film is determined by the point where the carbon concentration in the residual austenite is $x_{T_0'}$. (b) Comparison of measured and calculated austenite film thicknesses for a variety of alloys. (c) Austenite film thickness versus that of the adjacent bainite sub-unit (Chang and Bhadeshia, 1995).

the steel composition and transformation temperature. In one example the bainite reaction stopped in a matter of minutes, with pearlite growing from the residual austenite after some 32 h at the transformation temperature of 450 °C. In another example, isothermal reaction to lower bainite at 478 °C was completed within 30 min, but continued heat treatment for 43 days caused the incredibly slow reconstructive transformation to two different products. One of these was alloy-pearlite which nucleated at the austenite grain boundaries and which developed as a separate reaction (Fig. 4.5a). The other involved the irregular, epitaxial and reconstructive growth of ferrite from the existing bainite. The extent of ferrite growth in 43 days was comparable to the thickness

[12:17 3/9/01 C:/3B2 Templates/keith/3750 BAINITE.605/3750-005.3d] Ref: 0000 Auth: Title: Chapter 00 Page: 127 117-128

of the bainite plates, which took just a few seconds to form (Bhadeshia, 1981b, 1982b).

The two-stage decomposition of austenite is more difficult to establish for plain carbon steels where the reaction rates are large, with the pearlite reaction occurring a few seconds after bainite (Klier and Lyman, 1944).

5.5 Summary

The thermodynamic description of the bainite reaction is linked to its mechanism of growth and depends on the behaviour of solute atoms during transformation. By far the largest contribution to the stored energy of bainite is due to the invariant-plane strain shape deformation. The contributions from interfacial area are by comparison negligible during the growth stage. The dislocation density of bainite has its origins in the plastic accommodation of the shape change. The energy of the dislocations is therefore already accounted for in the estimate of an elastically accommodated shape change.

Substitutional solutes do not partition at all during the bainite reaction. Their primary effect is through their influence on the relative thermodynamic stabilities of the austenite and ferrite phases. The trapping of solutes in the bainite raises its free energy.

The fact that the transformation stops well before equilibrium is achieved is consistent with a mechanism in which growth is diffusionless, although the carbon atoms are partitioned soon afterwards from supersaturated ferrite.

[12:17 3/9/01 C:/3B2 Templates/keith/3750 BAINITE.605/3750-005.3d] Ref: 0000 Auth: Title: Chapter 00 Page: 128 117-128

6 *Kinetics*

There are three distinct events in the evolution of bainite (Fig. 6.1). A sub-unit nucleates at an austenite grain boundary and lengthens until its growth is arrested by plastic deformation within the austenite. New sub-units then nucleate at its tip, and the sheaf structure develops as this process continues. The average lengthening rate of a sheaf must be smaller than that of a sub-unit because of the delay between successive sub-units. The volume fraction of bainite depends on the totality of sheaves growing from different regions in the sample. Carbide precipitation influences the reaction rate by removing carbon either from the residual austenite or from the supersaturated ferrite.

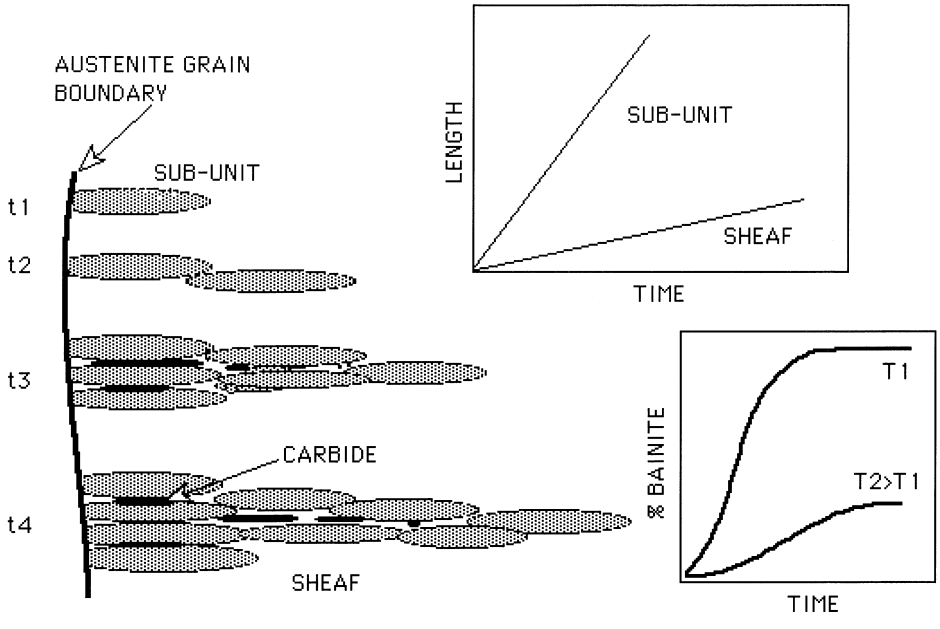

Fig. 6.1 The microstructural features relevant in the kinetic description of a bainitic microstructure. There is the lengthening of sub-units and of sheaves, the latter by the repeated nucleation of sub-units, the precipitation of carbides, and the change in volume fraction as a function of time and temperature.

6.1 Thermodynamics of Nucleation

It was shown in Chapter 5 that the equilibrium compositions $x^{\alpha\gamma}$ and $x^{\gamma\alpha}$ of ferrite and austenite respectively, are obtained using the common tangent construction. The same construction can be used to determine the change in free energy $\Delta G^{\gamma\rightarrow\gamma'+\alpha}$ when austenite of composition $\overline{x}$ decomposes into the equilibrium mixture of ferrite and carbon-enriched austenite (γ'), Fig. 6.2a.

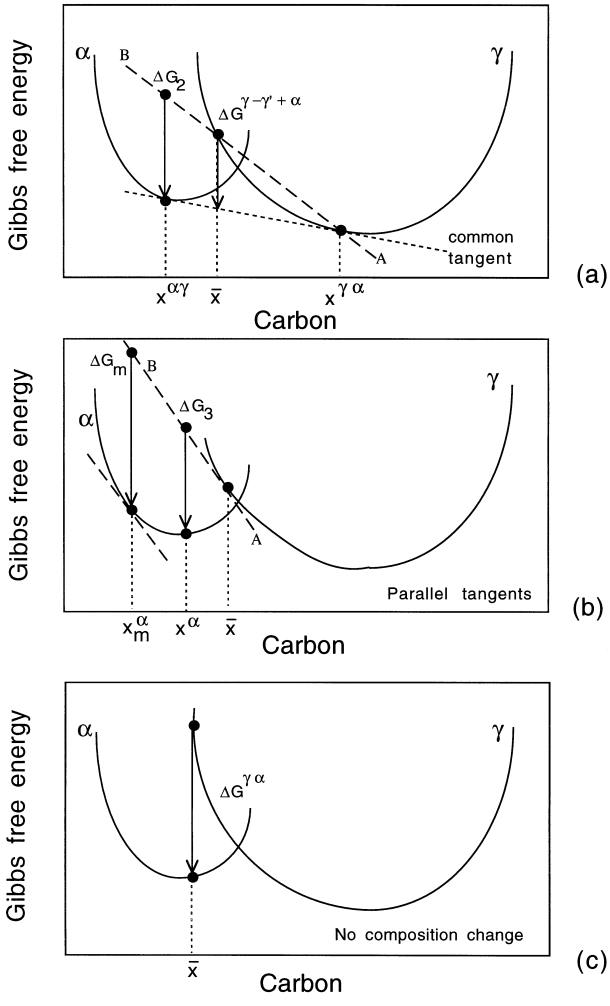

Fig. 6.2 Free energy diagrams illustrating the chemical free energy changes during the nucleation and growth of ferrite from austenite of composition $\overline{x}$. The term γ' refers to austenite which is enriched in carbon as a result of the decomposition of austenite of composition $\overline{x}$ into a mixture of ferrite and austenite.

The equilibrium fraction of ferrite is given by the lever rule as $(x^{\gamma\alpha} - \overline{x})/(x^{\gamma\alpha} - x^{\alpha\gamma})$. It follows that the free energy change per mole of ferrite is

$$\Delta G_2 = \Delta G^{\gamma \rightarrow \gamma' + \alpha} \times \frac{x^{\gamma\alpha} - x^{\alpha\gamma}}{x^{\gamma\alpha} - \overline{x}}$$

(Fig. 6.2a).

There is a significant change in the chemical composition of the austenite when it changes into the equilibrium mixture of ferrite and austenite. A ferrite nucleus on the other hand has such a small volume that it hardly affects the composition of the remaining austenite. The calculation of the free energy change associated with nucleation must therefore take into account that only a minute quantity of ferrite is formed. Consider the change ΔG_2 as austenite decomposes to a mixture of ferrite and enriched austenite of composition $x^{\gamma} = x^{\gamma\alpha}$. As the fraction of ferrite is reduced, x^{γ} and $\overline{x}$ move towards each other causing the line AB to tilt upwards. In the limit that $x^{\gamma} = \overline{x}$, AB becomes tangential to the curve at $\overline{x}$. The free energy change for the formation of a mole of ferrite nuclei of composition x^{α} is then given by ΔG_3, Fig. 6.2b.

The greatest reduction in free energy during nucleation is obtained if the composition of the ferrite nucleus is set to a value x_m, given by a tangent to the ferrite free energy curve which is parallel to the tangent to the austenite free energy curve at $\overline{x}$, as shown in Fig. 6.2b. This maximum possible free energy change for nucleation is designated ΔG_m.

There is simplification when the transformation occurs without composition change (Fig. 6.2c). The change $\Delta G^{\gamma \rightarrow \alpha}$ is the vertical distance between the austenite and ferrite free energy curves at the composition of interest.

6.1.1 Transformation-Start Temperature

It is a common observation that the Widmanstätten ferrite-start (W_S) and bainite-start (B_S) temperatures are more sensitive to the steel composition than is the Ae_3 temperature. This indicates that the influence of solutes on the nucleation of Widmanstätten ferrite and bainite is more than just thermodynamic (Fig. 6.3a).

Some clues to this behaviour come from studies of time-temperature-transformation diagrams, which consist essentially of two C-curves. The lower C-curve has a characteristic flat top at a temperature T_h, which is the highest temperature at which ferrite can form by displacive transformation (Fig. 6.3b). The transformation product at T_h may be Widmanstätten ferrite or bainite.

The driving force ΔG_m available for nucleation at T_h, is plotted in Fig. 6.4a, where each point comes from a different steel. The transformation product at T_h can be Widmanstätten ferrite or bainite, but it is found that there is no need to distinguish between these phases for the purposes of nucleation. The same

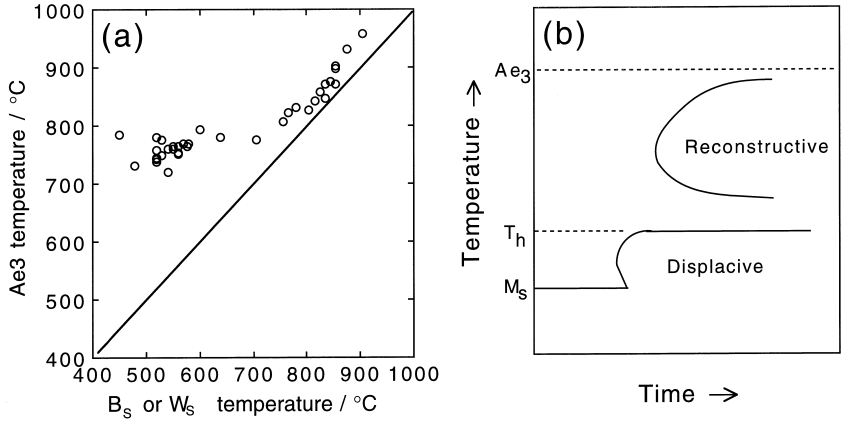

Fig. 6.3 (a) The variation of the Widmanstätten ferrite-start and bainite-start temperatures as a function of the Ae_3 temperature of the steel concerned (Ali, 1990). (b) Schematic TTT diagram illustrating the two C-curves and the T_h temperature.

nucleus can develop into either phase depending on the prevailing thermodynamic conditions. The analysis proves that carbon must partition during the nucleation stage in order always to obtain a reduction in free energy. The situation illustrated in Fig. 6.4b is not viable since diffusionless nucleation would in some cases lead to an increase in the free energy.

The plots in Fig. 6.4 are generated using data from diverse steels. Figure 6.4a represents the free energy change ΔG_m at the temperature T_h where displacive transformation first occurs. The free energy change can be calculated from readily available thermodynamic data. It follows that Fig. 6.4a can be used to estimate T_h for any steel. The equation fitted to the data in Fig. 6.4a is (Ali and Bhadeshia, 1990):

$$G_N = C_1(T - 273.18) - C_2 \qquad \mathrm{J\,mol^{-1}} \tag{6.1}$$

where the fitting constants are found to be $C_1 = 3.637 \pm 0.2\,\mathrm{J\,mol^{-1}\,K^{-1}}$ and $C_2 = 2540 \pm 120\,\mathrm{J\,mol^{-1}}$ for the temperature range 670–920 K. G_N is to be regarded as a *universal nucleation function*, because it defines the minimum driving force necessary to achieve a perceptible nucleation rate for Widmanstätten ferrite or bainite in any steel.

6.1.2 *Evolution of the Nucleus*

The nucleus is identical for Widmanstätten ferrite and for bainite; it must therefore be growth which distinguishes them. But what determines whether the nucleus evolves into bainite or Widmänsstatten ferrite?

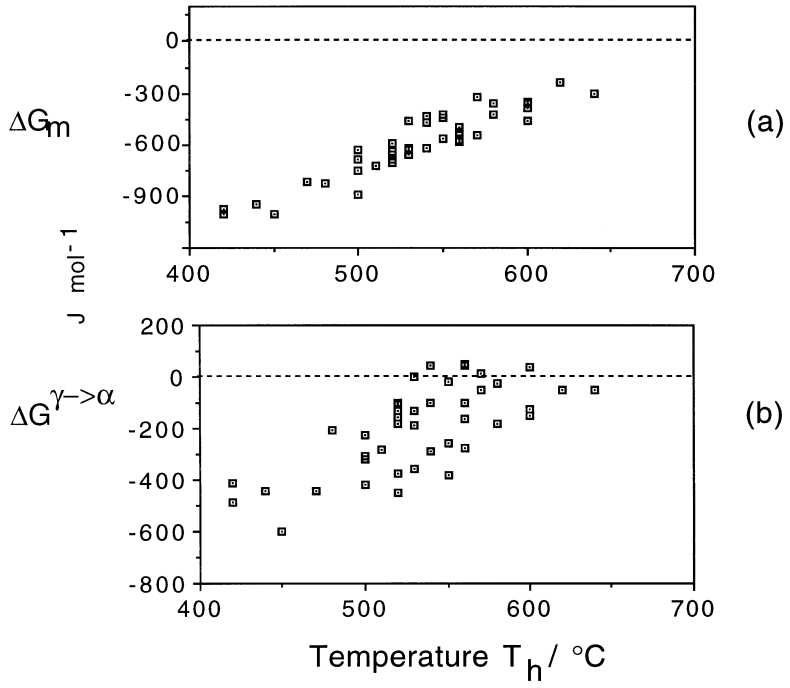

Fig. 6.4 The free energy change necessary in order to obtain a detectable degree of transformation. Each point represents a different steel and there is no distinction made between Widmanstätten ferrite or bainite. (a) Calculated assuming the partitioning of carbon during nucleation. (b) Calculated assuming that there is no change in composition during nucleation. After Bhadeshia, 1981a.

The answer is straightforward. If diffusionless growth cannot be sustained at T_h then the nucleus develops into Widmanstätten ferrite so that T_h is identified with W_S. A larger undercooling is necessary before bainite can be stimulated. If, however, the driving force at T_h is sufficient to account for diffusionless growth, then $T_h = B_S$ and Widmanstätten ferrite does not form at all.

It follows that Widmänsstatten ferrite forms below the Ae_3 temperature when:

$$\begin{aligned} \Delta G^{\gamma\rightarrow\gamma'+\alpha} &< -G_{SW} \\ \Delta G_m &< G_N \end{aligned} \qquad (6.2)$$

where G_{SW} is the stored energy of Widmanstätten ferrite (about 50 $\mathrm{J\,mol^{-1}}$). The first of these conditions ensures that the chemical free energy change exceeds the stored energy of the Widmanstätten ferrite, and the second that there is a detectable nucleation rate.

Bainite is expected below the T_0' temperature when:

$$\Delta G^{\gamma\rightarrow\alpha} < -G_{SB} \tag{6.3}$$

$$\Delta G_m < G_N \tag{6.4}$$

where G_{SB} is the stored energy of bainite (about 400 J mol^{-1}). The universal function, when used with these conditions, allows the calculation of the Widmanstätten ferrite-start and bainite-start temperatures from a knowledge of thermodynamics alone.

In this scheme, carbon is partitioned during nucleation but in the case of bainite, not during growth which is diffusionless. There is no inconsistency in this concept since a greater fraction of the free energy becomes available as the particle surface to volume ratio, and hence the influence of interfacial energy, decreases. The theory explains why both Widmanstätten ferrite and bainite can form during the early stages of isothermal transformation at temperatures close to B_S (Chang, 1999).

The scheme is illustrated in Fig. 6.5 which incorporates an additional function $G_N^{\alpha'}$ representing the critical driving force $\Delta G^{\gamma\rightarrow\alpha}\{M_S\}$ needed to stimulate martensite by an athermal, diffusionless nucleation and growth mechanism. Whereas it is reasonable to set $G_N^{\alpha'}$ to a constant value for low alloy steels

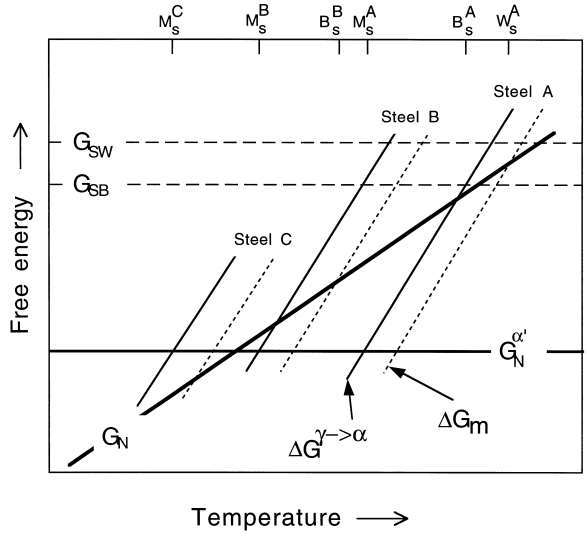

Fig. 6.5 Free energy curves for a low (A), medium (B) and high (C) alloy steel showing the conditions necessary for the nucleation and growth of Widmanstätten ferrite, bainite and martensite.

(Bhadeshia, 1981c,d) a function dependent on the strength of the austenite has to be used for steels containing large concentrations of solute (Ghosh and Olson, 1994).

The three common displacive transformations in steels include Widmanstätten ferrite, bainite and martensite. It is intriguing that they are not all found in every steel. Only martensite occurs in Fe–28Ni–0.4C wt%, whereas only bainite and martensite are found in Fe–4Cr–0.3C wt%. This is readily explained: steels *A*, *B* and *C* in Fig. 6.5 contain increasing quantities of austenite stabilising elements, with the driving force for transformation decreasing as the alloy content increases. In steel *A*, all three transformations are expected in turn as the temperature is reduced. For steel *B*, the temperature at which Widmanstätten ferrite nucleation becomes possible also corresponds to that at which bainite can grow. Bainite has a kinetic advantage so Widmanstätten ferrite does not form. Further alloying increases the stability of the austenite so much that the nucleation of Widmanstätten ferrite and bainite is suppressed to temperatures below M_S in which case they do not form at all.

The nucleation condition for bainite (eq. 6.4) becomes redundant for any steel in which Widmanstätten ferrite precedes bainite because they have a common nucleation mechanism.

An interesting prediction emerges from this rationale. For some steels the thermodynamic characteristics are such that the ΔG_m curve intersects the G_N function at two points, Fig. 6.6a (Bhadeshia and Svensson, 1989c). Widmanstätten ferrite then occurs at high temperatures, there is an intermediate temperature range where neither Widmanstätten ferrite nor bainite can nucleate, until bainite formation becomes possible at a lower temperature. The lower *C*-curve thus splits into two segments, one for Widmanstätten ferrite and a lower temperature segment for bainite (Fig. 6.6b). This prediction from theory has been confirmed experimentally (Ali and Bhadeshia, 1991).

Finally, because G_N decreases linearly with T_h, it is expected that the W_S and B_S temperatures are depressed to a greater extent by solute additions than the Ae_3 temperature. A larger driving force is needed to achieve a given rate of nucleation when the transformation is depressed to lower temperatures by alloying. A justification for the form of the universal nucleation function G_N is given in the next section.

6.2 Possible Mechanisms of Nucleation

Phase fluctuations occur as random events due to the thermal vibration of atoms. An individual fluctuation may or may not be associated with a reduction in free energy, but it can only survive and grow if there is a reduction. There is a cost associated with the creation of a new phase, the interface energy,

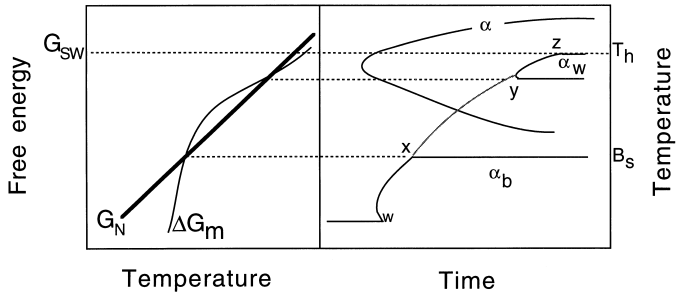

Fig. 6.6 (a) Free energy curves for the nucleation of Widmanstätten ferrite and bainite in a low alloy steel for which the ΔG_m and G_N curves exhibit a double intersection. (b) Calculated TTT diagram for the same steel, showing how Widmanstätten ferrite and bainite form separate C curves. The Widmanstätten ferrite and bainite C curves would ordinarily be just one curve, joined by the line *wxyz*. After Ali and Bhadeshia (1991).

a penalty which becomes smaller as the particle surface to volume ratio decreases. In a metastable system this leads to a critical size of fluctuation beyond which growth is favoured.

Consider the homogeneous nucleation of α from γ. For a spherical particle of radius r with an isotropic interfacial energy $\sigma_{\alpha\gamma}$, the change in free energy as a function of radius is:

$$\Delta G = \frac{4}{3}\pi r^3 \Delta G_{CHEM} + \frac{4}{3}\pi r^3 \Delta G_{STRAIN} + 4\pi r^2 \sigma_{\alpha\gamma} \qquad (6.5)$$

where $\Delta G_{CHEM} = G_V^{\alpha} - G_V^{\gamma}$, G_V is the Gibbs free energy per unit volume of α and G_{STRAIN} is the strain energy per unit volume of α. The variation in ΔG with size is illustrated in Fig. 6.7; the activation barrier and critical size obtained using equation 6.5 are given by:

$$G^* = \frac{16\pi\sigma_{\alpha\gamma}^3}{3(\Delta G_{CHEM} + \Delta G_{STRAIN})^2} \qquad \text{and} \qquad r^* = \frac{2\sigma_{\alpha\gamma}}{\Delta G_{CHEM} + \Delta G_{STRAIN}} \qquad (6.6)$$

The important outcome is that in classical nucleation the activation energy varies inversely with the square of the driving force. And the mechanism involves random phase fluctuations. It is questionable whether this applies to cases where thermal activation is in short supply. In particular, an activation barrier must be very small indeed if the transformation is to occur at a proper rate at low temperatures.

One mechanism in which the barrier becomes sufficiently small involves the spontaneous dissociation of specific dislocation defects which are already present in the parent phase (Christian, 1951; Olson and Cohen, 1976). The disloca-

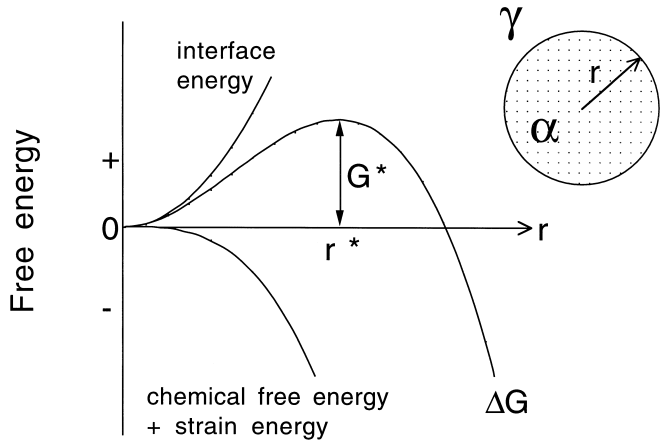

Fig. 6.7 The activation energy barrier G^* and the critical nucleus size r^* according to classical nucleation theory based on heterophase fluctuations.

tions are glissile so the mechanism does not require diffusion. The only barrier is the resistance to the glide of the dislocations. The nucleation event cannot occur until the undercooling is sufficient to support the faulting and strains associated with the dissociation process that leads to the creation of the new crystal structure (Fig. 6.8).

The free energy per unit area of fault plane is:

$$G_F = n_P \rho_A (\Delta G_{CHEM} + G_{STRAIN}) + 2\sigma_{\alpha\gamma}\{n_P\} \tag{6.7}$$

where n_P is the number of close-packed planes participating in the faulting process, ρ_A is the spacing of the close-packed planes on which the faulting is assumed to occur. The fault energy can become negative when the austenite becomes metastable.

For a fault bounded by an array of n_P dislocations each with a Burger's vector of magnitude b, the force required to move a unit length of dislocation array is $n_P \tau_o b$. τ_o is the shear resistance of the lattice to the motion of the dislocations. G_F provides the opposing stress via the chemical free energy change ΔG_{CHEM}; the physical origin of this stress is the fault energy which becomes negative so that the partial dislocations bounding the fault are repelled. The defect becomes unstable, i.e. nucleation occurs, when

$$G_F = -n_P \tau_o b \tag{6.8}$$

Take the energy barrier between adjacent equilibrium positions of a dislocation to be G_o^*. An applied shear stress τ has the effect of reducing the height of this barrier (Conrad, 1964; Dorn, 1968):

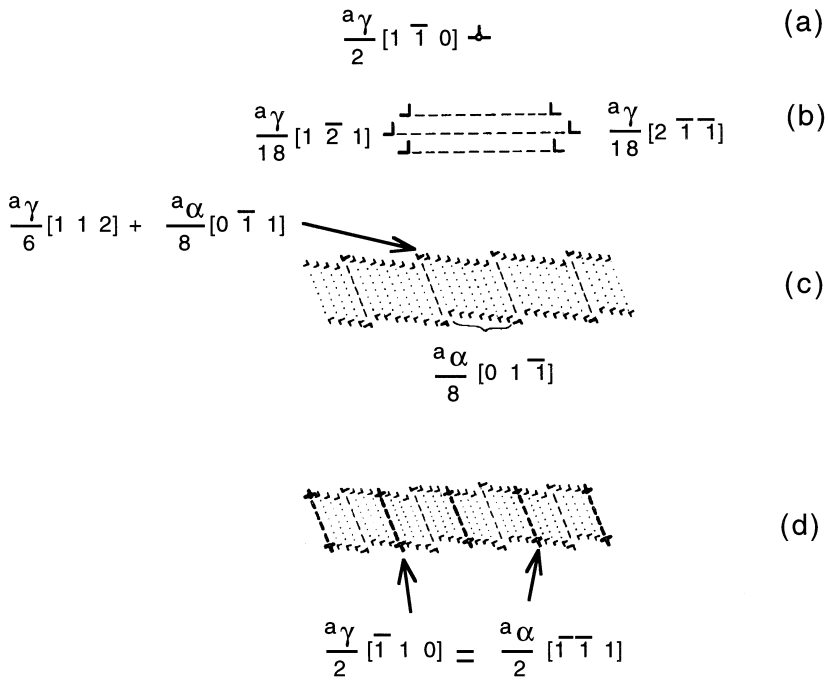

Fig. 6.8 Olson and Cohen model for the nucleation of α martensite. (a) Perfect screw dislocation in austenite. (b) Three-dimensional dissociation over a set of three close-packed planes. The faulted structure is not yet that of α. (c) Relaxation of fault to a body-centred cubic structure with the introduction of partial dislocations in the interface. (d) Addition of perfect screw dislocations which cancel the long range strain field of the partials introduced in (c).

$$G^* = G_o^* - (\tau - \tau_\mu)v^* \tag{6.9}$$

where v^* is an activation volume and τ_μ is the temperature independent resistance to dislocation motion (Fig. 6.9). In the context of nucleation, the stress τ is not externally applied but comes from the chemical driving force. On combining the last three equations we obtain

$$G^* = G_o^* + \left[\tau_\mu + \frac{\rho_A}{b}G_{STRAIN} + \frac{2\sigma}{n_P b}\right]v^* + \frac{\rho_A v^*}{b}\Delta G_{CHEM} \tag{6.10}$$

It follows that with this model of nucleation the activation energy G^* will decrease *linearly* as the magnitude of the driving force ΔG_{CHEM} increases. This direct proportionality contrasts with the inverse square relationship of classical theory.

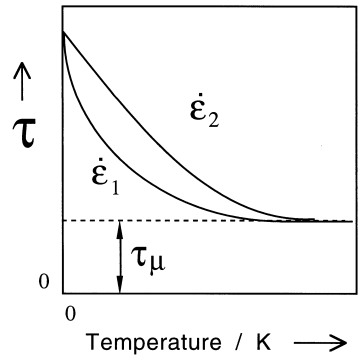

Fig. 6.9 Temperature dependence of the applied stress necessary to move a dislocation at two different strain rates ($\dot{\epsilon}_2 > \dot{\epsilon}_1$). τ_μ is the athermal resistance which never vanishes. After Conrad (1964).

6.3 Bainite Nucleation

The linear relationship between G_N and T_h (Fig. 6.4) can be used to deduce whether nucleation involves dislocation dissociation or heterophase fluctuations (Bhadeshia, 1981a). The nucleation rate I_V will have a temperature dependence due to the activation energy:

$$I_V \propto \nu \exp\{-G^*/RT\} \tag{6.11}$$

where ν is an attempt frequency. It follows that

$$-G^* \propto \beta T \qquad \text{where} \qquad \beta = R \ln\{I_V/\nu\} \tag{6.12}$$

We now assume that there is a specific nucleation rate at T_h, irrespective of the type of steel, in which case β is a constant, negative in value since the attempt frequency should be larger than the actual rate. This gives the interesting result that

$$G_N \propto \beta T \tag{6.13}$$

which is precisely the relationship observed experimentally. This is evidence for nucleation by the dissociation of dislocations with the activation energy proportional to the driving force, as opposed to the inverse square relationship predicted by classical theory. The activation energy G^* in this model comes from the resistance of the lattice to the motion of dislocations.

Nucleation corresponds to a point where the slow, thermally activated migration of glissile partial dislocations gives way to rapid, breakaway dissociation. This is why it is possible to observe two sets of transformation units, the first consisting of very fine embryo platelets below the size of the operational nucleus, and the second the size corresponding to the rapid growth

to the final size. Intermediate sizes are rarely observed because the time period for the second stage is expected to be much smaller than that for the first. Figure 6.10 shows that in addition to the fully growth sub-units (a few micrometers in length), there is another population of much smaller (submicron) particles which represent the embryos at a point in their evolution prior to breakaway dissociation.

6.4 Empirical Equation for the Bainite-Start Temperature

Steven and Haynes (1956) measured the bainite-start temperature by isothermally transforming a large number of engineering steels with chemical composition in the range (wt%):

Carbon	0.1–0.55	Nickel	0.0–5.0
Silicon	0.1–0.35	Chromium	0.0–3.5
Manganese	0.2–1.7	Molybdenum	0.0–1.0

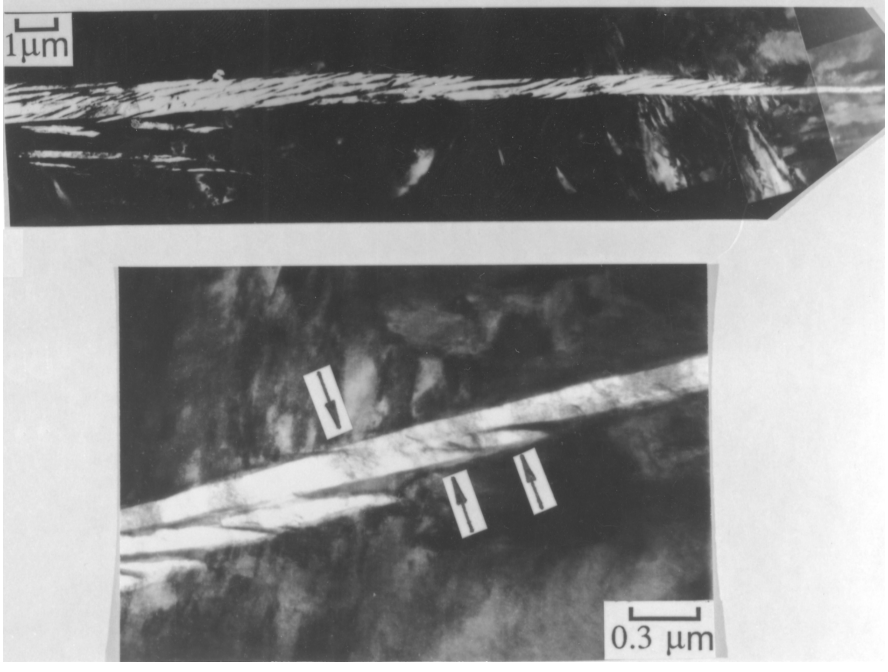

Fig. 6.10 Transmission electron micrograph of a sheaf of bainite in a partially transformed sample. A region near the tip of the sheaf in (a) is enlarged in (b). The arrows in (b) indicate possible sub-operational embryos which are much smaller than the fully grown sub-units seen in (a). After Olson *et al*. (1989).

and expressed their results empirically as:

$$B_S{}^{\circ}\mathrm{C} = 830 - 270w_C - 90w_{Mn} - 37w_{Ni} - 70w_{Cr} - 83w_{Mo} \tag{6.14}$$

where w_i is the wt% of element i in solid solution in austenite.

6.5 The Nucleation Rate

The linear dependence of the activation energy for nucleation on the driving force can be substituted into a nucleation rate equation to obtain:[†]

$$\begin{aligned} I_V &= C_3 \exp\left\{ -\frac{G^*}{RT} \right\} \\ &= C_3 \exp\left\{ -\frac{C_4 + C_5 \Delta G_m}{RT} \right\} \end{aligned} \tag{6.15}$$

where ΔG_m is the maximum value of ΔG_{CHEM} (Fig. 6.2c) and C_i are positive constants. The nucleation rate at T_h is obtained by setting $\Delta G_m = G_N$

$$I_{T_h} = C_3 \exp\left\{ -\frac{C_4 + C_5 G_N}{RT_h} \right\} \tag{6.16}$$

It follows that

$$I_V = I_{T_h} \exp\left\{ -\frac{C_4 \Delta T}{RTT_h} - \frac{C_5}{R}\left(\frac{\Delta G_m}{T} - \frac{G_N}{T_h} \right) \right\} \tag{6.17}$$

with $\Delta T = T_h - T$. Recall that the G_N function was justified with martensite nucleation theory assuming that the nucleation rate I_{T_h} is the same for all steels at T_h. For two different steels A and B,

$$\frac{I_{T_h^A}}{I_{T_h^B}} = \exp\left\{ -\frac{(C_4 - C_2C_5)(T_h^A - T_h^B)}{RT_h^A T_h^B} \right\} \tag{6.18}$$

Since $I_{T_h^A} = I_{T_h^B}$ it follows that $C_4 = C_2 \times C_5$ so that

$$I_V = C_3 \exp\left\{ -\frac{C_4}{RT} - \frac{C_4 \Delta G_m}{C_2 RT} \right\} \tag{6.19}$$

In this equation the constant C_2 is known since it comes from the slope of the G_N function (equation 6.1) so the two unknowns are C_3 and C_4 which are obtained by fitting to experimental data. The pre-exponential factor C_3 is the product of a number density of nucleation sites (N_V^0) and an attempt frequency (ν).

[†]Bhadeshia (1982b); Rees & Bhadeshia (1992); Chester & Bhadeshia (1997); Singh (1998).

6.6 Growth Rate

The displacement of an interface requires the atoms of the parent to transfer into and adopt the crystal structure of the product phase. The ease with which this happens determines the interface mobility. There may also be a partitioning of solutes in which case diffusion may limit the movement of the interface. The two processes of diffusion and mobility are in series; the velocity as calculated from the interface mobility must therefore match that due to the diffusion of solute ahead of the interface. Both processes dissipate the available free energy, so motion is always under mixed control. However, a process is said to be diffusion-controlled when most of the free energy is dissipated in the diffusion of solute. Interface-controlled growth occurs when the larger proportion of the free energy is consumed in the transfer of atoms across the interface. The compositions of the phases at the moving interface during diffusion-controlled growth are given approximately by a tie-line of the phase diagram, and other circumstances are illustrated in Fig. 6.11.

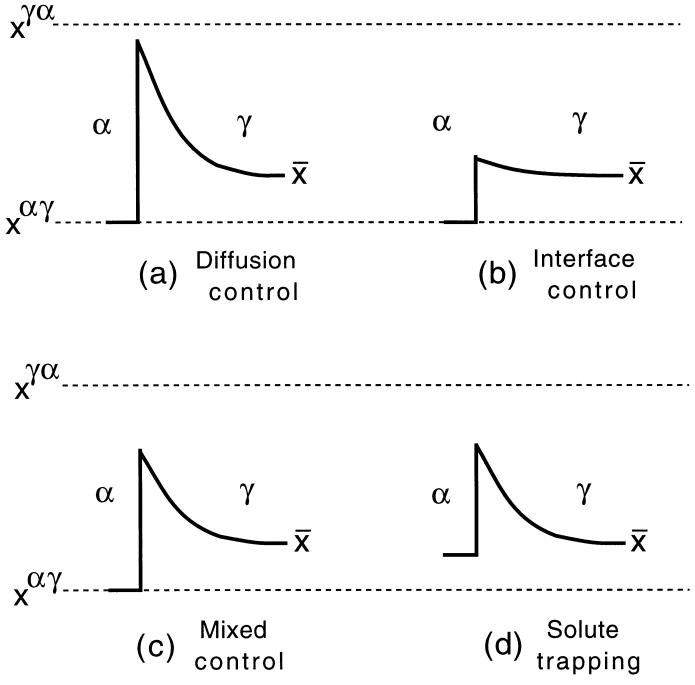

Fig. 6.11 Carbon concentration profiles at a moving α/γ interface. The terms $x^{\alpha\gamma}$, $x^{\gamma\alpha}$ and $\bar{x}$ refer to the equilibrium concentrations in the ferrite and austenite respectively, and the average concentration in the alloy as a whole. (a) Diffusion control. (b) Interface control. (c) Mixed control. (d) Solute trapping (discussed later).

6.6.1 Theory for the Lengthening of Plates

Particle dimensions during diffusion-controlled growth vary parabolically with time when the extent of the diffusion field increases with particle size. The growth rate thus decreases because the solute has to diffuse over ever increasing distances to reach the far-field concentration. Plates or needles can however grow at a constant rate because solute can be partitioned to their sides.

The partitioning of interstitial elements during displacive transformation should lead to diffusion-controlled growth because the glissile interface necessary for such transformation has the highest mobility. Iron and any substitutional solute atoms do not diffuse so their role is purely thermodynamic.

Trivedi (1970) has solved for the diffusion-controlled growth of plates whose shape approximates that of a parabolic cylinder (Fig. 6.12). The plate lengthening rate V_l at a temperature T for steady state growth is obtained by solving:

$$f_1 = \frac{x_r - \overline{x}}{x_r - x^{\alpha\gamma}}$$

$$f_1 = (\pi p)^{0.5} \exp\{p\}\mathrm{erfc}\{p^{0.5}\}\left[1 + \frac{V_l}{V_c} f_1 S_1\{p\} + \frac{r_c}{r} f_1 S_2\{p\}\right] \tag{6.20}$$

where the Péclet number is

$$p = V_l r / 2\overline{D} \tag{6.21}$$

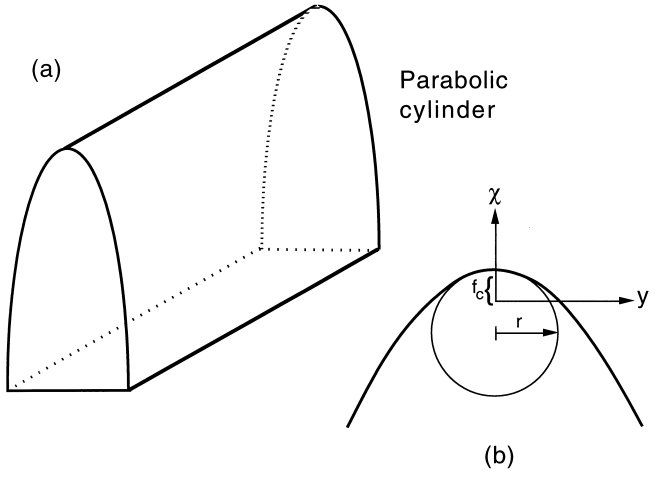

Fig. 6.12 (a) An illustration of the shape of a parabolic cylinder. (b) Definitions of the tip radius r, the focal distance f_c and the coordinates.

The weighted-average diffusion coefficient $\overline{D}$ for carbon in austenite is given by integrating D (the diffusivity at a specific concentration) over the range $\overline{x}$ to x_r, and then dividing the integral by this range.

The function $S_2\{p\}$ of equation 6.21 depends on the Péclet number (Fig. 6.13); it corrects for variation in composition due to changing curvature along the interface and has been evaluated numerically by Trivedi. The term containing S_1 is prominent when growth is not diffusion-controlled; V_c is the interface-controlled growth velocity of a flat interface. For diffusion-controlled growth, which is discussed first, V_c is very large when compared with V_l and the term containing it can be neglected.

x_r is the carbon concentration in the austenite at the plate tip. It may differ from the equilibrium carbon concentration $x^{\gamma\alpha}$ because of the Gibbs–Thompson capillarity effect (Christian, 1975); x_r decreases as interface curvature increases, and growth ceases at a critical radius r_c when $x_r = \overline{x}$. For a finite plate tip radius,

$$x_r = x^{\gamma\alpha}[1 + (\Gamma/r)] \tag{6.22}$$

where Γ is the capillarity constant given by (Christian, 1975):

$$\Gamma = \frac{\sigma^{\alpha\gamma} V_m}{RT} \frac{(1 - x^{\gamma\alpha})}{(x^{\alpha\gamma} - x^{\gamma\alpha})} \left[1 + \frac{d(\ln f_C\{x^{\gamma\alpha}\})}{d(\ln x^{\gamma\alpha})}\right]^{-1} \tag{6.23}$$

where $\sigma^{\alpha\gamma}$ is the interfacial energy per unit area, f_C is the activity coefficient of carbon in austenite, and V_m is the molar volume of ferrite. This assumes that the ferrite composition is unaffected by capillarity, since $x^{\alpha\gamma}$ is always very small. The critical plate tip radius r_c can be obtained by setting $x_r = \overline{x}$.

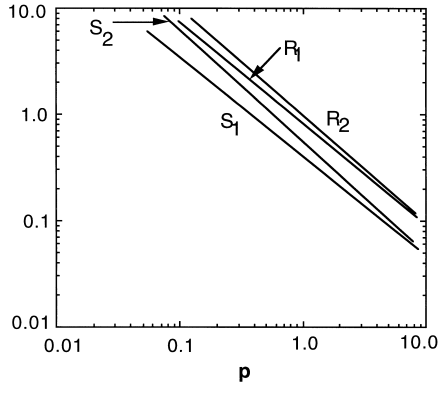

Fig. 6.13 Dependence of Trivedi's functions S_1, S_2, R_1 and R_2 on the Péclet number p.

Trivedi's solution for diffusion-controlled growth assumes a constant shape, but the solution is not strictly shape-preserving. The concentration x_r varies over the surface of the parabolic cylinder which should lead to a deviation from the parabolic shape. Trivedi claims that the variation in x_r has a negligible effect provided the tip radius is greater than $3r_c$.

Plate growth theory provides a relation between velocity and tip radius (Fig. 6.14). Additional theory is required to enable the choice of a particular tip radius and hence to fix V_l. Small tip radii favour fast growth due to the point effect of diffusion, but this is counteracted by the capillarity effect. Zener proposed that the plate should tend to adopt a tip radius which allows V_l to be maximised but this remains a hypothesis. Work on the dendritic growth of solid from liquid (formally an almost identical problem) has shown that the dendrites do not select the radius corresponding to the maximum velocity. The radius is determined instead by a shape stability criterion (Glicksman *et al*., 1976; Langer and Muller-Krumbhaar, 1978). If these results can be extrapolated to displacive transformations, and it is doubtful that they can given that the shape is constrained by strain energy minimisation, then calculated velocities would be greatly reduced. This does not fit experimental data where the lengthening rate is slightly higher that the maximum velocity predicted theoretically (Bhadeshia, 1985a).

The shape of ferrite plates is sometimes more needle-like (lath) than plate-like. Trivedi has obtained a steady-state solution for the diffusion-controlled growth of paraboloids of revolution (i.e. needles):

$$f_1 = p\exp\{p\}\mathrm{Ei}\{p\}\left[1+\frac{V_l}{V_c}f_1R_1\{p\}+\frac{r_c}{r}f_1R_2\{p\}\right] \qquad (6.24)$$

The tip radius r_c is twice as large as that for plates because there are two radii of curvature for a needle tip.

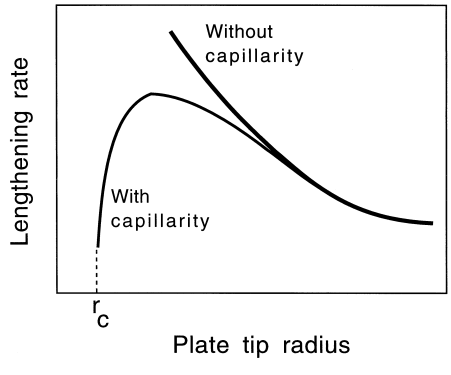

Fig. 6.14 Variation in lengthening rate as a function of the plate tip radius.

6.6.2 Growth Rate of Sheaves of Bainite

After nucleating at austenite grain surfaces, sheaves of bainite propagate by the repeated formation of sub-units, each of which grows to a limited size. New sub-units are favoured near the tips of existing platelets; nucleation in adjacent positions occurs at a much lower rate. Therefore, the overall shape of the sheaf is also that of a plate in three dimensions with growth limited only by austenite grain or twin boundaries.

Most direct observations have used optical microscopy and hence monitor the growth of *sheaves* rather than of the transformation unit which is only about 0.2 μm in thickness. Suppose that a sub-unit reaches its limiting size in a time period t_C, and that a time interval Δt elapses before the next one is stimulated, then the lengthening rate, V_S, of a sheaf is given by:

$$V_S = V_l\left(\frac{t_C}{t_C + \Delta t}\right) \tag{6.25}$$

where V_l is the average lengthening rate of a sub-unit.

Bainite sheaves lengthen at a constant rate although the data show considerable scatter, attributed to stereological effects (Speich and Cohen, 1960; Goodenow *et al*., 1963; Hawkins and Barford, 1972). Greater concentrations of carbon, nickel or chromium concentration reduce V_S. The growth of sheaves seems to occur at a constant aspect ratio although thickening continues when lengthening has stopped. This is not surprising since the sheaf can continue to grow by the sub-unit mechanism until the T_0' condition is achieved.

An assessment of sheaf data shows that the lengthening rate is greater than expected from diffusion-controlled growth, Fig. 6.15. This includes measurements on Fe–Ni–C alloys which are frequently (incorrectly) used to justify the existence of some sort of a solute drag effect.

6.6.3 Growth Rate of Sub-Units of Bainite

The growth rate of martensite can be so fast as to be limited only by the speed of sound in the metal. Although bainite grows rapidly, the lengthening rate is much smaller than that for martensite. The interface moves relatively slowly even though it is glissile. This is probably because of the plastic work that is done as the bainite grows. A good analogy is to compare brittle failure in a glass where cracks propagate rapidly, with cleavage failure in metals which is not as rapid because of the plastic zone which has to move with the crack tip.

The lengthening rate of sub-units has been measured using hot-stage photoemission electron microscopy. Electrons are excited from the surface of the sample using incident ultraviolet radiation, and it is these photo-emitted electrons which form the image. The technique can resolve individual sub-units of

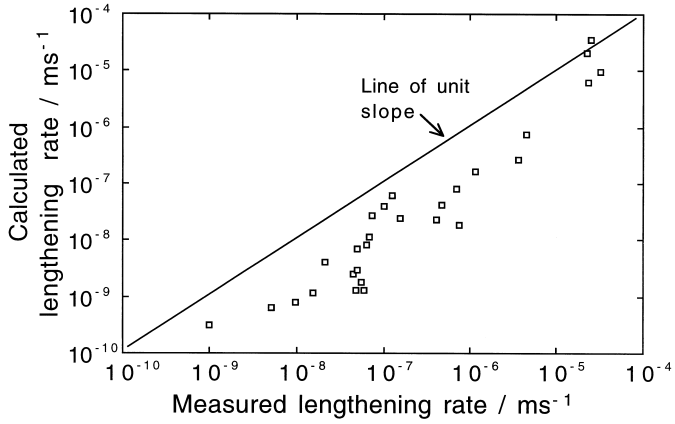

Fig. 6.15 Comparison of published data on the lengthening rate of bainite sheaves against those calculated assuming paraequilibrium carbon-diffusion controlled lengthening (Ali and Bhadeshia, 1989).

bainite. Fig. 6.16 illustrates a series of photoemission electron micrographs taken at 1 s intervals, showing the growth of bainite sub-units. The measured lengthening rate of the arrowed sub-unit is $75\,\mu\mathrm{m\,s^{-1}}$. This is many orders of magnitude larger than calculated assuming paraequilibrium at the transformation front ($0.083\,\mu\mathrm{m\,s^{-1}}$). Lengthening occurs at a rate much faster than expected from carbon diffusion-control growth.

There are interesting observations on the thickening of bainite sub-units. The thickness can increase even after lengthening has halted. An elastically accommodated plate tends to adopt the largest aspect ratio consistent with a balance between the strain energy and the free energy change driving the transformation, Fig. 6.17, in order to achieve thermoelastic equilibrium (Olson and Cohen, 1977).

Bainite plates are not elastically accommodated but it should be possible for the thickness of a plate to increase at constant length if the process is captured at an early stage. Fig. 6.17b shows a large plate of bainite which formed first followed by smaller orthogonal plates. The larger plate is seen to bow between the smaller plates whose tips act as pinning points. The smoothly curved regions of the interface between the pinning points prove that the interface moves continuously rather than by a step mechanism.

6.6.4 Solute Drag

Solute drag is a process in which free energy is dissipated in the diffusion of solute atoms *within the interface*; these are the atoms which in a stationary

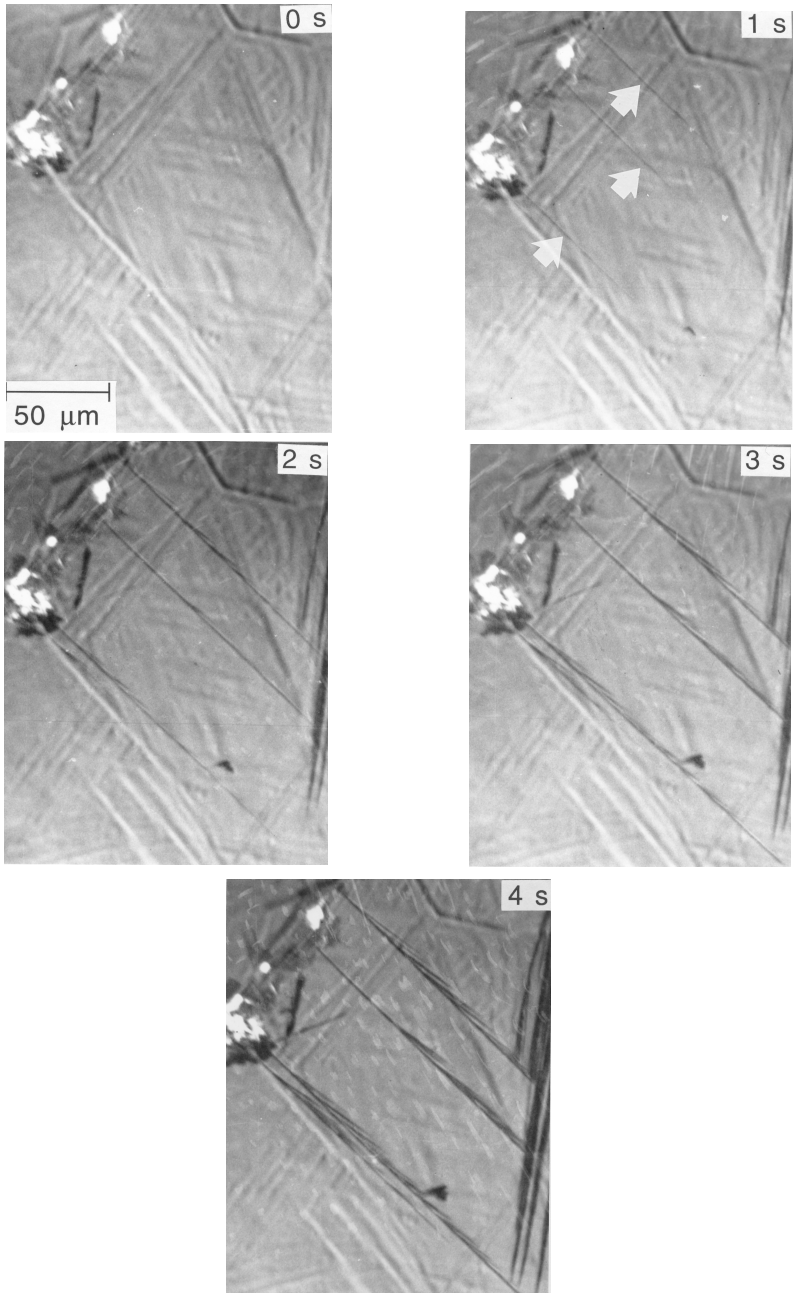

Fig. 6.16 Photoemission electron microscope observations on the growth of individual sub-units in a bainite sheaf (Bhadeshia, 1984). The pictures are taken at 1 s intervals during transformation at 380 °C in a Fe–0.43C–2.02Si–3Mn wt% alloy. The micrograph at 0 s is fully austenitic, the relief being a residue from an earlier experiment.

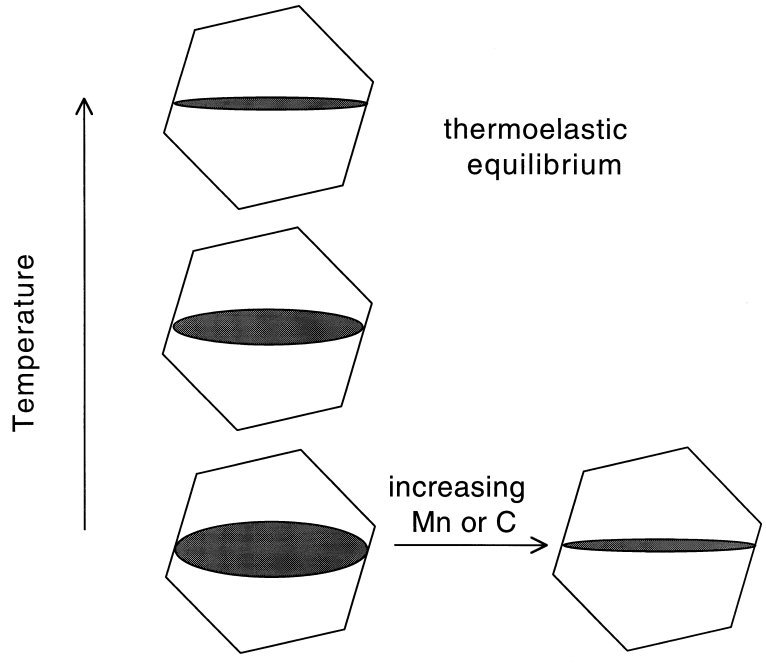

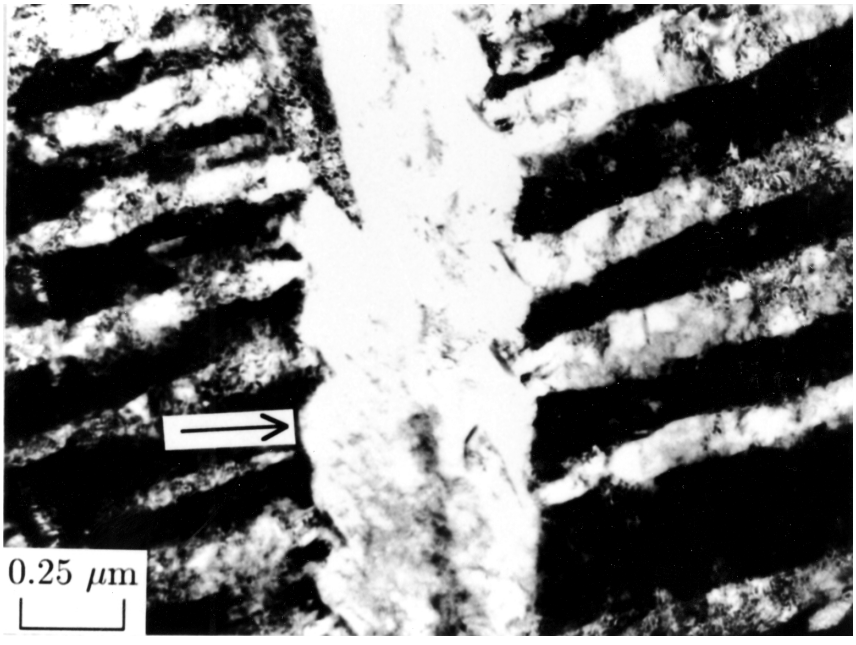

Fig. 6.17 (a) Effect of thermoelastic equilibrium on the aspect ratio of a plate with a fixed length. (b) Bowing of α_b/γ interface at strong pinning points, particularly prominent in regions identified by arrows (Chang and Bhadeshia, 1995b).

interface are said to be segregated or desegregated in the structure of the interface. The phenomenon is similar to the drag on dislocations when atoms are attracted to the dislocation cores. Chapter 2 contains a discussion of the atomic resolution experiments which show that there is no excess concentration of solute at the bainite/austenite interface. Consequently, there is no reason to expect solute drag effects during the bainite reaction.

6.7 Partitioning of Carbon from Supersaturated Bainitic Ferrite

It is better for the carbon that is trapped in bainite to partition into the residual austenite where it has a lower chemical potential. Consider a plate of thickness w with a one-dimensional flux of carbon along z which is normal to the α/γ interface, with origin at the interface and z defined as positive in the austenite (Kinsman and Aaronson, 1967). A mass conservation condition gives (Bhadeshia, 1988):

$$\frac{1}{2}w(\overline{x} - x^{\alpha\gamma}) = \int_0^\infty [x_\gamma\{z, t_d\} - \overline{x}]dz \tag{6.26}$$

where $x^{\alpha\gamma}$ and $x^{\gamma\alpha}$ are the paraequilibrium carbon concentrations in α and γ respectively, allowing for stored energy. Since the diffusion rate of carbon in austenite is slower than in ferrite, the rate of decarburisation will be determined by the diffusivity in the austenite. The concentration of carbon in austenite at the interface remains constant for times $0 < t < t_d$, after which it steadily decreases as homogenisation occurs. The concentration profile in the austenite is given by:

$$x_\gamma = \overline{x} + (x^{\gamma\alpha} - \overline{x})\text{erfc}\left\{\frac{w}{2(\overline{D}t_d)^{\frac{1}{2}}}\right\} \tag{6.27}$$

which on integration gives:

$$t_d^{\frac{1}{2}} = \frac{w(\overline{x} - x^{\alpha\gamma})\pi^{\frac{1}{2}}}{4\overline{D}^{\frac{1}{2}}(x^{\gamma\alpha} - \overline{x})} \tag{6.28}$$

Some results from this analysis are illustrated in Fig. 6.18.

Equation 6.28 does not allow for the coupling of fluxes in the austenite and ferrite. It assumes that the diffusivity in the ferrite is so large, that any gradients there are eliminated rapidly. A flux balance must in general be satisfied as follows:

$$D_\alpha \frac{\partial x^\alpha}{\partial z} = \overline{D}\frac{\partial x^{\gamma\alpha}}{\partial z} \tag{6.29}$$

where D_α is the diffusivity of carbon in the ferrite, x^α is the concentration of carbon in the ferrite at the interface with the gradients evaluated at the interface. Since $D_\alpha \gg D_\gamma$, x^α will inevitably deviate from $x^{\alpha\gamma}$ in order to maintain the flux balance. It will only reach the equilibrium value towards the end of the partitioning process. The gradients in the ferrite must also increase with $x^{\gamma\alpha}$; the partitioning process could then become limited by diffusion in the ferrite. As a consequence, the diffusion time as predicted by the finite difference method becomes larger than that estimated by the approximate analytical equation when the transformation temperature is decreased or $x^{\gamma\alpha}$ increased, as illustrated in Fig. 6.18. Typical concentration profiles that develop during the partitioning process are illustrated in Fig. 6.19.

The assumption throughout that during the decarburisation process $x^{\gamma\alpha}$ is fixed at the value given by paraequilibrium between ferrite and austenite is hard to justify since $x^\alpha \neq x^{\alpha\gamma}$. Hillert *et al*. (1993) have avoided this assumption; it is interesting that the results they obtain are not essentially different from those presented above.

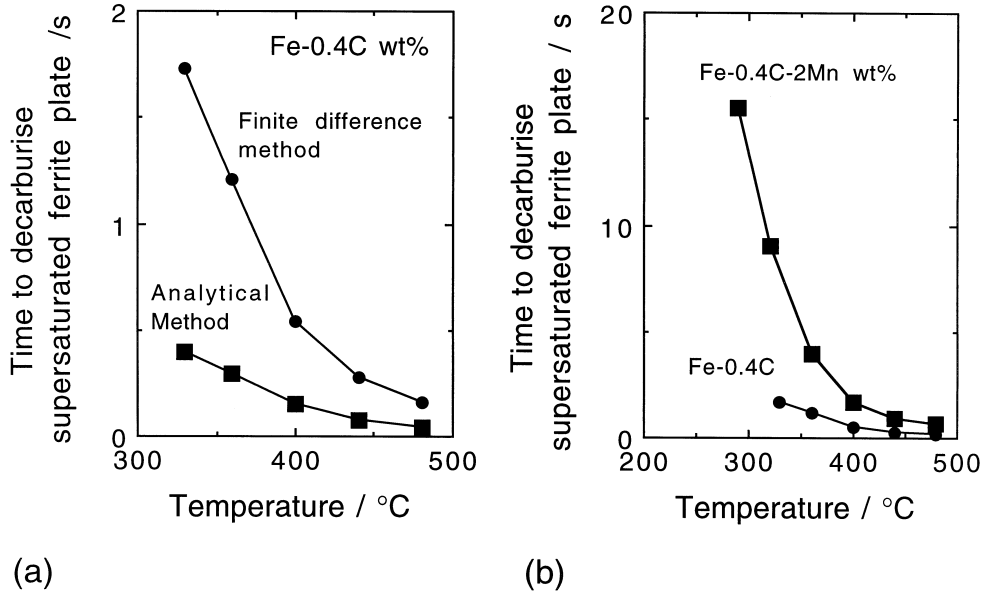

Fig. 6.18 (a) The time to decarburise a plate of thickness 0.2 μm. Calculations using the analytical and finite difference methods are illustrated. (b) The effect of adding an austenite stabilising substitutional solute on the decarburisation time (Mujahid and Bhadeshia, 1992).

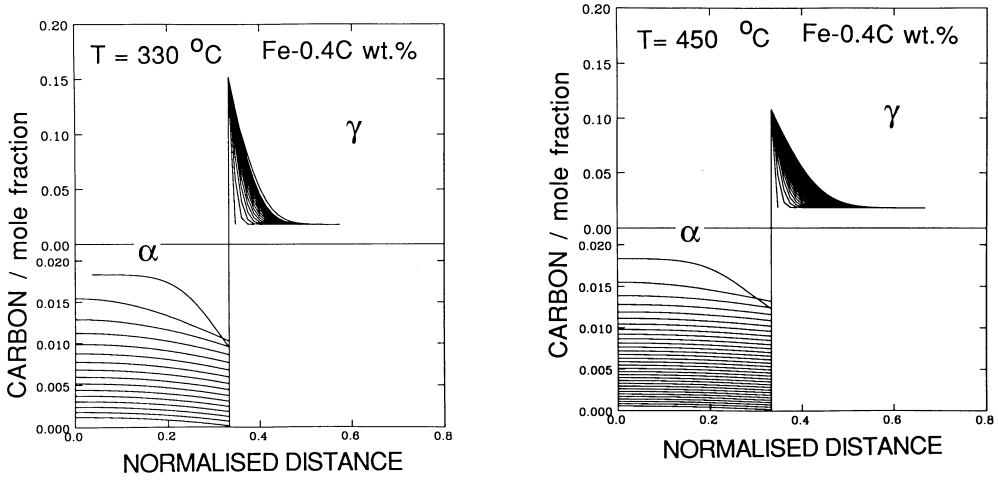

Fig. 6.19 The concentration profiles that develop in ferrite and and austenite during the partitioning of carbon from supersaturated bainite (Fe–0.4C wt%, plate thickness 0.2 μm). (a) 330 °C, the time interval between the concentration contours in each phase being 0.094 s. (b) 450 °C, the corresponding time interval is 0.007 s. (Mujahid and Bhadeshia, 1992).

6.8 Growth with Partial Supersaturation

(i) A transformation can occur without any composition change as long as there is a reduction in the free energy. The chemical potential is then nonuniform across phase boundaries for all of the atomic species. A net reduction in free energy is still possible because some of the species are trapped in the parent phase and others in the product. Thus, martensitic transformation of steel involves the trapping of carbon in the martensite and iron in the austenite.

(ii) Equilibrium transformation requires the partitioning of solutes between the phases until the chemical potential for each species is uniform in all locations.

(iii) In paraequilibrium only carbon has a uniform chemical potential - the substitutional and iron atoms are trapped in the parent or product phases.

These three cases of composition-invariant, equilibrium and paraequilibrium transformation are well-defined. We now deal with the case where the extent of carbon partitioning is between paraequilibrium and composition-invariant transformation:

$$x^{\alpha\gamma} \leq x^{\alpha} \leq \overline{x} \qquad \text{and} \qquad \overline{x} \leq x^{\gamma} \leq x^{\gamma\alpha}$$

Some of the carbon is trapped in the product phase but a proportion partitions so that the differences in chemical potential are reduced. The ferrite grows with a *partial supersaturation*, the level of which is fixed by kinetic constraints which we shall now consider.

6.8.1 Stability

In Fig. 6.20, x_m represents the maximum concentration of carbon that can be tolerated in ferrite which precipitates from austenite of composition $\overline{x}$. A higher concentration cannot be sustained because there would be an increase in free energy on transformation.

Growth with partial supersaturation, such as the case where the interface compositions are given by $x^\alpha = x_m$ and $x^\gamma = \overline{x}$ is expected to be unstable to perturbations since the concentration field must tend to adjust towards lower free energy states. The assembly should then irreversibly cascade towards the equilibrium partitioning of carbon with $x^\alpha = x^{\alpha\gamma}, x^\gamma = x^{\gamma\alpha}$. Experimental evidence supports this conclusion since the growth rate of Widmanstätten ferrite is found to be consistent with the paraequilibrium partitioning of carbon at all transformation temperatures. These considerations do not necessarily rule out the possibility of carbon trapping because some other physical phenomenon could provide the necessary stabilising influence (Christian and Edmonds, 1984).

There are many processes, including diffusion, which occur in series as the ferrite grows. Each of these dissipates a proportion of the free energy available for transformation. For a given process, the variation in interface velocity with dissipation defines a function which in recent years has been called an *interface*

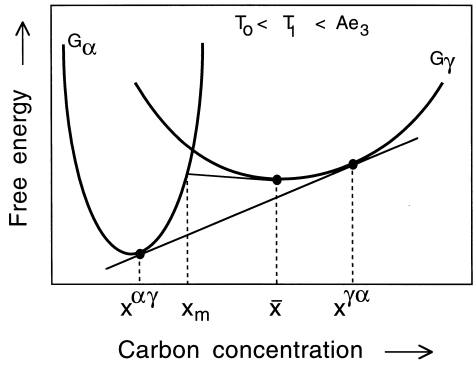

Fig. 6.20 Austenite and ferrite free energy curves illustrating the unstable nature of an assembly in which the ferrite forms with a partial supersaturation of carbon.

response function. The actual velocity of the interface depends on the simultaneous solution of all the interface response functions, a procedure which fixes the composition of the growing particle.

Figure 6.21 shows an electrical analogy; the resistors in series are the hurdles to the movement of the interface. They include diffusion in the parent phase, the transfer of atoms across the interface, solute drag, etc. The electrical-potential drop across each resistor corresponds to the free energy dissipated in each process, and the current, which is the same through each resistor, represents the interface velocity. The relationship between the current and potential is different for each resistor, but the actual current is obtained by a simultaneous solution of all such relations.

Following on from this analogy, the available free energy can be partitioned into that dissipated in the diffusion of carbon, a quantity expended in the transfer of atoms across the interface, and in any other process determining the motion of the interface. There are three unknowns: the austenite composi-

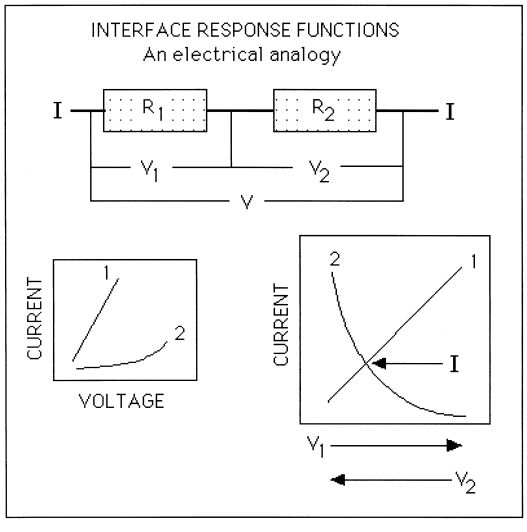

Fig. 6.21 An electrical analogy illustrating the dissipations due to processes which occur in series as the transformation interface moves. The resistors in series are the hurdles to the motion of the interface, the voltage the driving force and the current the interface velocity. The way in which voltage (driving force) is dissipated as a function of current (velocity) across each resistor is different, since each resistor represents a separate physical process. There is only one interface so all these processes must yield the same velocity, as indicated by the identical current passing through all the resistors.

tion at the interface, the supersaturation and the velocity, so it is necessary to exploit at least three interface response functions. If the tip radius of the plate is considered to be a variable, then the number of unknowns is four; for displacive transformations the radius can be assumed to be fixed by strain energy minimisation. The necessary three interface velocity functions are, therefore, the diffusion field velocity, the velocity determined from interface mobility and a carbon trapping function. Each of these is now discussed in detail.

But to summarise first, the response functions all give different velocities for a given free energy dissipation. The total driving force has to be partitioned into the individual dissipations in such a way that all the response functions give an identical velocity.

6.8.2 The Interface Response Functions

6.8.2.1 The Interface Mobility (Martensitic Interface)

The interfacial mobility is formulated using the theory for thermally activated motion of dislocations (Olson *et al.*, 1989, 1990). This is justified because a glissile interface consists of an array of appropriate dislocations. The interfacial velocity V_i is then given by:

$$V_i = V_o \exp\left\{ -\frac{G*}{kT} \right\} \tag{6.30}$$

where G^* is an activation free energy and the pre-exponential factor V_o can be taken to be $30\,\mathrm{m\,s^{-1}}$ based on experimental data from single-interface martensitic transformations (Grujicic *et al.*, 1985). The activation energy G^* is a function of the net interfacial driving force G_{id} through the relation (Kocks *et al.*, 1975):

$$G^* = \int_{G_{id}}^{G'_{id}} v^* dG \tag{6.31}$$

where G'_{id} is the maximum resistance to the glide of interfacial dislocations and v^* is the activation volume swept by the interface during a thermally activated event. For a wide range of obstacle interactions, the function $G^*\{G_{id}\}$ can be represented by:

$$G^* = G_o^* \left[1 - \left(\frac{G_{id}}{G'_{id}} \right)^y \right]^z \tag{6.32}$$

where G_o^* is the activation free energy barrier to dislocation motion in the absence of an interfacial driving force. The constants y and z define the shape of the force-distance function and for solid-solution interactions in the

Labusch limit (where hardening is due to the average effect of many strain centres), it may be assumed that $y = 0.5$ and $z = 1$ (Nabarro, 1982).†

Analysis of kinetic data for the interface-controlled nucleation of martensite gives

$$G_o^* = 0.31\mu\Omega \tag{6.33}$$

where μ is the shear modulus of the matrix and Ω is the volume per atom. Based on the behaviour of Fe–Ni–C alloys (Olson, 1984), G'_{id} is taken to be:

$$G'_{id} = 1.22 \times 10^{-3}\mu \tag{6.34}$$

6.8.2.2 The Interface Mobility Based on Absolute Reaction Rate Theory

An empirical model is sometimes used to represent the interface mobility for displacive transformations (Hillert, 1960; Ågren, 1989). It uses chemical rate theory, one of the assumptions of which is that the 'reaction' consists of the repetition of unit steps involving the interaction of a small number of atoms. Whereas this may be justified for a process like solidification, the assumptions of chemical rate theory are unlikely to be applicable to displacive transformations in which a large number of atoms move in a disciplined manner.

The interface velocity is given by (Christian, 1975):

$$V_i = \delta_b f^* \exp\left\{-\frac{G^*}{RT}\right\}\left[1 - \exp\left\{-\frac{G_{id}}{RT}\right\}\right] \tag{6.35}$$

where δ_b is the thickness of the interface, and f^* is an attempt frequency for atomic jumps across the interface. For small G_{id} the equation simplifies to

$$V_i = MG_{id} \tag{6.36}$$

where M is a mobility, estimated by Hillert (1975) for reconstructive transformations to be:

$$M = 0.035 \exp\left\{-\frac{17700}{T}\right\} \qquad \mathrm{m^4\,J^{-1}\,s^{-1}} \tag{6.37}$$

6.8.2.3 The Diffusion Field Velocity

The diffusion field velocity depends on the compositions of the phases at the interface. These compositions are illustrated in Fig. 6.22, on a free energy diagram as a function of the amount G_{dd} of free energy dissipated in the diffusion

†The relationship between the activation energy and driving force is here nonlinear, compared with equation 6.10 of the nucleation theory. The nonlinear function is a better approximation but the linear relation of equation 6.10 suffices for most purposes.

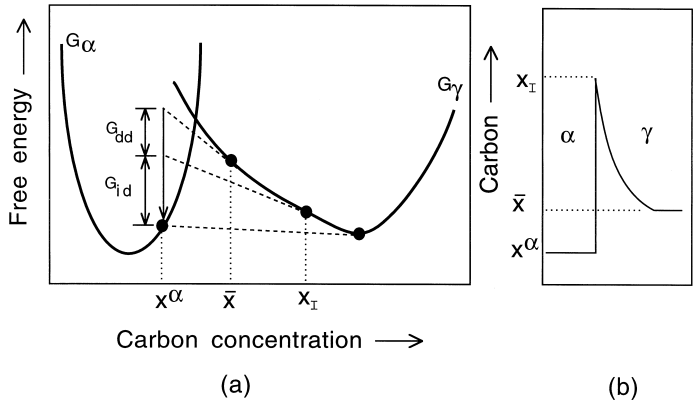

Fig. 6.22 (a) Constant temperature free-energy curves showing the quantities G_{dd} and G_{id} for the case where the interface compositions are as illustrated in (b). Note that the net free energy available for interfacial motion *after* allowing for strain energy and interface energy contributions is ΔG, which is the sum of the two dissipations G_{dd} and G_{id}.

of solute ahead of the interface. The concentrations x^α and x_I are not independent because the choice of either fixes the value of the other uniquely.

The Trivedi solution for plates is probably the best available for diffusion-controlled growth, but there are more convenient approximations. One of these is due to Ivantsov (1947), in which the growth of a parabolic cylinder shaped particle is treated without the inclusion of interface mobility and capillarity effects. The velocity V_d for steady state growth of ferrite of constant composition x^α in a steel of composition $\overline{x}$ is given by:

$$\frac{\overline{x} - x_I}{x^\alpha - x_I} = (\pi p)^{\frac{1}{2}} \exp\{p\} \mathrm{erfc}\{p^{\frac{1}{2}}\} \tag{6.38}$$

where x_I is the carbon concentration in the austenite at the interface and p is the Péclet number.

6.8.2.4 Solute Trapping Law

Atoms are forced into the product phase during martensitic transformation. The chemical potential of some of these atoms increases as they are engulfed by the martensite. Similarly, during paraequilibrium transformation some of the immobile substitutional-solutes are forced into the growing crystal. A solute or solvent is said to be trapped when its chemical potential increases on transfer across the interface. The term *solute trapping* is relatively recent (Baker and Cahn, 1969, 1971) but the phenomenon has been known for much longer in the context of transformations in steels.

Figure 6.23 illustrates a transformation front between the shaded and unshaded crystals, in a binary alloy containing A (solvent) and B (solute) atoms. The smaller solute atoms prefer to be in the parent phase (γ). The atoms in the central layer have to move along the vectors indicated in order to transform into the product phase (α). λ is a typical diffusion jump distance for the solute atom; the motions required for the atoms in the interfacial layer to adjust to the new crystal structure are rather smaller.

Solute will be trapped if the interface velocity V_k is greater than that at which solute atoms can diffuse away. The maximum diffusion velocity is approximately D/λ since λ is the minimum diffusion distance, so that trapping occurs when $V_k > D/\delta_s$.

The Aziz model (1982, 1983) relates interfacial velocity to the partitioning coefficient k_p, which is the ratio of the concentration in the product phase at the interface to that in the parent phase at the interface:

$$k_p = x^\alpha / x_I \tag{6.39}$$

and $k_p = k_e$ where k_e is the equilibrium partition coefficient.

There are two basic mechanisms of interface displacement, one involving propagation by the displacement of steps, and the other by the displacement of

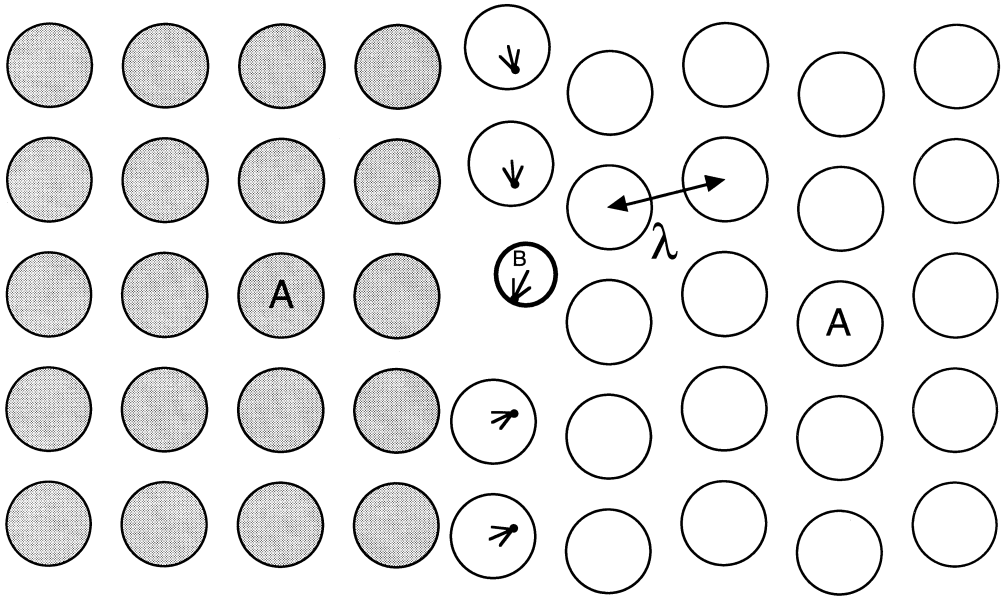

Fig. 6.23 Choreography of solute trapping, adapted from Aziz (1982). The solvent is labelled A, solute B and the product phase is shaded dark. The transformation front is advancing towards the right.

all elements of the boundary; this latter mechanism is called 'continuous' motion. Aziz has derived slightly different trapping models for these two cases. The step model only permits transformation below the T_0' temperature of the austenite in the vicinity of the interface. This is in general too restrictive and certainly inapplicable for transformations at temperatures above the T_0' temperature, of the type being considered here. Goldman and Aziz (1987) have proposed another model for stepped growth, which they call the *aperiodic step model*, in which the steps are assumed to pass at random intervals with transformation restricted to below the T_0' temperature of the parent phase at the interface. The trapping law turns out to be the same as for the continuous growth model which is suitable for transformation above T_0'.

The trapping model gives a velocity function of the form

$$V_k = \frac{D\{x_I\}}{\lambda} \frac{k_p - k_e}{1 - k_p} \tag{6.40}$$

where λ, the intersite jump distance is about 0.25 nm and $D\{x_I\}$ is the diffusion coefficient of carbon in austenite of composition x_I. The quantity $D\{x_I\}/\lambda$ is the diffusion velocity of carbon and trapping becomes prominent when the interface velocity approaches this value. Since the carbon atoms execute jumps across a glissile semi-coherent interface it is appropriate to take the coefficient for volume diffusion of carbon.

We now have the third interface response function (equation 6.40) which varies smoothly with x^α and x_I. Note that as x^α approaches $\overline{x}$, the diffusion field velocity diverges (tends towards infinity) and the interfacial dissipation then imposes the condition that $x_I = \overline{x}$ such that the trapping velocity V_k also tends towards infinity in the full trapping limit.

6.8.3 *Calculated Data on Transformation with Partial Supersaturation*

We now consider results from the two main models for growth involving a partial supersaturation of carbon, that due to Olson *et al*. (1987, 1989, 1990) and, due to Hillert (1960, 1975) and Ågren (1989).

With the three interface response functions, the diffusion field velocity (Ivantsov model, with a plate-tip radius fixed at 1.5 nm), the glissile-interface mobility function and the Aziz solute trapping function, Olson *et al*. solved for the interfacial velocity and phase compositions as a function of transformation temperature. Some of their results are presented in Fig. 6.24a, for a Fe–0.4C wt% alloy, illustrating how the supersaturation might vary with the transformation temperature for both the nucleation and growth stages. With a variety of assumptions about the strain energy of transformation and about the

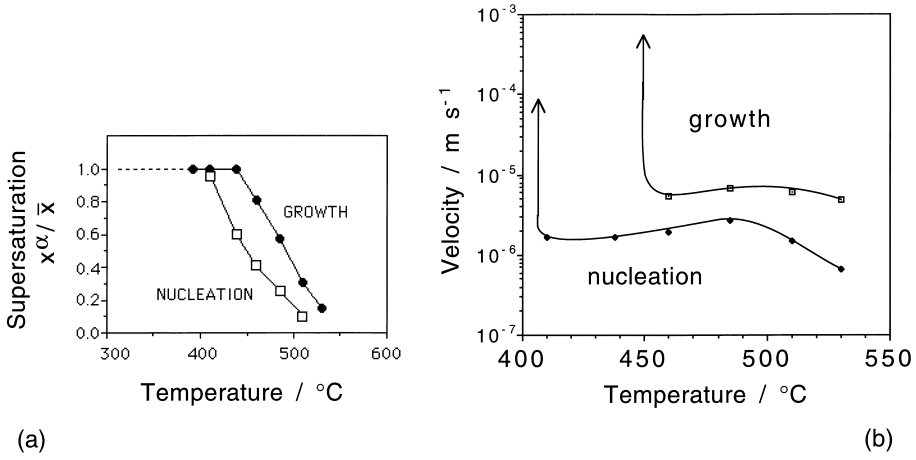

Fig. 6.24 (a) Plot of calculated normalised supersaturation $(x^\alpha/\bar{x})$ of carbon in ferrite versus the isothermal transformation temperature, for a Fe–0.4C wt% alloy, with the data obtained by the simultaneous solution of the interfacial mobility, diffusion field velocity and trapping velocity functions. Martensitic transformation is when both nucleation and growth become diffusionless. (b) The interfacial velocities during the 'nucleation' and growth processes.

nucleation behaviour, the model has been shown to compare favourably with the measured TTT diagram.

The calculations have been extended to cover a wider range of carbon concentrations. Malecki (1990) found that for high carbon steels the model is not able to predict the acceleration of the bainite reaction at temperatures just above M_S, first noted by Howard and Cohen (1948) and discussed later in this Chapter. Mujahid and Bhadeshia (1993) found that the M_S temperature is predicted accurately if it is assumed that both nucleation and growth are diffusionless for martensite. The variation in the B_S temperature as a function of the carbon concentration could also be estimated. However, the absolute values of B_S could only be brought into agreement with experimental data by allowing the stored energy to be a function of temperature.

The model by Hillert and Ågren is founded on the theory for reconstructive transformations. The interface mobility function used relies on absolute reaction rate theory, which is not appropriate for glissile interfaces. The radius of curvature at the plate tip is treated as a free variable. It is assumed that the curvature adopted is that which gives the highest growth rate. Strain energy due to the mechanism of transformation is neglected. To solve for the three unknowns (austenite and ferrite compositions and the interfacial velocity), a

solute drag function due to Hillert and Sundman (1976) is utilised in addition to the interface mobility and diffusion field velocity response functions. It is predicted that there is a gradual transition from diffusion-controlled to diffusionless growth as the driving force is increased, although the plate shape is then lost because diffusionless growth occurs with zero interface curvature, i.e. a flat interface!

6.8.4 Summary

Both of the models predict an increase in carbon trapping as the transformation temperature is reduced. They establish the possibility that the transition from bainite to martensite is gradual. However, there remain numerous difficulties.

An increasing supersaturation with undercooling is inconsistent with the fact that the bainite reaction stops when the carbon concentration of the residual austenite approaches the T_0' curve. According to the calculations the carbon concentration of the austenite when transformation stops should be that given by the Ae_3'' phase boundary at high temperatures but by the T_0' curve at low temperatures.

It is assumed that the supersaturation in the ferrite is constant for any given isothermal transformation temperature. On the other hand, there is no reason why the supersaturation should not decrease continuously towards equilibrium as the fraction of transformation increases at a constant temperature. This simply does not happen, e.g. we do not see martensite evolving into Widmanstätten ferrite. In other words, the models are theoretically elegant but do not reflect reality.

6.9 Cooperative Growth of Ferrite and Cementite

Ferrite and cementite grow together with a common transformation front during the formation of a pearlite colony. Hultgren (1947) proposed that the essential difference between pearlite and bainite is that in the latter case the cementite and ferrite do not grow cooperatively (Fig. 6.25). The microstructural evolution illustrated is now known to be incorrect, but it is nevertheless often argued that bainite is simply the product of a non-lamellar eutectoid reaction in which the component phases no longer share a common front with the austenite. This is doubtful for a variety of reasons, one of which is that bainitic ferrite can form without any carbide precipitation at all.

There have been attempts to revitalise Hultgren's ideas by adopting a generalised definition of bainite as the product of a non-lamellar, noncooperative

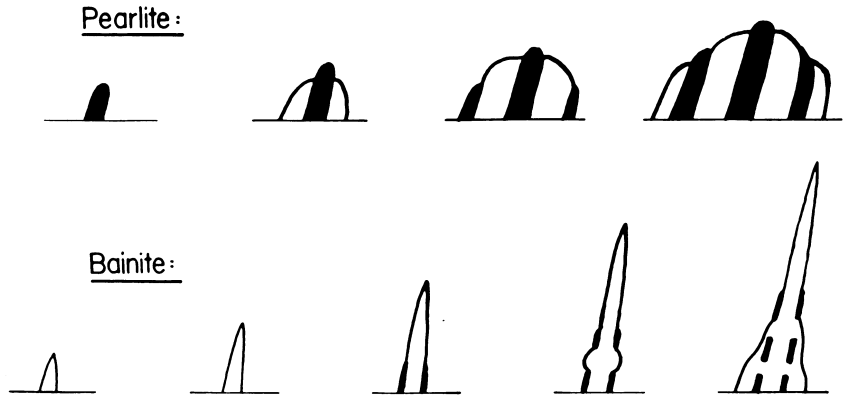

Fig. 6.25 Hultgren's interpretation of the cooperative and noncooperative growth modes of pearlite and bainite respectively.

mode of eutectoid decomposition. It is further assumed that both pearlite and bainite grow by a reconstructive mechanism in which the transformation front propagates by a ledge mechanism (Lee *et al.*, 1988). It is then claimed that the transition from pearlite to bainite occurs when the cementite and ferrite can no longer grow at the same rate from austenite. The ferrite and cementite cease to grow at the same rate when:

$$\frac{h_\alpha}{\lambda_\alpha} \neq \frac{h_\theta}{\lambda_\theta} \tag{6.41}$$

where h and λ represent the height and interledge spacing respectively. The phases can grow with a common front as long as this ratio is identical for both. The ledges are supposed to move in a direction parallel to the transformation front. They are therefore shared, i.e., they can traverse both ferrite and cementite. Cooperative growth fails when:

$$\frac{h_\alpha v^s_\alpha}{\lambda_\alpha} \neq \frac{h_\theta v^s_\theta}{\lambda_\theta} \tag{6.42}$$

where v^s is the step velocity. The ledge velocity must change when it moves from the ferrite to the cementite phase to account for the change in the phases which are in local equilibrium, but this is neglected in the analysis.

It is doubtful whether this criterion identifies the essential difference between bainite and pearlite. The character of the transformation interface, whether it is glissile or sessile, is not a part of the analysis.

6.10 Overall Transformation Kinetics

6.10.1 Isothermal Transformation

A model for a single transformation begins with the calculation of the nucleation and growth rates, but an estimation of the volume fraction requires impingement between particles to be taken into account. This is generally done using the extended volume concept of Johnson, Mehl, Avrami, and Kolmogorov (Christian, 1975). Referring to Fig. 6.26, suppose that two particles exist at time t; a small interval δt later, new regions marked a, b, c & d are formed assuming that they are able to grow unrestricted in extended space whether or not the region into which they grow is already transformed. However, only those components of a, b, c & d which lie in previously untransformed matrix can contribute to a change in the real volume of the product phase (α):

$$dV^{\alpha} = \left(1 - \frac{V^{\alpha}}{V}\right) dV_e^{\alpha} \tag{6.43}$$

where it is assumed that the microstructure develops randomly. The subscript e refers to extended volume, V^{α} is the volume of α and V is the total volume. Multiplying the change in extended volume by the probability of finding untransformed regions has the effect of excluding regions such as b, which clearly cannot contribute to the real change in volume of the product. For a random distribution of precipitated particles, this equation can easily be integrated to obtain the real volume fraction,

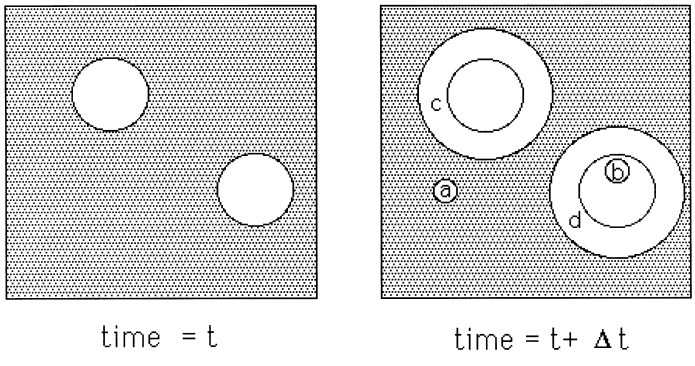

Fig. 6.26 An illustration of the concept of extended volume. Two precipitate particles have nucleated together and grown to a finite size in the time t. New regions c and d are formed as the original particles grow, but a & b are new particles, of which b has formed in a region which is already transformed.

$$\frac{V^\alpha}{V} = 1 - \exp\left\{ -\frac{V_e^\alpha}{V} \right\}$$

The extended volume V_e^α is straightforward to calculate using nucleation and growth models and neglecting completely any impingement effects. Consider a simple case where the α grows isotropically at a constant rate G and where the nucleation rate per unit volume is I_V. The volume of a particle nucleated at time τ is given by

$$v_\tau = \frac{4}{3}\pi G^3 (t-\tau)^3$$

The change in extended volume over the interval τ and $\tau + d\tau$ is

$$dV_e^\alpha = \frac{4}{3}\pi G^3 (t-\tau)^3 \times I_V \times V \times d\tau$$

On substituting into equation 6.43 and writing $\xi = V^\alpha/V$, we get

$$\begin{aligned} dV^\alpha &= \left(1 - \frac{V^\alpha}{V}\right)\frac{4}{3}\pi G^3 (t-\tau)^3 I_V \, d\tau \\ \text{so that} \qquad -\ln\{1-\xi\} &= \frac{4}{3}\pi G^3 I_V \int_0^t (t-\tau)^3 d\tau \\ \text{and} \qquad \xi &= 1 - \exp\{-\pi G^3 I_V t^4/3\} \end{aligned} \tag{6.44}$$

This equation has been derived for the specific assumptions of random nucleation, a constant nucleation rate and a constant growth rate. There are different possibilities but they often reduce to the general form:

$$\xi = 1 - \exp\{-k_A t^n\} \tag{6.45}$$

where k_A and n characterise the reaction as a function of time, temperature and other variables. This equation is frequently used empirically as an economic way of representing experimental data (Radcliffe *et al.*, 1963; Okamoto and Oka, 1986). The temptation to deduce mechanistic information from an empirical application of the Avrami equation should be avoided even when the equation accurately fits the data, since the fitting parameters can be ambiguous.

6.10.2 *Mechanistic Formulation of the Avarmi Equation*

Reasonable trends can be obtained using an Avrami model founded on the mechanism of the bainite (Singh, 1998). Each nucleus is assumed to transform into one sub-unit of bainite of volume u. The time required to nucleate is considered to be much greater than that for growth so that the change in extended volume over the interval τ and $\tau + d\tau$ is given by

$$dV_e^\alpha = I_V V u \, d\tau$$

If ξ is defined as a normalised fraction of bainite, i.e. the fraction of bainite divided by its maximum fraction:

$$\xi = \frac{V^\alpha}{V} \Big/ V_{max} \qquad \text{where} \qquad V_{max} \simeq \frac{x_{T_0'} - \overline{x}}{x_{T_0'} - x^{\alpha\gamma}}$$

then the conversion from extended to real volume becomes

$$\begin{aligned} dV^\alpha &= (1-\xi) dV_e^\alpha \\ &= (1-\xi) V u I_V \, d\tau \\ \text{or} \quad V_{max} d\xi &= (1-\xi) u I_V \, d\tau \end{aligned} \tag{6.46}$$

For every successful nucleation event, a further number p of nucleation sites is introduced autocatalytically. It follows that over a period τ there will be $pI_V\tau$ new nucleation sites introduced in addition to those originally present. The total number density N_V^T of sites at time τ therefore becomes

$$N_V^T = N_V^0 + pI_V\tau$$

where N_V^0 is the initial number density[†]. The nucleation rate (equation 6.15) therefore becomes time-dependent:

$$I_V = N_V^0 \nu \exp\left\{ -\frac{G^*}{RT} \right\} + N_V^0 \nu^2 \tau p \exp\left\{ -\frac{2G^*}{RT} \right\}$$

On substitution into equation 6.46 we get

$$\frac{V_{max}}{u N_V^0 \nu} \int_0^\xi \frac{d\xi}{\exp\{-\frac{G^*}{RT}\}} = \int_0^t \left[1 + p\tau\nu \exp\left\{ -\frac{G^*}{RT} \right\} \right]$$

which after integration and manipulation gives the time t to achieve a specified amount of transformation as:

$$t = \frac{-1 + \sqrt{1 - \frac{V_{max}}{u N_V^0} p \ln\{1-\xi\}}}{p\nu \exp\{-\frac{G^*}{RT}\}} \tag{6.47}$$

Some example calculations are shown in Fig. 6.27 which illustrates the advantages of formulating the Avrami theory on the basis of transformation mechan-

[†]Tzeng (2000) has attempted to introduce autocatalysis differently, by considering nucleation at the bainite/austenite surface. However, his mathematical derivations are wrong because his model is formulated to allow nucleation on *extended area* rather than real area. This is why his calculation of the bainite/austenite surface per unit volume tends to infinity. Similarly, w in his equations is an extended volume which should not be multiplied by I_0.

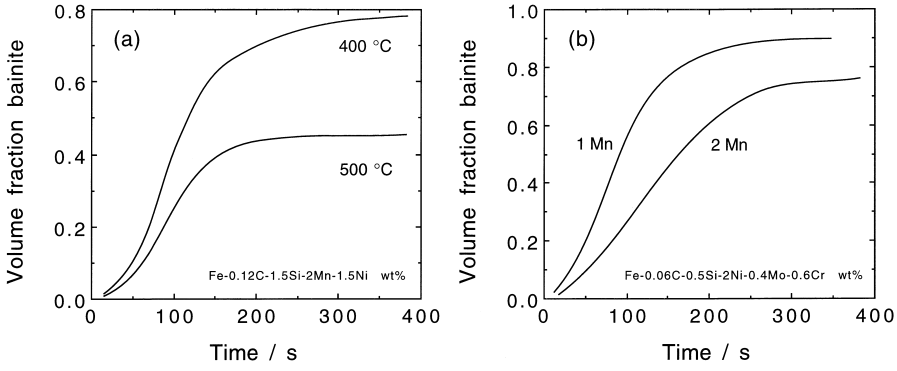

Fig. 6.27 The calculated influence of (a) transformation temperature and (b) manganese concentration on the kinetics of the bainite reaction (Singh, 1998).

ism. The maximum fraction decreases as the transformation temperature is raised towards the B_S temperature, consistent with the incomplete transformation phenomenon. Similarly an increase in the stability of the austenite (change in manganese) retards transformation.

6.10.3 Austenite Grain Size Effect

The bainite transformation is much less sensitive to the austenite grain size than is pearlite (Umemoto *et al.*, 1980). Furthermore, elements like boron, which increase the hardenability by segregating to the grain boundaries, have a much smaller effect on bainite than on ferrite. This is because for each bainite plate nucleated at a grain surface, there are a number which are autocatalytically stimulated; the majority of plates in a sheaf do not touch the austenite grain boundaries.

A reduction in the austenite grain size should, nevertheless, lead to an increase in the rate of transformation because of the greater number density of grain boundary nucleation sites (Barford and Owen, 1961). However, Davenport (1941) argued that the grain size has no appreciable effect on the transformation kinetics. By contrast, Graham and Axon (1959) suggested that because the growth of a bainite plate is resisted by the matrix, a smaller grain size should retard growth.

The austenite grain size is best defined by its mean line lineal intercept $\overline{L}$ because it is related inversely to the grain surface per unit volume S_V and hence to the number density of nucleation sites N_V^0:

$$S_V = \frac{2}{\overline{L}} \qquad \text{and therefore,} \qquad N_V^0 \propto \frac{1}{\overline{L}} \tag{6.48}$$

It follows that the nucleation rate must increase as the austenite grain size decreases. If this is the only effect then the overall rate of transformation must increase as $\overline{L}$ decreases.

There is, however, another effect since the maximum volume V^S_{max} of a sheaf which starts from each grain boundary nucleus must be constrained by the grain size, i.e.

$$V^S_{max} \propto \overline{L}^3$$

If this effect is dominant then the overall rate will decrease as the austenite grain size is reduced. Thus, it has been demonstrated experimentally that there is an acceleration of transformation rate as $\overline{L}$ is reduced when the overall

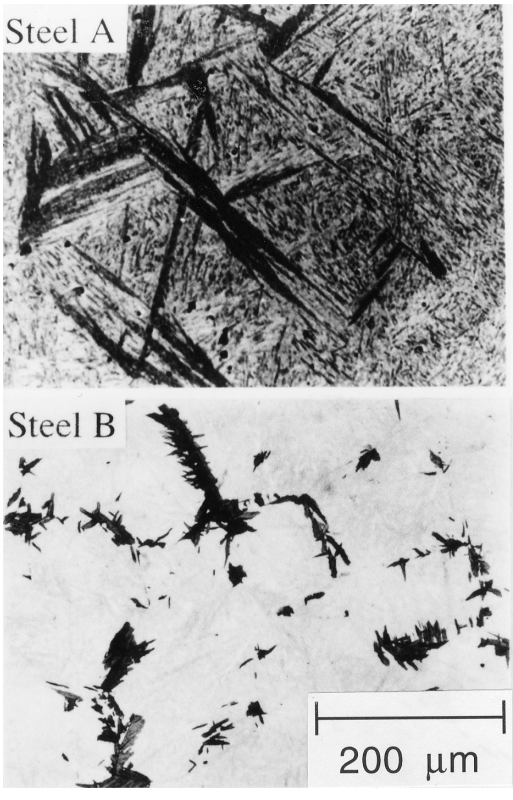

Fig. 6.28 (a) Bainite in a steel where nucleation is sparse and sheaf-growth is rapid. The austenite grains constrain the amount of transformation that each nucleus can cause. Reducing the austenite grain size then causes a net reduction in the overall rate of transformation. (b) Bainite in a steel where the growth rate is small so that the effect of the austenite grain size is simply to promote the nucleation rate. After Matsuzaki and Bhadeshia (1999).

reaction is limited by a slow growth rate, i.e. when the sheaf volume remains smaller than V^S_{max} and hence is unconstrained by the grain size. Conversely, for rapid growth from a limited number of nucleation sites, a reduction in the austenite grain size reduces the total volume transformed per nucleus and hence retards the overall reaction rate. The two circumstances are illustrated in Fig. 6.28.

6.10.4 *Anisothermal Transformation Kinetics*

A popular method of converting between isothermal and anisothermal transformation data is the *additive reaction rule* of Scheil (1935). A cooling curve is treated as a combination of a sufficiently large number of isothermal reaction steps. Referring to Fig. 6.29, a fraction $\xi = 0.05$ of transformation is achieved during continuous cooling when

$$\sum_i \frac{\Delta t_i}{t_i} = 1 \tag{6.49}$$

with the summation beginning as soon as the parent phase cools below the equilibrium temperature.

The rule can be justified if the reaction rate depends solely on ξ and T. Although this is unlikely, there are many examples where the rule has been empirically applied to bainite with success (e.g. Umemoto *et al.*, 1982). Reactions for which the additivity rule is justified are called isokinetic, implying that the fraction transformed at any temperature depends only on time and a single function of temperature (Avrami, 1939; Cahn, 1956).

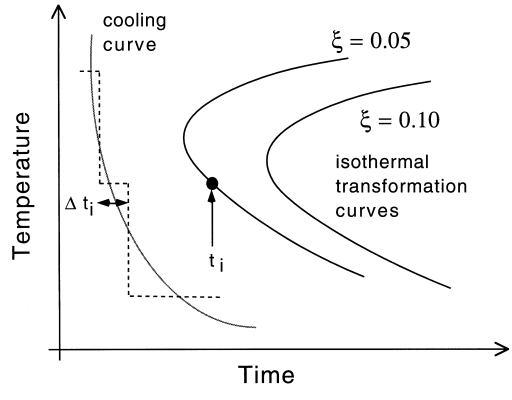

Fig. 6.29 The Scheil method for converting between isothermal and anisothermal transformation data.

6.11 Simultaneous Transformations

A simple modification for two precipitates (α and β) is that equation 6.43 becomes a coupled set of two equations,

$$dV^{\alpha} = \left(1 - \frac{V^{\alpha} + V^{\beta}}{V}\right) dV_e^{\alpha} \qquad \text{and} \qquad dV^{\beta} = \left(1 - \frac{V^{\alpha} + V^{\beta}}{V}\right) dV_e^{\beta} \quad (6.50)$$

This can be done for any number of reactions happening together (Robson and Bhadeshia, 1997; Jones and Bhadeshia, 1997). The resulting set of equations must in general be solved numerically, although a few analytical solutions are possible for special cases which we shall now illustrate (Kasuya *et al.*, 1999).

6.11.1 Special Cases

For the simultaneous formation of two phases whose extended volumes are related linearly:

$$V_e^{\beta} = BV_e^{\alpha} + C \qquad \text{with} \qquad B \geq 0 \qquad \text{and} \qquad C \geq 0 \qquad (6.51)$$

then with $\xi_i = V_i/V$, it can be shown that

$$\xi^{\alpha} = \int \exp\left\{ -\frac{(1+B)V_e^{\alpha} + C}{V} \right\} \frac{dV_e^{\alpha}}{V} \qquad \text{and} \qquad \xi^{\beta} = B\xi^{\alpha} \qquad (6.52)$$

If the isotropic growth rate of phase α is G and if all particles of α start growth at time $t = 0$ from a fixed number of sites N_V per unit volume then $V_e^{\alpha} = N_V \frac{4\pi}{3} G^3 t^3$. On substitution of the extended volume in equation 6.52 gives

$$\xi^{\alpha} = \frac{1}{1+B} \exp\left\{ -\frac{C}{V} \right\} \left[1 - \exp\left\{ -\frac{(1+B)N_V \frac{4\pi}{3} G^3 t^3}{V} \right\} \right] \quad \text{with} \quad \xi^{\beta} = B\xi^{\alpha} \qquad (6.53)$$

The term $\exp\{-C/V\}$ is the fraction of parent phase available for transformation at $t = 0$; it arises because $1 - \exp\{-C/V\}$ of β exists prior to commencement of the simultaneous reaction at $t = 0$. Thus, ξ^{β} is the additional fraction of β that forms during simultaneous reaction. It is emphasised that $C \geq 0$. A case for which $C = 0$ and $B = 8$ is illustrated in Fig. 6.30.

For the case where the extended volumes are related parabolically (Kasuya *et al.*, 1999):

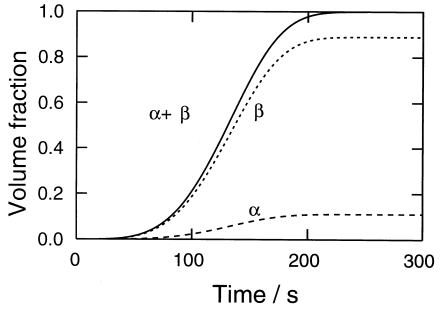

Fig. 6.30 Simultaneous transformation to phases $\alpha \equiv 1$ and $\beta \equiv 2$ with $C = 0$ and $B = 8$.

$$\xi^{\alpha} = \exp\left\{-\frac{C}{V}\right\}\left[\sqrt{\frac{\pi}{4A}}\exp\left\{\frac{(1+B)^2}{4A}\right\}\left(\mathrm{erf}\left\{\frac{1+B}{\sqrt{4A}}+\sqrt{A}V_e^{\alpha}\right\}\right.\right.$$
$$\left.\left.-\mathrm{erf}\left\{\frac{1+B}{\sqrt{4A}}\right\}\right)\right] \qquad (6.54)$$
$$\xi^{\beta} = \exp\left\{-\frac{C}{V}\right\}\left[1-\exp\left\{-\frac{A(V_e^{\alpha})^2+(1+B)V_e^{\alpha}}{V}\right\}\right]-\xi^{\alpha}$$

The volume fractions ξ^i again refer to the phases that form *simultaneously* and hence there is a scaling factor $\exp\{-C/V\}$ which is the fraction of parent phase available for coupled transformation to α and β.

6.11.2 Precipitation in Secondary Hardening Steels

Whereas the analytical cases described above are revealing, it is unlikely in practice for the phases to be related in the way described. This is illustrated for secondary hardening bainitic and martensitic steels of the kind used commonly in the construction of power plant. The phases interfere with each other not only by reducing the volume available for transformation, but also by removing solute from the matrix and thereby changing its composition. This change in matrix composition affects the growth and nucleation rates of all the participating phases.

The calculations must allow for the simultaneous precipitation of M_2X, $M_{23}C_6$, M_7C_3, M_6C and Laves phase. M_3C is assumed to nucleate instantaneously with the paraequilibrium composition. Subsequent enrichment of M_3C as it approaches its equilibrium composition is accounted for. All the phases, except M_3C, are assumed to form with compositions close to equili-

brium. The driving forces and compositions of the precipitating phases are calculated using standard thermodynamic methods.

The interaction between the precipitating phases is accounted for by considering the change in the average solute level in the matrix as each phase forms. This is frequently called the *mean field approximation*. It is necessary because the locations of precipitates are not predetermined in the calculations.

A plot showing the predicted variation of volume fraction of each precipitate as a function of time at 600 °C is shown in Fig. 4.16. It is worth emphasising that there is no prior knowledge of the actual sequence of precipitation, since all phases are assumed to form at the same time, albeit with different precipitation kinetics. The fitting parameters common to all the steels are the site densities and interfacial energy terms for each phase. The illustrated dissolution of metastable precipitates is a natural consequence of changes in the matrix chemical composition as the equilibrium state is approached.

Consistent with experiments, the precipitation kinetics of $M_{23}C_6$ are predicted to be much slower in the 2.25Cr1Mo steel compared to the 10CrMoV and 3Cr1.5Mo alloys. One contributing factor is that in the 2.25Cr1Mo steel a relatively large volume fraction of M_2X and M_7C_3 form prior to $M_{23}C_6$. These deplete the matrix and therefore suppress $M_{23}C_6$ precipitation. The volume fraction of M_2X which forms in the 10CrMoV steel is relatively small, so there remains a considerable excess of solute in the matrix, allowing $M_{23}C_6$ to precipitate rapidly. Similarly, in the 3Cr1.5Mo steel the volume fractions of M_2X and M_7C_3 are insufficient to suppress $M_{23}C_6$ precipitation to the same extent as in the 2.25Cr1Mo steel.

It is even possible in this scheme to treat precipitates nucleated at grain boundaries separately from those nucleated at dislocations, by taking them to be different phases in the sense that the activation energies for nucleation will be different.

6.11.3 Time-Temperature-Transformation (TTT) Diagrams

Transformation curves on TTT diagrams tend to have a C shape because reaction rates are slow both at high and at low temperatures. The diffusion of atoms becomes difficult at low temperatures whereas the driving force for transformation is reduced as the temperature is raised. The phase diagram thus sets the thermodynamic limits to the decomposition of austenite (Fig. 6.31).

Most TTT diagrams can be considered to consist essentially of two C curves, one for high temperatures representing reconstructive transformations to ferrite or pearlite. The other is for the lower temperatures where substitutional atoms take too long to diffuse, so that reconstructive transformations are replaced by displacive transformations such as Widmanstätten ferrite and

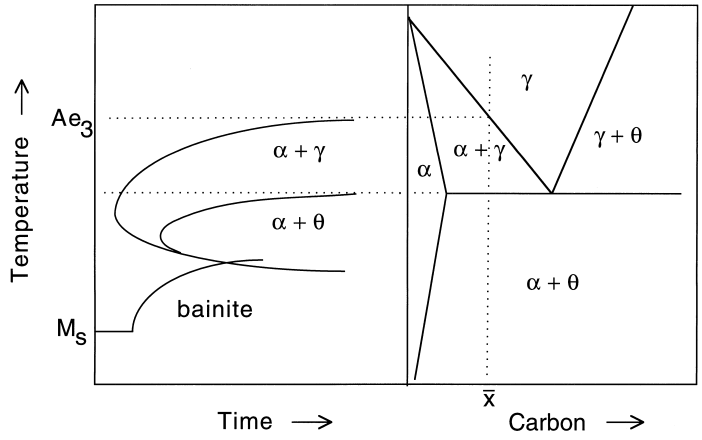

Fig. 6.31 The relationship between a TTT diagram for a hypoeutectoid steel with a concentration $\bar{x}$ of carbon, and the corresponding Fe-C phase diagram.

bainite. The martensite-start temperature generally features on a TTT diagram as a horizontal line parallel to the time axis (Cohen, 1940).

There are two major effects of alloying additions on transformation kinetics. Solutes which decrease the driving force for the decomposition of austenite retard the rate of transformation and cause both of the C curves to be displaced to longer times. At the same time they depress the martensite-start temperature (Fig. 6.32). The retardation is always more pronounced for reconstructive reactions where all atoms have to diffuse over distances comparable to the size of the transformation product. This diffusional drag exaggerates the effect of solutes on the upper C curve relative to the lower C curve.

For steels where the reaction rate is rapid, it becomes difficult experimentally to distinguish the two C curves as separate entities. For plain carbon and very low-alloy steels, the measured diagrams take the form of just a single C curve over the entire transformation temperature range. This is because the different reactions overlap so much that they cannot easily be distinguished using conventional experimental techniques (Hume-Rothery, 1966). Careful experiments have shown this interpretation to be correct (Brown and Mack, 1973; Kennon and Kaye, 1982). Sometimes the degree of overlap between the different transformation products decreases as the volume fraction of transformation increases (Fig. 6.33). This is because the partitioning of solute into austenite has a larger effect on reconstructive transformations.

As predicted by Zener (1946), when the two curves can be distinguished clearly, the lower C curve has a flat top. This can be identified with the Widmanstätten ferrite-start or bainite-start temperature, whichever is the larger in magnitude (Bhadeshia, 1981a).

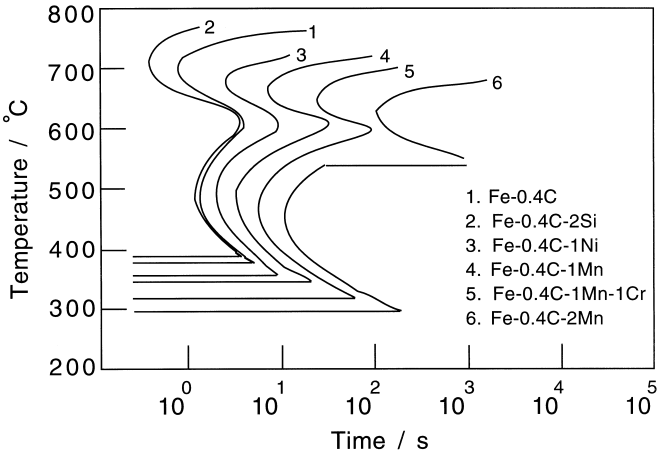

Fig. 6.32 Calculated TTT diagrams showing the C-curves for the initiation of reactions for a variety of steels.

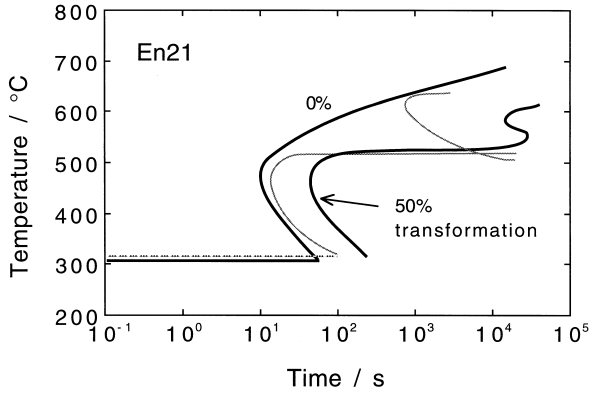

Fig. 6.33 TTT diagram for Steel En21 (BISRA, 1956). The continuous lines are experimental. The separation of the two constituent C curves, which is not apparent for the 0% curve is revealed as the extent of reaction increases. The dashed curves are calculated for 0% transformation.

There is more detail than implied in the two C curve description. The upper and lower bainite reactions can be separated on TTT diagrams (Schaaber, 1955; White and Owen, 1961; Barford, 1966; Kennon, 1978; Bhadeshia and Edmonds, 1979a). There is even an acceleration of the rate of isothermal transformation just above the classical M_S temperature, due to the formation of isothermal

martensite (Howard and Cohen, 1948; Schaaber, 1955; Radcliffe and Rollason, 1959; Smith *et al.*, 1959; Brown and Mack, 1973a,b; Babu *et al.*, 1976; Oka and Okamoto, 1986, 1988).

Isothermal martensite plates tend to be very thin and are readily distinguished from bainite. Although the overall rate of martensitic transformation appears isothermal, the individual plates are known to grow extremely rapidly. The isothermal appearance of the overall reaction is therefore due to the nucleation process (Smith *et al.*, 1959). The stresses caused by bainitic transformation seem to trigger induced isothermal martensite. The rate eventually decreases as the transformation temperature is reduced below the M_S temperature, giving the appearance of a C-curve with the peak transformation rate located below M_S (Fig. 6.34).

6.11.4 Continuous Cooling Transformation (CCT) Diagrams

Steels are not usually isothermally transformed. It is more convenient to generate the required properties during continuous cooling from the austenitic

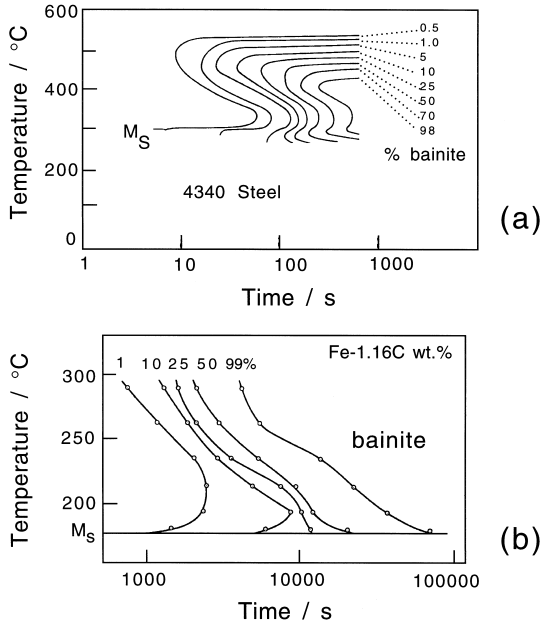

Fig. 6.34 (a) TTT diagram for a Fe–0.39C–0.70Mn–1.7Ni–0.76Cr–0.2Mo–0.28Si–0.22Cu wt% alloy austenitised at 900 °C for 15 minutes. Note the acceleration in the rate of transformation as the M_S temperature is approached (data from Babu *et al.*, 1976). (b) Similar data for a plain carbon steel (Howard and Cohen, 1948).

condition. Continuous-cooling-transformation (CCT) diagrams are then used to represent the evolution of microstructure (Fig. 6.35).

The rate of transformation in a given steel with a known austenite grain size can be described with just one TTT diagram. However, a different CCT diagram is required for cooling function, e.g. whether the cooling rate is constant or Newtonian. It is therefore necessary to plot the actual cooling curves used in the derivation of the CCT diagram (Fig. 6.35). Each cooling curve must begin at the highest temperature where transformation becomes possible (usually the Ae_3 temperature).

Each CCT diagram requires a specification of the chemical composition of the steel, the austenitisation conditions, the austenite grain size and the cooling condition. The diagrams are therefore specific to particular processes and lack the generality of TTT diagrams.

The CCT diagram is usually partitioned into domains of microstructure; Fig. 6.35 shows the conditions under which bainite and ferrite form. Mixed microstructures are obtained when a domain boundary is intersected by a cooling curve. The constant volume fraction contours must be continuous across the domain boundaries to avoid (incorrect) sudden changes in volume fraction as the boundary is crossed (e.g. points *a*, *b* on Fig. 6.36). The contours represent the fraction of austenite which has transformed into one or more phases. It follows that there are constraints on how the zero percent martensite and bainite curves meet, avoiding the double intersection with the cooling curve illustrated in Fig. 6.36b,c. Cooling curve *X* which leads to a fully martensitic

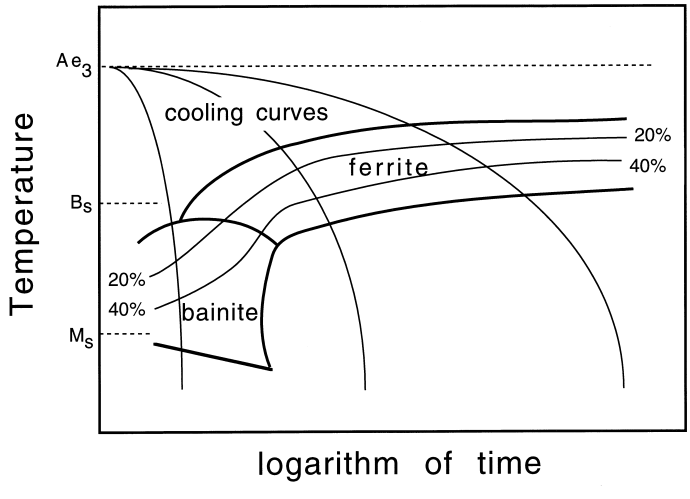

Fig. 35 CCT diagram illustrating the cooling curves, constant volume percent contours and transformation temperatures.

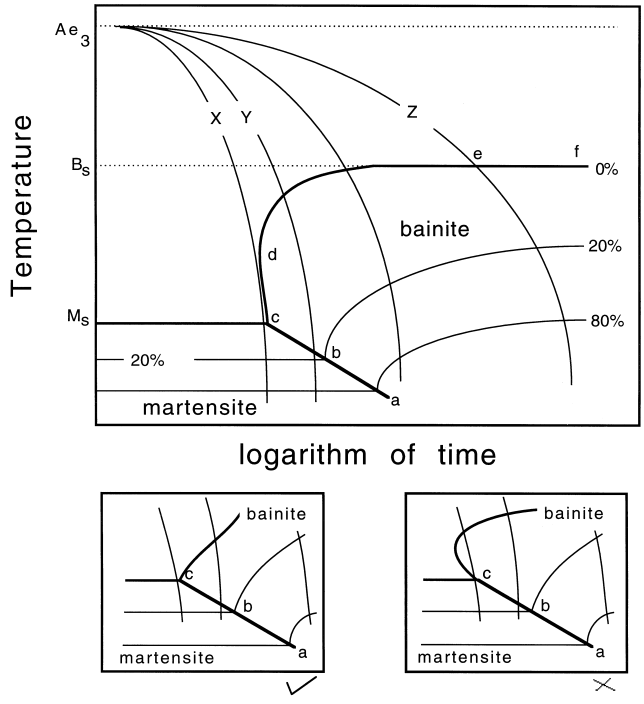

Fig. 6.36 Schematic CCT diagrams illustrating the continuity of constant volume percent contours across microstructure domain boundaries and the correct way in which the zero percent curves of different domains must meet at the point *c*.

microstructure, intersects the 0% transformation curve at just one point, without intersecting the region *cd*. Cooling curve *Y*, on the other hand, produces a mixed microstructure with less than 20% of bainite, the remaining austenite transforming to martensite on cooling. The temperature at which martensitic transformation begins (line *abc*) is depressed if bainite forms first and enriches the residual austenite with carbon.

The bainite curve in Fig. 6.36 approaches the B_S temperature asymptotically along *ef* as the cooling rate decreases consistent with the flat top of the bainite C curve in the TTT diagram. This is not always the case as shown schematically in Fig. 6.37. (Kunitake, 1971; Schanck, 1969; Lundin *et al.*, 1982). Any transformation which precedes bainite alters the chemical composition of the residual austenite. The main changes occur in the region associated with the vertical line 'c' in Fig. 6.37 The temperature at which the bainite first forms is depressed by the changed composition of the austenite. Because the ferrite and bainite domains are separated by a time gap, the continuity of constant volume fraction contours is interrupted. The contours must still be plotted so that

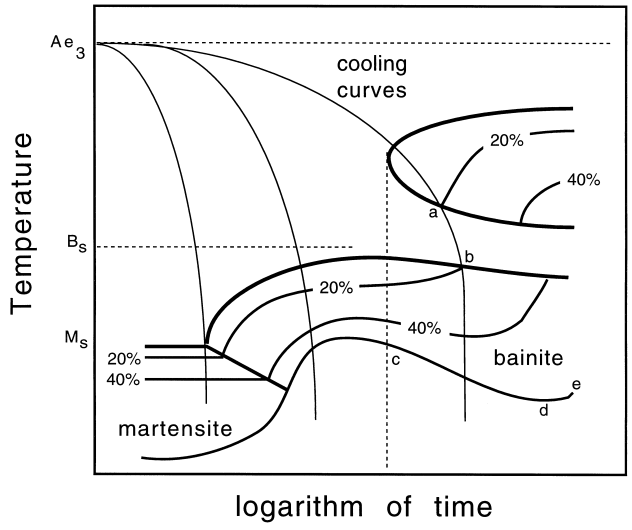

Fig. 6.37 TTT diagram in which the bainite region is strongly influenced by the initial formation of ferrite during continuous cooling transformation.

their loose ends are connected by a cooling curve as illustrated by 'ab' on Fig. 6.37.

Although bainite is depressed to lower temperatures by the prior formation of allotriomorphic ferrite as the cooling rate decreases, the temperature range over which bainite forms is eventually reduced. This is because very slow cooling rates give ample opportunity for transformation to be completed over a smaller temperature range as illustrated by the rising curve 'de' on Fig. 6.37.

All of the features described here can be found in actual TTT and CCT diagrams, for example, the measured diagrams for a '2.25Cr1Mo' steel which is used widely in the bainitic condition for power plant applications (Fig. 6.38).

6.11.5 Boron, Sulphur and the Rare Earth Elements

The early commercial development of bainitic steels relied on the effect of boron on the transformation characteristics of low-carbon steels (Chapter 1). Boron retards the heterogeneous nucleation of allotriomorphic ferrite at the austenite grain surfaces, to a greater degree than that of bainite (Fig. 6.39). This in turn permits boron-containing steels to be cooled continuously into fully bainitic microstructures. Elements like manganese are not suitable because they improve the martensite hardenability and hence favour a mixed microstructure of bainite and martensite.

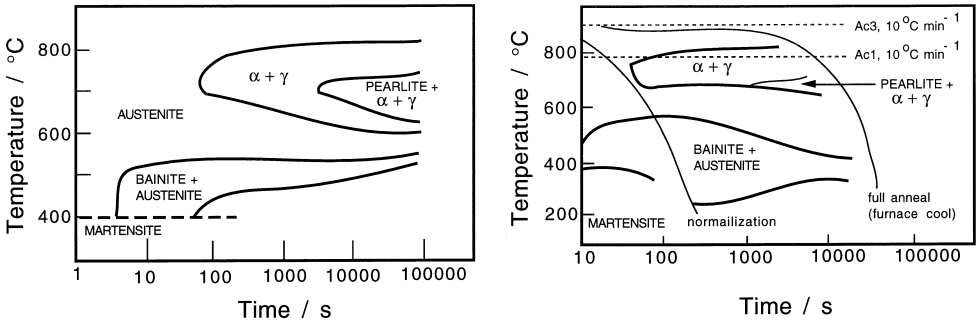

Fig. 6.38 Corresponding TTT and CCT diagrams for a 2.25Cr1Mo steel (Lundin *et al.*, 1982). The CCT diagram shows the terminology used in describing air-cooling from the austenitisation temperature (i.e., normalising) and furnace cooling (i.e. annealing).

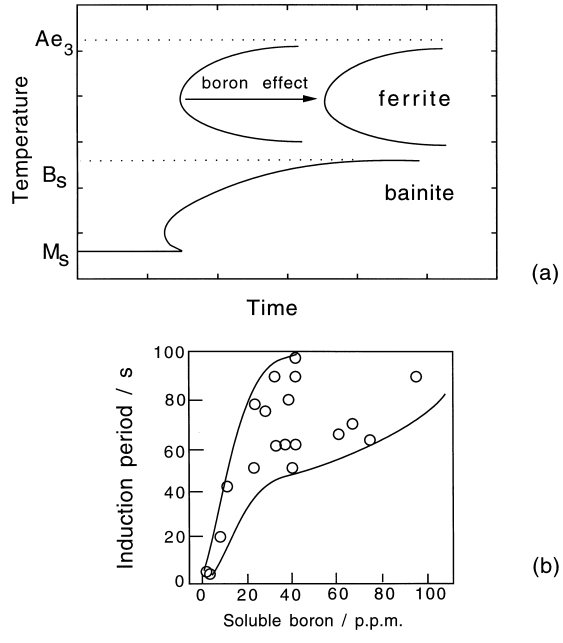

Fig. 6.39 (a) The effect of boron and its analogues (the rare earth elements) on the TTT diagram. There is a pronounced effect on the allotriomorphic ferrite transformation but only a minor retardation of bainitic reaction. (b) Change in the incubation time for the allotriomorphic ferrite reaction as a function of the soluble boron concentration. (After Pickering, 1978).

Boron segregates to austenite grain boundaries. In doing so it reduces the grain boundary energy and hence makes the boundaries less effective as heterogeneous nucleation sites. A typical boron addition of $\simeq 0.002$ wt% is sufficient to have a profound effect on transformation kinetics, although the exact amount must clearly depend on the austenite grain size. Too much boron precipitates as borides which stimulate the nucleation of ferrite. The boron is only effective in enhancing hardenability when present in solid solution, not when precipitated as oxides or nitrides (Fig. 6.40). It is for this reason that boron containing steels are usually deoxidised with aluminium. Titanium is added to tie up any nitrogen which may otherwise combine with the boron and render it impotent.

Carbon also tends to segregate to austenite grain boundaries. In low carbon steels, niobium or titanium forms carbides thereby reducing the quantity available for segregation. This leaves the boundaries open to receive boron (Tamehiro *et al.*, 1987a,b). Otherwise the boron can be displaced from the grain boundaries by the preferential segregation of carbon.

The efficacy of boron is influenced by the presence of nonmetallic inclusions, especially in steel welds or in inoculated steels where inclusions are added deliberately to induce the precipitation of desirable forms of bainite. For example, MnS and Al_2O_3 particles seem to act as heterogeneous nucleation sites for BN and $M_{23}C_6$ during fabrication (Saeki *et al.*, 1986). This reduces the free boron available for segregation to the ferrite nucleation sites (Dionne *et al.*, 1988).

Quite small concentrations of sulphur ($\simeq 0.005$ wt%) can sometimes stimulate the nucleation of bainite (Umemoto *et al.*, 1986b). Iron-rich sulphides precipitate at the austenite grain boundaries and form potent sites for the nucleation of bainite.

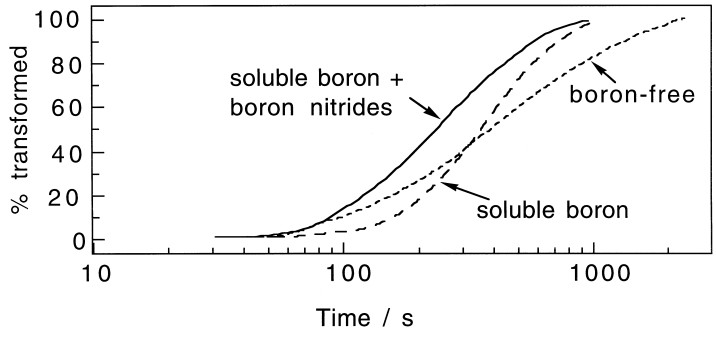

Fig. 6.40 Experimental data due to Ueda *et al.* (1980) for three steels. The rate of reaction is slow in the sample containing soluble boron and fast in the one containing boron nitride, compared with the boron-free steel.

Rare-earth elements including cerium, neodymium, lanthanum and yttrium are believed to act in a manner similar to boron (Jingsheng *et al.*, 1988). Attention has been focused on cerium additions of up to 0.134 wt%, where it is found that allotriomorphic ferrite formation is retarded relative to that of bainite. The mechanism is said to involve the segregation of cerium to the austenite grain boundaries. The effect of cerium is dramatically reduced if the phosphorous content exceeds $\simeq 0.02$ wt%, although the mechanism of this interaction is not yet established.

An indirect role of elements such as yttrium comes from their ability to getter sulphur, especially in the presence of sulphides which influence the nucleation frequency of ferrite (Abson, 1987).

6.12 Superhardenability

Transformations in a moderately hardenable steel can be retarded by superheating the melt to about 1650 °C during steelmaking, as long as the aluminium concentration is in the range 0.03–0.05 wt% (Brown and James, 1980). This phenomenon is dubbed the *superhardenability effect*; the effect on TTT diagrams is shown in Fig. 6.41.

The effect is most pronounced with high hardenability steels; it is also enhanced by increasing the aluminium concentration to about 0.06 wt% before it saturates (Mostert and van Rooyen, 1982). Superhardenability is not influenced by prolonged holding at the austenitisation temperature, as sometimes happens with hardenability increments due to boron additions. Some of the samples used in the original experiments were cast in air, the others in argon, and tests were carried out for both superheated (1650 °C) and conventional melts (1550 °C), at varying concentrations of aluminium. The superheated melts were held at 1650 °C for a few minutes and then cooled to 1550 °C, where alloying additions were made before casting.

The superheat apparently causes the breakdown of clusters of alloying atoms in the liquid and this influences hardenability (Sachs *et al.*, 1980). This fails to explain why holding a superheated melt at a lower temperature before casting does not reform the clusters and hence eliminate the superhardenability. Furthermore, superheating is not necessary when the melting is carried out under an inert atmosphere.

An alternative interpretation is based on nonmetallic inclusions such as manganese oxysulphides or titanium oxides in the steel. These can help nucleate ferrite and so reduce hardenability (Chapter 10). Aluminium is a stronger oxidising element than Mn, Si, or Ti. It forms alumina which is ineffective as a heterogeneous nucleation site for ferrite. The preferential formation of alumina would therefore lead to an increase in hardenability. This hypothesis explains several features of the superhardenability effect:

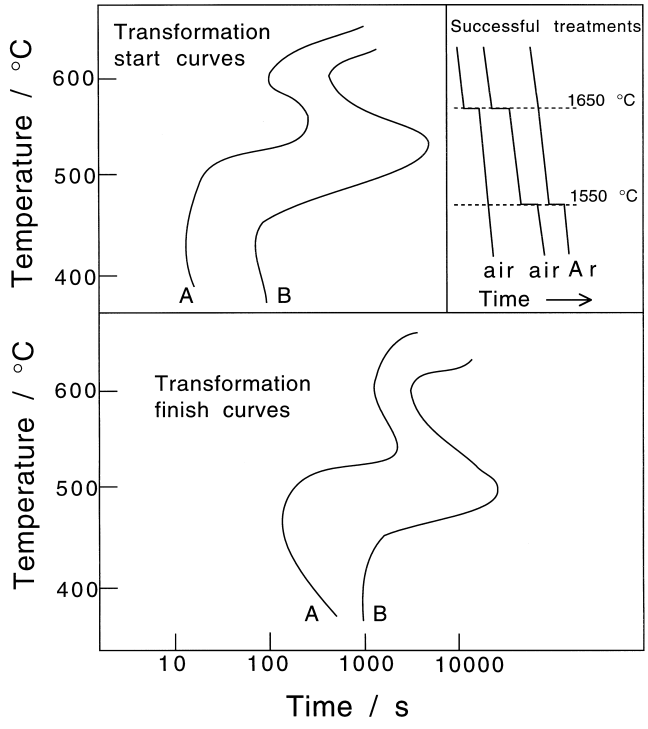

Fig. 6.41 The superhardenability effect. Curves *A* and *B* represent steels which were cast using melt temperatures of 1550 and 1650 °C respectively. The steels have similar compositions but their aluminium concentrations are 0.03 and 0.09 wt% respectively. After Mostert and van Rooyen (1982).

(i) The need to add aluminium.
(ii) That superheat is not needed when an inert gas cover is used during steelmaking. This would lead to a reduction in the oxygen concentration and hence the number density of the oxide nucleation sites.
(iii) Consistent with experimental data, an inclusion effect should not fade during prolonged austenitisation.
(iv) The additional nucleation sites on inclusions can only contribute significantly in steels which already have a reasonable hardenability, i.e. where any enhancement of nucleation kinetics would have a noticeable outcome.

The potent influence of inclusions is well established in welding metallurgy (Chapter 10). Controlled experiments are now needed, in which the trace element concentrations (Al, Ti, O, N, S, B) are carefully monitored.

6.13 The Effect of Chemical Segregation

Commercial steels do not have a uniform chemical composition. The thermomechanical processing used in the manufacturing process improves matters but the final product still is heterogeneous. Solute segregation can have a profound effect on the development of microstructure, for example, in the development of bands of transformation products (Fig. 6.42). The segregation structure of solidification is spread out into bands parallel to the rolling plane during deformation. The microstructural bands follow the segregation pattern because it is the local chemical composition that determines the onset of transformation.

The scale of segregation compares with the spacing of the secondary dendrite arms of the solidification microstructure, with a repeat distance of a few tens of micrometers. The peak concentrations are about factor of two of the mean values. Any coherency strains caused by variations in lattice parameter due to these composition gradients can therefore be neglected. Such strains become important in the theory of spinodal decomposition (or artificial multilayered structures) where the gradients are much larger.

It is the segregation of substitutional solutes which is the real cause of banding. Carbon diffuses rapidly and becomes homogeneous in the austenite; there may be small concentration variations as the carbon attempts to achieve a uniform chemical potential in the presence of substitutional solute gradients (Kirkaldy *et al*., 1962).

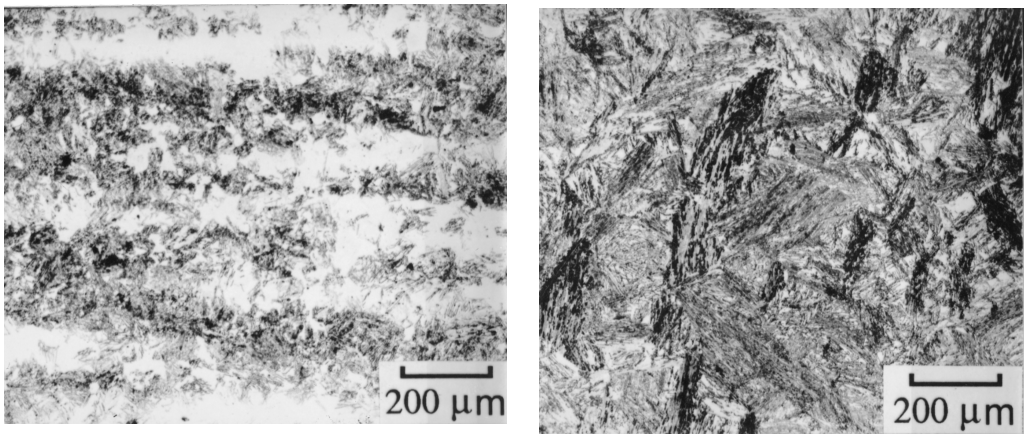

Fig. 6.42 (a) Optical micrograph illustrating the banded microstructure obtained in a heterogeneous steel (300M) after isothermal transformation to bainite; (b) corresponding optical micrograph for the sample which was homogenised prior to isothermal transformation to bainite (Khan and Bhadeshia, 1990a).

Although carbon is homogeneously distributed in the austenite, the preferential formation of ferrite in the substitutional-solute depleted regions causes a partitioning of carbon into the adjacent substitutionally-enriched regions. The resulting carbon-enriched bands have a profound influence on the development of microstructure, but it is important to realise that the redistribution of carbon is a consequence of solid state transformation and only indirectly due to the solidification process.

Davenport (1939) compared the isothermal transformation kinetics of steels containing banding with those which had been homogenised by annealing in the austenitic condition. It is expected that transformation should start first in the solute-depleted regions, and at a temperature which is higher than that for a homogenised steel. The early part of the TTT diagram of segregated steels is expected to reflect the behaviour of the solute-depleted regions. Conversely, the C curves for the later stages of transformation should reflect slower transformations in the solute-enriched regions. Davenport's experiments did confirm this; the C curves for the initiation of bainite in the segregated steels were frequently found to be at longer times when compared with homogenised steels.

The observations are summarised in Fig. 6.43. The reaction is faster in the heterogeneous sample at high transformation temperatures, but not as the undercooling below the B_S temperature increases. The rate is always found to be slower in the heterogeneous samples when considering the later stages of transformation. Experiments by Grange (1971) are consistent with these observations. The fact that the C curves of the homogeneous and heterogeneous

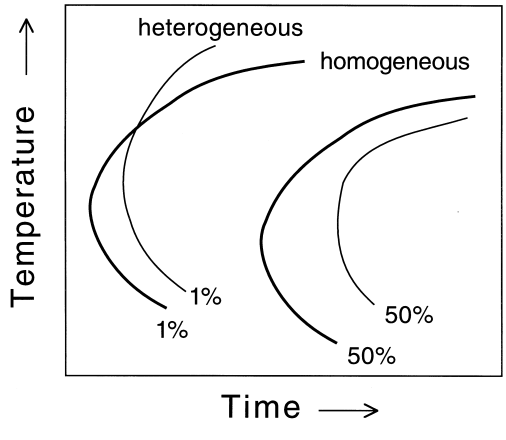

Fig. 6.43 The effect of chemical segregation on the bainite C curves of TTT diagrams.

samples cross is difficult to understand if it is argued that transformation should always be easier in the solute-depleted regions.

The peculiar behaviour illustrated in Fig. 6.43 has been explained quantitatively (Khan and Bhadeshia, 1990a). The segregated steel is able to transform in its solute-depleted regions at temperatures above B_S for the homogeneous alloy. This advantage is maintained at small undercoolings. However, at higher undercoolings the homogeneous steel is able to transform faster because bainite can nucleate uniformly in all regions, whereas it is only able to form in the depleted regions of the heterogeneous alloy.

The carbon partitioned during transformation is localised near the platelets so on a coarser scale it is more uniformly distributed in the homogeneous sample where the bainite grows everywhere. By contrast, most of the partitioned carbon remains in the substitutional solute depleted regions of the segregated sample and retards the development of transformation. The effect is prominent at large undercoolings because the maximum fraction of bainite that can form is greater. Anything which enables the distribution of carbon to become more uniform gives heterogeneous steels a kinetic advantage. For example, slow cooling through the transformation range (Fig. 6.44).

To summarise, when bainite forms during continuous cooling transformation, the reaction may begin at a higher temperature in segregated steels, but both the extent and rate of subsequent transformation should be larger in homogenised alloys.

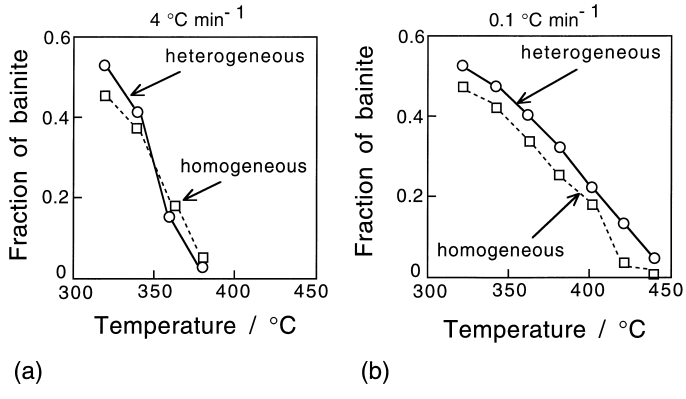

Fig. 6.44 Experiments on homogenised and heterogeneous steel samples in which bainitic transformation was obtained by continuous cooling: (a) $4\,^{\circ}\mathrm{C\,min^{-1}}$; (b) $0.1\,^{\circ}\mathrm{C\,min^{-1}}$. The slower cooling conditions permit a more uniform distribution of carbon in the residual austenite, in which case the heterogeneous sample transforms to a greater extent relative to the homogenised sample, at all temperatures.

6.14 Martensitic Transformation in Partially Bainitic Steels

The formation of bainite enriches the residual austenite and introduces strains and defect. This must influence the way in which the residual austenite transforms subsequently to martensite.

The progress of the athermal martensitic transformation is usually described empirically using the Koistinen and Marburger (1959) equation:

$$1 - \xi = \exp\{-C_6(M_S - T_Q)\} \tag{6.55}$$

where ξ is the volume fraction of martensite, T_Q is a temperature to which the sample is cooled below M_S and $C_6 \simeq 0.011\,\mathrm{K}^{-1}$ is a constant obtained originally by fitting to experimental data.

Magee (1970) justified this equation by assuming that the number density of new plates of martensite per unit volume of austenite, dN, is proportional to the change in the driving force $\Delta G^{\gamma\alpha}$ on cooling below M_S:

$$dN = -C_7 d(\Delta G^{\gamma\alpha})$$

where C_7 is a proportionality constant. The change in the volume fraction of martensite is therefore given by:

$$d\xi = \overline{V} dN_V$$

where dN_V is the change in the number of new plates of martensite formed per unit volume of sample, given by $dN_V = (1 - \xi)dN$. On combining these equations and substituting $[d(\Delta G^{\gamma\alpha})/dT]dT$ for $d(\Delta G^{\gamma\alpha})$ we get:

$$d\xi = -\overline{V}(1 - \xi)C_7 \frac{d(\Delta G^{\gamma\alpha})}{dT} dT$$

which on integration between the limits M_S and T_Q gives

$$\ln\{1 - \xi\} = \overline{V} C_2 \frac{d(\Delta G^{\gamma\alpha})}{dT} (M_S - T_Q)$$

or

$$1 - \xi = \exp\left\{\overline{V} C_2 \frac{d(\Delta G^{\gamma\alpha})}{dT} (M_S - T_Q)\right\} \tag{6.56}$$

which has a similar form as the equation used by Koistinen and Marburger.

6.41.1 Autocatalysis

The initial number density N_i^0 of the defects responsible for the nucleation of martensite is not large enough to explain the observed rate of martensitic

transformation (Shih *et al*., 1955; Pati and Cohen, 1951; Olson and Cohen, 1981). The extra defects necessary to account for the shortfall are obtained by *autocatalysis*. Each plate of martensite creates new embryos in the austenite. Their number density is given by integrating (Lin, 1987):

$$dN = dN_i + d(\xi p)$$

where N_i is the number density of original nucleation sites which survive at any stage of transformation:

$$N_i = (1 - \xi)N_i^0 p \tag{6.57}$$

where p is number of autocatalytic sites generated per unit volume of sample, assumed to be related linearly to the volume fraction of martensite and hence to ξ,

$$p = C_8 + C_9\xi$$

$$\text{so that} \qquad dN = (-N_i^0 + C_8 + 2C_9\xi)d\xi$$

Since $\overline{V}$ is assumed to be constant,

$$d\xi/\overline{V} = (1 - \xi)dN$$

so that

$$\int \frac{d\xi}{\overline{V}(1-\xi)} = \int (-N_i^0 + C_3 + 2C_4\xi)d\xi. \tag{6.58}$$

Integration gives

$$p = N_i^0 - \frac{\ln\{1-\xi\}}{\xi\overline{V}} \tag{6.59}$$

It is found experimentally that:

$$p - N_i^0 = C_{10} + C_{11}(M_S - T_Q)$$

On setting $M_S - T_Q = 0$, it is found that $C_{10} = 1/\overline{V}$. It follows that

$$-\frac{\ln\{1-\xi\}}{\xi} = 1 + \overline{V}C_6(M_S - T_Q) \equiv 1 + C_{12}(M_S - T_Q) \tag{6.60}$$

This is an alternative kinetic model for the development of martensitic transformation as a function of undercooling below the M_S temperature. It has been used to rationalise martensite transformation kinetics in fully austenitic samples as well as those which are first partially transformed to bainite.

Although a reasonable fit has been demonstrated (Fig. 6.45), the model tends to overestimate the fraction transformed when the amount of martensite is small.

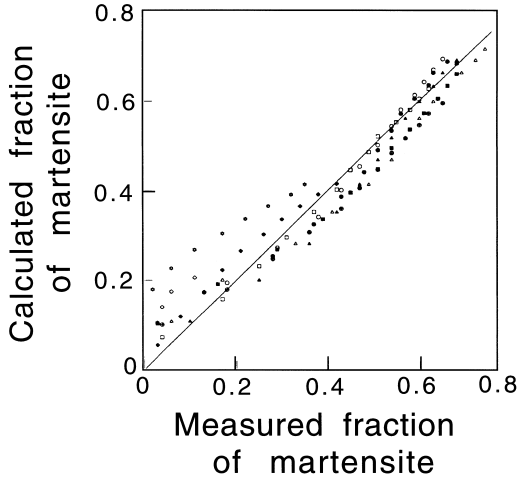

Fig. 6.45 Comparison of experimental results with those calculated by fitting equation 6.60 to the experimental data. After Khan and Bhadeshia, 1990b.

6.15 Summary

Both the individual platelets and the sheaves of bainite lengthen at rates much faster than permitted by the diffusion of carbon. It must be concluded that they grow with a supersaturation of carbon, the ferrite inheriting the composition of the parent austenite. The excess carbon is soon afterwards partitioned into the residual austenite or precipitates as carbides.

It is possible that not all the carbon is trapped in the ferrite during transformation. However, neither the experimental evidence nor the theory for growth with partial supersaturation is convincing.

Carbon must partition during the nucleation of bainite. The nucleation probably occurs by a displacive mechanism akin to martensite, but with the most potent sites confined to the austenite grain surfaces. Autocatalytic nucleation plays a role but it is not as prominent for bainite as it is for martensite. The activation energy for nucleation varies linearly with the driving force. Nucleation does not therefore rely on heterophase fluctuations, but rather on the dissociation of dislocation clusters. The activation energy is in these circumstances from the resistance to interfacial motion.

The calculation of overall transformation kinetics remains challenging. Whereas some important trends are reproduced, accurate predictions using few parameters are not yet possible. This indicates that important variables remain to be identified. A qualitative result is that bainitic transformation is less sensitive to the austenite grain size when compared with pearlite. This is

because sheaf growth occurs by the propagation of sub-units at sites away from the austenite grain surfaces.

Except at temperatures close to B_S, homogeneous steels transform more rapidly than those containing chemical segregation. The martensitic decomposition of austenite left untransformed after the growth of bainite can be described adequately by the theory for the martensitic decomposition of fully austenitic samples.

7 *Upper & Lower Bainite*

Although there have been attempts at generalising the definition of bainite, the most appropriate description remains that the microstructure consists of a non-lamellar mixture of ferrite and carbides, which can be classified further into upper and lower bainite. This latter distinction is of value because there are clear differences in the mechanical properties of upper and lower bainite. The two microstructures can easily be distinguished using transmission electron microscopy and hence can be discussed in the context of mechanical properties and the growth mechanism.

Lower bainite is obtained by transformation at relatively low temperatures. Both upper and lower bainite form as aggregates of small plates or laths (sub-units) of ferrite. The essential difference between them is in the nature of the carbide precipitates. Upper bainitic ferrite is free of precipitation, any carbides growing from the carbon-enriched residual austenite between the plates of ferrite. In addition to this kind of precipitation, there are carbide particles present inside lower bainitic ferrite. We shall see that the precipitates in lower bainitic ferrite can be any of the carbides reported to occur during the tempering of martensite, for example, ϵ, η, χ or cementite.

7.1 The Matas and Hehemann Model

The transition between upper and lower bainite is believed to occur over a narrow range of temperatures. It is possible for both forms to occur simultaneously during isothermal transformation near the transition temperature (Pickering, 1967). Matas and Hehemann (1961) proposed that the difference between upper and lower bainite comes from a competition between the rate at which carbides can precipitate from ferrite and the speed with which carbon is partitioned from supersaturated ferrite into austenite (Fig. 7.1). Upper bainite forms at higher temperatures, permitting the excess carbon to partition before it can precipitate in the ferrite. In lower bainite, the slower diffusion associated with the reduced transformation temperature provides an opportunity for some of the carbon to precipitate in the supersaturated ferrite.

A corollary is that upper bainite should not form when the carbon concentration is large. This is indeed found to be the case in a Fe–7.9Cr–1.1C wt% alloy which has a B_S temperature of just 300 °C (Srinivasan and Wayman,

[13:31 3/9/01 C:/3B2 Templates/keith/3750 BAINITE.605/3750-007.3d] Ref: 0000 Auth: Title: Chapter 00 Page: 189 189-200

1968a), and in a Fe–4.08Cr–0.3C wt% alloy which has a B_S temperature of 490 °C. Ohmori and Honeycombe (1971) have shown that in a series of high purity Fe–0.16–0.81C wt% alloys, lower bainite is not obtained when the carbon concentration is less than about 0.4 wt%. Tsuzaki *et al.* (1991) found a similar result for Fe–Si–C alloys; only upper bainite formed in a Fe–2Si–1Mn–0.34C wt% steel, whereas both upper and lower bainite could be observed when a higher carbon variant (0.59 wt%) was examined. A thorough piece of work by Oka and Okamoto (1986) on high purity, high carbon Fe–0.85–1.8C wt% steels has shown the absence of upper bainite in all cases. The formation of pearlite was in each case found to give way directly to that of lower bainite.

The model illustrated in Fig. 7.1 has been expressed quantitatively by comparing the time required to decarburise supersaturated ferrite against cementite precipitation kinetics (Takahashi and Bhadeshia, 1990).

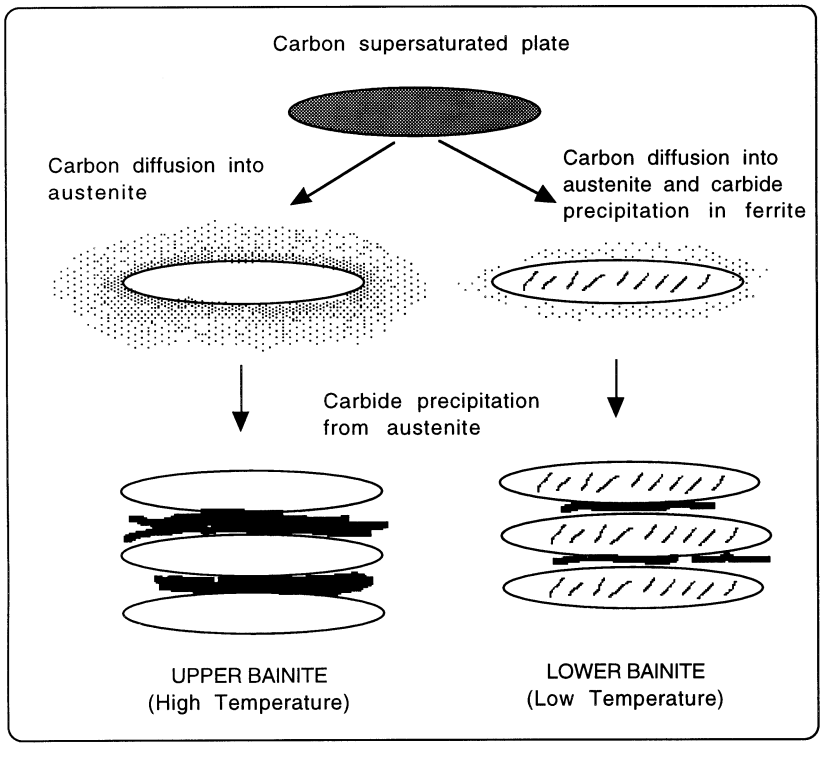

Fig. 7.1 Schematic representation of the transition from upper to lower bainite. After Takahashi and Bhadeshia (1990).

[13:31 3/9/01 C:/3B2 Templates/keith/3750 BAINITE.605/3750-007.3d] Ref: 0000 Auth: Title: Chapter 00 Page: 190 189-200

7.2 Quantitative Model

7.2.1 Time to Decarburise Supersaturated Ferrite

The theory for the partitioning of carbon from a supersaturated plate of ferrite has been presented in Chapter 6. The diffusion coefficient of carbon in ferrite is greater than that in austenite. This, together with the assumption that there is local paraequilibrium at the α/γ interface, gives the time t_d required to decarburise a plate of a specified thickness (equation 6.28). Some results for plain carbon steels are presented in Fig. 7.2. In each case, t_d is found to go through a minimum as a function of the transformation temperature. This is because the diffusion coefficient of carbon decreases with temperature (leading to an increase in t_d), while at the same time, the amount of carbon that the austenite can tolerate increases at lower temperatures.

7.2.2 Kinetics of Cementite Precipitation

It is not yet possible to estimate the rate of cementite precipitation from supersaturated ferrite as a function of time, temperature and chemical composition.

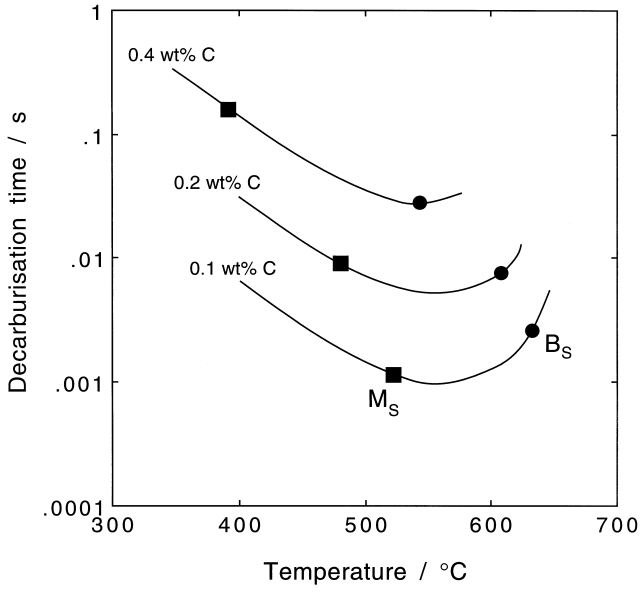

Fig. 7.2 Calculated time for the decarburisation of supersaturated ferrite plates (of thickness 0.2 μm) in plain carbon steels with 0.1, 0.2 and 0.4 wt% carbon respectively. The calculated martensite-start and bainite-start temperatures are also indicated.

[13:31 3/9/01 C:/3B2 Templates/keith/3750 BAINITE.605/3750-007.3d] Ref: 0000 Auth: Title: Chapter 00 Page: 191 189-200

However, for plain carbon steels, and in some cases for alloy steels, martensite tempering data can be adapted to derive reasonable functions for the purpose of predicting the transition from upper to lower bainite (Takahashi and Bhadeshia, 1990, 1991).

The first change that happens during the tempering of supersaturated martensite is that the excess carbon precipitates in the form of carbides. Prolonged annealing can also lead to recovery, recrystallisation and the coarsening of cementite precipitates. To derive a function representing precipitation alone, it is necessary to focus on the early stages of tempering.

Speich (1969) reported that the change in hardness of martensite in plain carbon steels after an hour of tempering at temperatures above 320 °C, includes significant contributions from recovery, recrystallisation and coarsening of cementite particles (Fig. 7.3). The data representing hardness changes during tempering below 320 °C can be used to derive a function which expresses the change in the volume fraction of cementite precipitation as a function of time and temperature. An Avrami equation can then be used empirically to represent the tempering reaction:

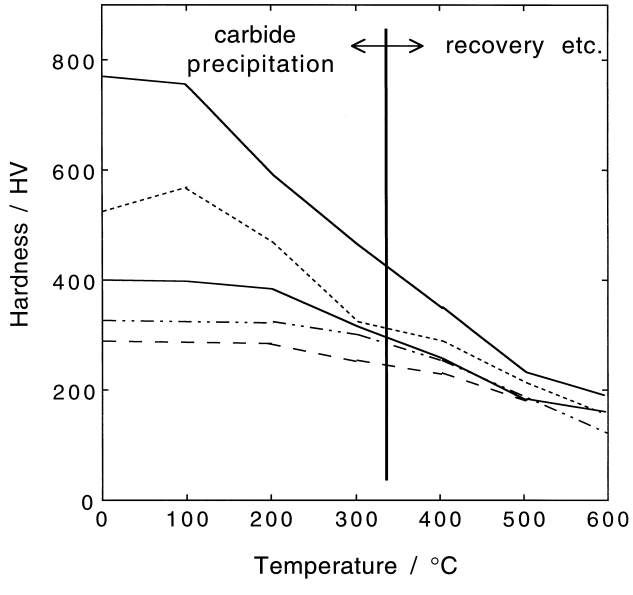

Fig. 7.3 Hardness curves for iron–carbon martensitic samples which were tempered for 1 hour at the temperatures indicated; the five curves represent steels with different carbon concentrations (data due to Speich, 1969). The data to the left of the vertical line reflect changes due to the precipitation of carbides rather than recovery or coarsening processes.

[13:31 3/9/01 C:/3B2 Templates/keith/3750 BAINITE.605/3750-007.3d] Ref: 0000 Auth: Title: Chapter 00 Page: 192 189-200

$$\xi\{t\} = 1 - \exp\{-k_A t^n\} \tag{7.1}$$

where $\xi\{t\}$ is the volume fraction of cementite normalised by its equilibrium volume fraction at the reaction temperature, t is the time, and k_A and n are rate constants determined from the experimental data. Since it is assumed that $\xi\{t\}$ is related at any time to the hardness of the martensite, $H\{t\}$, it follows that:

$$\xi\{t\} = (H_0 - H\{t\})/(H_0 - H_F) \tag{7.2}$$

H_0 is the hardness of the as-quenched virgin martensite, H_F is its hardness when all the carbon has precipitated but before any significant recovery, recrystallisation or coarsening has occurred. The assumption here is that the amount of carbon precipitated is related linearly to the change in hardness during the early stages of tempering.

Using the values of hardness for plain carbon martensite tempered for 1 hour at 320 °C, reported by Speich, H_F can be expressed empirically as a function of the initial hardness and average carbon concentration $\overline{x}$ (mole fraction), as follows:

$$H_F = H_0[1 - 1.731\overline{x}^{0.34}] \tag{7.3}$$

This equation is valid for plain carbon steels containing less than 0.4 wt% carbon, the value of H_F becoming constant thereafter. The hardness H_0 of plain carbon martensite (< 0.4 wt% carbon) before tempering can be also be deduced from the data reported by Speich:

$$H_0 = 1267(\text{weight \%} \quad \text{carbon})^{0.9} + 240 \tag{7.4}$$

where the hardness of martensite in pure iron is 240 HV (Leslie, 1982). This equation gives the hardness of virgin martensite in plain carbon steels as a function of dissolved carbon. There is evidence that the effect of carbon tends eventually to saturate, so H_0 should be set not exceed about 800 HV irrespective of the carbon concentration (Bhadeshia and Edmonds, 1983a,b). Having established all the data necessary to estimate the amount of cementite precipitated, it remains to evaluate the terms k_A and n of the Avrami equation in order to calculate the time t_θ for the formation of a specified fraction of cementite as a function of time, temperature and carbon concentration. This can easily be done by fitting the Avrami equation to experimental data on the tempering of martensite.

There are more elaborate theories available for the change in the strength of low-carbon martensite due to the precipitation of cementite, making it possible to estimate $H_0 - H_F$ independently of the empirical approach described above. The change can be expressed in terms of the decrease in solid solution strengthening as carbon is incorporated into cementite, and a lesser increase in strength as the cementite particles precipitation harden the martensite. Thus,

the yield strength of martensite, σ_y, is expressed as a combination of the intrinsic yield strength, the effect of the dislocation cell structure, and precipitation hardening by cementite (Daigne *et al*., 1982):

$$\sigma_y = \sigma_0 + k_\epsilon \epsilon_1^{-1} + k_p \Delta^{-1}, \text{MPa} \tag{7.5}$$

where σ_0 is the intrinsic strength of martensite (including solid solution strengthening due to carbon), ϵ_1 is the average transverse thickness of the cell structure, and Δ is the average distance between a particle and its two or three nearest neighbours. The data needed to evaluate the equation are well-founded. A comparison of the calculated strength and measured strength after tempering should give a good idea of the extent of cementite precipitation. When this is done, the relation between hardness and the amount of the precipitation (thus the decrease in solute carbon) is found not to be linear as was assumed in the empirical approach, but the predicted changes in hardness are found to be remarkably consistent with those measured by Speich for the early stages of tempering. This justifies the assumption that much of the hardness change can be attributed to the precipitation of carbon rather than due to other annealing effects such as tempering.

7.2.3 *Quantitative Estimation of the Transition Temperature*

Following the gist of the Matas and Hehemann proposal, a comparison of the time t_d required to decarburise a plate of ferrite, with the time interval t_θ necessary to obtain a detectable amount of cementite precipitation in the ferrite should give a good indication of whether upper or lower bainite is expected during isothermal transformation. If $t_d < t_\theta$ then it may be assumed that upper bainite is obtained, and vice versa (Fig. 7.4). A weakness of this theoretical model is that decarburisation and precipitation should really be coupled. A disposable parameter in the model as it stands is the 'detectable amount' of cementite precipitation, which has to be fixed by comparison with experimental data.

Some calculated data on the plain carbon steels are presented in Fig. 7.5. They indicate that lower bainite should not be observed in plain carbon steels with carbon concentrations less than 0.32 wt%. Furthermore, only lower bainite (i.e. no upper bainite) is expected in steels with carbon concentrations exceeding 0.4 wt%. Steels containing between 0.32 and 0.4 wt% of carbon should exhibit both both upper and lower bainite, depending on the reaction temperatures. Finally, at low temperatures where t_θ and t_d both become large, the times required for precipitation or redistribution of carbon exceed that to complete transformation, consistent with the fact that untempered martensite

[13:31 3/9/01 C:/3B2 Templates/keith/3750 BAINITE.605/3750-007.3d] Ref: 0000 Auth: Title: Chapter 00 Page: 194 189-200

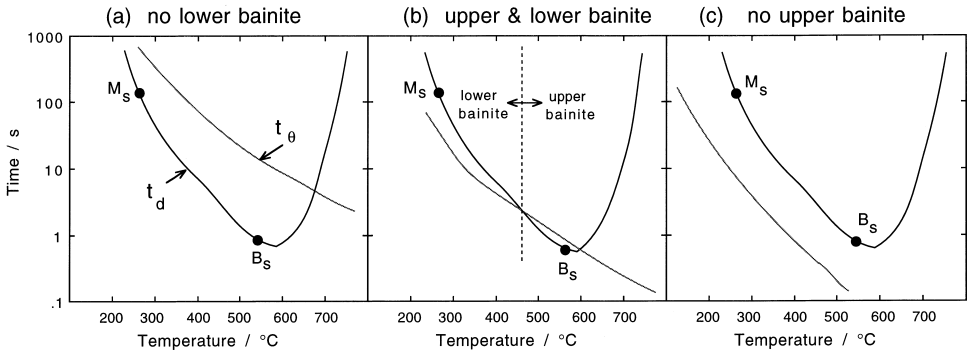

Fig. 7.4 Illustration of how differences in the relative variation of the decarburisation time t_d and the precipitation time t_θ can lead to: (a) a steel which is incapable of transforming to lower bainite; (b) a steel which should, under appropriate conditions, be able to transform to upper or lower bainite; (c) a steel in which bainitic transformation always leads to the formation of lower bainite.

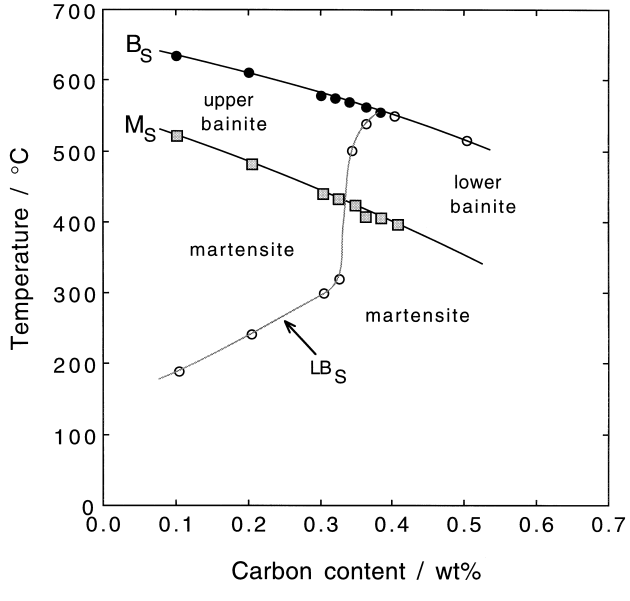

Fig. 7.5 Calculated lower bainite transformation start temperatures for plain carbon steels, as a function of transformation temperature. The calculated martensite-start and bainite-start temperatures are also presented. After Takahashi and Bhadeshia, 1990.

[13:31 3/9/01 C:/3B2 Templates/keith/3750 BAINITE.605/3750-007.3d] Ref: 0000 Auth: Title: Chapter 00 Page: 195 189-200

can be obtained at temperatures near M_S, with the degree of autotempering of the martensite decreasing as M_S is reduced.

7.2.4 Comparison of Theory and Experimental Data

The general behaviour indicated by the calculations for plain carbon steels, is found to be that observed experimentally. Some interesting work by Oka and Okamoto (1986) proves that there is no upper bainite in plain carbon steels with more than 0.8 wt% of carbon; the only bainite observed in their experiments was classical lower bainite at all temperatures above the M_S temperature (Fig. 7.6a).

Ohmori and Honeycombe (1971), in a study of plain carbon steels, showed that during isothermal transformation above M_S, only upper bainite could be obtained in samples containing less than 0.4C wt% (Fig. 7.6b). This is consistent with theory, although their observation that upper bainite can be obtained in steels with a carbon concentration up to about 0.85C wt% is not consistent with the theory, nor with the data reported by Oka and Okamoto (1986).

7.3 Mixed Microstructures Obtained By Isothermal Transformation

According to the analysis presented above, only lower bainite is expected in plain carbon steels with more than 0.32 wt% of bulk carbon content. However, the calculations are for ferrite plates whose carbon concentration is at first identical to that of the bulk alloy. As transformation proceeds the austenite becomes enriched in carbon. The bainite which grows from this enriched austenite will inherit a higher than bulk concentration of carbon. This leads to the possibility of upper bainite being followed by lower bainite during isothermal transformation. Mixed microstructures should therefore be obtained in plain carbon steels containing less than 0.32 wt% carbon, especially if the rate of carbide precipitation from the austenite is slow enough to allow the austenite to become enriched.

The maximum carbon concentration that can be tolerated in residual austenite before the bainite reaction stops is given by the T_0' curve. Therefore if the carbon concentration in residual austenite at the T_0' curve (i.e. $x_{T_0'}$) is greater than 0.32 wt%, lower bainite can form during the later stages of transformation.

However, the formation of cementite from the residual austenite also becomes possible if $x_{T_0'} > x^{\gamma\theta}$, where $x^{\gamma\theta}$ is a point on the $\gamma/(\gamma+\theta)$ phase boundary, since the austenite will then be supersaturated with respect to the cementite. The fact that a curve showing the carbon concentration in austenite which is in equilibrium with cementite in plain carbon steels crosses the T_0'

[13:31 3/9/01 C:/3B2 Templates/keith/3750 BAINITE.605/3750-007.3d] Ref: 0000 Auth: Title: Chapter 00 Page: 196 189-200

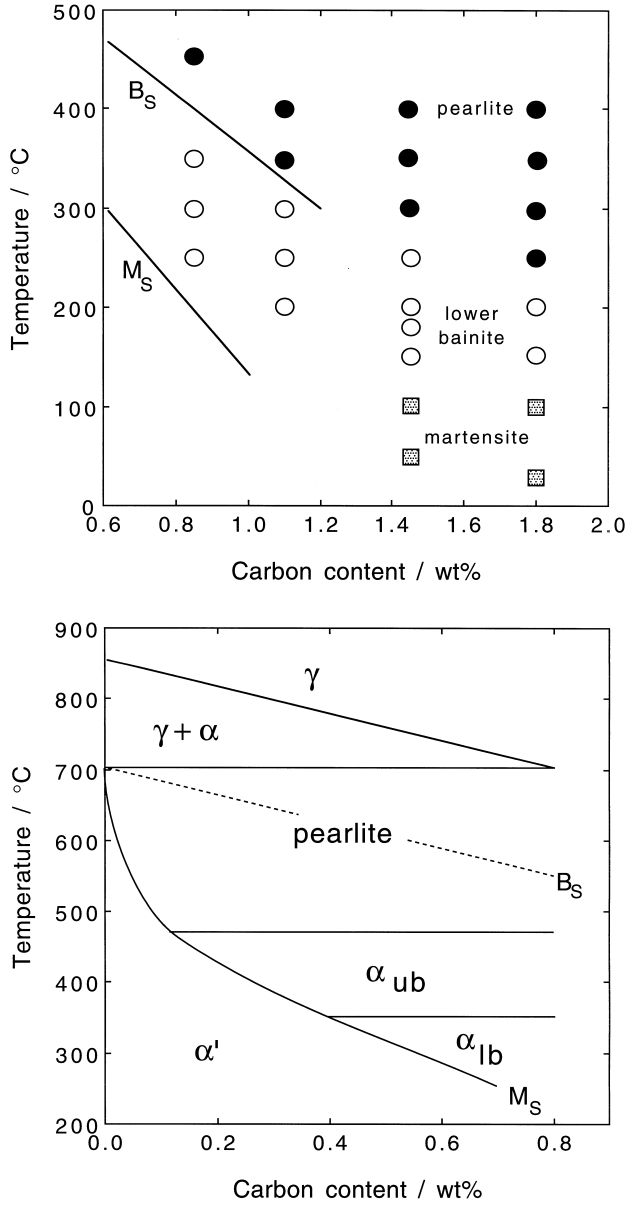

Fig. 7.6 (a) Experimental data (Oka and Okamoto, 1986) illustrating the temperatures at which fine nodules of pearlite, classical lower bainite and martensite were obtained by isothermal transformation of plain carbon steels. The lines represent calculated bainite-start and martensite-start temperatures (Takahashi and Bhadeshia, 1990). (b) The effect of carbon concentration on the temperature range where each microstructure is formed (Ohmori and Honeycombe, 1971).

[13:31 3/9/01 C:/3B2 Templates/keith/3750 BAINITE.605/3750-007.3d] Ref: 0000 Auth: Title: Chapter 00 Page: 197 189-200

curve at 0.4 wt% of carbon concentration (560 °C), leads to the identification of three regimes for bainite on the Fe–C phase diagram (Fig. 7.7). In steels with more than 0.4 wt% of the initial bulk carbon content (region B), lower bainite is to be expected from the earliest stages of transformation. For steels whose composition lies in region A, lower bainite is expected to be absent during isothermal transformation at all temperatures above M_S, and this behaviour is valid for any stage of transformation since the austenite cannot be supersaturated with cementite as far as regime A is concerned. The behaviour in the region marked C should be more complex. The residual austenite for these steels (region C) may at some stage of transformation contain enough carbon to precipitate cementite. If the kinetics of cementite precipitation from austenite are rapid, then lower bainite may not be obtained in steels with an average carbon concentration less than 0.32 wt%, but otherwise, a mixed microstructure of upper and lower bainite might arise.

Two of the trends described above have been verified by Chang (1999) who not only found that the lower bainie start temperature L_S could be depressed by retarding the precipitation of cementite, but also showed that a mixture of upper and lower bainite can be obtained by transformation at temperatures just above L_S.

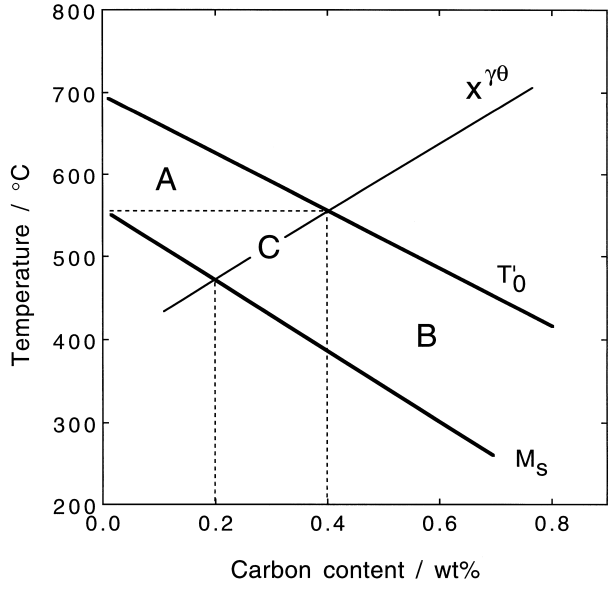

Fig. 7.7 Identification of regimes A, B and C, in which the progress of isothermal transformation can lead to changes in the nature of the transformation product. The line marked $x^{\gamma\theta}$ is the calculated $\gamma/(\gamma+\theta)$ phase boundary.

7.4 Other Consequences of the Transition

The growth of bainite plates stops when the glissile interface is clogged by plastic accommodation induced defects. For a given defect density, lower-bainite plates should be longer than those of upper bainite, since the driving force for transformation increases with the undercooling. At lower transformation temperatures the matrix is able to support higher strains without plastic deformation so that the defect density *in the matrix* is expected to be smaller. Step quenching experiments in which an alloy is first partially transformed to lower bainite and then heated rapidly into the upper bainite transformation range are consistent with this since the growth of lower bainite ceases on reaching the higher temperature (Goodenow and Hehemann, 1965). This also happens when specimens partially transformed to lower bainite experience an increase in temperature within the lower bainite transformation range (White and Owen, 1961).

7.5 Comparison with the Tempering of Martensite

We have seen that the transition from upper to lower bainite can be predicted on the basis of a simple model which compares the rates of decarburisation and precipitation. Lower bainite is in effect generated by a process of auto-tempering. It follows that there should be a strong comparison with the microstructure of tempered martensite.

When high-carbon martensite is tempered, the first precipitate is usually a transition phase such as ϵ-carbide, which is replaced eventually by the more stable cementite. Similarly, when lower bainite forms in high carbon steels, it contains ϵ-carbide which subsequently transforms into cementite during prolonged holding at the isothermal transformation temperature (Matas and Hehemann, 1961).

The chances of obtaining ϵ-carbide (instead of cementite) in lower bainite increase as the transformation temperature is reduced for the same steel (see Table II, Matas and Hehemann, 1961). As the transformation temperature is reduced, the time required to decarburise a supersaturated plate of bainite increases. A high carbon concentration can persist in the ferritic matrix for a time period long enough to allow the formation of ϵ-carbide, which does not form if the carbon concentration is less than about 0.25 wt%, (Roberts *et al.*, 1957). This explains why a medium carbon Fe–0.43C–3Mn–2Si wt% steel transforms to lower bainite containing cementite particles, although when quenched to martensite, gives ϵ-carbide on tempering (Bhadeshia and Edmonds, 1979a, 1983a). Some of the carbon is in the former case is lost to the austenite by diffusion, thus preventing the formation of ϵ-carbide.

7.6 Summary

A comparison between the times required to decarburise supersaturated ferrite plates with that required to precipitate cementite within the plates is a reasonable way to interpret the transition from upper to lower bainite. If the decarburisation process dominates, upper bainite is predicted whereas relatively rapid carbide precipitation within the ferrite leads to the microstructure of lower bainite.

A number of predictions from this theory are in agreement with experimental data. Thus, lower bainite cannot form in plain carbon steels containing less than about 0.3 wt% carbon. Similarly, upper bainite is predicted and found to be absent in plain carbon steels containing more than 0.4 wt% carbon.

[13:31 3/9/01 C:/3B2 Templates/keith/3750 BAINITE.605/3750-007.3d] Ref: 0000 Auth: Title: Chapter 00 Page: 200 189-200

8 *Stress and Strain Effects*

A displacive transformation can justifiably be regarded as a mode of deformation of the parent phase, with the additional characteristic that the crystallographic structure of that phase is altered in the deformed region (Table 8.1). For this reason, the permanent strain is called *transformation plasticity*. A phase transformation can be triggered by cooling below a certain transformation-start temperature, by the application of a stress in appropriate circumstances or by a combination of these factors. In the latter case, where the chemical driving force and stress act in concert, transformation plasticity can be obtained at stresses which are much smaller than the yield strength of the stable parent phase.

Table 8.1 Characteristics of different modes of deformation.

	Slip deformation	Mechanical twinning	Displacive transformation	Reconstructive transformation
Permanent deformation?	Yes	Yes	Yes	Yes
Invariant-plane strain with large shear?	Yes	Yes	Yes	No
Crystallographic orientation altered?	No	Yes	Yes	Yes
Lattice change?	No	No	Yes	Yes
Density change?	No	No	Yes	Yes

Just as a combination of a plane and a direction constitutes a deformation system for slip or twinning, the habit plane and displacement vector of an invariant-plane strain describe the deformation system for transformation plasticity. There will in general be 24 of these systems per austenite grain and they may operate simultaneously with varying contributions. Unlike ordinary slip, the different variants of transformation cannot intersect except in special circumstances where intervariant transformations are possible. The ordinary notion of work hardening does not therefore apply. Work hardening

[13:34 3/9/01 C:/3B2 Templates/keith/3750 BAINITE.605/3750-008.3d] Ref: 0000 Auth: Title: Chapter 00 Page: 201 201-224

nevertheless manifests itself via an increase in the stability of the austenite as it becomes more finely divided.

Given the large number of transformation variants available per grain, the Taylor criterion leads to the conclusion that transformation plasticity can cause or accommodate any externally imposed, arbitrary shape change assuming that there is sufficient austenite available to cope with the imposed strain. It follows that polycrystalline samples can remain intact at grain boundaries when transformation plasticity is the sole mode of deformation. Furthermore, the transformation plasticity can cause anisotropic changes in shape even in polycrystalline samples transformed without applied stress if the parent phase is crystallographically textured.

8.1 The Mechanical Driving Force

Given that displacive transformations in steels cause large strains, it is natural to expect an interaction between any applied stress and the progress of the transformation, in a manner which is related uniquely to the transformation mechanism. The total driving force can be partitioned into a *mechanical* and the more usual *chemical* components (Patel and Cohen, 1953; Delaey and Warlimont, 1975; Christian, 1982). The physical reasoning behind this idea is that the movement of a glissile interface is a combined deformation and transformation process. The work done by the external stress may be added to the chemical free energy change in order to obtain the total free energy difference. The mechanical driving force is assumed to be given by the work done (ΔG_{MECH}) by the external stress system in producing the macroscopic shape deformation:

$$\Delta G_{MECH} = \sigma_N \zeta + \tau s \tag{8.1}$$

where σ_N is the normal stress on the habit plane and τ is the component of the shear stress on the habit plane which is parallel to the direction along which the shear displacements of the shape deformation occur (Fig. 8.1). The strains ζ and s have previously been defined as the dilatational and shear components of the shape deformation. Given a free choice of some 12 to 24 crystallographic variants of the transformation product in a grain of austenite, the work done by the shear stress is always expected to be positive, whereas that due to the dilatational component depends on the sign of σ_N. For steels where this latter component is small, the observed stress effects reflect the dominant role of the shear component. The exception is when τ is small or zero, as would be the case when the applied stress is a hydrostatic pressure.

It follows from the equation 8.1, that since the shear stress remains positive irrespective of whether the sample is pulled in tension or uniaxially compressed, and since the shear component of the shape change is large, a

[13:34 3/9/01 C:/3B2 Templates/keith/3750 BAINITE.605/3750-008.3d] Ref: 0000 Auth: Title: Chapter 00 Page: 202 201-224

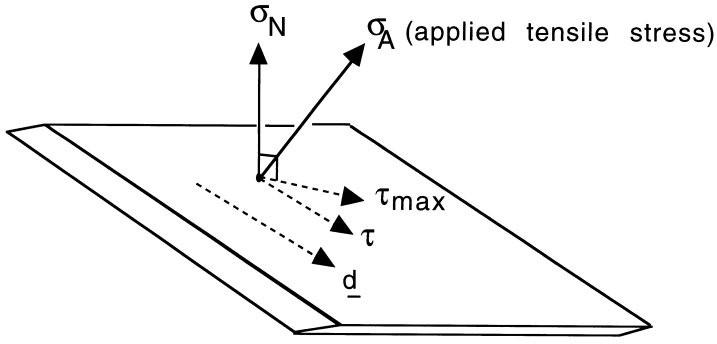

Fig. 8.1 Resolution of the applied stress σ_A. The normal stress σ_N, and the shear stress τ, both act on the habit plane. The vector $\underline{d}$ is the direction along which the shear displacements of the shape deformation lie. τ_{MAX} is the maximum shear stress on the habit plane, but τ is given by resolving τ_{MAX} along $\underline{d}$. Note that $\underline{d}$ differs slightly from the displacement vector of the invariant-plane strain, which includes a dilatational component in addition to the shear.

uniaxial stress will always cause an increase in the transformation temperature for displacive transformations in steels. Hydrostatic stress, on the other hand, has no deviatoric components and consequently only interacts with the dilatational component of the shape change. Thus, hydrostatic compression is expected to lead to a decrease in the transformation temperature (Fig. 8.2).

Shear stresses, unlike pressures, cannot strictly be considered as state variables so their use in thermodynamic equations is uncertain (Christian, 1982). This difficulty is unimportant provided irreversible processes such as diffusion or dislocation motion do not act to relieve the shear stresses during the time scale of the experiment. In practice, this means that in the absence of transformation, the state of the system should not be altered if the shear stress is changed and then restored to its original value.

A second complicating factor could arise if the stress influences the very nature of the transformation product, either by stimulating the formation of a metastable phase or by decoupling groups of self-accommodating variants which would form in the absence of stress (Christian, 1982). This would lead to a modification of the chemical driving force term, and as discussed later, there is some evidence to show that there are significant microstructural changes when bainite grows under the influence of an externally applied stress.

Assuming that the interaction of the applied stress is with the macroscopic shape deformation, the stress must favour the growth of those variants for which ΔG_{MECH} is maximised. Hence, for a tensile stress, plates which have their habit planes inclined at approximately 45° to the tensile axis will tend to

[13:34 3/9/01 C:/3B2 Templates/keith/3750 BAINITE.605/3750-008.3d] Ref: 0000 Auth: Title: Chapter 00 Page: 203 201-224

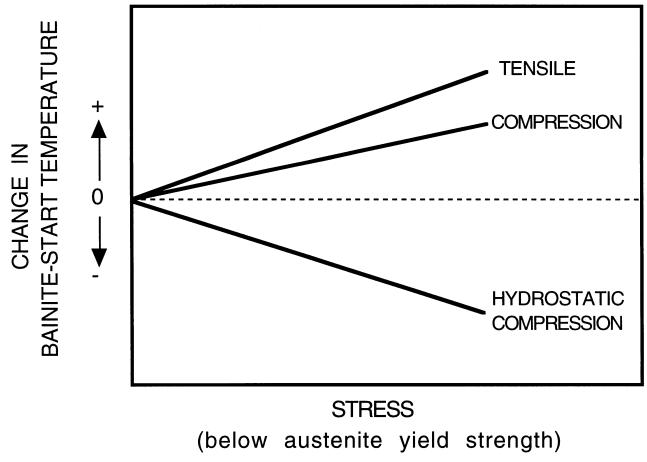

Fig. 8.2 An indication of how the bainite-start temperature should vary as a function of the nature and magnitude of the applied stress.

be favoured.[†] This does assume that the applied stress interacts solely with the growth process whereas its interaction with nucleation events could lead to a different criterion for variant selection (Christian, 1982). Indeed, efforts at predicting the martensitic transformation texture from the crystallographic texture of the parent austenite, are apparently more successful if it is assumed that variant selection depends on the Bain strain rather than on the macroscopic shape deformation (Ray and Jonas, 1990). The IPS deformation is unlikely to have developed at the nucleation stage, where the particle might be too small to sustain a lattice-invariant deformation. The Bain strain is essential to accomplish the lattice change, so the texture prediction work suggests that variant selection may depend on the interaction of the applied stress with the nucleation process.

8.2 The B_d Temperature

The highest temperature at which martensite forms during the cooling of austenite is the M_S temperature. This can be increased by the application of a suitable stress (Patel and Cohen, 1953). The maximum temperature at which martensite grows under the influence of stress is called the M_d temperature.

[†]The angle will not be exactly 45° because the displacement vector of the IPS is not quite parallel to the habit plane whenever ζ is finite.

[13:34 3/9/01 C:/3B2 Templates/keith/3750 BAINITE.605/3750-008.3d] Ref: 0000 Auth: Title: Chapter 00 Page: 204 201-224

There are no similar experiments for bainite but it is possible to piece together evidence to show that the behaviour is similar to that of martensite.

The transformation stresses associated with the growth of lower bainite are known to stimulate upper bainite at temperatures just above B_S, proving that stress can indeed raise the bainite-start temperature (Goodenow *et al*., 1969). It should in principle be possible to define a B_d temperature. Thus, Drozdov *et al*. (1962) found that no amount of deformation causes the austenite to transform to bainite when the temperature is sufficiently greater than B_S, i.e.$T > B_d$.

The expected stress effects are illustrated in Fig. 8.3, which is based on similar ideas for martensitic transformations. The net driving force available for transformation, ΔG, is given by:

$$\Delta G = \Delta G_{CHEM} - \Delta G_{MECH} \tag{8.2}$$

It is assumed that the critical value needed to trigger bainitic transformation at zero stress (i.e. $\Delta G_{CHEM}\{B_S\}$) remains constant over the temperature range of

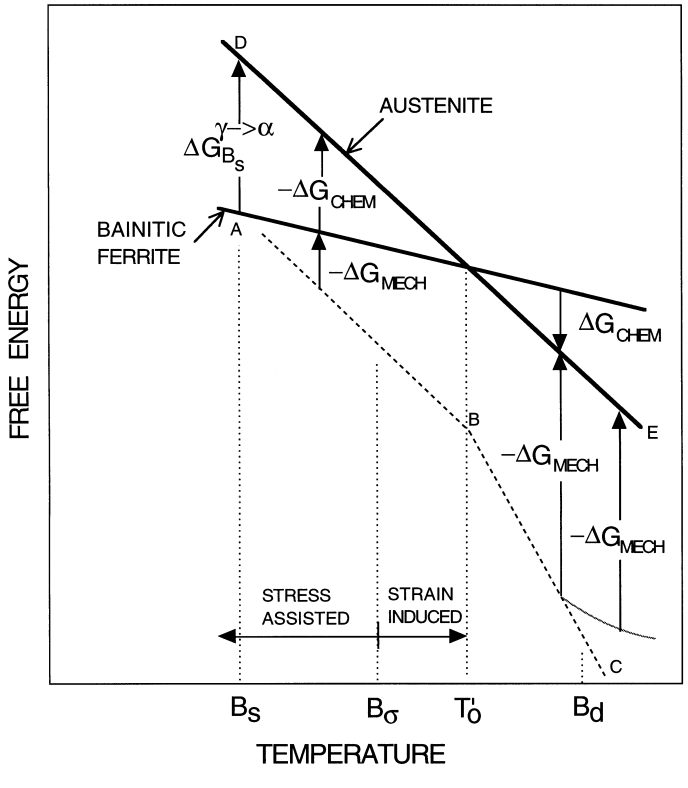

Fig. 8.3 Illustration of the stress-modified B_S, B_σ and B_d temperatures.

[13:34 3/9/01 C:/3B2 Templates/keith/3750 BAINITE.605/3750-008.3d] Ref: 0000 Auth: Title: Chapter 00 Page: 205 201-224

interest. The application of a tensile or compressive stress assists the transformation by boosting the overall driving force ΔG with the term $-\Delta G_{MECH}$, so that the B_S temperature rises continuously with the magnitude of the applied stress.

Consider a temperature B_σ corresponding to an applied stress σ, where σ becomes greater than the yield strength of the austenite. It is difficult to justify a thermodynamic analysis when the austenite undergoes plastic deformation prior to transformation. The dislocations and other defects generated during plastic deformation will nevertheless influence the progress of transformation. Following the terminology established for martensitic transformations, the region below B_σ is said to represent *stress-assisted* transformation, whereas *strain-induced* transformation describes the regime where the yield stress of the parent phase is exceeded.

The B_S temperature continues to increase as the stress is raised beyond the yield stress of the austenite. When the T_0' temperature is reached, the chemical driving force *opposes* transformation so that the mechanical component has to be larger than $\Delta G_{CHEM}\{B_S\}$. The yield strength of austenite is smaller at high temperatures so a point is reached where the austenite can no longer support a stress large enough to stimulate bainitic transformation; that temperature is B_d (Fig. 8.3).

8.3 General Observations

8.3.1 Externally Applied Stress

There are many independent observations which suggest that stress has a large effect on the progress of transformation (Fig. 8.4). Deformation during the thermomechanical processing of steels accelerates the rate of the bainite reaction.[†] There rate of reaction also increases with the rate of deformation (Drozdov *et al*., 1962; Mutui *et al*., 1977). A tensile stress during transformation even stimulates bainite beyond that expected from the T_0 condition (Cottrell, 1945).

8.3.2 Internally Generated Stress

The stress influencing transformation need not be applied externally. Internal stresses generated by other transformations also have an effect. Early studies

[†]Cottrell, 1945; Jepson and Thompson, 1949; Drozdov *et al*., 1962; Duckworth, 1966; Dubrov, 1969; Freiwillig *et al*., 1976; Mutui *et al*., 1977; Umemoto *et al*., 1986a; Tsuzaki *et al*., 1989; Yang *et al*., 1995, 1996; Larn and Yang, 2000.

[13:34 3/9/01 C:/3B2 Templates/keith/3750 BAINITE.605/3750-008.3d] Ref: 0000 Auth: Title: Chapter 00 Page: 206 201-224

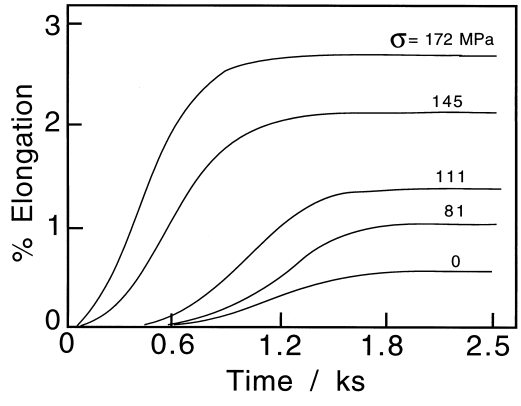

Fig. 8.4 The overall kinetics of bainitic transformation as a function of an externally applied tensile stress. Assuming that the degree of transformation is related to the elongation, the data show an increase in the rate of reaction as a function of the magnitude of the applied stress (after Umemoto *et al.*, 1986a).

indicated an acceleration in the rate at which upper bainite forms in specimens which are first transformed partially at a lower temperature (Lange and Mathieu, 1938; Jellinghaus, 1952). Martensite is the first phase to form on cooling a steel below the M_S temperature, but after the initial burst of transformation and a suitable incubation period, the austenite undergoes accelerated decomposition to bainite (Howard and Cohen, 1948). This is because it is deformed by the martensitic transformation. Supporting evidence is found in magnetometric studies, which have revealed that isothermal reaction below the M_S temperature leads first to the formation of the usual athermal martensite, followed by a small amount of isothermal martensite, an accelerated decomposition to bainite (Ericsson *et al.*, 1976). Similar results have been obtained by Radcliffe and Rollason (1959) and it has been shown that the upper bainite reaction is accelerated in the presence of lower bainite (Fig. 8.5).

A revealing observation is that both the nucleation and growth rates of bainite are accelerated by the proximity of a free surface (Ko, 1953; Hawkins and Barford, 1972). This is because the shape change can be accommodated better at a free surface where the constraint is reduced.

8.4 Plastic Deformation and Mechanical Stabilisation

It has been emphasised that displacive transformations involve the coordinated movement of atoms and that such movements cannot be sustained against strong defects such as grain boundaries. Thus, martensite plates, which form by a displacive mechanism, cannot cross austenite grain bound-

[13:34 3/9/01 C:/3B2 Templates/keith/3750 BAINITE.605/3750-008.3d] Ref: 0000 Auth: Title: Chapter 00 Page: 207 201-224

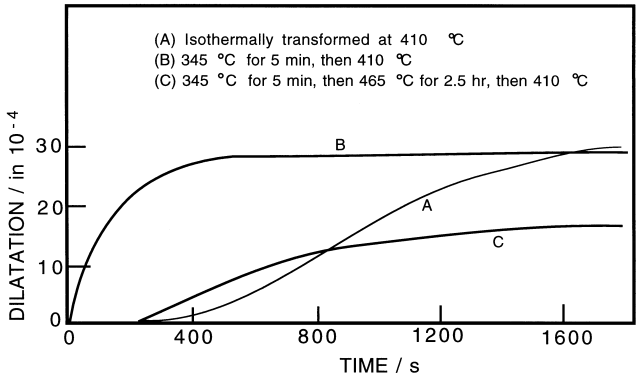

Fig. 8.5 The influence of internal stresses on the rate of transformation at 410 °C, in a Fe–0.31C–0.3Si–0.76Mn–3.07Ni–1.22Cr–0.49Mo wt% alloy. Curve A represents isothermal transformation to upper bainite; curve B is for a sample which was first partially transformed to lower bainite and then to upper bainite, showing an acceleration of reaction rate at 410 °C due to the internal stresses generated by the presence of lower bainite; curve C shows how annealing above the B_S temperature removes the stresses, and their accelerating influence on transformation kinetics (Goodenow *et al*., 1969).

aries. Smaller defects such as isolated dislocations hinder the progress of such transformations, but can often be incorporated into the martensite lattice. However, severe deformation of austenite prior to its transformation hinders the growth of martensite, causing a reduction in the fraction of transformation in spite of an increased number density of nucleation sites. This applies to all martensitic transformations, irrespective of material; apart from steels, the phenomenon is, for example, known to occur for martensitic transformations in lithium (Maier *et al*., 1997), in brass (Spielfeld, 1999) and during mechanical twinning (Christian and Mahajan, 1995).

This retardation of transformation by plastic deformation is called *mechanical stabilisation* and can be explained in terms of the structure of the transformation interface. Displacive transformations occur by the advance of glissile interfaces which can be rendered sessile when they encounter dislocation debris. Thus, whereas an appropriate stress can stimulate displacive transformation in the same way that it enables normal deformation, mechanical stabilisation actually retards the decomposition of the austenite (Bhadeshia, 1999).

Most of the work on mechanical stabilisation effects has been on martensitic transformations with few studies on bainite. Some early experimental data based on hot-rolling experiments can be interpreted to show that bainitic transformation is retarded in deformed austenite, as illustrated in Fig. 8.6.

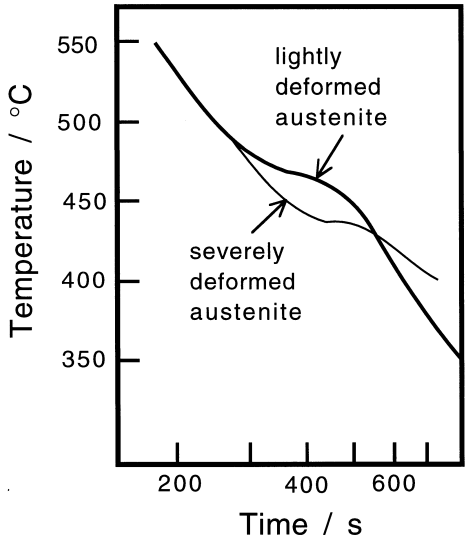

Fig. 8.6 Plots of temperature versus time for samples undergoing bainitic transformation during cooling. The deviations from linearity indicate the onset of transformation. The reaction is retarded in the austenite deformed to a greater degree before transformation, indicative of mechanical stabilisation (data from Davenport, 1977).

Direct evidence comes from the work of Tsuzaki *et al*. (1989) who found that although deformed austenite transformed faster, the net volume fraction of bainite decreased when compared with undeformed austenite, Fig. 8.7. This effect did not occur at higher temperatures, presumably because the amount of bainite that can form is then reduced. Stabilisation therefore only manifests itself when the 'easy' regions of austenite are exhausted, i.e. those regions left unaffected by the imposed deformation which is inevitably inhomogeneous. The nonuniformity of stabilisation is reflected in the microstructure. The bainite tends to align along specific directions within individual austenite grains (Fig. 8.8).

As is often the case with martensite in ausformed alloys, bainite plates sometimes follows a curved path. This is because of the deformation-induced lattice curvature present in the parent austenite grains prior to transformation (Fig. 8.8).

In recent work it has been demonstrated using metallography that the bainite transformation can be mechanically stabilised in a manner identical to the mechanical stabilisation of martensite in steels (Fig. 8.9). The mechanism appears to be that the growth of bainite is retarded by the deformation debris in the austenite. Heterogeneous nucleation becomes more frequent as defects

[13:34 3/9/01 C:/3B2 Templates/keith/3750 BAINITE.605/3750-008.3d] Ref: 0000 Auth: Title: Chapter 00 Page: 209 201-224

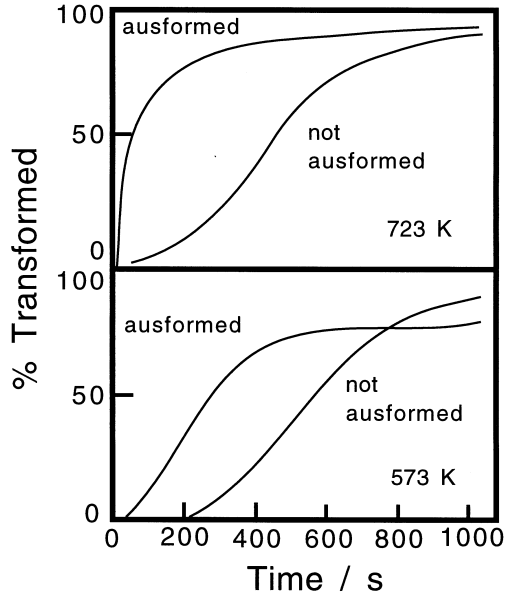

Fig. 8.7 The effect of ausforming on the kinetics of the bainite reaction in a Fe–0.59C–2.01Si–1.02Mn wt% alloy.

are introduced into the austenite, but their growth by a displacive mechanism is stifled as the interface encounters forests of dislocations. Heavily deformed austenite therefore transforms to a smaller quantity of bainite than undeformed austenite, and any bainite that forms is more refined.

Mechanical stabilisation is evident in quantitative experiments (Singh and Bhadeshia, 1996; Larn and Yang, 2000). There are two intriguing features illustrated in Fig. 8.10, first that transformation from deformed austenite leads to a smaller terminal fraction of bainite. Secondly, although the transformation rate is at first accelerated by deformation, it is eventually retarded relative to the undeformed sample. If this initial acceleration is explained by increasing the number density of nuclei then it is not possible to reach a smaller terminal fraction given that each nucleus transforms a fixed volume of austenite. On the other hand, if it is assumed that the smaller limiting fraction is due to the reduction in volume transformed per nucleus, then it is not possible to explain the initial acceleration. There are other complications described elsewhere, all of which can only be resolved by arguing that the austenite is inhomogeneously deformed (Singh, 1998). The lightly deformed regions transform more rapidly relative to undeformed austenite because of the increase in the defect density. The nucleation rate is larger in the heavily

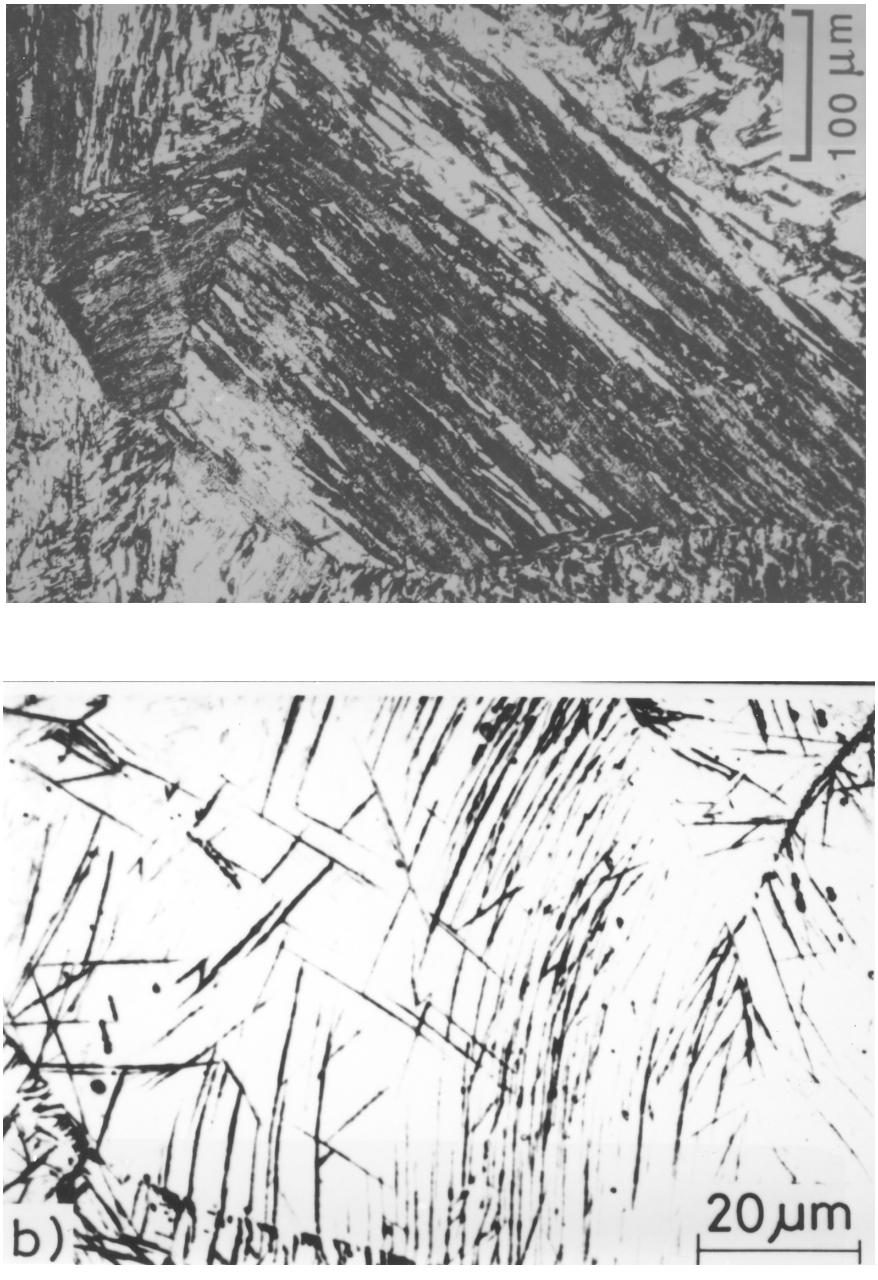

Fig. 8.8 Optical micrographs illustrating the microstructure of an ausformed bainitic steel: (a) alignment of sheaves of bainite in individual austenite grains; (b) curved bainite sheaves reflecting the deformation-induced misorientations within the austenite grains (Tsuzaki *et al.*, 1989).

[13:34 3/9/01 C:/3B2 Templates/keith/3750 BAINITE.605/3750-008.3d] Ref: 0000 Auth: Title: Chapter 00 Page: 211 201-224

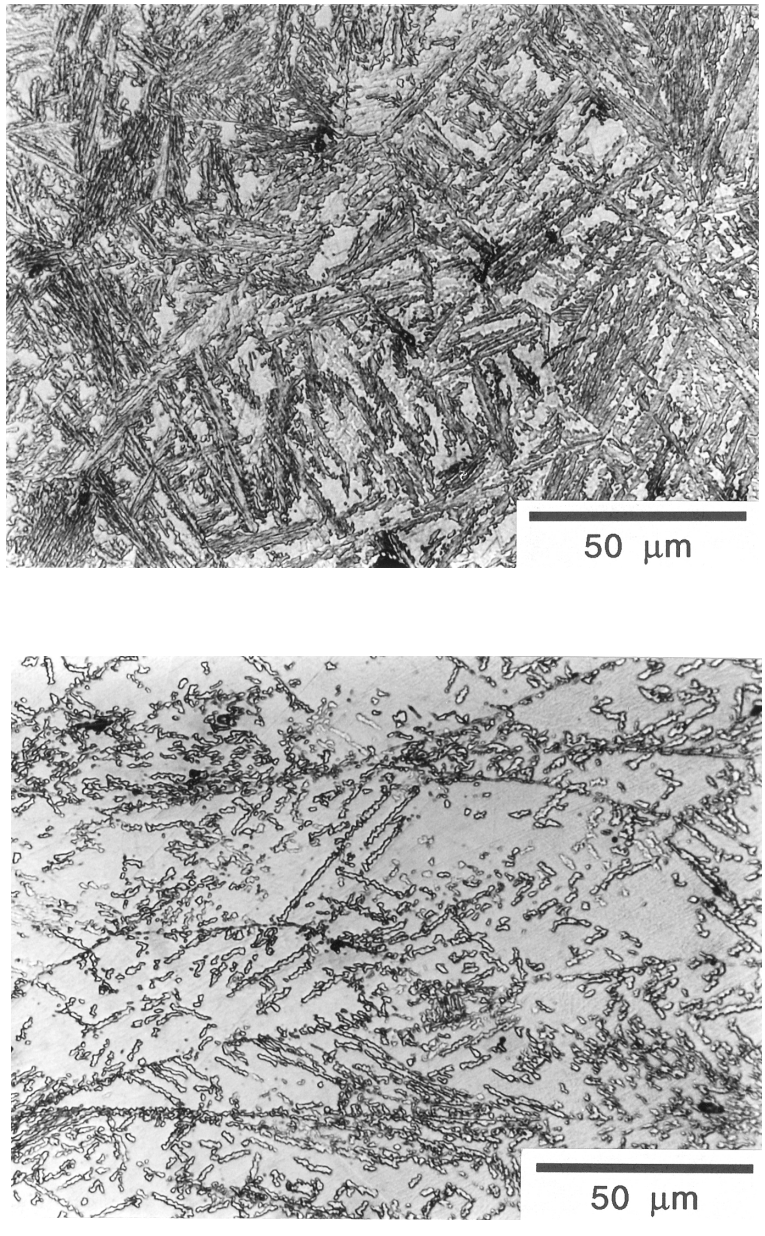

Fig. 8.9 Optical micrographs showing the large effect of mechanical stabilisation in refining the microstructure and in reducing the amount of bainite: (a) transformation from undeformed austenite; (b) transformation from plastically deformed austenite (Shipway and Bhadeshia, 1995).

[13:34 3/9/01 C:/3B2 Templates/keith/3750 BAINITE.605/3750-008.3d] Ref: 0000 Auth: Title: Chapter 00 Page: 212 201-224

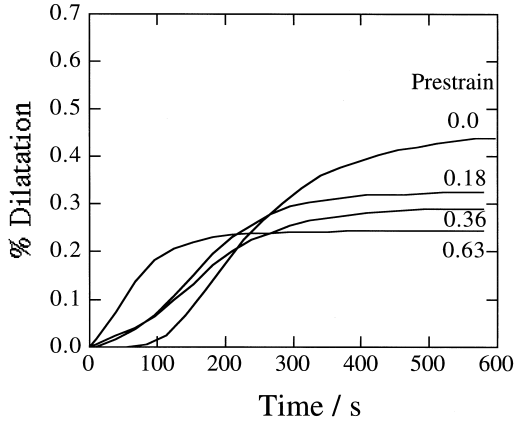

Fig. 8.10 Change in radial dilatation during isothermal transformation to bainite as a function of time and prestrain (the strain in the austenite prior to transformation); values of the prestrain are indicated next to individual curves. After Singh and Bhadeshia, 1996.

deformed regions but the overall rate of transformation is reduced because each nucleus then transforms to a smaller volume due to mechanical stabilisation of the interface.

These qualitative ideas need to be developed and backed by direct metallographic observations of the distribution of bainite sub-unit sizes, which should be bimodal. The importance of such work cannot be overemphasised given the increasing use of thermomechanical processing of bainitic steels.

Mechanical stabilisation has been found for all of the plate-shaped ferritic phases that occur in steels. This includes Widmanstätten ferrite (Shipway and Bhadeshia, 1997; Larn and Yang, 1999, 2000), bainite and martensite, all of which are displacive shear transformations. Mechanical stabilisation has been shown to occur in materials as diverse as lithium (Pichl and Krystian, 1999) and brass (Hornbogen, 1999). By contrast, reconstructive transformations are without exception accelerated if the parent phase is deformed prior to transformation. This is because of the increase in the number density of nucleation sites, and because the defects introduced by deformation are destroyed as the new phase grows, rather as in recrystallisation. The elimination of the defects contributes to the driving force for reconstructive transformation. In displacive transformations the defects are *inherited* by the growing phase and hence do not supplement the driving force. With these general observations it is possible to define a disarmingly simple criterion to distinguish these two mechanisms of transformation:

There is no mechanism by which plastic deformation can retard reconstructive transformation. Likewise, only displacive transformations can be mechanically stabilised.

8.4.1 Technological Implications of Mechanical Stabilisation

There are now many structural steels which have a bainitic microstructure but are manufactured using the same thermomechanical processing routes that have been applied so successfully to the ferrite–pearlite steels (Chapter 13). However, this has been done without the realisation that whereas the ferrite and pearlite reactions are accelerated by deforming the austenite, the bainite transformation can be retarded by the same action. The consequences of this for structural steels have simply not been explored.

It is possible to deduce evidence from the published literature of the consequences of mechanical stabilisation in commercial bainitic steels. Tsuji *et al*. (1999) found that the effect of forcing the bainite to grow in severely deformed austenite is to increase the quantity of untransformed austenite. This is precisely what is expected from mechanical stabilisation. Furthermore, they observed that although ferrite and pearlite are refined, their hardness does not increase greatly because they grow from deformed austenite. A much bigger increase in hardness was observed for the bainite. These observations are expected since ferrite and pearlite, both of which are reconstructive transformations, do not inherit the defect structure of the deformed austenite. The bainite on the other hand, acquires all the crystallographic errors present in the deformed austenite since its growth does not involve any diffusion.

8.5 The Effect on Microstructure

An applied stress will tend to favour the development of crystallographic variants which comply with that stress. This is analogous to the selective operation of a few of the available slip systems in a crystal under stress; it is the systems with the largest Schmid factors which are favoured. Assuming that variant selection is similarly controlled by the interaction of the applied stress with the shape deformation, the stress should cause an alignment of the plates at roughly 45° to the tensile axis. This alignment has been observed in many experiments involving martensitic transformations (e.g. Bhadeshia, 1982a). The observations are more difficult for bainite, partly because of the rapid rate of reaction under the influence of stress. The experiments have to be conducted at high temperatures. Further transformation may occur as the sample cools to

[13:34 3/9/01 C:/3B2 Templates/keith/3750 BAINITE.605/3750-008.3d] Ref: 0000 Auth: Title: Chapter 00 Page: 214 201-224

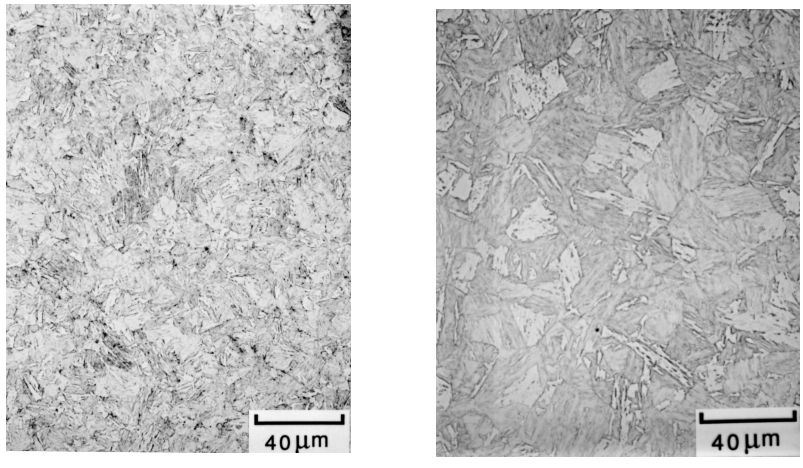

Fig. 8.11 Light micrographs of bainitic microstructures generated in a Fe–0.12C–0.27Si–0.84Mn–0.14Ni–1.48Mo–2.86Cr wt% alloy, by isothermal transformation at 400 °C under the influence of stress. (a) Zero stress; (b) 95 MPa.(after Bhadeshia *et al.*, 1991).

ambient temperature, confusing the interpretation of the microstructure. Nonetheless, good evidence for microstructural alignment has been reported for bainite platelets especially at relatively large stresses (Bhattacharyya and Kehl, 1955; Umemoto *et al.*, 1986a). All of these observations are based on polycrystalline samples, but that does not substantially alter the conclusions. There are so many variants available per austenite grain that there is a high probability of a plate orientation lying close to the optimum orientation with respect to the stress.

There are more subtle effects of stress on microstructure, even in the absence of any obvious plate alignment, at stress levels as small as 45 MPa. Variant selection leads to the development of a less chaotic microstructure (Jepson and Thompson, 1949; Dubrov, 1969; Bhadeshia *et al.*, 1991). Without stress, each grain of austenite transforms into many different orientations of bainite. Fewer variants develop per austenite grain under the influence of stress, so that the selected orientations can grow unhindered and form thick packets of bainite plates. The sheaves then are longer and their number density per grain smaller when variant selection operates (Fig. 8.11).

A further effect on microstructure is when the austenite has been plastically deformed prior to transformation. Heterogeneous nucleation then occurs not only at the original austenite grain boundaries, but apparently also intragranularly on slip bands or other deformation heterogeneities (Dubrov, 1969).

8.6 The Effect of Hydrostatic Pressure

There is general agreement that the application of hydrostatic pressure causes a retardation of the bainite reaction (Jellinghaus and Friedewold, 1960; Radcliffe *et al.*, 1963; Nilan, 1967). The effect on the time–temperature–transformation diagram is illustrated in Fig. 8.12. The observed retardation is not in itself a feature unique to bainite. All transformations which are accompanied by a reduction in density are expected to be retarded by hydrostatic pressure, which opposes a volume expansion. The effect of hydrostatic pressure is two fold: it reduces the diffusion coefficients by decreasing the available free volume (although the details remain to be established), and it influences the free energy change for transformation. If ΔG_m is the molar Gibbs free energy change for a reaction, then since

$$\left(\frac{\partial G}{\partial P}\right)_T = V$$

it follows that:

$$\Delta G_m\{P\} - \Delta G_m\{1\} = \int_1^P \Delta V_m \, dP' \tag{8.3}$$

where ΔV_m is the change in molar volume on transformation, V is the volume and P is the pressure. The way in which the free energy change for transformation is influenced by the pressure determines how the transformation temperature changes as a function of pressure. An alternative way of expressing this relationship is the Clausius–Clapyeron equation, whence the change in transformation temperature is given by

$$dT^{\gamma\alpha} = T^{\gamma\alpha}\Delta V_m / \Delta H^{\gamma\alpha} \tag{8.4}$$

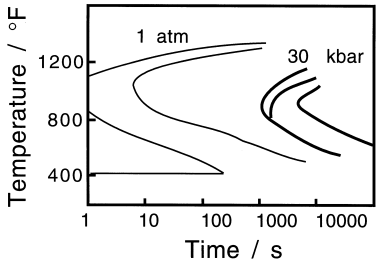

Fig. 8.12 Isothermal transformation diagrams of Fe–0.82C wt% at 1 atmosphere and at 30 kbar pressure (after Nilan, 1967).

[13:34 3/9/01 C:/3B2 Templates/keith/3750 BAINITE.605/3750-008.3d] Ref: 0000 Auth: Title: Chapter 00 Page: 216 201-224

where $\Delta H^{\gamma\alpha}$ is the enthalpy change on transformation at the transition temperature $T^{\gamma\alpha}$. The equation is approximate in that its derivation depends on the assumption that the enthalpy change does not vary with temperature. With typical values of all the parameters, the variation in transition temperature with pressure should be approximately $-0.01\,\mathrm{K\,MPa^{-1}}$ (Denis *et al*., 1985).

Radcliffe *et al*. also found that the bainite transformation could be suppressed completely by the application of hydrostatic pressure ($\simeq 15$ kbar) but Nilan, using similar steels could obtain conventional bainite at the maximum pressures he used (34 kbar). Why these experiments are contradictory is not clear, but Nilan concluded that the transformations at high pressures do not differ substantially from those at ambient pressure.

8.7 Mechanical Stability of Retained Austenite

In steels where the precipitation of carbides during the bainite reaction is slow, the residual austenite becomes enriched in carbon and a large proportion is retained on cooling to ambient temperature. The austenite, if it decomposes under the influence of stress, can be detrimental to the steel concerned since the

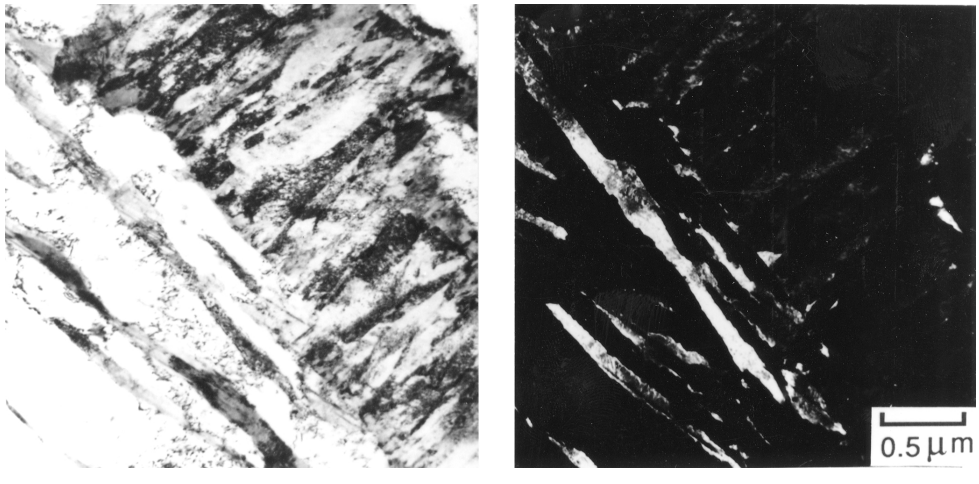

Fig. 8.13 Electron micrographs illustrating the effect of applied stress (850 MPa) on a sample which initially had a microstructure of bainitic ferrite and retained austenite (Bhadeshia and Edmonds, 1983a). The larger regions of austenite transform to martensite but the films are preserved. (a) Bright field image showing a large region of stress-induced martensite; (b) corresponding austenite dark field image. The sample was tempered prior to the application of stress in order to distinguish the martensite which forms during cooling from the bainite transformation temperature, from that which is induced by stress.

resulting high-carbon, untempered martensite is expected to be brittle. There is ample evidence that the austenite retained to ambient temperature after isothermal formation of bainitic ferrite, especially the larger blocky austenite, can decompose to martensite even at relatively small stresses, Fig. 8.13 (Horn and Ritchie, 1978; Kar *et al*., 1979; Bhadeshia and Edmonds, 1983a,b; George *et al*., 1985; Tsukatani *et al*., 1991). The mechanical stability of retained austenite is therefore important in obtaining good toughness in bainitic steels.

Miihkinen and Edmonds (1987b) have shown that for high silicon steels in which the bainite reaction is allowed to proceed until it stops, the mechanical stability of the retained austenite decreases as the isothermal transformation temperature is increased. The mechanical stability was defined as the ratio of retained austenite content after 2% plastic deformation in a tensile test, to the original content. Given that the bainite reaction in such steels ceases when the carbon concentration of the residual austenite x_γ approaches x_{T_0}, and that x_{T_0} increases with decreasing temperature, the austenite on the basis of its composition is theoretically expected to be more stable as the bainite formation temperature is reduced (Bhadeshia and Edmonds, 1983a,b). Furthermore, if the T_0 curve can be shifted to higher carbon concentrations by modifying the substitutional solute content then the stability of the austenite is expected to increase, and this has also been confirmed experimentally.

8.8 Transformation under Constraint: Residual Stresses

Residual stresses are mostly introduced unintentionally during fabrication. They are of particular importance in welded structures where they have a detrimental effect. Jones and Alberry (1977a,b) conducted an elegant series of experiments to illustrate the interaction between transformations and residual stress. Using bainitic, martensitic and stable austenitic steels, they demonstrated that transformation plasticity during the cooling of a uniaxially constrained sample from the austenite phase field, acts to relieve the build up of thermal stress as the sample cools. By contrast, the non-transforming austenitic steel exhibited a continuous increase in residual stress with decreasing temperature, consistent with the degree of thermal contraction. On the other hand, with the steels which transformed to bainite or martensite, the transformation strain compensated for the thermal contraction strains. Significant residual stresses developed only after transformation was completed, and the specimens approached ambient temperature (Fig 8.14).

The interpretation of experimental data of the kind illustrated in Fig. 8.14 is difficult. The view that the volume change during transformation gives the major contribution to transformation plasticity is almost certainly incorrect for displacive transformations such as bainite. The shape change due to transformation has a shear which is much larger than the volume strain.

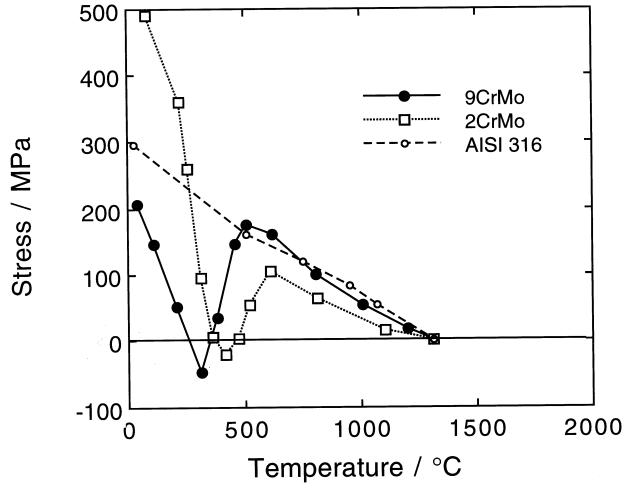

Fig. 8.14 Development of stress as a function of temperature as a constrained sample is cooled from the austenite phase field, for a martensitic (9CrMo), bainitic (2CrMo) and austenitic steel (AISI 316). After Alberry and Jones.

Admittedly, this shear component should on average cancel out in a fine grained polycrystalline sample containing plates in many orientations. However, the very nature of the stress effect is to favour the formation of selected variants in which case, the shear component rapidly begins to dominate the transformation plasticity.

8.9 Anisotropic Strain due to Transformation Plasticity

During their attempts to study the isothermal transformation of austenite using dilatometry, Davenport and Bain (1930) had noticed already that 'the volume change (due to transformation) is not necessarily uniformly reflected in linear change in all dimensions'. They even found that the thickness of flat disc specimens actually decreased as the volume increased! These results were stated without interpretation but it is now clear that in polycrystalline samples which are crystallographically textured, anisotropic transformation plasticity can be detected even in the absence of an applied stress (Bhadeshia *et al.*, 1991). When an unstressed polycrystalline sample of austenite is transformed, the shear components of the individual shape deformations of the large number of variants which form along any dimension should tend to cancel out on a macroscopic scale. Similarly, the dilatational component of the IPS shape deformation should average leaving an isotropic volume expansion. If the sample is not random, i.e. it is crystallographically textured, then the

possibility of the individual shape deformations cancelling out over large distances is correspondingly reduced. Transformation will then lead to a large anisotropy in the strains even in the absence of an applied stress (Fig. 8.15).

8.10 Stress-Affected Carbide Precipitation

The idea that cementite at low temperatures precipitates by a displacive mechanism with only the partitioning of carbon is not unnatural – this mechanism has been demonstrated for the precipitation of vanadium hydride (Bowles *et al.*, 1977). The evidence for cementite has been discussed in Chapter 3. Although the shape deformation associated with precipitation has yet to be measured, it is believed to be an invariant-plane strain with a shear of 0.211 parallel to the habit plane and a dilatational strain of 0.157 normal to the habit plane (Taylor *et al.*, 1989b).

The effect of the shape change can be revealed by the precipitation microstructure when it is generated under the influence of an externally applied

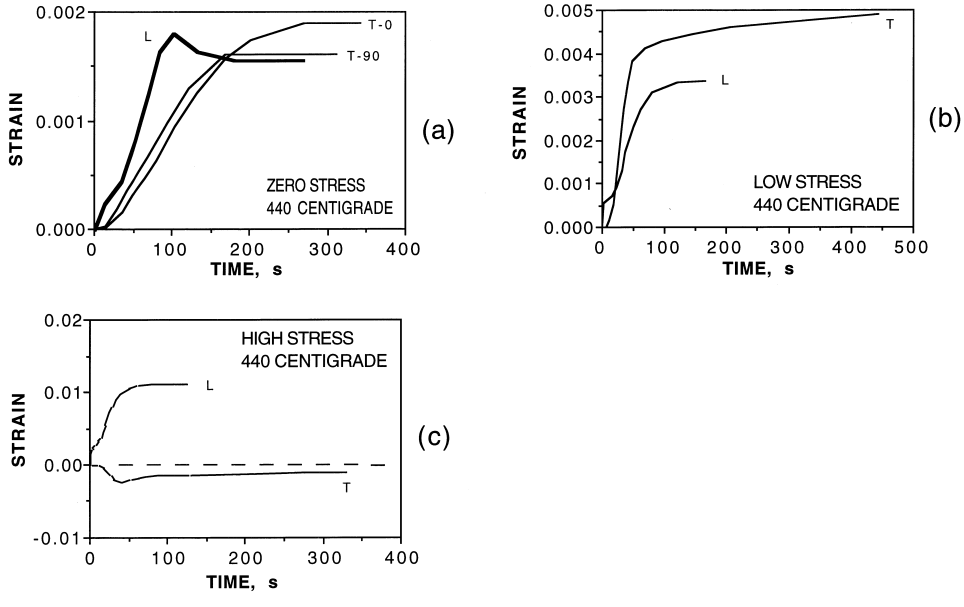

Fig. 8.15 Dilatometric curves showing the dimensional changes during transformation to bainite in a cylindrical sample. T-0 and T-90 refer to the strains monitored along orthogonal transverse directions, and L to the strain along the longitudinal direction: (a) transformation in the absence of an applied stress; (b) transformation under the influence of a tensile stress of about 45 MPa; (c) 90 MPa (Bhadeshia *et al.*, 1991).

stress (Matsuzaki *et al.*, 1992; Stewart *et al.*, 1994). When martensite is tempered in a stress-free condition, the carbides precipitate in several crystallographic variants in any given plate, in the so-called Widmanstätten pattern. When the tempering is carried out under a uniaxial stress, the variant which presumably complies best with the external stress begins to dominate the microstructure. Eventually, when the stress is large enough, it is only a dominant crystallographic variant is found in any plate of martensite (Fig. 8.16).

The response of the carbide microstructure to the applied stress is precisely that expected from the interaction with the transformation strain. In experiments reported in the literature, the mechanical driving force is similar in magnitude to the chemical driving force for the precipitation of cementite. Thus, $\Delta G_{MECH} \simeq 730\,\mathrm{J\,mol^{-1}}$ for a stress of 500 MPa, and $1380\,\mathrm{J\,mol^{-1}}$ for 950 MPa. This compares with $\Delta G_{CHEM} \simeq 1300\,\mathrm{J\,mol^{-1}}$ at the tempering temperature.

Figure 8.17 shows that the chemical driving force is sensitive to the carbon concentration of the martensite and to the tempering temperature. It follows that the effect of stress on the development of the carbide microstructure (and the tendency to precipitate a single variant) will be most prominent at low carbon concentrations or at high tempering temperatures. We note that the stress need not be applied externally; it is equally valid to consider the influence of internal stresses due to transformation from austenite.

Lower bainite forms at higher temperatures than martensite so ΔG_{CHEM} for carbide precipitation is smaller; any partitioning of carbon into austenite reduces ΔG_{CHEM} further. Therefore, lower bainite plates are more likely to contain only a single carbide variant than martensite, as observed experimentally.

8.11 Summary

There is little doubt that the bainite reaction is influenced by externally applied stress, and by stresses generated internally due to transformation or heat-treatment. This interaction with stress appears to be related to the displacive mechanism of transformation with its invariant-plane strain shape deformation with its large shear component. Stress-assisted transformation can lead to anisotropic dimensional changes whose magnitudes and senses are impossible to explain on the assumption of a reconstructive transformation mechanism. Transformation plasticity is readily detected during the growth of bainite under the influence of stress, the magnitude of the observed effect being excess of that expected from volume change criteria alone.

There is evidence that the response of bainite to stress is similar to that of martensite. The bainite-start temperature is raised by the application of a tensile stress, lowered by hydrostatic compression, and there exists a B_d tempera-

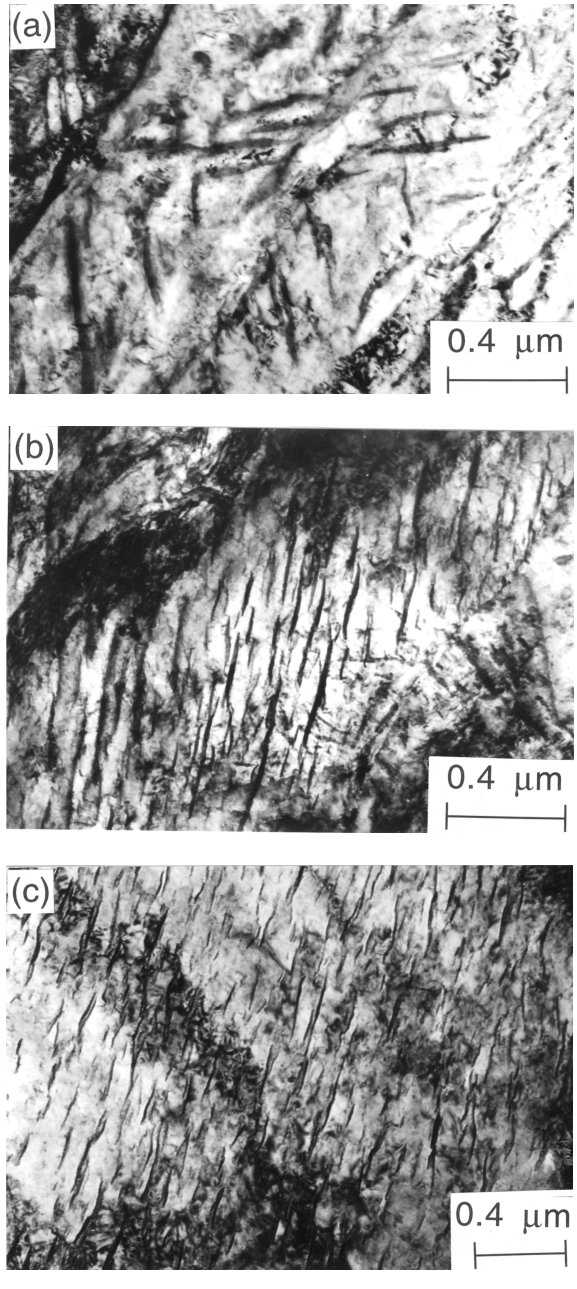

Fig. 8.16 The microstructure of martensite which is tempered under the influence of a uniaxial stress. The number of cementite variants in any given martensite plate decreases at the stress is increased: (a) zero stress; (b) 500 MPa; (c) 950 MPa. The stress is in all cases below the macroscopic yield strength of the sample at the tempering temperature. After Stewart *et al.*, 1994.

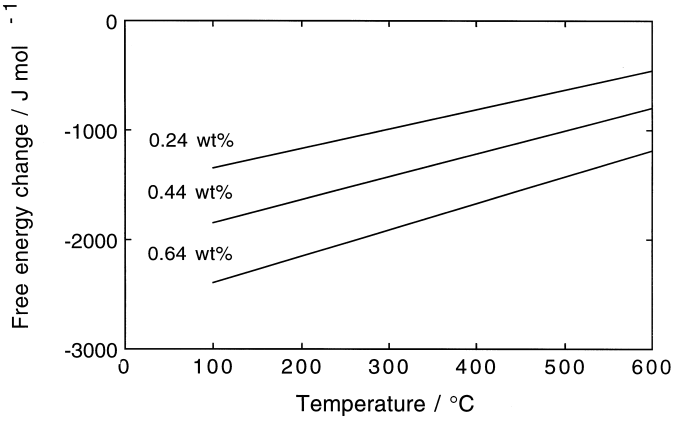

Fig. 8.17 Free energy change accompanying the precipitation of cementite from supersaturated ferrite, as a function of the carbon concentration and temperature (Stewart *et al.*, 1994).

ture beyond which the reaction will not occur whatever the magnitude of the stress. The microstructure of bainite responds to the applied stress, with clear evidence that the growth of certain crystallographic variants is favoured over others. The number of different sheaves per austenite grain decreases, causing the formation of large packets of parallel sheaves; this microstructure may be detrimental to toughness. Further work remains to be done in order to establish the criteria determining variant selection during stress-influenced transformation. Bainite also shows characteristics similar to those associated with the mechanical stabilisation of martensite, when the austenite is deformed prior to the growth of bainite.

Transformation to bainite accelerates under the influence of stress; whether this is predominantly due to enhanced nucleation or growth remains to be resolved. The extent to which the rate of reaction is accelerated increases with the rate of application of stress. On the other hand, heavy deformation of austenite prior to transformation causes mechanical stabilisation, another phenomenon associated uniquely with displacive transformations.

The primary effect on microstructure during transformation under stress is that of variant selection, which at low stresses reduces the number of sheaves per austenite grain. Variant selection does not lead to an obviously aligned microstructure until larger stresses are applied, in which case the sheaves probably form on habit plane variants which are most parallel to the planes of maximum shear stress. Although deviations from the random microstructures that form in the absence of applied stress are often not easily detectable,

they reveal themselves unambiguously in the form of anisotropic dimensional changes during transformation.

The response of bainitic transformation to stress is therefore essentially similar to that of martensite, although there are some exceptions because of the higher transformation temperatures. Irreversible processes such as plastic deformation by lattice dislocations or the partitioning of carbon, are routine with bainite. This rules out the possibility of reversing the motion of the interface by reversing the stress, making phenomena like shape memory effects or rubber elasticity are extremely unlikely with bainite.

There is no doubt at all that the growth of bainite is stifled when the austenite is severely plastically deformed prior to transformation. The transformation can therefore be mechanically stabilised. This feature is impossible to explain except by a displacive transformation mechanism in which the interface motion is glissile.

9 *From Bainite to Austenite*

Many commercial processes cause the steel to revert into the austenitic condition. The transformation of low-temperature ferrite into high-temperature austenite differs from the case where the latter transforms during cooling. Transformation during cooling follows a C curve kinetics in which the overall transformation rate goes through a maximum as a function of the undercooling below the equilibrium temperature. This is because diffusion coefficients decrease but the driving force increases as the temperature is reduced. By contrast, both the diffusivity and driving force for austenite formation increase as a ferritic microstructure is superheated. The rate of transformation increases indefinitely as the temperature is raised, Fig. 9.1.

This kinetic behaviour has several interesting consequences. It is commonly observed that reconstructive transformations can be suppressed by cooling rapidly to a low temperature where the lack of atomic mobility prevents further transformation. Austenite can therefore be retained by rapid cooling to ambient temperature, even though it is not thermodynamically stable. It should be impossible to similarly retain ferrite to high temperatures in the γ–phase field during a heating experiment, since atoms become more mobile at higher temperatures.

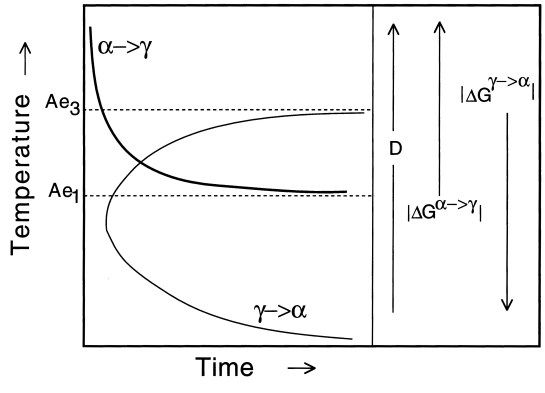

Fig. 9.1 The TTT curves for the $\gamma \rightarrow \alpha$ reaction, and for the reverse $\alpha \rightarrow \gamma$ transformation.

Austenite is not always retained when quenched from an elevated temperature. It may transform by a mechanism which does not require diffusion (martensitic). When the $\alpha \rightarrow \gamma$ transformation occurs during heating, the temperatures involved are usually high enough to permit the rapid reconstructive transformation. It is therefore rare for austenite to grow by a martensitic mechanism.

In compendiums of time–temperature–transformation diagrams, the kinetics of austenite decomposition are presented as a function of the chemical composition and the austenite grain size. The number of variables to be considered when presenting similar data for transformation to austenite is much larger: the initial microstructure can vary widely. The sophistication with which it is necessary to specify the starting microstructure remains to be determined, but factors such as particle size, the distribution and composition of individual phases, homogeneity of the microstructure, the presence of nonmetallic inclusions, etc. should all be important.

There are two particular examples where a detailed knowledge of austenitisation could be exploited to considerable advantage. During fusion welding, an optimum microstructure is required immediately after deposition from the liquid state. The luxury of homogenisation or other thermomechanical treatments is simply not available or practical. The welding process dissipates heat into the surrounding metal, with regions in the immediate proximity of the fusion surface being heated to temperatures high enough to cause austenitisation. Another example where austenitisation theory could be usefully applied is in the development of new wrought steels (Fe–Ni–Ti), where attempts are being made to utilise microstructures which have been partially austenitised.

There clearly is work to be done on all aspects of the formation of austenite, but the discussion in this chapter is confined to the austenitisation of bainitic microstructures.

9.1 Heating a Mixture of Austenite and Upper Bainitic Ferrite

When an iron–carbon alloy is heated to a temperature within the $\alpha + \gamma$ phase field until equilibrium is established, a small rise or fall in temperature leads to the growth or dissolution respectively, of the austenite until the volume fractions once again satisfy the lever rule (Tsuzaki *et al.*, 1988). The transformation of austenite into allotriomorphic ferrite is in this sense reversible, and exhibits little or no hysteresis. A much larger hysteresis occurs for the martensite to austenite transformation because the martensite tempers during heating and because its growth involves dissipation in the form of irreversible plastic

deformation. A substantial hysteresis effect is found experimentally when a mixture of bainitic ferrite and austenite is heated (Fig. 9.2).

If carbides precipitate during the bainite reaction then the final microstructure is unlikely to contain retained austenite. The sample must then be heated into the $\alpha + \gamma$ phase field before austenite can nucleate first and then grow. Of course, if austenite exists in the starting microstructure, and if it remains stable during heating, then it can begin growth as soon as the free energy change becomes negative. For bainite, this may nevertheless require a substantial superheat because the transformation remains incomplete, i.e. it stops when $x_\gamma \simeq x_{T_0'}$ rather than when $x_\gamma = x_{Ae3}$. The temperature therefore has to be raised until the carbon concentration of the residual austenite becomes equal to that given by the *Ae*3 phase boundary before the austenite can grow (Fig. 9.2).

These concepts can be revealed in steels which transform to bainite without the precipitation of carbides (Yang and Bhadeshia, 1989b). We have argued above that when a mixture of bainitic ferrite and carbon-enriched austenite is heated sufficiently rapidly to a high enough temperature, the existing austenite can grow without there being a need for nucleation (Fig. 9.3).†

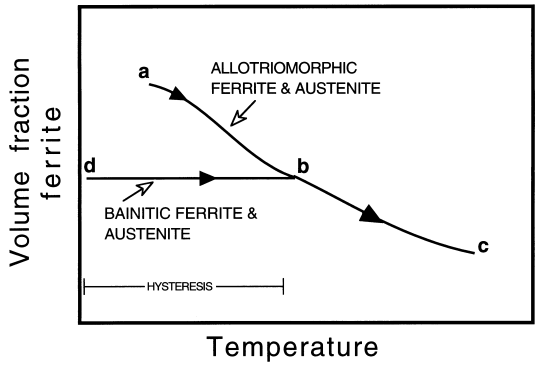

Fig. 9.2 The growth of austenite when mixtures of ferrite and austenite are heated. An equilibrium mixture of allotriomorphic ferrite and austenite begins to transform immediately the temperature is raised, whereas a large superheat is needed when a mixture of bainitic ferrite and austenite is heated.

†This does not preclude new nuclei of austenite; thus, Kessler and Pitsch (1965) found that new regions of austenite nucleated when a mixture of martensite and retained austenite was heated. Whether new nuclei form in microstructures which already contain retained austenite must depend on the superheat since nucleation is most difficult at low driving forces.

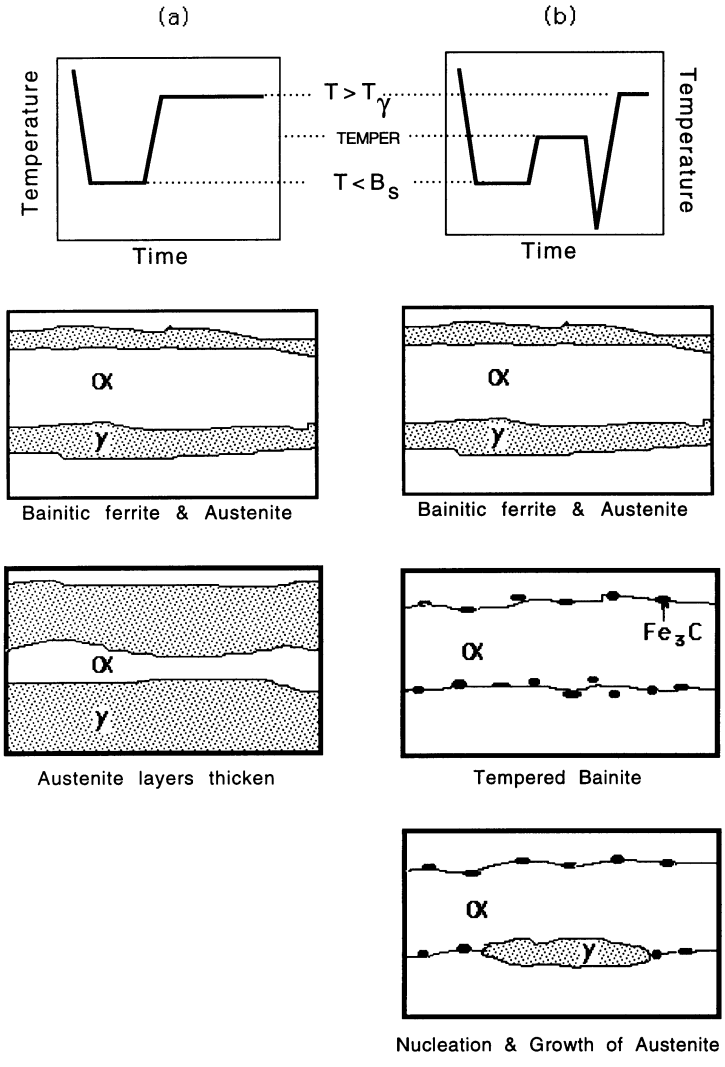

Fig. 9.3 (a) A mixture of bainitic ferrite and austenite is generated by isothermal transformation at a temperature below B_S; this microstructure is then reheated to an elevated temperature to permit the austenite to grow. (b) A tempering heat-treatment eliminates austenite. It is then necessary to nucleate austenite before it can grow.

Experiments like these have shown that the austenite in low-alloy steels grows by a reconstructive process at all but the fastest of heating rates. A large difference is found between the B_S and A_S (austenite-start) temperatures. The austenite only begins to grow when the *Ae*3 temperature of the *residual*

austenite is reached. Its fraction then increases from that at the A_S temperature, to complete transformation at the austenite-finish (A_F) temperature, which is the Ae_3 temperature of the alloy as a whole.

The observed austenitisation behaviour can be understood as follows (Yang and Bhadeshia, 1987, 1988). When carbide precipitation is avoided, bainite stops to form when the $x_\gamma = x_{T'_0}$ (Fig. 9.4). We shall designate this value of x_γ as the initial value x_γ^I obtained by transformation at the temperature T_i, i.e.

$$x_\gamma^I = x_{T'_0}\{T_i\} \tag{9.1}$$

as indicated by the point **a** in Fig. 9.4. Furthermore, we note that:

$$x_\gamma^I \ll x_{Ae3}\{T_i\} \tag{9.2}$$

where $x_{Ae3}\{T_i\}$ is marked as point **b** in Fig. 9.4. Bainite does not form if $x_\gamma > x_{T'_0}$ but at that point, x_γ is far less than the equilibrium or paraequilibrium concentration. Another way of stating this is to say that the fraction of austenite at T_i is greater than expected from equilibrium, so there is no tendency for the austenite to grow. This remains the case until the temperature is high enough to satisfy the equation:

$$x_\gamma^I = x_{Ae3}\{A_S\} \tag{9.3}$$

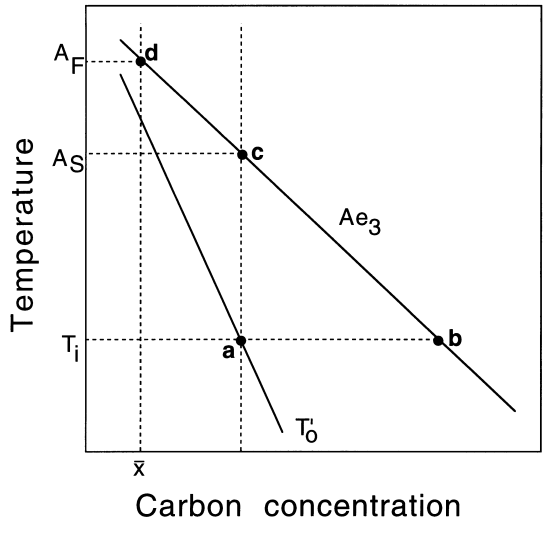

Fig. 9.4 Schematic phase diagram illustrating the theory for austenite growth when the initial microstructure is a mixture of bainitic ferrite and carbon-enriched residual austenite.

The austenite only begins to grow at A_S corresponding to the point **c** in Fig. 9.4. The required superheat $A_S - T_i$ is a direct effect of the incomplete reaction phenomenon.

The theory predicts that when $T_\gamma > A_S$, the $\alpha_b \rightarrow \gamma$ transformation should stop when

$$x_\gamma = x_{Ae3}\{T_\gamma\}. \tag{9.4}$$

Neglecting differences in the densities of austenite and ferrite, and assuming that $x_\alpha = 0$, the equilibrium volume fraction of austenite at T_γ is then given by:

$$V_\gamma\{T_\gamma\} = \overline{x}/x_{Ae3}\{T_\gamma\}. \tag{9.5}$$

The alloy becomes fully austenitic when $x_{Ae3}\{T_\gamma\} = \overline{x}$ (point **d**, Fig. 9.4). The corresponding temperature is designated A_F so for all $T_\gamma > A_F$, the alloy transforms completely to austenite.

9.1.1 One-Dimensional Growth from a Mixture of Austenite and Bainitic Ferrite

As discussed earlier, austenite need not nucleate when mixture of ferrite and austenite is heated. Transformation can occur by the thickening of the austenite films between the bainite plates. This effectively is one-dimensional growth, which we shall assume is diffusion-controlled. The redistribution of carbon must occur inside the austenite during its growth, assuming that its solubility in ferrite can be neglected. Microanalysis has shown that substitutional solutes may partition during austenite formation (Yang and Bhadeshia, 1987, 1988, 1989b). The extent of partitioning decreases as the transformation temperature T_γ, and hence the driving force, increases. It could be assumed that local equilibrium exists at the interface for low T_γ, with a tendency towards zero bulk partitioning, (i.e., negligible-partitioning local equilibrium or paraequilibrium) as $T_\gamma \gg Ae_3$. This makes a full analysis difficult because there are many possibilities between the states of local equilibrium and paraequilibrium.

If local equilibrium is achieved at the interface, the growth rate assuming carbon diffusion-control may give an estimate of the factors influencing the kinetics of transformation. This is the basis of the model presented below, which assumes that substitutional solute gradients do not affect the carbon (Kirkaldy, 1958). There is a further assumption that the tie-line of the equilibrium phase diagram, which determines the interface compositions, passes through the average composition of the alloy, which is unlikely in concentrated alloys. Any effects of soft impingement are also neglected.

One-dimensional diffusion-controlled growth leads to a parabolic thickening of films of austenite. The increase in the half-thickness q of the film is given by:

$$dq = \frac{1}{2}\alpha_1 t^{-\frac{1}{2}} dt \tag{9.6}$$

where α_1 is the one-dimensional parabolic thickening rate constant. The geometry assumed for the thickening of austenite layers is based on the shape of the bainite or acicular ferrite plates which bound the layers. If c is the largest dimension of such a plate, idealised as a rectangular parallelepiped with sides of length a, b and c, with $c = b \gg a$, then when both of the sides of a ferrite plate are penetrated by the growing austenite, the total area of the γ/α interface which advances into the plate of ferrite is $2c^2$. This reduces the thickness of the plate by $\Delta a/2$ from either side. If the minimum detectable change in volume fraction is ΔV_v, then it follows that:

$$\Delta V_v = 2N_v c^2 \int_0^{\Delta a/2} dq \tag{9.7}$$

where N_v is the initial number of particles of austenite per unit volume, and Δa_m is the minimum detectable increase in thickness. It follows that

$$\Delta V_v = 2N_v c^2 \int_0^{\tau} \frac{1}{2}\alpha_1 t^{-\frac{1}{2}} dt \tag{9.8}$$

where τ is the time taken to achieve the minimum detectable degree of transformation. After integration, equation 9.8 becomes:

$$\Delta V_v = 2\alpha_1 N_v c^2 \tau^{\frac{1}{2}} \qquad \text{or} \qquad \tau = \left(\frac{\Delta V_v}{2\alpha_1 N_v c^2}\right)^2 \tag{9.9}$$

$$\text{Since} \qquad 2N_v c^2 = S_v = 2/\overline{L}_3 \qquad \text{it follows that} \qquad \tau = \left(\frac{\Delta V_v}{\alpha_1 S_v}\right)^2 \tag{9.10}$$

where S_v is surface area of γ/α boundary per unit volume, and $1/\overline{L}_3$ is the mean number of intercepts of γ/α boundary per unit length of test line (DeHoff and Rhines, 1968). It is clear from equation 9.10, that τ is dependent not only on α_1 but also on the surface area of γ/α interface per unit volume S_v for a specific amount of austenitisation.

For the same initial microstructure and a fixed degree of transformation, τ should decrease rapidly T_γ. The microstructure affects τ via S_v. This explains experimental observations of the different rates at which mixtures of $(\alpha_b + \gamma)$ and $(\alpha_a + \gamma)$ austenitise (Fig. 9.5a). The distribution of plates in an acicular ferrite microstructure is such that S_v is smaller than in bainite, making the transformation to austenite relatively slow. It has also been verified experimentally that τ is proportional to α_1^{-2} (Fig. 9.5c).

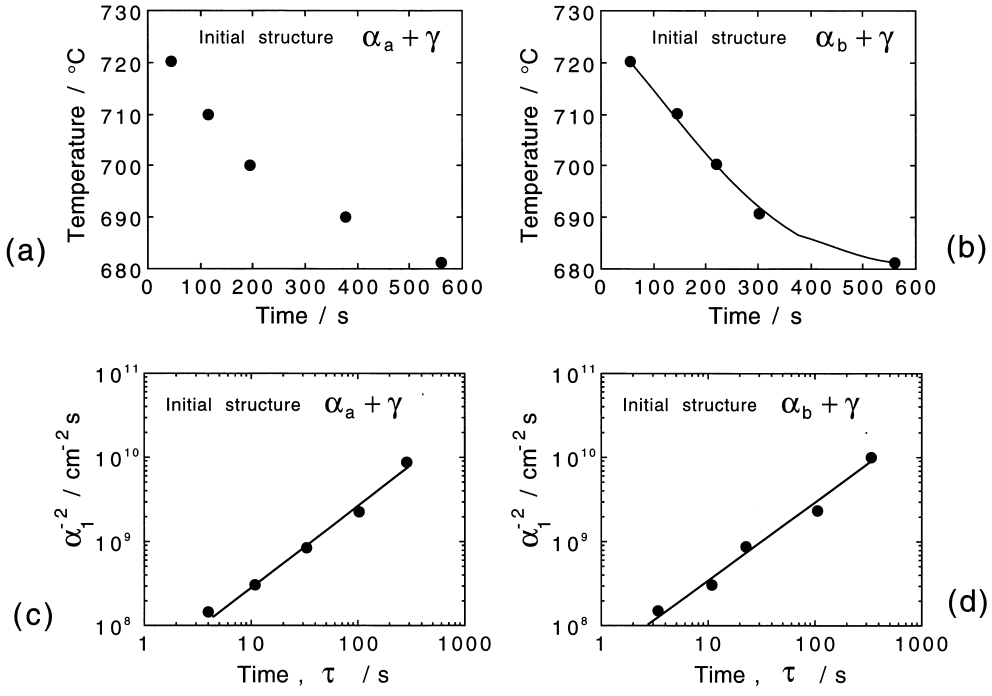

Fig. 9.5 (a,b) TTT diagrams for the growth of austenite from equivalent mixtures of acicular ferrite/austenite, and bainitic ferrite/austenite. (c,d) Linear relationship between the time τ taken for a constant volume fraction of austenite growth, versus α_1^{-2}, where α_1 is the one-dimensional parabolic thickening rate constant for austenite growth (Yang and Bhadeshia, 1989b).

9.1.2 Estimation of the Parabolic Thickening Rate Constant

The parabolic rate constant α_1 can be calculated using existing theory for the $\gamma \rightarrow \alpha$ transformation (Zener, 1949; Dubé, 1948; Bhadeshia, 1985b). Fig. 9.6 shows the carbon concentration profiles in α and γ before and during austenite growth. The austenite must become more dilute in carbon as it grows, the rate of interface motion being determined by the diffusion of carbon in the austenite behind the interface. In Fig. 9.6, x_γ^I is the initial carbon concentration in the austenite, given by $x_\gamma^I = x_{T'_0}$. The carbon concentration of γ at the γ/α interface during austenitisation is $x^{\gamma\alpha}$ and that of austenite far away from the interface is assumed to remain constant at x_γ^I, as is $x^{\alpha\gamma}$. The coordinate z is normal to the γ/α interface.

The flux of carbon in the austenite, towards the γ/α interface, at the position of interface is from Fick's first law given by:

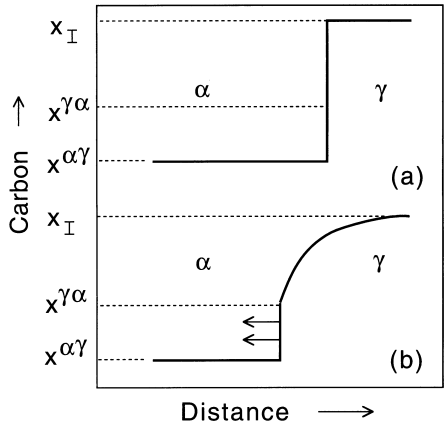

Fig. 9.6 The distribution of carbon, (a) before austenitisation from a mixture of bainitic ferrite and austenite, and (b) during the growth of austenite.

$$J = -D\{x^{\gamma\alpha}\}\frac{\partial x}{\partial z}\bigg|_{z=Z} \tag{9.11}$$

The rate at which the carbon concentration of austenite is diluted is:

$$R_d = V_d(x_\gamma^I - x^{\alpha\gamma}) \tag{9.12}$$

where V_d is the velocity of interface (the diffusion-field velocity). Given that

$$Z = \alpha_1 t^{\frac{1}{2}},$$

it follows that:

$$V_d = \frac{dZ}{dt} = \frac{1}{2}\alpha_1 t^{-\frac{1}{2}} \tag{9.13}$$

Consequently, the rate at which the carbon concentration of austenite is diluted is given by:

$$R_d = \frac{1}{2}\alpha_1 t^{-\frac{1}{2}}(x_\gamma^I - x^{\alpha\gamma}) \tag{9.14}$$

Making the approximation that the concentration dependence of the diffusion coefficient of carbon can be represented by its weighted average diffusivity $\overline{D}$, conservation of mass at the interface requires that:

$$\frac{1}{2}\alpha_1 t^{-\frac{1}{2}}(x_\gamma^I - x^{\alpha\gamma}) = -\overline{D}\left(\frac{\partial x}{\partial Z}\right)\bigg|_{z=Z} \tag{9.15}$$

This equation expresses the condition that as the austenite becomes dilute as its size increases, the change in concentration at the interface is compensated by a diffusion flux of carbon towards the γ/α interface. The differential equation for the matrix is:

$$\frac{\partial x}{\partial t} = \frac{\partial(\overline{D}\partial x/\partial Z)}{\partial Z} \tag{9.16}$$

subject to the boundary conditions $x = x^{\gamma\alpha}$ at $z = Z\{t\}$, and $x = x_\gamma^I$ at $t = 0$. Its solution leads to the following relationship from which α_1 can be determined (Zener, 1949; Dubé, 1948; Atkinson, 1967):

$$f_1 = \frac{x_\gamma^I - x^{\gamma\alpha}}{x_\gamma^I - x^{\alpha\gamma}} = H_1\{\overline{D}\} \tag{9.17}$$

where

$$H_1\{\overline{D}\} = \left(\frac{\pi}{4\overline{D}}\right)^{\frac{1}{2}} \alpha_1 \operatorname{erfc}\left\{\frac{\alpha_1}{2\overline{D}^{\frac{1}{2}}}\right\} \exp\left\{\frac{\alpha_1^2}{4\overline{D}}\right\} \tag{9.18}$$

9.2 Anisothermal Transformation

Heat treatments are rarely isothermal in commercial practice. A continuous heating curve can be expressed as a series of small isothermal steps i, each occurring at a successively higher temperature, with a time interval t_i associated with each step. With Scheil's rule, a specified increment of transformation is achieved during continuous heating when the sum of all the ratios of time steps to incubation periods equals unity:

$$\sum_{i=1}^{n} \frac{t_i}{\tau_i} = 1 \tag{9.19}$$

where τ_i is the time required to reach the specified fraction of transformation at the temperature T_i. This additivity rule assumes that the reaction is *isokinetic*, meaning that the fraction transformed is dependent only on the time and on a single function of temperature. This is unlikely to be true except in special cases where for example, nucleation is stifled by site saturation.

9.3 Heating a Mixture of Cementite and Bainitic Ferrite

Austenite grows with an equiaxed shape when the initial microstructure is pearlite, but in the form of layers between plates of ferrite when the initial microstructure is bainite or martensite (Nehrenberg, 1950). However, there are contradictory observations showing austenite nucleating at the prior austenite

grain boundaries from initial microstructures which are bainitic or martensitic (Law and Edmonds, 1980). What is clear, is that when the austenite forms as layers between the ferrite plates, the steel exhibits a *memory effect*. In this, the original austenite grain structure is regenerated when the transformation to austenite is completed, both with respect to shape and crystallography (Sadovskii, 1956; Kimmins and Gooch, 1983). Naturally, the austenite grain structure cannot be refined by repeated thermal cycling of the sample into the austenite phase field when the memory effect operates.

The memory arises from films of retained austenite in the starting bainitic or martensitic microstructure (Kimmins and Gooch, 1983). The films grow and coalesce to regenerate the original austenite grain structure. The memory effect vanishes if the initial microstructure is first annealed to eliminate any retained austenite. Allotriomorphs of austenite are nucleated when these annealed samples are heated into the austenite phase field (Wada and Eldis, 1982).

Retained austenite can decompose during slow heating to the austenitisation temperature, thus destroying the memory effect. Very rapid heating can also eliminate the memory by inducing the nucleation of new austenite grains (Kimmins and Gooch, 1983). The memory is enhanced if the steel contains impurities such as arsenic, phosphorus or tin, which segregate to the prior austenite grain boundaries (Kimmins and Gooch, 1983). The segregation reduces the grain boundary energy, making them less likely as heterogeneous nucleation sites.

9.4 Irradiation-Induced Rapid Heating

Surface layers of a steel containing ferrite and pearlite, when irradiated with high-energy electrons, transform into austenite. The effective heating and cooling rates are large because the irradiation effect is confined to a thin surface layer. As a consequence, the carbon concentration in the austenite which grows from pearlite is found to be much larger than in the remainder of the austenite because the rapid thermal cycle does not permit homogenisation over the scale of the microstructure. During cooling, martensite forms in the high carbon regions and bainite in the regions which were originally ferrite (Choi *et al.*, 1999). Rapid inductive heating also leads to an inhomogeneous distribution of carbon in the austenite, so that cooling produces mixed microstructures of ferrite and bainite (Weidig *et al.*, 1999).

9.5 Summary

Microstructures containing a mixture of bainitic ferrite and austenite when heated do not require the nucleation of new austenite. Nevertheless, they have to be superheated over a large temperature range before the austenite

begins to grow. This is because the bainite reaction stops before equilibrium is achieved so that the fraction of austenite in the initial microstructure is greater than required by equilibrium.

The nucleation of austenite is necessary when the original microstructure does not contain retained austenite. In this case, nucleation generally occurs preferentially at the prior austenite grain boundaries rather than between the ferrite plates. When a microstructure containing retained austenite is heated rapidly, the austenite grows and regenerates the original austenite grain structure, giving the so-called memory effect. This memory can only be destroyed by eliminating the retained austenite either by slow heating or by suitably tempering the initial microstructure (Fig. 9.7).

For any reasonable heating rate, the austenite grows by a reconstructive mechanism with the diffusion of substitutional solutes. The extent of solute partitioning decreases with the superheat above the equilibrium transformation temperature, but cannot as yet be predicted theoretically.

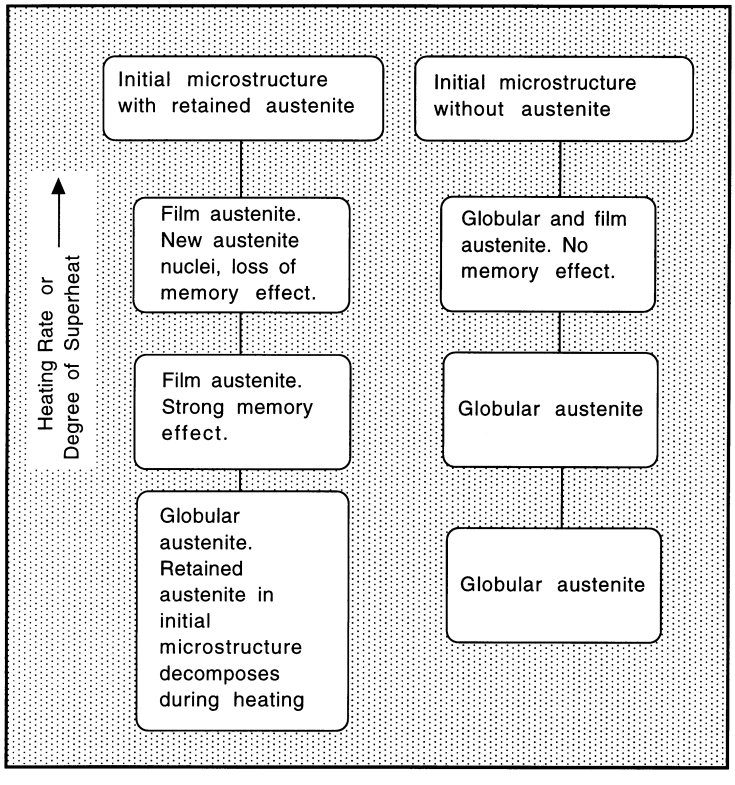

Fig. 9.7 The effects of heating rate and starting microstructure on the morphology of austenite and on the tendency for a memory effect.

10 *Acicular Ferrite*

10.1 General Characteristics and Morphology

Highly organised microstructures can often be found in steels; for example, ferrite plates frequently grow in the form of packets containing parallel plates which are in the same crystallographic orientation. This can be harmful to mechanical properties because cleavage cracks can propagate readily across the packets.

Some of the most exciting recent developments in wrought and welded steel technology have involved *acicular ferrite* (Grong and Matlock, 1986; Abson and Pargeter, 1986). Far from being organised, this microstructure is better described as chaotic. The plates of acicular ferrite nucleate heterogeneously on small nonmetallic inclusions and radiate in many different directions from these point nucleation sites (Fig. 10.1). Crystallographic data show highly misoriented plates nucleated on the same inclusion (Gourgues *et al*., 2000). Propagating cracks are then deflected on each encounter with a differently oriented acicular ferrite plate. This gives rise to superior mechanical properties, especially toughness.

Acicular ferrite is therefore widely recognised to be a desirable microstructure. This chapter deals with the mechanism by which it forms and with the role of inclusions in stimulating its formation.

The term *acicular* means shaped and pointed like a needle but this is misleading because the true shape is that of a lenticular plate. The aspect ratio of the plates has never been measured but in random planar sections, they are typically about 10 μm long and approximately 1 μm wide, so that the true aspect ratio is likely to be much smaller than 0.1.

An arc-weld deposit typically contains some $10^{18}\,m^{-3}$ inclusions of a size greater than 0.05 μm, with a mean size of about 0.4 μm, distributed throughout the microstructure. Inclusions form as oxygen in the liquid weld metal reacts with strong deoxidising elements such as silicon, aluminium and titanium. Slag-forming compounds which form a part of the system designed to protect weld metal from the environment, may also become trapped in the solid at the advancing δ-ferrite/liquid interface. Inclusions promote intragranular nucleation of acicular ferrite plates and hence improve toughness without

[13:35 3/9/01 C:/3B2 Templates/keith/3750 BAINITE.605/3750-010.3d] Ref: 0000 Auth: Title: Chapter 00 Page: 237 237-276

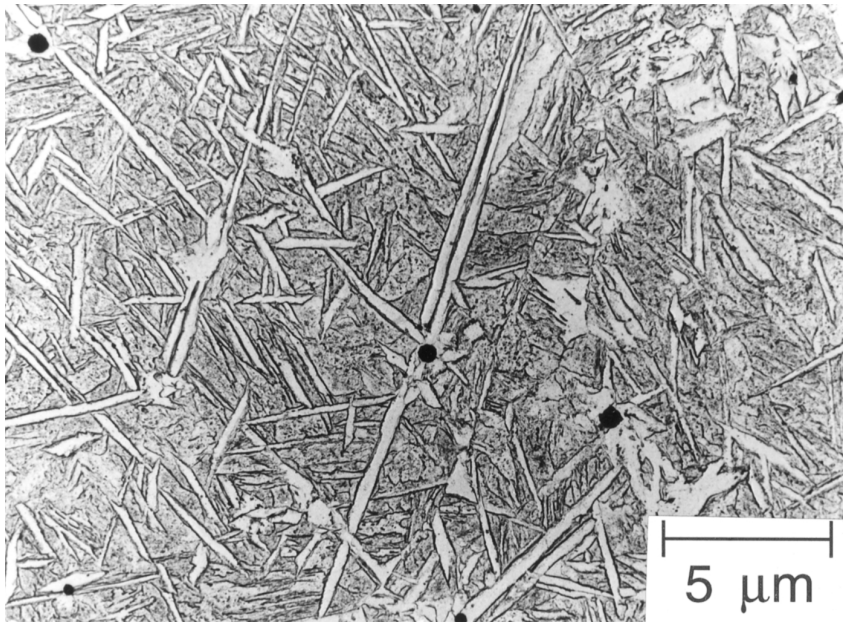

Fig. 10.1 Replica transmission electron micrograph of acicular ferrite plates in a steel weld deposit (Barritte, 1982).

compromising strength. But they also are responsible for the nucleation of voids during ductile fracture, or the nucleation of cleavage cracks during brittle fracture. Achieving a balance between these conflicting factors is the essence of good design. The inclusion microstructure is particularly important in this respect (Fig. 10.2). For example, nonmetallic particles in certain submerged arc weld deposits consist of titanium nitride cores, encapsulated in a glassy phase containing manganese, silicon and aluminium oxides, with a thin layer of manganese sulphide titanium oxide partly covering the surface of the inclusions (Barbaro *et al*., 1988). The development of this complex microstructure has been modelled using nucleation and growth theory (Babu *et al*., 1995).

Inclusions can be oxides or other compounds but the important point is that they may stimulate acicular ferrite (Ito and Nakanishi, 1976). The nucleation of a single plate on an inclusion can in turn stimulate others to nucleate autocatalytically, so that a one-to-one correspondence between the number of active inclusions and the number of acicular ferrite plates is not expected (Ricks *et al*., 1982).

The shape change accompanying the growth of acicular ferrite has been characterised qualitatively as an invariant-plane strain (Fig. 10.3). Like bainite, the shape deformation causes plastic deformation in the adjacent austenite. The

[13:36 3/9/01 C:/3B2 Templates/keith/3750 BAINITE.605/3750-010.3d] Ref: 0000 Auth: Title: Chapter 00 Page: 238 237-276

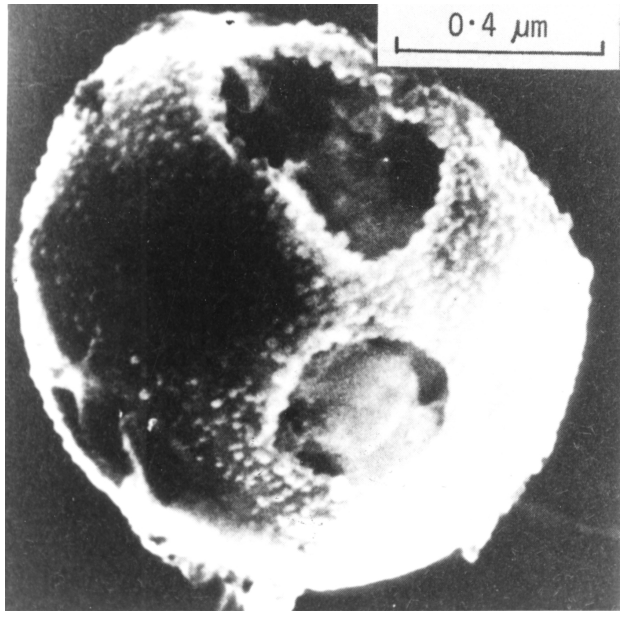

Fig. 10.2 Scanning transmission electron micrograph of a nonmetallic inclusion in a steel weld metal. The inclusion surface is very irregular, and it features many phases (after Barritte, 1982).

resulting dislocations are inherited by the acicular ferrite as it grows, giving a dislocation density which is typically at $10^{14}\,\mathrm{m}^{-2}$, and which contribute some 145 MPa to its strength. The stored energy of acicular ferrite is similar to that of bainite at about $400\,\mathrm{J\,mol}^{-1}$ (Strangwood and Bhadeshia, 1987; Yang and Bhadeshia, 1987). Consistent with the observed shape change, microanalysis experiments prove that there is no long-range partitioning of substitutional solutes during the formation of acicular ferrite (Strangwood, 1987); indeed, atomic resolution experiments have demonstrated that there is no partitioning on the finest conceivable scale (Chandrasekharaiah *et al.*, 1994).

Acicular ferrite clearly grows by a displacive mechanism so there are other consequences on the development of microstructure. Thus, plates of acicular ferrite are confined to the grains in which they grow because the coordinated movement of atoms associated with the displacive transformation mechanism cannot be sustained across grain boundaries. The α_a/γ orientation relationship is *always* found to be one in which a close-packed plane of the austenite is nearly parallel to the most densely packed plane of α_a. Corresponding close-packed directions within these planes are found to be within a few degrees of each other (Strangwood and Bhadeshia, 1987). As with bainite, the size of the acicular ferrite plates increases with transformation temperature; Horii

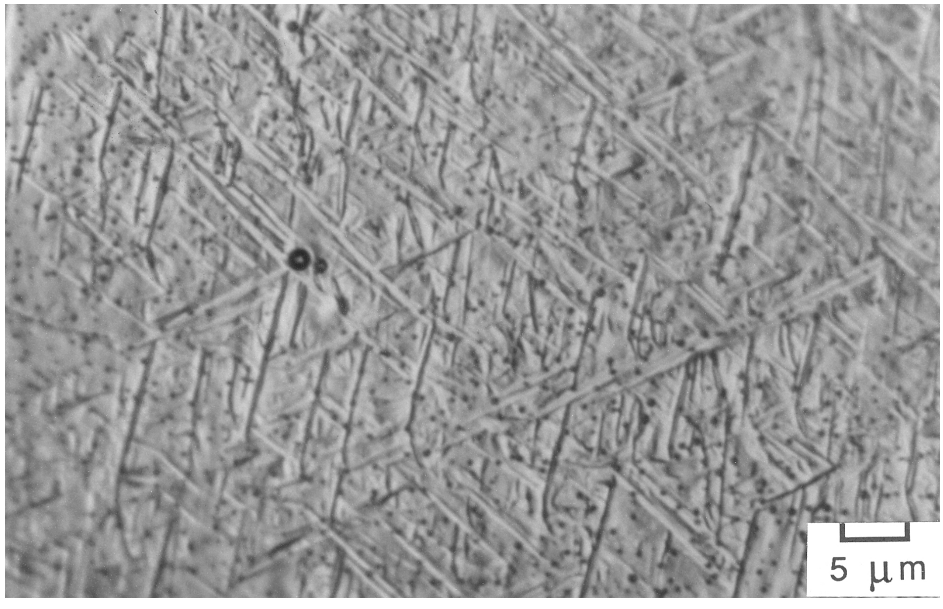

Fig. 10.3 Nomarski interference contrast micrograph illustrating the displacements associated with the formation of acicular ferrite (Strangwood and Bhadeshia, 1987).

et al.(1988) reported that the apparent plate thickness and length changed from about 1 to 2 μm as the weld cooling rate was reduced.

10.2 Mechanism of Growth

The acicular ferrite transformation exhibits the incomplete-reaction phenomenon, an important characteristic of bainite. The extent of reaction decreases towards zero as the transformation temperature is increased towards B_S (Yang and Bhadeshia, 1987; Strangwood and Bhadeshia, 1987). Isothermal transformation stops when the carbon concentration of the residual austenite exceeds the T_0' curve (Fig. 10.4). This implies that acicular ferrite grows supersaturated with carbon, but the excess carbon is shortly afterwards rejected into the remaining austenite.

Acicular ferrite is intragranularly nucleated bainite so it should be possible to switch between these two morphologies by controlling the nucleation site. A bainitic microstructure can be replaced by one containing acicular ferrite by increasing the oxygen, and hence the inclusion content (Ito *et al*., 1982). After all, the appearance of the acicular ferrite microstructure is only different from

[13:36 3/9/01 C:/3B2 Templates/keith/3750 BAINITE.605/3750-010.3d] Ref: 0000 Auth: Title: Chapter 00 Page: 240 237-276

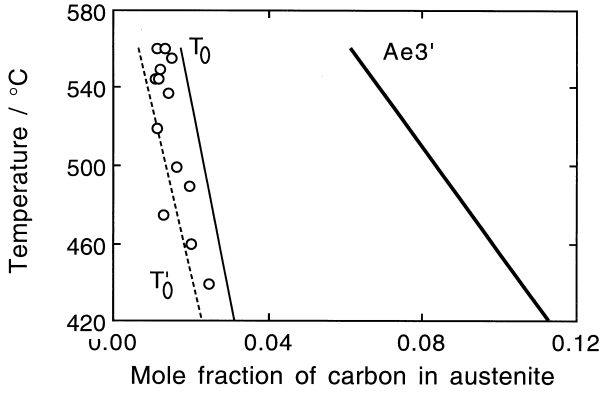

Fig. 10.4 Data from experiments in which the austenite is transformed isothermally to acicular ferrite, showing that the reaction stops when the carbon concentration of the austenite reaches the T_0' curve (Strangwood and Bhadeshia, 1987).

that of bainite because it nucleates intragranularly in steels containing a greater number density of inclusions than austenite grain surface nucleation sites (Yang and Bhadeshia, 1986). Acicular ferrite does not grow in sheaves because their development is stifled by impingement between plates nucleated independently at adjacent sites. Indeed, both microstructures can be obtained under identical isothermal transformation conditions in the same inclusion-containing steel. Bainite forms when the austenite grain size is small because nucleation then predominates at the grain boundaries. Subsequent growth then swamps the interiors of the austenite grains, preventing the development of acicular ferrite. When the austenite grain size is large, the number density of inclusions becomes large relative to boundary nucleation sites promoting the formation of acicular ferrite at the expense of bainite (Fig. 10.5).

This basic theory explains many observations on welds where the heat due to welds produces a gradient of austenite grain size in the heat affected zone (HAZ), with the largest grains adjacent to the fusion surface. When steels containing appropriate inclusions are welded, the ratio of acicular ferrite to bainite is the highest in the HAZ nearest the fusion boundary where the austenite grain size is at a maximum (Fig. 10.6a). In the absence of inclusions, the acicular ferrite content is always very small, Fig. 10.6b (e.g. Imagumbai *et al.*, 1985).

In another supporting experiment, Harrison and Farrar (1981) removed the inclusions by vacuum remelting a weld; when cooled, the steel transformed into bainite instead of the original acicular ferrite microstructure.

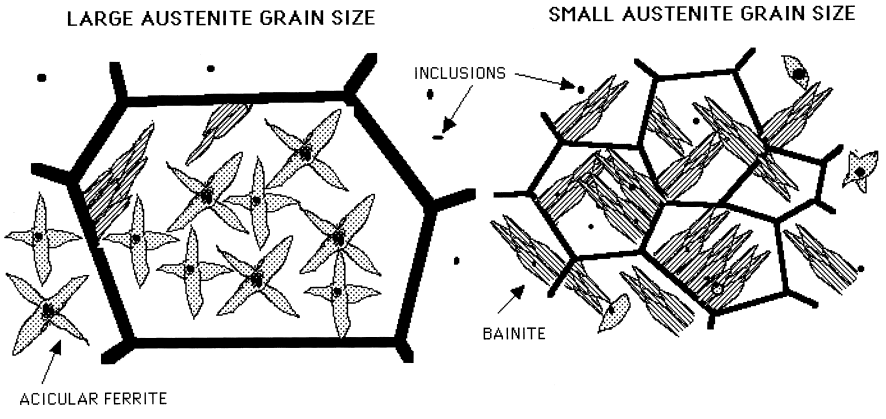

Fig. 10.5 The effect of austenite grain size on the development of microstructure in an inclusion-containing steel. A small grain sized sample has a relatively large number density of grain boundary nucleation sites so bainite dominates the microstructure, whereas a relatively large number density of intragranular nucleation sites leads to a microstructure consisting predominantly of acicular ferrite.

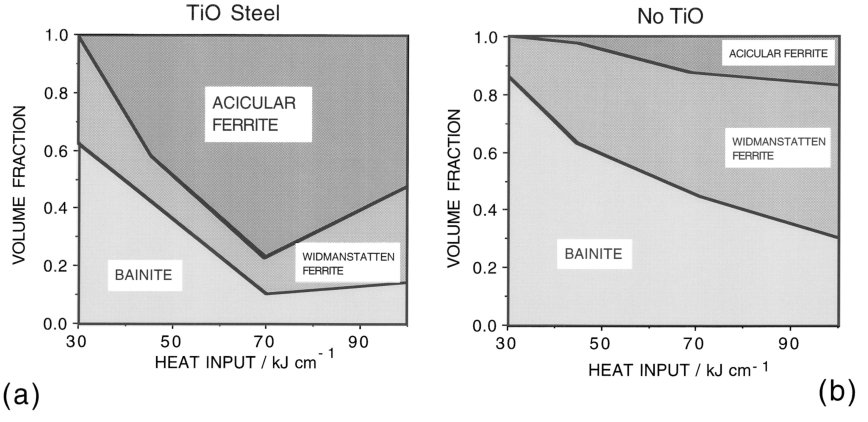

Fig. 10.6 Changes in the microstructure of the heat affected zone of welds, as a function of the heat input during welding: (a) steel containing titanium oxide particles; (b) ordinary steel without inclusion inoculation (after Chijiiwa *et al*., 1988).

We have emphasised that the transformation mechanism for acicular ferrite is identical to that for bainite. However, all phases can nucleate on inclusions, including Widmanstätten ferrite (Dubé, 1948; Ali and Bhadeshia, 1991). Thewlis *et al*. (1997) have argued that in some welds the so-called acicular

[13:36 3/9/01 C:/3B2 Templates/keith/3750 BAINITE.605/3750-010.3d] Ref: 0000 Auth: Title: Chapter 00 Page: 242 237-276

ferrite may predominantly be intragranularly nucleated Widmanstätten ferrite rather than bainite. They reached this conclusion by noting that the estimated bainite-start (B_S) temperature was lower than that at which coarse plates nucleated on very large inclusions (3–9 μm diameter). Although there is uncertainty in their calculated B_S values, the conclusion that a mixed microstructure of intragranularly nucleated Widmanstätten ferrite and intragranularly nucleated bainite (i.e. acicular ferrite) was obtained seems justified. Intragranularly nucleated Widmanstätten ferrite can be distinguished readily from bainite by the scale of the optical microstructure.

Widmanstätten ferrite plates are always much coarser than bainite because what appears as a single plate using optical microscopy is in fact a pair of self accommodating plates. The shape deformation consists of two adjacent invariant-plane strains which mutually accommodate and hence reduce the strain energy, thus allowing the plates to be coarse (Bhadeshia, 1981a).

Acicular ferrite is sometimes considered to be intragranularly nucleated Widmanstätten ferrite on the basis of the observation of 'steps' at the transformation interface, which are taken to imply a ledge growth mechanism (Ricks *et al*., 1982). The step mechanism of interfacial motion does not necessarily indicate the mechanism of *transformation*. The observations are in any case weak; perturbations of various kinds can always be seen on transformation interfaces between ferrite and austenite. Such perturbations do not, however, necessarily imply a step mechanism of growth. Evidence that the residual austenite is enriched in carbon is sometimes quoted in support of the contention that α_a is Widmanstätten ferrite but as pointed out above, the enrichment can occur during or after the transformation event.

The weight of the evidence is that the acicular ferrite recognised in most weld microstructures is intragranularly nucleated bainite. And that the term acicular ferrite should be reserved for this fine microstructure. If coarse Widmanstätten ferrite forms on inclusions then it can be called 'intragranularly nucleated Widmanstätten ferrite'. The names given to phases are important because they imply a mechanism of transformation which can be used in theoretical models. It is particularly important to avoid naming mixtures of microstructures.

10.3 Mechanism of Nucleation

A popular treatment of acicular ferrite nucleation based on classical heterophase fluctuation theory is due to Ricks *et al*. (1981,1982). It relies on the occurrence of chance fluctuations in crystal structure. The activation energy (G^*) for a fluctuation which is large enough to stimulate critical nucleus depends on the inverse square of the chemical driving force $G^* \propto \Delta G^{-2}$ (Chapter 6). With this theory it is possible to explain why larger spherical non-metallic inclusions are

more effective for heterogeneous nucleation. An embryo which forms in contact with the surface will have a smaller curvature and a corresponding smaller surface-to-volume ratio when the inclusion is large. A flat austenite grain surface is therefore expected to be a more potent heterogeneous nucleation site than a spherical inclusion. Furthermore, the energy of the interface between the ferrite and the inclusion is likely to be larger relative to the case when ferrite nucleates on austenite grain surfaces. It follows that the activation energy for nucleation on an inclusion, relative to that for nucleation on an austenite grain surface should vary as illustrated in Fig. 10.7.

An alternative interpretation uses the bainite nucleation theory discussed in Chapter 6. Nucleation is said to occur when an appropriate array of dislocations is able to dissociate rapidly. The activation energy is that for the migration of the embryo/austenite interface; it decreases linearly as the driving force increases. The driving force must be calculated to allow for the diffusion of carbon although the overall mechanism of nucleation remains displacive since the dislocation array considered is glissile.

It follows that the driving force available for nucleation at the highest temperature at which transformation occurs (T_h) should be proportional to T_h (Chapter 6). This is found to be the case as illustrated in Fig. 10.8, which is comparable to Fig. 6.4a. The line is identified with the universal nucleation

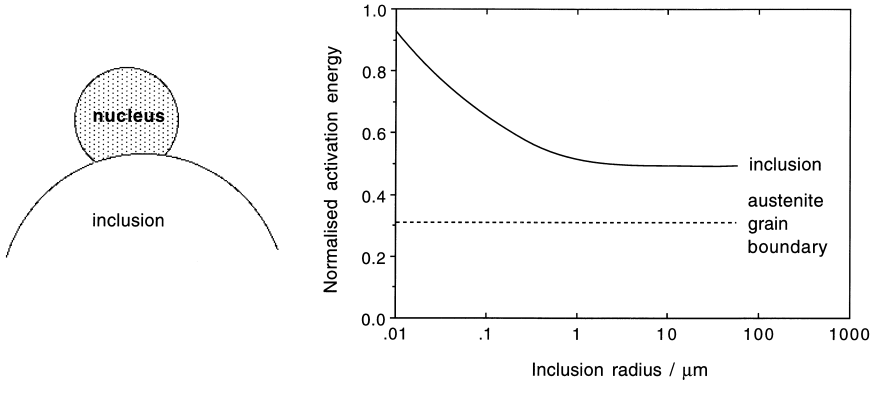

Fig. 10.7 The formation of a truncated spherical nucleus on a spherical inclusion. The activation energy for nucleation has been normalised with respect to that for homogeneous nucleation. The calculations assume that the interfacial energy between austenite and ferrite is the same as that for an austenite grain boundary; that the inclusion/ferrite and inclusion/austenite interface energies are identical and that these are both greater than an austenite grain boundary energy. After Ricks *et al*. (1981, 1982).

function G_N that can be used to estimate the acicular ferrite start-temperature for any alloy.

The experiments shown in Fig. 10.8 included both bainite and acicular ferrite, the change in microstructure being achieved by controlling the austenite grain size. It is evident that both bainite and acicular ferrite can be represented by the same line, emphasising the conclusion that acicular ferrite is simply intragranularly nucleated bainite.

The displacive mechanism of nucleation relies on the existence of arrays of dislocations. It is conceivable that such arrays are generated in the proximity of non-metallic inclusions due to stresses caused by differential thermal expansion. Such stresses are more difficult to accommodate for larger inclusions, making large inclusions more potent nucleation sites. Arrays of dislocations are readily found at grain boundaries, accounting for the observation that austenite grain surfaces are most effective as nucleation sites.

10.4 Nucleation and The Role of Inclusions

Non-metallic inclusions in steels have complex multiphase microstructures which make controlled experiments designed to reveal nucleation phenomena rather difficult. A popular idea is that the most potent nucleants have a good *lattice match* with ferrite. There may then exist reproducible orientation relationships between inclusions and the ferrite plates that they nucleate (Mills *et al.*, 1987). The lattice matching is expressed as a mean percentage planar misfit κ (Bramfitt, 1970). Suppose that the inclusion is faceted on $(h\,k\,l)_I$ and

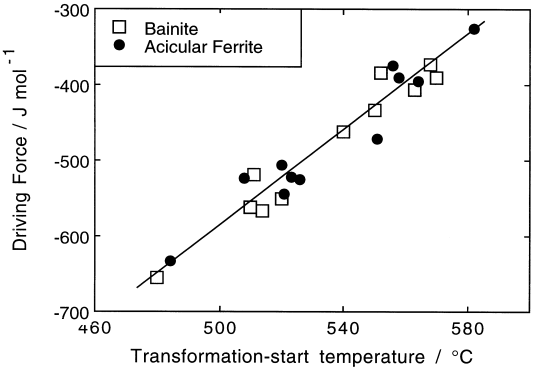

Fig. 10.8 Plot of the driving force available for the nucleation of bainite or acicular ferrite at the temperature T_h, versus T_h for a series of welding alloys. Note that each pair of bainite and acicular ferrite points represents a different alloy. After Rees and Bhadeshia, 1994.

that the ferrite deposits epitaxially with $(h\,k\,l)_\alpha \| (h\,k\,l)_I$, with a pair of corresponding rational directions $[u\,v\,w]_I$ and $[u\,v\,w]_\alpha$ inclined at an angle ϕ to each other. The interatomic spacings d along three such directions within the plane of epitaxy are examined to obtain:

$$\kappa = \frac{100}{3} \sum_{j=1}^{3} \frac{|d_j^I \cos\phi - d_j^\alpha|}{d_j^\alpha} \tag{10.1}$$

Data calculated in this manner, for a variety of inclusion phases, are presented in Table 10.1. A description of the relationship between two crystals with cubic lattices requires five degrees of freedom, three of which are needed to specify the relative orientation relationship, and a further two in order to identify the plane of contact between the two crystals. Mills *et al*. considered nine different kinds of epitaxy, confined to planes of low crystallographic indices: $\{0\,0\,1\}$, $\{0\,1\,1\}$ & $\{1\,1\,1\}$. The orientation relationships considered are listed in Table 10.1: the Bain orientation implies $\{1\,0\,0\}_\alpha \| \{1\,0\,0\}_I$ and $< 1\,0\,0 >_\alpha \| < 0\,1\,1 >_I$. The Cube orientation occurs when the cell edges of the two crystals are parallel.

Table 10.1 Misfit values between different substrates and ferrite. The data are from a more detailed set published by Mills *et al.* (1987) and include all cases where the misfit is found to be less than 5%. The inclusions all have a cubic-F lattice; the ferrite is body-centred cubic (cubic-I).

Inclusion	Orientation	Plane of Epitaxy	Misfit %
TiO	Bain	{1 0 0}	3.0
TiN	Bain	{1 0 0}	4.6
γ-alumina	Bain	{1 0 0}	3.2
Galaxite	Bain	{1 0 0}	1.8
CuS	Cube	{1 1 1}	2.8

A comparison with experiments requires not only the right orientation relationship, but the inclusion must also be faceted on the appropriate plane of epitaxy. Experiments, however, demonstrate that the ferrite/inclusion orientation relationship tends to be random (Dowling *et al*., 1986). The inclusions, which form in liquid steel, are randomly orientated but there is a fixed α_a/γ orientation so it follows that the inclusion/ferrite orientation relation must be random (Fig. 10.9). A contrary view is due to Kluken *et al*. (1991), who claim that the δ-ferrite grains sometimes nucleate on inclusions in the melt. The

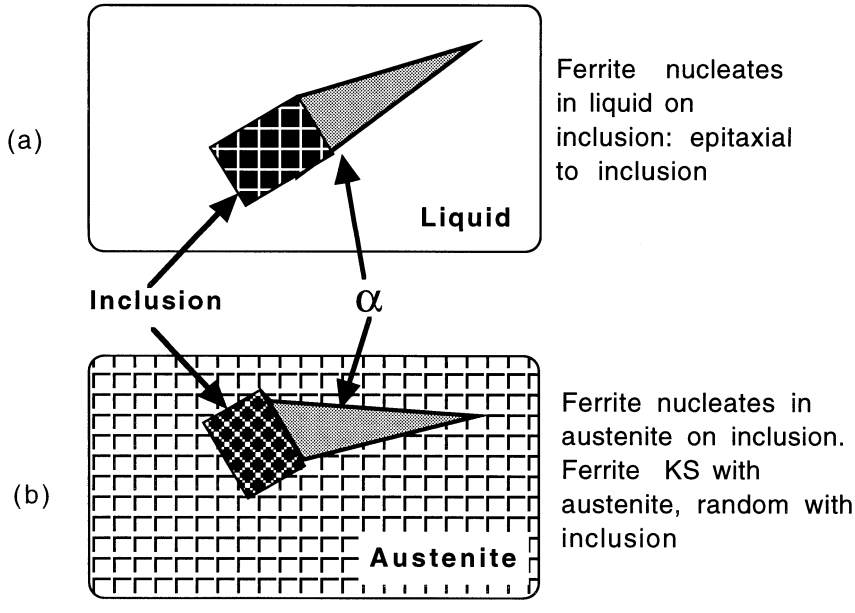

Fig. 10.9 Illustration of the orientation relationship that might develop between acicular ferrite and an inclusion. (a) When ferrite nucleates on an inclusion, with both phases surrounded by liquid; it is possible for the ferrite to adopt a favoured relationship to the inclusion since it is not limited by the liquid. (b) The inclusion, which grows from liquid, is randomly orientated to the austenite. The acicular ferrite, which has fixed orientation relationship with the austenite, must therefore be randomly orientated to the inclusion.

acicular ferrite should then bear an orientation relationship with the inclusions since it will be related to the δ-ferrite via the austenite. Textural measurements have been cited in support of this hypothesis.

Other ways in which inclusions may assist nucleation include stimulation by thermal strains, chemical heterogeneities in the vicinity of the inclusion/matrix interface; alternatively, they may simply be inert sites for heterogeneous nucleation. Pressure bonded ceramic–steel composites have been studied to reveal the potency of pure ceramic phases in stimulating the nucleation of bainite, Table 10.2 (Strangwood and Bhadeshia, 1988; Gregg and Bhadeshia, 1994a,b). A rather simple model emerges from these experiments, that those ceramics which chemically interact with the adjacent steel are most effective in nucleating bainite. A significant exception is TiO, which remains inert and yet enhances bainite formation.

There is clear evidence from the bond experiments that some minerals act as sources of oxygen which cause the steel in their vicinity to decarburise, which

[13:36 3/9/01 C:/3B2 Templates/keith/3750 BAINITE.605/3750-010.3d] Ref: 0000 Auth: Title: Chapter 00 Page: 247 237-276

Table 10.2 List of ceramics found to be chemically active in experiments designed to test for ferrite nucleation at ceramic/steel bonds.

Chemically Active	Chemically Inactive
TiO_2	TiO, Ti_2O_3, TiC, TiB_2, TiN
$Al_2Si_2O_7$	Al_2O_3
MnO_2	MnO
SiC, Si	Si_3N_4, SiO_2
CoO, V_2O_5	ZrO_2, FeS, Y_2O_3

in turn stimulates the nucleation of bainite. One such mineral is TiO_2. Structural and behavioural analogues of TiO_2 (SnO_2, MnO_2 and PbO_2) are also found to stimulate bainite in the same manner. TiO_2 and related minerals tend to form oxygen vacancy defects at elevated temperatures, thus releasing oxygen, which can penetrate the adjacent steel. On this hypothesis, all oxygen producing minerals would be expected to react with the steel, and enhance bainite formation, while non-oxygen producing minerals would not. This contrast in nucleation potential due to differences in the ability to release oxygen is illustrated by examining the nucleation potency of the perovskite structural group of ceramics. *Normal* perovskites (ABO_3 type) are structurally similar to *defect* perovskites (BO_3 type) but the ability of defect perovskites to produce oxygen is much greater. Therefore, WO_3, which is a defect perovskite is effective in nucleating bainite whereas the normal perovskite $CaTiO_3$ is found to be ineffective. Indeed, any oxygen source, for example KNO_3, is found to be effective in stimulating the nucleation of bainite.

Neither Ti_2O_3 nor TiO are oxygen sources but nevertheless stimulate bainite. Ti_2O_3 does this by absorbing manganese and hence causing a dramatic depletion in the manganese concentration in the adjacent steel. Since manganese stabilises austenite, its depletion stimulates bainite formation. By contrast, TiO remains completely inert so the mechanism by which it stimulates nucleation is not clear. It could be argued that it offers a good lattice match with ferrite. However, so does TiN, which is not particularly useful in nucleating bainite. The nucleation mechanisms are summarised in Table 10.3.

10.4.1 Aluminium and Titanium Oxides

There is evidence that titanium oxides (TiO, Ti_2O_3, TiO_2) are potent acicular ferrite nucleating agents whereas Al_2O_3 is not. Aluminium is a stronger oxidising agent than titanium so it is expected that alumina forms first, followed by

[13:36 3/9/01 C:/3B2 Templates/keith/3750 BAINITE.605/3750-010.3d] Ref: 0000 Auth: Title: Chapter 00 Page: 248 237-276

Table 10.3 Mineral classification according bainite nucleation potency.

Effective: oxygen sources	Effective: other mechanisms	Ineffective
TiO_2, SnO_2	Ti_2O_3	TiN, $CaTiO_3$
MnO_2, PbO_2	TiO	$SrTiO_3$, $\alpha - Al_2O_3$
WO_3, MoO_3		$\gamma - Al_2O_3$, $MnAl_2O_4$
KNO_3		NbC

titania, which can form as a coating on the alumina particles. Titanium oxide formation requires that there is excess oxygen left after the aluminium has combined with oxygen (Horii *et al*., 1986, 1988). The aluminium concentration should therefore be kept to a minimum, otherwise, titanium oxides do not form even if the steel contains a titanium addition Ringer *et al*., (1990).

Titanium nitride is an effective nucleant but is less thermodynamically stable at high temperatures when compared with Ti_2O_3.

$$Ti + O_2 \rightleftharpoons TiO_2 \quad G^O = -9.2 \times 10^5 - 50.2\,T \ \ J\,mol^{-1} \tag{10.2}$$

$$Ti + N \rightleftharpoons TiN \quad G^O = -3.4 \times 10^5 - 30.1\,T \ \ J\,mol^{-1} \tag{10.3}$$

where G^O is the standard free energy of formation (Kubaschewski and Evans, 1950). Nevertheless, titanium nitride is often the first to precipitate from the liquid phase.

Notwithstanding this anomaly, considerable progress can be made by assuming that the dissolved elements in a sequence consistent with their oxidising potential. For welds, this usually means that aluminium has the first call on the available oxygen, followed by titanium (Horii *et al*., 1988). Oxygen can be depleted from the melt by an excess of aluminium, preventing the formation of desirable titanium oxides. A minimisation of the aluminium content has the additional advantage that the total oxygen (and hence the inclusion content) can be reduced whilst keeping the same titanium oxide content. Nitrogen must be controlled to prevent the formation of titanium nitride, perhaps by adding boron as a nitrogen gettering agent. Trace elements like calcium, cerium and other rare earth elements, at the concentrations used for inclusion shape control in wrought alloys, do not influence the development of the acicular ferrite microstructure (Horii *et al*., 1986, 1988). These elements might enter the weld metal via the fused base metal, particularly during high heat input welding where dilution is exaggerated (Fig. 10.10).

Small concentrations of dissolved aluminium seem to promote Widmanstätten ferrite; the mechanism of this is effect is not understood

[13:36 3/9/01 C:/3B2 Templates/keith/3750 BAINITE.605/3750-010.3d] Ref: 0000 Auth: Title: Chapter 00 Page: 249 237-276

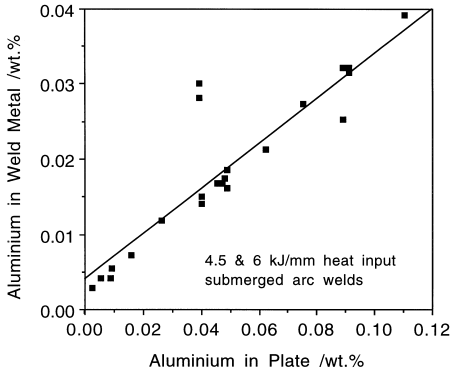

Fig. 10.10 A plot of the aluminium concentration in the weld metal versus that in the steel, illustrating the incorporation of trace elements from the base plate into the weld fusion zone during high heat input welding (Horii *et al*. 1988).

(Abson, 1987; Grong *et al*., 1988; Thewlis, 1989a,b). It may be that the presence of soluble aluminium correlates with a large overall aluminium concentration, in which case the aluminium oxide becomes γ-alumina instead of galaxite. The former is not an effective nucleant for acicular ferrite, thus allowing grain boundary nucleated Widmanstätten ferrite to grow unhindered.

The mean size of non-metallic inclusions in welds changes only a little with the aluminium concentration (Thewlis, 1989a; Evans, 1990). Although inclusions are essential for improved weld microstructure, they can also nucleate fracture. A compromise level of inclusions is required, but it seems likely most weld deposits contain more oxygen than is necessary. For example, concentrations less than 120 p.p.m. are adequate in producing an acicular ferrite microstructure in suitably alloyed wrought steels.

The character of inclusions alters with increasing aluminium concentration. The oxide particles being predominantly $MnOSiO_2$ at low Al concentrations, to be replaced by galaxite which is a mixed spinel (Al_2O_3MnO) and finally by $\gamma - Al_2O_3$ at higher aluminium concentrations (Thewlis, 1990). Galaxite has a good lattice match with ferrite and so is the desired oxide form (Table 10.1).

10.4.2 Sulphur

Manganese sulphide (MnS) particles sometimes act as heterogeneous nucleation sites. Using a steel containing 0.07 wt% of sulphur and 0.1 wt% vanadium, Ochi *et al*. (1988) produced a fine dispersion of MnS particles on which they obtained the successive precipitation of vanadium nitride, vanadium carbide and finally, idiomorphic ferrite:

[13:36 3/9/01 C:/3B2 Templates/keith/3750 BAINITE.605/3750-010.3d] Ref: 0000 Auth: Title: Chapter 00 Page: 250 237-276

$$MnS \rightarrow VN \rightarrow V_4C_3 \rightarrow \alpha_I$$

On the other hand, in more recent work, the nitride has been shown to lead directly to the nucleation of ferrite via the lattice-matching mechanism (Ishikawa *et al*., 1994).

The sulphide can itself stimulate ferrite. Thus, Yamamoto *et al*. (1987) in their titanium-containing steel, found that MnS precipitates on titanium oxides and then stimulates the nucleation of acicular ferrite. The acicular ferrite fraction decreased when the sulphur concentration was reduced to less than 0.001 wt%. However, there are contradictory results. Chijiiwa *et al*. (1988) found an increase in the acicular ferrite fraction as the sulphur concentration from was reduced from 0.005 to 0.001 wt%. Ringer *et al*. (1990) showed that Ti_2O_3 particles without any surrounding MnS films can nevertheless be effective in stimulating the intragranular nucleation of ferrite. Abson (1987) has concluded that the presence of MnS at the surface of oxide particles inhibits the nucleation of ferrite, and furthermore, that the addition of elements which getter sulphur makes the inclusions more effective.

It is therefore difficult to reach a conclusion, but it is likely that manganese sulphide can act as a substrate for the nucleation of ferrite. MnS is commonly present in commercial steels but it precipitates in the solute-enriched interdendritic regions of the solidification microstructure. These regions are rich in manganese which retards ferrite formation. Realising this, Ueshima *et al*. (1989) produced uniform distributions of MnS particles by inducing them to nucleate on oxide particles. High purity melts, each containing 0.004 wt.% of sulphur, were deoxidised using one of Al, Ti, Zr, La, Ce, Hf or Y. Of these, aluminium and titanium additions were found to be the most uniformly dispersed and insensitive to the killing time within the range 30–600s (Fig. 10.11).[†] All of the deoxidising elements studied were able to promote MnS nucleation (Fig. 10.11), but Ti_2O_3 and zirconia were particularly effective, with aluminium being the least potent in this respect. The MnS precipitated in the solid-state over a temperature range estimated to be 1050–1400°C. Whilst these results do not help resolve the role of sulphides in stimulating ferrite nucleation, they establish methods of controlling the sulphide size, distribution and precipitation. Ueshima *et al*. estimated, using diffusion theory, that the formation of MnS would lead to a manganese-depleted zone in its close proximity, a zone in which the tendency to form ferrite would be enhanced.

It is obvious that manganese depletion can only help the nucleation of ferrite. An elegant study by Mabuchi *et al*. (1996) has proved that depletion zones are

[†]During *killing*, the oxygen concentration in the molten steel is reduced by the addition of metallic elements which have a strong affinity for oxygen. The resulting oxides usually float off into the slag, although fine particles are retained. The killing time is the interval between the addition of the deoxidising element and the solidification of the steel.

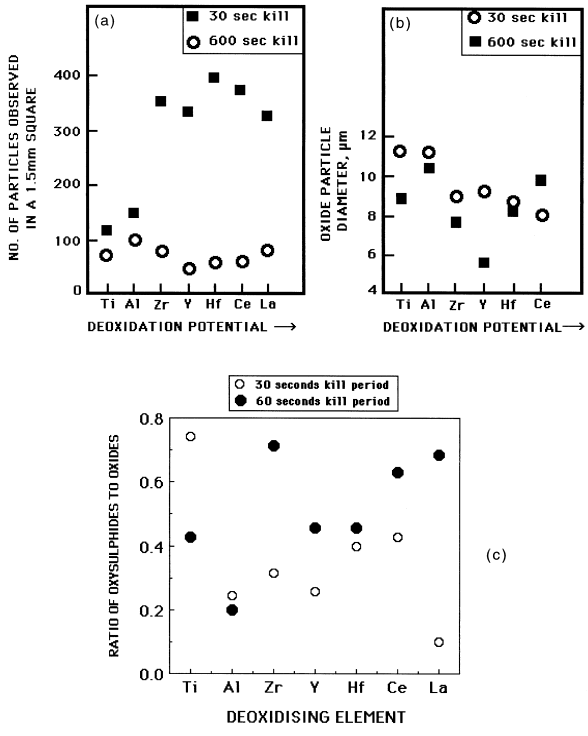

Fig. 10.11 The effects of a variety of deoxidising elements on the nature of oxide and oxysulphide precipitation in steel (Ueshima *et al*., 1989): (a) number density of oxide particles; (b) size of oxide particles; (c) propensity of the oxide to stimulate the solid-state nucleation of sulphide.

indeed to be found in the vicinity of MnS which precipitates from austenite, but the zones are rapidly homogenised soon after the precipitation is completed. The MnS is therefore only active in stimulating ferrite nucleation if the latter occurs shortly after MnS formation. Any prolonged holding in the austenite phase field homogenises the manganese concentration. For the same reason, MnS particles might be active as heterogeneous nucleation sites on the first occasion that they precipitate, but their potency is reduced if the sample is then reheated into the austenite phase field. This has significant implications for the large number of experiments based on reheated weld metals and may explain why the early results are contradictory.

10.4.3 Phosphorus

Phosphorus is another impurity element which is rarely deliberately added to steels because of its well known tendency to embrittle grain boundaries. Its concentration is usually kept below 50 p.p.m., but in welds the average

[13:36 3/9/01 C:/3B2 Templates/keith/3750 BAINITE.605/3750-010.3d] Ref: 0000 Auth: Title: Chapter 00 Page: 252 237-276

concentration can exceed 100 p.p.m. Solidification induced segregation can locally raise the concentration to 500 p.p.m. This may alter the kinetics of transformation and hence influence the development of acicular ferrite microstructure in weld deposits (Kluken and Grong, 1989b; Kluken *et al*., 1990).

The thermodynamic effect of phosphorus is to raise the Ae_3 temperature by about 460 °C per wt%, over the concentration range of interest (Bastien, 1957), although the consequences of such a big effect are not as large as might be expected (Kirkaldy *et al*., 1962).

During weld solidification, the phosphorus segregates between the δ-ferrite dendrites and cells. When solidification is complete, the δ-ferrite transforms to austenite which nucleates heterogeneously at the δ/δ grain boundaries. Kluken and Grong suggest that the austenite grain boundaries coincide with the phosphorus rich regions so this stimulates the formation of acicular ferrite; when they do not do so, ferrite plates grow from the grain boundaries and consume most of the austenite before the intragranular acicular ferrite has a chance to develop.

This hypothesis is then used to explain why the acicular ferrite content of welds decreases suddenly as the ratio of the precipitated aluminium to oxygen concentrations reaches a value of 1.13 (Fig. 10.12a). Beyond that limiting value, the nonmetallic inclusions become pure γ-alumina (Fig. 10.12b), and these apparently stimulate austenite directly from the melt. The resulting austenite

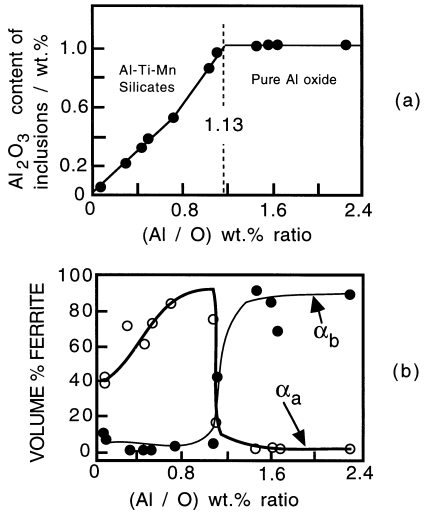

Fig. 10.12 (a) Variation in the volume fraction of acicular ferrite as a function of the precipitated-Al : oxygen ratio; (b) variation in the inclusion chemistry with the same ratio.

[13:36 3/9/01 C:/3B2 Templates/keith/3750 BAINITE.605/3750-010.3d] Ref: 0000 Auth: Title: Chapter 00 Page: 253 237-276

grain boundaries are no longer coincident with the phosphorus rich regions, thus leading to Widmanstätten ferrite formation.

These ideas are inconsistent with the fact that phosphorus increases the driving force for the transformation of austenite. A second difficulty is that in a weld, the temperature isotherms change position during cooling, so that the fastest growth direction of the austenite does not coincide with that of the δ-ferrite (Dadian, 1987).

10.4.4 Nitrogen, Titanium and Boron

Nitrogen is not often a deliberate alloying addition to steels and weld deposits. It is detrimental to the toughness even at concentrations as low as 20–120 p.p.m. The mechanism of embrittlement is strain age-hardening solid-solution hardening effects, both of which increase the yield strength and hence the ability of the material to absorb energy by plastic deformation during fracture (Lancaster, 1986; Keown *et al*., 1976; Judson and McKeown, 1982; Oldland, 1985).

Some studies suggest that nitrogen has no detectable influence on the acicular ferrite content of welds (Mori *et al*., 1981), whereas others (Okabe *et al*., 1983; Ito and Nakanishi, 1975) claim significant changes due to nitrogen. At the small concentrations of nitrogen in ferritic steels, it is unlikely that nitrogen has any significant thermodynamic effect on the $\gamma \rightarrow \alpha$ transformation. Its influence must be kinetic, perhaps via some interaction with the inclusion phases.

In practice, the effect of nitrogen in weld metals has to be considered alongside that of titanium and boron, both of which form nitrides. It appears that nitrogen, in the absence of boron, has no detectable effect on the development of microstructure (Horii *et al*., 1986, 1988; Lau *et al*., 1987, 1988). Boron is added to render austenite grain boundary nucleation sites impotent and hence to promote acicular ferrite. By contrast, nucleation at the interface between Ti_2O_3 and austenite is not retarded by boron; its diffusion into the oxide, which contains cation vacancies, leaves behind a boron-depleted zone (Yamamoto *et al*., 1996). Titanium has the function of protecting the boron from oxidation during transfer across the welding arc. It also prevents boron from combining with nitrogen to form boron nitride. Boron must be in solid solution if it is to segregate to and reduce the energy of the austenite grain surfaces, making them less effective nucleation sites.

For a given oxygen and boron concentration, the aluminium and titanium concentrations have to be large enough to getter all the available oxygen. Furthermore, there has to be enough titanium left over to combine with any nitrogen to permit boron to remain in solid solution. A method for making rational decisions during the design of titanium and boron containing deposits is illustrated in Fig. 10.13.

The assumptions involved are illustrated by the work of Kluken and Grong (1989a), whose ideas are reproduced below in an explicit formalism. The total volume fraction V_I of inclusions is approximately (Franklin, 1969):

$$V_I \simeq 0.05 w_O + 0.054(w_S - w_S^{sol}) \tag{10.4}$$

where w_i is the concentration of element i in units of weight percent and w_S^{sol} the soluble sulphur concentration, usually assumed to be about 0.003 wt%. The mass fraction of inclusions is:

$$m_I = V_I \frac{\rho_I}{\rho_S} \tag{10.5}$$

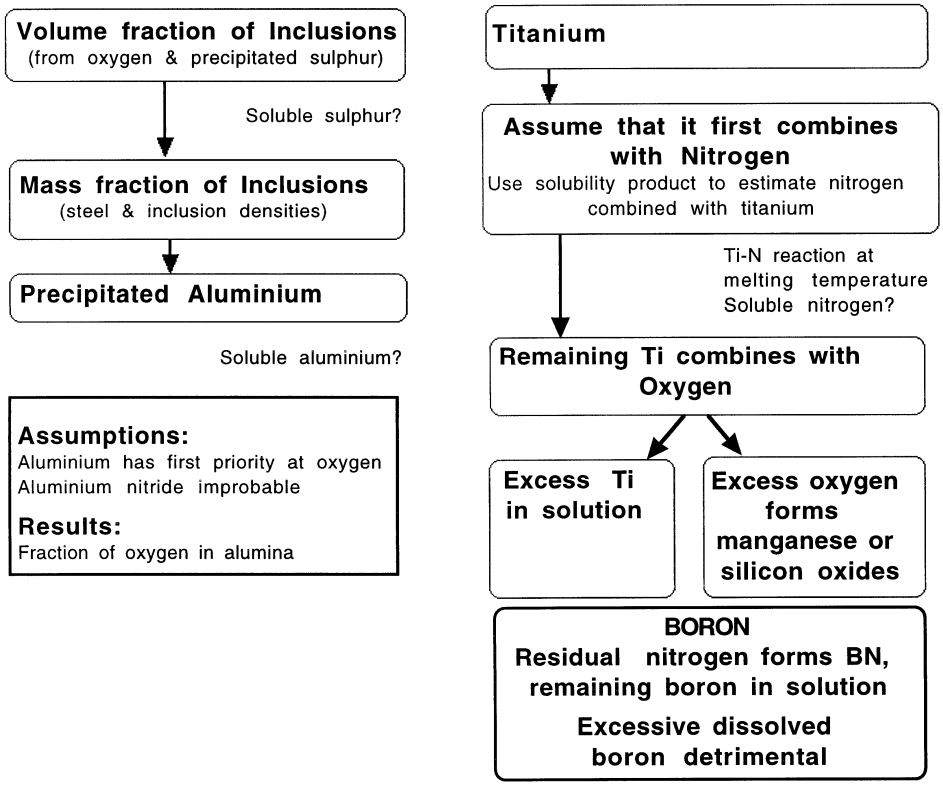

Fig. 10.13 Procedure for the estimation of inclusion microstructure. The assumptions and difficulties associated with the method are placed outside of the main boxes.

[13:36 3/9/01 C:/3B2 Templates/keith/3750 BAINITE.605/3750-010.3d] Ref: 0000 Auth: Title: Chapter 00 Page: 255 237-276

where ρ_S and ρ_I are the steel and inclusion densities, about 7.8 and 4.2 $\mathrm{g\,cm^{-3}}$ respectively. It follows that the concentration of Al in the inclusions is given by:

$$w_{Al}^{I} = \left(w_{Al}^{T} - w_{Al}^{sol}\right)/m_I \tag{10.6}$$

where w_{Al}^{T} and w_{Al}^{sol} represent the total and soluble aluminium concentrations respectively. It is reasonably assumed here that none of the aluminium is in the form of aluminium nitride.

It may be assumed that the titanium reacts first with oxygen, and that any residual titanium can then proceed to combine with nitrogen. In the absence of active oxygen, the titanium nitride can be estimated by calculating the nitrogen in solution using a solubility product (Matsuda and Okumura, 1978):

$$\log\left\{\left[w_{Ti}^{sol}\right]\left[w_{N}^{sol}\right]\right\} = \frac{8000}{T} + 0.32 \tag{10.7}$$

assuming that the concentration of dissolved titanium is known. The temperature for which the calculation is to a good approximation the melting temperature of the steel. The quantity of titanium nitride in the inclusion (w_{Ti}^{I-N}), is then given by:

$$w_{Ti}^{I-N} = A_{Ti}\left(w_{N}^{T} - w_{N}^{sol}\right)/\left(m_I A_N\right) \tag{10.8}$$

where A_i represents the atomic weight of element i. It follows that the titanium in the inclusions, tied up as oxide (w_{Ti}^{I-O}) is given by

$$w_{Ti}^{I-O} = \left(w_{Ti}^{T} - w_{Ti}^{I-N} m_I - w_{Ti}^{sol}\right)/m_I \tag{10.9}$$

This differs from equation 13a of Kluken and Grong, which does not account for the titanium nitride. The sulphur content of the inclusion is similarly given by:

$$w_{S}^{I} = \left(w_{S}^{T} - w_{S}^{sol}\right)/m_I \tag{10.10}$$

Assuming that the sulphur is incorporated in the inclusion as manganese sulphide, the concentration of Mn in the inclusion as MnS is given by

$$w_{Mn}^{I-S} = A_{Mn} w_{S}^{I}/A_S. \tag{10.11}$$

The next step involving the calculation of the SiO_2 and MnO contents of the inclusion requires some assumption about the relative proportions of these two phases.

$$\text{If} \qquad \theta = \text{wt\% } SiO_2/\text{wt\% MnO} \tag{10.12}$$

$$\text{and} \qquad \beta = \frac{\left(\frac{A_{Mn}}{A_O} + 1\right)\theta}{\left(\frac{A_{Si}}{2A_O} + 1\right) + \left(\frac{A_{Mn}}{A_O} + 1\right)\theta} \tag{10.13}$$

$$\text{then} \qquad w_{Si}^{I} = \beta A_{Si}\left(w_O^T - m_I w_O^{I-Al} - m_I w_O^{I-Ti}\right)/(2m_I A_O) \tag{10.14}$$

where w_O^{I-Al} and w_O^{I-Ti} are the concentrations of oxygen in the inclusion, tied up as alumina and titania respectively. It follows that:

$$w_{Mn}^{I-O} = (1-\beta)A_{Mn}\left(w_O^T - m_I w_O^{I-Al} - m_I w_O^{I-Ti}\right)/(m_I A_O) \tag{10.15}$$

These estimates require a knowledge of the dissolved Al, Ti and S concentrations and assume that the oxidation state of the titanium is known. Titanium compounds such as TiN, TiC and TiO have similar lattice parameters and crystal structures and are difficult to distinguish using diffraction. Common microanalytical techniques can readily identify titanium but not the light elements. Even when oxygen can be detected, the stoichiometry is difficult to determine since absorption and other corrections are not known for complex shapes. Lau *et al*. assumed that the Ti is in the form of TiO_2 whereas Kluken and Grong assumed it to be combined as Ti_2O_3. Abson (1987a) on the other hand, assumes that in weld deposits, the titanium oxide is TiO. The major weakness, however, is the method of partitioning oxygen between the different metallic elements. It can for example, be demonstrated that manganese and silicon oxides are found in systems where oxygen is expected to combine completely with Al and Ti. Moreover, the silicon concentration has been known to influence the ability of titanium to combine with oxygen (Lee and Pan, 1992a).

The real picture is evidently complex, but the sequence of reactions should at least determine the microstructure of the inclusions, with the first compounds to precipitate being located at the inclusion core, Fig. 10.14. It is the least reactive elements which should end up at the inclusion surface. Indeed, non-metallic particles in some submerged arc weld deposits have been identified with titanium nitride cores, surrounded by a glassy phase containing manganese, silicon and aluminium oxides, with a thin layer of manganese sulphide partly covering the inclusion surface (Barbaro *et al*., 1988). Similarly, in a weld free from aluminium or titanium, the inclusion core was found to be MnO–SiO_2 whereas the addition of only 40 p.p.m. of aluminium introduced alumina in the core (Es-Souni and Beaven, 1990). On the other hand, both these investigations reported the presence of unspecified titanium compounds over a part of the inclusion surface. It is possible that this reflects an incomplete coverage of the titanium compound core by subsequent phases.

10.4.5 Boron and Hydrogen

Experiments using secondary ion mass spectroscopy have revealed a tendency for boron to form a BH+ complex with hydrogen when both are in solution in steel (Pokhodnya and Shvachko, 1997). A consequence of this is that the mobi-

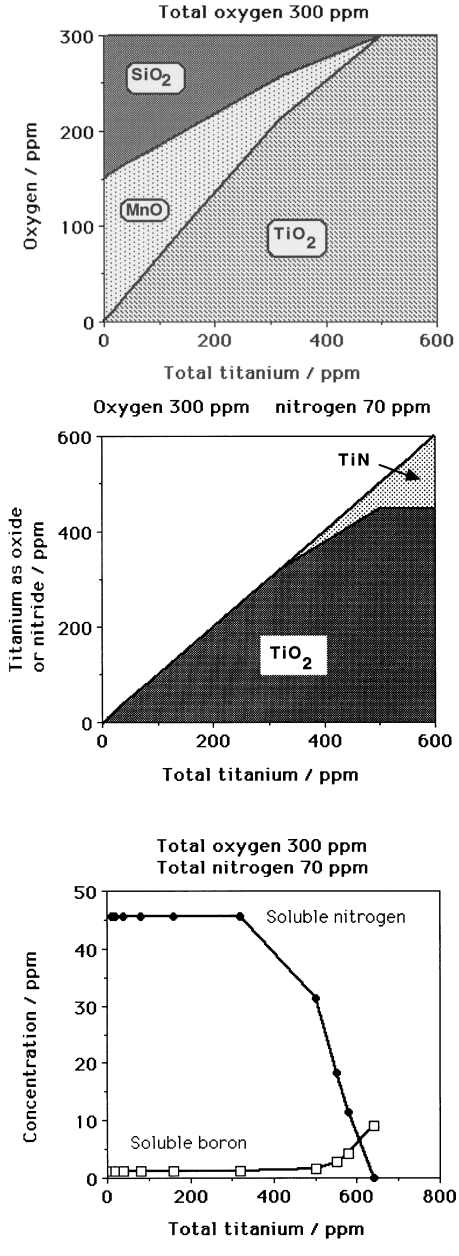

Fig. 10.14 Calculations showing how the components of inclusions in welds change as the chemical composition is altered. Manganese and silicon oxides are progressively replaced by titanium oxide. When the oxygen has reacted completely with titanium, the latter begins to combine with nitrogen and helps to liberate boron.

[13:36 3/9/01 C:/3B2 Templates/keith/3750 BAINITE.605/3750-010.3d] Ref: 0000 Auth: Title: Chapter 00 Page: 258 237-276

lity of both the boron and hydrogen is reduced. Furthermore, more of the hydrogen gets trapped resulting in a strong correlation between the boron and hydrogen concentrations, as shown in Fig. 10.15.

10.4.6 Stereological Effects

There is no doubt that plates of acicular ferrite nucleate on inclusions, although once the process begins, other plates can be stimulated autocatalytically. A one-to-one correspondence between the plates of acicular ferrite and inclusions is therefore not expected. It is difficult to establish the presence of an inclusion in a plate using metallography. By analogy with the procedure used by Chart *et al*. (1975) for aluminium alloys, if the volume of a typical plate of acicular ferrite is taken to be $10^{-16}\,m^3$, and that of a spherical inclusion $4 \times 10^{-20} m^3$, then of all the grains examined, only 7.4% can be expected to display the nucleating particle. When a particle is detected, its intercept on the plane of section will in general be smaller than its diameter. The estimate by Chart *et al*. is strictly valid when the grains of the major phase are spherical, which acicular ferrite plates are not. If the acicular ferrite is approximated as a square plate of side 10 μm and thickness $t = 1$ μm, containing an inclusion of radius $r = 0.2$ μm, the ratio of the mean linear intercepts of the two phases is given by $4r/6t$ (Myers, 1953; Mack, 1956). If every plate contains an inclusion, some 13% will show the nucleating particle in a plane section which is large enough.

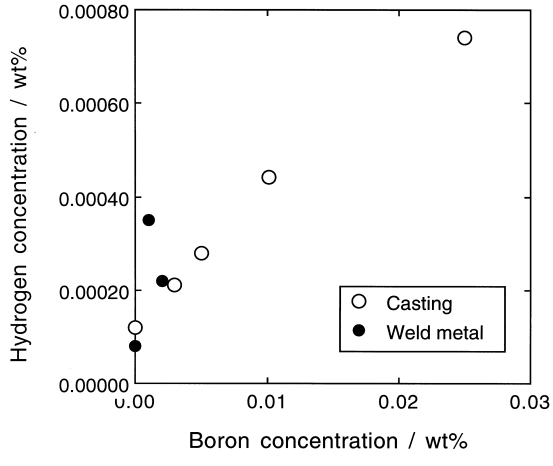

Fig. 10.15 The correlation between the residual hydrogen concentration and the total boron concentration in a series of castings and weld deposits (after Pokhodnya and Shvachko, 1997).

[13:36 3/9/01 C:/3B2 Templates/keith/3750 BAINITE.605/3750-010.3d] Ref: 0000 Auth: Title: Chapter 00 Page: 259 237-276

The estimate assumes that each plate contains just one inclusion, and more importantly, that each observed inclusion is responsible for nucleating the plate in which it is found, i.e. it has not been incorporated accidentally into the plate as a consequence of growth. It is not safe to assume that the observation of a particle in the plate implies that it was responsible for originating the plate when the total fraction of acicular ferrite is large.

An alternative way of establishing the role of autocatalysis is by examining the orientation relationships between adjacent plates in clusters of acicular ferrite plates. The clusters have been found to contain similarly oriented plates with a probability which is larger than random, implying autocatalysis (Yang and Bhadeshia, 1989a).

10.5 Effect of Inclusions on the Austenite Grain Size in Welds

A microstructure with large austenite grains has a better chance of transforming to acicular ferrite because the number density of grain boundary nucleation sites is reduced. It is sometimes assumed that the austenite grain size is determined by Zener pinning by inclusions. This analogy is, however, not justified since the austenite grains form by the *transformation* of δ-ferrite grains which evolve during solidification, whereas Zener pinning deals with the hindrance of grain boundaries during grain growth. The driving force for grain growth typically amounts to just a few Joules per mole, whereas that for transformation from δ-ferrite to austenite increases indefinitely with undercooling below the equilibrium transformation temperature. Pinning of δ/γ interfaces cannot then be effective. A mechanism in which inclusions pin the columnar austenite grain boundaries is also inconsistent with the *shape* of these grains, since the motion of the of the δ/γ interfaces along the steepest temperature gradients is clearly not restricted; if pinning were effective, the austenite grains that evolve should be isotropic.

10.6 Influence of Other Transformation Products

In weld deposits, acicular ferrite is one of the last transformation products to form after the growth of allotriomorphic and Widmanstätten ferrite. As a consequence, it is bound to be influenced by prior transformation products. Indeed, its volume fraction during continuous cooling transformation of such welds can in many cases be estimated simply by calculating the volume fractions of allotriomorphic and Widmanstätten ferrite, and assuming that the remainder of the austenite transforms to acicular ferrite (Bhadeshia *et al.*, 1985). For the same reason, it is found that in wrought alloys with mixed microstruc-

tures, the amount of acicular ferrite decreases with the austenite grain size, as grain boundary nucleated phases such as allotriomorphic ferrite become more dominant (Barbaro *et al*., 1988). The dependence of the volume fraction of acicular ferrite on the austenite grain size becomes less pronounced as the cooling rate (from the austenite phase field) is increased, since at slow cooling rates, much of the austenite is consumed during the higher temperature formation of allotriomorphic ferrite.

This dependence of the acicular ferrite content on the austenite grain size, in a mixed microstructure of acicular ferrite and allotriomorphic ferrite, can for isothermal reaction be expressed precisely using the relationship:

$$\ln\{1-\xi\} \propto S_V \tag{10.16}$$

where ξ is the volume fraction of allotriomorphic ferrite divided its equilibrium volume fraction at the temperature concerned and S_V is the amount of austenite grain surface per unit volume of sample. If a number of reasonable assumptions are made (Bhadeshia *et al*., 1987) the proportionality can be applied to continuous cooling transformation in low-carbon, low-alloy steels, in which case, $(1-\xi)$ is approximately equal to the volume fraction of acicular ferrite, thus relating the latter to the austenite grain size.

An interesting observation reported by Dallum and Olson (1989) is that in samples containing mixtures of allotriomorphic ferrite, Widmanstätten ferrite and acicular ferrite, a relatively small austenite grain size leads to a coarser acicular ferrite microstructure. They attributed this to an reduction in the α_a nucleation rate, caused by some unspecified interaction with the prior transformation products (α and α_w). An alternative explanation could be that with a smaller austenite grain size, the volume fractions of α and α_w that form are correspondingly larger, thereby causing a higher degree of carbon enrichment in the residual austenite and hence a significant reduction in the acicular ferrite nucleation rate. A reduction in the nucleation frequency would then permit the fewer plates to grow to larger dimensions before hard impingement with other plates in the vicinity.

Effects like these are of considerable importance in the development of mixed microstructures, but the coarsening of acicular ferrite without any change in shape *per se* is unlikely to lead to any drastic changes in the strength of weld deposits (Bhadeshia and Svensson, 1989a,b). This is because the mean slip distance in a plate does not change much as the plate becomes larger. Of course, it remains to be demonstrated whether toughness is sensitive to small variations in the size and distribution of acicular ferrite.

10.6.1 Some Specific Effects of Allotriomorphic Ferrite

We now proceed to consider a particular role of allotriomorphic ferrite formation in influencing the development of acicular ferrite in mixed microstructures. The effect is especially prominent in chromium- and molybdenum-containing steels. At relatively high concentrations of chromium (> 1.5 wt%) or molybdenum (> 0.5 wt%), the columnar austenite grains of steel weld deposits transform into bainite instead of acicular ferrite. The bainite is in the form of classical sheaves emanating from the austenite grain surfaces, often with layers of austenite left untransformed between the individual platelets of bainitic ferrite. This is in spite of the presence of nonmetallic inclusions, which usually serve to intragranularly nucleate the plates of acicular ferrite. The effect is probably a consequence of the fact that as the amount of allotriomorphic ferrite decreases with increasing solute concentrations, the austenite grain boundaries are freed to nucleate bainite (Fig. 10.16). The observations of Sneider and Kerr

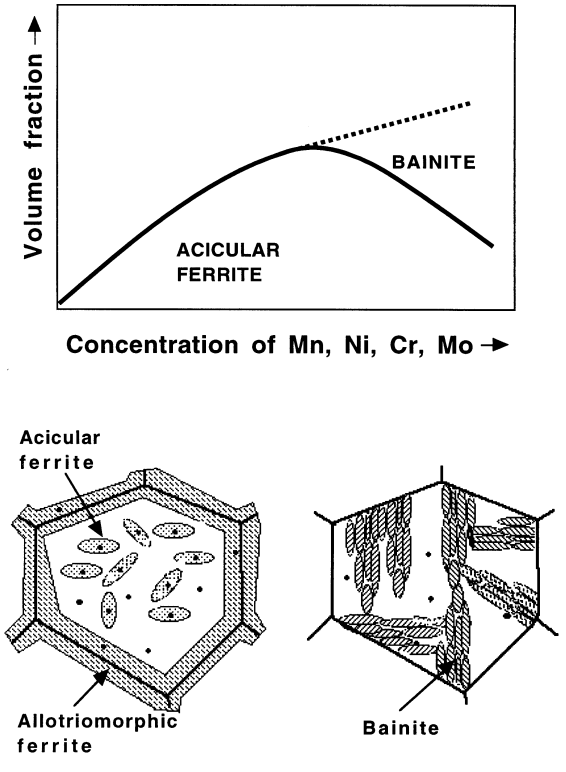

Fig. 10.16 Schematic illustration of the mechanism by which the presence of allotriomorphic ferrite at the austenite grain surfaces induces a transition from a bainitic to acicular ferrite microstructure.

[13:36 3/9/01 C:/3B2 Templates/keith/3750 BAINITE.605/3750-010.3d] Ref: 0000 Auth: Title: Chapter 00 Page: 262 237-276

(1984) could be interpreted to support this conclusion. In welds containing a variety of chromium concentrations, with microstructures which are predominantly acicular ferrite, the amount of bainite increased directly as the volume fraction of allotriomorphic ferrite decreased. In addition, bainite was not found when the allotriomorphic ferrite volume fraction was greater than 0.08, presumably because in their welds, that quantity was sufficient to completely cover the austenite grain surfaces, and prevents the grain boundary nucleation of bainite at a lower transformation temperature.

It may not be necessary to entirely cover the austenite grain surfaces with allotriomorphic ferrite, because the ferrite will tend to form at the most potent nucleation sites, thereby disabling the most active areas of the grain surfaces.

Some interesting quantitative data have also been reported by Evans (1986); he found that as the chromium or molybdenum concentration of low-carbon weld deposits is increased, the amount of allotriomorphic ferrite decreases. The volume fraction of acicular ferrite goes through a maximum as a function of concentration. The volume fraction of the remainder of the microstructure, which is described as 'ferrite with aligned second phase' therefore increases with concentration (Fig. 10.17). This is the terminology used in the welding industry to describe a microstructure in which parallel plates of ferrite are separated by regions of residual phase such as retained austenite. It really refers to packets of parallel plates of Widmanstätten ferrite or to sheaves of

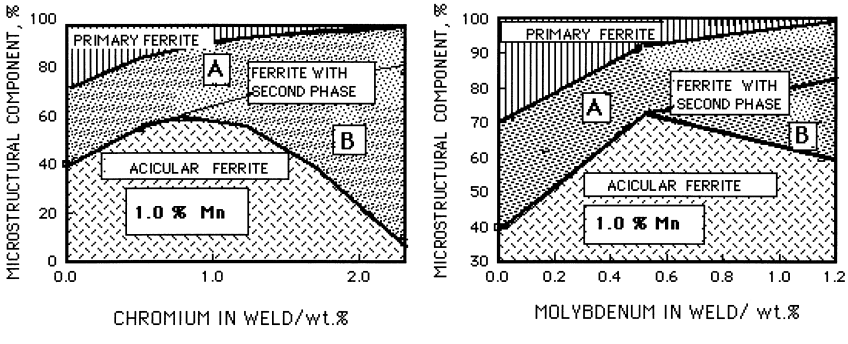

Fig. 10.17 Changes in the as-deposited microstructure of steel welds as a function of chromium or molybdenum concentration (after Evans). Notice that in each case, the fraction of acicular ferrite goes through a maximum as the Cr or Mo concentration increases. The region labelled 'ferrite with aligned second phase' by Evans has been subdivided schematically into regions A and B, to represent the Widmanstätten ferrite and bainite microstructures respectively. The maximum occurs because at large alloy concentrations, acicular ferrite is progressively replaced by austenite grain boundary nucleated bainite.

bainitic ferrite. There is some evidence (Bhadeshia *et al*., 1986b) that in typical welds deposits of the type studied by Evans, the fraction of Widmanstätten ferrite decreases to small values (0.04–0.1) as the chromium or molybdenum concentration increases, so that most of the increase in the volume fraction of the 'ferrite with aligned second phase' can be ascribed to an increase in the volume fraction of bainite (Fig. 10.17). The fact that bainite is obtained when the austenite grain boundaries are free from other transformation products is also consistent with the observation that Fe–2.25Cr–1Mo wt% weld deposits used in the power generation industry are well known to have an almost fully bainitic microstructure (variously referred to as conventional bainite or granular bainite) in the as-deposited condition, with classical sheaves in which the platelets of bainitic ferrite are partially separated by films of retained austenite or martensite (Klueh, 1974b; Wada and Eldis, 1982; Kar and Todd, 1982; Lundin *et al*., 1986; Vitek *et al*., 1986; McGrath *et al*., 1989). The large alloy concentration in this steel prevents the growth of allotriomorphic ferrite under normal heat-treatment conditions.

It appears therefore, that at relatively large concentrations of chromium and/or molybdenum, acicular ferrite is in increasing proportions, replaced by classical bainite, until eventually, the microstructure becomes almost entirely bainitic. This effect cannot be attributed to any drastic changes in the austenite grain structure, nor to the inclusion content of the weld deposits (Babu and Bhadeshia, 1990). It turns out in fact, that the Cr and Mo alloys have highlighted a more general condition associated with welds containing high concentrations of alloying additions. Several cases have been reported in the literature, where a similar transition from an acicular ferrite microstructure to one containing a greater amount of bainite is found to occur as the concentration of elements other than Cr or Mo is increased so that the amount of allotriomorphic ferrite is reduced. Horii *et al*. (1988) found that in a series of low-alloy steel welds, when the manganese or nickel concentrations exceeded about 1.5 and 2.9 wt% respectively, the weld microstructure was found to exhibit significant quantities of bainite. Interestingly, in the case of the nickel-containing steels, the toughness nevertheless improved since nickel in solid solution has a beneficial intrinsic effect on the toughness of iron. It apparently increases the stacking fault energy of body-centred cubic iron; since the dislocations in such iron are three-dimensionally dissociated, the change in stacking fault energy reduces the stress required for plastic flow at low temperatures, relative to that necessary for cleavage fracture (see Leslie, 1982).

To summarise, many experiments have indirectly revealed that the cause for the transition from a predominantly acicular ferrite microstructure to one containing substantial amounts of bainite, may be related to the reduction in the coverage of austenite grain boundaries by layers of allotriomorphic ferrite, as the solute concentration exceeds a certain value (Babu and Bhadeshia, 1990).

Below that concentration, the steel hardenability is low enough to ensure that the austenite grain surfaces are completely covered by uniform layers of allotriomorphic ferrite, thereby rendering them useless for bainite nucleation, and consequently allowing the development of acicular ferrite by intragranular transformation. As the concentration of austenite stabilising elements is increased, some of the austenite grain surface is left bare and becomes available for the nucleation of bainite sheaves as soon as the temperature falls within the bainite transformation range.

These ideas have been verified directly in experiments on Cr-containing steels, which demonstrated that the microstructure can be changed from bainite to acicular ferrite simply by introducing thin layers of allotriomorphic ferrite at the austenite grain surfaces (Fig. 10.18). It appears that the allotriomorphic ferrite/austenite boundaries, even when the α/γ orientation is appropriate, cannot develop into bainite because the adjacent austenite is enriched in carbon, to an extent which drastically reduces its bainite start temperature. A transformation-free zone is therefore found ahead of the allotriomorphic ferrite/austenite interfaces.

10.7 Lower Acicular Ferrite

We have seen that acicular ferrite and bainite seem to have similar transformation mechanisms. The microstructures might differ in detail because bainite sheaves grow as a series of parallel platelets emanating from austenite grain *surfaces*, whereas acicular ferrite platelets nucleate intragranularly at *point* sites so that parallel formations of plates cannot develop. Some of the similarities between bainite and acicular ferrite are:

1. They both exhibit the invariant-plane strain shape deformations with large shear components, during growth. Consequently, the growth of a plate of acicular ferrite or bainite is confined to a single austenite grain (i.e. it is hindered by a grain boundary) since the coordinated movement of atoms implied by the shape change cannot in general be sustained across a border between grains in different crystallographic orientations. A further implication is that plates of acicular ferrite, like bainite, *always* have an orientation relationship with the parent phase, which is within the Bain region. This is not necessarily the case when the transformation occurs by a reconstructive mechanism.
2. There is no substitutional solute partitioning during the growth of either bainite or acicular ferrite (Strangwood, 1987; Chandrasekharaiah *et al.*, 1994).
3. Both reactions stop when the austenite carbon concentration reaches a value where it becomes thermodynamically impossible to achieve

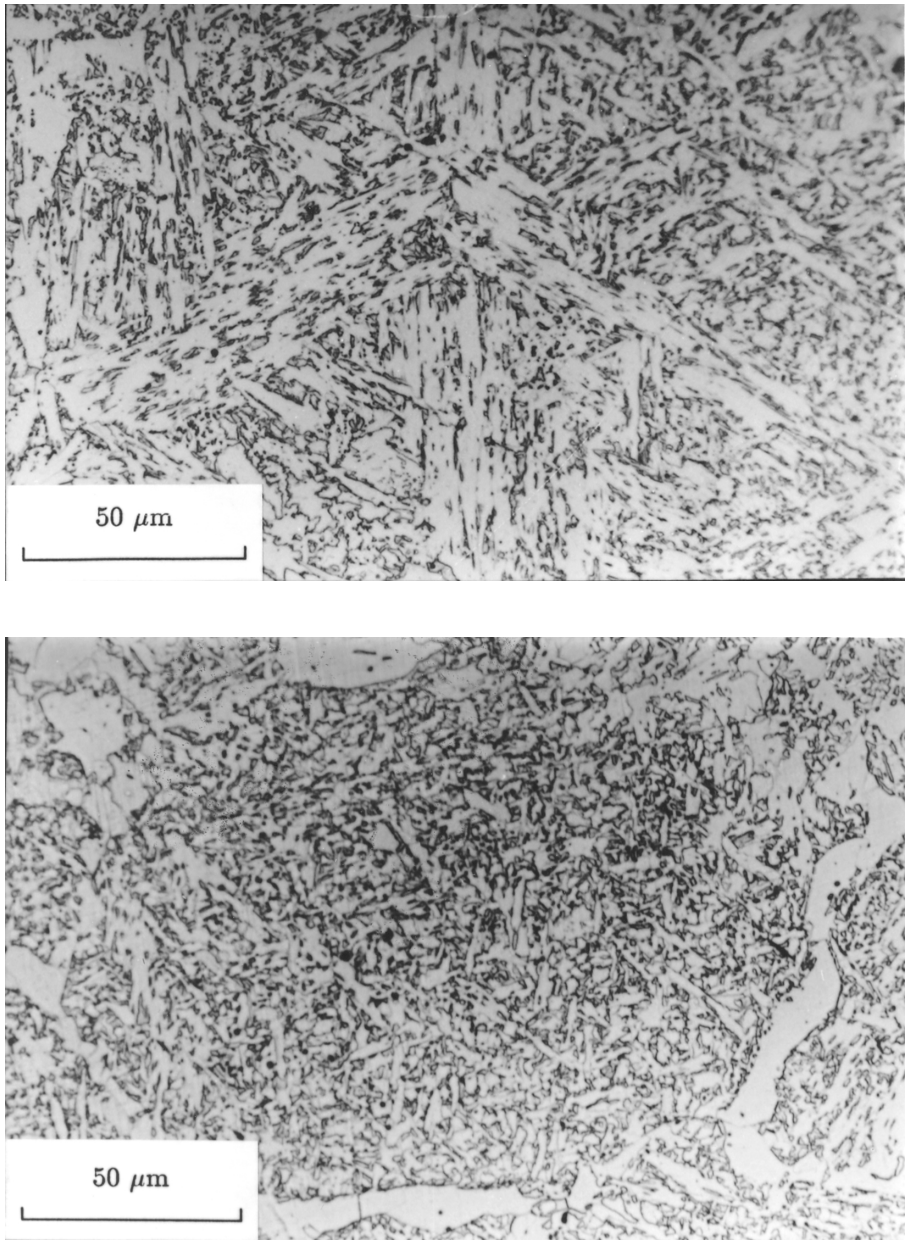

Fig. 10.18 The change from a bainitic microstructure (a) to one which is predominantly acicular ferrite (b), induced by the introduction of a thin layer of allotriomorphic ferrite at the austenite grain surfaces. Both the acicular ferrite and bainite were otherwise obtained by isothermal transformation under identical conditions (after Babu and Bhadeshia, 1990).

diffusionless growth (Yang and Bhadeshia, 1987b; Strangwood and Bhadeshia, 1987a). Any redistribution of carbon from the supersaturated ferrite plates occurs after growth. Growth is thus diffusionless, but is followed immediately afterwards by the rejection of carbon into the residual austenite.

4. Acicular ferrite only forms below the bainite-start temperature.
5. There is a large and predictable hysteresis in the temperature at which austenite formation begins from a mixed microstructure of acicular ferrite and austenite, or bainite and austenite (Yang and Bhadeshia, 1987a).
6. The removal of inclusions from a weld deposit, without changing any other feature, causes a change in the microstructure from acicular ferrite to bainite (Harrison and Farrar, 1981).
7. An increase in the number density of austenite grain surface nucleation sites (relative to intragranular sites) causes a transition from acicular ferrite to bainite (Yang and Bhadeshia, 1987a).
8. The elimination of austenite grain surfaces by decoration with inert allotriomorphic ferrite leads to a transition from a bainitic to an acicular ferritic microstructure (Babu and Bhadeshia, 1990).

These and other similarities emphasise the point that bainite and acicular ferrite have the same growth mechanisms. There is one anomaly. Like conventional lower bainite in wrought steels, there ought to exist a *lower* acicular ferrite microstructure, in which the intragranularly nucleated plates of α_a contain plates of cementite inclined at an angle of about 60° to the habit plane (Bhadeshia & Christian, 1990). The transition from upper to lower bainite occurs when the partitioning of carbon from supersaturated bainitic ferrite into austenite becomes slow compared with the precipitation of carbides in the ferrite, Fig. 7.1 (Hehemann, 1970; Takahashi and Bhadeshia, 1990). Consequently, if the carbon concentration of a steel weld is increased sufficiently (Fig. 7.2), then for similar welding conditions, the microstructure should undergo a transition from acicular ferrite to lower acicular ferrite. An experiment designed to test this, using an exceptionally high carbon weld, has detected lower acicular ferrite (Sugden & Bhadeshia, 1989b), supporting the conclusion that acicular ferrite is simply intragranularly nucleated bainite (Fig. 10.19). Lower acicular ferrite is only found when the weld carbon concentration is large enough to permit the precipitation of carbides from the acicular ferrite, before much of the carbon can partition into the residual austenite. This means that in reality, lower acicular ferrite is unlikely to be of technological significance in welds which necessarily have low carbon equivalents. On the other hand, lower acicular ferrite has been detected in a laser welded high-carbon steel (Hall, 1990).

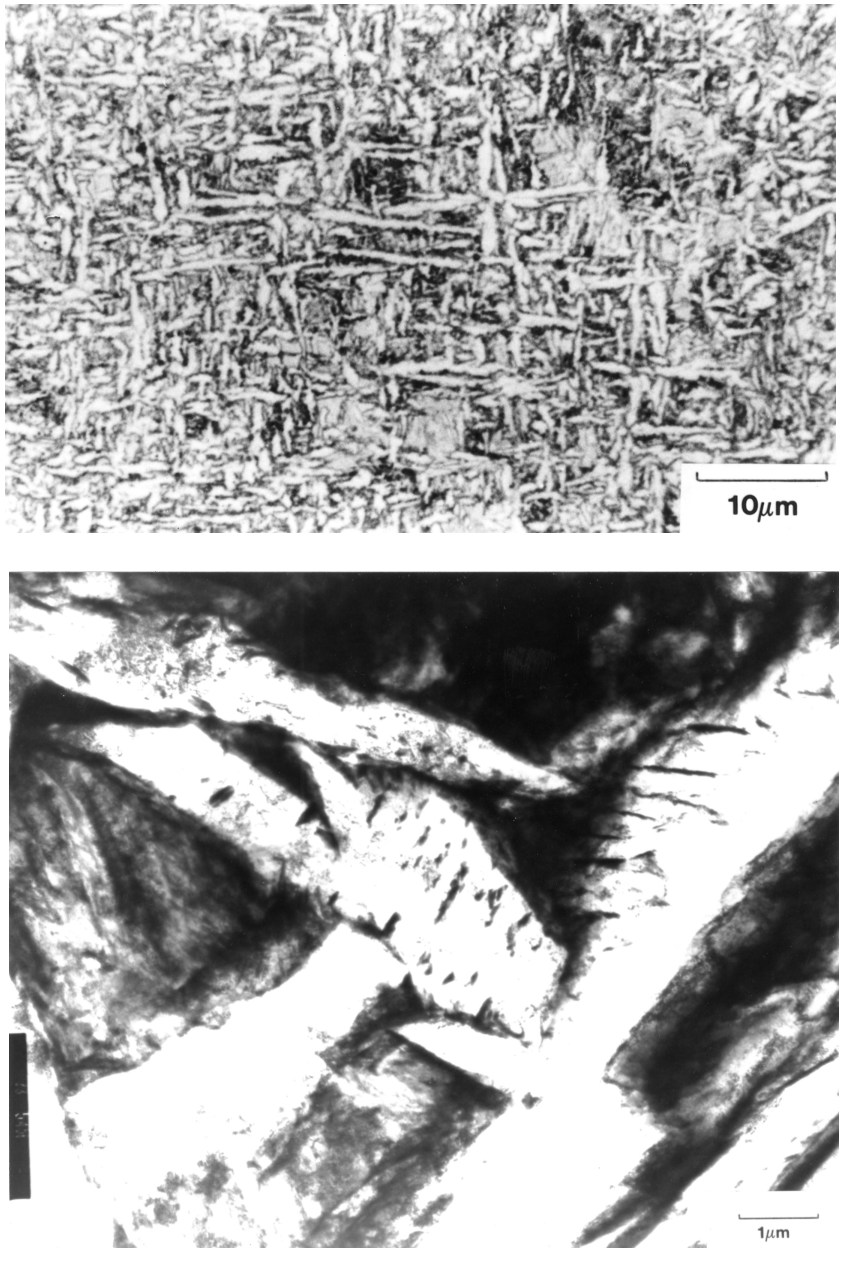

Fig. 10.19 (a) Light micrograph of lower acicular ferrite in an experimental high-carbon steel weld deposit (Sugden and Bhadeshia, 1989b). (b) Corresponding transmission electron micrograph illustrating the carbide particles in the acicular ferrite, in the single crystallographic variant typical of lower bainite in conventional microstructures.

10.8 Stress-Affected Acicular Ferrite

Welded fabrications are prone to the development of residual stresses whose magnitudes may approach the yield stress. This may have consequences on the development of the acicular ferrite microstructure during the cooling of the weld to ambient temperature. Dallum and Olson (1989) have shown that stress has little influence on the overall volume fraction of acicular ferrite. Nevertheless, an externally applied stress accelerates transformation and alters the morphology of acicular ferrite as shown in Fig. 10.20. This is not surprising given the displacive character of the transformation.

10.9 Effect of Strain on the Acicular Ferrite Transformation

The distinguishing feature of acicular ferrite is that it must nucleate intragranularly on inclusions. The amount of acicular ferrite is reduced if the number density of grain boundary nucleation sites is increased relative to the number density of inclusions.

The effect of deforming austenite prior to its transformation is to increase the nucleation potency and number density of the austenite grain boundaries. This is not helpful in promoting acicular ferrite. This is why the thermomechanical processing of austenite prior to its transformation discourages the formation of acicular ferrite (Shim *et al.*, 2000).

10.10 Inoculated Acicular Ferrite Steels

We have seen that acicular ferrite in weld deposits is intragranularly nucleated bainite. An acicular ferrite microstructure appears different from that of bainite because its plates nucleate from point sites, the non-metallic inclusions present in the steel. Adjacent plates of acicular ferrite tend to radiate in many directions from each nucleation site. A propagating crack is therefore frequently deflected as it encounters plates in different crystallographic orientations, leading to an improvement in the toughness.

Bainite and acicular ferrite can be obtained under identical isothermal transformation conditions in the same inclusion-rich steel. Bainite dominates when the austenite grain size is small, i.e. the number density of grain boundary nucleation sites is large relative to the number density of inclusions. Conversely, acicular ferrite is not easily obtained in clean steels.

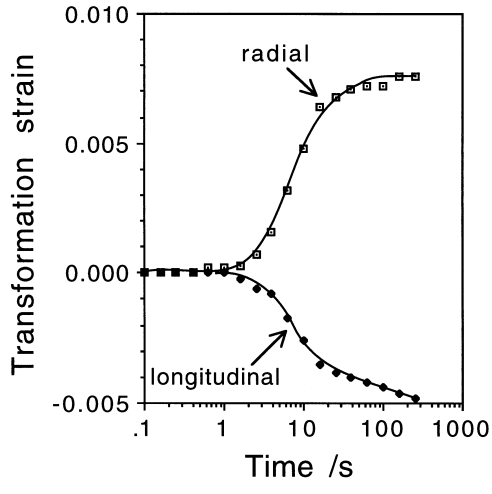

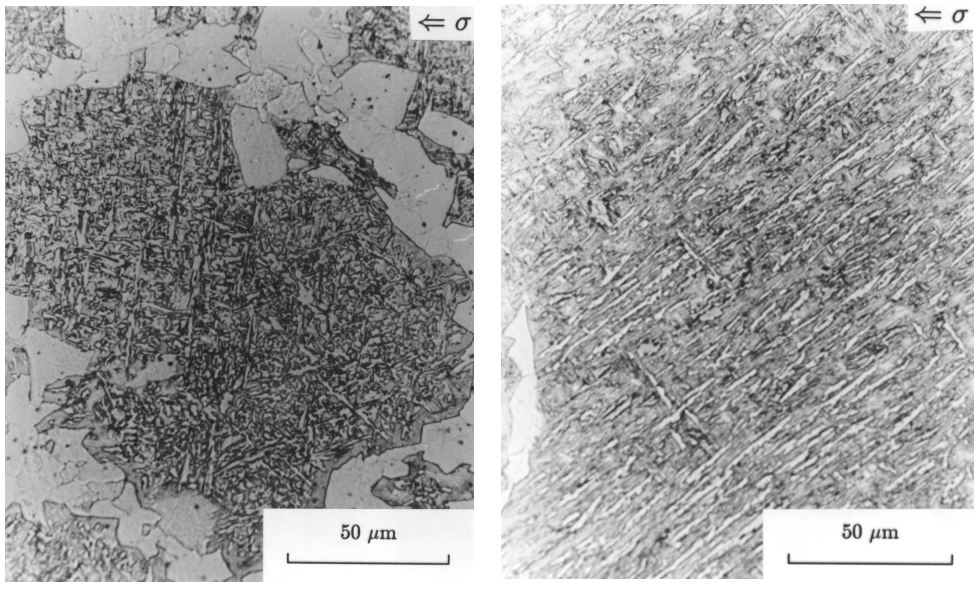

Fig. 10.20 (a) Dilatometric data monitored along orthogonal directions, showing the displacive character of the acicular ferrite reaction, and the acceleration of transformation by the applied stress. (b) The microstructure obtained in the absence of stress. (c) The aligned microstructure generated by the formation only of those acicular ferrite variants which are favoured by the applied stress. The transformation conditions for (b) and (c) are otherwise identical (after Babu).

10.10.1 Structural Steel

It is more than ten years now since the invention of steels with deliberate additions of oxide particles to induce the formation of acicular ferrite and hence to achieve better toughness (Nishioka and Tamehiro, 1988).† More than 100,000 tonnes of these inoculated steels have been marketed for applications in the offshore oil and gas industries, and for constructions in hostile, deep and cold environments. Steels destined for the Arctic regions must have adequate toughness at temperatures as low as $-80\,^{\circ}C$. In some cases, the steels have to be amenable to high heat-input welding ($4\,kJ\,mm^{-1}$) typical in ship construction. It follows that the designed microstructure must be left unchanged by any heat originating from the welding process. Regions of the heat-affected zone which become austenitic must transform back into an appropriate microstructure which is tough.

Inoculated steels have many advantages in this context. The coarse austenite grain structures found in the heat-affected zone adjacent to the fusion boundary favour the development of acicular ferrite plates on the titanium oxides and nitrides.

A typical composition of an inoculated structural steel is Fe–0.08C–0.2Si–1.4Mn–0.012Ti–0.002Al–0.002N wt%. Small concentrations of boron may be added to discourage grain boundary allotriomorphic ferrite and to fix free nitrogen which reduces toughness via a strain hardening mechanism.

The oxide particles effective in stimulating nucleation are about 2 μm in size. They are introduced during steel making by controlling the deoxidation practice. Each particle is generally a mixture of many compounds [MnS, Al_2O_3, (Mn,Si)O etc.] but the key phase responsible for the nucleation of ferrite is Ti_2O_3, although the published experimental evidence is rather limited (Homma *et al*., 1987; Nishioka and Tamehiro, 1998).

Aluminium has a strong affinity for oxygen; its concentration must be kept below about 30 p.p.m. to allow titanium to combine with oxygen. The fraction of the total oxide content which is due to titanium decreases as the aluminium concentration increases (Fig. 10.21).

Aluminium dissolved in austenite promotes Widmanstätten ferrite at the expense of acicular ferrite, the fraction of which decreases sharply at concentrations greater than about 70 p.p.m. (Fig. 10.22a). The mechanism of this effect is unknown and the concentration of dissolved aluminium is difficult to

†Prior to the advent of the oxide-inoculated wrought steels, high-strength low-alloy steels were sometimes called 'acicular ferrite HSLA' steels (Krishnadev and Ghosh, 1979). However, their microstructure consisted of parallel, heavily dislocated laths in identical crystallographic orientation. It is modern practice to restrict the term acicular ferrite to more chaotic microstructures.

[13:36 3/9/01 C:/3B2 Templates/keith/3750 BAINITE.605/3750-010.3d] Ref: 0000 Auth: Title: Chapter 00 Page: 271 237-276

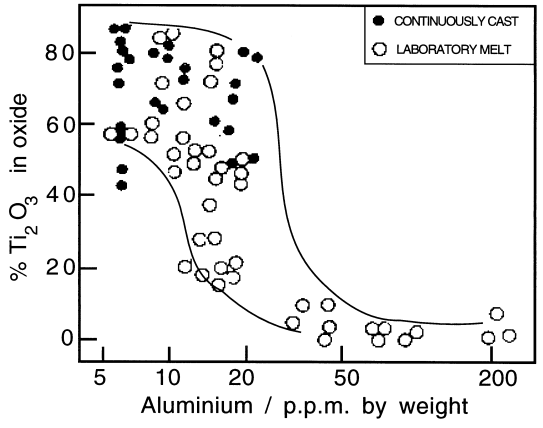

Fig. 10.21 The effect of aluminium concentration on the proportion of Ti_2O_3 in the total oxide content of the steel (Chijiiwa *et al*., 1988).

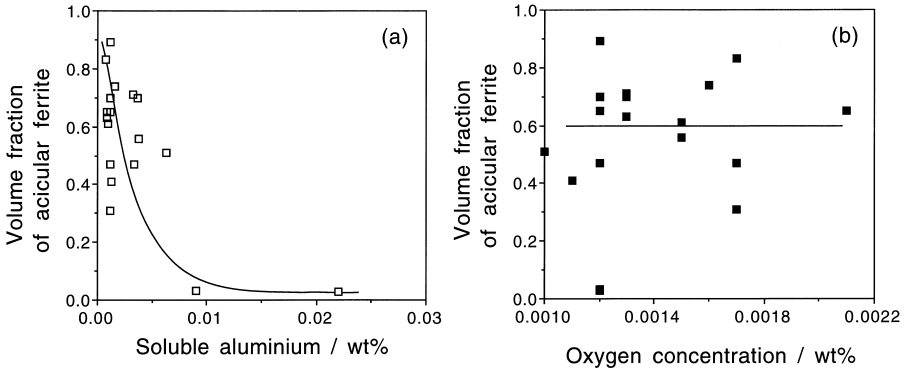

Fig. 10.22 (a) The volume fraction of acicular ferrite as a function of the soluble aluminium concentration; (b) the volume fraction of acicular ferrite as a function of the total oxygen concentration (data from Imagumbai *et al*., 1985).

control in practice. There is little correlation between the total aluminium concentration and that in solution (Thewlis, 1989a,b).

The effect of inclusions in promoting acicular ferrite saturates at about 120 p.p.m. of oxygen (Fig. 10.22b). The oxide content of the steel should be kept to the minimum consistent with the development of acicular ferrite, because any excess contributes towards the initiation of fracture. This is why inoculated steel contains the same amount of oxygen as a fully killed steel; it is the nature of the oxide that is more important than the total concentration of oxygen (Imagumbai *et al*., 1985).

The nitrogen concentration of inoculated steels must be controlled to avoid the formation of TiN which is not as effective as the oxide in stimulating intragranular nucleation. TiN is also not as stable as the oxide and tends to dissolve in the region of the heat-affected zone adjacent to the fusion boundary of a weld.

The design of inoculated steels includes a consideration of hardenability since phases such as allotriomorphic ferrite and Widmanstätten ferrite must be avoided. This ensures that there is sufficient untransformed austenite available for conversion into acicular ferrite. The hardenability can be enhanced by the careful use of microalloying elements such as Nb, Mo and B, thereby minimising the carbon equivalent of the steel. The silicon concentration should be kept below about 0.2 wt% to avoid large oxide particles.

10.10.2 Acicular Ferrite Forging Steels

Forging steels contain a high carbon concentration and hence are not welded. Titanium nitride can therefore be used to produce an acicular ferrite microstructure instead of the more usual mixture of ferrite and pearlite (Linaza *et al.*, 1993). The heat-treatment temperatures are never high enough to take the nitride into solution.

The steels listed in Table 10.4 under normal conditions have the microstructure illustrated in Fig. 10.23a, consisting mainly of pearlite and a small quantity of allotriomorphic ferrite. The same steel, when cooled rapidly transforms to acicular ferrite rather than bainite (Fig. 10.23b,c) because the titanium nitride particles present in the austenite provide abundant sites for intragranular nucleation. The toughness improves but the change is not large at comparable

Table 10.4 Chemical compositions (wt%) and representative mechanical properties of some titanium alloyed forging steels (Linza *et al.*, 1993).

Alloy	C	Mn	Si	V	Al	Ti	N
Ti–V	0.37	1.45	0.6	0.11	0.024	0.015	0.0162
Ti	0.35	1.56	0.33	–	0.027	0.028	0.0089

Alloy	Microstructure	Yield Strength/MPa	K_{IC}/MPa $m^{\frac{1}{2}}$
Ti–V	Acicular ferrite	560–666	133–155
Ti–V	Ferrite & Pearlite	590–650	134–139
Ti	Acicular ferrite	519	169–176
Ti	Ferrite & Pearlite	440	162–169

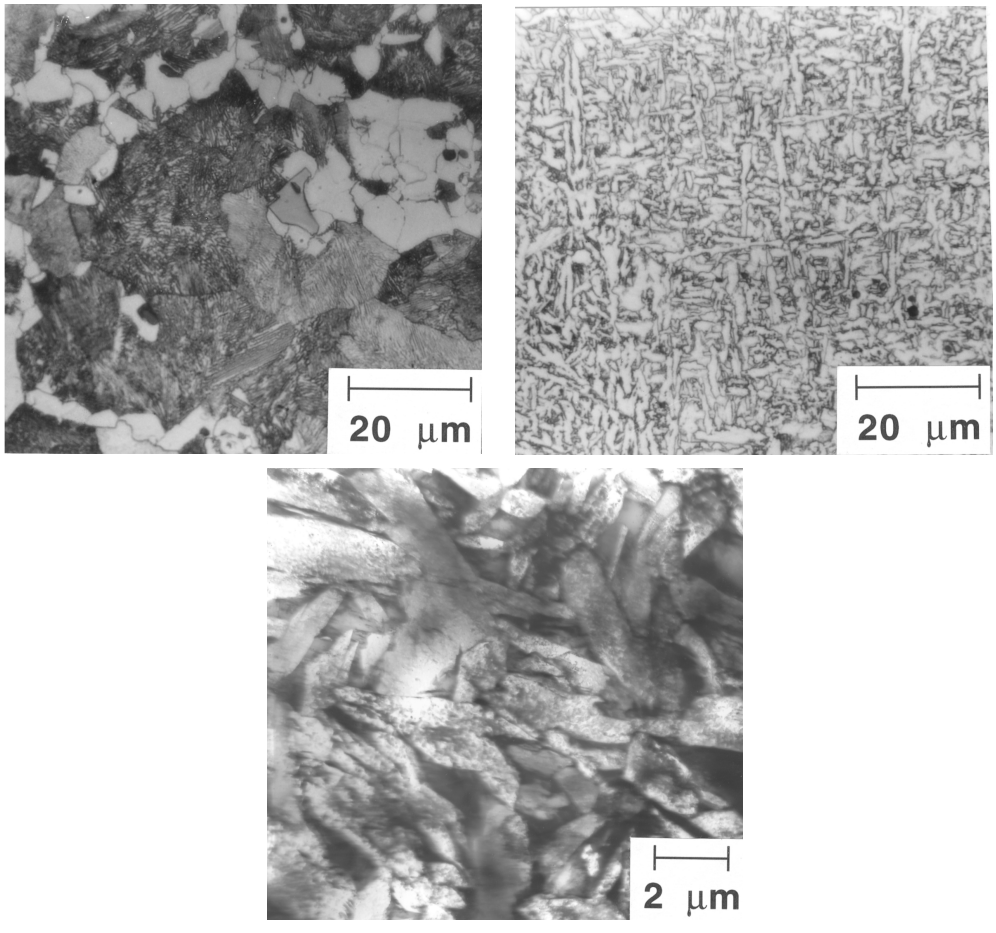

Fig. 10.23 The microstructures of a Ti–V forging steel: (a) optical micrograph showing a mixture of ferrite and pearlite; (b) optical micrograph showing the acicular ferrite microstructure; (c) transmission electron micrograph showing the acicular ferrite microstructure.

yield strength (Table 10.4). This is because some of the TiN particles can be coarse, greater than 2 μm. They are also brittle and hence act to initiate cracks (Rodriguez-Ibabe, 1998).

10.10.3 Steelmaking Technology for Inoculated Alloys

The details of the manufacturing practice for inoculated steels have not been published but the aim is to incorporate titanium oxide (Ti_2O_3) rather than TiN

which is less stable at high temperatures. The steelmaking involves deoxidation with titanium, whilst avoiding other strong deoxidisers such as Al, Ca or the rare earth elements. The oxygen concentration in the molten steel should be between 60 and 120 p.p.m., depending on application. High toughness levels demand a small inclusion (and hence oxygen) content. The steel must otherwise be clean with a minimal concentration of sulphur.

The active inclusions form in the melt or during the solidification stage (Pan and Lee, 1994). The titanium oxide might be added as powder into the melt, or during the casting stage (Ohno *et al*., 1985). However, the oxide then tends to cluster making the distribution of particles uneven. Alternatively, elemental titanium or ferro-titanium may be added to the melt or casting (Nishioka and Tamehiro, 1988; Chijiiwa *et al*., 1988). The titanium then combines with any dissolved oxygen. With this second method, the steel must not be aluminium killed because alumina then forms in preference to titanium oxides, as illustrated in Fig. 10.20. Aluminium-free molten steel is therefore titanium-killed in order to produce an inoculated alloy (Lee and Pan, 1991a, 1991b, 1992, 1993).

10.11 Summary

It is ironic that bainite, when it was first discovered, was called *acicular ferrite* by Davenport and Bain (1930). The terms acicular ferrite and bainite were often used interchangeably for many years after 1930 (see for example, Bailey, 1954). There is good evidence that the microstructure which we now call acicular ferrite, consists simply of intragranularly nucleated bainite. Conventional bainite grows in the form of sheaves of parallel plates which nucleate at austenite grain *surfaces*. By contrast, acicular ferrite plates emanate from *point* nucleation sites and hence grow in many different directions; the development of a sheaf microstructure is prevented by impingement between plates which have nucleated from adjacent inclusions.

The transformation has otherwise been verified to show all the characteristics of the bainite reaction: the incomplete reaction phenomenon, the absence of substitutional solute partitioning during transformation, an invariant-plane strain shape deformation accompanying growth, a large dislocation density, a reproducible orientation relationship within the Bain region, the lower acicular ferrite etc.

Any factor which increases the number density or potency of intragranular nucleation sites at the expense of austenite grain boundary sites favours a transition from a bainitic to an acicular ferrite microstructure. The transition can in practice be obtained by increasing the austenite grain size, by decorating the grain boundaries with thin, inactive layers of allotriomorphic ferrite, by increasing the inclusion content or by rendering the boundaries impotent with elements like boron. It is well understood that these microstructural factors can

only be useful if enough austenite is left untransformed for the development of acicular ferrite – the grain boundary nucleated phases must therefore be kept to a minimum).

[13:36 3/9/01 C:/3B2 Templates/keith/3750 BAINITE.605/3750-010.3d] Ref: 0000 Auth: Title: Chapter 00 Page: 276 237-276

11 *Other Morphologies of Bainite*

Upper and lower bainite are established terms describing microstructures which can easily be distinguished using routine microscopy, and whose mechanisms of formation are well understood. There are, however, a number of other descriptions of steel microstructures which include the word 'bainite'. These additional descriptions can be useful in communicating the form of the microstructure. But this must be done with care, avoiding the natural tendency to imagine a particular mechanism of transformation, simply because someone has chosen to coin the terminology.

11.1 Granular Bainite

Of all the unusual descriptions of bainitic microstructures, granular bainite is probably the most useful and frequently used nomenclature. During the early 1950s, continuously cooled low-carbon steels were found to reveal microstructures which consisted of 'coarse plates and those with an almost entirely granular aspect', together with islands of retained austenite and martensite, Fig. 11.1 (Habraken, 1956, 1957, 1965; Ridal and McCann, 1965; Habraken and Economopolus, 1967). Habraken and coworkers called this granular bainite and the terminology became popular because many industrial heat-treatments involve continuous cooling rather than isothermal transformation. The energy generation industry in particular uses enormous quantities of bainitic microstructures generated by allowing large steel components to cool naturally (Chapter 12). Granular bainite is supposed to occur only in steels which have been cooled continuously; it cannot be produced by isothermal transformation.

The coarse ferrite plates referred to earlier, do not really exist. They are in fact, sheaves of bainitic ferrite with very thin regions of austenite between the sub-units because of the low carbon concentration of the steels involved (Leont'yev and Kovalevskaya, 1974; Josefsson and Andren, 1989). Hence, on an optical scale, they give the appearance of coarse plates (Fig. 11.1a). Many of the original conclusions were reached from microstructural observations which were not of sufficient resolution to establish the fine structure within the sheaves of bainite. Indeed, evidence of this interpretation of so-called coarse plates appeared in the literature as early as 1967 when thin foil TEM

[13:37 3/9/01 C:/3B2 Templates/keith/3750 BAINITE.605/3750-011.3d] Ref: 0000 Auth: Title: Chapter 00 Page: 277 277-284

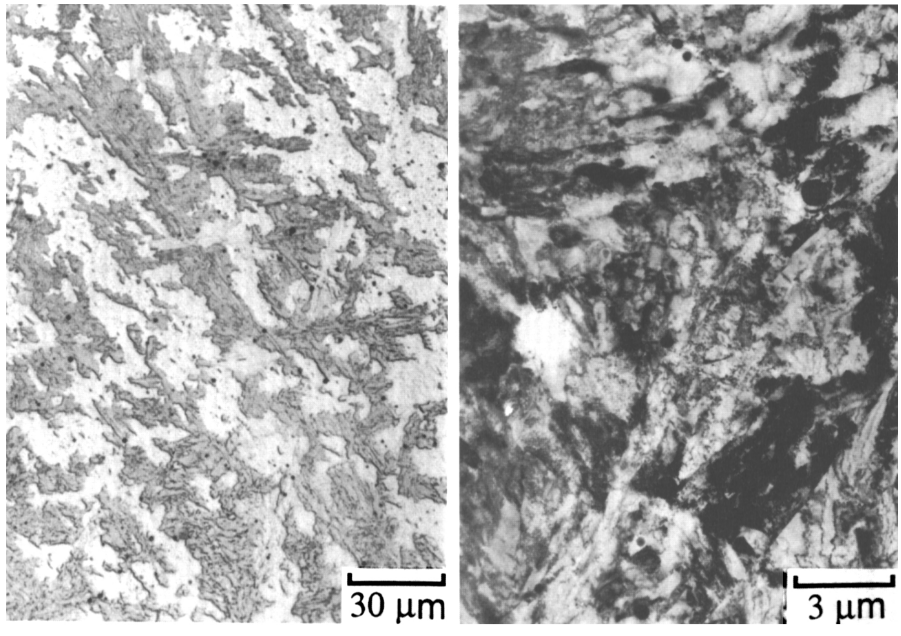

Fig. 11.1 Granular bainite in a Fe–0.15C–2.25Cr–0.5Mo wt.% steel: (a) light micrograph; (b) corresponding transmission electron micrograph (after Joseffson, 1989).

observations were made by Habraken and Economopolus, revealing the fine bainitic ferrite platelets within the sheaves.

A characteristic (though not unique) feature of granular bainite is the lack of carbides in the microstructure. The carbon that is partitioned from the bainitic ferrite stabilises the residual austenite, so that the final microstructure contains both retained austenite and some high-carbon martensite. Consistent with observations on conventional bainite, there is no redistribution of substitutional solutes during the formation of granular bainite (Tenuta-Azevedo and Galvao-da-Silva, 1978).

The extent of transformation to granular bainite is found to depend on the undercooling below the bainite-start temperature (Habraken and Economopolus, 1967). This is a reflection of the fact that the microstructure, like conventional bainite, exhibits an incomplete reaction phenomenon.

The evidence therefore indicates that granular bainite is not different from ordinary bainite in its mechanism of transformation. The peculiar morphology is a consequence of two factors: continuous cooling transformation and a low carbon concentration. The former permits extensive transformation to bainite during gradual cooling to ambient temperature. The low carbon concentration ensures that any films of austenite or regions of carbide that might exist

[13:37 3/9/01 C:/3B2 Templates/keith/3750 BAINITE.605/3750-011.3d] Ref: 0000 Auth: Title: Chapter 00 Page: 278 277-284

between sub-units of bainite are minimal, making the identification of individual platelets within the sheaves rather difficult using light microscopy.

Finally, it is interesting that in an attempt to deduce a mechanism for the formation of granular bainite, Habraken (1965) proposed that the austenite prior to transformation divides into regions which are rich in carbon, and those which are relatively depleted. These depleted regions are then supposed to transform into granular bainite. The idea is the same as that of Klier and Lyman (1944) and has been shown to be thermodynamically impossible in steels (Aaronson *et al*., 1966a).

11.2 Inverse Bainite

Ferrite is the dominant phase in conventional bainite; carbide precipitation when it occurs is a secondary event. In the so-called 'inverse bainite' which is found in hypereutectoid steels, it is the cementite which is the first phase to form (Hillert, 1957). A central plate-like spine of cementite grows directly from austenite (Hehemann, 1970) and then becomes surrounded by a layer of ferrite (Fig. 11.2). The term 'inverse' reflects the fact that, unlike conventional bainite, cementite is the first phase to precipitate from austenite.

The mechanism of the transformation is virtually unknown; there is no evidence that the growth of the ferrite occurs by a coordinated movement of atoms, and no crystallographic or chemical composition data. Judging from the shape alone, the ferrite probably forms by a reconstructive transformation mechanism. It is premature to classify the transformation as bainite.

11.3 Columnar Bainite

'Columnar bainite' is a description of a non-lamellar aggregate of cementite and ferrite, the overall shape of which is like an irregular and slightly elongated colony (Fig. 11.3). The distribution of cementite particles within the colony is rather peculiar, the majority of needle-shaped particles being aligned to the longer dimension of the colony. This latter region is surrounded by a layer of a different microstructure, in which the coarse cementite particles meet the austenite/ferrite interface edge on (Nilan, 1967). The structure is normally observed in hypereutectoid steels (Greninger and Troiano, 1940; Vilella, 1940; Jellinghaus, 1957; Speich and Cohen, 1960) but has been found in lower carbon steels transformed at high pressures (Nilan, 1967). It may be relevant to point out that the eutectoid composition is shifted to lower carbon concentrations by hydrostatic pressure.

The microstructure can be obtained at transformation temperatures comparable with those associated with conventional bainite, but there is no invariant-plane strain surface relief accompanying the growth of 'columnar bainite'. It is

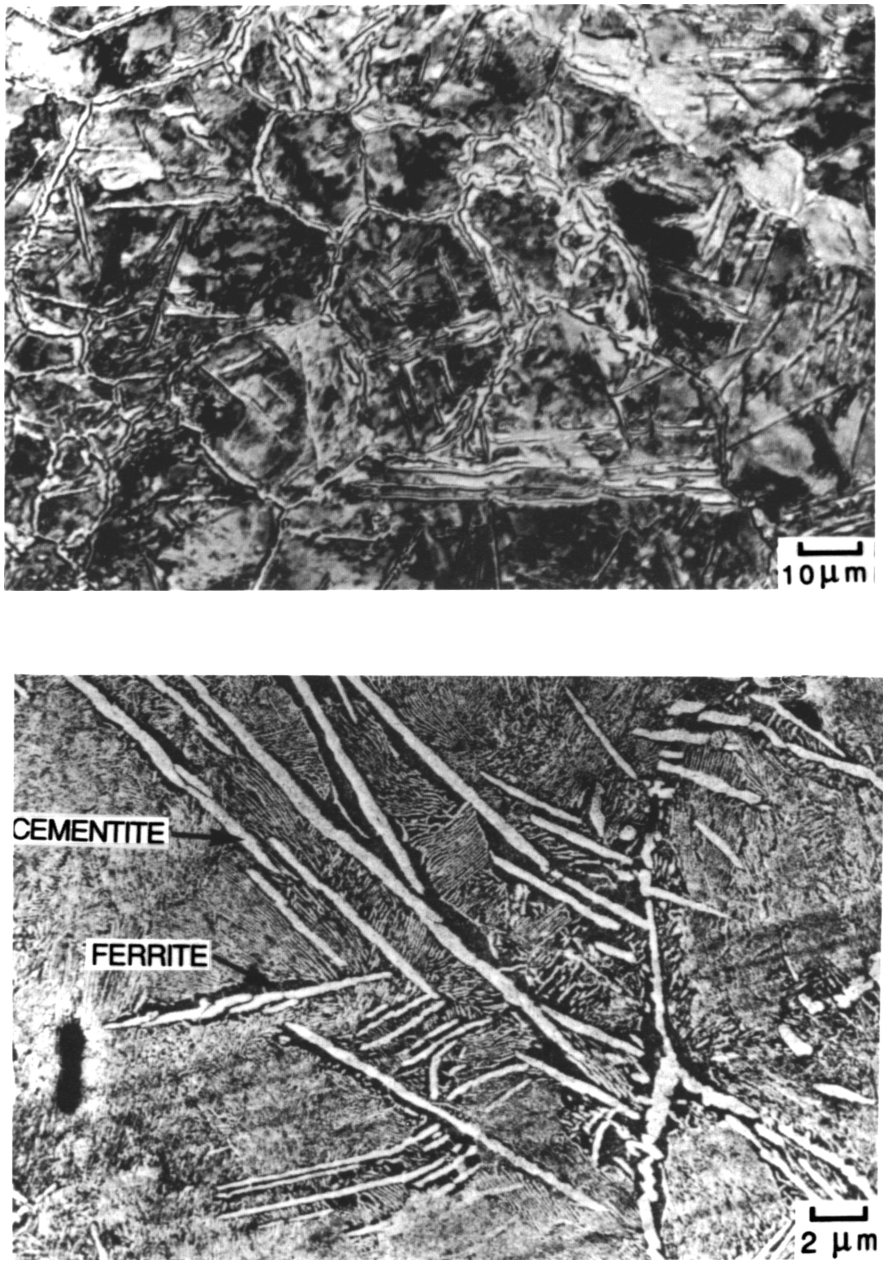

Fig. 11.2 Inverse bainite in a hypereutectoid steel: (a) light micrograph; (b) transmission electron micrograph (after Farooque and Edmonds).

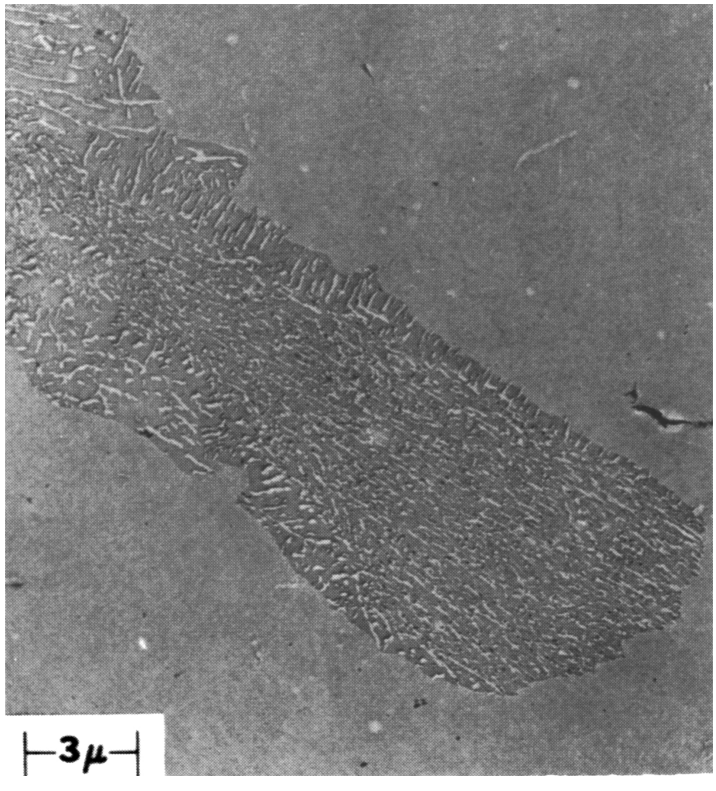

Fig. 11.3 Electron micrograph, obtained using a replica technique, showing a colony of 'Columnar Bainite' in an Fe–0.82C wt.% following isothermal transformation at 288 °C and at a pressure of 30 kbar (after Nilan, 1967).

probable that columnar bainite is more akin to pearlite than bainite, but further investigations are needed to make any sensible decisions about the mechanism of growth.

11.4 Pearlitic Bainite

In steels containing strong carbide-forming elements, it is possible to obtain pearlite, in which the carbide phase is an alloy carbide (such as M_7C_3) instead of cementite. The alloy pearlite can form at temperatures above B_S, or somewhat below that temperature but only after holding at the transformation temperature for very long time periods (usually many days). On the scale of light microscopy, the pearlite etches as dark nodules (Fig. 11.4), but the colonies tend to have crystallographic facets rather than the nicely rounded

[13:37 3/9/01 C:/3B2 Templates/keith/3750 BAINITE.605/3750-011.3d] Ref: 0000 Auth: Title: Chapter 00 Page: 281 277-284

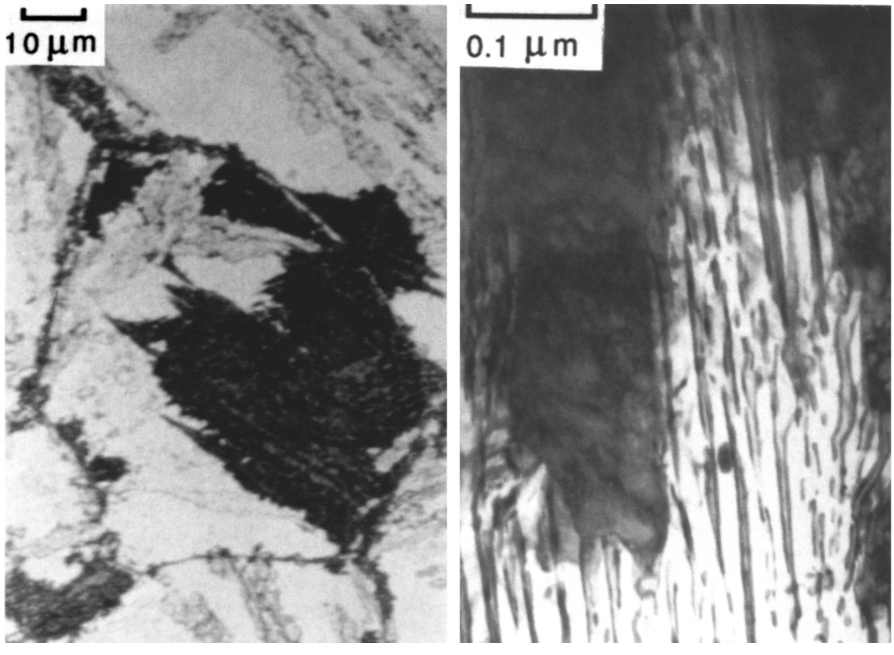

Fig. 11.4 Microstructure of the so-called 'pearlitic bainite', which is really just a pearlite with alloy carbide (in this case M_7C_3) instead of cementite: (a) light micrograph; (b) transmission electron micrograph.

colonies of normal pearlite. This is probably a reflection of the orientation dependence of the interfacial energy of the alloy carbide.

Because of this faceting, transmission electron microscopy observations can be misleading. The crystallographically faceted nodules of pearlite at a high resolution give the appearance of parallel ferrite plates with intervening carbides, a microstructure on that scale similar to upper bainite. The terminology 'pearlitic bainite' given to this transformation product is misleading. There is gross partitioning of substitutional solutes during the transformation, there is no surface relief effect, the carbide and ferrite phases grow cooperatively, and there is no reason to associate this microstructure with bainite.

11.5 Grain Boundary Lower Bainite

Bainite nucleation in most steels occurs heterogeneously at the austenite grain boundaries. The nucleation rate of lower bainite can be large at temperatures close to M_S; the austenite grain surfaces then become covered by lower bainite sub-units (Fig. 11.5). The rate at which carbon partitions from supersaturated

[13:37 3/9/01 C:/3B2 Templates/keith/3750 BAINITE.605/3750-011.3d] Ref: 0000 Auth: Title: Chapter 00 Page: 282 277-284

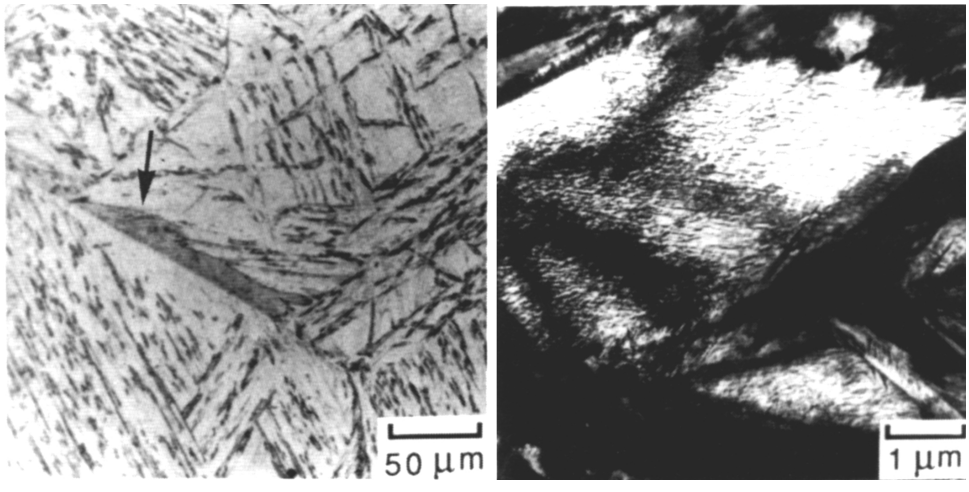

Fig. 11.5 The microstructure of grain boundary lower bainite: (a) light micrograph; (b) transmission electron micrograph.

ferrite is slow when transformation is at such low temperatures. Therefore, the sub-units are able to form in arrays without any intervening austenite (Bhadeshia and Edmonds, 1979a). These layers of sub-units have the overall form of allotriomorphs, but there is no doubt that they form individually.

The microstructure has caused some concern in the context of 300M, which is an ultrahigh-strength steel used in the quenched and tempered condition (Padmanabhan and Wood, 1984). The alloy has a very high hardenability – 10 cm diameter sections can be made martensitic by air cooling from the austenitisation temperature. However, optical microscopy revealed the surprising presence of allotriomorphs, which on detailed examination turned out to be the grain boundary lower bainite described above.

11.6 Summary

Granular bainite is basically ordinary bainite generated by continuous cooling transformation of low-carbon steels. The mechanism of inverse bainite is unclear, but it involves the formation of cementite as the primary phase. It is not clear whether the ferrite, when it eventually forms and engulfs the cementite, forms by a reconstructive or displacive mechanism.

Whilst there is some doubt about the mechanism of inverse bainite, the terms columnar and pearlitic bainite are undoubtedly misnomers and are best avoided. Columnar bainite is simply an aggregate of cementite and ferrite

[13:37 3/9/01 C:/3B2 Templates/keith/3750 BAINITE.605/3750-011.3d] Ref: 0000 Auth: Title: Chapter 00 Page: 283 277-284

which grows by a reconstructive transformation mechanism. Pearlitic bainite is simply a crystallographically faceted alloy pearlite.

At high supersaturations, arrays of lower bainite sub-units can rapidly decorate the austenite grain surfaces, giving the appearance of allotriomorphs. This 'grain boundary lower bainite' is much harder than allotriomorphic ferrite, and hence is easily distinguished.

12 *Mechanical Properties*

12.1 General Introduction

Many years elapsed after the work of Davenport and Bain before the commercial exploitation of bainitic steels. There were difficulties in obtaining fully bainitic microstructures in sizable samples of steel. It has long been recognised that the influence of bainite on the mechanical behaviour of a steel is difficult to understand because of the inability to attain fully bainitic microstructures at all transformation temperatures, a consequence of the incomplete reaction phenomenon (Hehemann *et al.*, 1957). Isothermal transformation to bainite was considered impractical on a commercial scale, continuous cooling being the preferred heat treatment. Furthermore, continuous cooling at a rate greater than $\simeq 50\,\mathrm{K\,s^{-1}}$ during transformation was also believed impractical. In these circumstances, lean steels gave mixed microstructures of allotriomorphic ferrite and bainite, whereas richly alloyed steels transformed only partly to bainite, the remaining microstructure consisting of martensite and retained austenite. It was not until low-alloy, low-carbon steels, containing small amounts of boron and molybdenum to suppress proeutectoid ferrite were developed that the potential for commercial exploitation became realistic (Irvine and Pickering, 1957).

Boron is effective in retarding proeutectoid ferrite formation but has a negligible effect on the bainite reaction, allowing bainitic microstructures to be obtained over a wider range of cooling rates. The segregation of boron to the austenite grain boundaries leads to a reduction in their energy, thereby making them less favourable as sites for the heterogeneous nucleation of ferrite. The reason why the effect is more pronounced for allotriomorphic ferrite than for bainite has not been investigated, but it may be associated with the fact that for bainite, which grows in the form of sheaves of small platelets, the vast majority of platelets nucleate autocatalytically after the initial formation of some platelets at the austenite grain boundaries (Chapter 6). Boron thus increases the bainite hardenability. The level of other alloying additions can, in the presence of boron, be kept low enough to avoid the formation of martensite. Steels of typical composition Fe–0.0033B–0.52Mn–0.54Mo–0.11Si–0.10C, wt% were found to yield fully bainitic microstructures with very little martensite during

normalising (i.e. air cooling from the austenitising temperature), and permitted the characterisation of the mechanical properties of bainite in isolation.

Many investigations of the mechanical properties fail to recognise that the microstructures studied were not fully bainitic. In the discussion that follows, attention is restricted to cases where the microstructure has been characterised thoroughly, and where it plays a significant role in determining the mechanical properties.

12.2 The Strength of Bainite

The strength of bainite can in principle be factorised into components consisting of the intrinsic strength of pure annealed iron (σ_{Fe}), substitutional solid solution strengthening contributions (σ_{SS}), strengthening due to carbon in solid solution (σ_C), and a variety of microstructural components including dislocation strengthening, particle effects and grain size effects. Thus,

$$\sigma = \sigma_{Fe} + \sum_i \sigma_{SS}^i + \sigma_C + k_\epsilon(\overline{L}_3)^{-1} + k_P\Delta^{-1} + C_{10}\rho_d^{0.5} \qquad (12.1)$$

where ρ_d is the dislocation density and Δ the average distance between a cementite particle and its two or three nearest neighbours. From measurements done on martensite, k_ϵ is approximately 115 MPa m; assuming that the cementite particles are spherical and of a uniform size, k_P is given approximately by $0.52\,V_\theta$ MPa m, where V_θ is the volume fraction of cementite (Daigne *et al.*, 1982). Dislocation theory for body-centred cubic metals gives $C_{10} = 0.38\,\mu b \simeq 7.34$ Pam (Keh and Weissmann, 1963). The carbon and substitutional solutes are listed separately because their solid solution strengthening contributions vary differently with concentration. For carbon, the strengthening varies with the square root of concentration (Speich and Warlimont, 1968; Christian, 1971), whereas for the substitutional solutes there is a direct relationship (Leslie, 1982). Equation 12.1 illustrates the form of the relationships, it is in practice difficult to decipher the microstructural contributions because parameters such as grain size and particle spacing cannot be varied independently. Figure 12.1 illustrates the magnitudes of the terms involved, together with some typical data for a fully bainitic microstructure.

12.2.1 Hardness

The hardness of bainite increases linearly with carbon concentration, by approximately 190 HV per wt% (Irvine and Pickering, 1965). This contrasts with a change of about 950 HV per wt% in the case of carbon-supersaturated martensite. The austenitising temperature does not influence the hardness unless it is not high enough to dissolve all the carbides (Irvine and

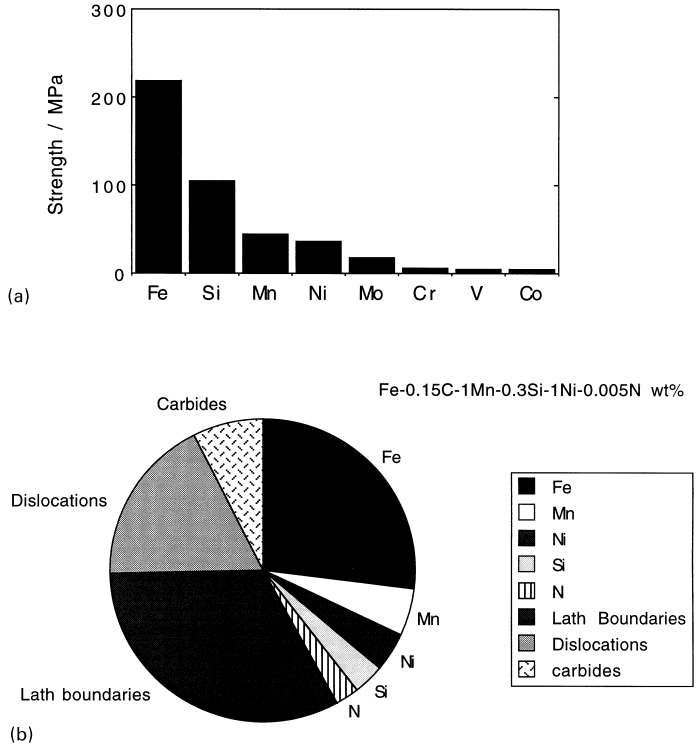

Fig. 12.1 The tensile yield strength of bainite at 25 °C and a strain rate of 0.0025 s^{-1}: (a) typical solid solution strengthening contributions per wt% of solute in ferrite; the intrinsic strength of pure iron is also included (data from Leslie, 1982); (b) estimated contributions to the strength of a fully bainitic sample.

Pickering, 1965). For mixed microstructures, the hardness depends on the transformation temperature and composition. This is because the stability of the residual austenite to martensitic transformation changes with its carbon concentration, the limiting value of which depends on the transformation temperature via the T_0' curve of the phase diagram.

Reconstructive transformations become incredibly slow below B_S in high-alloy steels. Hence, any austenite left untransformed during the bainite reaction either decomposes into untempered high-carbon martensite or is retained to ambient temperature. In low-alloy steels the residual austenite may transform into some form of degenerate pearlite. These secondary transformations have for a long time been known to influence the hardness of the microstructure. Lyman and Troiano (1946) found that for a series of Fe–Cr–C alloys the hardness for the 0.08 wt% C alloy was insensitive to the isothermal transformation temperature (Fig. 12.2). The low carbon concentration ensures that the

[13:37 3/9/01 C:/3B2 Templates/keith/3750 BAINITE.605/3750-012.3d] Ref: 0000 Auth: Title: Chapter 00 Page: 287 285-342

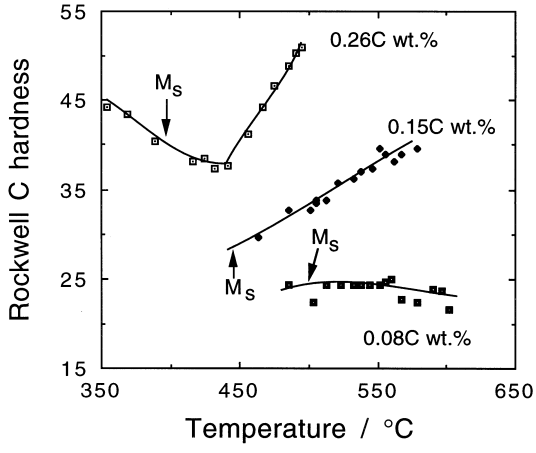

Fig. 12.2 Variation in hardness as a function of the isothermal transformation temperature (after Lyman and Troiano, 1946.)

microstructure is almost fully bainitic for all of the temperatures studied. This contrasts with higher carbon alloys, where the hardness first decreases as the transformation temperature is reduced; this is because the fraction of bainite increases at the expense of residual phases like martensite and degenerate pearlite.[†]

The *microhardness* of bainite, in a mixed microstructure of bainite and pearlite obtained by isothermal transformation, is found to be less than that of the pearlite, Fig. 12.3. This remains the case even when the pearlite and bainite have been generated at the same temperature. This behaviour is easy to explain once it is realised that the pearlite grows from *carbon-enriched* austenite and hence contains a much larger fraction of cementite than the bainite.

The hardness of bainite is insensitive to the austenite grain size, even though the latter influences the bainite sheaf thickness (Kamada *et al*., 1976). This is expected since the bainite sub-unit size is hardly influenced by the austenite grain size (Chapter 2). Since the sub-units are much smaller they exert an overriding influence on strength. For the same reason, the hardness of fully bainitic microstructures is not sensitive to the austenitising temperature (Irvine and Pickering, 1965; Kamada *et al*., 1976).

[†]This happens even though the dislocation density of bainitic ferrite increases as the transformation temperature decreases (Smith, 1984). The reduction in the quantity of hard phases (martensite, pearlite) compensates for the increase in dislocation density.

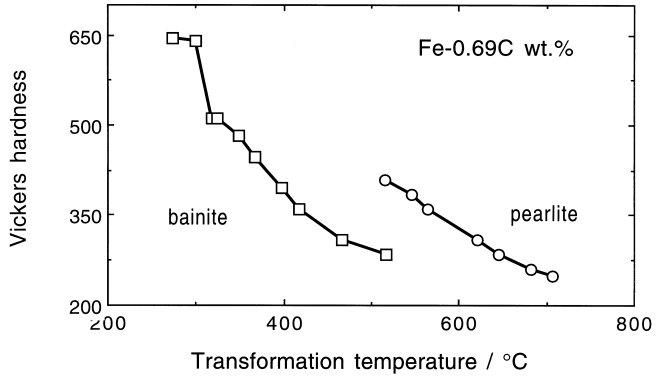

Fig. 12.3 Microhardness data from plain carbon steels transformed isothermally to a mixture of bainite and pearlite (after Ohmori and Honeycombe, 1971).

12.2.2 Tensile Strength

Although there is evidence that bainitic ferrite retains an excess concentration of carbon even after annealing (Bhadeshia and Waugh, 1981, 1982; Stark *et al.*, 1988), the majority of dislocations in bainite are believed to be mobile. Sharp yield points are not observed during tensile tests. The main effect of carbon on strength is through carbide precipitation. Cementite is the most common carbide; it precipitates in a coarse form without substantial coherency strains. Matrix dislocations have to bypass the cementite particles because they are unable to cut through them. It follows that the effect of carbon on the strength of bainite is rather small, approximately 400 MPa per 1 wt% of carbon (Irvine *et al.*, 1957).

Plates of bainitic ferrite are typically 10 μm in length and about 0.2 μm in thickness. This gives a small mean free path for dislocation glide because the probability of the slip parallel to the plate is small. The effective grain size of the plate is then about twice the plate thickness. There is only one other method, mechanical alloying (Benjamin, 1970), which can give a similarly small grain size in bulk materials. It is not surprising that the main microstructural contribution to the strength of bainite is from its fine grain size (Irvine *et al.*, 1957).

There have been many attempts at an analysis of the grain size contribution to the strength of bainite, most of them being based on the Hall–Petch relationship. This predicts a linear relationship between the strength and the reciprocal of the square root of the grain size. Although most data on bainite can be fitted to the Hall–Petch relation with $\sigma_y \propto (\overline{L})^{-1/2}$ (Siriwardene, 1955; Pickering, 1967), the results are difficult to interpret because the platelet size cannot be

[13:37 3/9/01 C:/3B2 Templates/keith/3750 BAINITE.605/3750-012.3d] Ref: 0000 Auth: Title: Chapter 00 Page: 289 285-342

altered without influencing other variables such as the dislocation density and the number density of carbide particles.

The Hall–Petch relationship relies on a description of macroscopic yielding in which a dislocation pile-up generates a large enough stress concentration to stimulate a dislocation source in an adjacent grain, thereby transmitting deformation across grains. If the grain size is large, then the number of dislocations that can participate in the pile-up increases. The larger stress field of the pile-up makes it easier to stimulate distant sources, thereby leading to a reduction in the yield strength.

This is an unlikely description of events when the grain size is fine. The slip plane dimensions become too small to allow the existence of pile-ups. Yielding is then determined by the stress necessary to expand a dislocation loop across a slip plane (Langford and Cohen, 1969, 1970, 1975). The yield stress in these circumstances varies as the inverse of the grain size, $\sigma_y \propto (\overline{L})^{-1}$. The strength of heavily cold-deformed iron and of martensitic samples has been interpreted using such a relationship (Langford and Cohen, 1969, 1970, 1975; Naylor, 1979; Daigne *et al.*, 1982). The changeover from the Hall–Petch to the Langford–Cohen relation should occur when the slip plane dimensions become $\simeq 1\mu m$.

An attempt has been made to separate the effect of bainite grain size and particle strengthening using multiple regression analysis (Gladman, 1972). The results indicate that carbides do not contribute much to the strength of bainite. This probably is a reasonable conclusion, but it has been pointed out that the analysis includes empirical constants which are difficult to justify (Honeycombe and Pickering, 1972).

12.2.3 Effect of Austenite Grain Size

We have seen already that the hardness of bainite is insensitive to the austenite grain structure. There have, nevertheless, been many investigations on the role of the austenite grain size and the bainite packet (sheaf) size on the strength. Both of these features are much coarser than the lath size which is probably the parameter with the greatest influence on flow stress. Published plots showing a Hall–Petch dependence of strength on austenite grain size or bainite packet size are probably fortuitous. Experiments have demonstrated that for martensite, the strength does not depend on the austenite grain size in low carbon steels (Brownrigg, 1973). Whether this applies to bainite depends on the effectiveness of the low-misorientation boundaries that exist between neighbouring platelets within a sheaf, in hindering dislocation motion. If there are films of austenite, or carbides separating the platelets within a sheaf, then they should be much more formidable barriers than implied by the small crystallographic misorientations between the sub-units. Since this is the case for most bainitic

steels, it is unlikely that the austenite grain size or the packet size have any significant effect on strength.

12.2.4 Effect of Tempering on Strength

The hardness and tensile strength of fully bainitic microstructures decrease during tempering, the rate of change being larger for lower bainite, which has a higher starting hardness. As might be expected, it is the highest strength steels which undergo the largest changes in strength during tempering (Bush and Kelly, 1971). After all, low-strength steels are not much stronger than the strength of the fully tempered microstructure.

The strength at any stage of tempering correlates well with the interparticle spacing, irrespective of the thermal history of the bainite (Deep and Williams, 1975). However, the grain size, particle size and distribution and dislocation density are not independent parameters. For example, studies using low carbon bainitic steels have established that the combined strengthening effects of dislocation density and the ultrafine bainitic ferrite grain size are substantial (McEvily and Magee, 1968). In bainitic steels containing retained austenite, the yield strength is found to be low due to the relative softness of the austenite. Tempering these steels at temperatures as high as 540 °C does not lead to a reduction in yield strength, the general softening of the microstructure being compensated by the removal of the soft austenite which decomposes diffusionally into a harder mixture of ferrite and carbides (Kalish *et al*., 1956).

There are interesting empirical relationships between strength and transformation characteristics, particularly for low carbon, low alloy, fully bainitic steels. Irvine *et al*. (1957) found a negative linear correlation between tensile strength and the 'temperature of maximum rate of transformation', indicating that the alloying element effect on strength can be rationalised simply on the basis of transformation kinetics (Fig. 12.4). For similar steels, the tensile strength is also found to correlate with the B_S temperature (Coldren *et al*., 1969). These results may be explained qualitatively: the bainite obtained at lower transformation temperatures should have a finer plate size and a larger dislocation density.

12.2.5 The Strength Differential Effect

Plastic deformation in metals becomes easier when the sense of the deformation is suddenly reversed. Thus, when the loading is changed from compression to tension (or vice versa), the deformation occurs more easily than would have been the case had it continued in the compressive mode. This is called the

[13:37 3/9/01 C:/3B2 Templates/keith/3750 BAINITE.605/3750-012.3d] Ref: 0000 Auth: Title: Chapter 00 Page: 291 285-342

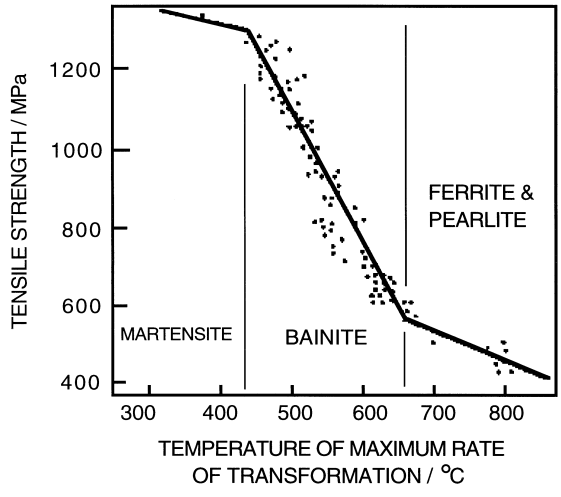

Fig. 12.4 Variation in the tensile strength of structural steels as a function of the temperature at which the rate of transformation is greatest during continuous cooling heat treatment (Irvine *et al*., 1957).

Bauschinger effect. A simple explanation is that deformation creates reversible features such as dislocation pile-ups, which relax and hence aid flow in the reverse direction when the sense of the load is changed. The effect therefore becomes less prominent as the total plastic strain increases, since the general build up in defect density makes it difficult for relaxation to occur.

Careful experiments on steels containing either martensite, bainite or Widmanstätten ferrite show that they have a higher yield stress in compression than in tension. This *strength differential effect* (Rauch and Leslie, 1972) persists even at large plastic strains, is independent of the starting sense of the deformation, and is not influenced by cyclic prestraining. It is believed to be associated with microstructures containing a high density of dislocations. It is not, for example, found in annealed ferrite or in ferrite–pearlite mixtures (Leslie, 1982). It has been shown to be inconsistent with an internally induced Bauschinger effect. Since the elastic modulus is similar in both tension and compression, the results cannot be explained in terms of the opening of microcracks during tension but not in compression (Rauch and Leslie, 1972).

There is no complete explanation for the phenomenon (Kennon, 1974), but it may be related to the presence of a nonlinear elastic interaction between dislocations and interstitial carbon atoms, the interaction being asymmetric in tension and compression (Hirth and Cohen, 1970). But it is not clear why the effect should be confined to microstructures with large dislocation densities.

12.2.6 Temperature Dependence of Strength

With the exception of creep-resistant alloys, most bainitic steels are used at ambient temperature. However, austempered ductile cast irons, which have a microstructure which is a mixture of graphite, bainitic ferrite, martensite and retained austenite, have found applications in automobile engines where the operating temperature might reach between 400–600 K. The strength of the iron hardly changes with temperature up to about 550 K; deformation is resisted by strain ageing due to interstitial carbon atoms in the bainitic ferrite (Shieh *et al*., 1993, 1995). Serrated stress–strain curves are observed during deformation at higher temperatures, consistent with the classical Portevin–Le Chatelier effect. Thus, the solute atoms are sufficiently mobile to migrate to moving dislocations, which then have to break away, the process repeating during the test. The serrations disappear at even higher temperatures where the carbon can diffuse fast enough to migrate with the dislocation.

12.3 Ratio of Proof Stress to Ultimate Tensile Strength

If a material does not exhibit a sharp yield point, then it is necessary to define a proof stress which is the stress needed to produce a specified amount of plastic strain (usually 0.2%). The strain rate of the test should also be defined but this is usually neglected because for steels there is only a 10% increase in the flow stress with an order of magnitude change in strain rate (Knott, 1981). Sharp yield points are not observed in stress–strain curves of bainite so it is usual to specify the yield strength in terms of a proof stress. The proof-stress to UTS ratio increases as dislocation motion becomes more difficult at lower temperatures, typically from about $0.67 \rightarrow 0.80$ over the range $300 \rightarrow 70$ K (Krishnadev and Ghosh, 1979).

It is desirable in high-strength steels to have a proof-stress to UTS ratio, r_1, which is less than about 0.8. This helps to ensure that there is substantial plastic deformation prior to ductile fracture. A small value of r_1 in many cases correlates with good fatigue resistance. The disadvantage is that the value of the stress that can be used in design is reduced. Unfortunately, many bainitic steels have r_1 values much lower than 0.8 even though the UTS may be large (Irvine and Pickering, 1965). The internal strains caused by the displacive transformation and the resultant mobile dislocations ensure a low proof stress. Tempering of bainite at 400 °C has only a minor effect on the microstructure but its recovery raises r_1.

The gradual yielding behaviour sometimes persists after stress-relief heat-treatments. The microstructure of bainite is heterogeneous, with fine carbide particles which concentrate stress and hence lead to gradual yielding. There is also a variety of obstacles to dislocation motion, (solute atoms, precipitates

[13:38 3/9/01 C:/3B2 Templates/keith/3750 BAINITE.605/3750-012.3d] Ref: 0000 Auth: Title: Chapter 00 Page: 293 285-342

of different sizes, boundaries), each with a different ability to obstruct plastic deformation. Many of the obstacles are not uniformly distributed so there will exist obstacle-free areas into which dislocations can penetrate at low stresses, thus giving rise to a gradual deviation from elastic deformation (Kettunen and Kocks, 1972; Kettunen and Lepistö, 1976).[†] Another scale of heterogeneity can arise when a large fraction of a phase harder or softer than bainite is included in the microstructure (Hehemann *et al*., 1957). Plastic deformation at first focuses in the softer phase whose yield strength is effectively reduced (Tomota *et al*., 1976). The hard phase only begins to deform when the softer phase has strain hardened sufficiently to transfer load. Small values of r_1 for so-called bainitic steels can frequently be explained by the presence of martensite, or retained austenite in the predominantly bainitic microstructure (Coldren *et al*., 1969). In particular, bainitic steels with austenite yield gradually and hence fail to meet some established industrial specifications which are based on steels with sharp yield points. The specifications need to be modernised to take into account the deformation

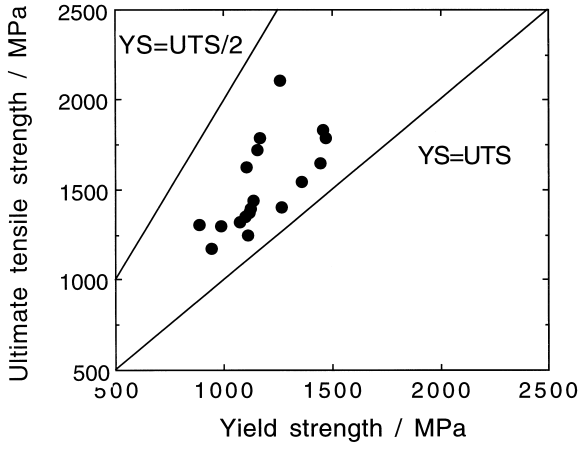

Fig. 12.5 The relationship between the ultimate tensile strength (UTS) and yield strength (YS) in steels with a mixed microstructure of bainitic ferrite, carbon-enriched retained austenite and some martensite.

[†]The deformation behaviour of a microstructure as complex as that of bainite is qualitatively consistent with the statistical theory of slip (Kocks, 1966). In this, a crystal is assumed to contain a random distribution of obstacles of differing strength. Dislocations have a finite probability of overcoming obstacles even when the applied stress σ is below the macroscopic yield stress σ_y. The mean free slip area A_s for dislocation glide varies with σ/σ_y and when dislocations can sweep right across the specimen, $\sigma = \sigma_y$.

behaviour of such steels, which strain harden rapidly and hence meet the ultimate strength requirements with ease. There is direct evidence that low values of r_1 correlate with large amounts of retained austenite in the microstructure, Fig. 12.5 (Sandvik and Nevalainen, 1981).

Retained austenite can in part be transformed into martensite by refrigeration in liquid nitrogen, or by tempering the steel to form ferrite and carbides. The reduction in retained austenite content leads to an increase in yield strength after both of these thermal treatments. The ultimate tensile strength is hardly affected, because the retained austenite in any case decomposes by stress-induced martensitic transformation during the early stages of deformation in a tensile test (Kalish *et al*., 1965).

Gradual yielding is advantageous in forming operations where it helps to avoid 'stretcher strains'. These represent Luders fronts between yielded and unyielded metal. Dual-phase steels are designed to take advantage of the gradual yielding associated with mechanically heterogeneous microstructures. They consist of mixtures of soft proeutectoid ferrite and a hard phase which may be bainite, martensite or indeed, a mixture of three phases.

However, it has been found that intercritically annealed steels containing allotriomorphic ferrite and bainite produced by isothermal transformation can cause discontinuous yielding behaviour because the ferrite strain ages at the temperature where bainite forms (Choi *et al*., 1988). The ageing occurs because of the difference in the solubility of interstitials, between the intercritical annealing temperature and the bainite transformation temperature. It may therefore be possible to avoid quench ageing by generating the required microstructure using continuous cooling heat treatment, thus allowing the interstitials to equilibrate during cooling.

Choi *et al*. have also shown that discontinuous yielding can be avoided if the hard phase is a mixture of bainite and martensite. This is because the latter forms during cooling from the isothermal transformation temperature and generates fresh interstitial-free dislocations allowing the gradual yielding behaviour to be recovered.

Bainitic dual phase steels are weaker than those containing martensite and they have a large r_1 ratio. But they have the advantage of better formability and fatigue strength (Sudo *et al*., 1982, 1983). It follows that r_1 is not always a reliable indicator of fatigue performance.

The required magnitude of the proof-stress/UTS ratio must be assessed for each application. For pipe-line alloys which are low-carbon bainitic steels, used for the conveyance of oil or gas under pressure, the fabricated pipe is hydrotested prior to service. This involves pressurisation to 125% of the planned operating pressure. If the value of r_1 is too low, there is a possibility of gross plastic deformation with failure during hydrotesting. It is common therefore to specify a minimum value of r_1 which is in the range 0.85–0.90 (Jones and

Johnson, 1983). On the other hand, steel columns used in the construction of buildings in earthquake areas are required to absorb energy without failure; a low r_1 value is then an advantage.

12.4 Ductility

It was noticed as early as 1957 by Irvine and Pickering, that low-carbon bainitic or martensitic steels always show superior tensile ductility when compared with their high-carbon counterparts, even when the comparison is made at identical strength. Their subsequent work (1965) confirmed that ductility can be improved by reducing the carbon concentration of a fully bainitic microstructure while maintaining its strength using substitutional solid solution strengthening.

Ductile fracture in good quality commercial steels which do not contain many nonmetallic inclusions propagates via the nucleation, growth and coalescence of voids. Macroscopic fracture occurs when the voids link on a large enough scale. If the number density of voids is large, then their mean separation is reduced and coalescence occurs rapidly, giving very little plastic deformation before fracture, i.e. a small overall ductility (Fig. 12.6). The number of carbide particles per unit volume increases with the carbon concentration of

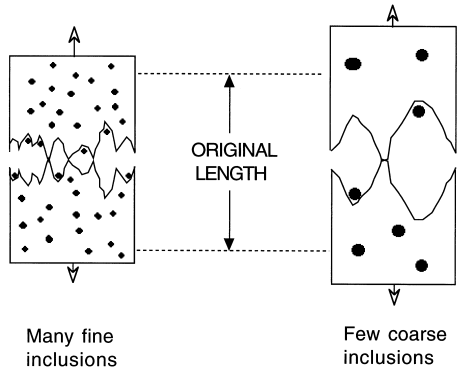

Fig. 12.6 An illustration of how a large density of void nucleating particles can result in fracture with a low overall ductility, even though the material fails by gross plastic deformation on a microscopic scale.

[†]The term *clean* implies the absence of nonmetallic inclusions of a size larger than cementite particles. High-carbon steels, where the cementite particle size may be expected to be large, can be air-melted, and yet be classified as clean. For low-carbon bainitic steels, significant differences in toughness are obtained for the air-melted and vacuum-refined conditions (McEvily and Magee, 1968), so that only the latter can be considered clean.

bainitic steels (Pickering, 1958). It is these carbides which are responsible for void nucleation in clean steels, so it follows that ductility must decrease with increasing carbon concentration even if the strength remains constant or decreases (Bhadeshia and Edmonds, 1983a,b).[†]

In steels which do not transform completely to bainite, ductile void formation initiates at the hard regions of untempered martensite which result from transformation of carbon-enriched residual austenite (McCutcheon *et al*., 1976). Presumably, the brittle failure of martensite provides the nuclei for void growth. This is why the elongation of fully bainitic low-carbon steels is always better than that of tempered martensite of the same strength, whereas the situation reverses when the comparison is made at high carbon concentrations (Irvine and Pickering, 1965). It is more difficult to obtain fully bainitic microstructures free from untempered martensite when the carbon concentration is large.

The linking of voids is associated with internal necking between adjacent voids. Since the necking instability depends on the rate of work hardening, the ductility should decrease if the work hardening rate is small. Experimental results do not bear this out. Deep and Williams (1975) have shown that tempered upper bainite strain hardens more rapidly than tempered lower bainite. And yet, the two microstructures have identical ductilities even when the interparticle spacing and mean carbide size are kept constant. Thus, the effect of work hardening, and indeed of the yield stress, on the ductile failure of bainitic steels is not yet understood.

The tensile elongation of fully bainitic, low-carbon steels is better than that of quenched and tempered martensitic steels of equivalent strength but the reverse is true at high carbon concentrations (Irvine and Pickering, 1965). The reduction of area is, on the other hand, always worse for bainitic steels. These results are not easily explained. Ductility trends as indicated by elongation data are inconsistent with reduction of area measurements. Martensitic steels almost always have larger reductions of area in tensile tests against comparable bainitic steels.

12.4.1 Ductility: The Role of Retained Austenite

Both the total elongation, and its uniform component, reach a maximum as a function of the fraction of retained austenite, when the latter is varied by altering the degree of isothermal transformation to bainitic ferrite (Sandvik and Nevalainen, 1981). The difference between the uniform and total elongation decreases as an optimum volume of retained austenite is reached. Further increases in retained austenite content are associated with tensile failure which occurs before the necking instability, in which case the difference between uniform and total elongation vanishes.

The best elongation behaviour is observed when the retained austenite is present mainly in the form of films between the sub-units of bainite, rather than as blocky regions between the sheaves of bainite (Sandvik and Nevalainen, 1981). The optimum austenite content increases as the transformation temperature decreases; this is because a finer microstructure incorporates more of the austenite in film form for a given fraction of bainite. For the same reason, elongation becomes less sensitive to retained austenite content as the transformation temperature is reduced. While mechanically unstable austenite causes a reduction in toughness for bainitic steels (Horn and Ritchie, 1978; Bhadeshia and Edmonds, 1983a,b), the ductility improves via the TRIP effect because of lower strain rates involved in measuring elongation.

It must be emphasised that all these results have yet to be interpreted quantitatively. Changes in retained austenite content cannot easily be made without altering other factors such as the tensile strength and the distribution of the austenite. For example, Miihkinen and Edmonds (1987b) have reported a monotonic increase in the uniform and total ductility with retained austenite content. The latter was varied by altering the transformation temperature, so that the strength increased as the austenite content decreased.

12.5 Impact Toughness

The concept of toughness as a measure of the energy absorbed during fracture is well-developed. It is often measured using notched-bar impact tests of which the most common is the Charpy test. A square section notched bar is fractured under specified conditions and the energy absorbed during fracture is taken as a measure of toughness. The notch is blunt; it concentrates stress thereby increasing plastic constraint, making brittle fracture more likely. The tests are conducted over a range of temperatures, and a plot of the impact toughness versus temperature is called an impact transition curve, which has a sigmoidal shape (Fig. 12.7a). The flat region of the curve at high temperatures is the *upper shelf* which represents ductile failure. The corresponding flat region at lower temperatures is called the *lower shelf* and represents cleavage failure. In between these is the transition region with mixed cleavage and ductile fracture. The impact transition temperature (T_t) is usually defined that at which the fracture surface shows 50% cleavage fracture.

The Charpy test is empirical in that the data cannot be used directly in engineering design. It does not provide the most searching mechanical conditions. The sample has a notch, but this is less than the atomically sharp brittle crack. Although the test involves impact loading, there is a requirement to start a brittle crack from rest at the tip of the notch, suggesting that the test is optimistic in its comparison against a propagating brittle crack (Cottrell,

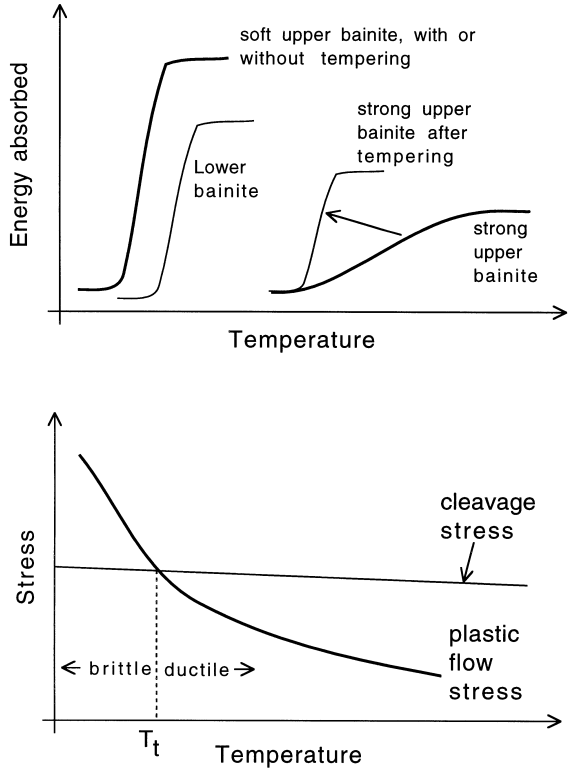

Fig. 12.7 Schematic illustration of impact transition curves (a) and of the cause of the ductile/brittle transition temperature (b) in body-centred cubic metals where the plastic flow stress is much more sensitive to temperature than the cleavage stress.

1995). Most materials can be assumed to contain sub-critical cracks so that the initiation of a crack seems seldom to be an issue.

The Charpy test is nevertheless a vital quality control measure which is specified widely in international standards, and in the ranking of samples in research and development exercises. It is the most common first assessment of toughness and in this sense has a proven record of reliability. The test is usually carried out at a variety of temperatures in order to characterise the ductile–brittle transition intrinsic to body-centred cubic metals with their large Peierls barriers to dislocation motion. In such metals, the cleavage stress is insensitive to temperature, the stress required for plastic flow rises rapidly as the temperature decreases (Fig. 12.7b). The increase in plastic flow stress is partly a consequence of the large Peierls barrier but also because of the

[13:38 3/9/01 C:/3B2 Templates/keith/3750 BAINITE.605/3750-012.3d] Ref: 0000 Auth: Title: Chapter 00 Page: 299 285-342

ubiquitous presence of traces of interstitial elements which interact strongly with dislocation motion.

The curves representing the cleavage and flow stress cross at the transition temperature, on a plot of stress versus temperature. Below T_t, cleavage is easier than plastic flow and vice versa. Any effect which raises the plastic yield stress (such as constraint caused by a notch) without influencing the nucleation or growth of cleavage cracks inevitably leads to an increase in T_t. Cleavage fracture is fast, occurs with little warning, absorbs minimal energy and is undesirable; a low transition temperature is therefore an important aim in safe design.

12.5.1 Fully Bainitic Structures

Irvine and Pickering (1963) conducted a major study of the Charpy impact properties of normalised low-carbon bainitic steels (typical composition Fe–0.003B–0.5Mn–0.5Mo–0.1C wt%). Their results are important and simple to interpret because the samples studied were free from proeutectoid ferrite and almost free of martensite.[†]

The impact properties of soft upper bainite were found not to be sensitive to tempering at temperatures as high as 925 K for 1 hr, as long as the ferrite retained its plate shape. After all, the upper bainite was obtained by transformation at high temperatures where tempering occurs during transformation, so that imposed tempering has only minor further effects on the microstructure.

When strong upper bainite is obtained by transformation at lower temperatures, T_t increases but the upper shelf energy decreases. The ductile–brittle transition becomes less well-defined, the region of the impact curve between the upper and lower shelves extends over a larger temperature range (Fig. 12.7a). This temperature range becomes narrower, and T_t and σ_y decrease, on tempering. The larger sensitivity to tempering is consistent with the lower degree of autotempering expected in bainite generated by transformation at low temperatures.

Even higher strength can be obtained by transforming to lower bainite, which surprisingly has good toughness, comparable to the low strength upper bainite. This is because carbide particles in lower bainite are much finer than in upper bainite. Cementite is brittle and cracks under the influence of the stresses generated by dislocation pile-ups (Hahn *et al.*, 1959). The crack may then propagate into the ferrite under appropriate conditions of stress and temperature. The cracks from fine cementite particles are smaller and hence

[†]It is the combination of low carbon and low substitutional solute concentration, the ease of cementite precipitation in these steels, and the continuous cooling heat treatment which allow the bainite reaction to consume all of the austenite.

more difficult to propagate into ferrite, which is the reason for the higher toughness of lower bainite when compared with upper bainite.

Consider a microcrack nucleus as a through thickness Griffith crack of length c. The cleavage stress σ_F is given (McMahon and Cohen, 1965) by:

$$\sigma_F = \left[\frac{4E\sigma_p}{\pi(1-\nu^2)c}\right]^{\frac{1}{2}} \tag{12.2}$$

where E is the Young's Modulus of ferrite, ν is its Poisson's ratio and σ_p is the plastic work of fracture per unit area of crack surface, an effective surface energy. If c is now set equal to the carbide particle thickness c_o, then the fracture stress is found to vary as $c_o^{-\frac{1}{2}}$. The details of this relationship must of course vary with the shape of carbide particles but the general relationship between σ_F and c remains the same; for example, when considering mixtures of ferrite and spheroidal carbides, the stress σ_F necessary to propagate cleavage fracture through the ferrite has been shown to be given by (Curry and Knott, 1978):

$$\sigma_F = \left[\frac{\pi E\sigma_p}{(1-\nu^2)c_d}\right]^{\frac{1}{2}} \tag{12.3}$$

where c_d is the diameter of the penny-shaped crack resulting from the cleavage of the spheroidal carbide particle.

The identification of the crack length c with the carbide particle thickness c_o is a vital assumption which can be justified experimentally for mild steels containing a microstructure of equiaxed ferrite and cementite particles. This is a carbide-controlled fracture mechanism, but the alternative possibility is a grain-size controlled fracture mechanism, in which the fracture stress is that required to propagate cleavage across grains. The parameter c must then be identified with a grain size dimension, and in the case of bainite, with a packet size. Brozzo *et al*. (1977) have demonstrated that for low-carbon bainitic steels (containing 0.025–0.50 C wt%) the covariant bainite packet size is the microstructural unit controlling cleavage resistance. It is nevertheless possible that the carbide size controls the cleavage fracture of high-carbon bainitic steels.

12.6 Fracture Mechanics Approach to Toughness

Most bainitic steels are used in high-strength applications and failure is not usually accompanied by a large amount of plasticity; they are in this sense 'brittle' materials. It is therefore a good approximation to use elasticity theory to represent the stresses in the vicinity of a sharp crack, even though cleavage crack propagation in metals always involves a degree of plastic deformation at the crack tip. Making the further assumption of *linear* elasticity, we have the

linear-elastic-fracture-mechanics (LEFM) approximation. One definition of a sharp crack is that the inevitable plastic zone at the crack tip is small enough to permit the LEFM approximation.

A fracture mechanics approach is more reliable than impact testing because a toughness value is obtained which is a material property, essentially independent of specimen geometry effects. The pre-cracked test samples and conditions such as the strain rate are similar to the conditions experienced during service. The results can be used quantitatively to predict whether a structure is likely to fail catastrophically under the influence of the design stress. There are excellent books and reviews on the subject but a brief introduction is necessary for an adequate discussion of the work on bainite.

Using LEFM, it is possible to show that when a uniaxial tensile stress σ is applied, the stress σ_r at a distance r ahead of a sharp crack tip is given by

$$\sigma_r = K_I(2\pi r)^{-\frac{1}{2}} \tag{12.4}$$

where K_I is a stress intensification factor in mode I (tensile) loading. K_I is a function of the applied stress σ and of the specimen geometry:

$$K_I = \sigma Y\{c/W\} \tag{12.5}$$

where Y is a compliance function which depends on the crack length c and on the specimen width W. For a body of infinite extent, containing a central through-thickness crack of length $2c$, normal to σ, $Y = (\pi c)^{\frac{1}{2}}$. For brittle materials, K_I at fracture takes a unique *critical* value K_{IC}. The latter is then independent of W or other dimensional variables; it is a material constant which can be used to design against catastrophic failure in service.

12.6.1 Microstructural Interpretation of K_{IC}

In considering the role of microstructure in fracture, it is necessary to distinguish between 'large' and 'small' particles. With small particles, the phenomenon controlling fracture is the propagation of particle-sized microcracks into the surrounding ferrite matrix. For larger particles the cracking of the particle represents the critical event, after which the crack propagates into the matrix and across grain boundaries (Gibson, 1988; Burdekin, 1990). For the most part, high-strength steels such as bainitic or martensitic alloys should, if manufactured properly, lie in the small particle regime, where we shall focus attention.

It is sometimes possible to relate K_{IC} values to microstructural and micromechanistic parameters. It can be argued that the critical value of stress intensity which leads to failure must be associated with corresponding critical values of stress σ_C and distance r_C (Knott and Cottrell, 1963; Knott, 1966; Ritchie *et al*., 1973; Knott, 1981):

[13:38 3/9/01 C:/3B2 Templates/keith/3750 BAINITE.605/3750-012.3d] Ref: 0000 Auth: Title: Chapter 00 Page: 302 285-342

$$K_{IC} = \sigma_C (2\pi r_c)^{\frac{1}{2}} \tag{12.6}$$

where σ_C is usually identified with σ_F (eq. 12.2), the local stress required to propagate a microcrack nucleus. σ_F varies with carbide thickness, or more generally, with the size of the microcrack nuclei resulting from the fracture of a brittle phase in the steel; it is relatively independent of temperature.

The interpretation of the distance r_C is less straightforward. The sample used in a fracture toughness test contains a machined notch, but to make the specimen representative of failure during service, it is fatigue loaded to form a sharp crack which grows slowly from the root of the notch. Fatigue loading is stopped as soon as a uniform crack front is established. The specimen is then ready for toughness testing. The fatigue crack tip is sharp, but not as sharp as the tip of a cleavage crack. It does not therefore propagate when the specimen is tensile loaded for the K_{IC} test. Instead, the stress field extending from the fatigue crack tip causes brittle particles within a distance r_C of the tip to fracture. The resulting microcrack nuclei are atomically sharp and propagate into the matrix if the stress σ_C is exceeded. The cleavage cracks then link up with the original fatigue crack and failure occurs rapidly across the specimen section.

It is emphasised that both r_C and σ_C are for most materials, statistically averaged quantities, since all microstructural features exhibit variations in size, shape and distribution. If the carbide particle size and spatial distribution is bimodal, due perhaps to the presence of a mixture of microstructures, then the K_{IC} values obtained are likely to show much scatter. The stress field extending from the crack tip effectively samples a finite volume and it is the microstructure of that volume which determines toughness. Bowen *et al*. (1986) found that K_{IC} values determined for mixed microstructures of upper and lower bainite (the former containing coarser cementite) exhibited a large degree of scatter when compared with a microstructure of just upper bainite or just martensite.

The microstructural interpretation of K_{IC} evidently requires a knowledge of a local tensile stress and a microstructural distance. This approach has been successful in explaining the toughness of mild steels with a microstructure of ferrite and grain boundary cementite (McMahon and Cohen, 1965; Smith, 1966, Knott, 1981) and to a limited extent of steel weld-deposits which have complex microstructures containing nonmetallic inclusions which initiate failure (Tweed and Knott, 1983; McRobie and Knott, 1985). In some of these cases, the critical microstructural features controlling cleavage fracture resistance have been identified directly, giving faith in the r_C concept.

Difficulties arise when attempts are made to use this approach for clean bainitic or martensitic structures. The carbides particles are so fine as to make a direct identification of r_C impossible. The fracture stress σ_F can never-

theless be measured and if it is shown to be constant, then σ_F itself can be used as a measure of 'toughness' (Bowen *et al*., 1986), although it is not clear how possible variations in r_C can be accounted for. A constant σ_F indicates that the critical step in the fracture process is the propagation of a microcrack.

Bowen *et al*. used this approach, together with K_{IC} studies to explain the toughness of tempered martensite and bainite in a low-alloy steel. In all cases, K_{IC} values were found to increase with the test temperature over the range 77–300 K. For the same temperature range, the proof stress decreased with increasing temperature. For a given proof stress, the toughness of bainite was always lower than that of tempered martensite (Fig. 12.8). The fracture stress σ_F was in all cases found to be independent of test temperature, but bainite had a lower σ_F than martensite. The results were explained in terms

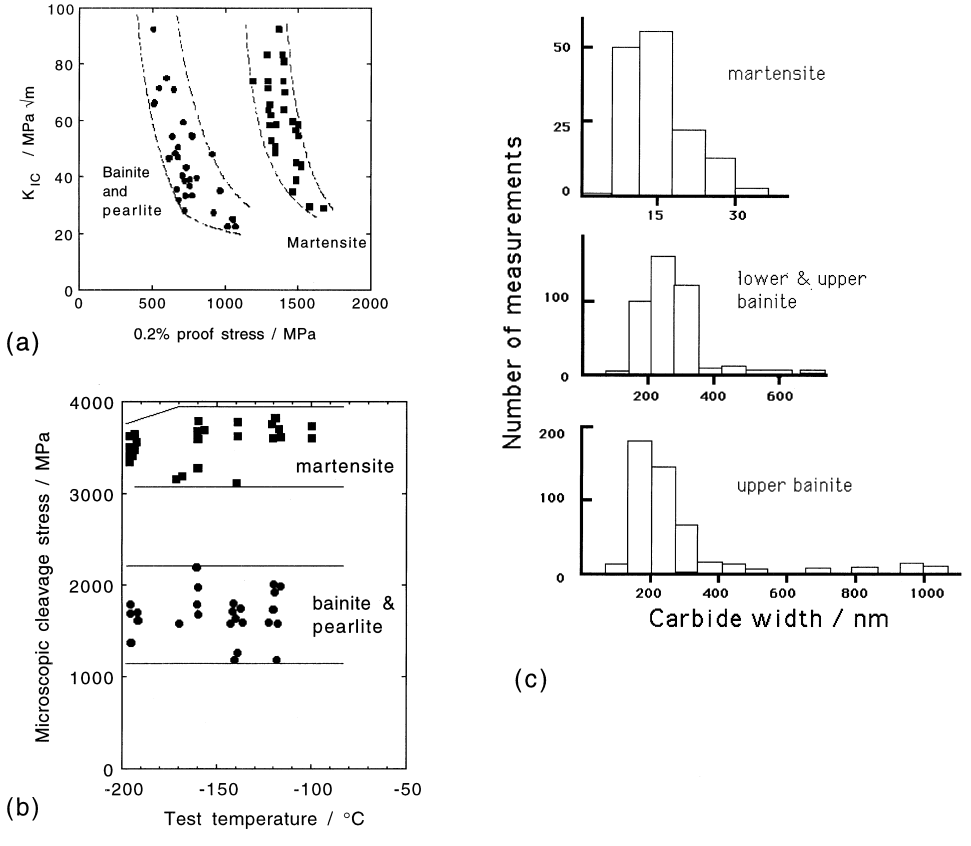

Fig 12.8 (a) K_{IC} values plotted against corresponding values of the 0.2% proof stress. (b) σ_F values plotted against test temperatures. (c) Carbide size distributions obtained from martensitic and bainitic microstructures (after Bowen *et al*.).

of measured cementite particle size distributions (Fig. 12.8). They showed that it is not the mean carbide particle size which determines toughness, but the coarsest particles to be found in the microstructure. A plot of σ_F versus the reciprocal square root of the coarsest carbide thickness gave a straight line as predicted by the modified Griffith equation (eq. 12.2); deviations from this equation occurred at small particle sizes. On this basis, for a given proof stress, the toughness is expected (and found) to increase in the order upper bainite, lower bainite and tempered martensite. Trends like this are also important in the design of welding processes and materials, and there are many qualitative results which confirm that the toughness increases in that order for microstructures in the heat affected zones of steel welds (Inagaki and Hiroyuki, 1984; Harrison and Farrar, 1989).

The reason why the modified Griffith equation fails at small particle sizes is not clear but it means that σ_F becomes relatively insensitive to carbide thickness when the latter is less than about 450 nm.

It must not be assumed that these results spell doom for bainitic microstructures; they need not always have poor toughness relative to tempered martensite. The size of bainitic carbides can be controlled using suitable alloying additions. Indeed, the carbides can be eliminated completely by adding sufficient Si or Al to the steel. The results are valid only for clean steels in which the fracture mechanism is carbide-nucleated and growth-controlled. That the coarseness of carbides controls the toughness of bainite in clean steels is emphasised by the observation that lower bainite with its finer carbides and higher strength nevertheless has a better toughness than the softer upper bainite. All other things being equal, toughness is expected to improve as the strength is reduced, making plastic deformation easy.

The micromechanistic model for the toughness of bainite contains the terms σ_C and r_C, the former defining the stress to propagate a microcrack in a cementite particle, and the latter the distance over which the stress is large enough to cause carbide cracking. The distance r_C is expected to be small in comparison with the width of a bainite sheaf, so the toughness of bainite or martensite should not be dependent on the austenite grain size or the bainite packet size. This prediction has been demonstrated to be the case for tempered martensite (Bowen *et al*.) but contradictory results exist for bainite. Naylor and Krahe (1974) using notched-bar impact tests have shown that a refinement in the bainite packet size leads to an improvement in toughness. The impact transition temperature of bainitic steels is also found to decrease as the austenite grain size decreases (Fig. 12.9), although this might be because the packet size becomes finer at small austenite grain sizes. The austenite grain size in Irvine and Pickering's experiments was varied by controlling the temperature at which hot-rolling finished, or by reheating into the austenite phase field, before the steel was continuously cooled to bainite.

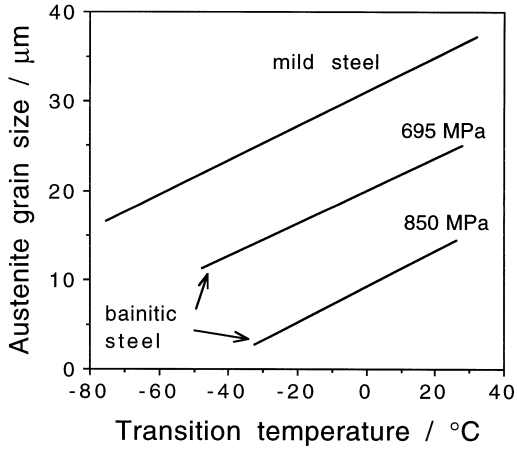

Fig. 12.9 Variation in the impact transition temperature as a function of the austenite grain size (after Irvine and Pickering, 1963).

The fracture stress σ_F and the critical distance r_C do not vary much with temperature, although K_{IC} for bainite is found experimentally to increase as the test temperature rises. This apparent contradiction arises because of the LEFM approximation. In practice, the effect of temperature is to reduce the yield strength. The size of the plastic zone at the crack tip increases so that more work is done as the crack propagates, leading to an increase in K_{IC} (Ritchie *et al.*, 1973).

Finally, it is worth noting that the austenite grain size cannot always be varied independently. Some carbides may not dissolve if the required grain size is achieved using a low austenitising temperature; these carbides can be detrimental to toughness (Tom, 1973). As the solubility of the carbides increases with austenitising temperature, so does the average carbon concentration in the austenite; more of the austenite is therefore retained to ambient temperature after partial transformation to martensite or bainite (Mendiratta *et al.*, 1972; Kar *et al.*, 1979). Variations in austenite grain size also influence hardenability; a fine grain structure can be detrimental if it causes the formation of transformation products such as allotriomorphic ferrite during cooling of a high strength steel (Parker and Zackay, 1975).

12.6.2 Cleavage Fracture Path

Microstructural observations have demonstrated that during cleavage failure, the cracks propagate undeviated across individual packets of bainite (Pickering, 1967).[†] Similar results have been reported for weld deposits,

where cleavage has been shown to propagate undeflected across packets of bainite, reinitiating only at packet boundaries (Chandel *et al*., 1985). The size of cleavage facets obtained by brittle fracture correlates well with the width of the packets (Naylor and Krahe, 1974), although there are also many results which indicate that the undeflected crack path is some 1.5 times larger than the width of bainite packets (Ohmori *et al*., 1974; Brozzo *et al*., 1977). The larger size of the crack path is because even though adjacent packets of bainite are different crystallographic variants of the orientation relationship, there is a high probability that their cleavage planes are fairly parallel (Brozzo *et al*., 1977). The cleavage crack path can lie on {1 1 0}, {1 0 0}, {1 1 2} or {1 2 3} ferrite planes (Naylor and Krahe, 1975).

The correlation between the cleavage facet size and packet size are for low-carbon, low-alloy steels where the fraction of bainitic ferrite that forms is large and that of cementite, martensite or retained austenite, small. The platelets of ferrite within a packet of bainite therefore touch each other at low misorientation boundaries over large areas, thus giving the crystallographic continuity essential for undeviated cleavage crack propagation. In richly-alloyed steels, the intervening layers of retained austenite may hinder the crack as it passes through a packet. It has yet to be established as to how this effect manifests in the context of a fracture path.

12.7 Temper Embrittlement

There are three kinds of embrittlement phenomena associated with quenched and tempered steels, each of which leads either to a minimum in the toughness as a function of tempering temperature, or to a reduction in the rate at which the toughness improves as the tempering temperature is increased:

12.7.1 650 °C Reversible Temper Embrittlement

Tempering at temperatures around 650 °C promotes the segregation of impurity elements such as phosphorous to the prior austenite grain boundaries, leading to intergranular failure along these boundaries. The reversibility arises because the impurity atmospheres at the grain boundaries can be evaporated by increasing the tempering temperature. Quenching from the higher temperature avoids the resegregation of impurities during cooling, thus eliminating embrittlement.

[†]The terms *packet* and *sheaf* are used interchangeably. The former is conventional terminology in mechanical property studies.

In fact, one of the tests for the susceptibility of bainitic microstructures to impurity-controlled embrittlement involves a comparison of the toughness of samples which are water quenched from a high tempering temperature (680 °C) with those cooled slowly to promote impurity segregation (Bodnar *et al*., 1989).

Studies of creep resistant bainitic steels show that phosphorus and tin, and to a lesser extent manganese and silicon, are all embrittling elements (Bodnar *et al*., 1989). Manganese is known to reduce intergranular fracture strength (Grabke *et al*., 1987). Silicon, on the other hand, enhances the segregation of phosphorus to the austenite grain boundaries (Smith, 1980), and can itself cosegregate with nickel to the grain surfaces (Olefjord, 1978). There are also smaller effects due to arsenic, antimony and sulphur. The tendency for embrittlement correlates strongly with an empirical 'J' factor:

$$J = Mn + Si + 10^4(P + Sn) \tag{12.7}$$

where the concentrations of elements are in weight percent Fig. 12.10.

To summarise, the impurity-controlled temper embrittlement occurs in bainite as it does in martensite; after all, neither of these transformation products cross austenite grain surfaces and hence leave them open for impurity segregation. By comparison, reconstructive transformations products such

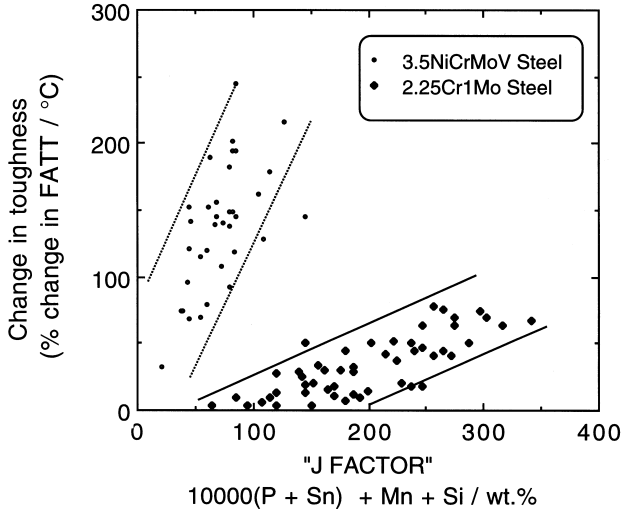

Fig. 12.10 Correlation between the tendency to embrittle and an empirical 'J' factor which is a function of chemical composition (Watanabe and Murakami, 1981; Bodnar *et al*., 1989).

as allotriomorphic ferrite, can grow across and consume the austenite grain surfaces, thereby removing them entirely from the final microstructure.

Finally, it is worth noting that although the science of the embrittlement is well understood, for reasons of cost, commercial steels always contain more impurities than is desirable. Steps must therefore be taken to mitigate the impurity effects, for example by alloying with molybdenum to pin down the phosphorus and prevent it from segregating.

12.7.2 300→350 °C Temper Embrittlement

Fracture is again intergranular with respect to the prior austenite grain boundaries which become decorated with coarse cementite particles during tempering. At the same time, the grain boundaries are weakened by impurity segregation. The cementite particles crack under the influence of an applied stress and in this process concentrate stress at the weakened boundaries. These factors combine to cause embrittlement.

12.7.3 300→350 °C Tempered-Martensite Embrittlement

This effect is common in clean steels, with fracture occurring transgranularly relative to the prior austenite grain boundaries. It is attributed to the formation of cementite particles at the martensite lath boundaries and within the laths. During tempering, the particles coarsen and become large enough to crack, thus providing crack nuclei which may then propagate into the matrix. As a consequence, untempered low-carbon martensitic steels sometimes have a better toughness than when they are tempered, even though the untempered steel is stronger (Fig. 12.11). The cementite behaves like a brittle inclusion.

Both of the impurity-controlled embrittlement phenomena can be minimised by adding about 0.5 wt% molybdenum to the steel. The Mo associates with phosphorus atoms in the lattice thereby reducing mobility and hence the extent to which they segregate to boundaries. Larger concentrations of molybdenum are not useful because precipitation occurs.

In many bainitic microstructures, tempering even at temperatures as high as 550 °C has only a small effect on cementite size and morphology. Consequently, the low-temperature embrittlement phenomena are not found in conventional bainitic microstructures (Ohmori *et al.*, 1974).

When bainite in carbon-containing iron alloys is free from carbides, its microstructure consists of bainitic ferrite, martensite and carbon-enriched retained austenite. In such microstructures, there is a special 'embrittlement' effect associated with the decomposition of the austenite during tempering (Bhadeshia and Edmonds, 1983a,b). The effect is specific to clean steels and is associated with a large reduction in the work of fracture even though the

[13:38 3/9/01 C:/3B2 Templates/keith/3750 BAINITE.605/3750-012.3d] Ref: 0000 Auth: Title: Chapter 00 Page: 309 285-342

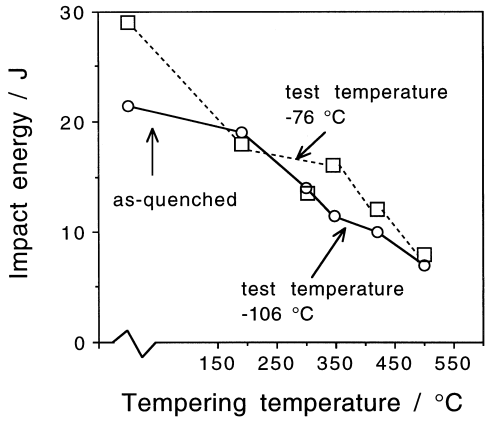

Fig. 12.11 Plot of toughness versus tempering temperature for a high-purity martensitic steel, illustrating that the toughness is reduced even though the strength decreases on tempering (Bhadeshia and Edmonds, 1979b).

failure mode is microscopically ductile. Ductile failure occurs by the nucleation and linkage of microvoids. In the absence of carbide particles, the number of voids nucleated is small, so that the total plastic strain before the voids link is large since they are widely spaced (Fig. 12.6). When the austenite decomposes, the resulting carbides increase the number density of void nucleation sites; the smaller spacing between the voids then reduces the plastic strain to failure, even though the bainite weakens on tempering. The effect is obvious from an examination of fracture surfaces: those from untempered bainite exhibit larger dimples, indicative of widely spaced void nucleation sites (Fig. 12.12). Similar reductions in the ductility and toughness have been correlated versus the decomposition of austenite to carbides in high-silicon bainitic cast irons (Dubensky *et al.*, 1985; Gagne, 1985; Shieh *et al.*, 1993, 1995). Other work has indicated that even the presence of carbides within the lower bainitic ferrite can impair toughness (Miihkinen and Edmonds, 1987c).

12.8 Fatigue Resistance of Bainitic Steels

There are few studies of fatigue phenomena in bainitic steels because they have not had many structural applications when compared with martensitic alloys. Notable exceptions are the creep-resistant alloys used in the power generation industry, where high cycle fatigue is an issue for rotating parts and thermal fatigue resistance becomes important for plant designed to operate intermittently. Fatigue crack propagation in hydrogen-containing environments (chemical or coal conversion plant and pressure vessels) can be life limiting

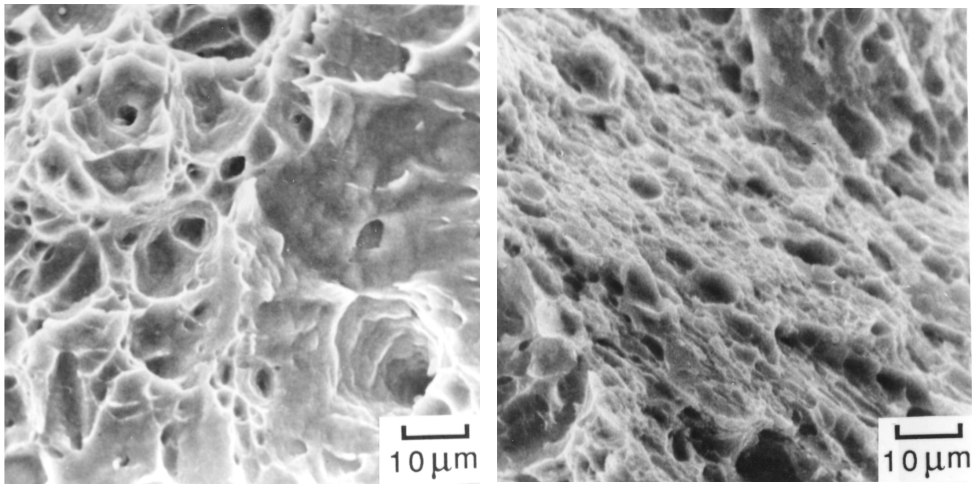

Fig. 12.12 Scanning electron micrographs of the fracture surfaces of untempered (a) and tempered (b) samples, showing the much reduced dimple size in the latter sample which contains numerous carbide particles which help nucleate voids.

and so there are more studies in this area for bainitic alloys. Sub-surface fatigue caused by rolling-contact stresses can similarly limit the life of rails in the transportation industries.

12.8.1 Fatigue of Smooth Samples

Fatigue tests on smooth samples give information on the sensitivity of the specimen to fatigue crack initiation. Such tests are mostly relevant for materials which are clean, i.e. they are free from defects which might propagate under the influence of the applied alternating stress. The results from tests on smooth samples are expressed in the form of an $S-N$ curve, which is a plot of $\ln\{\sigma_a\}$ versus $\ln\{N\}$, where σ_a is the alternating stress amplitude and N the number of cycles to failure (Fig. 12.13).

Materials which strain-age show a *fatigue limit*, which is a value of the alternating stress amplitude below which fatigue failure does not occur. The fatigue limit is the stress below which fatigue cracking never develops, and is usually ascribed to dynamic strain-aging in which the mobile dislocations are pinned by interstitials. Another view is that the limit should be identified with the need for plasticity to spread across grain boundaries for the successful propagation of cracks (Wilson and Oates, 1964; Mintz and Wilson, 1965; Petch, 1990). Fatigue cracks are said not to develop when plasticity is confined to the surface regions of the samples. This alternative interpretation is supported by the fact

[13:38 3/9/01 C:/3B2 Templates/keith/3750 BAINITE.605/3750-012.3d] Ref: 0000 Auth: Title: Chapter 00 Page: 311 285-342

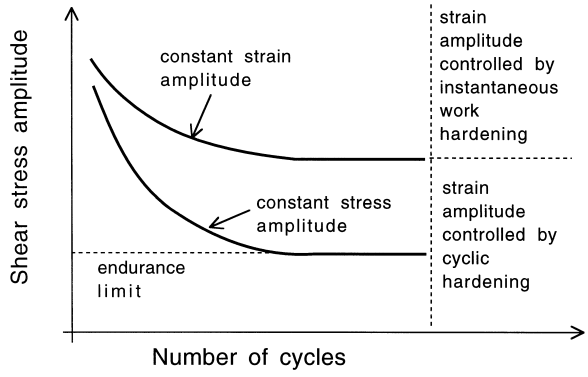

Fig. 12.13 Schematic *S–N* curves for fatigue.

that a fatigue limit can be found even when the test temperature is so low that interstitials can hardly be mobile enough to enable dynamic strain aging. At the same time the role of interstitials is recognised as an additional factor since the fatigue limit actually rises as the temperature is raised to a point where ageing becomes possible (Petch, 1990).

Notice that even smooth samples will have non-uniformities at the surface. These develop into cracks which are small in comparison with the microstructure but they do not grow when the stress amplitude is below the fatigue limit. The cracks are halted by strong microstructural barriers. Chapetti *et al*. (1998) which have defined the nature of the non-propagating crack and of the microstructural feature which acts as a strong barrier, which must be overcome by raising the stress amplitude beyond the fatigue limit (Table 12.1).

Table 12.1 Microstructural observations from smooth specimen fatigue crack growth tests done at stress amplitudes close to the fatigue limit. The non-propagating crack is present at stresses below the fatigue limit but is stopped from advancing by a strong microstructural barrier. After Chapetti *et al.* (1998).

Microstructure	HV	Non-propagating crack	Strong barrier
Ferrite–Pearlite $(\alpha + P)$	127	Across α grain	α/α or α/P grain boundary
Ferrite–Bainite $(\alpha + \alpha_b)$	181	Across α grain	α/α_b boundary
Bainite–Martensite $(\alpha_b + \alpha')$	288	Across packets of laths	Austenite grain boundary

[13:38 3/9/01 C:/3B2 Templates/keith/3750 BAINITE.605/3750-012.3d] Ref: 0000 Auth: Title: Chapter 00 Page: 312 285-342

Mild steels with a microstructure of equiaxed proeutectoid ferrite exhibit a fatigue limit. For other materials, an *endurance limit* is defined as the value of the stress amplitude corresponding to a fatigue life of say $N = 10^8$. It is worth noting that fatigue stresses are in practice less than half the ultimate tensile strength of the steel, so that the plastic strain per cycle can be small.

Fatigue tests on smooth samples can be carried out with the stress amplitude maintained constant for all cycles, or with the plastic strain amplitude fixed for each cycle (Fig. 12.14). The test chosen depends on the nature of the application, but the two kinds of experiments can reveal different information on the relationship between microstructure and fatigue properties. Clearly, when the strain per cycle is a fixed quantity, the alternating stress amplitude needed to maintain the strain increases with the number of cycles as the material fatigue hardens during the test. The hardening eventually reaches a saturation level after many cycles and the stress σ_a does not then vary with N (Fig. 12.14). During each half cycle σ_a has to be raised to the instantaneous flow stress σ_{iy} which can be determined experimentally by interrupting the test at any stage. As the test proceeds, σ_{iy} can be expected to increase as instantaneous work hardening occurs. If σ_s is the value of σ_{iy} at saturation, the ratio $r_2 = \sigma_a/\sigma_s$ is always expected to be close to unity because the applied stress σ_a has to rise to the value of σ_{iy} (Kettunen and Kocks, 1967).

For a test in which the alternating stress amplitude is kept constant, the plastic strain per cycle decreases as the material *cyclically hardens*, until it eventually reaches an approximately constant value. In cyclic hardening, σ_a is constant but σ_{iy} rises, whereas in fatigue hardening $\sigma_a \simeq \sigma_{iy}$ (Kettunen and Kocks, 1972). During the test, σ_{iy} increases due to cyclic hardening as the mean free slip area for dislocations (A_s) decreases. σ_{iy} eventually reaches the saturation value σ_s and at that stage, A_s remains approximately constant with N.

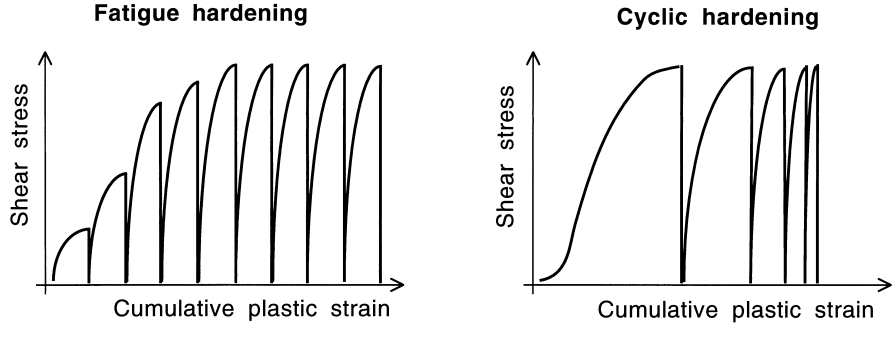

Fig. 12.14 Schematic illustration of constant plastic strain and constant stress fatigue tests (after Kettunen and Kocks, 1967).

[13:38 3/9/01 C:/3B2 Templates/keith/3750 BAINITE.605/3750-012.3d] Ref: 0000 Auth: Title: Chapter 00 Page: 313 285-342

The area A_s at saturation may be larger than the mean slip area per obstacle in which case the to and fro movement of dislocations causes an accumulation of damage which eventually may eventually lead to fatigue failure. However, if A_s is of the order of the mean free slip area per obstacle, because σ_a is low, then the dislocations bow between obstacles, a process which leads to energy dissipation but not to damage accumulation. The applied stress σ_a at which this happens is the endurance limit and fatigue failure does not then occur for many millions of cycles. For cyclic stressing, the ratio r_2 varies with σ_a, but its value corresponding to the endurance limit (i.e. r_e) is predicted to be $\simeq 0.65 - 0.75$ for single crystal specimens (Kocks, 1967). For polycrystalline specimens of lower bainite, $r_e \simeq 0.51 - 0.55$, depending on the way in which the saturation flow stress σ_s is defined. Bainite yields gradually so a saturation *proof* stress has to be substituted for σ_s, and the proof stress has to be measured after an arbitrary (though small) plastic strain. Kettunen and Lepistö (1976) found that the saturation proof stress defined at a strain of 0.02 gives the best agreement with theory. The stress was measured by testing specimens which had first been fatigue cycled to about 20% of their fatigue life to be sure that the specimens are in a state of saturation. It is a good approximation for lower bainite to take $r_2 = (\sigma_a/\sigma_y)$ where σ_y is the proof stress obtained from an ordinary uniaxial tensile test, even though the microstructure is then not in the saturated condition.

Cyclic hardening correlates with the rate of work hardening in monotonic tensile tests. The rate decreases during both fatigue tests and during monotonic tensile testing. The endurance limit can be identified with the onset of a critical (low) value of the rate of work hardening, associated with the approach to saturation in the context discussed above. Since the ultimate tensile strength is also determined by the point at which a reduced rate of hardening cannot keep up with increasing stress due to reduction of area, the endurance limit should correlate well with the UTS, and this is experimentally found to be the case (Kettunen and Kocks, 1967, 1972). This correlation should remain valid as long as the failure mode is ductile.

12.8.2 Fatigue Crack Growth Rate

For many engineering applications, the steels used can be assumed to contain subcritical cracks, in which case the initiation of cracks is not a controlling feature of fatigue life. The lifetime of the component then depends on the rate at which these cracks can grow slowly to a critical size leading to catastrophic failure. If the plastic zone at the crack tip is small when compared with the characteristic dimensions of the specimen, then most of the material surrounding the tip behaves elastically. Linear elastic fracture mechanics can be used to estimate the stress intensity range ΔK felt at the crack tip due to the alternating

stress. The stress intensity range can be related to the crack growth rate da/dN, which is the average distance advanced by the crack front per cycle.

Experiments indicate that there is a minimum threshold value of ΔK below which subcritical cracks do not propagate (Fig. 12.15). For many applications, the majority of fatigue life is spent at near threshold levels of stress intensity since the crack growth rates there can be incredibly small, the average advance of the crack front sometimes being less than an interatomic spacing per cycle. Beyond the threshold regime, the crack growth rate increases with ΔK, until the 'Paris Law' regime is reached (Fig. 12.15) the relationship between the stress intensity range and the crack growth rate is empirically found to be of the form:

$$\frac{da}{dN} = C_4 \Delta K^m \tag{12.8}$$

where C_4 is a constant and m is called the Paris constant.

The crack growth rates in regime A where the stress intensity range is near the threshold value are found to be most sensitive to microstructure, mean stress and environment (Ritchie, 1979). The threshold region is of practical

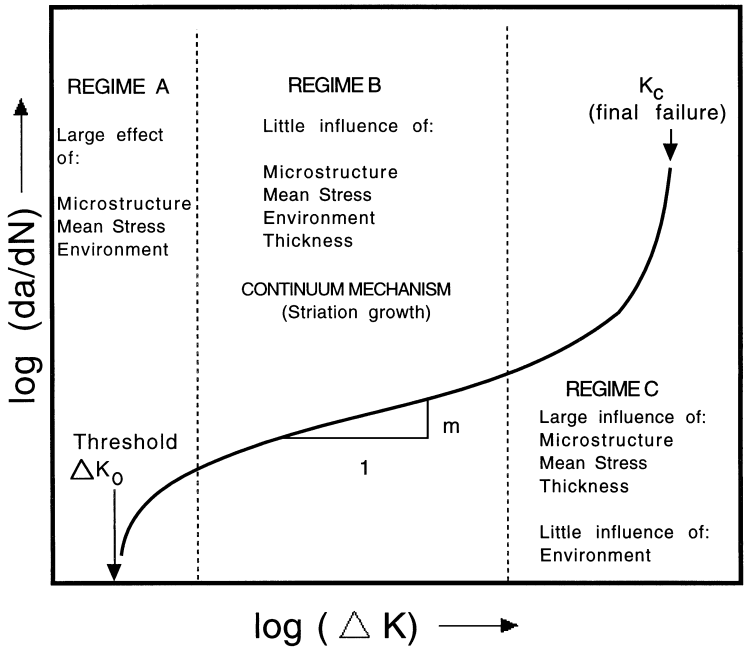

Fig. 12.15 Schematic illustration of the variation in fatigue crack growth rate as a function of the stress intensity range (after Ritchie, 1979.)

[13:38 3/9/01 C:/3B2 Templates/keith/3750 BAINITE.605/3750-012.3d] Ref: 0000 Auth: Title: Chapter 00 Page: 315 285-342

significance because many cracked components spend a good proportion of their fatigue life in that region. The threshold value of ΔK (i.e. ΔK_0) correlates directly with the *cyclic* yield strength (Fig. 12.16) which is in general less than the yield strength as measured in a uniaxial tensile test (Ritchie, 1979). The sensitivity of ΔK_0 to strength decreases as the mean stress amplitude increases.[†] This correlation is expected because the plastic zone at the fatigue crack tip is subject to alternating stresses; cyclic deformation of this kind must be different from monotonic strain hardening. Cyclic softening in quenched and tempered martensitic steels is usually attributed to rearrangements of the dislocation substructure and to a reduction in the dislocation density with alternating load. The softening occurs also because some of the plastic strain is reversible, a phenomenon analogous to the Bauschinger effect.

With some microstructures, the cyclic yield strength is found to be larger than the ordinary yield strength. In lightly tempered martensitic steels, the cyclic hardening is believed to occur due to dynamic strain ageing (Thielen

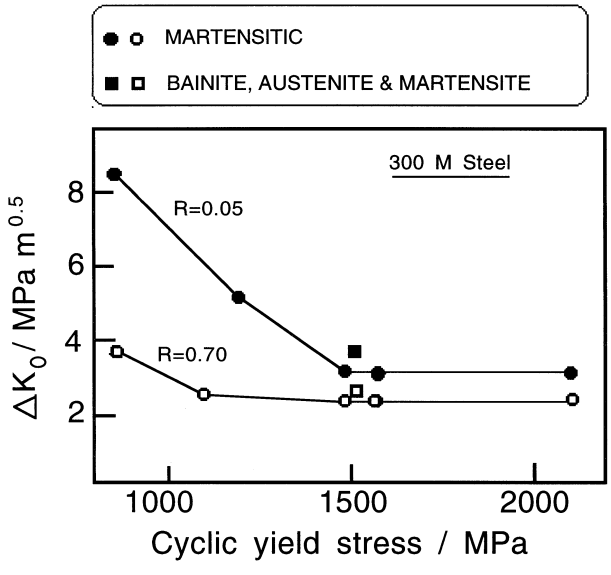

Fig. 12.16 Correlation of the threshold stress intensity range for fatigue crack propagation versus the cyclic yield stress for fully martensitic, and mixed microstructures at two values of R, which is the ratio of the minimum to maximum stress intensity (Ritchie, 1977a).

[†]This behaviour contrasts with the fatigue or endurance limit for steels, which increases with strength since it becomes more difficult to initiate cracks in smooth samples as the strength increases. The threshold value of ΔK on the other hand, depends on the ability of existing long cracks to grow, an ability which is enhanced by an increase in strength.

et al., 1976). For a high strength steel transformed isothermally to a mixed microstructure of bainite, martensite and retained austenite, Ritchie (1977a) found that the deformation-induced transformation of retained austenite to martensite reduced the reversibility of plastic strain during cyclic deformation, causing the cyclic yield strength to exceed the ordinary yield strength and consequently leading to a reduction in ΔK_0 (Fig. 12.17). Later work on metastable austenitic stainless steel has confirmed that fatigue induced martensitic transformation is accompanied by drastic cyclic hardening (Bayerlein *et al.*, 1992).

Cyclic softening therefore improves the near threshold fatigue crack growth resistance as long as the overall tensile strength is not reduced by a modification of the microstructure. Consistent with this, it is found that in a Fe–0.5Cr–0.5Mo–0.25V wt% steel, coarse grained precipitation hardened ferritic microstructures show significantly lower fatigue crack growth rates near ΔK_0, than higher strength bainitic or martensitic microstructures in the same alloy (Benson and Edmonds, 1978). In all cases, the crack path was found to be predominantly transgranular, with the bainite or martensite lath boundaries bearing no obvious relationship with the fracture surface.

A major reason why the threshold region is microstructure sensitive is that at higher stress intensities, the plastic zone size at the crack tip can be many times

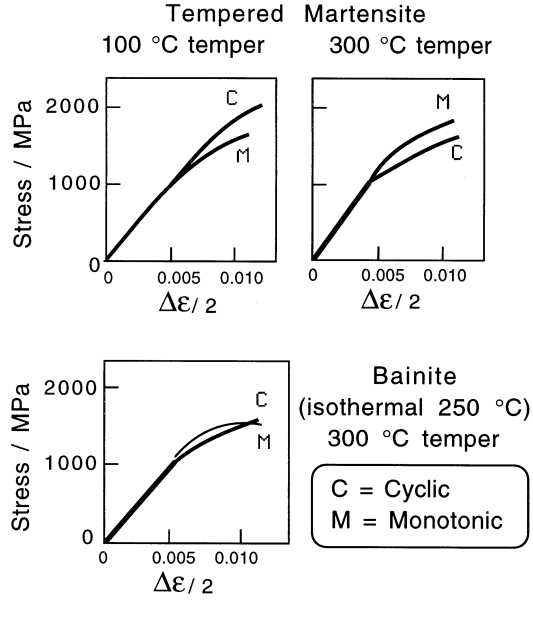

Fig. 12.17 Data illustrating the differences between the cyclic and monotonic yield behaviours for tempered martensite and bainite in 300M steel (Ritchie, 1977a).

[13:38 3/9/01 C:/3B2 Templates/keith/3750 BAINITE.605/3750-012.3d] Ref: 0000 Auth: Title: Chapter 00 Page: 317 285-342

greater than the grain size or other microstructural feature. Benson and Edmonds showed that in the threshold region, the maximum plastic zone size was about 3–5 times the ferrite grain size, and comparable with the austenite grain size in the case of the bainitic and martensitic microstructures (i.e. a few times larger than the lath or packet size).

In the Paris Law regime (regime B, Fig. 12.15), the material behaves essentially as a continuum with little demonstrable influence of microstructure or mean stress. For ductile materials, the crack advances by a striation mechanism although other modes of fracture might occur at the same time in embrittled materials, giving values of m which are much larger than the $m = 2$ value expected theoretically. As the crack continues to grow at increasing ΔK, the maximum stress intensity begins to approach the critical value K_{IC} characteristic of final failure. The growth rate then becomes microstructurally sensitive, the dependency on microstructure reflecting its relationship with toughness. Thus, the austenite associated with bainitic microstructures can be beneficial to fatigue in Regime C (Fig. 12.15). The fracture modes in this regime replicate those found in static fracture, e.g. cleavage or intergranular failure.

12.8.3 Fatigue in Laser-Hardened Samples

Surface layers of steel components can be heat-treated with minimal distortion using lasers. The action of the laser is to swiftly heat a thin surface layer which then cools rapidly by the transfer of heat into the underlying material, a process known as 'self-quenching'. A motivation for surface treatments of this kind is to improve the resistance to fatigue. The microstructure of the surface layer can be martensitic or bainitic depending on the composition and shape of the steel, together with the parameters controlling the laser treatment. The general principles discussed above apply, that the fatigue crack growth rate is insensitive to the microstructure in the Paris law regime, but varies with the microstructure when the stress intensity range is close to the threshold value.

In the threshold regime, Tsay and Lin (1998) have shown that for equivalent hardness, a lower bainitic microstructure has better resistance to cleavage crack propagation than one containing tempered martensite. This is because the latter is more sensitive to grain boundary embrittlement leading to intergranular failure during fatigue at ΔK values as low as $25\,\mathrm{MPa\,m^{\frac{1}{2}}}$. Since the tempering temperature was only $300\,^{\circ}\mathrm{C}$, the weakness of the prior austenite grain boundaries must be associated with coarse cementite particles as discussed in section 12.7. The tendency to form such particles at the prior austenite grain boundaries is reduced for a lower bainitic microstructure since the cementite precipitates during the course of transformation.

It is interesting to note that Tsay and Lin induced the formation of lower bainite during laser treatment by preheating the steel to a temperature of 300 °C, a method used widely in the welding industry.

12.8.4 Fatigue and Retained Austenite

Fatigue cracks propagate as damage is accumulated during the cyclic straining of the material at the crack tip. It is natural to expect metastable austenite in the vicinity of the crack tip to transform into martensite, leading effectively to an increase in the strain hardening rate. A high strain hardening rate leads to more rapid crack propagation (Cottrell, 1965), because the ability of the material to accommodate plastic strain then becomes exhausted more readily. The formation of hard martensite in a ductile matrix also decreases the strain preceding fracture.

It might therefore be concluded that the presence of austenite is not beneficial to the fatigue properties. However, this neglects the work that has to be done by the applied stress to induce martensitic transformation (Chanani *et al*., 1972). Stable austenite might also improve the fatigue properties by increasing the ductility of the microstructure.

Figure 12.18 shows fatigue crack propagation data from two samples of carbide-free bainitic microstructures in which the strength was altered by varying the isothermal transformation temperature. It is seen that the threshold stress-intensity increases and the crack propagation rate decreases, as the fraction of retained austenite increases. This is in spite of the fact that the yield strength of the sample with less austenite is in fact larger[†]

12.8.5 Corrosion Fatigue

There are few corrosion fatigue data available for bainitic microstructures, but it is known that environmental effects can accelerate fatigue cracks via a conjoint action of stress and corrosion. Many of the effects are attributable to hydrogen embrittlement. The fresh fracture surfaces created as the crack propagates are vulnerable to environmental attack, as long as there is sufficient time available for the hydrogen to diffuse into the region ahead of the crack front. Consequently, corrosion fatigue is less detrimental at high frequencies of cyclic loading.

Corrosion during fatigue also leads to a reduction in the threshold stress intensity, below which normal fatigue crack growth does not occur, to a value designated K_{CRIT}. The reduction may be so drastic as to make K_{CRIT} of little use

[†]It is sometimes considered that the crack growth increment per cycle should be inversely proportional to the cyclic yield strength. This is because the crack tip opening displacement will be smaller when the yield strength is large. This is opposite to the behaviour illustrated in Fig. 12.18, providing evidence for the beneficial effect of retained austenite.

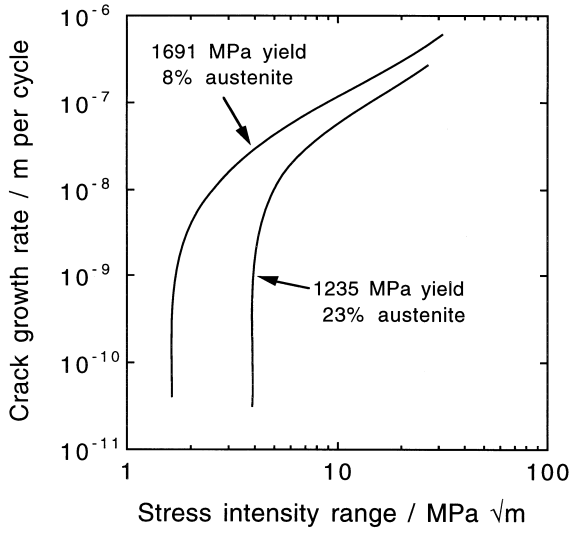

Fig. 12.18 The fatigue crack propagation rate as a function of the stress-intensity range. The chemical composition of the steel is Fe–0.6C–2.3Si–1.5Mn–0.6Cr wt%. The microstructures each consist of a mixture of retained austenite, bainitic ferrite and high-carbon martensite. The high and low yield strength samples are obtained by isothermal transformation at 573 and 643 K respectively (Wenyan *et al.*, 1997).

as a design parameter, since the section sizes necessary to reduce the design stresses to a level at which crack propagation does not occur may be unrealistically large. In such circumstances, the components are assigned service lives calculated using known corrosion fatigue data.

Although it is intuitively reasonable that corrosion should, by chemical degradation, enhance the crack growth rate, there are complications which sometimes lead to an overall reduction in the rate of crack propagation (Dauskardt and Ritchie, 1986). When the stress intensity range and mean stress is low, any corrosion products that form can isolate the crack tip from its environment. Thus, fatigue crack growth in a moist environment occurs at a lower rate than in dry hydrogen (Ritchie *et al.*, 1980; Suresh *et al.*, 1981). Specimens which have been damaged by hydrogen bubble formation prior to fatigue testing can fail more rapidly relative to those in which the bubbles form in the vicinity of the crack front during testing. The expansion associated with bubble formation then induces crack tip closure (Fig. 12.19). All other factors being equal, low strength steels are better at resisting crack growth because plasticity leads to crack tip closure.

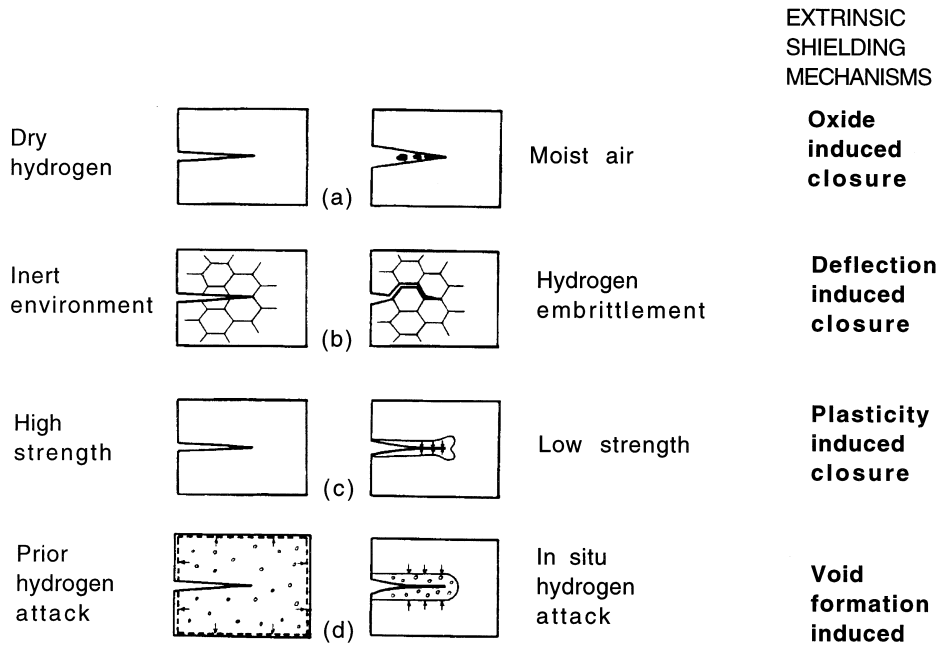

Fig. 12.19 An illustration of the micromechanisms of crack tip shielding, as discussed in the text (Dauskardt and Ritchie, 1986.)

12.8.6 Stress Corrosion Resistance

Cleavage fracture occurs when a critical stress is exceeded over a region ahead of the crack tip, such as to stimulate the growth of an existing microcrack. This critical stress can be reduced by environmental effects. Cleavage fracture then occurs at a critical stress intensity K_{ISCC} which is about a third of K_{IC}. This means that stress corrosion can severely limit the effective use of high strength steels. The effect of corrosion manifests primarily via hydrogen embrittlement, the hydrogen being generated by cathodic reaction at the crack surface. It then diffuses to regions of highest dilatation ahead of the crack tip, leading to a reduction in the cohesive strength (Pfeil, 1926; Troiano, 1960; Oriani and Josephic, 1974).

It is difficult to comment on the relationship of K_{ISCC} with microstructure but it appears that the presence of retained austenite reduces the stress corrosion crack growth rates, by hindering the diffusion of hydrogen to the sites of triaxial tension ahead of the advancing crack front (Parker, 1977; Ritchie *et al.*, 1978). The diffusivity of hydrogen through austenite can be many orders of magnitude smaller than that in ferrite (Shively *et al*. 1966). The permeation of

[13:38 3/9/01 C:/3B2 Templates/keith/3750 BAINITE.605/3750-012.3d] Ref: 0000 Auth: Title: Chapter 00 Page: 321 285-342

hydrogen in high strength steels has been studied using electrochemical techniques (Tsubakino and Harada, 1997). The diffusivity derived from permeation curves is found to be smaller, and the activation energy larger, for steels with retained austenite.

Comparative experiments at constant yield strength, on tempered martensite and on a mixed microstructure of lower bainite, martensite and retained austenite, revealed that the sample containing the greater quantity of austenite exhibited better stress corrosion resistance in a NaCl solution (Ritchie *et al*., 1978). While both samples failed at the prior austenite grain surfaces, the proportion of ductile tearing was greater in the bainitic samples. This was attributed to the ability of retained austenite to act as sinks for impurities thereby reducing segregation to boundaries (Marschall *et al*., 1962). Embrittled boundaries are more susceptible to stress corrosion (Ritchie, 1977b).

These investigations emphasise the role of retained austenite in improving the resistance to stress corrosion, but the conditions under which the austenite is beneficial are limited (Solana *et al*., 1987; Kerr *et al*., 1987). The austenite has to continuously surround the plates of ferrite in order to hinder the diffusion of hydrogen. There are other effects which are more important than that of austenite. Any microstructural modifications which lead to a high density of hydrogen traps (e.g. interfaces between cementite and ferrite) lead to large improvements in stress corrosion resistance.

Kerr *et al*. and Solana *et al*. were able to establish some general principles relating microstructure and stress corrosion resistance (SCR). The sensitivity to microstructure was largest at yield strengths less than about 1000 MPa, and when failure occurred by a transgranular mechanism. Furthermore, the largest improvements obtained did not correlate with the presence of retained austenite. Twinned martensite was deleterious to SCR, presumably because twinned martensite is associated with high carbon concentrations and poor toughness; the twins themselves are innocuous. Mixtures of ferrite and martensite were found to be better, correlating with extensive crack branching due to the high density of interphase interfaces. The presence of lower bainite also led to improved SCR, but the effect could not be separated from any due to the associated drop in yield strength. All other factors being equal, reductions in yield strength correlated strongly with improved SCR (Fig. 12.20). Alloy specific effects were also observed and attributed to differences in the density of hydrogen traps. Indeed, any feature of the microstructure which enables the hydrogen to be dispersed, or which promotes crack branching, improves SCR.

There is recent work using secondary-ion mass spectroscopy on an acicular ferrite microstructure, which suggests that dissolved boron atoms form stable complexes with hydrogen, thereby reducing its mobility (Pokhodnya and Shvachko, 1997).

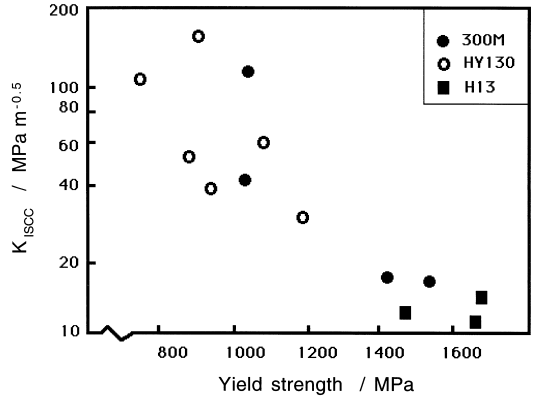

Fig. 12.20 The correlation of stress corrosion cracking resistance versus the yield strength for a variety of steels (Solana *et al.*, 1987)

12.9 The Creep Resistance of Bainitic Steels

Creep-resisting steels used in power plant or in the petrochemical industries are based on low-carbon, low-alloy steels containing chromium, molybdenum, tungsten or vanadium as the significant alloying additions. Low-chromium steels, such as the classical $2\frac{1}{4}$Cr1Mo or 1CrMoV alloys have formed the backbone of the power generation and petrochemical industries for at least five decades, for operating temperatures of 565 °C or less. The $2\frac{1}{4}$Cr1Mo is essentially bainitic, whereas the 9Cr1Mo type alloys developed much later, for higher temperatures and greater corrosion/oxidation resistance, are martensitic. The major applications are in the fabrication of pressure vessels, boiler steam pipes, steam generating and handling equipment, high pressure tubes with thick walls, turbine rotors, superheater tubes, coal to methane conversion plants, petrochemical reactors for the treatment of heavy oils and tar sands bitumen, etc. In addition to creep, they have to be resistant to oxidation and hot-corrosion, sometimes in environments containing hydrogen and sulphur. The pressure vessels in large coal liquefaction and gasification plant may be required to contain mixtures of hydrogen and hydrogen sulphide at pressures up to 20 MPa at 550 °C. The steels have to be weldable and cheap.

Given the demands for service at high temperatures and over 30–50 years, the microstructures must be resistant to other phenomena, such as graphitisation. Protection against graphitisation is one of the reasons why the aluminium concentration is limited to less than 0.015 wt%, and why chromium and molybdenum are used together as alloying additions, because molybdenum on its own promotes the tendency to graphitisation (Hrivnak, 1987). Ambient temperature properties are relevant because the fabricated components must

be safe during periods where elevated temperature operation is interrupted. Fatigue resistance is important to bear in mind but the tolerance to cyclic stresses can frequently be managed by proper engineering design.

The steels might typically be used within the temperature range 480–565 °C, the service stresses being of the order of 15–40 MPa ($\sigma/E \simeq 1\text{–}3\times10^{-4}$). The maximum tolerable creep strain rate is about $3 \times 10^{-11}\,\mathrm{s}^{-1}$. In power plant, the stresses normally originate from a combination of internal steam pressure and the dead weight of the components in large assemblies. The most important property requirement is creep resistance. A greater creep strength can be exploited to reduce the component wall thickness; the resulting reduction in weight allows the support structures to be reduced in scale. It is often the case that the hoop stresses generated by the pressurised steam can be comparable to those due to the weight of the steam pipes, providing the incentive for weight reduction. Higher alloy steels can be used without additional expense, if they have a higher creep strength. Welding also becomes simpler and cheaper for smaller section sizes. Thermal stresses induced by temperature differences between the inner and outer surfaces of any component are smaller with section size, thereby mitigating any thermal fatigue problems associated with the irregular use of the power plant, due for example to variations in electricity demand. Such flexibility can make a substantial difference to the economic performance of electricity-generating plant.

Typical chemical compositions of bainitic steels used for their creep resistance the given in the upper half of Table 12.2; those listed in the lower half represent are corresponding martensitic steels presented for comparison. The newer steels tend to contain less manganese in order reduce their susceptibility to temper embrittlement and banding due to chemical segregation. The hardenability is maintained at reduced manganese concentrations by the overall increase in the concentration of other elements, for example chromium.

The actual chemical composition can in practice vary significantly from the typical value. The specified composition range is generally not tight from a metallurgical point of view (Table 12.2). Indeed, the American Society for Testing Materials has at least twelve standards for the $2\frac{1}{4}$Cr1Mo steel for different applications (Lundin *et al.*, 1986). It is unfortunate that many publications refer only to the nominal designation, and sometimes do not even mention the carbon concentration of the steel concerned. It is now recognised that very small and apparently innocuous variations in chemical composition can explain large variations in the mechanical properties of creep-resistant steels (Kimura *et al.*, 1997).

An interesting reason for keeping the carbon concentration as low as possible, is that it is often necessary to join these steels to stainless steels. There is then a carbon chemical potential gradient which exists at the junction,

Table 12.2 Compositions (wt%) of creep-resistant steels with typical specification ranges. The upper and lower sections of the table represent bainitic and martensitic steels respectively. The sulphur concentration is usually within the range 0.005–0.02 wt%, and that of phosphorus within the range 0.005–0.025 wt%

Designation	C	Si	Mn	Ni	Mo	Cr	V	Others
0.25CrMoV	0.15	0.25	0.50	0.05	0.50	0.30	0.25	–
range	<0.18	0.10–0.60	0.40–0.65	–	0.45–0.65	0.25–0.35	0.20–0.30	–
1Cr MoV	0.25	0.25	0.75	0.70	1.00	1.10	0.35	–
range	0.24–0.31	0.17–0.27	0.74–0.81	0.60–0.76	0.65–1.08	0.98–1.15	0.27–0.36	–
2.25Cr1Mo	0.15	0.25	0.50	0.10	1.00	2.30	0.00	–
range	<0.16	<0.05	0.3–0.6	–	0.9–1.1	2.0–2.5	–	–
Mod. 2.25Cr1Mo	0.1	0.05	0.5	0.16	1.00	2.30	0.25	Ti = 0.03 B = 0.0024
3.0Cr1.5Mo	0.1	0.2	1.0	0.1	1.5	3.0	0.1	–
range	<0.16	<0.5	0.30–0.60	–	0.45–0.65	4.0–6.0	–	–
3.5NiCrMoV	0.24	0.01	0.20	3.50	0.45	1.70	0.10	–
range	<0.29	<0.11	0.20–0.60	3.25–4.00	0.25–0.60	1.25–2.00	0.05–0.15	
9Cr1Mo	0.10	0.60	0.40	–	1.00	9.00	–	–
range	<0.15	0.25–1.00	0.30–0.60	–	0.90–1.10	8.00–10.00	–	–
Mod. 9Cr1Mo	0.1	0.35	0.40	0.05	0.95	8.75	0.22	Nb = 0.08 N = 0.05
range	0.08–0.12	0.20–0.50	0.30–0.60	<0.2	0.85–1.05	8.00–9.50	0.18–0.25	Nb 0.06–0.10 N 0.03–0.07 Al <0.04
$9Cr\frac{1}{2}MoWV$	0.11	0.04	0.45	0.05	0.50	9.00	0.20	W = 1.84 Nb = 0.07 N = 0.05
range	0.06–0.13	<0.50	0.30–0.60	<0.40	0.30–0.60	8.00–9.50	0.15–0.25	Nb 0.03–0.10 N 0.03–0.09 Al <0.04
12CrMoV	0.20	0.25	0.50	0.50	1.00	11.25	0.30	–
range	0.17–0.23	<0.5	<1.00	0.30–0.80	0.80–1.20	10.00–12.50	0.25–0.35	–
12CrMoVW	0.20	0.25	0.50	0.50	1.00	11.25	0.30	W = 0.35
range	0.17–0.23	<0.5	<1.00	0.30–0.80	0.80–1.20	10.00–12.50	0.25–0.35	W <0.70
12CrMoVNb	0.15	0.20	0.80	0.75	0.55	11.50	0.28	Nb 0.30 N 0.06

causing it to migrate during service at high temperatures (Fig. 12.21). The migration occurs from the low-alloy to the high-alloy steel, causing a decarburised layer to develop in the former and an intense region of carbide precipitation in the latter. The overall integrity of the joint is therefore jeopardised (Klueh, 1974a; Lundin *et al.*, 1982). Naturally, a reduced carbon concentration also leads to inferior creep properties given that the steels rely on alloy carbides for their resistance to creep so that a compromise is necessary (Klueh, 1974a,b).

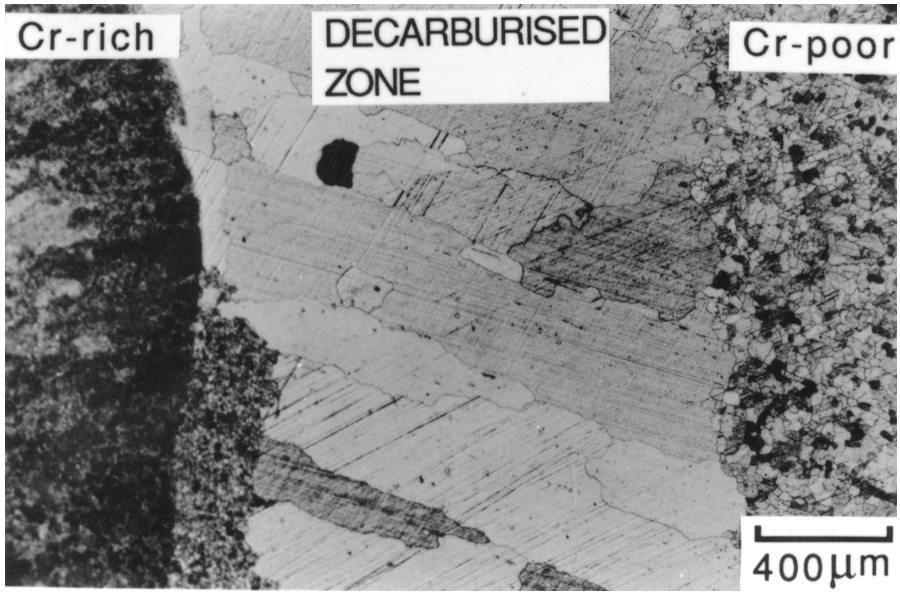

Fig. 12.21 Optical micrograph of a junction between mild steel and a $2\frac{1}{4}$Cr1Mo alloy, showing the development of a decarburised zone in the mild steel side of the joint after tempering (Race, 1990).

The standard alloys sometimes contain trace additions of boron and titanium, added presumably to enhance the bainitic hardenability in the manner discussed in Chapter 6. Unintentional trace impurities such as tin and antimony are also known to have disproportionate effects on creep strength for reasons which are not well understood (Collins, 1989). The alloys are usually fabricated by welding, and the filler material used can be chemically different from the parent plate; the CrMoV steels are usually welded with $2\frac{1}{4}$Cr1Mo fillers in order to ensure good creep properties in the weld metal.

12.9.1 Heat Treatment

For power plant applications, the steels are usually air cooled ('normalised') after austenitisation. The component thickness may vary from 12–120 mm; the thickness determines the heat treatment time in order to allow the component to achieve uniform temperature. On the other hand, heat flow analysis shows that the specified periods are excessive and could in principle be reduced (Greenwell, 1989). The temperature to which the steels are heated for austenitisation is usually about 100 °C above the Ae_3 temperature, or 50 °C above the Ac_3 temperature when the heating rate is about 1 °C per minute. Lower temperatures lead to correspondingly smaller austenite grain sizes,

[13:38 3/9/01 C:/3B2 Templates/keith/3750 BAINITE.605/3750-012.3d] Ref: 0000 Auth: Title: Chapter 00 Page: 326 285-342

which can be beneficial to mechanical properties. The creep mechanism in service is not controlled by grain boundary diffusion or sliding, but rather by the motion of dislocations past precipitates.

Given that it is impossible to achieve uniform cooling in large components, it is reasonable to expect variations in the microstructure and mechanical properties as a function of position. For a typical range of chemical compositions encountered within the $2\frac{1}{4}$Cr1Mo designation, the normalised microstructures consist of mixtures of allotriomorphic ferrite and bainite, with the fraction of bainite in the range 0.34–0.94 (Murphy and Branch, 1971). The effect on the mechanical properties due to these variations is pronounced during the early stages of service, but the differences in creep strength vanish over the long term.

After normalisation, the steels are given a stress-relief treatment by tempering at 660–700 °C for some 2–14 h, depending on application and component size. This not only produces the required microstructure containing relatively stable carbides, but also mitigates residual stresses arising from welding operations. These heat treatments are so severe that the precipitates are in an overaged condition (Pilling and Ridley, 1982).

12.9.2 $2\frac{1}{4}$Cr1Mo Type Steels

This is a popular steel which has been used reliably for many decades. Its creep resistance, like that of many low-alloy steels used in the power generation industry, comes from fine and stable dispersions of alloy carbides together with contributions from solid solution strengthening. The latter is especially important in the long term when the carbide dispersions have become ineffective due to coarsening. Molybdenum is particularly effective as a solid solution strengthening element (Lundin *et al*., 1982, 1986). The alloy design should be such as to avoid tying up all of the molybdenum in the form of carbides. The carbon concentration should therefore be controlled carefully to achieve the best compromise between the need for carbides and solution strengthening. Typical values of the creep rupture strength of $2\frac{1}{4}$Cr1Mo steel are illustrated in Fig. 12.22.

Investigations have shown that the ferrite/bainite microstructure in $2\frac{1}{4}$Cr1Mo steel is stronger in creep than martensite because M_2C, which is replaced eventually by more stable carbides during service, persists for shorter times in a martensitic microstructure (Baker and Nutting, 1959; Murphy and Branch, 1971). M_2C is more stable in ferrite when compared with bainite or martensite. These observations have yet to be explained.

12.9.3 1CrMoV Type Steels

These steels have been used in the manufacture of rotors for steam turbine power generating plant. 1CrMoV steels are austenitised at temperatures within

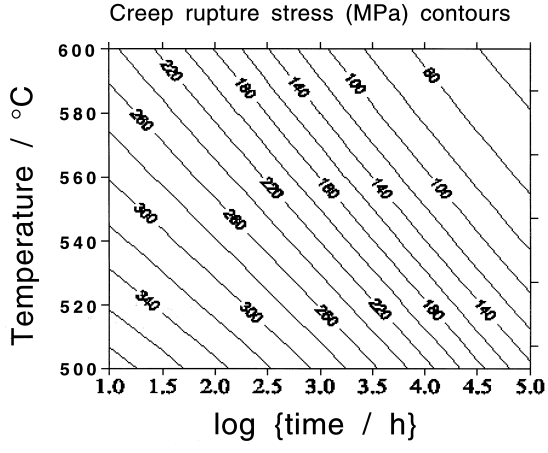

Fig. 12.22 Creep rupture strength of $2\frac{1}{4}$Cr1Mo steel as a function of temperature and time.

the range 950–1000 °C for 1–14 h and air cooled or furnace cooled to give a fully bainitic or a mixed microstructure of ferrite and bainite (Myers *et al*., 1968; Murphy and Branch, 1969; Strang *et al*., 1994). Tempering is in the range 690–710 °C for time periods up to 20 h. The resulting microstructure is a fine dispersion of V_4C_3 particles (about $\simeq 12$ nm size) in a matrix of ferrite.[†] Other carbides such as M_3C and $M_{23}C_6$ may also form when the carbon concentration is in excess of that required to react with the vanadium. These other carbides are coarse and precipitate mainly at the prior-austenite or ferrite grain boundaries.

The alloy is martensitic in the quenched condition; tempering at 690 °C for 20 h converts the martensite into ferrite containing V_4C_3 but for some unknown reason the carbide particles are much coarser with a typical size of 50 nm (Buchi *et al*., 1965; Myers *et al*., 1968). The creep strength of 1CrMoV steels in the tempered bainite condition is higher than in a tempered martensitic state, but this may not be due to the finer carbides in the tempered bainite. The observed activation free energy for creep is inconsistent with a process controlled by the climb of dislocations; the spacing between particles is too close to allow dislocation bowing (Myers *et al*., 1968). It is suggested that it is the interaction of dissolved vanadium with dislocations which controls creep deformation. The finer carbides in the tempered bainite leave a larger concentration of dissolved vanadium since the solubility of solute increases with interface curvature via the Gibbs–Thompson capillarity effect. The greater

[†]The V_4C_3 precipitates contain some iron, manganese molybdenum and chromium in solid solution, although vanadium is by far the major carbide-forming constituent (Senior, 1988).

concentration of soluble vanadium is claimed to be responsible for the better creep strength of tempered bainite. The interaction of vanadium atoms with dislocations must be important, but so must the dispersions of particles since it is unlikely that Fe–V solid solutions would have good creep properties in their own right.

The uniformity of the V_4C_3 dispersion depends on the form of M_3C present (Buchi *et al*., 1965). If the vanadium and carbon concentrations are stoichiometrically balanced, then M_3C is eliminated during tempering and the V_4C_3 dispersion is uniform. Otherwise, the regions around M_3C particles are found to be free from V_4C_3. Since the M_3C particles are mostly located at prior austenite or ferrite grain boundaries, V_4C_3-free zones form at the boundaries. This results in poor creep properties (Buchi *et al*., 1965; Murphy and Branch, 1969).

12.9.4 $\frac{1}{4}$CrMoV Type Steels

$\frac{1}{4}$CrMoV steels have a low hardenability so they are used with microstructure of allotriomorphic ferrite and a small fraction of pearlite. Fine V_4C_3 dispersions form on tempering. These steels have a higher creep ductility than the 1CrMoV alloys at a slightly lower creep strength. The lower creep ductility of 1CrMoV steels is because creep cavitation occurs at both the ferrite/ferrite and ferrite/bainite boundaries, whereas the $\frac{1}{4}$CrMoV cavitates mainly at the ferrite/pearlite which are not as susceptible to cavitation (Murphy and Branch, 1969). It is also argued that a larger fraction of ferrite permits a greater relaxation of stresses, thereby inhibiting cavity nucleation and growth (Jones and Pilkington, 1978).

12.9.5 Enhanced Cr–Mo Bainitic Steels

Many attempts have been made to improve on the properties of the low-alloy creep-resistant steels, especially in the context of pressure vessels in hydrogen environments. A higher concentration of alloy carbide-forming elements can reduce the stability of cementite, which is prone to hydrogen problems (Ritchie *et al*., 1984; George *et al*., 1985). Those alloys containing unstable carbides such as cementite and Mo_2C react with ingressed hydrogen, leading to decarburisation, cavitation and to the formation of methane bubbles at interfaces. Damage by hydrogen is thought to occur in three stages (Vagarali and Odette, 1981; Shewmon, 1976). The first stage, during which the microstructure and macroscopic mechanical properties are largely unaffected, involves the nucleation and growth of bubbles. This is followed by rapid attack as methane bubbles grow and coalesce into fissures at the grain boundaries, leading to swelling and a deterioration of mechanical properties. The final stage is

[13:38 3/9/01 C:/3B2 Templates/keith/3750 BAINITE.605/3750-012.3d] Ref: 0000 Auth: Title: Chapter 00 Page: 329 285-342

extensive decarburisation with the dissolution of carbides as the system attempts to maintain an equilibrium carbon concentration in the ferrite.

Thick steel plates (300–400 mm) are required in applications such as coal conversion plant. Conventional steels do not have adequate hardenability so attention has been focussed on improving the popular bainitic $2\frac{1}{4}$Cr1Mo steel, with the aim of extending the temperature range over which the alloy can be utilised, whilst maintaining the bainitic microstructure. Modifications include microalloying to improve elevated temperature strength, larger concentrations of chromium for improved resistance to hydrogen embrittlement, carbide stabilising additions such as vanadium and niobium, and nickel, boron and carbon additions for improved bainitic hardenability (Wada and Eldis, 1982; Wada and Cox, 1982, 1984; Ishiguro *et al*., 1982, 1984; Kozasu *et al*., 1984; Parker *et al*., 1984; Klueh and Swindeman, 1986).

Ishiguro *et al*. (1982) developed an alloy which differs from $2\frac{1}{4}$Cr1Mo steel in that it has a negligible silicon concentration, a lower carbon concentration (0.1 wt%) and 0.25V–0.02Ti–0.002B wt%. It is designated the 'Modified $2\frac{1}{4}$Cr1Mo' steel, with improved creep strength, impact toughness and resistance to temper embrittlement. The titanium combines with nitrogen, so that the boron can remain in solution and increase hardenability; boron otherwise forms a nitride which is less stable than that of titanium. The creep strength is improved because of vanadium carbides which make the bainitic microstructure more resistant to tempering (Klueh and Swindeman, 1986).

An alloy which has received a lot of attention has the chemical composition Fe–3Cr–1.5Mo–0.1V–1Mn–0.1C wt% developed by Wada and coworkers (1982, 1984). After austenitisation at about 1000 °C for two hours and air cooling, it has a microstructure which is essentially a mixture of bainitic ferrite and austenite/martensite, of the kind normally associated with the $2\frac{1}{4}$Cr1Mo steel discussed earlier. The extra alloying elements add to solution hardening, an important factor determining the long-term creep strength.

An advantage of the higher chromium concentration is that cementite is replaced more rapidly by carbides such as M_7C_3, $M_{23}C_6$ and M_6C, thus rendering the microstructure less susceptible to severe hydrogen attack. Bainite in $2\frac{1}{4}$Cr1Mo steel is far more sensitive to a high pressure hydrogen embrittlement than a tempered martensitic microstructure (Chung *et al*., 1982). This is because the carbon-enriched retained austenite associated with bainite decomposes into intense clusters of cementite particles which react with hydrogen. The cementite in tempered martensite is more uniformly distributed. At higher chromium concentrations, for example in the 3.5Cr1Mo bainitic steels, the cementite is quickly replaced by $M_{23}C_6$ making the alloy less sensitive to hydrogen exposure (George *et al*., 1985).

Manganese and silicon contribute to austenite grain boundary embrittlement (Bodnar *et al*., 1989). A bainitic steel in which the concentration of these

elements is minimised is the 3.5Ni3CrMoV alloy which is insensitive to hydrogen and temper embrittlement effects when compared with the $2\frac{1}{4}$Cr1Mo steel (Ritchie *et al*., 1984). The larger concentration of chromium and vanadium leads to the dissolution of cementite during tempering at 700 °C, thereby improving the resistance to hydrogen effects. Hydrogen sometimes reacts with carbon dissolved in ferrite producing gases such as methane, which precipitate as bubbles under conditions of severe hydrogen attack. This is another reason why 3.5Ni3CrMoV steel performs better because the concentration of carbon in the ferrite which is in equilibrium with alloy carbides is reduced.

The nickel in 3.5Ni3CrMoV steel improves toughness; it also increases the hardenability, allowing sections as thick as 0.4 m to transform into fully bainitic microstructures. The reduction in the Ae_3 temperature due to nickel permits the use of lower austenitisation temperatures; the resulting refinement of the austenite grain size is beneficial to toughness. Many other steels with lower nickel concentrations have been investigated and found to possess better properties over the conventional $2\frac{1}{4}$Cr1Mo alloy (Spencer *et al*., 1989).

12.9.6 Tungsten-Strengthened Steels

The heat associated with the welding of steels introduces a heat-affected zone (HAZ) in the solid metal adjacent to the weld; the heating and cooling cycle within this zone may induce undesirable microstructures such as untempered martensite. Post-weld heat treatments are then used to render any martensite in the HAZ harmless. However, this is not practical for large constructions, which also cannot be heated prior to welding in order to avoid the formation of brittle martensite.

A new bainitic steel, known commercially as *HCM2S*, has been developed to address these difficulties (Komai *et al*., 1999; Table 12.3). It is a modification of the $2\frac{1}{4}$Cr1Mo alloy with the molybdenum substituted with tungsten; combined with a reduction in the carbon concentration, this leads to a bainitic microstructure without martensite, allowing welding without pre- or post-weld heat treatment. The maximum hardness obtained for typical cooling rates is

Table 12.3 The chemical composition (wt%) of a tungsten-strengthened creep-resistant steel known commercially as *HCM2S*. The concentration of aluminium refers to that dissolved in the ferrite.

C	Si	Mn	P	S	Cr	Mo	W	V	Nb	N	Al	B
0.05	0.2	0.5	0.015	0.001	2.2	0.1	1.6	0.25	0.05	0.008	0.008	0.004

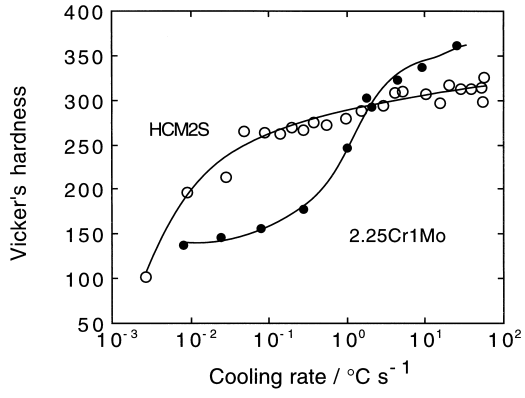

Fig. 12.23 A comparison between the hardness of a tungsten strengthened creep-resistant steel and the classical $2\frac{1}{4}$Cr1Mo alloy. The cooling rate is an average value in the range 800–300 °K s^{-1}. Data from Komai *et al.* (1999).

reduced to about 300 HV which is some 50 HV below that of $2\frac{1}{4}$Cr1Mo steel (Fig. 12.23). The insensitivity of the hardness to the cooling rate is claimed to be desirable in the design of joints.

The microstructure of the steel after normalising is bainite and in the tempered condition consists of tempered bainitic ferrite with cementite, $M_{23}C_6$, and vanadium or niobium carbonitrides. The addition of boron has the effect of stabilising $M_{23}C_6$ and $M_{23}(C,B)_6$ on grain boundaries, thereby retarding dynamic recrystallisation during creep (Miyata *et al.*, 1999). All this makes the alloy creep resistant, so much so that tolerable stress at 600 °C is about twice that of $2\frac{1}{4}$Cr1Mo, and almost matches the more expensive and difficult-to-weld 9Cr1Mo martensitic steels (Fig. 12.24).

The tungsten-strengthened bainitic steel has now performed satisfactorily in service for more than three years. Monitoring tests have shown that the alloy performs better than other steels such as $2\frac{1}{4}$Cr1Mo (Masuyama *et al.*, 1998). Recent work has suggested that a reduction in the manganese concentration can lead to further improvements in the creep strength (Miyatat et al., 1999). This is because M_6C precipitation is slower at low manganese concentrations, thus allowing more tungsten to remain dissolved in, and strengthen the solid solution. A reduction in manganese from 0.5 to 0.01 wt% led to an increase in the creep rupture strength by almost 50 MPa.

12.9.7 Regenerative Heat Treatments

Cavitation and other irreversible creep damage occurs at the late stages in the life of creep-resistant steels. During that period, any loss in properties is due

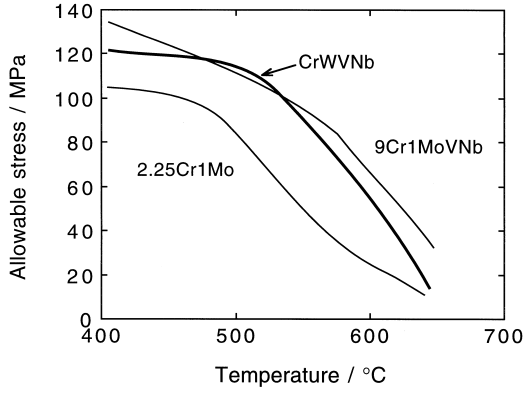

Fig. 12.24 Comparison of the allowable stress, as a function of temperature, for the tungsten-strengthened steel, $2\frac{1}{4}$Cr1Mo and a 9Cr1Mo martensitic steel. After Komai *et al*. (1999).

largely to microstructural changes such as carbide coarsening, changes in the configuration of dislocations, and the general approach of the microstructure towards equilibrium. These microstructural changes can, in principle, be reversed by heating the component back into the austenite phase field and then allowing it to transform back into the original microstructure. However, such a heat treatment involves high temperatures which may not be feasible with large components.

A possible alternative is to regenerate just the carbides, by annealing the steel at a temperature ($\simeq$700 °C) above the service temperature, but below that at which austenite can form (Senior, 1988). Some of the carbides would then dissolve to reprecipitate in a fine form during ageing at a lower temperature, thereby regenerating a semblance of the original microstructure.

12.9.8 Comparison with Martensitic Creep-Resistant Steels

Modern ferritic creep-resistant steels start with a microstructure which is martensitic. On the other hand, the best established steels of this kind rely on allotriomorphic ferrite or bainite as the starting microstructure. It is therefore pertinent to ask why modern heat-resistant steels are based on martensite.

The probable answer to this has little to do with microstructure. Indeed, when compared under identical conditions, the 9Cr1Mo steel is not better in creep than $2\frac{1}{4}$Cr1Mo (Fig. 12.25); it is only when these alloys are modified with elements such as niobium, vanadium, cobalt and tungsten that they begin to outperform the lower alloy steels.

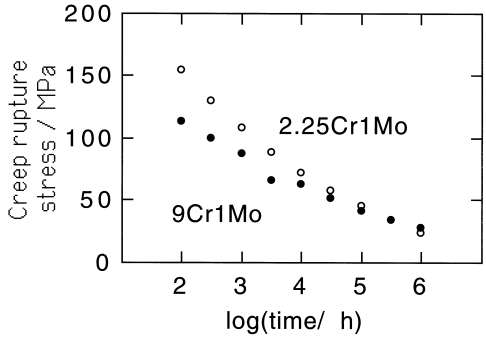

Fig. 12.25 A comparison of the creep rupture strengths of $2\frac{1}{4}$Cr1Mo and 9Cr1Mo steels given identical heat treatments (Bhadeshia, 2000).

The 9Cr1Mo alloys were developed for higher temperatures and greater corrosion/oxidation resistance. A greater chromium concentration is needed to obtain the oxidation and corrosion resistance necessary for higher service temperatures. The chromium must then be balanced by other solutes to avoid an excessive fraction of δ-ferrite. The net solute content then becomes so large that the steels cannot transform to bainite and hence the martensitic microstructure. This is illustrated by the time–temperature transformation diagrams for 2.3, 4.3 and 9.3 wt% chromium steels shown in Fig. 12.26.

It could be argued that a martensitic microstructure, which has a large number density of defects, encourages the precipitation of more numerous and finer carbide particles which are better at resisting creep. Figure 12.27 shows a comparison between bainite and martensite in the same steel; whereas the kinetics of precipitation are not identical in the two cases, the differences are very small over the temperature range of interest (500–650 °C). A martensitic microstructure is not therefore necessary in heat-resistant steels; bainite is adequate.

To summarise, the modern trend towards martensitic creep-resistant steels is associated more with the need to improve the environmental resistance of the alloys rather than microstructural considerations. Indeed, there are well known disadvantages to high hardenability martensitic steels when it comes to weldability.

12.9.9 Transition Metal Joints

It is sometimes necessary in steam turbine assemblies to join the low-alloy ferritic steels to austenitic steels which are more suited for corrosive environments. The joints are usually between tubular elements although thicker joints

[13:38 3/9/01 C:/3B2 Templates/keith/3750 BAINITE.605/3750-012.3d] Ref: 0000 Auth: Title: Chapter 00 Page: 334 285-342

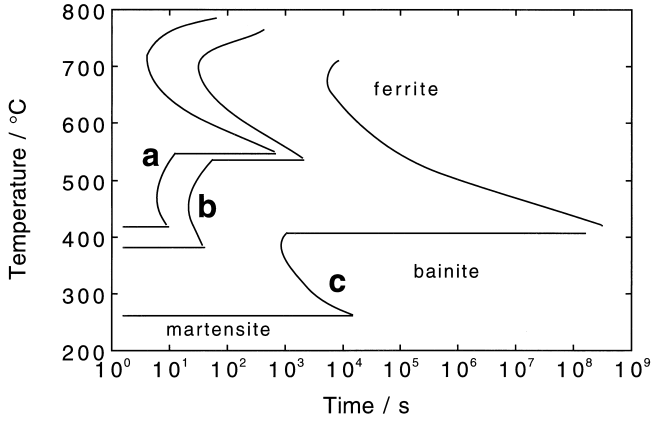

Fig. 12.26 Calculated time-temperature transformation diagrams for steels **x** (0.15C–0.25Si–0.5Mn–1Mo–2.3Cr wt%), **y** (4.3Cr) and **z** (9.3Cr). The transformation curves refer to zero percent reaction. In each case the upper curve represents diffusional transformation whereas the lower curve represents bainite. After Bhadeshia (2000).

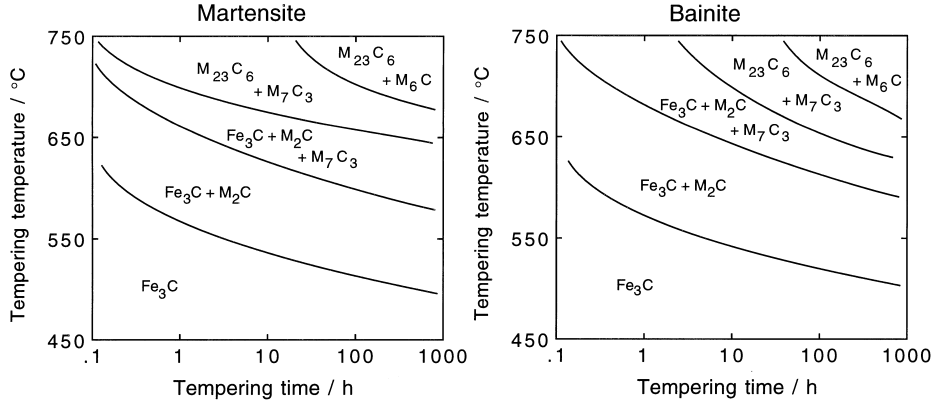

Fig. 12.27 Measured isothermal transformation diagrams for carbide precipitation reactions in $2\frac{1}{4}$Cr1Mo steel: (a) martensitic starting microstructure; (b) bainitic starting microstructure. Adapted from Baker and Nutting (1959).

are occasionally needed. The welds between these dissimilar steels are made using a filler material which is either an austenitic stainless steel, or a nickel-base alloy such as 'Inconel'. The filler material/ferritic steel interface is quite abrupt when the nickel-base filler is used, even though a true metallurgical bond is achieved.

The ferritic steel is usually the $2\frac{1}{4}$Cr1Mo alloy. The chances of a dissimilar metal joint failing during service are large when compared with other welds between like metals. Nath (1982) has suggested that this is because of the complex stresses arising from the different creep properties of the filler, the HAZ and the ferritic base plate. The stresses are such as to intensify creep damage in the vicinity of the weld/base-plate junction.

The microstructure of $2\frac{1}{4}$Cr1Mo is essentially bainite, but after welding, that of the heat-affected zone can contain allotriomorphic ferrite. On the other hand, the coarser austenite grain structure in the HAZ adjacent to the fusion boundary has a higher hardenability and hence transforms into bainite. The allotriomorphic ferrite-containing region which is weak in creep, and is located sandwiched between two stronger regions, the original plate microstructure far away from the weld and the bainite at the fusion boundary. Furthermore, the austenitic (or Inconel) filler material is relatively rigid. This focus-ses the strain in the ferrite, causing the transition joints to fail prematurely. The joints are sometimes heat treated at 700 °C for 30 minutes after welding for stress-relief, but this does lead to a homogenisation of mechanical properties.

Nath (1984) attempted to overcome these problems by reheating the entire welded joint into the austenite phase field at 950 °C for 1 h, followed by air cooling, with the aim of regenerating a fully bainitic microstructure throughout the parent material, including the heat-affected zone. The treatment was successful in improving the creep properties, but the overall performance was still less than that of the unwelded steel. The austenitising heat treatment caused the migration of carbon, which in the case of the ferritic/austenitic joint caused a decarburised zone on the ferrite side of the dissimilar metal interface and a carbon-enriched zone in the austenite on the other side. The carbon migration is driven by the chemical potential gradient resulting from the different chemical compositions of the ferritic and austenitic steels.

12.10 Reduced-Activation Steels

The formation of voids during irradiation with neutrons causes the swelling of metals. Irradiation damage involves the creation of both interstitials and vacancies in equal concentrations, but the former anneal out more rapidly than the latter. The resulting excess concentration of vacancies is relieved by condensation into voids.

Ferrite has a much higher resistance to void swelling than austenite, although nickel base alloys rank alongside the ferritic steels (Little, 1991). Point defects introduced by irradiation condense at *neutral* or *biassed* sinks. The latter are typically dislocations with large Burgers vectors, attracting more interstitials than vacancies. It follows that a large density of neutral sinks enhances the swelling resistance.

It is believed that in ferritic steels, irradiation induces the formation of two kinds of dislocations, one of which is strongly biased whereas the other is neutral. This provides sinks for both interstitials and vacancies, resulting in a smaller excess of void-forming vacancies. There are differences in the void swelling resistance of creep-resistant ferritic steels because of variations in their microstructures. For a given vacancy concentration, a larger number density of vacancy traps leads to a smaller tendency for swelling. Lath boundaries or oxide particles are good vacancy traps.

It is for their swelling resistance that ferritic steels have been considered for structural applications in the construction of the first wall and blanket structures of fusion reactors. But in addition, there is a search for specific alloys whose radioactivity decays most rapidly once they are removed from the radioactive environment. These are the so-called *reduced activation* alloys which have minimal concentrations of Mo, Ni, Nb, Cu and nitrogen, all of which have long-lived radioactive isotopes (Abe *et al*., 1990; Klueh *et al*., 1995). Some of these elements are key constituents of creep-resistant steels, but can be eliminated by using tungsten instead of molybdenum and by substituting vanadium and tantalum for niobium. Some examples of steels which have been studied specifically for their reduced activation are listed in Table 12.4.

Table 12.4 Chemical compositions (wt%) of reduced activation steels (Klueh *et al*., 1995). All of these steels are bainitic with the exception of the 9Cr and 12Cr steels which are martensitic. The chemical compositions of the first group of steels are nominal.

Steel	C	Si	Mn	Cr	V	W	Ta	B
$2\frac{1}{2}$Cr–V	0.1			2.25	0.25			
$2\frac{1}{4}$Cr–1WV	0.1			2.25	0.25	1		
$2\frac{1}{4}$Cr–2W	0.1			2.25		2		
$2\frac{1}{4}$Cr–2WV	0.1			2.25	0.25	2		
Cr–2WV	0.1			5	0.25	2		
9Cr–2WV	0.1			9	0.25	2		
9Cr–2WVTa	0.1			9	0.25	2	0.07	
12Cr–2WV	0.1			12	0.25	2		
$2\frac{1}{4}$Cr–2WVTa	0.1	0.12	0.40	2.41	0.24	2.03	0.05	
$2\frac{1}{4}$Cr–2WVTB	0.090	0.12	0.38	2.37	0.24	2.04		0.005
$2\frac{1}{4}$Cr–2WVTaB	0.093	0.12	0.38	2.36	0.24	2.04	0.05	0.005
2.6Cr–2WVTa	0.11	0.11	0.39	2.59	0.25	2.02	0.05	
2.6Cr–2WVTaB	0.11	0.11	0.39	2.60	0.25	2.07	0.05	0.004
$2\frac{1}{2}$Cr–2W	0.11	0.15	0.39	2.48		1.99		
$2\frac{1}{4}$Cr–2WV	0.11	0.20	0.42	2.41	0.24	1.98		
9Cr–2WVTa	0.10	0.23	0.43	8.72	0.23	2.09	0.07	

Early studies revealed that of the first group of steels listed in Table 12.4, the 9Cr–2WVTa alloy in its martensitic condition has a high strength, good toughness and is able to retain its impact properties after irradiation (Fig. 12.28). On the other hand, the low-chromium bainitic steels do not require a post-weld heat treatment which can be difficult to implement in complex fabricated structures.

Although the high Cr steels show only modest shifts in the ductile-brittle transition temperature following irradiation (Fig. 12.28), difficulties arise when the displacement damage is accompanied by the production of helium by the transmutation of traces of nickel. The helium is insoluble in the matrix and precipitates as small bubbles which embrittle the material. Suppose that the bubble has a radius r, then for an ideal gas the pressure inside the bubble is $P = 2\sigma/r$ where σ is the interface energy per unit area. A small bubble can therefore hold a lot more gas under high-pressure than a large bubble. Typically, a 100 Å bubble holds gas at a pressure of 10^3 atmospheres whereas the pressure is only 1 atmosphere in a bubble which is 10^5 Å in size. Swelling can obviously be minimised by increasing the number density of bubble nucleation sites (Thompson, 1969). Carbide particles are bubble nucleation sites but the high chromium steels form coarse $M_{23}C_6$ particles in contrast to the larger numbers of fine MC or M_2C particles in the lower chromium alloys,

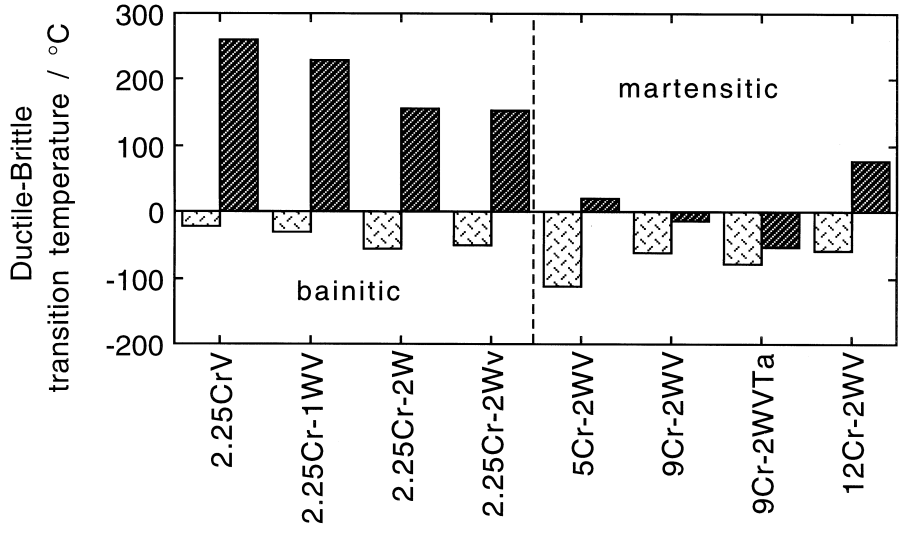

Fig. 12.28 The ductile–brittle transition temperature for normalised and tempered 3 mm diameter bar samples which have been irradiated to about 14 dpa. The 12Cr steel contains some δ-ferrite in addition to martensite. Some of the bainitic steels may also contain allotriomorphic ferrite. After Klueh and Alexander (1999).

making the latter more suitable for fusion reactor applications. On the other hand, the microstructures of the bainitic steels are much more sensitive to the cooling rate from the austenitic condition. Care has to be taken to ensure that the required fine distribution of carbides is obtained in practice.

Some of the steels listed in Table 12.4 are designed with low chromium concentrations to enhance the impact toughness in the irradiated condition. Klueh and co-workers found that the hardenability could be increased with a slight increase in the chromium concentration supported by additions of B and Ta; this resulted in a refined bainitic microstructure with improved toughness and tempering resistance. Indeed, the 2.6Cr–2WVTaB alloy is found to have mechanical properties comparable to those of the best 9Cr steels.

A fine distribution of carbides promotes toughness whether or not the steel is irradiated. The iron carbides which form in the early stages of tempering can be refined by increasing the silicon or aluminium concentration. It is these carbides which set the scene for the subsequent formation of alloy carbides, so there should be a consequential refinement of the entire carbide microstructure. This idea would be worth exploring in the context of reduced-activation steels.

12.11 Steels with Mixed Microstructures

Mixed microstructures consisting of bainite and martensite are usually a consequence of inadequate heat-treatment or the use of steels with insufficient martensitic hardenability.

Early research suggested that bainite in an otherwise martensitic microstructure leads to a deterioration in ductility, toughness and strength (Bailey, 1954; Hehemann *et al*., 1957). The impairment of properties becomes less severe as the bainite forms at lower transformation temperatures, and is related to the difference in strength between martensite and bainite. As this difference decreases, so does the reduction in properties (Hehemann *et al*., 1957).

Tempering homogenises the strength so bainite in a tempered martensite microstructure has less of an effect on the overall properties (Triano and Klinger, 1952; Hehemann *et al*., 1957). For the same reason, a mixture of martensite and lower bainite has better properties than one consisting of upper bainite and martensite. The strength of lower bainite more closely matches that of martensite.

There are, however, circumstances in which mixed microstructures are beneficial. Edwards (1969) observed that after tempering, mixtures of lower bainite and martensite were tougher than either martensite or bainite. There are considerable recent data that following tempering, the presence of bainite in a predominantly martensitic microstructure leads to a higher strength and toughness relative to the single phase samples, Fig. 12.29 (Tomita and

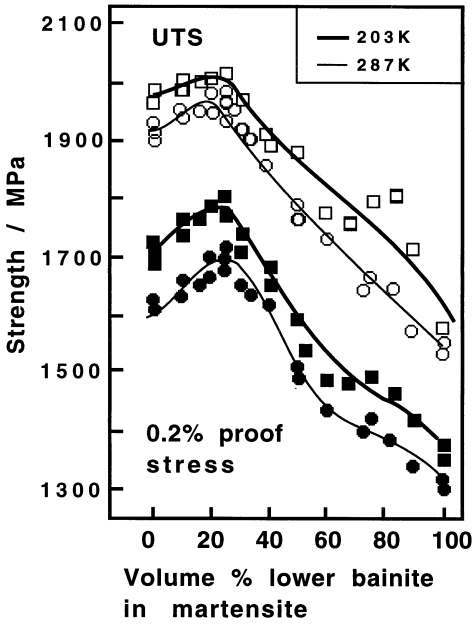

Fig. 12.29 Variation in the 0.2% proof stress as a function of the volume fraction of lower bainite in a mixed, tempered microstructure of lower bainite and martensite. The different curves represent data collected at the temperatures indicated on the diagram.

Okabayashi, 1983a,b 1985a,b, 1987, 1988; Tomita, 1991, 2000). This is because the bainite partitions the austenite, thus refining the size of the martensite packets that form subsequently (Mutui *et al.*, 1977). The refined martensite is stronger, and furthermore, the strength of the bainite is increased by constraint from the strong martensite. But a further point that should be taken into account is that the martensite grows from austenite which is enriched in carbon due to the bainite transformation; it will therefore be expected to be harder.

It is particularly interesting that the strength of a tempered mixture of lower bainite and martensite can exceed that of the martensite alone, and yet can be tougher (Fig. 12.30).

12.12 Summary

The anisotropic, thin-plate shape of bainite ensures that the mean free path for slip is comparable to the plate thickness rather than to the plate length. This means that the major microstructural contribution to strength is via the fine sub-unit size, rather than the sheaf or austenite grain size which are of minor

[13:38 3/9/01 C:/3B2 Templates/keith/3750 BAINITE.605/3750-012.3d] Ref: 0000 Auth: Title: Chapter 00 Page: 340 285-342

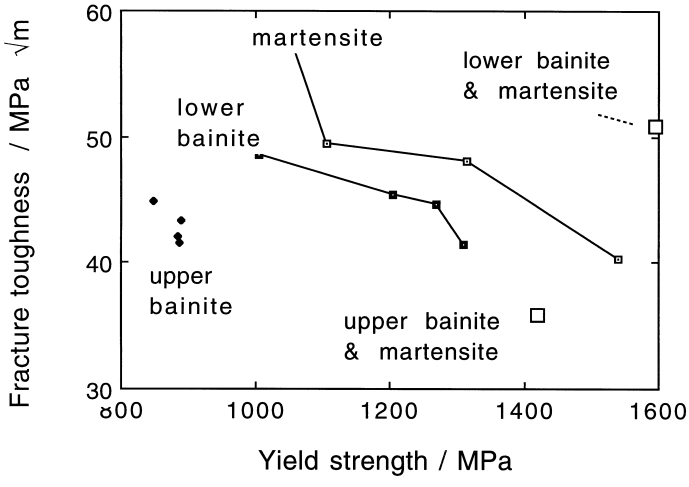

Fig. 12.30 Plot of toughness versus strength for a variety of microstructures in an ultra-high strength steel (data from Tomita, 1988).

importance as far as the strength is concerned. The sub-unit size is so small, that the Hall–Petch relation does not apply; yield is instead controlled by the stress required to expand dislocation loops. This gives a linear relationship between the yield strength and the inverse of the sub-unit size.

Bainitic steels usually exhibit continuous yielding behaviour, with proof stress to UTS ratios which can be much smaller than 0.8. This gradual yielding is a consequence of mobile dislocations, the presence of heterogeneities in the microstructure and residual stresses due to transformation. The ratio can be increased by annealing at low temperatures, although there is not much of a change if the bainite transformation temperature is comparable to the annealing temperature.

There is no doubt that higher carbon concentrations lead to a deterioration of ductility, primarily because of the void nucleating tendency of cementite particles. The presence of large regions of untempered martensite in the microstructure can reduce ductility, whereas retained austenite can in some circumstances enhance it.

The impact toughness of upper bainite deteriorates as its strength increases, but that of lower bainite which has much finer carbides is superior at the same strength level. An interpretation in terms of fracture toughness theory has demonstrated that it is the coarsest carbides in the microstructure which control toughness. Consistent with theory, the fracture strength correlates directly with the reciprocal of the square root of the coarsest carbide size. The scatter in toughness data increases as the microstructure becomes more heterogeneous;

[13:38 3/9/01 C:/3B2 Templates/keith/3750 BAINITE.605/3750-012.3d] Ref: 0000 Auth: Title: Chapter 00 Page: 341 285-342

mixed microstructures of bainite and martensite show greater scatter than fully bainitic samples. During fracture, the cleavage facet dimensions are found to be comparable to those of bainite packets. A refinement of the austenite grain size also reduces the packet size, and consequently leads to an improvement in toughness. All of the impurity controlled temper embrittlement phenomena normally associated with martensite, are found in bainitic steels.

The endurance limit during the fatigue testing of smooth samples correlates well with the UTS of bainitic steels. The threshold stress intensity range for fatigue crack growth is reduced by the presence of retained austenite, because its transformation to martensite prevents the reversal of plastic strain during cyclic deformation. Stable austenite on the whole leads to an improvement in fatigue properties via the ductility it confers to the microstructure.

Retained austenite can lead to an improvement in the stress corrosion cracking resistance, by hindering the diffusion of hydrogen. However, comparable benefits can be achieved by any method which increases the number density of hydrogen traps in the microstructure.

Creep-resistant alloys containing strong carbide-forming elements represent one of the most successful industrial applications of bainitic microstructures. They achieve their creep strength via solid solution strengthening and with the help of fine dispersions of alloy carbides. The most modern of these steels is such that it can be welded without the need for post-weld heat treatments.

Finally, there are now considerable data to suggest that mixed microstructures of bainite and martensite can offer higher strength and toughness than fully martensitic alloys. The mechanism behind this remains to be established.

[13:38 3/9/01 C:/3B2 Templates/keith/3750 BAINITE.605/3750-012.3d] Ref: 0000 Auth: Title: Chapter 00 Page: 342 285-342

13 *Modern Bainitic Steels*

Steels with yield strengths in excess of 1000 MPa are important in certain applications, but the biggest commercial markets are for lower strength varieties, where the total alloy content rarely exceeds 2 wt%. The alloy design therefore has to be careful with a proper balance of hardenability in the context of large scale steel production technologies. Lean steels tend to transform into mixtures of allotriomorphic ferrite and bainite, whereas any attempt to improve hardenability usually leads to partly martensitic microstructures. The solution therefore lies in low-alloy, low-carbon steels, containing small amounts of boron and molybdenum to suppress allotriomorphic ferrite formation, principles established originally by Irvine and Pickering. Boron increases the bainitic hardenability. Other solute additions can, in the presence of boron, be kept at sufficiently low concentrations to avoid the formation of martensite. Steels like these (Alloy 1, Table 13.1), when normalised, are found to transform almost completely into bainite with only small fractions of martensite or other residual phases.

The other alloys listed in Table 13.1 are examples of some of the latest commercial bainitic steels. A striking feature of the list is that they don't look particularly different in chemical composition. This impression is misleading because each steel has distinct mechanical properties. Trace element concentrations are vital in determining the details of the microstructure as are the thermomechanical processing routes used in their manufacture.

Any alloy development or 'advanced material' needs to be considered in the context of what already exists. For this reason, we first discuss the incredibly successful ferrite–pearlite microalloyed steels which set the standard by which any new alloy system must be assessed.

13.1 Alternatives to the Ferrite–Pearlite Microstructure

The most popular microstructure in the context of structural steels has undoubtedly been a mixture of ferrite and pearlite. There are hundreds of millions of tonnes of this manufactured annually. Typical chemical compositions are given in Table 13.2 together with an indication of the usual mechanical properties. Figure 13.1 shows that the main effect of microalloying and the associated thermomechanical processing is to refine the microstructure. The

[13:39 3/9/01 C:/3B2 Templates/keith/3750 BAINITE.605/3750-013.3d] Ref: 0000 Auth: Title: Chapter 00 Page: 343 343-396

Table 13.1 Typical compositions of advanced bainitic steels (wt%). Notice that the steels are fairly similar in composition with respect to the major alloying additions, although there are significant differences with respect to carbon and trace element concentrations. The fabrication procedure is also of vital importance in giving a large variation in properties in spite of the similarities of chemical composition. In the inoculated steels, the titanium oxide-bearing steel is the most effective.

No.	C	Si	Mn	Ni	Mo	Cr	Nb	Ti	B	Al	N	Others	Steel Type
1	0.100	0.25	0.50	–	0.55	–	–	–	0.0030	–	–	–	Early bainitic
2	0.039	0.20	1.55	0.20	–	–	0.042	0.015	0.0013	0.024	0.0030	–	Rapidly cooled bainitic
3	0.081	0.25	1.86	0.20	0.09	–	0.045	0.016	–	0.025	0.0028	–	Rapidly cooled bainitic
4	0.110	0.34	1.51	–	–	–	0.029	–	–	–	–	–	Rapidly cooled bainitic
5	0.100	0.25	1.00	–	–	–	–	–	–	–	–	–	Bainitic dual phase
6	0.040	–	0.40	–	–	–	–	–	–	0.05	–	–	Triple phase
7	0.150	0.35	1.40	–	–	–	0.022	0.011	–	0.035	–	–	Bainitic dual phase
8	0.120	1.50	1.50	–	–	–	–	–	–	0.045	0.0035	–	TRIP-assisted
9	0.020	0.20	2.00	0.30	0.30	–	0.050	0.020	0.0010	–	0.0025	–	ULCB
10	0.028	0.25	1.75	0.20	–	0.30	0.100	0.015	–	0.030	0.0035	Cu 0.3, Ca 0.004	ULCB
11	0.080	0.20	1.40	–	–	–	–	0.012	–	0.002	0.0020	O 0.0017	acicular ferrite, TiO_x
12	0.080	0.20	1.40	–	–	–	–	0.008	0.0015	0.038	0.0028	–	acicular ferrite, TiB
13	0.080	0.20	1.40	–	–	–	–	0.019	–	0.018	0.0050	–	acicular ferrite, TiN
14	0.15	0.80	1.40	–	0.20	–	–	–	–	–	–	V 0.15	Forging (high strength)
15	0.09	0.25	1.00	0.50	1.00	–	0.10	0.02	0.002	0.04	0.006	–	Forging (100% bainitic)
16	0.09	0.40	1.40	–	–	–	0.07	–	–	0.04	0.010	V 0.06	Forging (Nb + V)
17	0.09	0.25	1.40	–	–	–	0.07	0.02	0.002	0.04	0.006	–	Forging (Nb + B)
18	0.012	–	1.60	–	–	–	0.08	–	0.004	–	–	–	Cold-heading

Table 13.2 Typical ferrite–pearlite structural steels in both the standard and niobium microalloyed conditions.

Type	Composition, wt.%				Stress, MPa				
	C	Si	Mn	Nb	σ_y^l	σ_y^u	UTS	Elongation %	C_V (−20 °C), J
Standard	0.11	0.21	1.24		285	320	480	36	55–90
Microalloyed	0.11	0.30	1.40	0.034	395	430	525	32	100–190

Type	Ferrite %	Pearlite %	Ferrite grain size	Pearlite interlammellar spacing
Standard	76	24	15 μm	0.22 μm
Microalloyed	78	22	9 μm	0.22 μm

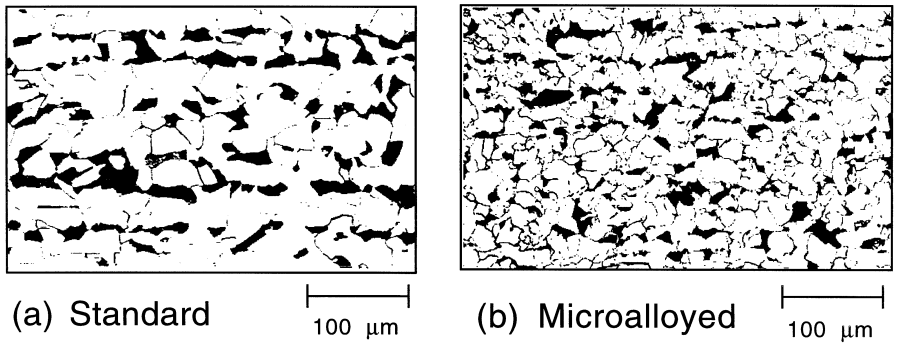

Fig. 13.1 Optical micrographs of banded ferrite–pearlite microstructures in (a) standard, (b) niobium microalloyed structural steel.

niobium carbonitrides that form also strengthen the ferrite by interphase precipitation or by strain-induced precipitation (Pickering, 1978, 1992; Honeycombe and Bhadeshia, 1995; Gladman, 1997).

Some of the major applications of structural steels include: oil and gas pipelines ($\sigma_y = 350$–485 MPa), drilling rigs and production platforms (345–415 MPa), ships (315–450 MPa), pressure vessels and tubing, earth-moving equipment (345–550 MPa), heavy goods vehicles and automobile components, high-rise buildings (415–530 MPa), bridges (345–485 MPa), transmission towers, fuel and other storage tanks and reinforcement bars for concrete (Pickering, 1992; Bodnar *et al*., 1997). A few of the attributes that are consistent with these applications include the low cost, ability to produce a variety of forms, weldability, fabricability, reliability under extreme conditions (such as fire and earthquakes and other *force majeures*).

It seems unlikely in this context that the dominant position of the ferrite–pearlite steels will ever be challenged by alternative steel microstructures, let alone other materials! Nevertheless, we shall describe rivals based on bainite because such steels can be produced using a similar production route and without any additional heat treatments.

13.2 Strength

Strength is a basic engineering specification; steels can be made stronger by transforming the austenite at ever decreasing temperatures (Fig. 12.4) or by increasing hardenability. There are many other strengthening mechanisms available. Unfortunately, toughness does not necessarily increase with strength. The weldability may also deteriorate because the excessive use of alloying elements can cause the formation of untempered hard-phases in the austenitised regions of the heat-affected zone or there may be excessive softening in the tempered regions of the HAZ.

[13:39 3/9/01 C:/3B2 Templates/keith/3750 BAINITE.605/3750-013.3d] Ref: 0000 Auth: Title: Chapter 00 Page: 345 343-396

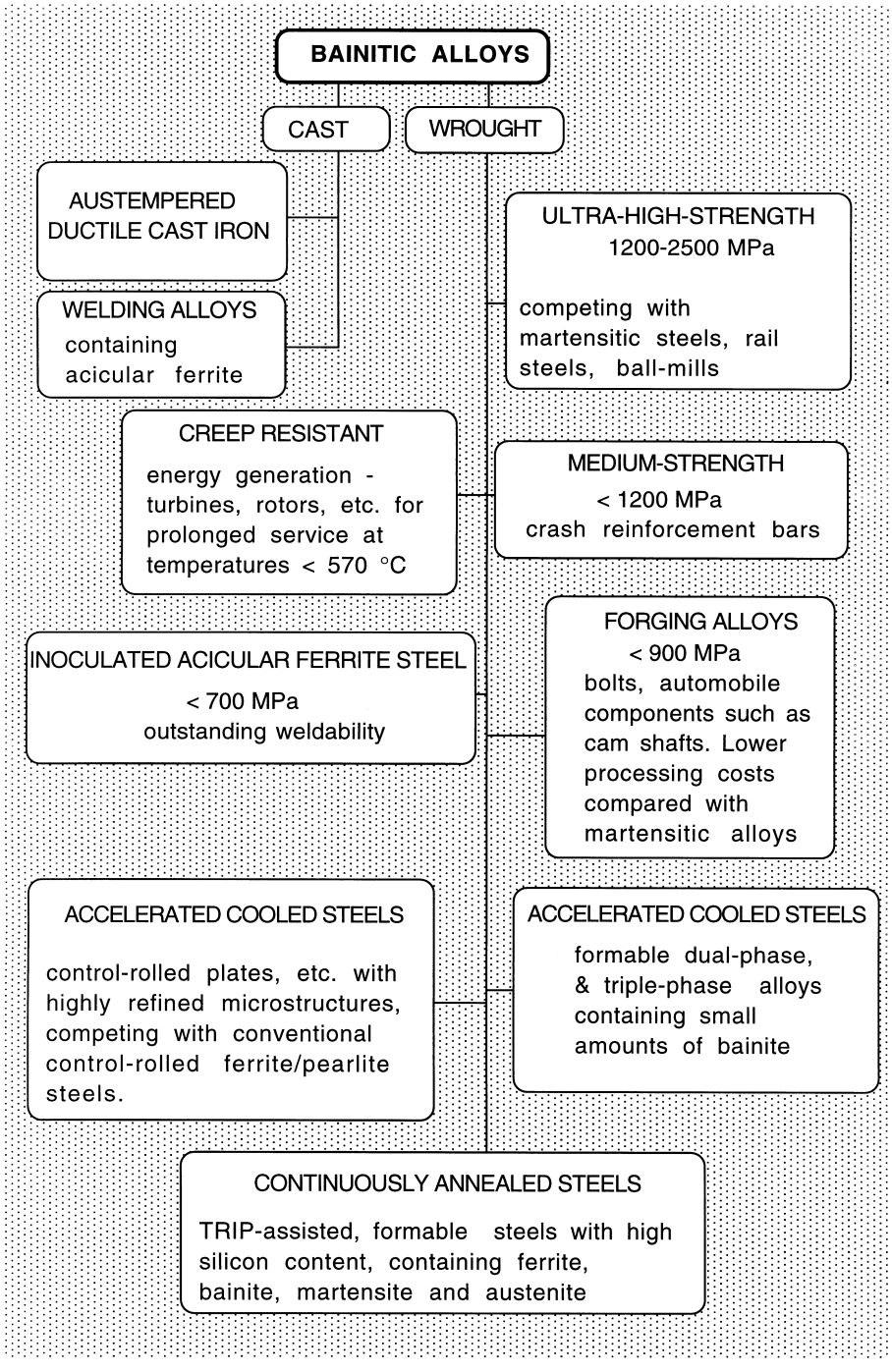

Fig. 13.2 The range of bainitic steels currently available on a commercial basis. *TRIP* stands for transformation-induced plasticity.

The tendency to soften depends on how far the original microstructure deviates from equilibrium (Table 13.3). Large deviations naturally lead to greater rates of softening because the driving force for tempering is the energy stored within the material; the heat simply provides the thermal activation needed to bump the structure to lower energies. Higher strength steels are therefore more likely to be difficult to weld.

13.3 Bainitic Steels

It is evident that ferrite/pearlite steels are outstanding on any performance criterion which includes cost and reliability. They will certainly not be threatened by the alternative microstructures to be discussed here. On the other hand, the novel microstructures offer a better set of properties for high performance applications where their additional cost is not an issue.

The steels developed by Irvine and Pickering exhibited quite reasonable combinations of toughness and strength, but in time proved to fall short of the best quenched and tempered martensitic steels. Nevertheless, the physical metallurgy principles established during their development have been applied in the metallurgical design of a new generation of bainitic steels, in which the emphasis is on reductions in carbon and other alloying element concentrations, and on processing designed to refine the microstructure. We now proceed to describe developments in these high-technology steels and cast irons based on bainitic microstructures. Many of the lower alloy content steels are thermomechanically processed prior to their transformation so it is appropriate to begin

Table 13.3 The stored energy as a function of microstructure, relative to the equilibrium state defined as a mixture of ferrite, cementite and graphite (Bhadeshia, 1998). The phases in cases 1 and 2 involve a partitioning of all elements so as to minimise free energy. In cases 3–5 the iron and substitutional solute are configurationally frozen (for martensite even the interstitial elements are frozen). Case 6 refers to an iron-base mechanically alloyed oxide-dispersion strengthened (ODS) sample which has the highest reported stored energy prior to recrystallisation (Bhadeshia, 1997)

Phase Mixture in Fe–0.2C–1.5Mn wt% at 300 K	Stored Energy, J mol^{-1}
1. Ferrite, graphite & cementite	0
2. Ferrite & cementite	70
3. Paraequilibrium ferrite & paraequilibrium cementite	385
4. Bainite and paraequilibrium cementite	785
5. Martensite	1214
6. Mechanically alloyed ODS metal	55

[13:39 3/9/01 C:/3B2 Templates/keith/3750 BAINITE.605/3750-013.3d] Ref: 0000 Auth: Title: Chapter 00 Page: 347 343-396

with a description of the key industrial processes in the context of bainite. The range of bainitic alloys currently in use is summarised in Fig. 13.2; the inoculated acicular ferrite steels have already been dealt with in Chapter 10.

13.4 Controlled-Rolling of Bainitic Steels

The strengthening of iron via a reduction in grain size is an attractive option because a small grain size leads also to an improvement in toughness. This simple fact has led to the development of impressive thermomechanical processing technology capable of refining the austenite grain structure prior to its transformation to ferrite (Fig. 13.3). A fine austenite grain size leads to a correspondingly refined ferrite grain structure. The *controlled-rolling* process

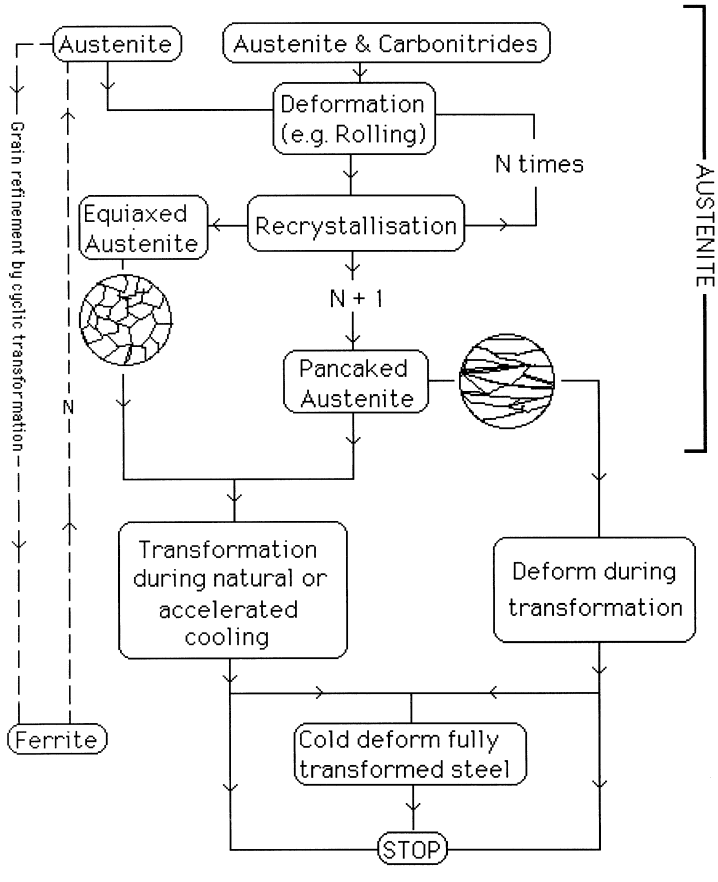

Fig. 13.3 Flow chart illustrating some of the thermomechanical processing routes available for the manufacture of steels.

involves a sophisticated rolling deformation of austenite. The subject has been reviewed by Speich *et al*. 1984), where the complex procedures and the variety of rolling and alloying practices are discussed in detail. The essence of the process is the reduction of ingots by hot-rolling in the austenite phase field, such that the austenite is induced to recrystallise many times before the finish-rolling temperature is reached. This gives a fine recrystallised austenite grain structure. The growth of these grains during the hot-rolling process is hindered by the use of microalloying additions such as niobium or titanium. These elements are added in small concentrations ($\simeq 0.01$–0.03 wt%) to form stable carbides or carbonitrides which impede austenite grain growth. As will be seen later, it can be an advantage if the austenite grains are pancaked (flattened) because such grains transform into finer ferrite. A typical chemical composition of a steel suitable for control-rolling into a ferritic microstructure is Fe–0.08C–0.3Si–1Mn–0.03Nb–0.004N wt%.

Controlled-rolling has been used successfully for over 40 years to produce steels with a ferrite and pearlite microstructure; it has since been adapted for bainitic alloys (Nakasugi *et al*., 1980, 1983). There are two ways in which a bainitic microstructure can be obtained: the first involves an increase in the cooling rate in order to allow the austenite to supercool into the bainite transformation range. The second is to modify the steel hardenability without substantially changing the processing conditions. Alloying elements such as manganese are boosted in order to retard the formation of allotriomorphic ferrite relative to bainite. Unlike conventional steels for control-rolling, TiN particles (of size $\simeq 0.02\,\mu$m) are induced to precipitate during solidification and subsequent cooling to ambient temperature. The precipitation of fine TiN is stimulated by increasing the cooling rate of the molten steel during continuous casting. Slabs of the material are then reheated to a low austenitisation temperature of 1150 °C, the TiN particles inhibiting austenite grain growth. The grain size is reduced during repeated recrystallisation due to control-rolling. By inhibiting grain growth, the particles also help to produce a uniform grain structure than is obtained in conventional processes. Finish rolling is carried out at a temperature where recrystallisation does not occur within the time scale of the rolling sequence; the austenite grains are therefore pancaked and have a deformed microstructure just before they start to transform into bainite.

The details of the steelmaking process are important in determining the final properties of control-rolled steels. The higher quality steels are dephosphorised, desulphurised and vacuum degassed prior to casting. Typical concentrations of phosphorous and sulphur after these treatments are 0.015 and 0.0015 wt% respectively. In circumstances where formability and uniform ductility are important, the steel is usually treated with calcium which has the effect of fixing sulphur and of modifying the shape of the sulphide inclusions.

[13:39 3/9/01 C:/3B2 Templates/keith/3750 BAINITE.605/3750-013.3d] Ref: 0000 Auth: Title: Chapter 00 Page: 349 343-396

13.4.1 Crystallographic Texture

Polycrystalline materials do not in general contain grains which are randomly oriented. The crystals tend to align along particular orientations determined by the thermomechanical history of the material. This alignment is called *crystallographic texture* and its most important manifestation is in the development of anisotropic mechanical properties. The anisotropy may be exploited, as in deep-drawing steels where the texture is optimised to reduce plastic strain in the thickness direction. It can, on the other hand, be detrimental if the cleavage planes show a tendency to align because the fracture path becomes continuous across many grains.

In wrought steels, it is deformation, recrystallisation or phase transformation which can cause crystallographic texture. All of these processes occur during control-rolling. There are excellent reviews on the subject (Tanaka, 1981; Ray and Jonas, 1990), but the purpose here is to highlight the differences of crystallographic texture which arise between conventional and bainitic control-rolled steels.

A convenient (though incomplete) way of representing the texture in rolled sheet is by stating the set $\{h\,k\,l\} < u\,v\,w >$, where $\{h\,k\,l\}$ are the Miller indices of the planes which lie roughly parallel to the rolling plane, and $< u\,v\,w >$ the Miller indices of the direction in $\{h\,k\,l\}$, which tends to be parallel to the rolling direction. The texture can sometimes be deconvoluted into components:

$$\text{texture} = \sum_i \lambda_i \{h\,k\,l\}_i < u\,v\,w >_i \qquad (13.1)$$

where λ represents the weighting given to a particular type of texture. The major components of the deformation texture of austenite are $\{1\,1\,0\} < 1\,\overline{1}\,2 >$ and $\{1\,1\,2\} < 1\,1\,\overline{1} >$, the so-called *brass* and *copper* textures respectively.

Because ferrite has an orientation relationship with the austenite, the brass texture gives rise to a $\{3\,3\,2\} < 1\,1\,\overline{3} >$ ferrite texture, and the copper texture to a $\{1\,1\,3\} < 1\,\overline{1}\,0 >$ ferrite component (Fig. 13.4). It is found experimentally that the $\{3\,3\,2\} < 1\,1\,\overline{3} >$ ferrite texture is beneficial to the deep drawing qualities of steels and for strength and toughness. Control-rolling should therefore aim to maximise the brass texture component of austenite.

The texture of steel obtained from recrystallised austenite is made up predominantly of $\{1\,0\,0\} < 0\,1\,1 >$ ferrite, originating from the $\{1\,0\,0\} < 0\,0\,1 >$ *cube* recrystallisation texture of the parent austenite. This variety of ferrite texture can in principle be detrimental to the through thickness mechanical properties of rolled steels, since the $\{1\,0\,0\}$ ferrite cleavage planes tend to align with the rolling plane. The fraction of $\{1\,0\,0\}$ normals within 10° of the plate normal tends to increase as the finish rolling temperature decreases, but there does not appear to be any systematic correlation with measures of toughness

[13:39 3/9/01 C:/3B2 Templates/keith/3750 BAINITE.605/3750-013.3d] Ref: 0000 Auth: Title: Chapter 00 Page: 350 343-396

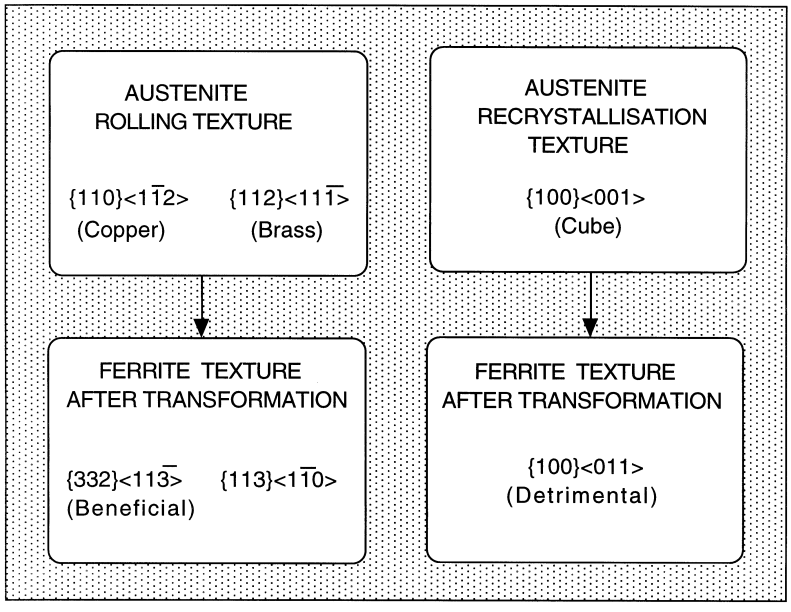

Fig. 13.4 Summary of crystallographic texture phenomena in wrought steels (adapted from Ray and Jonas, 1990).

(Davies *et al*., 1977). It is possible that the texture is not uniform on a local scale. In fact, the cleavage process itself is not well defined for fine microstructures such as bainite, where the mode of brittle fracture is more accurately described as *quasi-cleavage*. In this, the cleavage planes are frequently disrupted by fibrous fracture at finely spaced plate boundaries. The complete story is therefore likely to be more complex given that inclusions such as MnS also tend to align parallel to the rolling plane. Whatever the detailed explanation, both the texture and inclusions make it easier for the steel to delaminate parallel to the rolling plane. The texture enhances the toughness along the length and width directions at the expense of the through-thickness properties. It is important therefore to ensure that the austenite is in a deformed, rather than in its recrystallised state just before it begins to transform.

Transformation textures associated with martensitic or bainitic microstructures (or acicular ferrite) are much more pronounced when compared with the case where the austenite transforms into allotriomorphic ferrite (Fig. 13.5). It is however, difficult to gauge the significance of the observations as far as delamination is concerned. Although the texture increases in intensity when the austenite transforms by a displacive mechanism, all of the components are strengthened. Any deleterious influence of the $\{1\,0\,0\} < 0\,1\,1 >$ ferrite component may therefore be masked by stronger components, and

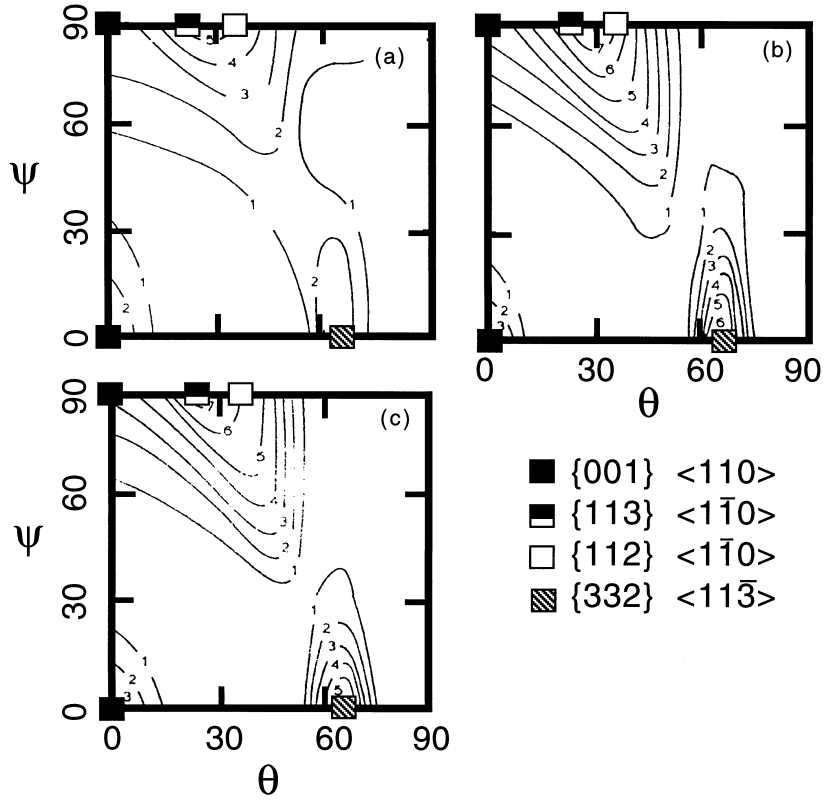

Fig. 13.5 Sections along $\phi = 45^\circ$ of the crystal orientation distribution functions showing transformation textures of control-rolled steels with a variety of microstructures (Yutori and Ogawa, 1979). For steels the most important features of the orientation distribution function are in the section of Euler space at $\phi = 45^\circ$ because it contains orientations of the form $\{1\,0\,0\} < u\,v\,w >$ and the fibre textures $\{h\,k\,l\} < 1\,1\,0 >$ and $\{1\,1\,1\} < u\,v\,w >$. (a) Allotriomorphic ferrite/pearlite; (b) acicular ferrite; (c) martensite. The points represent the exact textures indicated on the diagrams.

there do not seem to be any mechanical property data to indicate that bainitic steels which have been control-rolled have a greater propensity for delamination. Indeed, results to the contrary have been reported by Tamehiro *et al.* (1985b), who demonstrated that the delamination tendency is greater for conventional control-rolled steels, when compared with the more modern accelerated-cooled ferrite/bainite steels.

The observed differences in the strength of transformation textures are due to the displacive growth mechanisms of martensite, bainite and acicular ferrite;

the experimental data have been critically assessed by Ray and Jonas (1990). It appears to be a general result that when the transformation mechanism is reconstructive, all possible variants of the austenite/ferrite orientation relationship occur during transformation. There is therefore no *variant selection* during reconstructive transformations. On the other hand, attempts at predicting the product texture during displacive transformation, without assuming variant selection, have been unsuccessful in explaining experimental observations. The stresses and strains due to deformation favour the formation of particular variants in individual grains.

13.5 Rapidly Cooled Control-Rolled Steels

It was suggested in the previous section that bainitic microstructures can be generated in control-rolled steel either by increasing the hardenability or by changing the cooling rate during processing. The latter is the preferred route because the weldability deteriorates as the hardenability increases. The technology of rapid cooling during controlled-rolling is not trivial given the speed of production, the kinetics of transformation, the need to avoid distortion and nonuniform cooling. Progress has nevertheless been made and the rapidly cooled steels described here are commercially available. It is worth noting that rapidly cooled steels are often referred to as *accelerated cooled steels*.

Accelerated cooling plate mills are not essentially different from conventional rolling mills (Bodnar *et al.*, 1997). The distance from the finishing mill to the point where the plate can be removed from the mill can vary from 12–116 m. The cooling unit uses up to about 45 m of this distance with a variety of water and air systems to achieve a controlled cooling rate which can be as high as $100\,\mathrm{K\,s^{-1}}$ for a plate which is 10 mm thick.

13.5.1 Pipeline and Plate Steels

There is a demand for a reduction in the wall-thickness and an increase in the diameter of pipelines for gas transmission. Thinner walls permit faster and less troublesome girth-welding operations. Thinner sections can be achieved by increasing the strength of the steels used, as long as toughness and weldability are not sacrificed in the process. When thickness considerations are not paramount, an increase in strength has the further advantage that the gas can be transmitted more efficiently under increased pressure ($\simeq$ 10 MPa).

It is found that if, after thermomechanical processing, the steel is cooled at a rate which is high enough to reduce the amount of allotriomorphic ferrite, but

low enough to avoid martensite, then a fine-grained microstructure which is a mixture of allotriomorphic ferrite and bainite is obtained. Such a microstructure has the required higher yield strength and toughness. The cooling rates involved are larger (10–40 $^{\circ}C\,s^{-1}$ over the temperature range 800–500 $^{\circ}C$) than those appropriate for normal control-rolling (Fig. 13.6). The accelerated cooling is achieved using water spray curtains directed on either side of the hot plate such that distortion is avoided; the plates can be as thick as 15 mm. The rapid cooling of thicker plate requires different technology with careful control of water pouring and to cope with the slow rate at which the plate moves through the mill.

It has been demonstrated that the microstructure of these rapidly cooled steels consists of a mixture of ferrite and bainite (Graf *et al.*, 1985). The bainite consists of sheaves of platelets of submicron thickness with a large dislocation density of $1.7 \times 10^{14}\,m^{-2}$, compared with $0.4 \times 10^{14}\,m^{-2}$ in allotriomorphic ferrite. In fact, the dislocation density of the allotriomorphic ferrite in rapidly cooled steels is known to be about four times larger than in other steels containing ferrite, possibly because of plastic deformation caused by the formation of bainite (DeArdo, 1988). The volume fraction of bainite can vary from about $0.2 \rightarrow 1.0$ depending on the steel composition and cooling conditions. Typical compositions for accelerated-cooled alloys are given as Alloys 2–4 in Table 13.3. Of these, Alloy 2 is the leanest and can be expected to contain the smallest amount of bainite.

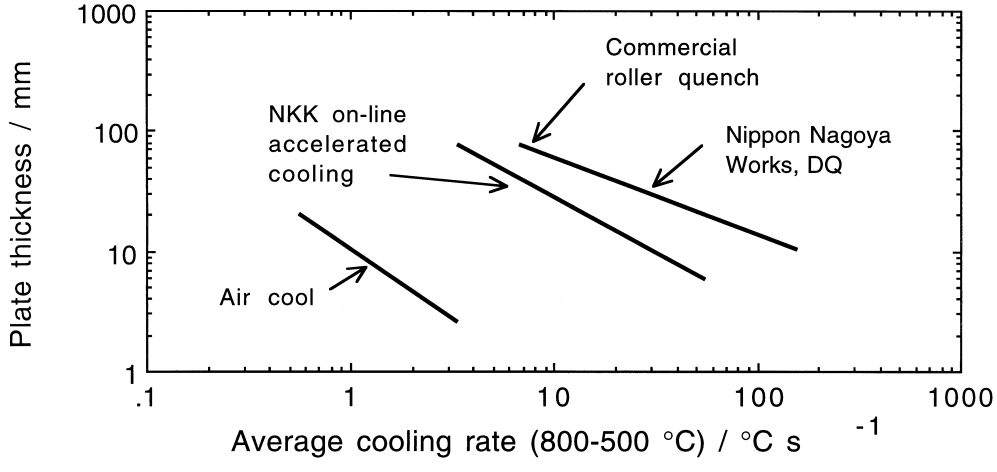

Fig. 13.6 An illustration of the average cooling rates associated with the manufacture of steels for structural applications (Gross *et al.*, 1995).

[13:39 3/9/01 C:/3B2 Templates/keith/3750 BAINITE.605/3750-013.3d] Ref: 0000 Auth: Title: Chapter 00 Page: 354 343-396

The production of the steels is not a continuous process of casting and control-rolling followed directly by accelerated cooling. Instead, cast ingots are first allowed to cool to ambient temperature and then reheated for the thermomechanical treatment. This ensures that the coarse austenite grain structure which evolves during ingot cooling is disrupted by transformation to ferrite. The processing involves the reheating of thick ingots to 1150 °C, followed by rolling during cooling of the ingot to 740 °C, with the total reduction in thickness being more than 600%, followed by accelerated cooling at 20 °C s^{-1} to around 450 °C before allowing natural cooling. This treatment alters the normal microstructure, which is a mixture of ferrite and pearlite, to one which consists of ferrite and bainite, resulting in a better combination of mechanical properties. The tensile strength achieved is typically 700 MPa which is about 50–70 MPa higher than that of conventional control-rolled steels; the Charpy impact toughness can be an impressive 160-200 J at −20 °C. The extra strength is attributed to the fine size of bainite plates, although Morikawa *et al*. (1985) have demonstrated that the strength of the allotriomorphic ferrite also increases with the accelerated cooling, probably because of the dislocation density increase described above. The steels show gradual yielding, although the relevance of this to pipeline applications is not clear (Collins *et al*., 1985).

13.5.2 Process Parameters

There are many processing variables which influence the properties of steel (Graf *et al*., 1985; Tamehiro *et al*., 1985a; Collins *et al*., 1985). For example, a high ingot reheating temperature allows more of the niobium carbonitrides to dissolve in the austenite; the niobium may subsequently precipitate during the $\gamma \rightarrow \alpha$ reaction to give fine dispersions of interphase precipitates within the ferrite, thereby increasing its strength.

The temperature at which the rolling operation finishes is critical because it should leave the austenite grains in an unrecrystallised, pancake shape. This not only helps refine the microstructure but also helps avoid the undesirable recrystallisation texture of austenite. If the finish rolling temperature is too low then transformation happens during deformation; the deformed ferrite then is stronger but less tough. The finish rolling temperature (T_R) also influences the variation in mechanical properties through the thickness of heavy gauge plates (Fig. 13.7). The surfaces, where the cooling rates are greatest, are harder compared with the central regions of the plates. The differences diminish as T_R is reduced because rolling deformation becomes focused at the plate surfaces, which then transform more rapidly, counteracting the effect of the higher surface cooling rates (Tanaka, 1988).

[13:39 3/9/01 C:/3B2 Templates/keith/3750 BAINITE.605/3750-013.3d] Ref: 0000 Auth: Title: Chapter 00 Page: 355 343-396

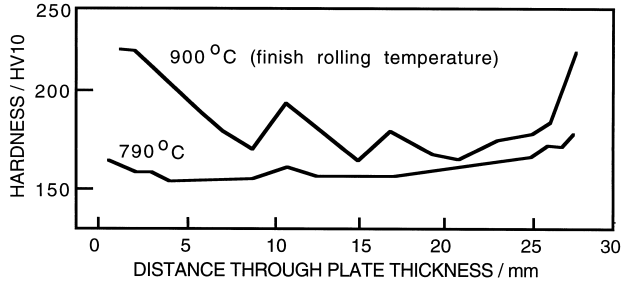

Fig. 13.7 The effect of the temperature at which rolling is completed, on the variation in hardness of a Fe–0.16C–0.63Mn wt% accelerated cooled steel (Tamukai *et al*., 1981).

Some of the steels processed using accelerated cooling have a high hardenability which introduces martensite into the microstructure with an accompanying reduction in toughness and increase in plate distortion. To avoid this, the cooling is arrested by cutting off the water sprays at temperatures between $600 \rightarrow 450\,^{\circ}\mathrm{C}$. This has the effect of permitting more bainite to form thus reducing the amount of martensite that can form.

Another related problem occurs in alloys with high hardenability, for example, those containing more than about 1.4 wt% manganese. Thermomechanical processing actually reduces the yield strength even though the tensile strength increases (Fig. 13.8a, Shiga *et al*., 1983; Amano *et al*., 1988). This is because martensite replaces bainite as the dominant hard phase so yielding becomes a gradual process, giving the reduction in the proof strength. Although this has clear advantages for applications involving forming operations, the lowering of yield strength is a disadvantage for pipeline and heavy plate fabrications where the design thickness is calculated using yield criteria.

Assuming that the difficulty can be avoided by limiting martensite formation, a two-stage accelerated cooling process has been developed to promote bainite over martensite, while at the same time retaining the high cooling rate required to refine the allotriomorphic ferrite that forms first (Fig. 13.8b). After thermomechanical processing in the austenitic condition, the steel is cooled rapidly ($25\,\mathrm{K\,s^{-1}}$) through the ferrite temperature range in order to obtain the fine ferrite grain size, but the cooling rate is then reduced to about $3\,\mathrm{K\,s^{-1}}$) over the temperature range where bainite forms, thereby reducing martensite. The temperature T_F at which the forced cooling is stopped to allow the steel to air cool in the second stage of the process is important. The mechanical properties are less sensitive to T_F for the two-stage process presumably because much of the bainitic transformation is completed at a relatively high temperature during the second stage (Fig. 13.8). The process

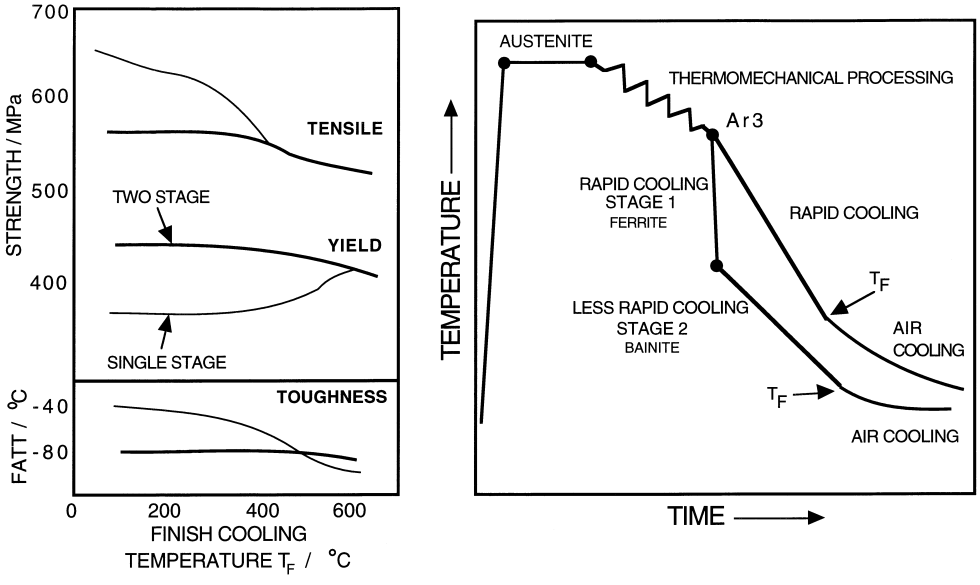

Fig. 13.8 (a) The relationship between the tensile and yield strength, and toughness of accelerated cooled steels as a function of the temperature at which the forced cooled is stopped, for the single and double stage processes. (b) Schematic illustration of the thermomechanical cycles associated with the two-stage accelerated cooling process (Amano *et al.*, 1988).

succeeds in raising the yield stress of the steel when compared with the conventional accelerated cooling procedure.

A general problem with accelerated cooled steels is that the toughness and microstructure are not maintained in the heat-affected zones due to welding (Nishioka and Tamehiro, 1988). The steels are nevertheless about 50 MPa stronger than conventional control-rolled plates. When this additional strength is not required the carbon-equivalent of the steel can be reduced to improve weldability (Fig. 13.9). Accelerated cooling is not appropriate for heavy gauge plates (20–30 mm thick) because it is not possible to ensure uniform cooling; the central regions of thick plates transform into a ferrite and pearlite microstructure rather than the desired bainite (Collins *et al.*, 1985).

In control-rolled steels, thick plates which are cooled slowly after rolling develop a coarse ferrite grain structure at the surfaces. This is a consequence of the recrystallisation of ferrite grains deformed by rolling in the $(\alpha + \gamma)$ phase field, due to heterogeneous deformation. Accelerated cooling avoids this difficulty because it inhibits recrystallisation, particularly at the surface (Tamehiro *et al.*, 1985a).

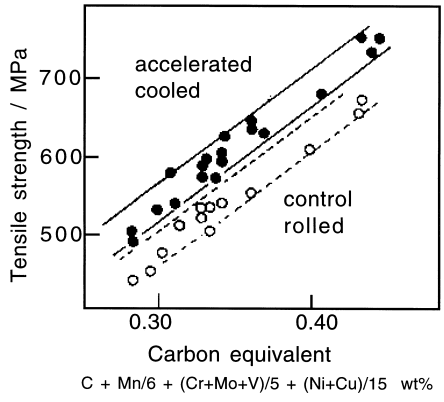

Fig. 13.9 Relationship between the carbon equivalent and tensile strength for conventionally produced control-rolled steels and accelerated cooled steels; the latter have a mixed microstructure of ferrite and bainite (Tamehiro *et al*., 1985a).

13.5.3 Chemical Segregation

Control-rolled steels are cast continuously so they contain pronounced chemical segregation along the mid-thickness of the plate. For example, the manganese concentration at the centre can reach twice the average value. Ferrite naturally forms first in the manganese-depleted regions; the carbon partitioned as the ferrite grows ends up in the manganese-rich regions of austenite. This exaggerates the hardenability of the manganese-rich regions which transform into bands of hard microstructure.

These bands are susceptible to hydrogen cracking. Hydrogen can be infused into the steel through corrosion reactions or other phenomena. An advantage of the accelerated cooled steels is that they are more microstructurally homogeneous (Fig. 13.10); this is because the ferrite and bainite form at a larger undercooling during accelerated cooling, so transformation occurs everywhere, even in the manganese-rich regions. The gross banding characteristic of ferrite–pearlite microstructures is therefore minimised or avoided altogether (Graf *et al*., 1985; Tamehiro *et al*., 1985a). The resulting lower hardness in the segregated zone makes the steel less susceptible to hydrogen-induced cracking. Cracking ceases to be a problem because the hardness in all regions becomes less than about 250 HV (Tamehiro *et al*., 1985).

13.6 Steels with High Formability

The oil crisis of the seventies led to the development of the *dual phase* steels in an effort to reduce the weight of cars and make them fuel efficient.

[13:39 3/9/01 C:/3B2 Templates/keith/3750 BAINITE.605/3750-013.3d] Ref: 0000 Auth: Title: Chapter 00 Page: 358 343-396

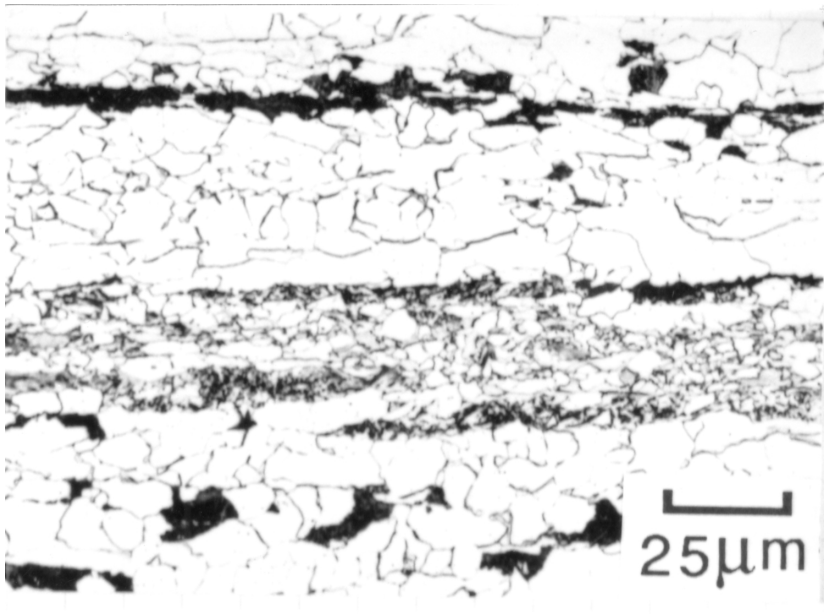

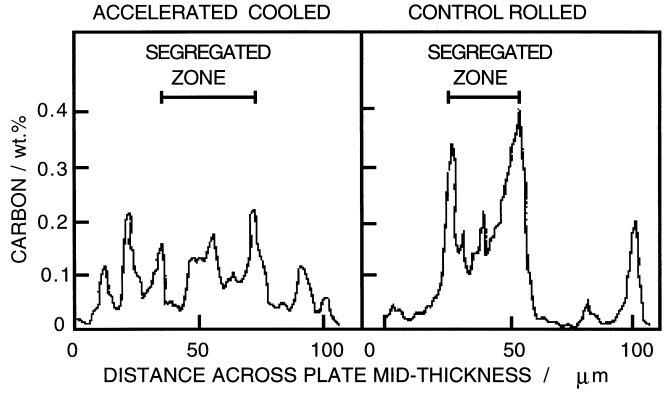

Fig. 13.10 (a) A light micrograph illustrating the effect of chemical segregation along the mid-thickness of heavy gauge plate. (b) Distribution of carbon concentration in the segregated zone for conventional control-rolled and rapidly cooled steel plates (Tamehiro *et al.*, 1985c).

Conventional automobile steels consist either of mixtures of ferrite and small amounts of pearlite, or wholly of ferrite, with a tensile strength of $\simeq 420$ MPa and sufficient formability. In the context of automobile manufacture, formability includes the effects of operations like deep drawing, bending and stretching.[†]

Ordinary steels are troublesome in forming operations because they exhibit discontinuous yielding behaviour, which causes the formation of unsightly stretcher strains on the finished products. Dual-phase steels are similar in composition to conventional alloys, but are heat-treated to generate a mixed microstructure of ferrite and martensite. Their mechanical properties are haracterised by continuous yielding, a small proof to tensile strength ratio and a high uniform elongation (Fig. 13.11). The free dislocations in martensite, the strain induced in the ferrite due to martensitic transformation, and the large difference in hardness between the phases all contribute to yielding behaviour. Although the 0.2% proof stress can be small, the dual phase steels strain harden rapidly so the ultimate tensile strength can be quite large at 500–650 MPa, without loss of formability. More details on dual phase steels can be found in a review by Owen (1980). A typical dual-phase steel would have a chemical composition Fe–0.09C–0.6Si–1.0Mn wt% and would be heat-treated to give a mixed microstructure containing about 20% martensite and 80% ferrite. The high silicon concentration is known to enhance formability; alloying elements such as chromium are sometimes added in small concentrations ($\simeq 0.5$ wt%) for hardenability and solid solution strengthening. The carbon concentration is normally less than 0.2 wt% to avoid brittle spot-welds.

One method of heat treatment involves annealing of strip at a temperature in the two phase $(\alpha + \gamma)$ field, followed by cooling at a rate which ensures that the austenite transforms to martensite. However, it is less expensive to integrate the heat treatment into the steel production process, by adjusting the conditions to allow the required microstructure to develop immediately after the hot rolling and coiling process.

There are difficulties associated with the ferrite–martensite dual phase steels. They do not have sufficient stretch flangeability and can suffer from localised necking in the heat-affected zones of flash butt welds. The final coiling

[†]A common test involves the measurement of a *hole expansion limit* which is the ratio of the hole radius before and after expansion. The test can be carried out using a cone or a flat punch. Hole expandability increases with the difference between the total elongation and uniform elongation, and depends on the cleanliness of the steel. Since local necking and local-fracture limit the ability of the hole to expand, it is the freedom of the steel from inclusions which often determines acceptability. Microstructures without cementite are, for the same reason, favoured. High strength fully bainitic or martensitic steels which have more homogeneous microstructures, show better hole expandability than, for example, dual-phase steels.

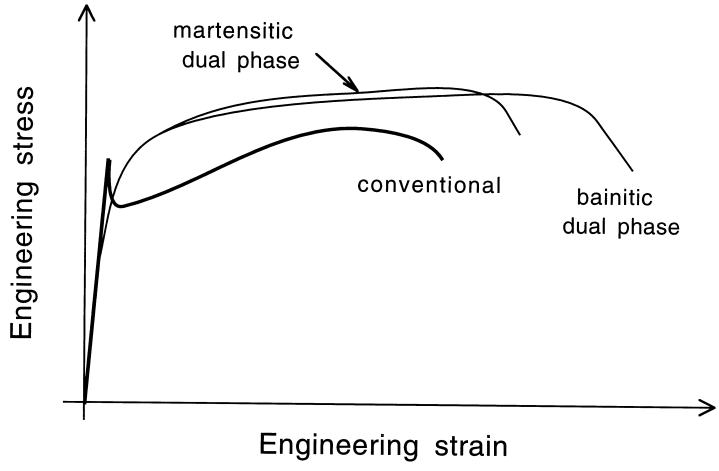

Fig. 13.11 Schematic stress–strain curves comparing the deformation behaviour of conventional high-strength, low-alloy automobile steel and that of dual phase steels. The bainitic dual-phase steel fares better because of its high retained austenite content.

temperature has to be below M_S with a sufficiently large cooling rate; this is technically difficult to attain at high mill speeds. Also, the liberal use of alloying elements is costly and the silicon causes scale formation on the steel surface during the manufacturing stage.

Attempts have therefore been made to create dual phase steels in which the hard phase is bainite instead of martensite (Esaka *et al.*, 1985). These new dual phase steels are simple in composition (Alloy 5, Table 13.1). They are hot-rolled in the austenite phase field to give a fine austenite grain size, cooled rapidly into the bainite transformation region (typically 400 °C) and coiled in that temperature range to promote bainite. The ferrite forms during the cooling operation, and the cooling rate ($40 \rightarrow 100\,\mathrm{K\,s^{-1}}$) determines the fraction of bainite, which may vary from 0.2–1.0 depending on the cooling conditions and composition. A coiling temperature below M_S can induce martensite as well, giving a triple phase steel.

The new steels have better weldability because the bainite which forms in the heat-affected zone is softer than martensite. The martensite does not form in the HAZ because of the lower carbon equivalent of the new steels.

Although conventional dual phase steels have been used in automobile manufacture, but not for body panels where their formability is inadequate. Bainitic dual phase steels have superior formability, but because the difference between the hardness of bainite and martensite is relatively small, they sometimes exhibit discontinuous yielding. A compromise solution would be

a triple phase steel containing some martensite in addition to bainite and ferrite, to promote gradual yielding. Sudo and coworkers (1981, 1982) have demonstrated that triple phase steels (Alloy 6, Table 13.3) do have the best combination of mechanical properties for press forming applications. Notice that their triple phase steel is leaner in alloy content than the dual phase alloys; the development of the required microstructure therefore depends on more difficult heat treatment practice.

Bainitic dual phase steels have recently been developed for the building industry, specifically to exploit their low yield to tensile strength ratio (Terada *et al*., 1990). High-rise buildings require heavy gauge, strong and weldable steels. It is also necessary for earthquake-resistant design, to ensure that the steel has enough ductility after yielding to sustain localised deformation without collapse. Recent earthquakes have established that steel is the only cost-efficient construction material which imparts reliability to constructed structures (Williams, 1991). During an earthquake, the beams and columns of the building framework, which support axial loads, experience bending moments. The maximum bending moment that the beam can support before plastic collapse is reduced when the yield ratio is large. Conventional steels for these applications are quenched to a mixed microstructure of bainite and martensite, which is then tempered; any attempt to increase the yield strength unfortunately also increases the yield ratio. For reasons already discussed, this is not the case for dual-phase steels where the heterogeneity of the microstructure lowers the yield strength but increases the tensile strength. The bainitic dual phase steel developed for building purposes (Alloy 7, Table 13.1) has a yield ratio of about 0.7 compared with the quenched and tempered martensitic steel for which the ratio is 0.9. The steel is produced by controlled rolling, and the temperature where the forced cooling cycle commences determines the exact mix of phases and the precise mechanical properties. Typical properties of plates ranging in thickness from 12–80 mm, are 460 MPa yield strength, 600 MPa tensile strength, 35% elongation and > 200 J of Charpy impact energy at ambient temperature. These properties are not degraded by welding.

13.6.1 TRIP-Assisted Steels

These alloys are also referred to as 'continuously annealed steels' because the required microstructure can be generated using a complex heat treatment within a matter of seconds during the processing of steel strip. The ultimate microstructure consists of allotriomorphic ferrite as the major phase mixed with a total of 30–40% of bainite, martensite and carbon-enriched retained austenite. The chemical composition is typically Fe–0.12C–1.5Si–1.5Mn wt%

[13:40 3/9/01 C:/3B2 Templates/keith/3750 BAINITE.605/3750-013.3d] Ref: 0000 Auth: Title: Chapter 00 Page: 362 343-396

(Alloy 8, Table 13.3); the silicon prevents cementite precipitation so the carbon rejected by bainite enriches the austenite which is retained.

The alloys are used to improve the safety of automobiles without adding to their weight. The strong steel which connects the front bumper to the frame was in the past made of high-strength low-alloy steels with a UTS of about 400 MPa. These have now been replaced by the TRIP-assisted steels with an ultimate tensile strength of 600 MPa with consequent reductions in weight. Side-impact bars with similar microstructures are used with the UTS in the range 900–1500 MPa.

The large silicon concentration causes scale formation during hot-rolling, resulting in a poor surface finish. The steels are therefore confined to applications where the components are hidden from view.

There are two kinds of TRIP-assisted steels. In the first case a cold-rolled strip is heated rapidly from ambient temperature to form some austenite (Fig. 13.12). This stage is known as an 'intercritical anneal'.[†] The strip is then cooled at a controlled rate which may lead to the transformation of the

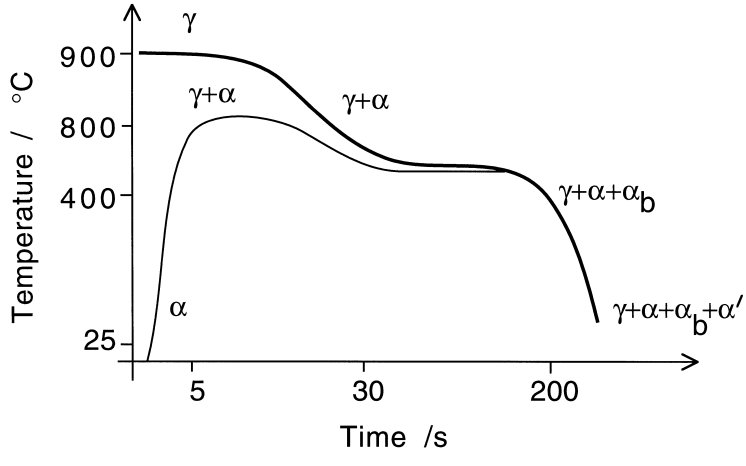

Fig. 13.12 Schematic illustration of the two kinds of heat treatment used to generate the microstructures of TRIP-assisted steels. Some typical times and temperatures are indicated on the graph axes. The lighter curve represents an intercritical annealing heat treatment whereas the bold curve involves transformation from a fully austenitic sample. The terms γ, α, α_b and α' represent austenite, allotriomorphic ferrite, bainite and martensite respectively.

[†]The Ae_1 and Ae_3 temperatures on the iron–carbon phase diagram are often identified as the 'critical temperatures'. The term 'intercritical annealing' refers to heat treatment in the temperature range $Ae_1 \rightarrow Ae_3$ when the alloy is in the $\alpha + \gamma$ phase field.

austenite first into allotriomorphic ferrite and subsequently into bainitic ferrite. This latter reaction causes the austenite to become enriched in carbon, some of which may decompose to martensite on cooling, although a fraction ($\simeq 0.05$) may be retained (Fig. 13.13). The details of the microstructure and mechanical properties can be altered by changing the cooling rate or varying the rate as a function of the temperature. For example, it is common practice to allow more time in the bainite transformation range than at the higher temperatures where allotriomorphic ferrite grows.

The second kind of heat treatment starts from a hot-rolled strip which is fully austenitic (Fig. 13.11) and forms both allotriomorphic ferrite and bainite during the cooling part of the thermal cycle. This has the advantage that the microstructure can be produced directly from the hot strip which has been rolled to its final dimensions. The process is cheap since the strip does not have to be heated to the intercritical annealing temperature. However, hot-rolling mills are restricted by rolling loads to strips thicker than about 3 mm, although there

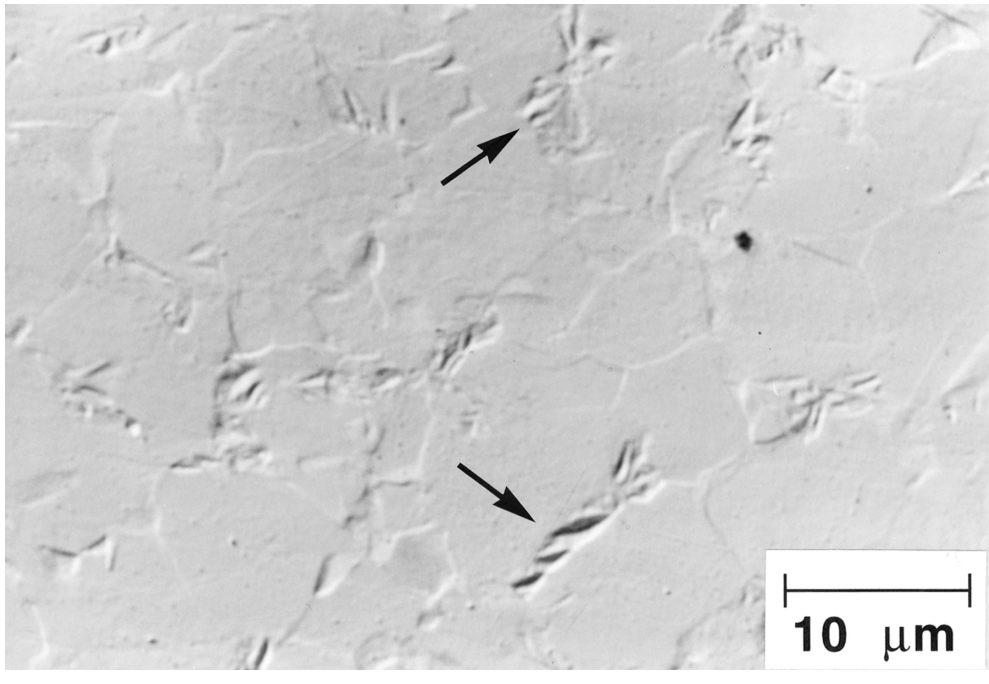

Fig. 13.13 A Nomarski interference micrograph of a TRIP-assisted steel. The sample was metallographically polished, protected against oxidation and then subjected to an intercritical anneal and subsequent partial transformation of the austenite into bainite. The latter phase is here identified by the displacements due to its growth mechanism. Micrograph provided by Jacques, 1999.

are modern mills which can cope with 1.4 mm thickness. Cold-rolled strips can, on the other hand, be made routinely into thinner gauges. Hot-rolled strips are preferred for automobile applications where cost is a prime factor in the choice of materials.

Virtually all such TRIP steels are based on the simple Fe–Si–Mn–C system with a narrow composition range. In spite of this, it is possible to obtain a great variety of combinations of the yield strength, ultimate tensile strength and uniform elongation by making subtle changes to the heat treatment (Fig. 13.14).

A common parameter used to assess formability in the context of TRIP-assisted steels is the product of the tensile strength and uniform elongation. The parameter is related in some way to retained austenite, but the formability must depend on many more variables including the stability of the austenite, the mechanical inhomogeneity of the microstructure, inclusions, carbide particles and the texture of the steel as a whole. The fact that some of the austenite transforms under stress must also be important. There is no satisfying quantitative interpretation of all these observations.

13.6.2 *Transformations During Intercritical Annealing*

The effect of intercritical annealing is to transform some of the initial microstructure into austenite. The part which does not transform is severely tempered, causing the ferrite to recrystallise. The quantity of austenite determines its chemical composition and stability (Fig. 13.15a–c). Austenite nucleates at cementite particles; it has a high carbon concentration to begin with but this becomes diluted as the austenite grows, raising its M_S temp-

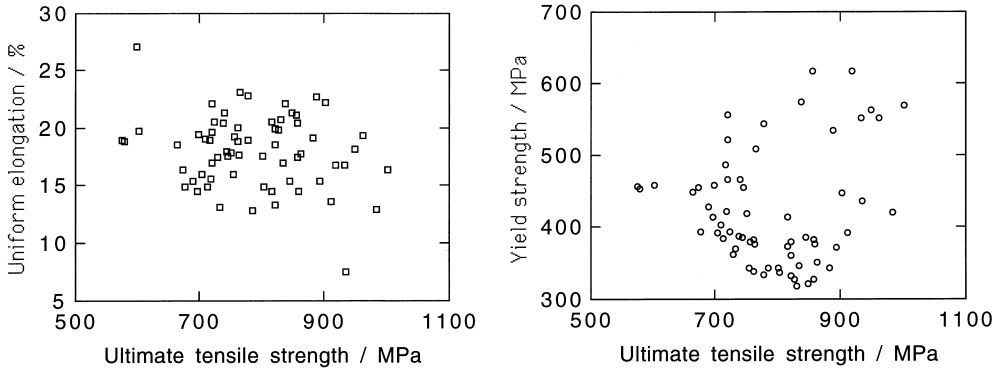

Fig. 13.14 The remarkable range of mechanical properties that can be obtained from TRIP-assisted steels containing allotriomorphic ferrite, bainite, martensite and retained austenite. The steels all are within the composition range 0.15–0.25C, 0.9–2.0Si and 1.4–1.8Mn wt% with a range of processing conditions.

[13:40 3/9/01 C:/3B2 Templates/keith/3750 BAINITE.605/3750-013.3d] Ref: 0000 Auth: Title: Chapter 00 Page: 365 343-396

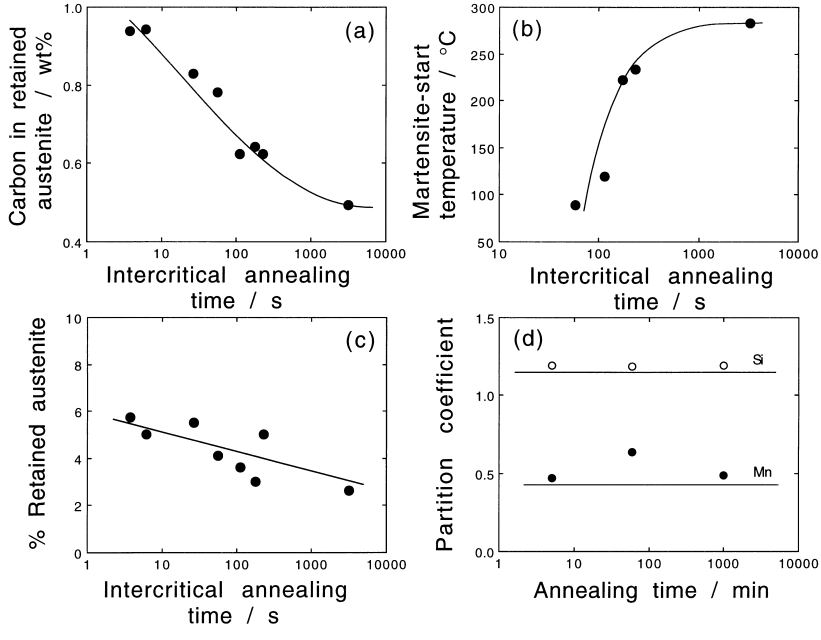

Fig. 13.15 (a–c) Some effects of intercritical annealing on a Fe–0.11C–1.5Si–1.53Mn wt% steel at 750 °C. Data from Samajdar *et al*. (1998). (d) Ratio of concentration of element in ferrite to that in austenite as a function of the intercritical annealing time, for a steel of approximate composition Fe–0.2C–1.5Si–1.5Mn annealed at 800 °C. The horizontal lines represent values calculated assuming equilibrium partitioning. Data from Minote *et al*. (1996).

erature and hence reducing the fraction that is retained on cooling to ambient temperature. The size of the austenite grains also influences their stability; larger grains transform more readily to martensite. Intercritical annealing can also lead to the redistribution of the substitutional solutes (Fig. 13.15d), the degree of partitioning depending on the annealing temperature and time.

The heat treatment influences also the crystallographic texture of both the austenite and the recrystallised ferrite (Samajdar *et al*., 1998). Newly formed austenite grains which nucleate at cementite particles do not show preferred orientation. The texture changes during annealing but the mechanism is not understood.

13.6.3 Dieless-Drawn Bainitic Steels

Wires or rods are conventionally made by drawing, in which a reduction in cross-sectional area is achieved by passing the stock through a die (Fig. 13.16).

The drawing reduction is determined by the ability of the thinner, work-hardened section which leaves the die, to sustain the drawing force without further deformation.

An alternative process achieves the reduction in section using inductive heating. The region of the rod which passes through the hot zone softens and is extended by the drawing force. It stops deforming on leaving the hot zone. The process avoids all the difficulties associated with die erosion and requires a smaller drawing force (Fig. 13.16) because there are no stresses due to die-constraint. Dieless drawing can be applied to a greater variety of shapes, for example, square rods or tubes. The thermomechanical processing combined with accelerated cooling can be used to selectively develop microstructures,

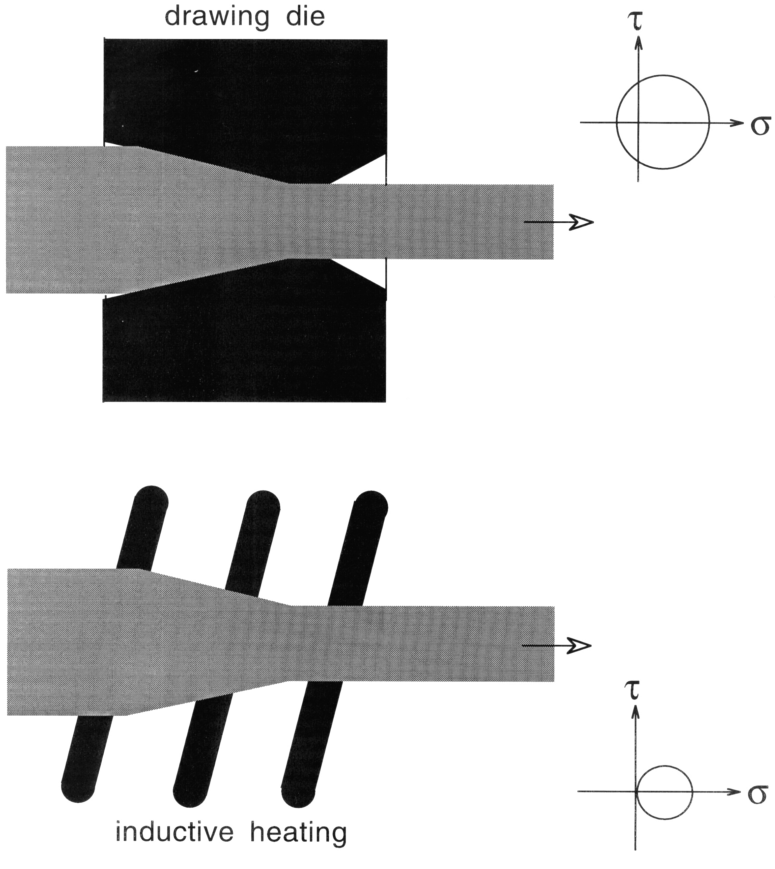

Fig. 13.16 A comparison of conventional drawing with dieless drawing. The Mohr's circle representations of stress are also presented; σ and τ represent the normal and shear stresses respectively (Weidig *et al.*, 1999).

including dual-phase mixtures of ferrite and bainite (Weidig *et al*., 1999). The technology has yet to see major applications but the absence of discontinuous yielding in the dual phase microstructure is an advantage when drawn tubes subsequently have to be formed into complex shapes. Weidig *et al*. have managed to produce predominantly bainitic microstructures using dieless drawing and accelerated cooling in a low-hardenability steel of chemical composition Fe–0.1C–0.14Si–0.7Mn wt%.

13.7 Ultra-Low-Carbon Bainitic Steels

Ever since Irvine and Pickering (1957), it has been apparent that good mechanical properties can be achieved in bainitic steels by reducing their carbon concentrations. Lower concentrations not only reduce the coarse cementite but also regions of untempered martensite which originate from the incomplete transformation of austenite to bainite. For this latter reason, large concentrations of substitutional solutes are also detrimental if they limit the extent of transformation to bainite. And yet, the steel must have sufficient hardenability to avoid phases which occur before bainite during continuous cooling transformation.

Irvine and Pickering compromised by choosing a low concentration of carbon at about 0.1 wt% but ensuring hardenability using boron and molybdenum. They were therefore able to produce fully bainitic steels by continuous cooling transformation. Carbon is a potent strengthener of ferrite but for the same reason, it can lead to embrittlement following welding. A low carbon concentration can therefore provide major economies in fabrication, often allowing welding to be carried out without preheat.

The *ultra-low carbon bainitic* (ULCB) bainitic steels use this philosophy (Alloys 9 and 10, Table 13.1). The carbon concentration is limited to the range 0.01–0.03 wt% (Nakasugi *et al*., 1980, 1983; Hulka *et al*., 1988). The steels are microalloyed so some of the carbon precipitates in austenite as niobium carbide, so that the actual concentration in the austenite prior to its transformation is even smaller than the average value. The resulting reduction in the fraction of martensite improves toughness without undue loss of strength (Fig. 13.17). The carbon concentration should not be reduced to less than 0.01 wt% since niobium carbide precipitation then decreases, with an accompanying loss of toughness. The niobium carbide and TiN prevent austenite grain growth during control-rolling operations and suppress $Fe_{23}CB_6$ and BN precipitation, thereby leaving the boron free to make its contribution to hardenability (Tamehiro *et al*., 1987a,b). In fact, $Fe_{23}CB_6$ particles should be avoided since they stimulate the nucleation of allotriomorphic ferrite.

Because there is insufficient carbon to combine with niobium in ULCB steels, a substantial proportion of the niobium remains dissolved in austenite. Since

[13:40 3/9/01 C:/3B2 Templates/keith/3750 BAINITE.605/3750-013.3d] Ref: 0000 Auth: Title: Chapter 00 Page: 368 343-396

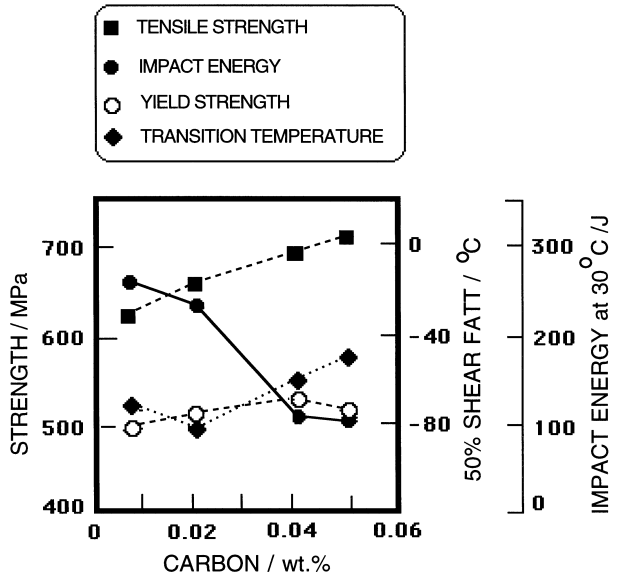

Fig. 13.17 Mechanical properties as a function of carbon concentration in thermomechanically processed ultra-low-carbon bainitic steels (Hulka *et al.*, 1988). The fracture assessed impact transition temperature (FATT), an indicator of the ductile-brittle transition temperature, begins to increase as the carbon concentration falls below about 0.02 wt%.

the equilibrium between niobium and carbon is temperature dependent, the finish rolling temperature T_R has a large influence on the state of the niobium (Fig. 13.18a). Less niobium remains in solution as T_R is reduced due to the greater propensity for strain-induced precipitation during deformation of the austenite at low temperatures.

Changes in the dissolved niobium concentration influence the evolution of microstructure in ULCB steels (Fig. 13.18b). The effect is unlikely to be purely thermodynamic given the small concentrations involved. Soluble niobium strongly retards allotriomorphic ferrite, permitting more bainite to be obtained in the final microstructure. The effect is not obvious in rapidly cooled steels because the ferrite is suppressed irrespective of the niobium concentration (Fig. 13.18b).

There is a synergistic effect between vanadium and niobium. Vanadium competes for carbon leaving more niobium in solution and thereby promoting a bainitic microstructure (Leber *et al.*, 1987).

ULCB steels have outstanding toughness, strength and weldability combinations so they find use in the construction of pipelines in Arctic or submarine environments. The highest strength values are obtained using low finishing

[13:40 3/9/01 C:/3B2 Templates/keith/3750 BAINITE.605/3750-013.3d] Ref: 0000 Auth: Title: Chapter 00 Page: 369 343-396

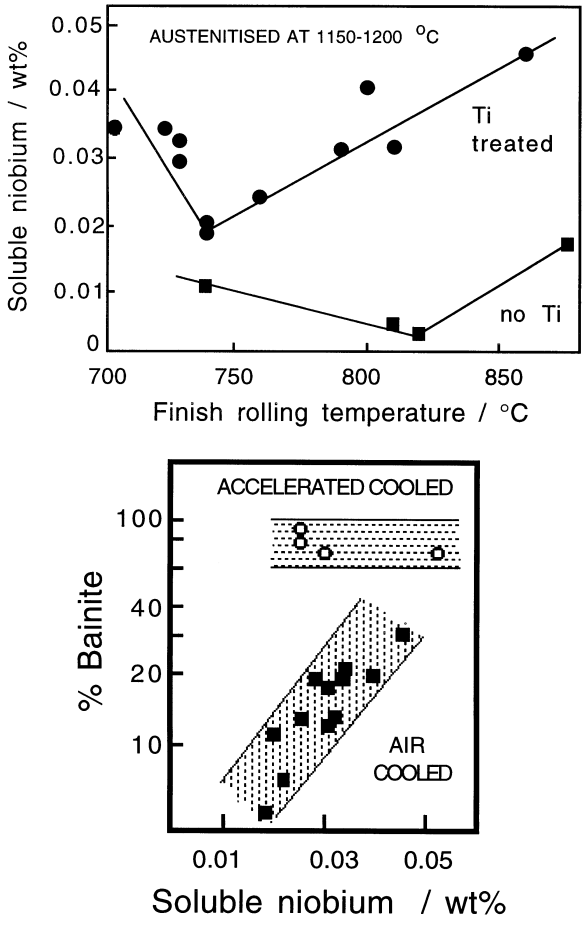

Fig. 13.18 Soluble niobium in ULCB steel (Hulka *et al.*, 1988). (a) Variation in the soluble niobium concentration as a function of the finish rolling temperature; (b) variation in microstructure as a function of the finish rolling temperature.

temperatures and accelerated cooling. The strength can be increased further by retarding cooling below 550 °C to allow NbC precipitation in the ferrite. This can be achieved by coiling or stacking the hot-steel product.

13.8 Bainitic Forging Steels

Forging is a method of working metal into the required shape by hot or cold plastic deformation. Large objects can be shaped using open forging-dies, whereas the mass production of precise components is done in closed dies

[13:40 3/9/01 C:/3B2 Templates/keith/3750 BAINITE.605/3750-013.3d] Ref: 0000 Auth: Title: Chapter 00 Page: 370 343-396

which are filled with solid metal using forge pressure. Forging is attractive as a manufacturing process because it reduces the machining costs and can enhance properties along directions consistent with the application. Typical components which are forged range from small scale items such as crankshafts, connecting rods, piston shafts, bolts, axles and fasteners to components which might weigh many tonnes, such as the rotor shafts in steam turbine generators.

Fe–C–Mn–Si mild steels have served the forging industry reliably for many decades. They have been available in two strength ranges, 350–450 MPa ferrite/pearlite alloys, and high strength (> 600 MPa) quench and tempered martensitic steels.[†] With the martensitic steels, the forged components have to be austenitised, quenched, tempered, manipulated to remove distortion due to heat treatment, and finally, stress-relieved (Fig. 13.19a). For large

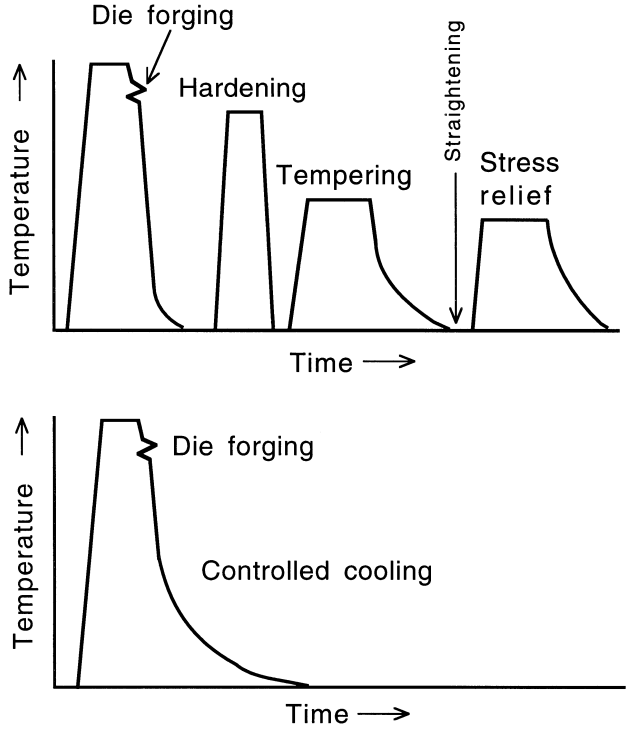

Fig. 13.19 An illustration of the heat-treatment procedures for forging steels (Wright *et al.*, 1987): (a) conventional quenched and tempered martensitic steels; (b) microalloyed forging steels.

[†]An excellent review on the subject has been published by Jones *et al*. (1985).

components, the steels has to be heavily alloyed to obtain martensite at all positions.

There have therefore been attempts to reduce costs by reducing the concentrations of alloying elements and by simplifying the heat treatments. Modern forging steels are microalloyed to produce either fine ferrite/pearlite microstructures, or are alloyed to give bainitic or predominantly bainitic microstructures. Unlike martensite, these microstructures can be produced by transformation during cooling from the forging temperature, with savings in heat treatment, handling and fabrication costs (Fig. 13.19b). Strength as high as 500–700 MPa are readily achieved without compromising toughness and with improved fatigue performance, machinability and weldability. The martensitic steels are still the toughest when it comes to medium carbon steels with a strength of 1200 MPa.

There are special considerations necessary when using directly transformed microalloyed steels; rapid induction heating is often used to heat the stock to forging temperature. The time at the austenitisation temperature has to be long enough to permit microalloying elements such as niobium to dissolve (Wright *et al*., 1987). The way in which the finished components are stacked after the final forging operation can determine their cooling rates.

The new alloys open up the possibility of *controlled forging*, which by analogy with controlled rolling, aims to refine the austenite grain structure prior to transformation (Jones *et al*., 1987). The final stages of forging are carried out at a temperature where the austenite does not recrystallise or alternatively, it recrystallises to a fine grain size. The disadvantage is that reductions in forging temperature cause an increase in the forging force necessitating more powerful production equipment. The increased stress also causes more rapid die wear.

Some of the new forging steels contain carbide-forming elements such as Nb, V, Mo (Alloys 14–18, Table 13.3). Tempering causes fine carbide precipitation which strengthens the final product. The response to tempering is related to the amount and type of bainite in the mixed microstructures of α, α_b and pearlite (Leber *et al*., 1988). The high dislocation density of bainite provides nucleation sites for the carbides, leading to rapid hardening. Predominantly bainitic microstructures are therefore preferred over those containing large fractions of allotriomorphic ferrite. Where niobium and boron additions are used to develop low carbon bainitic microstructures with high work hardening rates (Alloy 18, Table 13.3), cold deformation can be used to increase the strength of the final product. A good example is the series of steels developed for the production of high-strength bolts by cold heading operations (Heritier *et al*., 1984).

Strong, bainitic-forging steels containing high silicon and molybdenum concentrations have been developed for automobile applications, with a typical composition: Fe–1.4Mn–0.8Si–0.15V–0.2Mo wt% with 0.1–0.40 wt% C

(Heitmann and Babu, 1987; Grassl *et al.*, 1989). Such steels are intended to replace quenched and tempered martensitic alloys. The compositions are chosen to avoid the formation of carbides during bainitic transformation, carbides which can be detrimental to toughness. The toughness turns out to be better than that of ferrite–pearlite microstructures at comparable strength levels. However, at higher carbon concentrations the bainitic steels compare unfavourably with martensitic steels which have superior toughness (Fig. 13.20). Although this might militate against the use of bainitic-forging steels, their toughness is still more than adequate for many applications, where their cost advantage may be usefully exploited.

13.9 High Strength Bainitic Steels without Carbides

We have seen in Chapters 2 and 3 that an interesting microstructure results when a silicon or aluminium-alloyed steel is transformed into upper bainite. The carbon that is partitioned into the residual austenite does not precipitate as cementite, but remains there to make the austenite stable at ambient temperature. The microstructure obtained consists of fine plates of bainitic ferrite separated by carbon-enriched regions of austenite (Fig. 13.21).

The potential advantages of this mixed microstructure can be listed as follows:

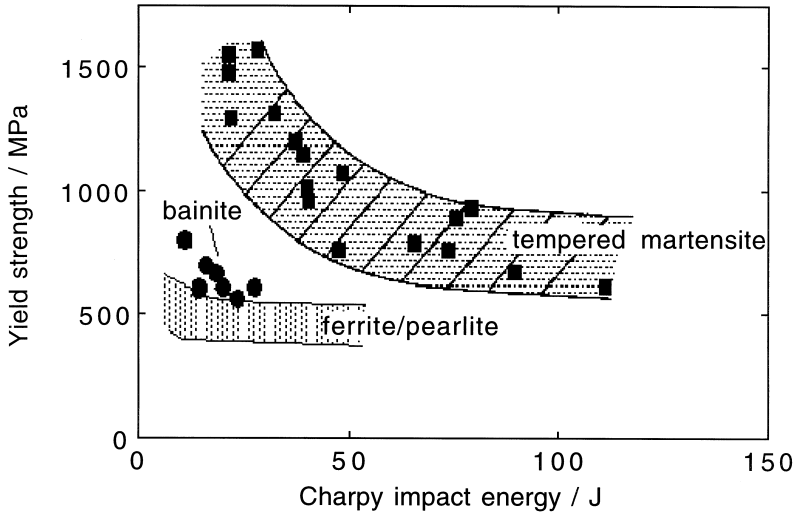

Fig. 13.20 A comparison of the properties of ferrite/pearlite, bainitic- and martensitic-forging steels (Grassl *et al.*, 1989).

[13:40 3/9/01 C:/3B2 Templates/keith/3750 BAINITE.605/3750-013.3d] Ref: 0000 Auth: Title: Chapter 00 Page: 373 343-396

(i) Cementite is responsible for initiating fracture in high-strength steels. Its absence is expected to make the microstructure more resistant to cleavage failure and void formation.

(ii) The bainitic ferrite is almost free of carbon, which intensely strengthens ferrite and hence embrittles it.

(iii) The microstructure derives its strength from the fine grain size of the ferrite plates, which are less than 1 μm in thickness. It is the thickness of these plates which determines the mean free slip distance, so that the effective grain size is less than a micrometer. This cannot be achieved by any other commercially viable process. Grain refinement is the only method available for simultaneously improving the strength and toughness of steels.

(iv) The ductile films of austenite which are intimately dispersed between the plates of ferrite have a crack blunting effect. They further add to toughness by increasing the work of fracture as the austenite is induced to transform to martensite under the influence of the stress field of a propagating crack. This is the TRIP, or transformation-induced plasticity effect (Chapter 12).

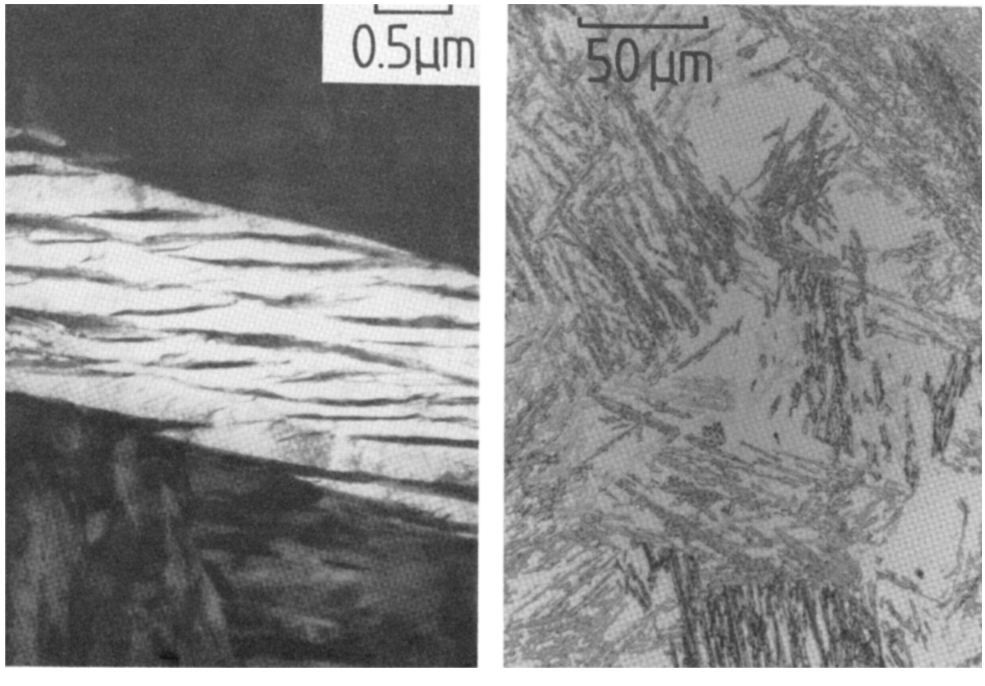

Fig. 13.21 (a) Transmission electron micrograph of bainitic ferrite plates separated by films of stable austenite. (b) Optical micrograph showing the large blocks of austenite left untransformed.

(v) The diffusion of hydrogen in austenite is slower than in ferrite. The presence of austenite can therefore improve the stress corrosion resistance of the microstructure.
(vi) Steels with the bainitic ferrite and austenite microstructure can be obtained without the use of expensive alloying. All that is required is that the silicon concentration should be large enough to suppress cementite.

In spite of these appealing features, the microstructure does not always give the expected good combination of strength and toughness. This is because the relatively large *blocky* regions of austenite between the sheaves of bainite (Fig. 13.21b) readily transform into high-carbon martensite under the influence of stress. This untempered, hard and coarse martensite regions severely embrittle the steel.

If it is assumed that a fraction ϕ of a sheaf consists of films of austenite, then the ratio of the fractions of film and blocky austenite (prior to any martensitic transformation) is given by:

$$\frac{V^{\gamma-F}}{V^{\gamma-B}} \simeq \frac{\phi V^{\alpha}}{V^{\gamma} - \phi V^{\alpha}} \tag{13.2}$$

where $V^{\gamma-F}$ and $V^{\gamma-B}$ are the volume fractions of film and blocky type retained austenite respectively, and V^{α} and V^{γ} the total volume fractions of bainitic ferrite and residual austenite respectively. It is found experimentally that both strength and toughness are optimised by achieving a ratio greater than 0.9. Any large blocks of austenite can be consumed by promoting the formation of bainite without precipitating carbides. The maximum fraction of bainite that can be obtained at any temperature is, from the lever rule,

$$V^{\alpha} \simeq \frac{x_{T_0} - \overline{x}}{x_{T_0}} \tag{13.3}$$

It follows that there are three ways of eliminating blocky austenite:

(i) By reducing the isothermal transformation temperature to increase x_{T_0}. The lower limit is set by either the lower bainite or martensite-start temperature.
(ii) By reducing the overall carbon concentration of the steel, so that the austenite reaches its limiting composition at a later stage of reaction.
(iii) By moving the T_0 curves of the phase diagram to larger carbon concentrations. This can be done by adjusting the concentration and type of substitutional solute (Fig. 13.22a).

[13:40 3/9/01 C:/3B2 Templates/keith/3750 BAINITE.605/3750-013.3d] Ref: 0000 Auth: Title: Chapter 00 Page: 375 343-396

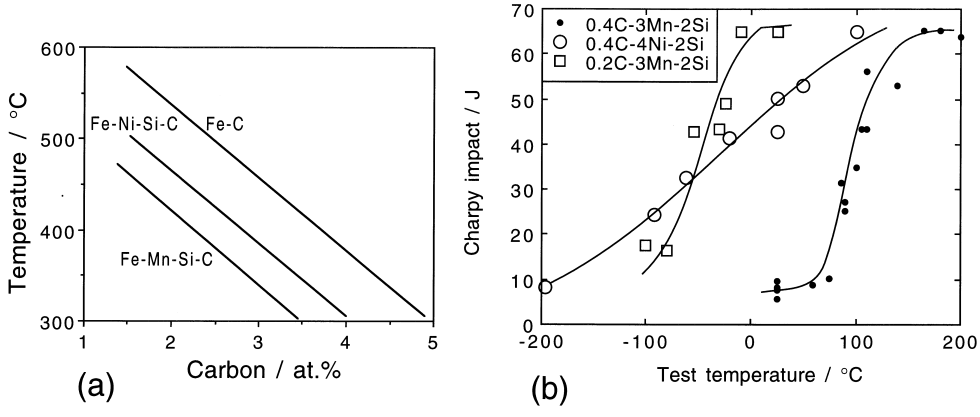

Fig. 13.22 (a) T_0 curves for the alloy-steels listed in Table 13.3, and a corresponding curve for a plain carbon steel. (b) Impact transition curves showing improved toughness without loss of strength, obtained by reducing the amount of blocky austenite in a mixed microstructure of bainitic ferrite and austenite. The Fe–0.43C–2Si–3Mn wt% alloy has $V^{\gamma-F}/V^{\gamma-B} = 0.5$. The reduced carbon Fe–Mn–Si–C steel and the Fe–Ni–Si–C steel both have $V^{\gamma-F}/V^{\gamma-B} > 1.5$. After Bhadeshia and Edmonds (1983a,b).

The effect on toughness in reducing the amount of blocky austenite is indicated in Fig. 13.22b, which shows the large changes in the impact transition temperatures as the ratio of film to blocky austenite is increased in the manner just described. Note that for a duplex $\alpha + \gamma$ microstructure, the strength actually increases as the fraction of bainitic ferrite increases, so that the better toughness is obtained without sacrificing strength.

Typical compositions of high-strength steels which show good toughness are given in Table 13.4; Fig. 13.23 shows how the mechanical properties compare

Table 13.4 Chemical compositions (wt%) of experimental high-strength steels with microstructures consisting of mixtures of bainitic ferrite and retained austenite. After Caballero *et al.* (2001).

C	Si	Mn	Ni	Cr	Mo	V	YS/MPa	UTS/MPa	K_{IC}/MPa m$^{1/2}$
0.3	1.5	2.0	–	1.3	0.25	0.1	1170	1800	
0.3	1.5	–	3.5	1.5	0.25	0.1	1150	1730	125
0.3	1.5	–	3.5	1.5	0.25	–	1100	1625	128

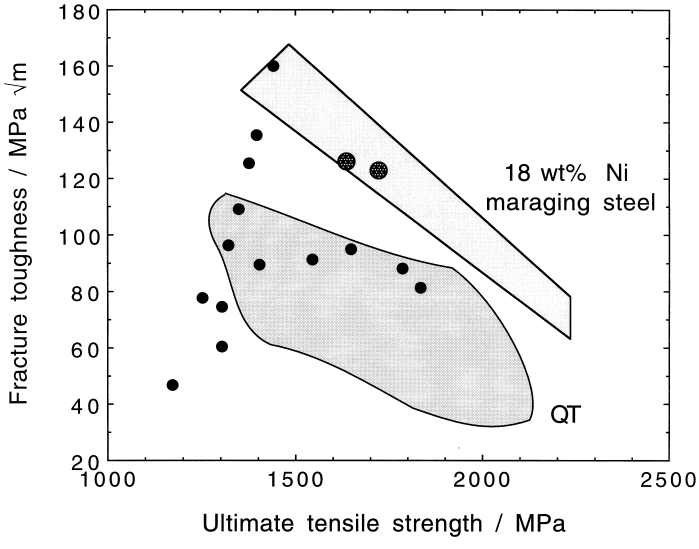

Fig. 13.23 Comparison of the mechanical properties of mixed microstructures of bainitic ferrite and austenite, versus those of quenched and tempered (QT) low-alloy martensitic alloys and marageing steels. The two large points refer to the latest bainitic steels, which match the marageing steel but are thirty times cheaper (about £900 per tonne compared with some £30,000 per tonne for marageing steels). Data from Miihkinen and Edmonds (1987c) and Caballero *et al*. (2001).

with quenched and tempered steels. It is evident that in some cases, the properties match those obtained from much more expensive marageing steels.

The properties of these steels do not change much when tempered at temperatures close to the transformation temperature at which the original bainite formed. However, annealing at elevated temperatures or prolonged periods at low temperatures can lead to the decomposition of the austenite into ferrite and carbides, with a simultaneous drop in strength and toughness, especially the upper shelf energy (Fig. 13.24). The latter effect can be attributed directly to the void nucleating propensity of carbide particles in the tempered microstructure, as illustrated by the much smaller void size evident in the fracture surface of the tempered sample (Fig. 12.11).

13.10 Thermomechanically Processed High-Strength Steels

The alloys described here are not terribly useful in practice, but the phenomena they reveal are interesting and add to the understanding of bainite.

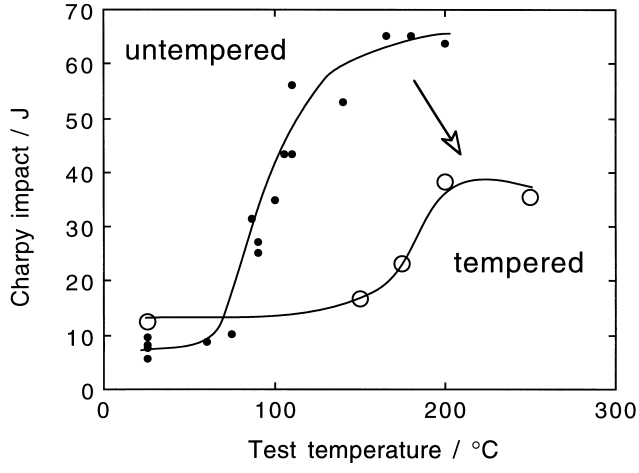

Fig. 13.24 Charpy impact toughness data for Fe–0.43C–2Mn–3Si wt% alloy transformed to a mixture of bainitic ferrite and carbon-enriched retained austenite. The data from the untempered microstructure are from Fig. 13.9. The other data were obtained after tempering the microstructure at 500 °C for 1 h to induce the decomposition of the austenite into a mixture of ferrite and carbides.

13.10.1 Ausformed Bainitic Steels

Ausforming is the deformation of austenite at temperatures well below Ae_3, followed by transformation to martensite or bainite. Its main effect is to increase the strength with a small loss in ductility. The deformation reduces the effective size of the austenite grains leading in turn to a more refined bainite (Kalish *et al*., 1965, Duckworth, 1966; Edwards and Kennon, 1974, 1978; Umemoto *et al*., 1986). The microstructure can become biased by the deformation which might favour particular crystallographic variants to form over others (Umemoto *et al*., 1986).

The bainite that grows from deformed austenite has a greater density of dislocations (Irani, 1967; Edwards and Kennon, 1978). This is because it inherits the dislocations present in the parent austenite. The bainite sheaves adopt a smaller aspect ratio in ausformed samples (Tsuzaki *et al*., 1989). Although there is an overall refinement of the microstructure, each grain of deformed austenite transforms into fewer variants of bainite. Indeed, an entire austenite grain can transform into a single packet of bainite, which may not be desirable from a toughness point of view (Tsuji *et al*., 1999). On the other hand, the refinement of cementite particles in ausformed bainite improves the toughness. As a rough estimate, each one percent increment of plastic deformation leads to a 5 MPa increase in strength.

Not all steels are suitable for ausforming because the austenite must remain stable during deformation at a low temperature. The steel must exhibit a deep bay in the region of the TTT diagram between the two C curves representing the reconstructive and displacive reactions (Table 13.5). Some of the alloying elements used to achieve the required hardenability in ausforming steels are also strong carbide formers. It is suspected that there is a precipitation of fine carbides in the austenite during its deformation; this must contribute further to the strength of ausformed samples (Duckworth *et al*., 1964, Thomas *et al*., 1965). When strong carbide-forming elements are absent, electrical resistivity measurements have shown that deformation does not affect the concentration of dissolved carbon in the austenite (Hoffman and Cohen, 1973).

Table 13.5 Chemical compositions (wt%) of bainitic steels that have been studied with respect to the ausforming process. The steels are not in some cases custom made for ausforming operations.

C	Si	Mn	Ni	Mo	Cr	V	Cu	W	
0.39	1.00	0.25	–	1.39	5.25	0.54	–	–	Kalish *et al*., 1965
0.48	0.25	0.86	0.18	0.04	0.98	–	0.09	–	Duckworth, 1966
0.85	–	1.39	–	–	0.59	–	–	0.53	Edwards & Kennon, 1978
0.59	2.01	1.02	–	–	–	–	–	–	Tsuzaki *et al*., 1989

The plastic deformation of austenite at low temperatures is rarely homogeneous. Slip tends to concentrate into narrow bands (Schmatz and Zackay, 1959; Evans and O'Neill, 1959; Freiwillig *et al*., 1976). The austenite in the bands then transforms into a peculiar narrow band of ferrite, whose transformation mechanism is not known, although the bands do act as nucleation sites for bainitic ferrite (Jepson and Thompson, 1949; Freiwillig *et al*., 1976; Edwards and Kennon, 1978). Transmission electron microscopy has shown the bands to consist of single crystals of ferrite, or parallel laths of ferrite whose long axes lie in the plane of the band, together with some retained austenite. The bands also contain carbides which assist the nucleation of ferrite by locally reducing the carbon concentration. It is likely that the microstructure of the band is simply some highly refined form of bainite (Edwards and Kennon, 1978).

The tempering behaviour of ausformed bainite is somewhat different from that of ordinary bainite. The dislocations in the ausformed bainite rearrange into cells, whereas those in the lower dislocation density ordinary bainite remain dispersed (Edwards and Kennon, 1978).

[13:40 3/9/01 C:/3B2 Templates/keith/3750 BAINITE.605/3750-013.3d] Ref: 0000 Auth: Title: Chapter 00 Page: 379 343-396

Ausformed steels are not commercially successful because of the expense of the thermomechanical treatment and because of the limited variety of shapes that can be produced. With the exception of some low-carbon bainitic steels, ausformable alloys are costly because of the alloying elements they contain; a typical ausforming steel which is transformed to bainite might contain 5Cr–2Mo–0.5V–0.3Mn–1.0Si wt%. In general, ausformed martensitic steels exhibit better combinations of toughness and strength when compared with ausformed bainitic steels (Kalish *et al.*, 1965). This is because of the coarser carbides bainitic steels; it is not therefore surprising that ausformed low-carbon bainitic steels are tougher than martensite in the same alloy (Durbin and Krahe, 1973).

There have been developments in ausformed bainitic steels. Silicon-rich steels respond well to thermomechanical processing because of the absence of cementite (Tsusaki *et al.*, 1989). A particularly promising application is in the manufacture of wire-springs; the shape of this product is ideal for thermomechanical processing. Ausformed lower bainite wires have a hardness of 650 HV which is higher than the same spring in its tempered martensitic condition (Tsuji *et al.*, 1999).

13.10.2 Strain-Tempered Bainitic Steels

Strain tempering involves the deformation of martensitic or bainitic microstructures, followed by an ordinary isothermal tempering heat-treatment. The steel compositions are similar to those of ausformed steel. The process leads to large increases in strength, with some loss in ductility and toughness. The strengthening that is obtained increases with the level of prior deformation, but is not just a reflection of the effects of deformation on the microstructure. The tempering causes an increase in strength as fine carbides precipitate on deformation-defects (Kalish *et al.*, 1965). The effect is greater for bainite than for martensite, because the retained austenite in the former microstructure undergo stress-induced transformation to harder martensite. Strain tempering is more effective as a method for increasing the yield strength than ausforming, but does reduce ductility.

13.10.3 Creep Tempering of Bainite

Both recovery and recrystallisation processes are accelerated when bainite is tempered during creep deformation (Ridal and Quarell, 1962; Murphy and Branch, 1971). The unstressed regions of creep test samples retain a higher hardness than those in the gauge length. In molybdenum-containing bainitic steels, the transition from $Mo_2C \rightarrow M_6C$ is accelerated by creep testing, the

[13:40 3/9/01 C:/3B2 Templates/keith/3750 BAINITE.605/3750-013.3d] Ref: 0000 Auth: Title: Chapter 00 Page: 380 343-396

change being most noticeable at low temperatures or high strain rates, i.e. when reaction kinetics for the $Mo_2C \rightarrow M_{23}C_6$ transition are slow.

It may be that the precipitation rate is increased by the greater number density of nucleation sites in a deformed sample, and by defect-assisted diffusion. However, there are complications in that the $Mo_2C \rightarrow M_{23}C_6$ reaction has been reported to be retarded when the microstructure is tempered martensite (Ridal and Quarell).

13.10.3.1 Orientation changes during creep tempering

Cold-deformation experiments show that once a dislocation cell structure is established, further strain leads to a decrease in the cell size and a corresponding increase in the crystallographic misorientation between adjacent cells (Langford and Cohen, 1975). The dislocations move and their density and distribution also changes during the course of creep deformation. These changes are more complex than those associated with straight annealing, since there is in fact a coarsening of the microstructure. There is certainly an increase in the misorientation between adjacent cells in bainite as shown in Fig. 13.25a but the bainite lath width actually increases with the creep strain (Fig. 13.25b).

The measurements are for a $2\frac{1}{4}$Cr1Mo steel with a bainitic microstructure. The cell structure is found to be much coarser in the same steel when the microstructure is a mixture of ferrite and pearlite, with smaller misorientations between cells. Minute misorientations develop between dislocation cells within individual ferrite grains over a scale of about 10 μm. This contrasts with the

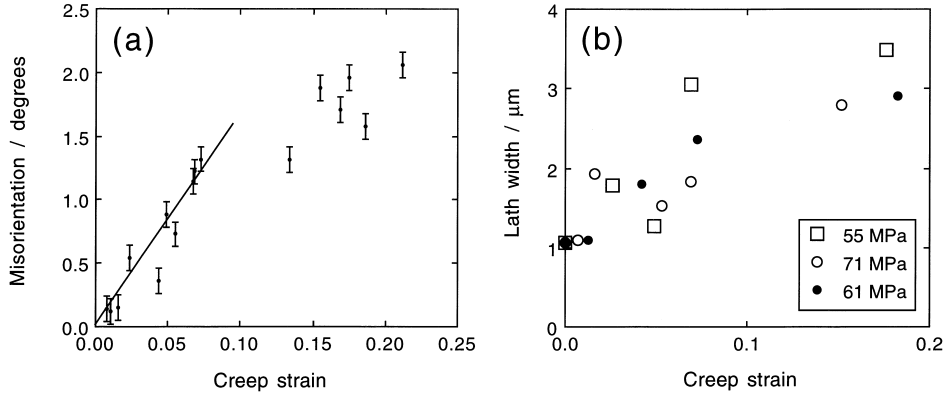

Fig. 13.25 (a) Crystallographic misorientation between adjacent laths of bainite in $2\frac{1}{4}$Cr1Mo steel as a function of the secondary-creep strain. The samples were tested at a variety of stresses and temperatures. (b) Corresponding variations in lath size (Lonsdale and Flewitt, 1979).

[13:40 3/9/01 C:/3B2 Templates/keith/3750 BAINITE.605/3750-013.3d] Ref: 0000 Auth: Title: Chapter 00 Page: 381 343-396

orientation differences between adjacent laths of bainite, which are over distances less than 1 μm.

13.11 Bainite in Rail Steels

Modern railway systems are subjected to intense use, with fast trains and increasing axle loads. Rails have to be more wear resistant and achieve higher standards of straightness and flatness in order to avoid the surface and internal defects which may lead eventually to failure. The shape of the manufactured rail depends to a large extent on the uniformity of thermomechanical processing; the most advanced mills are computer controlled with continuous feedback from the product during manufacture (Fitzgerald, 1991). In this section we consider advances in the steels used for making rails, particularly the bainitic steels.

13.11.1 Track Materials

Although a variety of loadings can adversely affect the life of rails, wear and plastic deformation can lead to unacceptable changes in the rail head profile, changes controlled primarily by a system of rolling contact stresses encountered during service. This system is dependent upon the relative motions of wheel and rail within a small contact zone of about one square centimeter. The motions lead to lateral and longitudinal surface tractions and a spin moment. The rate of rail degradation depends also on the exact location; rail head erosion is at a maximum in regions where the track curves.

Ordinary rail steels contain about 0.7 wt% of carbon and are pearlitic (Table 13.6). However, special grade steels have been considered for tracks carrying high axle loads or fast trains. Since the steels may be used in continuous welded track, they must be amenable to welding to other kinds of low-grade rail steels. Conventional welding processes include flash butt welding and the thermite process. The Hadfield cast austenitic manganese steels are excellent for wear resistance but are not weldable to ordinary rail steels (Sawley *et al.*, 1985).

Wear is a system property more than a material property, but it is nevertheless possible to identify material factors which are important. With eutectoid steels, the wear rate decreases as the hardness increases (Fig. 13.26), although exceptions have been reported (Kalousek *et al.*, 1985b). Figure 13.26 shows also that the microstructure influences wear; refining the microstructure prolongs the wear-limited rail life (Kalousek and Beynon, 1975).

The majority of rail steels are of eutectoid composition with a pearlitic microstructure. The pearlite colony size and interlamellar spacing can be refined by transformation at lower temperatures. But a higher level of refinement can be

Table 13.6 Compositions (wt%) of typical bainitic and pearlitic rail steels.

No	C	Si	Mn	Ni	Mo	Cr	V	Nb	B	Al	Ti		Other
1	0.55	0.25	1.00	–	–	–	–	–	–	–	–	–	Pearlitic rail steel
2	0.80	0.30	1.00	–	–	–	–	–	–	–	–	–	Pearlitic rail steel
3	0.70	1.90	1.50	–	–	–	–	–	–	–	–	–	Pearlitic rail steel
4	0.75	0.70	1.00	–	–	1.0	0.1	–	–	–	–	–	Special grade pearlitic rail steel
5	0.65	0.25	0.70	–	–	–	–	–	–	–	–	–	Pearlitic tyre steel
6	0.04	0.20	0.75	2.0	0.25	2.8	–	–	0.01	0.03	0.03	–	Bainitic rail steel
7	0.09	0.20	1.00	–	0.50	–	–	–	0.003	0.03	0.03	–	Experimental bainitic rail steel
8	0.07	0.30	4.50	–	0.50	–	–	0.1	–	–	–	–	Experimental bainitic rail steel
9	0.10	0.30	0.60	4.0	0.60	1.7	–	–	<0.01	0.03	0.03	–	Experimental bainitic rail steel
10	0.30	0.20	2.00	–	0.50	1.0	–	–	0.003	0.03	0.03	–	Experimental bainitic rail steel
11	0.30	1.00	0.70	–	0.20	2.7	–	0.1	–	–	–	–	Experimental bainitic rail steel
12	0.52	0.25	0.35	1.5	0.25	1.7	–	0.1	<0.01	–	–	–	Experimental bainitic rail steel
13	1.00	0.25	0.25	–	–	1.50	–	–	–	–	–	–	Roller bearing alloy

achieved by transforming instead to bainite. We shall consider first the conventional bainitic steels in which the microstructure contains carbides. These are in general found to perform worse than the pearlitic steels. Ghonem *et al*. (1982) compared the wear and toughness of pearlitic rails with that of an experimental bainitic rail containing chromium and molybdenum. The rail head microstructure consisted of 70% bainite and 30% pearlite but not only was the toughness unacceptable, so was the wear on the gauge face where there is rolling–sliding contact. Heller and Schweitzer (1980) compared the properties and service performance data from bainitic rail steels (alloys 8, 11, Table 13.6) with those from a pearlitic rail steel (alloy 4, Table 13.6). The bainitic

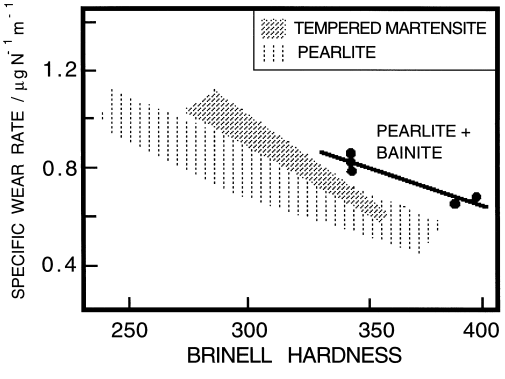

Fig. 13.26 The correlation of hardness with the wear rate for martensitic, bainitic and pearlitic microstructures (Hodgson and Preston, 1988).

[13:40 3/9/01 C:/3B2 Templates/keith/3750 BAINITE.605/3750-013.3d] Ref: 0000 Auth: Title: Chapter 00 Page: 383 343-396

steels achieved higher tensile and fatigue strengths and performed well in service. There were, however, unspecified problems during welding. Service trials subsequently revealed that the bainitic steels wore faster than conventional pearlitic steel rails, when comparisons were made at the same hardness (Heller and Schweitzer, 1982). Work on a low-carbon bainitic steel using laboratory tests involving rolling/sliding contact has indicated a wear rate some ten times faster than a pearlitic steel of the same hardness (Ichinose *et al.*, 1982). Other results confirm these general trends and indicate further that mixed microstructures consisting of bainite and pearlite are less wear resistant when compared with fully pearlitic steels Fig. 13.26 (Kalousek *et al.*, 1985a,b; Mutton, 1985).

By contrast, low-carbon bainitic steels (alloy 6, Table 13.6) have been tested successfully for railway crossing applications where impact erosion and fatigue of the crossing nose were the major wear problems with conventional pearlitic rail steels (Callender, 1983; Garnham, 1989). An advantage of low carbon concentrations is that it enables the steels to be welded easily. Tests using pure sliding, cooled, pin-ring tests has demonstrated that low-carbon bainitic steels might have comparable or superior wear resistance to the pearlitic steels, Fig. 13.27. Even when the pearlitic and bainitic steels have similar wear characteristics, the lower carbon concentration of bainitic steels ensures better ductility, toughness and weldability.

It has been argued that most of the early pessimistic results on bainitic steels could be challenged because they were not systematic investigations and the

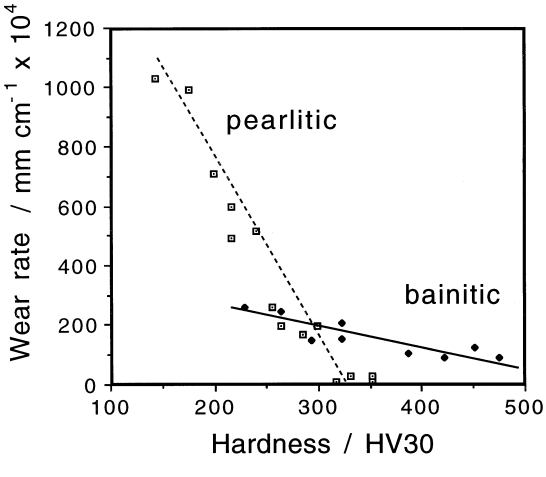

Fig. 13.27 Pin-ring wear rate versus hardness data for pearlitic and bainitic steels (Clayton *et al.*, 1987).

microstructures had been inadequately characterised (Clayton *et al*., 1987, 1990). Contradictory results can also be attributed to the different ways in which wear resistance was measured. The pin-ring test is not representative of service conditions where there is rolling–sliding wear. Using tests designed to simulate rolling–sliding wear, Garnham (1989) has demonstrated, using a variety of steels that carbide-free bainite has poor wear resistance relative to pearlite. Although carbide-containing bainitic steel performed better, it increased the wear of the mating pearlitic railway wheel steel so that the combined wear rates were generally no better than for pearlite–pearlite combinations. It may be concluded from Garnham's work that bainitic steel is not suitable for railway applications where rolling–sliding wear is the major cause of rail or wheel replacement.

The most recent work has been more systematic in the assessment of wear resistance (Devanathan and Clayton; 1990). Three steels with carbon concentrations ranging from 0.04 to 0.54 wt% (alloys 8, 9 & 12, Table 13.6) were examined in their bainitic condition. The lowest carbon steel, which also had the lowest starting hardness, outperformed pearlitic steels at the same hardness level. This is because the bainitic steel work hardened rapidly and had a greater ductility. The medium carbon steel was similar in its wear performance to pearlite, whereas the higher carbon steel was found to be worse. Microstructural observations (Fig. 13.28) revealed that the high carbon steel was chemically segregated, leading to bands of high carbon martensite separated by bainite; cracking initiated at the interfaces between these bands.

13.11.2 Silicon-rich Carbide-free Bainitic Rail Steels

We have seen that rail steels are largely based on high-carbon steels of near eutectoid composition and pearlitic microstructures. It is the carbide phase which is crucial in providing the necessary hardness. A different approach has been based on medium carbon bainitic alloys without any carbides, using precisely the same design philosophy as described for high-strength steels in section 13.9; much of the work is commercially sensitive and the subject of many patents, but there is a brief review article published by Yates (1996) and a paper by Jin and Clayton (1997). The steels contain a large silicon concentration and hence have a microstructure which is a mixture of bainitic ferrite, carbon-enriched retained austenite and some martensite. They have already been demonstrated to have a much improved wear resistance (Fig. 13.29) and rolling-contact fatigue resistance, together with a high toughness even at sub-zero temperatures. A typical composition for the new steel is Fe–0.4C–1.5Si–2.0Mn–0.25Mo wt%, the composition being decided using thermodynamic and kinetic theory as described in section 13.9. The hardness throughout the rail section is about 400 HV.

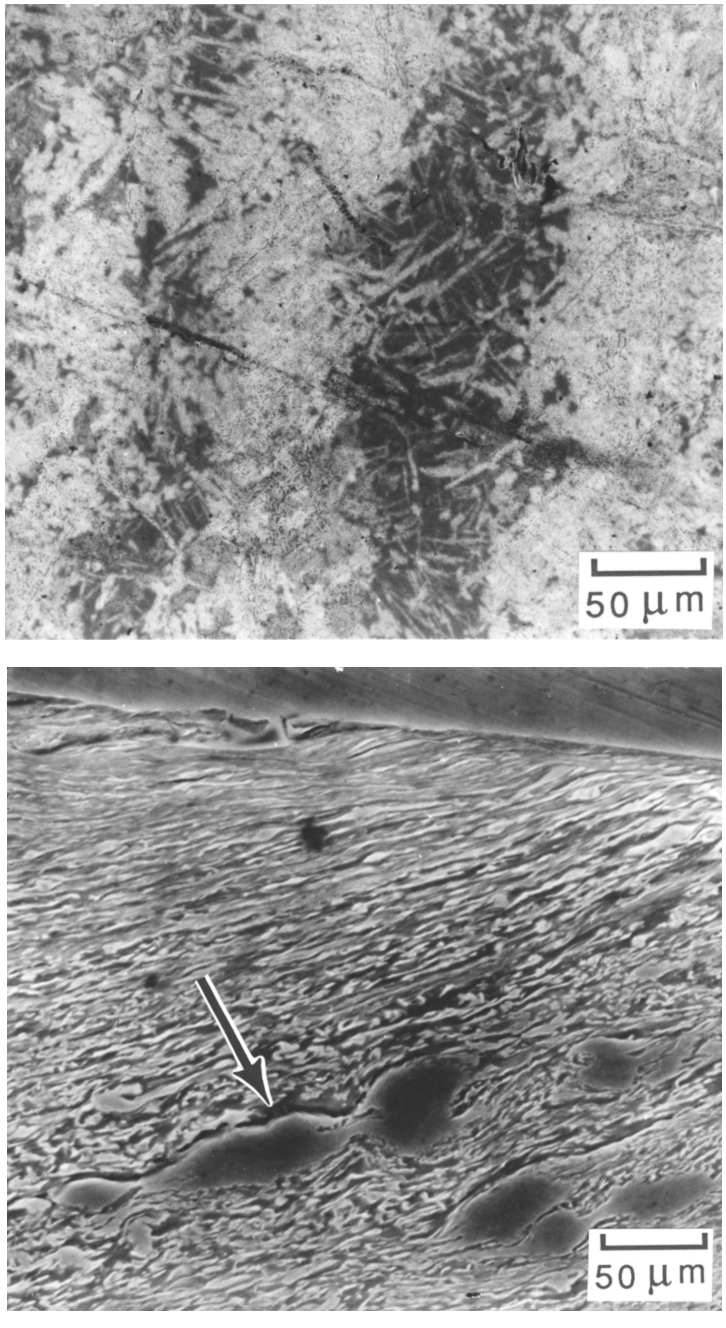

Fig. 13.28 (a) Banding apparent in a high carbon bainitic rail steel (Alloy 12, Table 13.6); (b) cracking at the interface between a pool of martensite and bainite (after Devanathan and Clayton, 1990).

[13:40 3/9/01 C:/3B2 Templates/keith/3750 BAINITE.605/3750-013.3d] Ref: 0000 Auth: Title: Chapter 00 Page: 386 343-396

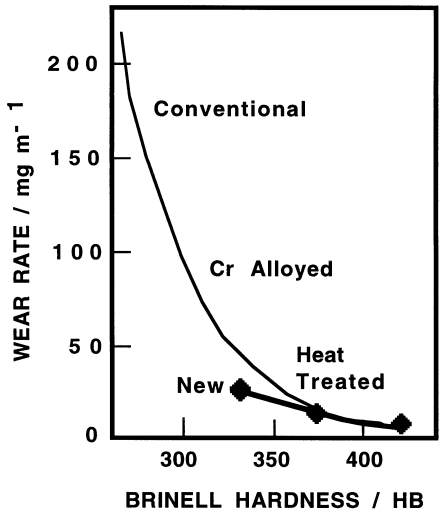

Fig. 13.29 Comparison of the wear rates and hardness levels of conventional rail steels against the new alloys which have a carbide-free microstructure of bainitic ferrite and austenite (Jerath *et al.*, 1991).

13.11.3 Wheels

It is possible that railway wheels will also in the future be based on a bainitic microstructure. A particular problem with wheels is that the alloys must be resistant to microstructural change due to *wheel spin burning*. This can lead to the formation of brittle martensite when material at the surface of a pearlitic steel is momentarily heated to a temperature high enough to cause austenite to form. The same material is then cooled rapidly as the heat is dissipated into the underlying bulk of the wheel, causing the austenite to transform into brittle martensite. This effect can be of greater importance than the rolling-sliding wear of the tread (Sawley *et al.*, 1988). Steels containing less carbon and a bainitic microstructure have been shown to outperform the pearlitic steels because their lower hardenability makes martensite formation less likely; if martensite does form, it is not as brittle given the low carbon concentration and high M_S temperature.

13.11.4 Bearing Alloys

Roller bearings represent another wear-related application in which bainitic microstructures might have an advantage over the traditional alloys used in the quenched and tempered condition (Akbasoglu and Edmonds, 1990). The

studies to date have focused on altering the microstructure of available alloys rather than starting from scratch. The standard bearing alloy is the Fe–1C–1.5Cr steel (Alloy 13, Table 13.5), austenitised at 850 °C for 20 min, oil quenched and then tempered at 175 °C for 1 h. The tempering temperature can be increased to 250 °C for better toughness, but at the expense of hardness. A lower bainitic microstructure can be produced by isothermal transformation below the B_S temperature (a typical heat-treatment might consist of 250 °C for 40 min).

For roller bearings, the main life-limiting factor is rolling contact fatigue, a parameter which can be sensitive to the environment (oil, water) in which the bearing operates. Maximum shear stresses arise under the outer surface of the bearing and can lead to severe spalling. When operating in water-based lubricants, hydrogen evolving from electrochemical reactions can cause embrittlement and can accelerate the fatigue crack growth. In these circumstances, bainitic microstructures fare better than the more hydrogen sensitive martensitic microstructures.

13.12 Bainitic Cast Irons

Cast irons typically contain 2–4 wt% of carbon with a high silicon concentrations and a greater concentration of impurities than steels. The *carbon equivalent* (CE) of a cast iron helps to distinguish the grey irons which cool into a microstructure containing graphite and the white irons where the carbon is present mainly as cementite. The carbon equivalent is defined as:

$$CE(\text{wt\% }) = C + \frac{Si + P}{3} \tag{13.4}$$

A high cooling rate and a low carbon equivalent favours the formation of white cast iron whereas a low cooling rate or a high carbon equivalent promotes grey cast iron.

During solidification, the major proportion of the carbon precipitates in the form of graphite or cementite. When solidification is just complete, the precipitated phase is embedded in a matrix of austenite which has an equilibrium carbon concentration of about 2 wt%. On further cooling, the carbon concentration of the austenite decreases as more cementite or graphite precipitates from solid solution. For conventional cast irons, the austenite then decomposes into pearlite at the eutectoid temperature. However, in grey cast irons, if the cooling rate through the eutectoid temperature is sufficiently slow, then a completely ferritic matrix is obtained with the excess carbon being deposited on the already existing graphite.

White cast irons are hard and brittle; they cannot easily be machined. When they are hypoeutectic (Fig. 13.30)

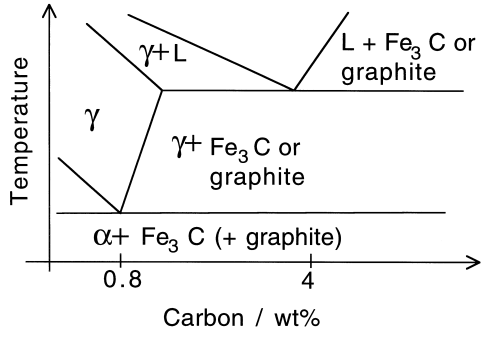

Fig. 13.30 Schematic representation of the iron-carbon phase diagram showing the eutectic and eutectoid reactions.

$$\text{Liquid} \rightarrow \underbrace{\gamma - \text{dendrites}} + \underbrace{\text{Liquid}}$$
$$\downarrow \qquad \downarrow$$
$$\underbrace{\gamma - \text{dendrites}} + \overbrace{\underbrace{\gamma} \quad + \text{Fe}_3\text{C (ledeburite eutectic)}}$$
$$\downarrow \qquad \downarrow$$
$$\text{pearlite} \qquad + \text{Fe}_3\text{C}$$

Grey cast irons are softer with a microstructure of graphite in transformed-austenite and cementite matrix. The graphite flakes, which are rosettes in three dimensions, have a low density and hence compensate for the freezing contraction, thus giving good castings free from porosity.

The flakes of graphite have good damping characteristics, good machinability but are stress concentrators, leading to poor toughness.

The addition of minute quantities of magnesium or cerium poisons preferred growth directions and leads to isotropic growth resulting in spheroids of graphite. This spheroidal graphite cast iron has excellent toughness and is used widely, for example in crankshafts.

13.12.1 Austempered Ductile Cast Irons

The latest breakthrough in cast irons is where the matrix of spheroidal graphite cast iron is not pearlite, but bainite (Fig. 13.31). This results in a major improvement in toughness and strength. The bainite is obtained by isothermal transformation of the austenite at temperatures below that at which pearlite forms.

[13:40 3/9/01 C:/3B2 Templates/keith/3750 BAINITE.605/3750-013.3d] Ref: 0000 Auth: Title: Chapter 00 Page: 389 343-396

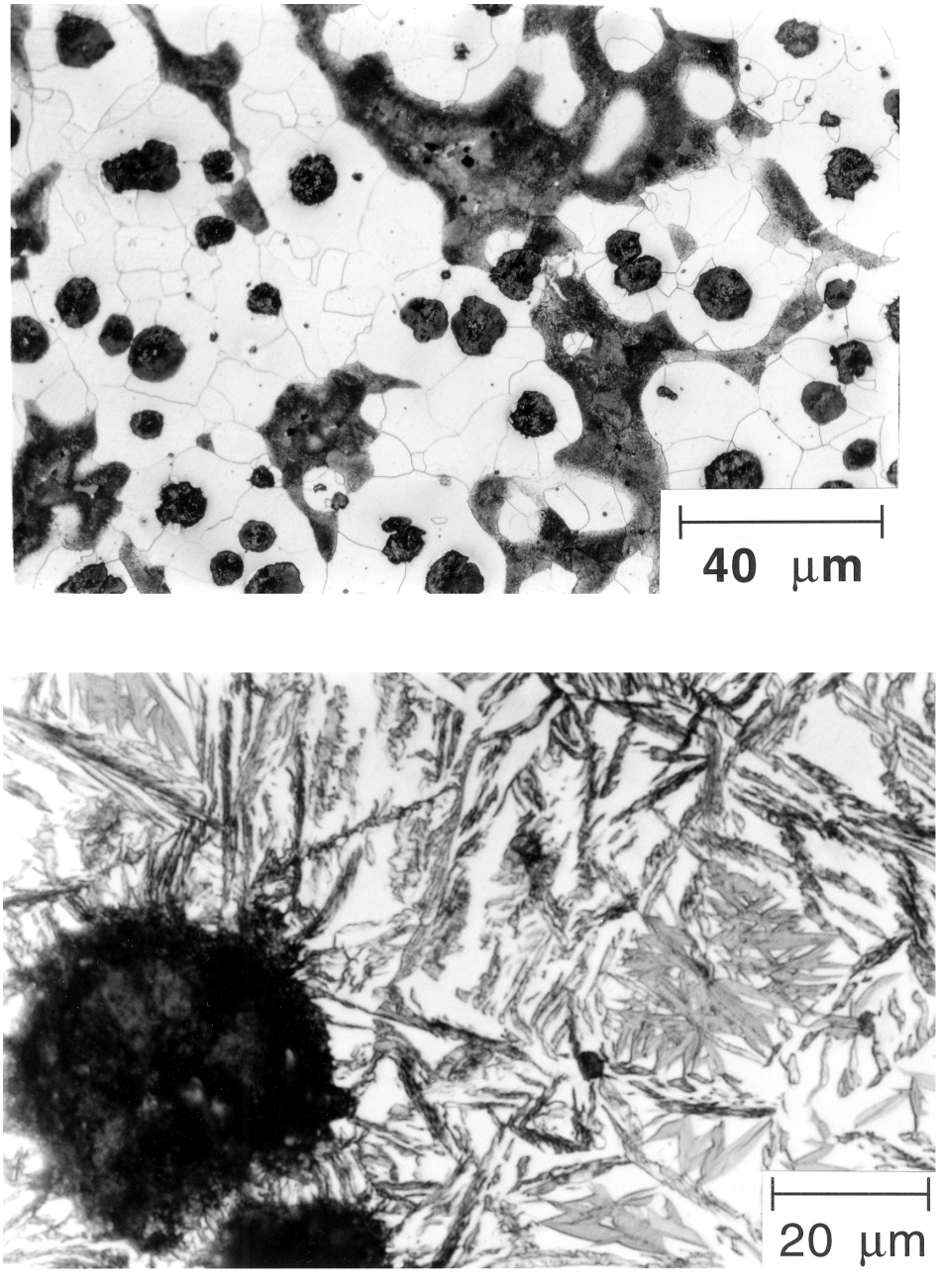

Fig. 13.31 Optical micrographs: (a) the microstructure before austempering; (b) the microstructure after austempering, with graphite in a matrix which is a mixture of bainitic ferrite, retained austenite and some martensite (after Yescas, 2000)

The isothermal heat treatment which leads to the formation of bainite is known as *austempering* and the resulting cast iron, which is known as *austempered ductile cast iron*, has much improved ductility and toughness (Dorazil *et al*., 1962; Blackmore and Harding, 1984; Moore *et al*., 1985a; Ueda and Takita, 1986; Shea and Ryntz, 1986; Franetovic *et al*., 1987a,b; Rundman *et al*., 1988), together with improved abrasion wear resistance (Shepperson and Allen, 1987; Lu and Zhang, 1989). The austempered ductile cast irons have a typical composition Fe–4.0C–2.0Si–0.5Mn–0.06Mg wt%, with a carbon equivalent of about 4.5 (Table 13.7). The nodular iron is prepared by treating the melt with magnesium which alters the flake graphite morphology associated with untreated melts to that of nodular graphite. The solidified iron is then held at 930 °C for 12 hours followed by slow cooling, to give a structure consisting of graphite nodules in a ferritic matrix.

Table 13.7 Typical compositions of austempered ductile casta irons.

	Chemical composition/wt%								
Type	C	Si	Mn	Mo	Cu	S	P	Mg	Reference
Typical	3.6	2.0	0.5	–	–	0.02	0.02	0.06	
Reduced manganese	3.44	2.41	0.15	–	–	0.007	0.0015	0.064	Putatunda & Gadicherla, 1999

Heat-treatment consists of austenitisation at around 950 °C followed by isothermal transformation of the austenite at temperatures where bainite is expected. Because the cast irons have a large silicon concentration (1–2 wt%), carbide precipitation is prevented during the formation of upper bainite so that the microstructure at the isothermal transformation temperature consists of a mixture of bainitic ferrite and carbon-enriched residual austenite. Some of the latter phase then decomposes into untempered martensite on cooling to ambient temperature (Moore *et al*., 1985a; Franetovic *et al*., 1987a).

One important feature of the heat treatment is that bainite is allowed to form until it reaches a maximum in its volume fraction, but the heat treatment must not go on so long that carbides begin to precipitate from the carbon-enriched austenite. This is why the carbon concentration of the residual austenite at the isothermal transformation temperature can be calculated using the T_0' boundary (James and Thomson, 1999). This is useful because not only can the carbon concentration of the austenite be calculated using the T_0 curve, but so can the maximum fraction of bainitic ferrite since:

[13:40 3/9/01 C:/3B2 Templates/keith/3750 BAINITE.605/3750-013.3d] Ref: 0000 Auth: Title: Chapter 00 Page: 391 343-396

$$V_{\alpha_b}^{max} \simeq \frac{\overline{x} - x^{\alpha}}{x_{T_0} - x^{\alpha}} \tag{13.5}$$

where $V_{\alpha_b}^{max}$ is the maximum fraction of bainitic ferrite, $\overline{x}$ is the average carbon concentration in the austenite before the formation of bainite, x_{T_0} is the concentration of carbon given by the T_0 curve of the phase diagram and x^{α} is the solubility of carbon in ferrite. Furthermore, this theory also explains why the carbon concentration of the austenite is independent of the starting concentration $\overline{x}$ (Moore *et al*., 1985b). Naturally, the calculations must all allow for the presence of chemical segregation in the cast iron.

As emphasised earlier, prolonged heat-treatment at the isothermal transformation temperature leads eventually to the diffusional decomposition of the residual austenite into carbides and more ferrite. The period between the achievement of a maximum volume fraction of bainitic ferrite and the onset of carbide precipitation is known as the heat-treatment window.

Austempered ductile cast iron behaves in the same manner as silicon-rich steels transformed to bainite, except that the carbon concentration of the austenite depends both on the time and temperature to which the cast iron is heated. This is because the austenite is in contact with graphite and the equilibrium between these phases depends on temperature; the time required to achieve equilibrium also depends on the austenitising temperature. An increase in austenitising time leads to a greater dissolution of the graphite into the austenite, thereby increasing the austenite carbon concentration to a maximum level consistent with the ($\gamma/\gamma + \text{graphite}$) phase boundary (Moore *et al*., 1987). Consequently, a cast iron isothermally transformed to bainite after holding at the austenitising temperature for a long period gives lower bainite (with η carbides within the bainitic ferrite) whereas the bainite obtained after a short austenitising treatment is upper bainite, free of carbides. This is consistent with the theory for the transition from upper to lower bainite (Chapter 7).

Cast irons need a long time (typically 2 h) at the austenitising temperature to reach equilibrium, when compared with steels (Rouns and Rundman, 1987). This is because the dissolution of graphite produces carbon concentration gradients in the matrix, leading to a heterogeneous microstructure. For reasons which are not clear, the ferrite also seems to take longer to dissolve at the austenitising temperature.

Consistent with the lower carbon level expected in the austenite following a low temperature austenitising treatment, the rate of formation of bainite is found to increase with a decrease in the austenitising temperature (Moore *et al*., 1985a,b). Of course, the austenite grain size also decreases with the austenitising temperature and may contribute to the acceleration of transformation, but the effect of carbon is expected to be the main factor responsible for the increased reaction rate.

A further effect of austenitising temperature that is peculiar to the cast irons is the mechanism by which phosphorous embrittles the austenite grain boundaries (Klug *et al.*, 1985). The phosphorous combines with magnesium to form particles (possibly Mg_3P_2) at the boundaries. The phase begins to redissolve at the grain boundaries if the austenitisation temperature is too high: for a Fe–3.74C–2.4Si–0.19Mn–0.15Mo–0.02P–0.045Mg wt% alloy, the redissolution becomes important at temperatures exceeding ~1050°C. The dissolving particles act as a source for free phosphorous which then spreads along the austenite grain. There is then a drop in toughness as fracture occurs preferentially at the embrittled austenite grain boundaries.

As is the case for bainitic steels containing large concentrations of silicon, austempered nodular graphite cast irons have the highest toughness when carbides are absent and when the retained austenite is mechanically stable (Moore *et al.*, 1985a; Franetovic *et al.*, 1986). The time at austenitising temperature therefore is important because it determines the matrix austenite carbon concentration, and hence its stability with respect to both carbide precipitation and martensitic decomposition.

The role of carbide precipitation in causing a reduction in the ductility of bainitic cast irons is not as clear cut as in the wrought alloys. The austempered cast irons contain numerous large graphite particles which should be the main sites for failure initiation. It seems unreasonable to suggest that the much smaller carbides associated with bainite can control failure initiation. It is probable that the reduction in austenite volume fraction and stability caused by carbide precipitation causes the reduced ductility. Fractography could establish this hypothesis.

Common defects in cast irons, such as shrinkage, slag inclusions and films, segregation, and certain eutectic products can negate the benefits achieved by the presence of austenite in the austempered ductile iron (Moore *et al.*, 1987). For example, the brittle interdendritic carbides which form when the molybdenum concentration is greater than 0.5 wt%, makes the iron brittle in spite of the austenite. The problems become more severe for larger castings where cooling rate variations might necessitate larger alloy concentrations at the risk of exaggerating segregation. There is a growing trend towards alloys with reduced concentrations of manganese and molybdenum (Table 13.7) because these have a greater tendency to segregate into the liquid phase when compared with solutes such as Si, Ni, and Cu which partition preferentially into the solid phase (Hayrynen *et al.*, 1988; Putatunda and Gadicherla, 1999).

It is a well-known result for bainitic steels that the retained austenite occurs in two forms. There are the films trapped between the platelets of bainitic ferrite, and the coarser blocky regions of austenite trapped between different bainite sheaves. The blocks tend to transform more easily to untempered

high-carbon martensite which causes embrittlement. Their volume fraction therefore needs to be minimised. Similar results have been obtained for the austempered ductile iron (Moore *et al*., 1987, Rouns and Rundman, 1987).[†] The ductility decreases as the amount of blocky austenite increases. A smaller fraction of this austenite can be achieved by allowing a longer time t_1 at the austempering temperature assuming that the reaction has not saturated. The difficulty is to ensure that the time t_2, when the residual austenite begins to decompose to carbides is longer than t_1. For example, it has been demonstrated that beyond a certain manganese concentration, t_2 is always found to be smaller than t_1 (Moore *et al*., 1986, 1987; Rouns and Rundman, 1987). This limiting manganese concentration is found to depend on the austenitising temperature which determines the carbon concentration in the austenite (Moore *et al*., 1987). Hence, a higher austenitising temperature should lead to more of the blocky austenite. With lower bainite, the volume fraction of blocky austenite is reduced because some of the carbon is then tied up as carbides in the bainitic ferrite (Moore *et al*., 1987). However, the higher strength causes a reduction in toughness. Cast irons containing upper bainite generally have a tensile strength in the range 960–1150 MPa with a tensile elongation up to 13%, whereas the corresponding data for lower bainite are 1310–1495 MPa and 5% elongation (Moore *et al*., 1987).

There are other special effects concerning the bainite transformation in cast irons. In wrought steels, bainite inevitably nucleates at the austenite grain boundaries. In cast irons, the nucleation of bainite is also found to occur at the austenite/graphite interfaces (Moore *et al*., 1985a). The interface between graphite and iron is weak, and it may in fact be the case that nucleation occurs at the free surface, produced by detachment of the graphite from the matrix. The regions where the nodules of graphite form are in general poorer in alloy concentration, and this might explain their ability to preferentially stimulate the nucleation of bainite (Rouns and Rundman, 1987). Cast irons usually contain chemical segregation which is more pronounced than in steels. Solute concentrations tend to be highest in the interdendritic and intercellular regions,

[†]The terminology used to identify the blocky regions is confusing. The regions are designated *untransformed austenite volumes (UAV)*, their volume fraction being measured using point counting on a light microscope. However, the films of austenite within the bainite sheaves are not included in this analysis, even though they are also untransformed. Hence, the volume fractions of austenite reported using X-ray diffraction analysis (which includes both films and blocks) are higher than the values reported for the UAV regions. A further difficulty is that the carbon concentration of the UAV regions is assumed to be unchanged by the formation of bainite (Moore *et al*., 1986); this is incorrect and must lead to an overestimation of carbon in the remaining microstructure, since some of the microstructural parameters are derived using mass conservation conditions.

which are the last to solidify (Moore *et al*., 1985a,b). The problem is made worse by the rather high mean alloy concentration of bainitic cast irons, necessitated by the need for the austenite to have sufficient hardenability to avoid the formation of pearlite, especially for applications where heavy section castings are required (Rundman *et al*., 1988). The presence of pearlite leads to poor mechanical properties when compared with bainite (Dorazil *et al*., 1962; Shiokawa, 1985). The effect of chemical segregation is to give a non-uniform distribution of bainite. Solute-rich regions which are unable to transform to bainite during austempering decompose into untempered, high-carbon martensite on cooling to ambient temperature and cause a marked decrease in ductility (Moore *et al*., 1985a; Rundman *et al*., 1988).

A more uniform distribution of bainite can be obtained in spite of the chemical segregation, by holding for a longer time at the isothermal transformation temperature. The regions rich in austenite-stabilising elements then have an opportunity to transform. A difficulty is that carbides might form in the regions which transform first to bainite (Moore *et al*., 1985a,b). Another procedure involves ausforming prior to austempering, the rate of transformation to bainite being higher everywhere, in lightly deformed austenite (Moore, 1985a). Ausforming is a specialised treatment involving austenite deformation before transformation and does not seem practicable for cast irons.

There is an effect of segregation which cannot be eliminated by any of the treatments discussed above. The good properties of austempered ductile irons are due to the stable austenite. A short austempering time leads to less carbon enrichment in the residual austenite, which consequently suffers from mechanical instability. Longer times, on the other hand, induce carbide precipitation. There is therefore an optimum austempering time which depends on alloy chemistry. Segregation causes this optimum time period to be different in different regions of the sample, making it impossible to obtain stable austenite throughout the sample (Rundman *et al*., 1988).

13.12.2 Wear of Bainitic Cast Irons

Many cast irons are used in situations where resistance to abrasive wear is an important requirement. The mechanical properties (high strength and ductility) of austempered cast irons, together with their cheapness, make them potential candidates for applications involving abrasive wear. Many investigations have now indicated that the austempered ductile cast irons have better abrasive wear resistance when compared with normalised cast irons of the same chemical composition (Lu and Zhang, 1989) or abrasion-resistant steels, including the Hadfield manganese steel, of equivalent hardness (Shepperson and Allen, 1987). It appears that the improved wear resistance is

at least partly a consequence of the stress-induced transformation of austenite into hard, high carbon martensite, together with the inherent ductility of the microstructure (Shepperson and Allen, 1987). The high work hardening rate usually associated with the transformation induced plasticity may also make a contribution.

[13:40 3/9/01 C:/3B2 Templates/keith/3750 BAINITE.605/3750-013.3d] Ref: 0000 Auth: Title: Chapter 00 Page: 396 343-396

14 *Other Aspects*

14.1 Bainite in Iron and its Substitutional Alloys

Bainite can be distinguished in high-purity iron or iron alloys which have an interstitial content that is less than 0.01 wt%. Kinetic experiments are difficult to conduct because the rate of reaction can be very large. The classification of microstructure therefore has to be based on limited evidence. The question arises as to whether there is any essential difference between martensite and bainite in interstitial-free alloys.

Many experiments have been conducted by monitoring the temperature during rapid cooling. The evolution of latent heat due to transformation can cause inflexions in the cooling curves, which in turn indicate the onset of transformation. Continuous cooling experiments on a Fe–14.43Ni–0.01C wt% alloy revealed two plateaux in a plot of the thermal arrest temperature versus the cooling rate (Wilson *et al.*, 1982). The plateau at the higher temperature was identified with bainite, the other with martensite but the microstructural evidence cited to support this interpretation was simply that the lath width was larger for the higher temperature arrest.

There does not seem to be satisfactory evidence to suggest that there is any difference in the mechanism of transformation between bainite and martensite in interstitial-free alloys. On the basis of the theory discussed in Section 6.1.2, the difference between bainite and martensite should vanish as the carbon concentration is reduced to zero.

14.2 The Weldability of Bainitic Steels

The region which is adjacent to the fusion zone of a weld is influenced by heat diffusion from the fusion zone. This region is the *heat-affected zone* (HAZ). Its boundaries need not be precisely defined because the definition depends on purpose. The heat dissipated into the HAZ can be detected as the temperature at any point rises to a maximum and then drops gently towards the far-field temperature. The severity of the heating or cooling cycles, and the peak temperature, depends on the location within the HAZ (e.g. Easterling, 1983;

Lancaster, 1986; Grong, 1997). For steels with a high hardenability, regions of the HAZ which have been austenitised by the heat pulse may transform during cooling into untempered martensite or to some other hard microstructure. These hard regions are susceptible to cold-cracking due to hydrogen embrittlement and other impurity effects.

This is the main reason why hardenable steels are difficult or impossible to weld (Fig. 14.1). The cooling rate can be reduced during welding, to avoid the formation of martensite in the HAZ. This can be done by heating the sample before welding begins. But this *preheating* adds to the cost of manufacture. It has been estimated, for example, that the cost of fabricating an aircraft carrier could be reduced by about £3 million if the number of panels requiring preheat can be reduced by 50% (Cullison, 1991).

The cold cracking susceptibility correlates empirically with a carbon equivalent (CE), which is a measure of hardenability. There are two popular formulae. The first one is a slightly modified version of the equation originally proposed by Dearden and O'Neill, and adopted by the International Institute for Welding. It is applied to steels containing less than 0.18 wt% of carbon:

$$\text{IIW} \quad > 0.18\,\text{wt\% C}$$

$$\text{CE} = \text{C} + \frac{\text{Mn} + \text{Si}}{6} + \frac{\text{Ni} + \text{Cu}}{15} + \frac{\text{Cr} + \text{Mo} + \text{V}}{5} \quad \text{wt\%} \qquad (14.1)$$

where all the concentrations are in wt%. The other equation, due to Ito and Besseyo, has been adopted by the Japanese Welding Engineering Society:

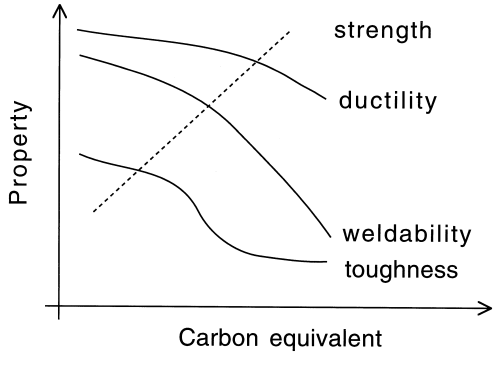

Fig. 14.1 Variation in mechanical properties of the heat-affected zone as a function of the carbon equivalent.

[13:41 3/9/01 C:/3B2 Templates/keith/3750 BAINITE.605/3750-014.3d] Ref: 0000 Auth: Title: Chapter 00 Page: 398 397-404

$$\text{Ito} - \text{Besseyo} \quad < 0.18\,\text{wt\% C}$$

$$\text{CE} = \text{C} + \frac{\text{Si}}{30} + \frac{\text{Mn} + \text{Cu} + \text{Cr}}{20} + \frac{\text{Ni}}{60} + \frac{\text{Mo}}{15} + \frac{\text{V}}{10} + 5\text{B} \quad \text{wt\%} \qquad (14.2)$$

It is generally accepted that if the carbon equivalent is between 0.35 and 0.55 wt%, then the sample must be preheated prior to welding (the preheat temperature can be as high as 400 °C), and when CE > 0.55, both preheating and postheating is considered essential to avoid cold-cracking and other difficulties.

The two equations give different values of CE, the Ito and Besseyo method taking a more conservative account of alloying additions. Equation 14.2 is appropriate for modern low-carbon, low-alloy steels such as the ultra-low-carbon bainitic steels (C $\simeq 0.01 \rightarrow 0.03$ wt%, e.g. Nakasugi *et al.*, 1980, Lorenz and Duren, 1983). For these alloys, the IIW CE gives a pessimistic assessment of weldability whereas the Ito and Besseyo equation works well. It has also been demonstrated (Lorenz and Duren, 1983) that for low carbon pipeline steels, the IIW CE overestimates the effects of alloying elements like manganese and molybdenum, a more realistic CE being given by:

$$\text{CE} = \text{C} + \frac{\text{Si}}{25} + \frac{\text{Mn} + \text{Cu}}{16} + \frac{\text{Cr}}{20} + \frac{\text{Ni}}{60} + \frac{\text{Mo}}{40} + \frac{\text{V}}{15} \quad \text{wt\%} \qquad (14.3)$$

for weld cooling times of 2–3 seconds over the temperature range 800–500 °C (these conditions are typical for girth welds in pipelines).

There are good reasons for supposing that the same CE should not apply to medium-carbon and low-carbon steels. There is a disproportionate increase in the growth rates of both allotriomorphic and Widmanstätten ferrite as the carbon concentration drops below $\simeq 0.06$ wt%, when compared with variations in carbon above this value (Bhadeshia *et al.*, 1985; Bhadeshia, 1990). This is because the average carbon concentration of the alloy approaches the equilibrium solubility of carbon in ferrite. The need to partition carbon into the austenite is thus reduced so that the diffusion-controlled velocity rises sharply.

14.3 Electrical Resistance

It follows from the Bloch theorem that anything which disrupts the periodic potential of the lattice causes an increase in the electrical resistance. Thermal vibrations, dislocations, solute atoms and other point defects therefore all contribute to electrical resistance.

The role of dissolved carbon has been modelled by Hoffman and Cohen (1973) using an analogy with the dynamic displacements associated with thermal vibrations. The analogy seems to work well even though the dis-

placements due to carbon are static. Thermal vibrations involve dynamic displacements whose mean square value $\overline{u_T^2}$ is given by the Debye theory as:

$$\overline{u_T^2} - \overline{u_0^2} = \frac{145}{MT_D}\left(\frac{T}{T_D}\right)^2 \int_0^{T/T_D} \frac{v\,dv}{\exp\{v\} - 1} \tag{14.4}$$

where $\overline{u_0^2}$ represent the zero-point quantum vibrations (the units of the displacements are in Å), M is the atomic weight of iron in grams, v is a dummy integration variable. Using equation 14.4, $\overline{u_T^2} - \overline{u_0^2}$ is found to be $3.25 \times 10^{-5}\,\text{nm}^2$ at 295 K at which temperature the measured resistivity $\rho_T = 9.8\,\mu\Omega\,\text{cm}$. The ratio of the resistivity to mean square displacement is to a good approximation found to be constant. If the static displacements due to carbon are known, then this ratio can be used to estimate its contribution to resistivity. The ratio is found to be about $30.3\,\mu\Omega\,\text{cm}$ per wt% C, in excellent agreement with a variety of experimental measurements on martensite.

Bainite is expected to have a lower electrical resistivity than martensite because it has less carbon in solid solution and a lower defect density. On the other hand, its dislocation density is larger than that of pearlite or allotriomorphic ferrite (Chapter 2). Therefore, the electrical resistivity of a specimen fully reacted to bainite is always found to be higher than that of pearlite at the same temperature (Radcliffe and Rollason, 1959). The resistivity decreases in the order austenite, martensite, bainite and pearlite for a given temperature; for a constant microstructure it decreases with temperature (Fig. 14.2).

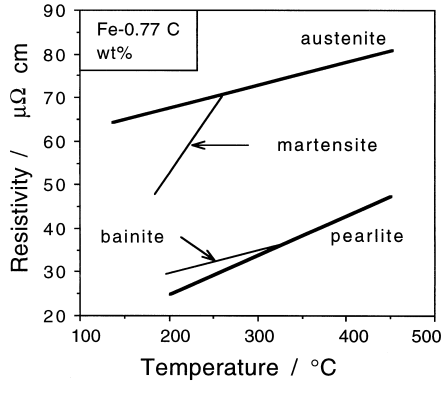

Fig. 14.2 Electrical resistivity of a variety of microstructures in steels (Radcliffe and Rollason, 1959).

14.4 Internal Friction

A material is said to be elastic when it exhibits a stress–strain curve which is fully reversible. The removal of stress eliminates the strain. The energy stored in the material when under stress is fully recovered. When such a material vibrates in a vacuum it may continue vibrating for an indefinite period of time.

Similar vibrations would decay naturally in an *anelastic* solid, since energy is dissipated by some process occurring within the sample during each vibration. The vibrations are said to be damped. An examination of the damping as a function of temperature and frequency can reveal information about the nature of the dissipative process. *Internal friction* measurements like these can be used to detect the onset of transformations, since moving interfaces can damp oscillations.

Internal friction measurements conducted during the continuous cooling transformation of a commercial steel to bainite have been interpreted to indicate a *prebainitic* microstructural change before the formation of bainite proper (Jihua *et al*., 1989). The argument is based on an observed rise in damping during continuous cooling, at temperatures above B_S. These experiments are not supported by microstructural evidence nor is the association with bainite proven.

The same experiments have demonstrated that the degree of damping decreases monotonically as the transformation progresses, indicating that the concentration of dissipative units (whatever they may be) varies directly with the extent of reaction. The damping at any instant of time, increases as the temperature is reduced below B_S. This is expected because the total amount of bainite that can form increases with undercooling below B_S.

14.5 Internal Stress

It has long been recognised that the transformation of austenite to martensite causes the development of stresses which are retained in the transformed specimen. These *residual stresses* are usually attributed to the volume change due to transformation (Buhler *et al*., 1932; Buhler and Scheil, 1933; Scheil, 1955; Buhler, 1955; Hildenwall, 1979).

The volume expansion is not unique to martensite; allotriomorphic ferrite, pearlite, Widmanstätten ferrite, and bainite all cause a decrease in density. There are no data for Widmanstätten ferrite, but the formation of bainite generates residual stresses (Radcliffe and Rollason, 1959; Diesburg *et al*., 1981). As a general rule, X-ray diffraction peaks from transformations which are displacive (martensite, bainite, Widmanstätten ferrite) are found to be more

diffuse than those from reconstructive reactions (allotriomorphic ferrite, pearlite). For example, Radcliffe and Rollason demonstrated a larger lattice strain with martensite and bainite than with pearlite. The diffusion that occurs during reconstructive transformation help accommodate the volume change, preventing the development of stresses.

The residual stresses develop mainly because transformation does not usually occur uniformly in all regions of the sample. This can be exploited for case-hardened components, where it is advantageous to have a compressive stress on the surface of the component. The compressive stress prolongs the fatigue life and makes the component more resistant to surface initiated fracture. In steels which are surface carburised and then quenched, the lower carbon core transforms at a higher temperature. The resulting core–volume expansion puts the still austenitic surface regions into tension, though the tensile stress is partly relaxed by plastic deformation. When the surface region eventually transforms to martensite on further cooling, its volume expansion causes stress reversal, so the surface ends up in compression relative to the core (Koistinen, 1958).

Because of the smaller volume expansion that accompanies the transformation to bainite (Goldak *et al*., 1985), and since plastic relaxation eases at higher temperatures, a bainitic case is not as effective in introducing a compressive stress at the surface when compared with a martensitic case (Diesburg *et al*., 1981). Samples containing bainite in the case have lower levels of compressive residual surface stresses. Thus, the performance of case-hardened samples can be improved by adding elements such as molybdenum which encourage martensite to form at the expense of bainite.

14.6 Bainite in Iron–Nitrogen Alloys

Both nitrogen and carbon exist in interstitial sites in iron and their respective binary phase diagrams with iron show eutectoid reactions in which austenite decomposes into a mixture of ferrite and carbide or ferrite and nitride (Fe_4N). It is therefore reasonable to expect similar sorts of phase transformations to occur in both alloy systems. It is well established that martensite can form in both Fe–C and Fe–N alloys, but the first report of bainite in an Fe–N alloy was by Bell and Farnell (1969). A Fe–1.8N wt% alloy when transformed isothermally at 350 °C was observed using light microscopy to contain ferrite and Fe_4N with an appearance similar to that of upper bainite in Fe–C alloys. The transformation products were stifled in their growth by austenite twin boundaries, consistent with growth in which there is a co-ordinated movement of atoms.

Foct *et al*. (1988) showed that in a Fe–9N at.% alloy, the transformation to bainite is sometimes preceded by the precipitation of Fe_4N. The resulting

localised depletion of nitrogen then stimulates the austenite to transform into bainitic ferrite and more Fe_4N, without any change in the lattice parameter of the residual austenite.

Whilst there is evidence for the existence of a bainite reaction in Fe–N alloys, it would be useful to conduct a detailed microstructural characterisation, thermodynamic analysis and crystallographic experiments including the study of surface relief.

14.7 Effect of Hydrogen on Bainite Formation

Hydrogen has a bad reputation in the context of steels because when in solution, it undoubtedly embrittles ferrite. However, there are examples in titanium metallurgy where it is introduced temporarily to enable processing, after which it is removed by heat treatment. With this in mind, Yalci and Edmonds (1999) conducted what is probably the first study on the influence of hydrogen on the microstructure and properties of upper bainite.

The studies were conducted on silicon-rich steels to avoid the formation of cementite. The hydrogen was introduced at a pressure of two atmospheres, whilst the alloys were in the austenite phase field. This was followed immediately by isothermal transformation in the bainite temperature range.

The introduction of hydrogen apparently led to a greater amount of upper bainite and the thickness of bainite plates was reduced from 0.31 ± 0.06 μm to 0.21 ± 0.09 μm in the hydrogenated alloy. The hardness of the hydrogenated samples was measured to be greater than those which were simply heat treated in helium (Table 14.1). The increase in hardness in the hydrogenated samples is consistent with an increase in the fraction of bainite, since ferrite is at low temperatures harder than austenite.

Table 14.1 Hardness of Fe–0.2C–3Mn–2.1Si wt% and Fe–0.4C–4.09Ni–1.99Si wt% alloy transformed isothermally at 390 °C after austenitisation at 920 °C for 30 min. The samples were sealed in chambers containing either helium or hydrogen at 2 atmospheres pressure throughout these heat-treatments. After Yalci and Edmonds (1999). HV_{30} refers to the Vicker's hardness measured using a 30 kg load.

Alloy	Mn-containing alloy		Ni-containing alloy	
Environment	Helium	Hydrogen	Helium	Hydrogen
HV_{30}	367	409	364	383

14.8 Magnetically-Induced Bainite

It has long been known the magnetic fields must influence the transformation from austenite to martensite (Krivoglaz and Sadovskii, 1964; Kekeshita *et al.*, 1985). The two phases have different magnetic properties so the application of a magnetic field encourages the formation of the ferromagnetic martensite.

Ohtsuka and coworkers (2000) have recently verified the same effect of an externally applied magnetic field on the bainite transformation. The major effect of the field is to accelerate transformation (Fig. 14.3).

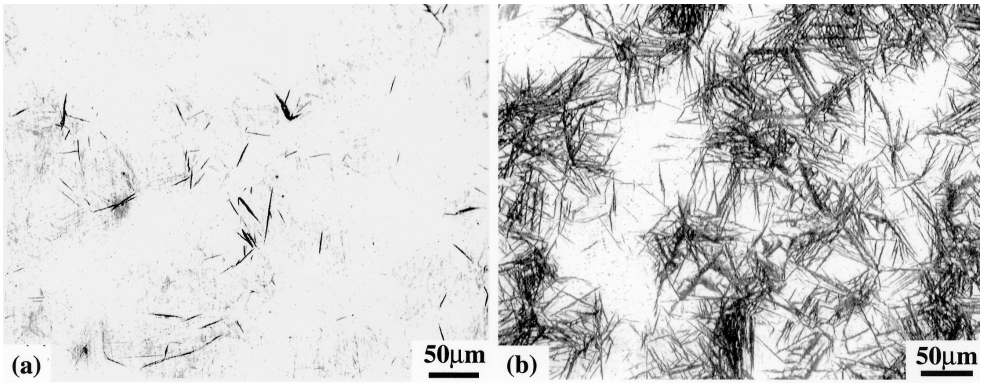

Fig. 14.3 A Fe–0.52C–0.24Si–0.84Mn–1.76Ni–1.27Cr–0.35Mo–0.13V wt% steel austenitised at 1273 K for 600 s and transformed isothermally to bainite at 573 K for 480 s, followed by helium quenching to ambient temperature: (a) zero magnetic field; (b) sample under the influence of a 10 Tesla magnetic field during transformation.

[13:41 3/9/01 C:/3B2 Templates/keith/3750 BAINITE.605/3750-014.3d] Ref: 0000 Auth: Title: Chapter 00 Page: 404 397-404

15 *The Transformations in Steel*

Probably the most interesting revelations are made when *all* of the decomposition reactions of austenite are examined together. And the most awkward question seeks to discover the difference between the variety of transformation products. This chapter is intended to be a brief picture of how these transformations fit together, in a way which is consistent with the available experimental and theoretical data (Fig. 15.1).

There is ample evidence that the different forms of ferrite can be categorised into those which grow by displacive transformation and the others which grow by a reconstructive mechanism. Amongst the displacive transformations are Widmanstätten ferrite, bainite, acicular ferrite and martensite, all of which are characterised uniquely by their plate or lath shapes and the striking invariant-plane strain surface relief which accompanies transformation. An important feature of this strain is the large shear component which is the dominant reason for the plate shape of the transformation product. There is no equilibrium at the transformation front; substitutional solutes do not partition between the parent and product phases.

Widmanstätten ferrite grows at high temperatures by a paraequilibrium mechanism in which the plates lengthen at a rate controlled by the diffusion of carbon in austenite. This diffusion does not contradict its displacive character because interstitials can migrate without affecting the IPS shape deformation. The transformation occurs at small driving forces, so that the shape change consists of two adjacent invariant-plane strains which tend to mutually accommodate and hence reduce the strain energy. This also explains the thin-wedge shape of Widmanstätten ferrite because the adjacent plates are different crystallographic variants (Fig. 15.2).

Carbon must diffuse during the nucleation of both Widmanstätten ferrite and bainite. Nucleation probably occurs by a process akin to the dissociation of arrays of dislocations. This follows from the observation that the activation energy for nucleation is directly proportional to the driving force, rather than the inverse square relationship implied by a heterophase fluctuation model of nucleation. Both Widmanstätten ferrite and bainite develop from the same nucleus; it develops into bainite if diffusionless growth is possible at the temperature where nucleation becomes possible. Otherwise it evolves into Widmanstätten ferrite.

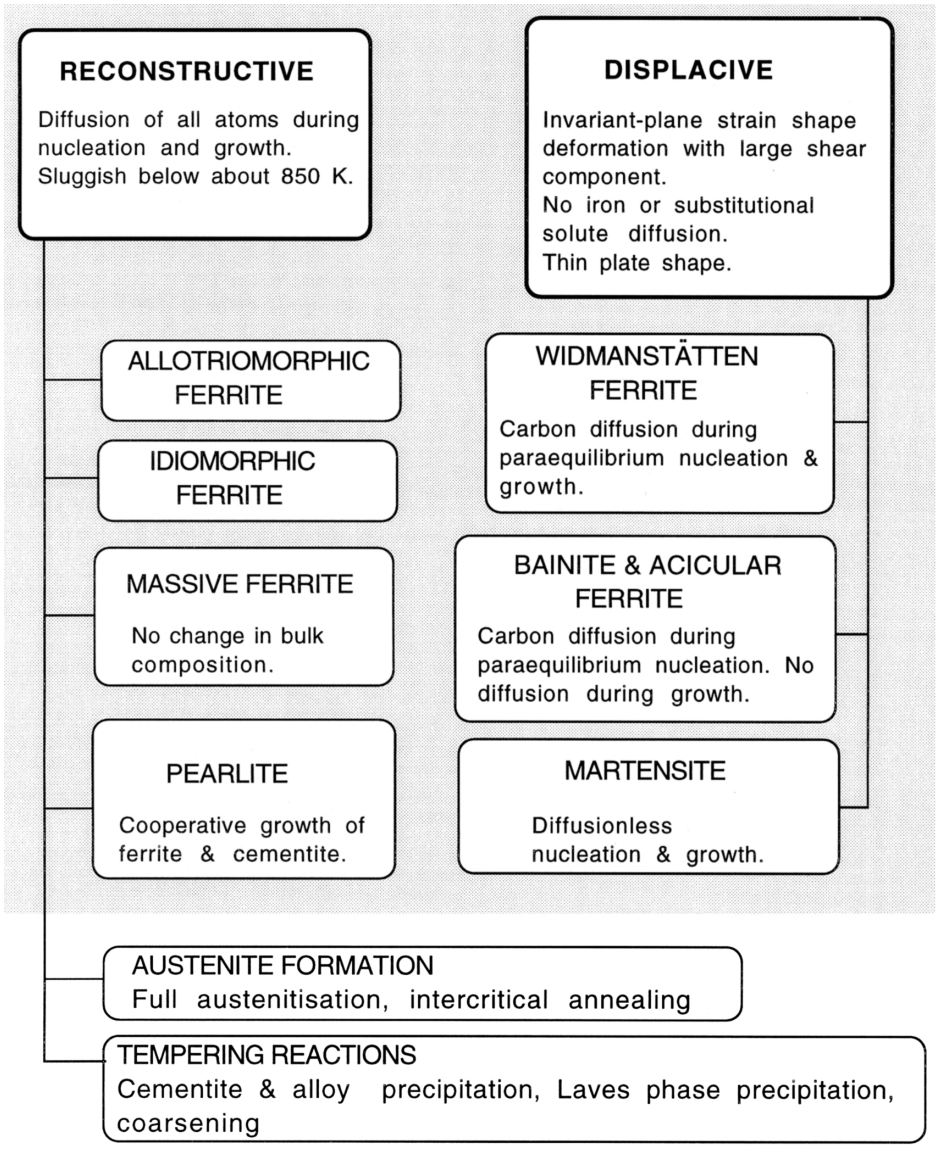

Fig. 15.1 Flowchart summarising the characteristics of transformations in steels.

Bainite probably grows without diffusion, but excess carbon is soon after transformation, rejected into the residual austenite. The partitioned carbon may then precipitate as carbides, giving the classical upper bainitic microstructure. At somewhat lower transformation temperatures where the

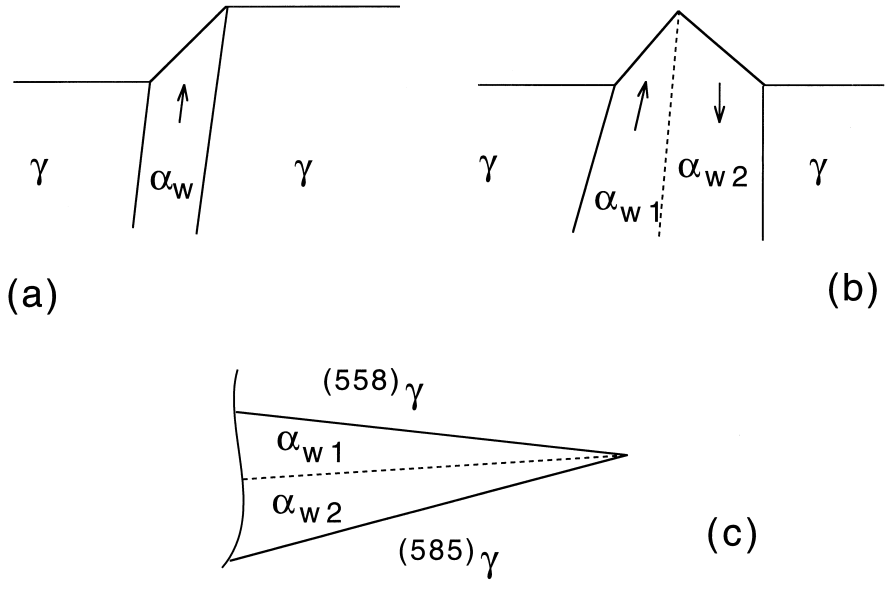

Fig. 15.2 (a) A single invariant-plane strain shape deformation. (b) The combined effect of two mutually accommodating, back-to-back IPS deformations. (c) The morphology of two plates, with different habit plane variants, growing together in a mutually accommodating manner.

partitioning of carbon is slower, a proportion of the excess carbon has the opportunity to precipitate inside the bainitic ferrite. This leads to the lower bainitic microstructure.

Bainite grows at temperatures where the austenite is mechanically weak and unable to elastically accommodate the shape deformation. As a result, the dislocations generated during the plastic deformation of the adjacent austenite, cause a loss of coherency at the α_b/γ interface. The growth of the bainite platelet therefore is arrested before it hits any hard obstacle such as an austenite grain boundary. Continued transformation therefore requires new platelets to form, giving rise to clusters of parallel sub-units with identical crystallographic orientation, habit plane and size. These clusters are known as sheaves of bainite. Acicular ferrite is an alternative, more chaotic morphology of bainite in which the plates are intragranularly nucleated on non-metallic inclusions and hence grow in many different directions from the nucleation site.

The possibility remains that the transition from Widmanstätten ferrite to bainite involves a gradual increase in carbon supersaturation, rather than a sudden change from paraequilibrium to diffusionless growth.

Martensitic transformation is diffusionless, both during nucleation and during growth.

The reconstructive transformations include allotriomorphic and idiomorphic ferrite, and pearlite in its various forms. It is important to appreciate that all elements, including iron, must diffuse during reconstructive transformation in order to achieve the structural change without the strains characteristic of displacive reactions. None of these transformations are associated with shear strains.

A prominent feature of the eutectoid decomposition reaction which leads to the formation of pearlite is that the ferrite and carbide phases grow with a common transformation front with the austenite. They are said to grow co-operatively.

Figure15.1 lists the growth of austenite by a reconstructive mechanism. This is not always the case. However, extraordinarily large heating rates are needed in all practical circumstances to change the growth mode into one which is displacive. The precipitation of alloy carbides undoubtedly occurs by reconstructive transformation with the long-range diffusion of substitutional solutes. However, this is not necessarily the case for the iron carbides, which can grow at temperatures where the diffusion of iron is inconceivable.

15.1 Key Characteristics of Transformations in Steels

Table 15.1 lists the key characteristics of phase transformations in steels. The nomenclature used for the transformation products is as follows: martensite (α'), lower bainite (α_{lb}), upper bainite (α_{ub}), acicular ferrite (α_a), Widmanstätten ferrite (α_w), allotriomorphic ferrite (α), idiomorphic ferrite (α_i), pearlite (P), substitutional alloying elements (X). Consistency of a comment with the transformation concerned is indicated by (=), inconsistency by ($\neq$); cases where the comment is only sometimes consistent with the transformation are indicated by a bullet ($\bullet$). The term *parent* γ implies the γ grain in which the product phase grows. Note that it is not justified to distinguish massive ferrite from α.

15.2 Notes Related to Table 15.1

Nucleation and growth reactions are of first order in the Ehrenfest classification; in all such reactions, the parent and product phases can coexist, and are separated by well-defined interfaces. Martensitic transformations, although they can be rapid, still involve a nucleation and growth process.

It is significant that all of the ferrite crystals which grow in the form of plates cause an invariant-plane shape deformation which is dominated by shear. The ferrite within pearlite does not have a plate morphology; Hillert showed some time ago that it is wrong to consider pearlite as alternating layers of ferrite and

Table 15.1 Characteristics of solid-state transformations in steels.

Comment	α'	α_{lb}	α_{ub}	α_a	α_w	α	α_i	P
Nucleation and growth reaction	=	=	=	=	=	=	=	=
Plate shape	=	=	=	=	=	≠	≠	≠
IPS shape change with large shear	=	=	=	=	=	≠	≠	≠
Diffusionless nucleation	=	≠	≠	≠	≠	≠	≠	≠
Only carbon diffuses during nucleation	≠	=	=	=	=	≠	≠	≠
Reconstructive diffusion during nucleation	≠	≠	≠	≠	≠	=	=	=
Often nucleates intragranularly on defects	=	≠	≠	=	≠	≠	=	≠
Diffusionless growth	=	=	=	=	≠	≠	≠	≠
Reconstructive diffusion during growth	≠	≠	≠	≠	≠	=	=	=
Atomic correspondence (all atoms) during growth	=	=	=	=	≠	≠	≠	≠
Atomic correspondence only for atoms in substitutional sites	=	=	=	=	=	≠	≠	≠
Bulk redistribution of X atoms during growth	≠	≠	≠	≠	≠	⊗	⊗	⊗
Local equilibrium at interface during growth	≠	≠	≠	≠	≠	⊗	⊗	⊗
Local paraequilibrium at interface during growth	≠	≠	≠	≠	=	⊗	⊗	≠
Diffusion of carbon during transformation	≠	≠	≠	≠	=	=	=	=
Carbon diffusion-controlled growth	≠	≠	≠	≠	=	⊗	⊗	⊗
Co-operative growth of ferrite and cementite	≠	≠	≠	≠	≠	≠	≠	=
High dislocation density	=	=	=	=	⊗	≠	≠	≠
Incomplete reaction phenomenon	≠	=	=	=	≠	≠	≠	≠
Necessarily has a glissile interface	=	=	=	=	=	≠	≠	≠
Always has an orientation within the Bain region	=	=	=	=	=	≠	≠	≠
Grows across austenite grain boundaries	≠	≠	≠	≠	≠	=	=	=
High interface mobility at low temperatures	=	=	=	=	=	≠	≠	≠
Displacive transformation mechanism	=	=	=	=	=	≠	≠	≠
Reconstructive transformation mechanism	≠	≠	≠	≠	≠	=	=	=

cementite – instead a colony of pearlite is an interpenetrating bicrystal of ferrite and cementite.

Reconstructive diffusion is the flow of matter necessary to avoid the strains characteristic of displacive transformations. A diffusional transformation may phenomenologically be regarded as a combination of a lattice change and a recrystallisation of the product phase, reconstructive diffusion being the flow necessary for the recrystallisation process.

In diffusionless transformations, it is possible to specify (in a localised region at least) how particular vectors, planes and unit cells of one structure (defined by an imaginary labelling of the individual atoms) are derived from *corresponding* vectors, planes and unit cells of the other structure. This is

termed a lattice correspondence and it defines a pure lattice deformation which carries the original lattice points, or some fraction of these points into points of the new lattice. When interstitial atoms are present, they may move over large distances during transformation without affecting the lattice correspondence; this is sometimes loosely expressed by stating that there is an atomic correspondence for the solvent and substitutional solute atoms but not for the interstitial atoms. A further relaxation of the condition is to allow the solvent and substitutional solute atoms to be displaced during transformation among the sites specified by the lattice correspondence, but not to create new sites or to destroy any specified sites; in this way the lattice correspondence is preserved but there is no longer an atomic correspondence. Note that in the classification presented above, the single atomic jumps of interstitial atoms needed to destroy Zener ordering (which is produced automatically by the Bain correspondence) are not taken into account.

Even though two crystals may have an identical *bulk* composition, it may not be concluded that their compositions at the transformation interface are identical. There are modes of transformation (e.g. negligible partitioning local equilibrium) where the bulk compositions are predicted to be identical but where the phases differ in the vicinity of the transformation interface. For plain carbon steels, there is no difference between equilibrium and paraequilibrium.

The incomplete reaction phenomenon implies that when a reaction can be studied in isolation, it stops before the phases reach their equilibrium or paraequilibrium compositions when stored energy terms have been accounted for.

An orientation within the Bain region means a reproducible relation which may be irrational but is close to the rational NW or KS relations.

Massive ferrite is not classified as a separate morphology since it can be included within allotriomorphic or idiomorphic ferrite.

References

Aaronson, H. I. *The Decomposition of Austenite by Diffusional Processes*, eds. V. F. Zackay and H. I. Aaronson, Interscience Publishers, New York (1962) 387–546.

Aaronson, H. I., Domian, H. A. and Pound, G. M. *Trans. Met Soc. AIME* **236** (1966a) 753–767.

Aaronson, H. I., Domian, H. A. and Pound, G. M. *Trans. Met Soc. AIME* **236** (1966b) 768–780.

Aaronson, H. I. and Domian, H. A. *Trans. Met Soc. AIME* **236** (1966) 781–796.

Aaronson, H. I. *The Mechanism of Phase Transformations in Crystalline Solids*, The Institute of Metals, London (1969) 270–281.

Aaronson, H. I. and Wells, C. *Trans. AIME* **206** (1956) 1216–1223.

Aaronson, H. I., Laird, C. and Kinsman, K. R. *Phase Transformations*, ASM, Metals Park, Ohio, USA (1970) 313–396.

Aaronson, H. I., Hall, M. G., Barnett, D. M. and Kinsman, K. R. *Scripta Metall.* **9** (1975) 705.

Aaronson, H. I., Plichta, H. R., Franti, G. W. and Russell, K. C. *Metall. Trans*. **9A** (1978) 363.

Aaronson, H. I., Enomoto, M. and Reynolds, W. T. *Advances in Phase Transitions,* eds. J. D. Embury and G. R. Purdy, Pergamon Press, Oxford (1988) 20–36.

Abe, F., Araki, H. and Noda, T. *Materials Science and Technology* **6** (1990) 714–723.

Abson, D. J. *Welding Institute Research Report 7931.01/86/544.3,* The Welding Institute Abington, Cambridge, (1986) pp. 1–30.

Abson, D. J. *Nonmetallic inclusions in ferritic steel weld metals – a review,* International Institute for Welding, Document IX–1486–87 (1987).

Abson, D. J. and Pargeter, R. J. *Int. Met. Rev.* **31** (1986) 141–194.

Adcock, J. N. *JISI* **200** (1962) 909–913.

Afrouz, A., Collins, M. J. and Pilkington, R. *Metals Tech.* **10** (1983) 461.

Agren, J. *Acta Metallurgica* **37** (1989) 181–189.

Akbasoglu, F. C. and Edmonds, D. V. *Metall. Trans. A* **21A** (1990) 889–893.

Alberry, P. J. and Jones, W. K. C. *Metals Technology* **11** (1977) 557–566.

Alberry, P. J. and Jones, W. K. C. *CEGB internal report R/M/R282*, Central Electricity Research Laboratories, Leatherhead, Surrey, U.K. (April 1979).

Alberry, P. J., Brunnstrom, R. R. L. and Jones, K. E. *Metals Technology* **10** (1983) 28.

Al-Salman, S. A. and Ridley, N. *Scripta Metall.* **18** (1984) 789–791.

Ali, A. PhD Thesis, University of Cambridge (1990).

Ali, A. and Bhadeshia, H. K. D. H. *Materials Science and Technology* **5** (1989) 398–402.

Ali, A. and Bhadeshia, H. K. D. H. *Materials Science and Technology* **6** (1990) 781–784.

Ali, A. and Bhadeshia, H. K. D. H. *Materials Science and Technology* **7** (1991) 895–903.

Allen, N. P. and Pfeil, L. B. *ISI Special Rep. 24*, London (1939) 369–390.

Allen, N. P., Pfeil, L. B. and Griffiths, W. T. *2nd Report, Alloy Steels Research Comm.*, Iron and Steel Institute, London (1939) 369.
Allten, A. G. *Discussion* to ?tf>Owen (1954).
Allten, A. G. and Payson, P. *Trans. ASM* **45** (1953) 498.
Amano, K., Haromura, T., Shiga, C., Enami, T. and Tanaka, T. *Accelerated Cooling of Rolled Steel*, eds. G. E. Ruddle and A. F. Crawley, Pergamon Press, Oxford, UK (1988) 43–56.
American Society for Metals *Atlas of Isothermal and Cooling Transformation Diagrams*, ASM, Ohio, USA (1977) 28.
American Society for Testing Materials *Special Technical Publication 155*, Metals Park, Ohio, USA (1955).
Andrews, K. W. *Acta Metall.* **11** (1963) 939–946.
Antia, D. P., Fletcher, A. and Cohen, M. *Trans. ASM* **32** (1944) 290.
Ashby, M. F. *Proc. Roy. Soc. Lond.* **A322** (1987) 393–407.
Ashby, M. F. and Easterling, K. E. *Acta Metallurgica* **32** (1982) 1969–1978.
Atkinson, C. *Acta Metallurgica* **15** (1967) 1207–1211.
Austin, A. E. and Schwartz, C. M. *Proc. ASTM* **52** (1952) 592–596.
Austin, A. E. and Schwartz, C. M. *Proc. ASTM* **55** (1955) 623–625.
Avrami, M. *J. Chem. Phys.* **7** (1939) 1103.
Avrami, M. *J. Chem. Phys.* **8** (1940) 212.
Azevedo, T. A. L. and Galvao-da-Silva, E. *Scripta Metall.* **12** (1978) 113–117.
Aziz, M. J. *Journal of Applied Physics* **53** (1982) 1158–1168.
Aziz, M. J. *Applied Physics Letters* **43** (1983) 552–554.
Babu, B. N. P., Bhat, M. S., Parker, E. R. and Zackay, V. F. *Metall. Trans. A* **7A** (1976) 17–22.
Babu, S. S. and Bhadeshia, H. K. D. H. *Materials Science and Technology* **6** (1990) 1005–1020.
Babu, S. S., Bhadeshia, H. K. D. H., and Svensson, L.-E. *Journal of Materials Science Letters* **10** (1991) 142–144.
Babu, S. S., Hono, K. and Sakuri, T. *Applied Surface Science* **67** (1993) 321–327.
Babu, S. S., David, S. A., Vitek, J. M., Mundra, K. and DebRoy, T. *Maaterials Science and Technology* **11** (1995) 186–199.
Bagaryatski, Y. A. *Dokl. Akad. Nauk. SSSR* **73** (1950) 1161.
Bailey, E. F. *Trans. A. SM* **46** (1954) 830–854.
Bain, E. C. *Chem. Met. Eng.* **25** (1921) 657–664.
Bain, E. C. *Trans. AIMME* **70** (1924) 25–46.
Bain, E. C. *Trans. AIMME* **100** (1932) 13.
Bain, E. C. *Alloying Elements in Steel*, ASM, Cleveland, Ohio, USA (1939).
Bain, E. C. *Sorby Centennial Symposium on the History of Metallurgy*, ed. C. S. Smith, Gordon and Breach Publisher, New York (1963) 121.
Baker, J. C. and Cahn, J. W. *Acta Metall.* **17** (1969) 575–578.
Baker, J. C. and Cahn, J. W. *Solidication*, ASM, Metals Park, Ohio, USA (1971) 23–54.
Baker, R. G. and Nutting, J. *JISI* **192** (1959) 257–268.
Bannova, M. I. *Fiz. Metal. Metlloved.* **41** (1976) 1104–1106.
Barbaro, F. J., Edwards, R. H. and Easterling, K. E. *7th National Conference of the Australian X-Ray Analysis Association (AXAA-88)*, University of Western Australia, (August 1988) 1–14.

Barbaro, F. J., Krauklis, P. and Easterling, K. E. *Materials Science and Technology* **5** (1989) 1057–1068.
Barford, J. *JISI* **204** (1966) 609–614.
Barford, J. and Owen, W. S. *JISI* **197** (1961) 146.
Barnard, S. J., Smith, G. D. W., Garratt-Reed, A. J. and Vander Sande, J. *Advances in the Physical Metallurgy and Applications of Steels*, Metals Society, London (1981) 33–38.
Barnard, S. J., Smith, G. D. W., Garratt-Reed, A. J. and Vander Sande, J. *Solid → Solid Phase Transformations*, TMS of AIME, Warrendale, PA, USA (1982) 881–885.
Barnard, S. J., Smith, G. D. W., Sarikaya, M. and Thomas, G. *Scripta Metall.* **15** (1981) 387.
Barritte, G. S. PhD Thesis, University of Cambridge (1982).
Barritte, G. S., Ricks, R. A. and Howell, P. R. *Quantitative Microanalysis with High Spatial Resolution*, The Metals Society, London (1982) 112–118.
Bastien, P. G. *JISI* **187** (1957) 281–291.
Bayerlein, M., Mughrabi, H., Kesten, M. and Meier, B. *Materials Science and Engineering* **A159** (1992) 35–41.
Benjamin, J. S. *Metall. Trans.* **1** (1970) 2943–2951.
Bee, J. V. and Honeycombe, R. W. K. *Metall. Trans.* **9A** (1978) 587.
Bell, T. and Farnell, B. C. *The Mechanism of Phase Transformations in Crystalline Solids*, Institute of Metals, London (1969) 282.
Benson, J. P. and Edmonds, D. V. *Metal Science* **12** (1978) 223–232.
Bhadeshia, H. K. D. H. *Acta Metall.* **28** (1980a) 1103–1114.
Bhadeshia, H. K. D. H. *Scripta Metall.* **14** (1980b) 821–824.
Bhadeshia, H. K. D. H. *Acta Metall.* **29** (1981a) 1117–1130.
Bhadeshia, H. K. D. H. *International Conference on Solid → Solid Phase Transformations*, eds. H. I. Aaronson *et al.*, TMS–AIME, Warrendale, PA, U.S.A. (1981b) 1041–1048.
Bhadeshia, H. K. D. H. *Metal Science* **15** (1981c) 175–177.
Bhadeshia, H. K. D. H. *Metal Science* **15** (1981d) 178–180.
Bhadeshia, H. K. D. H. *Journal of Materials Science* **17** (1982a) 383–386.
Bhadeshia, H. K. D. H. *J. de Physique* **43** (1982b) C4-437–441.
Bhadeshia, H. K. D. H. *Metal Science* **16** (1982c) 167–169.
Bhadeshia, H. K. D. H. *Journal of Materials Science* **18** (1983a) 1473–1481.
Bhadeshia, H. K. D. H. *Int. Conf. on Phase Transformations in Ferrous Alloys*, Marder A. R. and Goldstein, J. I. eds. A.S.M., Cleveland, Ohio, USA (1984) 335–340.
Bhadeshia, H. K. D. H. *Materials Science and Technology* **1** (1985a) 497–504.
Bhadeshia, H. K. D. H. *Progress in Materials Science* **29** (1985b) 321–386.
Bhadeshia, H. K. D. H. *Scripta Metall. Software Survey Section* **22** (1988a) I–IV.
Bhadeshia, H. K. D. H. *Proc. of Int. Conf. on Solid → Solid Phase Transformations*, Cambridge, ed. G. W. Lorimer, Institute of Metals, London (1988b) 309–314.
Bhadeshia, H. K. D. H. *Materials Science and Technology* **5** (1989) 131–137.
Bhadeshia, H. K. D. H. *Metallurgy, Welding, and Qualification of Microalloyed (HSLA) Steel Weldments*, eds. J. T. Hickey, D. G. Howden and M. D. Randall, American Welding Society, Florida, USA (1990) 34–69.
Bhadeshia, H. K. D. H. *Materials Science and Engineering A*, **A223** (1997) 64–77.
Bhadeshia, H. K. D. H. *Materials Science Forum* **284–286** (1998) 39–50.

Bhadeshia, H. K. D. H. *Materials Science and Engineering A* **273–275** (1999) 58–66.
Bhadeshia, H. K. D. H. *Proceedings of Ultra-Steel 2000*, National Research Insitute for Metals, Tsukuba, Japan (2000) 205–214.
Bhadeshia, H. K. D. H. and Edmonds, D. V. *Metall. Trans.* **10A** (1979a) 895–907.
Bhadeshia, H. K. D. H. and Edmonds, D. V. *Metal Science* **13** (1979b) 325–334.
Bhadeshia, H. K. D. H. and Edmonds, D. V. *Acta Metall.* **28** (1980a) 1265–1273.
Bhadeshia, H. K. D. H. and Edmonds, D. V. *Metal Science* **14** (1980b) 41–49.
Bhadeshia, H. K. D. H. and Waugh, A. R. *Proc. of Int. Conf. on Solid → Solid Phase Transformations*, Pittsburgh, ASM, Metals Park, Ohio, U.S.A. (1981) 993–998.
Bhadeshia, H. K. D. H. and Waugh, A. R. *Acta Metall.* **30** (1982) 775–784.
Bhadeshia, H. K. D. H. and Edmonds, D. V. *Metal Science* **17** (1983a) 411–419.
Bhadeshia, H. K. D. H. and Edmonds, D. V. *Metal Science* **17** (1983b) 420–425.
Bhadeshia, H. K. D. H., Svensson, L. E. and Gretoft, B.*Acta Metall.* **33** (1985) 1271–1283.
Bhadeshia, H. K. D. H., Svensson, L. E. and Gretoft, B. *J. Materials Science* **21** (1986a) 3947–3951.
Bhadeshia, H. K. D. H., Svensson, L. E. and Gretoft, B. *Proc. of the 4th Scand. Symposium on Materials Science,* University of Trondhiem, Norwegian Inst. of Technology, Trondheim, Norway (1986b) 153–157.
Bhadeshia, H. K. D. H., Svensson, L. E. and Gretoft, B. *Welding Metallurgy of Structural Steels,* ed. J. Y. Koo, AIME, Warrendale, Penn. (1987) 517–530.
Bhadeshia, H. K. D. H. and Svensson, L. E. *Joining and Materials* **2** (1989a) 182R–187R.
Bhadeshia, H. K. D. H. and Svensson, L. E. *Joining and Materials* **2** (1989b) 236R–238R.
Bhadeshia, H. K. D. H. and Svensson, L. E. *J. Materials Science* **24** (1989c) 3180–3188.
Bhadeshia, H. K. D. H. and Christian, J. W. *Metall. Trans. A* **21A** (1990) 467–497.
Bhadeshia, H. K. D. H., David, S. A., Vitek, J. M. and Reed, R. W. *Materials Science and Technology* **7** (1991) 686–698.
Bhadeshia, H. K. D. H. *Mathematical Modelling of Weld Phenomena 2*, ed. H. Cerjak, The Institute of Materials, London (1995) 71–118.
Bhadeshia, H. K. D. H. *Mathematical Modelling of Weld Phenomena 3*, ed. H. Cerjak, The Institute of Materials, London (1997) 229–284.
Bhadeshia, H. K. D. H., Strang, A., Gooch, D. J. *International Materials Reviews* **43** (1998) 45–69.
Bhat, M. S. *PhD Thesis*, Microstructure and Mechanical Properties of AISI 4340 Steel modified with Al and Si, Lawrence Berkley Laboratories, California (1977).
Bhattacharyya, S. and Kehl, G. L. *Trans. ASM* **47** (1955) 351–379.
Bilby, B. A. and Christian, J. W. *The Mechanism of Phase Transformations in Crystalline Solids*, Institute of Metals, London, Monograph No. 18 (1956) 121–171.
BISRA *Atlas of Isothermal Transformation Diagrams of BS En Steels*, Special Report 56, 2nd ed., The Iron and Steel Institute, London (1956).
Blackmore, P. A. and Harding, R. A. *Proc. 1st Int. Conf. on Austempered Ductile Iron*, ASM, Metals Park, Ohio, USA (1984) 117.
Bodnar, R. L., Ohhashi, T. and Jaffe, R. I. *Metall. Trans. A* **20A** (1989) 1445–1460.
Bodnar, R. L., Shen, Y., Lin, M., Elwood, D. W., Feher, F. C. and Roe, G. J. *Proc. Materials Solutions '97 on Accelerated Cooling/Direct Quenching Steels*, TMS–AIME, Warrendale, Pennsylvania, USA (1997) 3–13.

Bondt, De M. and Deruyttere, A. *Acta Metall.* **15** (1967) 993.
Bowen, P. and Knott, J. F. *Metall. Trans. A* **17A** (1986) 231.
Bowen, P., Druce, S. G. and Knott, J. F. *Acta Metall.* **34** (1986) 1121–1131.
Bowles, J. S. and MacKenzie, J. K. *Acta Metall.* **2**(1954) 129–234.
Bowles, J. S. and Kennon, N. F. *J. Aust. ISI* **5** (1960) 106–113.
Bowles, J. S., Muddle, B. C. and Wayman, C. M. *Acta Metall.* **25** (1977) 513–520.
Bowles, J. S. and Wayman, C. M. *Acta Metall.* **27** (1979) 833.
Bradley, J. R., Rigsbee, J. M. and Aaronson, H. I. *Metall. Trans. A* **8A** (1977) 323–333.
Bramfitt, B. L. *Metall. Trans.* **1** (1970) 1987–1995.
Bramfitt, B. L. and Marder, A. R. *Metall. Trans.* **4** (1973) 2291.
Brown, G. T. and James, B. A. *Metals Technology* **7** (1980) 261–268.
Brown, P. W. and Mack, D. J. *Metall. Trans.* **4** (1973a) 2639–2643.
Brown, P. W. and Mack, D. J. *Metall. Trans.* **4** (1973b) 2850–2851.
Brozz, P., Buzzichelli, G., Mascanzoni, A. and Mirabile, M. *Metal Science* **11** (1977) 123–129.
Buchi, G. J. P., Page, J. H. R. and Sidey, M. P. *JISI* **203** (1965) 291–298.
Buerger, M. J. *Phase Transformations in Solids*, Wiley, New York (1951) 183.
Buhler, H., Buchholz, H. and Schultz, E. H. *Arch. Eisenhuttenwes.* **5** (1932) 413.
Buhler, H. and Scheil, E. *Arch. Eisenhuttenwes.* **6** (1933) 283.
Buhler, H. *Arch. Eisenhuttenwes.* **26** (1955) 51.
Bunshah, R. F. and Mehl, R. F. *Trans. AIME* **193** (1953) 1251–1258.
Burdekin, F. M. *Advances in Physical Metallurgy*, eds. J. A. Charles and G. C. Smith, The Institute of Metals, London, (1990) 27–45.
Burgess, P. B. and Kennon, N. F. *Metals Forum* **4** (1978) 185–190.
Bush, M. E. and Kelly, P. M. *Acta Metall.* **19** (1971) 1363–1371.
Caballero, F. G., Bhadeshia, H. K. D. H., Mawella, Jones and Brown *Materials Science and Technology* **17** (2001) in press.
Cahn, J. W. *Acta Metall.* **4** (1956) 572.
Callender, W. R. PhD Thesis, University of Sheffield (1983).
Cameron, J. A. *JISI* **194** (1956) 260–267.
Cane, B. J. and Townsend, R. D. *Central Electricity Generating Board Report TPRD/L/2674/N84* Leatherhead, Surrey, UK (1984).
Carruthers, R. B. and Collins, M. J. *Quantitative Microanalysis with High Spatial Resolution*, Institute of Metals, London (1981) 108.
Carruthers, R. B. and Collins, M. J. *Metals Technology* **10** (1983) 461.
Chance, J. and Ridley, N. *Metall. Trans. A* **12** (1981) 1205.
Chandel, R. S., Orr, R. F., Gianetto, J. A., McGrath, J. T., Patchett, B. M. and Bicknell, A. C. *The Microstructure and Mechanical Properties of Narrow Gap Welds in 2.25Cr–1Mo Steel*, Report ERP/PMRL 85–16(OP–J) of the Physical Metallurgy Research Laboratories, CANMET, Energy, Mines and Resources Canada, Ottawa, Canada (1985).
Chanani, G. R., Antolovich, S. D. and Gerberich, W. W. *Metall. Trans.* **3** (1972) 2661–2672.
Chandrasekharaiah, M. N., Dubben, G. and Kolster, B. H. *American Welding Journal* **71** (1994) 247s–252s.

Chang, L. C. *Metallurgical and Materials Transactions A* **30A** (1999) 909–916.
Chang, L. C. and Bhadeshia, H. K. D. H. *Materials Science and Technology* **11** (1995a) 874–881.
Chang, L. C. and Bhadeshia, H. K. D. H. *Materials Science and Technology* **11** (1995b) 105–108.
Chapetti, M. D., Kitano, T., Tagawa, T. and Miyata, T. *Fatigue and Fracture of Engineering Materials and Structures* **21** (1998) 1525–1536.
Chart, T. G., Counsell, J. F., Jones, G. P., Slough, W. and Spencer, P. J. **20** (1975) 57–82.
Chester, N. A. and Bhadeshia, H. K. D. H. *Journal de Physique IV* **7**, **Colloque C5** (1997) 41–46.
Chevenard, P. and Portevin, A. *Rev. Met.* **28** (1931) 417.
Chijiiwa, R., Tamehiro, H., Hirai, M., Matsuda, H. and Mimura, H. *Offshore Mechanics and Arctic Engineering (OMAE)*, Houston, Texas (1988) 1–8.
Choi, B. Y., Krauss, G. and Matlock, D. K. *Scripta Metall.* **22** (1988) 1575–1580.
Choi, S. J., Kwon, S.-J., Choo, S.-H. and Lee, S. *Materials Science and Engineering A* **A165** (1999) 208–216.
Christian, J. W. *Acta Metall.* **6** (1958) 377–379.
Christian, J. W. *The Decomposition of Austenite by Diffusional Processes*, ed. V. F. Zackay and H. I. Aaronson, Interscience Publishers, New York (1962) 387–546.
Christian, J. W. *Physical Properties of Martensite and Bainite*, Iron and Steel Institute Spec. Rep. No. 93 (1965a) 1–19.
Christian, J. W. *Theory of Transformations in Metals and Alloys*, Pergamon Press, Oxford (1965b).
Christian, J. W. *Monogr. Ser. Inst. Metals*, Number 33, Institute of Metals, London **33** (1969) 129.
Christian, J. W. *Strengthening Methods in Crystals*, eds. A. Kelly and R. Nicholson, Elsevier, North-Holland, Amsterdam (1971) 261–329.
Christian, J. W. *Theory of Transformations in Metals and Alloys*, Part 1, 2nd. ed., Pergamon Press, Oxford, (1975).
Christian, J. W. *Phase Transformations*, Vol. 1, No.1, series 3, Institute of Metallurgists, London (1979a) 1–11.
Christian, J. W. *ICOMAT 79, International conference on martensitic transformations*, Cambridge, Massachusetts (1979b) 220–234.
Christian, J. W. and Crocker, A. G. *Dislocations in Solids*, ed. F. R. N. Nabarro, vol. 3, North–Holland, Amsterdam (1980).
Christian, J. W. *Metall. Trans. A* **13A** (1982) 509–538.
Christian, J. W. *Metall. Trans. A* **14A** (1983) 1237.
Christian, J. W. *Encyclopedia of Materials Science and Engineering*, Pergamon Press, Oxford (1986) 2741–2743.
Christian, J. W. *Metall. Trans. A* **21A** (1990a) 799–803.
Christian, J. W. *Materials Science and Engineering* **A127** (1990b) 215–227.
Christian, J. W. *Metallurgical and Materials Transactions A* **25A** (1994) 1821–1839.
Christian, J. W. *Progress in Materials Science* **42** (1997) 109–124.
Christian, J. W. and Edmonds, D. V. *Int. Conf. on Phase Transformations in Ferrous*

Alloys, eds. A. R. Marder and J. I. Goldstein, AIME, Cleveland, Ohio, USA (1984) 293–326.
Christian, J. W. and Mahajan, S. *Progress in Materials Science* **39** (1995) 1–157.
Chung, D. W., Todd, J. A., Youngs, J. K. and Parker, E. R. *Advanced Materials for Pressure Vessel Service with Hydrogen at High Temperatures and Pressures*, ed. M. Semchyshen, **MPA–18** (1982) 25.
Clark, H. M. and Wayman, C. M. *Phase Transformations*, ASM, Metals Park, Ohio, USA (1970) 59–114.
Clayton, P., Sawley, K. J., Bolton, P. J. and Pell, G. M. *Wear* **120** (1987) 199–220.
Coates, D. E. *Metall. Trans.* **3** (1972) 1203–1212.
Coates, D. E. *Metall. Trans.* **4** (1973a) 1077–1086.
Coates, D. E. *Metall. Trans.* **4** (1973b) 2313–2325.
Cohen, M. *Trans. ASM* **28** (1940) 537.
Cohen, M. Discussion to Troiano and Greninger (1946).
Cohen, M., Machlin, E. S. and Paranjpe, V. G. *Thermodynamics in Physical Metallurgy*, ASM, Cleveland, Ohio, USA (1950).
Coheur, P. and Habraken, L. *Rev. Univ. Min.* **94** (1951) 107.
Coldren, A. P., Cryderman, R. L., Semchysen, M. *Steel Strengthening Mechanisms*, Climax Molybdenum, Ann Arbor, USA, (1969) 17.
Collins, L. E., Knight, R. F., Ruddle, G. E. and Boyd, J. D. *Accelerated Cooling of Steel*, ed. P. D. Southwick, TMS–AIME (1985) 261–282.
Collins, M. *Materials Science and Technology* **5** (1989) 323–327.
Conrad, H. *J. Metals* (July 1964) 582.
Cotterell, B. *Trans. ASME, J. Basic. Eng.* **87** (1965) 230.
Cottrell, A. H. *JISI* **151** (1945) 93P–104P.
Cottrell, A. H. *International Journal of Pressure Vessels and Piping* **64** (1995) 171–174.
Cottrell, S. A. and Ko, T. *JISI* **173** (1953) 225.
Crosky, A., McDougall, P. G. and Bowles, J. S. *Acta Metall.* **28** (1980) 1495–1504.
Cullison, A. *American Welding Journal* **70** (1991) 80–82.
Curry, D. A. and Knott, J. F. *Metal Science* **12** (1978) 511.
Dadian, M. *Advances in Welding Science and Technology*, ed. S. A. David, ASM, Metals Park, Ohio, USA (1987) 101–117.
Daigne, J., Guttmann, M. and Naylor, J. P. *Mat. Sci. and Eng.* **56** (1982) 1–10.
Dallum, C. B. and Olson, D. L. *American Welding Journal* (1989) 198s–205s.
Darken, L. S. *Transactions AIME* **180** (1949) 430–438.
Dauskardt, R. H. and Ritchie, R. O. *ASME PVP* Vol. 114/MPC Vol. 27, American Society for Mechanical Engineers, New York, NY (1986) 17–28.
Davenport, A. S. *Trans. Met. Soc. AIME* **145** (1941) 301–340.
Davenport, A. T. *The Crystallography of Upper Bainite*, Republic Steel Research Rep. on Project 12051 (February 1974) 1–35.
Davenport, A. T. *The Hot Deformation of Austenite*, ed. J. B. Ballance, TMS–AIME, New York, USA (1977) 517–536.
Davenport, E. S. and Bain, E. C. *Trans. Met Soc. AIME* **90** (1930) 117–154; Also published in *Metall. Trans. A* **1** (1970) 3501–3530, as a Metallurgical Classic, with commentary by H. W. Paxton.

Davenport, E. S. *Trans. ASM* **27** (1939) 837–886.
Davies, G. J. and Garland, J. G. *International Metals Reviews* **20** (1975) 83–106.
Davies, G. J., Kallend, J. S. and Morris, P. P. *The Hot Deformation of Austenite*, ed. J. B. Ballance, TMS–AIME, New York, USA (1977) 599–626.
Davies, R. G. and Magee, C. L. *Proc. Second International Conference on the Strength of Metals and Alloys*, ASM (1970a) 817.
Davies, R. G. and Magee, C. L. *Metall. Trans.* **1** (1970b) 2927–2931.
Davies, R. G. and Magee, C. L. *Metall. Trans.* **2** (1971) 1939–1947.
Dearden, J. and O'Neill, H. *Trans. Inst. Weld.* **3** (1940) 203.
DeArdo, A. J. *Accelerated Cooling of Rolled Steel*, eds. G. E. Ruddle and A. F. Crawley, Pergamon Press, Oxford, UK (1988) 3–27.
Deep, G. and Williams, W. M. *Canadian Metall. Quart.* **14** (1975) 85–96.
Degang, Y., Dajun, C., Jinghong, Z., Yirong, H. E. and Fufa, S. *Acta Metallurgica Sinica* **2** (1989) 161–167.
DeHoff, R. T. and Rhines, F. N., eds. *Quantitative Microscopy*, McGraw–Hill Book Company, New York (1968).
Delaey, L. and Warlimont, H. *Shape Memory Effects in Alloys*, ed. J. Perkins, TMS–AIME, Plenum Press, New York, NY (1975) 89–114.
Deliry, J. *Mem. Sci. Rev. Metall.* **62** (1965) 527–550.
Denis, S., Gautier, E., Simon, A. and Beck, G. *Materials Science and Technology* **1** (1985) 805–814.
Devanathan, R. and Clayton, P. *Rolling/Sliding Wear Behaviour of Three Bainitic Steels*, Private communication (1990).
Diesburg, D. E., Kim, C. and Fairhurst, W. *Heat Treatment 81*, The Institute of Metals, London, (1981) 178.
Dionne, S., Krishnadev, M. R., Collins, L. E. and Boyd, J. D. *Accelerated Cooling of Rolled Steel*, eds. G. E. Ruddle and A. F. Crawley, Pergamon Press, Oxford, UK (1988) 71–84.
Dorazil, E., Barta, B., Munsterova, E., Stransky, L. and Huvar, A. *AFS Int. Cast Met. J.* (June 1962) 52–62.
Dorazil, E., Svejcar *Arch Eisenhuttenaves* **50** (1979) 293–298.
Dorn, J. E. *Dislocation Dynamics*, eds. A. R. Rosenfield, G. T. Hahn, A. L. Bement and R. I. Jaffee, McGraw-Hill, New York (1968) 27.
Dowling, J. M., Corbett, J. M. and Kerr, H. W. *Metall. Trans. A* **17A** (1986) 1611.
Drozdov, B. Ya., Kogan, L. I. and Entin, R. I. *Fiz. Metal. Metalloved.* **13**, No. 5 (1962) 776–779; English translation in *Physics of Metals and Metallography* **13** No. 5 (1962) 135–138.
Dubé C. A. PhD Thesis, Carnegie Institute of Technology (1948).
Dubé, C. A., Aaronson, H. I. and Mehl, R. F. *Rev. Met.* **55** (1958) 201.
Dubensky, W. J. and Rundman, K. B. *AFS Transactions* **93** (1985) 389–394.
Dubrov, V. A. *Fiz. Metal. Metalloved.* **28** (No. 2) (1969) 309–314; English translation in *Physics of Metals and Metallography* **28** No. 2 (1969) 126–131.
Duckworth, W. E. *Journal of Metals* **18** (1966) 915.
Duckworth, W. E., Taylor, P. R. and Leak, D. A. *JISI* **55** (1964) 135.
Dunne, D. P. and Wayman, C. M. *Metallurgical Transactions* **202** (1971) 2327–2341.

Durbin, M. and Krahe, P. R. *Processing and Properties of Low-Carbon Steel*, AIME, Warrendale, Pennsylvania, USA (1973) 109–31.
Easterling, K. E. *Introduction to the Physical Metallurgy of Welding*, Butterworths, London (1983).
Edwards, D. P. *JISI* **207** (1969) 1494–1502.
Edwards, R. H. and Kennon, N. F. *J. Aust. Inst. Metals* **19** (1974) 45.
Edwards, R. H. and Kennon, N. F. *Metall. Trans.* **9A** (1978) 1801.
Ehrenfest, P. *Proc. Acad. Sci. Amsterdam* **36** (1933) 153.
Entin, R. *Decomposition of Austenite by Diffusional Processes*, Interscience, New York (1962) 295–311.
Ericsson, C. E., Bhat, M. S., Parker, E. R. and Zackay, V. F. *Metall. Trans. A* **7A** (1976) 1800–1803.
Es-Souni, M. and Beaven, P. A. *Microanalysis of inclusion/matrix interfaces in weld metals*, International Institute of Welding Document II–A–815–90 (1990).
Esaka, K., Koyama, K., Matsumura, Y. and Tashiro, M. *HSLA Steels: Metallurgy and Applications*, eds. J. M. Gray, T. Ko, Z. Shouhua, W. Baorong and X. Xishan, Beijing, China, ASM International (1985) 959–968.
Eterashvili, T. V., Utevsky, L. M. and Spasskiy, M. N. *Phys. Met. Metall.* **48**(4) (1979) 113–121.
Evans, G. M. *International Institute of Welding Document II–A–666–86* (1986).
Evans, G. M. *International Institute of Welding Document II–A–739–86* (1988).
Evans, P. R. V. and O'Neill, H. *JISI* **191** (1959) 34.
Evans, G. M. *The effect of aluminium in shielded metal-arc C–Mn steel multi-run deposits,* International Institute of Welding Document II–1146–90 sub commission II–A–796–90 (1990) 1–14.
Farrar, R. A. and Harrison, P. L. *Journal of Materials Science* **22** (1987) 3812–3820.
Fisher, J. C. *Metals Transactions* **185** (1949) 688–700.
Fisher, J. C. *Thermodynamics in Physical Metallurgy*, ASM, Cleveland, Ohio, USA (1950).
Fisher, R. M. *Proc. Int. Conf. on Electron Microscopy*, Springer Verlag OHG, Berlin (1958) 579–588.
Fitzgerald, F. *Metals and Materials* **7** (1991) 378–387.
Fleck, N. A., Grong, O., Edwards, G. R. and Matlock, D. K. *Welding Journal* (1986) 113s–121s.
Foct, J., Rochegude, P. and Hendry, A. *Scripta Metallurgica* **23** (1988) 613–615.
Fondekar, M. K., Rao, A. M. and Mallik, A. K. *Metall. Trans.* **1** (1970) 885–890.
Forster, F. and Scheil, E. *Z. Metallkunde* **28** (1936) 245–247.
Forster, F. and Scheil, E. *Naturwissenschaften* **25** (1937) 439.
Forster, F. and Scheil, E. *Z. Metallkunde* **32** (1940) 165.
Fourlaris, G., Baker, A. J. and Papadimitriou, G. D. *Acta Materialia* **44** (1996) 4791–4805.
Fowler, R. H. and Guggenhiem, E. A. *Statistical Thermodynamics*, Cambridge University Press, New York (1939) 442.
Franetovic, V., Sachdev, A. K. and Ryntz, E. F. *Metallography* **20** (1987a) 15–37.
Franetovic, V., Shea, M. M. and Ryntz, E. F. *Materials Science and Engineering* **96** (1987b) 231–245.
Franklin, A. G. *J. Iron Steel Inst.* **207** (1969) 181–186.

Franti, G. W., Williams, J. C. and Aaronson, H. I. *Metall. Trans.* **9A** (1978) 1641.
Freiwillig, R., Kudrman, J. and Chraska, P. *Metall. Trans.* **7A** (1976) 1091.
Fridberg, J., Torndahl, L.-E. and Hillert, M. *Jernkont. Ann.* **153** (1969) 263–273.
Fujita, N. and Bhadeshia, H. K. D. H. *Materials Science and Technology* **15** (1999) 627–634.
Fullman, R. L. *Trans. AIMME* **197** (1953) 477, 1267.
Gagne, M. *AFS Transactions* **93** (1985) 801–812.
Garnham, J. University of Leicester, private communication (1989).
Garwood, R. D. *J. Inst. Met.* **83** (1954–1955) 64–68.
George, T., Parker, E. R. and Ritchie, R. O. *Materials Science and Technology* **1** (1985) 198–208.
Ghonem, H., Kalousek, J. and Stone, D. *Specialty Steels and Hard Materials*, Pretoria, South Africa, Pergamon Press, Oxford (1982) 259.
Ghosh, G. and Olson, G. B. *Acta Metallurgica et Materialia* **42** (1994) 3361–3370.
Ghosh, G., Campbell, C. E. and Olson, G. B. *Metallurgical and Materials Transactions A* **30A** (1999) 501–512.
Gibson, G. B. *Review of cleavage fracture mechanisms in ferritic steels*, UKAEA Report R13227, Harwell, Oxon (1988) referred to by Burdekin (1990).
Gladman, T. Private communication to Honeycombe and Pickering (1972).
Gladman, T. *Physical Metallurgy of Microalloyed Steels*, Inst. of Materials, London (1997) 1–360.
Gladman, T., Dulieu, D. and McIvor, I. D. *Proc. Conf. Microalloying 1975*, Washington, (1–3 October 1975).
Glicksman, M. E., Shaefer, R. J. and Ayres, J. D. *Metall. Trans. A* **7A** (1976) 1747–1759.
Goldak, J., Patel, B., Bibby, M. and Moore, J. *Computational Weld Mechanics*, Carelton University, Canada, private communication (1985).
Goldman, L. M. and Aziz, M. J. *J. Mater. Res.* **2** (1987) 524–527.
Goodenow, R. H. and Hehemann, R. F. *Discussion* to Speich (1962).
Goodenow, R. H., Matas, S. J. and Hehemann, R. F. *Trans. AIMME* (1963) 651–658.
Goodenow, R. H., Hehemann, R. F. *Trans. AIMME* **233** (1965) 1777.
Goodenow, R. H., Barkalow, R. H. and Hehemann, R. F. *ISI Spec. Rep. 93*, London (1969) 135–141.
Gorbach, V. G., Jelenkowski, J. and Filipiuk, J. *Materials Science and Technology* **5** (1989) 36–39.
Gordine, J. and Codd, I. *JISI* **207** (1969) 461–467.
Gourgues, A.-F., Flower, H. M. and Lindley, T. C. *Materials Science and Technology* **16** (2000) 26–40.
Grabke, H. J., Hennesen, K., Moller, R. and Wei, W. *Scripta Metall.* **21** (1987) 1329–1334.
Graham, L. W. and Axon, H. J. *JISI* **191** (1959) 361.
Graf, M. K., Hillenbrand, H. G., Peters, P. A. *Accelerated Cooling of Steel*, ed. P. D. Southwick, TMS–AIME (1985) 349–366.
Grange, R. A. *Metall. Trans.* **2** (1971) 417.
Grassl, K., Thompson, S. W. and Krauss, G. *New Options for Steel Selection for Automotive Applications*, Society of Automotive Engineers, Warrendale, USA, Technical Paper 890508 (March 1989) 1–13.
Greenwell, B. Private communication, NEI Parsons, Ltd., Newcastle, UK (1989).

Greenwood, G. W. *Acta Metall.* **4** (1956) 243.
Gregg, M. and Bhadeshia, H. K. D. H. *Metallurgical Transactions A* **25** (1994a) 1603–1611.
Gregg, M. and Bhadeshia, H. K. D. H. *Acta Metallurgica et Materialia* **42** (1994b) 3321–3330.
Gregory, E. and Simmons, E. N. *The Structure of Steel*, Blackie and Son Ltd. London (1947).
Greninger, A. B. and Troiano, A. R. *Trans. AIMME* **140** (1940) 307–336.
Griffiths, J. R. and Oates, G. *Metal Science* **11** (1977) 285–292.
Grong, O. *Metallurgical Modelling of Welding*, 2nd edition, Institute of Materials, London (1997) 1–602.
Grong, O. and Matlock, D. K. *Int. Met. Rev.* **31** (1986) 27–48.
Grong, O., Kluken, A. O. and Bjornbakk, B. *Joining and Materials* (1988) 164–169.
Gross, J. H., Stout, R. D. and Czyryca, E. J. *Welding Journal* **74** (1995) 53–62.
Grube, W. L. and Rouze, S. R. *High Temperature–High Resolution Metallography*, Gordon and Breach, New York (1967) 313.
Grujicic, M., Olson, G. B. and Owen, W. S. *Metall. Trans. A* **16A** (1985a) 1713–1722.
Grujicic, M., Olson, G. B. and Owen, W. S. *Metall. Trans. A* **16A** (1985b) 1723–1734.
Grujicic, M., Olson, G. B. and Owen, W. S. *Metall. Trans. A* **16A** (1985c) 1735–1745.
Gulyaev, A. P. *Metallurgy* **15** (1940) 43.
Gutierrez, I., Aranzabal, J., Castro, F. and Urcola, J. J. *Metall. and Materials Transactions A* **26A** (1995) 1045–1060.
Habraken, L. J. *Rev. Met.* **53** (1956) 930.
Habraken, L. J. *Compt. Rend.* **19** (1957) 126.
Habraken, L. J. *Proc. 4th Int. Conf. on Electron Microscopy*, Springer-Verlag, Berlin (1958) 621–628.
Habraken, L. *Physical Properties of Martensite and Bainite*, Special Report 93, Iron and Steel Institute, London (1965) 147.
Habraken, L. J. and Economopolus, M. *Transformation and Hardenability in Steels*, Climax Molybdenum, Ann Arbor, Michigan, USA (1967) 69–107.
Hägg, G. *Z. Kristallogr.* **89** (1934) 92.
Haezebrouck, D. M. Ph.D. Thesis entitled Nucleation and Growth of a Single Martensitic Particle, Massachusetts Institute of Technology (June 1987).
Hall, B. Ph.D. Thesis, University of Cambridge (1990).
Hall, D. J., Self, P. G. and Stobbs, W. M. *J. of Microscopy* **130** (1983) 215–224.
Hannemann, H., Hofmann, W. and Wiester, H. J. *Arch. Eisenhuttewesen* **6** (1932–1933) 199.
Harrison, P. L. and Farrar, R. A. *J. of Materials Science* **16** (1981) 2218–2226.
Harrison, P. L. and Farrar, R. A. *Int. Materials Rev.* **34** (1989) 35–51.
Hawkins, M. J. and Barford, J. *JISI* **210** (1972) 97–105.
Hayrynen, K. L., Moore, D. J. and Rundman, K. B. Presented at the 1988 American Foundry Society Conference, private communication to H. K. D. H. Bhadeshia (1988) 1–13.
Heckel, R. W. and Paxton, H. W. *Trans. ASM* **53** (1961) 539.
Hehemann, R. F., Luhan, V. J. and Troiano, A. R. *Trans. ASM* **49** (1957) 409–426.

Hehemann, R. F. *Phase Transformations*, ASM, Metals Park, Ohio, USA (1970) 397–432.
Hehemann, R. F., Kinsman, K. R. and Aaronson, H. I. *Metall. Trans.* **3** (1972) 1077.
Heitmann, W. F. and Babu, F. B. *Fundamentals of Microalloying Forging Steels*, eds. G. Krauss and S. K. Banerji, The Metallurgical Society of the AIME, Warrendale, Pennsylvania, U.S.A. (1987) 55–72.
Heller, W. and Schweitzer, R. *Railway Gazette International* (October 1980) 855–857.
Heller, W. and Schweitzer, R. *2nd Int. Conf. Heavy Haul Railways*, Colorado, USA (1982) 282–286.
Heritier, B. *et al. HSLA Steels – Technology and Applications*, ASM International, Ohio, U.S.A. (1984) 981–990.
Hildenwall, B. *Prediction of the Residual Stresses Created During Quenching*, PhD.Thesis, Linkoping University, Sweden **1** (1979).
Hillert, M. *Jernkontorets Ann.* **136** (1952) 25–37.
Hillert, M. *Paraequilibrium*, Internal Report, Swedish Inst. Met. Res., Stockholm, Sweden (1953).
Hillert, M. *Jernkontorets Ann.* **141** (1957) 757–764.
Hillert, M. *The Growth of Ferrite, Bainite and Martensite*, Internal Report, Swedish Inst. Met. Res., Stockholm, Sweden (1960).
Hillert, M. *Decomposition of Austenite by Diffusional Processes*, eds. V. F. Zackay and H. I. Aaronson, Interscience, New York (1962) 197–247.
Hillert, M. *Metall. Trans. A* **6A** (1975) 5–19.
Hillert, M. *Solid → Solid Phase Transformations*, TMS–AIME, Warrendale, PA, USA (1982) 789–806.
Hillert, M. and Sundman, B. *Acta Metall.* **24** (1976) 731–743.
Hillert, M., Höglund, L. and Ågren, J. *Acta Metallurgica et Materialia* **41** (1993) 1951–1957.
Hirotsu, K. C. S. and Nagakura, S. *Acta Metall.* **20** (1972) 645–655.
Hirth, J. P. and Cohen, M. *Metall. Trans.* **1** (1970) 3.
Hobbs, R. M., Lorimer, G. W. and Ridley, N. *JISI* **210** (1972) 757.
Hodgson, W. H. and Preston, R. R. *Bulletin of the Canadian Institute of Metals* CIM Bull. (October 1988) 95–101.
Hofer, W. E., Cohn, E. M. and Peebles, W. C. *J. Amer. Chem. Soc.* **71** (1949) 189.
Hoffman, D. W. and Cohen, M. *Acta Metallurgica* **21** (1973) 1215–1223.
Hollomon, J. H. and Jaffe, L. D. *Trans. TMS–AIME* **162** (1945) 223–249.
Homma, H., Ohkita, S., Matsuda, S. and Yamamoto, K. *American Welding Journal* (October 1987) 301s–309s.
Honeycombe, R. W. K. *Phase Transformations in Ferrous Alloys*, eds. A. R. Marder and J. I. Goldstein, The Metallurgical Society of the AIME, Warrendale, Pennsylvania (1984) 259–280.
Honeycombe, R. W. K. and Pickering, F. B. *Metall. Trans.* **3** (1972) 1099–1112.
Honeycombe, R. W. K. *Steels*, Edward Arnold, London (1981).
Honeycombe, R. W. K. *The Plastic Deformation of Metals*, 2nd edition, Edward Arnold, London (1984) 150–151.
Honeycombe, R. W. K. and Bhadeshia, H. K. D. H. *Steels*, 2nd edition, Edward Arnold, London (1995).

Horii, Y., Ohkita, S., Wakabayashi, M. and Namura, M. *Nippon Steel Technical Report* Nippon Steel Company, Japan (1986) 1–9.
Horii, Y., Wakabayashi, M., Ohkita, S. and Namura, M. *Nippon Steel Technical Report* No. 37, Nippon Steel Company, Japan (1988) 1–9.
Horn, R. PhD Thesis, University of California (1976).
Horn, R. M. and Ritchie, R. O. *Metall. Trans. A* **9A** (1978) 1039–1053.
Hornbogen, E. *Materials Science and Engineering A* **A273–275** (1999) 630–633.
Houdremont, E., Koch, E. and Wiester, H.–J. *Arch. Eisenhuttenwesen* **18** (1945) 147.
Houillier, R. Le, Begin, G. and Dubé, C. E. *Metall. Trans.* **2A** (1971) 2645–2653.
Howard, R. T. and Cohen, M. *Trans. AIMME* **176** (1948) 384–400.
Hrivank, I. *Guide to the welding and weldability of CrMo and CrMoV heat resistant steels*, International Institute for Welding Document IX–G–319/c–87 (1987) 1–61.
Huang, D. H. and Thomas, G. *Metall. Trans.* **8A** (1977) 1661.
Hulka, K., Heisterkamp, F. and Nachtel, L. *Processing, Microstructure and Properties of HSLA Steels*, ed. A. J. DeArdo, The Minerals, Metals and Materials Society, Warrendale, Pennsylvania, USA (1988) 153–167.
Hull, D. *Bulletin of the Institute of Metals* **2** (1954) 134–139.
Hultgren, A. *Trans. ASM* **39** (1947) 915–1005.
Hultgren, A. *Jernkontorets Ann.* **4** (1951) 403.
Hultgren, A. *Kungl. Ver. Akad. Handl.* **4** (1953) 1.
Hume-Rothery, W. *The Structures of Alloys of Iron*, Pergamon Press, Oxford (1966) 240–253.
Hume-Rothery, W., Raynor, G. V. and Little, A. T. *Arch Eisenhuttenwesen* **145** (1942) 143.
Hwang, J. R., Peng, K. P. and Wang, C. C. *Journal of Materials Science Letters* **15** (1996) 192–196.
Ichinose, H., Takehara, J. and Ueda, M. *1st Int. Conf. on Heavy Haul Railways*, Perth, Australia (1978).
Ichinose, H., Takehara, J. and Ueda, M. *2nd Int. Conf. on Heavy Haul Railways*, Colorado Springs, USA (1982) 178–186.
Imagumbai, M., Chijiiwa, R., Aikawa, N., Nagumo, M., Homma, H., Matsuda, S. and Mimura, H. *HSLA Steels: Metallurgy and Applications*, eds. J. M. Gray, T. Ko, Z. Shouhua, W. Baorong and X. Xishan, ASM Int., Ohio (1985) 557–566.
Inagaki, M. and Hiroyuki, M. *Quality and reliability in welding*, Hangzhou, China, Welding Institute of the Chinese Mechanical Engineering Society (1984).
Ion, J. C., Easterling, K. E. and Ashby, M. F. *Acta Metall.* **32** (1984) 1949–1962.
Irani, J. J. *British Iron and Steel Research Association Report No. MG/A/60/67*, BSIRA, London (1967).
Irvine, K. J. and Pickering, F. B. *JISI* **187** (1957) 292–309.
Irvine, K. J., Pickering, F. B., Heselwood, W. C. and Atkins, M. *JISI* **195** (1957) 54–67.
Irvine, K. J. and Pickering, F. B. *JISI* **188** (1958) 101.
Irvine, K. J., Llewellyn, D. T. and Pickering, F. B. *JISI* **199** (1961) 153.
Irvine, K. J. and Pickering, F. B. *JISI* **201** (1963) 518–531.
Irvine, K. J. and Pickering, F. B. *ISI Spec. Rep. 93*, London (1965) 110–125.
Isaichev, I. V. *Zhur Tekhn. Fiziki.* **17** (1947) 835.
Ishiguro, T., Murakami, Y., Ohnishi, K. and Watanabe, J. *ASTM-STP 755*, American Society for Testing Materials, Philadelphia, USA (1982) 129–147.

Ishiguro, T., Ohnishi, K., Murakami, Y., Mima, S. and Watanabe, J. *Research on Chrome-Moly Steels*, MPC-21, American Society of Mechanical Engineers, New York (1984) 43–52.

Ishikawa, F., Takahashi, T. and Ochi, T. *Metallurgical and Materials Transactions* **25A** (1994) 929–936.

Ito, Y. and Bessyo, K. *Int. Inst. of Welding Document IX–576–68* (1968).

Ito, Y. and Nakanishi, M. *International Institute for Welding Document XII–113–75* (1975).

Ito, Y. and Nakanishi, M. *Sumitomo Search* **15** (1976) 42–62.

Ito, Y., Nakanishi, M. and Komizo, Y. *Metal Constr.* **14** (1982) 472.

Ivantsov, G. P. *Dokl. Akad. Nauk. SSSR* **58** (1947) 567.

Jack, K. H. *Acta Cryst.* **3** (1950) 392.

Jack, K. H. *JISI* **169** (1951) 26–36.

James, J. S. and Thomson, R. C. *Solid→Solid Phase Transformations 1999*, eds. M. Koiwa, K. Otsuka and T. Miyazaki, Japan Institute for Metals, Tokyo, Japan (1999) 1473–1476.

Jana, S. and Wayman, C. M. *Metall. Trans.* **1** (1970) 2825.

Jellinghaus, W. *Arch. Eisenhuttenwesen* **23** (1952) 459.

Jellinghaus, W. *Arch. Eisenhuttenwesen* **28** (1957) 469.

Jellinghaus, W. and Friedewold, H. *Arch. Eisenhuttenwesen* **31** (1960) 309.

Jepson, M. D. and Thompson, F. C. *JISI* **162** (1949) 49–56.

Jerath, V., Mistry, K., Bird, P. and Preston, R. R. *British Steel Report* Collaborative research, University of Cambridge (H. Bhadeshia) and British Steel Corporation, Report SL/RS/R/S/1975/1/91A (1991) 1–43.

Jihua, Z., Shuchuan, C. and Hsu, T. Y. *Acta Metall.* **37** (1989) 241–246.

Jin, N. and Clayton, P. *Wear* **202** (1997) 202–207.

Jingsheng, Y., Zongsen, Y. and Chengjian, W. *J. of Metals* **40** (1988) 26–31.

Jones, W. K. C. and Alberry, P. J. *Ferritic Steels for Fast Reactor Steam Generators*, British Nuclear Engineering Society Conference, London (June 1977) paper 78, 1–4.

Jones, W. K. C. and Alberry, P. J. *Residual Stresses in Welds by Welded Construction and Their Effects*, London, UK (Nov. 1978) 15–25.

Jones, B. L. and Johnson, D. L. *Steels for Line–Pipe and Pipeline Fittings*, Metals Society, London (1983) 14.

Jones, B. L., DeArdo, A. J., Garcia, C. I., Hulka, K. and Luthy, H. *HSLA Steels: Metallurgy and Applications*, Proc. of an Int. Conf. on HSLA Steels '85, China, eds. J. M. Gray, T. Ko, Z. Shouhua, W. Baorong and X. Xishan, ASM International, Ohio, USA (1985) 875–884.

Jones, C. L. and Pilkington, R. *Metall. Trans. A* **9A** (1978) 865.

Jones, S. and Bhadeshia, H. K. D. H. *Acta Materialia* **45** (1997) 2911–2920.

Josefsson, B. 'Microscopy and Microanalysis of Bainitic Weld Metal', Licentiate Thesis, Chalmers University, Sweden (1989).

Josefsson, B., Kvist, A. and Andren, H. O. *J. de Physique Colloque C6* **48** (1987) C6–435–440.

Josefsson, B. and Andren, H. O. *Proc. of the 35th Int. Field Emission Symp.*, Oak Ridge, Tennessee, USA (July 1988) 18–22.

Josefsson, B. and Andren, H. O. *Advances in the Science and Technology of Welding*, eds. S. A. David and J. Vitek, ASM Int., Ohio, USA (1989) 243–247.
Judson, P. and McKeown, D. *Advances in the Control of Weld Metal Toughness*, The Welding Institute, Abington, Cambridge (1982).
Kakeshita, T., Shimizu, K., Kimima, S., Yu, Z. and Date, M. *Trans. JIM* **26** (1985) 630–637.
Kajiwara, S., Ogawa, K., Kikuchi, T., Okamoto, H. and Oka, M. *Int. Conf. Solid–Solid Phase Transformations 99 (JIMIC–3)*, eds. M. Koiwa, K. Otsuka and T. Miyazaki, Japan Inst. Metals, Tokyo (1999) 969–972.
Kalish, D., Kulin, S. A. and Cohen, M. *J. of Metals* (February 1965) 157.
Kalish, D. and Cohen, M. *Mater. Sci. and Engng.* **6** (1970) 156–166.
Kalousek, J. and Beynon, G. *Rail Metallurgy*, Canadian Pacific Technical Reports, No. S497–75 (1975).
Kalousek, J., Fegredo, D. M. and Laufer, E. E. *Wear* **105** (1985a) 199–222.
Kalousek, J., Fegredo, D. M. and Laufer, E. E. *Wear of Materials*, ed. K. C. Ludema, Amer. Soc. of Mech. Engineers, New York (1985b) 212–231.
Kamada, A., Koshizuka, N. and Funakoshi, T. *Trans. ISIJ* **16** (1976) 407.
Kang, M. K., Sun, J. L. and Yang, Q. M. *Metall. Trans. A* **21A** (1990) 853–858.
Kapadia, B. M. *Hardenability Concepts with Applications to Steel*, ed. D. V. Doane and J. S. Kirkaldy, The Metallurgical Society of the AIME, Warrendale, Pennsylvania, USA (1978) 448–480.
Kar, R. J., Horn, R. M. and Zackay, V. F. *Metall. Trans. A* **10A** (1979) 1711–1717.
Kar, R. J. and Todd, J. A. *Discussion on Transformation Characteristics*, ASTM STP 755, American Society for Testing Materials (1982) 361–362.
Kasuya, T., Ichikawa, K., Fuji, M. and Bhadeshia, H. K. D. H. *Materials Science and Technology*, **15** (1999) 471–473.
Kaufman, L. and Cohen, M. *Prog. in Metal Phys.* **7** (1958) 165–246.
Kaufman, L. and Radcliffe, S. V. *Decomposition of Austenite by Diffusional Processes*, eds. V. F. Zackay and H. I. Aaronson, Interscience, New York (1962) 313–351.
Keh, A. S. and Leslie, W. C. *Materials Science Research*, Plenum Press, New York **1** (1963) 208.
Keh, A. S. and Weissmann, S. *Electron Microscopy and the Strength of Crystals*, eds. G. Thomas and J. Washburn, Interscience, New York, USA (1963) 231–300.
Kelly, P. M. and Nutting, J. *Proc. Roy. Soc. London* **A259** (1960) 45–58.
Kennon, N. F. *J. Aust. ISI* **19** (1974) 3.
Kennon, N. F. *Metall. Trans.* **9A** (1978) 57.
Kennon, N. F. and Kaye, N. A. *Metall. Trans.* **13A** (1982) 975.
Keown, S. R., Smaill, J. S. and Erasmus, L. A. *Metals Technology* **3** (1976) 194.
Kerr, R., Solana, F., Bernstein, I. M. and Thompson, A. W. *Metall. Trans. A* **18A** (1987) 1011–1022.
Kessler, H. and Pitsch, W. *Acta Metall.* **13** (1965) 871–874.
Kettunen, P. O. and Kocks, U. F. *Scr. Metall.* **1** (1967) 13–17.
Kettunen, P. O. and Kocks, U. F. *Acta Metall.* **20** (1972) 95–103.
Kettunen, P. O. and Lepistö, T. *Trans. JIM* **17** (1976) 63.
Khan, S. A. and Bhadeshia, H. K. D. H. *Metall. Trans. A* **21A** (1990a) 859–875.

Khan, S. A. and Bhadeshia, H. K. D. H. *Materials Science and Engineering* **A129** (1990b) 257–272.
Kimmins, S. T. and Gooch, D. J. *Metal Science* **17** (1983) 519–532.
Kimura, K., Kushima, H., Abe, F., Yagi, K. and Irie, H. *Advances in turbine materials, design and manufacturing*, 4th Int. Charles Parsons Turbine Conference, eds A. Strang, W. M. Banks, R. D. Conroy and M. J. Goulette, Institute of Materials, London (1997) 257–269.
King, A. D. and Bell, T. *Metall. Trans. A* **6A** (1975) 1419.
King, J. F., David, S. A., Sims, J. E. and Nasreldin, A.M. *Welding Journal* (July 1986) 39–47.
Kinsman, K. R. and Aaronson H. I. *Discussion* to Oblak and Hehemann (1967).
Kinsman, K. R. and Aaronson H. I. *Metall. Trans.* **1** (1970) 1485–1488.
Kinsman, K. R., Eichen, E. and Aaronson, H. I. *Metall. Trans.* **2** (1971) 346–348.
Kinsman, K. R. and Aaronson, H. I. *Metall. Trans.* **4** (1973) 959–967.
Kinsman, K. R., Eichen, E. and Aaronson, H. I. *Metall. Trans.* **6** (1975) 303.
Kinsman, K. R., Richman, R. H. and Verhoeven, J. D. *Mater Sci. Symp. Abst.*, ASM (1974).
Kirkaldy, J. S. *Can. J. Phys.* **36** (1958) 899–925.
Kirkaldy, J. S., Forstmann, V. D. and Brigham, R. J. *Canadian Metall. Quart.* **1** (1962) 59–81.
Klier, E. P. and Lyman, T. *Trans. AIMME* **158** (1944) 394–422.
Klueh, R. L. *Journal of Nuclear Materials* **54** (1974a) 41–54.
Klueh, R. L. *Journal of Nuclear Materials* **54** (1974b) 55–63.
Klueh, R. L. and Nasreldin, A. M. *Metall. Trans. A* **18A** (1987) 1279–1290.
Klueh, R. L. and Swindeman, R. W. *Metall. Trans. A* **17A** (1986) 1027–1034.
Klueh, R. L., Alexander, D. J. and Kenik, E. A. *Journal of Nuclear Materials* **227** (1995) 11–23.
Klueh, R. L. and Alexander, D. J. *Journal of Nuclear Materials* **265** (1999) 262–272.
Klug, R. C., Hintz, M. B. and Rundman, K. B. *Metall. Trans. A* **16A** (1985) 797–805.
Kluken, A. O. and Grong, O. *Metall. Trans. A* **20A** (1989a) 1335–1349.
Kluken, A. O. and Grong, O. *Recent Trends in Welding Science and Technology*, eds. S. A. David and J. Vitek, ASM International, OH, USA (1989b) 781–786.
Kluken, A. O., Grong, O. and Rorvik, G. *Metall. Trans. A* **21A** (1990) 2047–2058.
Kluken, A. O., Grong, O. and Hjelen, J.*Metall. Trans. A* **22A** (1991) 657–663.
Knott, J. F. *JISI* **204** (1966) 104.
Knott, J. F. *Fundamentals of Fracture Mechanics*, Butterworths, London (1973).
Knott, J. F. *Advances in the Physical Metallurgy and Applications of Steels*, Metals Society, London (1981) 181
Knott, J. F. and Cottrell, A. H. *JISI* **201** (1963) 249–260.
Knowles, K. M. and Smith, D. A. *Acta Crystallographica* **A38** (1982) 34–40.
Koistinen, P. P. and Marburger, R. E. *Acta Metallurgica* **7** (1959) 59–60.
Komai, N., Masuyama, F., Ishihara, I., Yokoyama, T., Yamadera, Y., Okada, H., Miyata, K. and Sawaragi, Y. *Advanced Heat Resistant Steels for Power Generation*, San Sebastian, The Institute of Materials, London (1999) 96–108.
Konoval, G., Zwell, L., Gorman, L. A. and Leslie, W. C. *Nature* **184** (1959) 1862–1863.
Ko, T. *JISI* **175** (1953) 16–18.

Ko, T. and Cottrell, S. A. *JISI* **172** (1952) 307–313.
Kocks, U. F. *Phil. Mag.* **13** (1966) 541.
Kocks, U. F. *Can. J. Phys.* **45** (1967) 737.
Kocks, U. F., Argon, A. S. and Ashby, M. F. *Prog. Mater. Sci.* **19** (1975) 1.
Koistinen, D. P. *Trans. ASM* **50** (1958) 227.
Korenko, M. K. PhD thesis entitled 'Martensitic Transformations in High Magnetic Fields', Massachusetts Institute of Technology (1973).
Kostic, M. M., Hawbolt, E. B. and Brown, L. C. *Metall. Trans.* **7A** (1976) 1643.
Kostic, M. M., Hawbolt, E. B. and Brown, L. C. *Metall. Trans.* **10A** (1979) 165.
Kozasu, I., Suzuki, H., Yamada, M. and Tagawa, H. *Research on Chrome–Moly Steels*, MPC-21, American Society of Mechanical Engineers, New York (1984) 53–76.
Krivoglaz, M. A. and Sadovsky, V. D. *Fiz. Met. Metalloved.* **18** (1964) 502.
Kriesement, O. and Wever, F. *Mechanism of Phase Transformations in Metals*, Institute of Metals, Monograph and Rep. Ser. No. 18, London (1956) 253.
Krishnadev, M. R. and Ghosh, R. *Metall. Trans. A* **10A** (1979) 1941–1944.
Kubaschewski, O. and Evans, E. Li. *Metallurgical Thermochemistry*, Pergamon Press, Oxford, UK (1950).
Kunitake, T. *Reactor Steel Studies*, Cr–Mo Steels Research in Japan, ed. K. Ono (1971) Quoted in Lundin *et al*., 1982.
Kunitake, T., Terasaki, F., Ohmori, Y. and Ohtani, H. *Iron and Steel* (December 1972) 647–653.
Kurdjumov, G. V. *Trans. AIMME (Iron and Steel Div.)* **103** (1933) 253–255.
Kurdjumov, G. V. and Sachs, G. *Z. Phys.* **64** (1930) 325.
Lacher, J. R. *Proc. Cambridge Phil. Soc.* **33** (1937) 518.
Lai, G. Y. *Metall. Trans. A* **6A** (1975) 1469.
Lancaster, J. F. *Metallurgy of Welding*, 4th edition, Allen and Unwin, London (1986).
Lange, H. and Mathieu, K. *Mitt. K. W. I. Eisenforchung* **20** (1938) 125.
Langer, E. W. *Metal Science Journal* **2** (1968) 59.
Langer, J. S. and Muller–Krumbhaar *Acta Metall.* **26** (1978) 1681–1687.
Langford, G. and Cohen, M. *Trans. Am. Soc. Met.* **62** (1969) 625.
Langford, G. and Cohen, M. *Metall. Trans.* **1** (1970) 1478.
Langford, G. and Cohen, M. *Metall. Trans. A* **6A** (1975) 901.
Larn, R. H. and Yang, J. R. *Materials Science and Engineering A* **A264** (1999) 139–150.
Larn, R. H. and Yang, J. R. *Materials Science and Engineering A* **A278** (2000) 278–291.
Lau, T. W., Sadowsky, M. M., North, T. H. and Weatherly, G. C. *Welding Metallurgy of Structural Steels*, ed. J. Y. Koo, TMS–AIME, Warrendale, Penn., USA (1987) 349–365.
Lau, T. W., Sadowsky, M. M., North, T. H. and Weatherly, G. C. *Materials Science and Technology* **4** (1988) 52–61.
Laverroux, M. and Pineau, A. *Scripta Metall.* **8** (1974) 351–356.
Law, N. and Edmonds, D. V. *Metall. Trans. A* **11A** (1980) 33.
Leber, H., Luthy, H. and Form, W. *Fundamentals of Microalloying Forging Steels*, eds. G. Krauss and S. K. Banerji, The Metallurgical Society of the AIME, Warrendale, Pennsylvania, USA (1987) 189–206.

Leber, H. J., Garcia, C. I., Palmiere, E. J. and DeArdo, A. J. *Processing, Microstructure and Properties of HSLA Steels*, ed. A. J. DeArdo, The Minerals, Metals and Materials Society, Warrendale, Pennsylvania (1988) 425–437.
Lee, Y. J. PhD Thesis, Assessment of Creep Damage in Weldments of 1Cr–0.5Mo Steel, Monash University, Clayton, Victoria, Australia (1989).
Lee, H. J., Spanos, G., Shiflet, G. J. and Aaronson, H. I. *Acta Metall.* **36**(1) (1988) 1129–1140.
Leont'yev, B. A. and Kovalevskaya, G. V. *Fiz. Metall. Metalloved.* **38** (1974) 1050.
Leslie, W. C. *Physical Metallurgy of Steels*, McGraw-Hill Kogakusha, Tokyo, Japan (1982).
Lewis, D. *Journal of the Iron and Steel Institute* **119** (1929) 427.
Li, C. Y., Blakely, J. M. and Feingold, A. H. *Acta Metall.* **14** (1966) 1397.
Lifshitz, I. H. and Slyozov, V. Z. *Phys. Chem. Solids* **19** (1961) 35.
Lin, M. Research Proposal for PhD Thesis entitled 'Autocatalytic Kinetics of Martensitic Transformations', Massachusetts Institute of Technology (1987) private communication G. B. Olson.
Linaza, M. A. Romero, J L., Rodriguez-Ibabe, J. M. and Urcola, J. J. *Scripta Metallurgica and Materialia* **29** (1993) 1217–1222.
Llopis, A. M. PhD Thesis, referred to in E. R. Parker, *Metall. Trans.* **8A** (1977) 1025.
Lorenz, K. and Duren, C. *Steels for Line Pipe and Pipeline Fittings*, Metals Society, London (1983) 322.
Lonsdale, D. and Flewitt, P. E. J. *Metall. Trans. A* **9A** (1978) 1619–1623.
Lonsdale, D. and Flewitt, P. E. J. *Materials Science and Engineering* **39** (1979) 217–229.
Lu, G.-Z., Zhang, H. *Wear of Materials*, ed. K. C. Ludema, Amer. Soc. of Mech. Engineers, New York (1989) 225–231.
Lundin, C. D., Kruse, B. J. and Pendley, M. R. *Bulletin 277 of the Welding Research Council*, United Engineering Center, New York (May 1982) 1–27.
Lundin, C. D., Kelly, S. C., Menon, R. and Kruse, B. J. *Bulletin 315 of the Welding Research Council*, United Engineering Center, New York (June 1986) 1–66.
Lyman, T. and Troiano, A. R. *Trans. AIME* **162** (1945) 196.
Lyman, T. and Troiano, A. R. *Trans. ASM* **37** (1946) 402–448.
Mabuchi, H., Uemori, R. and Fujioka, M. *ISIJ International* **36** (1996) 1406–1412.
Mack, C. *Proc. Cambridge Phil. Soc.* **52** (1956) 246.
Magee, C. L. *Phase Transformations*, ASM, Metals Park, Ohio (1) (1970) 15–156.
Magee, C. L. *Metallurgical Transactions* **2** (1971) 2419–2430.
Maier, Ch., Blaschko, O. and Pichl, W. *Physical Review B* **55** (1995) 113–116.
Maki, T., Shimooka, S., Arimoto, T. and Tamura, I. *Trans. JIM* **14** (1973) 62–67.
Maki, T., Shimooka, S., Fujiwara, S. and Tamura, I. *Trans. JIM* **16** (1975) 36–41.
Maki, T. and Tamura, I. *Proceedings of an International Conference on Martensitic Transformations*, ICOMAT 86, Kyoto, Japan Institute of Metals (1986) 963–970.
Malecki, P. Private communication on a paper to be published in the proceedings of the 8th International Conference on Metallography, Leoben, Austria (1990).
Marder, A. R. and Krauss, G. *Trans. ASM* **60** (1967) 651.
Marschall, C. W., Hehemann, R. F. and Troiano, A. R. *Trans. ASM* **55** (1962) 135.
Masuyama, F., Komai, N., Yokoyama, T., Yamamoto, S., Miyata, K. and Igarashi, M. *JSME International Journal* **41** (1998) 1098–1104.

Matas, S. J. and Hehemann, R. F. *Nature* **187** (1960) 685–686.
Matas, S. J. and Hehemann, R. F. *Trans. Met Soc. AIME* **221** (1961) 179–185.
Matsuda, A. *Tetsu-tó-Hagane* **56** (1970) 1428.
Matsuda, S., Inoue, T. and Ogasaswara, M. *Trans. Japan Inst. Metals* **9** (1968) 343.
Matsuda, S., Inoue, T. and Ogasaswara, M. *Trans. ISIJ* **12** (1972) 325.
Matsuda, S. and Okumura, N. *Trans. ISIJ* **18** (1978) 198–205.
Matsuzaki, A., Bhadeshia, H. K. D. H. and Harada, H. *G. R. Speich symposium*, Iron and Steel Society, AIME, Warrendale, PA, USA (1992) 47–52.
Matsuzaki, A. and Bhadeshia, H. K. D. H. *Materials Science and Technology* **15** (1999) 518–522.
McCutcheon, D. B., Trumper, T. W. and Embury, J. D. *Revue de Metallurgie* (Feb. 1976) 143–174.
McEvily, A. J. and Magee, C. L. *Low Alloy Steels*, Iron and Steel Institute, London (1968) 111–117.
McGrath, J. T., Chandel, R. S., Orr, R. F. and Gianetto, J. A. *Canadian Metall. Quarterly* **28** (1989) 75–83.
McMahon Jnr., C. J., Cohen, M. *Acta Metall.* **13** (1965) 591.
McRobie, D. E. and Knott, J. F. *Mater. Sci. Tech.* **1** (1985) 137.
Meggers, K., Priesmeyer, H. G., Trela, W. J., Bowman, C. D. and Dahms, M. *Nuclear Instruments and Methods in Physics Research* **88** (1994) 423–429.
Mehl, R. F. *Hardenability of Alloy Steels*, ASM, Cleveland, Ohio, USA (1939) 1.
Mehl, R. F. *JISI* **159** (1948) 113–129.
Mendiratta, M. G., Sasser, J. and Krauss, G. *Metall. Trans. A* **3** (1972) 351–353.
Miihkinen, V. T. T. and Edmonds, D. V. *Mat. Sci. and Tech.* **3** (1987a) 422–431.
Miihkinen, V. T. T. and Edmonds, D. V. *Mat. Sci. and Tech.* **3** (1987b) 432–440.
Miihkinen, V. T. T. and Edmonds, D. V. *Mat. Sci. and Tech.* **3** (1987c) 441–449.
Miller, R. F., Benz, W. G. and Unverzagt, W. E. *Proc. ASTM* **40** (1940) 771–781.
Mills, A. R., Thewlis, G. and Whiteman, J. A. *Mat. Sci. and Tech.* **3** (1987) 1051–1061.
Minote, T., Torizuka, S., Ogawa, A. and Niikura, M. *ISIJ International* **36** (1996) 201–207.
Mintz, B. and Wilson, D. V. *Acta Metall.* **13** (1965) 947.
Miyata, K., Igarashi, M. and Sawaragi, Y. *ISIJ International* **39** (1999) 947–954.
Moore, D. J., Rouns, T. N. and Rundman, K. B. *J. Heat Treating* **4** (1985a) 7.
Moore, D. J., Rouns, T. N. and Rundman, K. B. *AFS Transactions* **93** (1985b) 705–718.
Moore, D. J., Rouns, T. N. and Rundman, K. B. *AFS Transactions* **94** (1986) 255–264.
Moore, D. J., Rouns, T. N. and Rundman, K. B. *AFS Transactions* **95** (1987) 765–773.
Morgan, E. R., Dancy, T. E. and Korchynsky, M. *Blast Furnace and Steel Plant* **53** (1965) 921–929.
Mori, N., Homma, H., Okita, S. and Wakabayashi, M. *International Institute for Welding, Document IX–1196–80* (1980).
Morikawa, H. and Hasegawa, T. *Accelerated Cooling of Steel*, ed. P. D. Southwick, TMS–AIME (1985) 83–96.
Morniroli, J., Grosse, E. and Gantois, M. *Phil. Mag. A* **48** (1983) 311.
Mostert, R. J. and van Rooyen, G. T. *Specialty Steels and Hard Materials*, Pretoria, S. Africa, Pergamon Press, Oxford (1982) 229.

Mujahid, S. A. and Bhadeshia, H. K. D. H. *Acta Metall. et Mater.* **40** (1992) 389–396.
Mujahid, S. A. and Bhadeshia, H. K. D. H. *Acta Metall. et Mater.* **41** (1993) 967–973.
Murakami, T. and Imai, Y. *Sci. Rep. Res. Inst. Tohoku Univ., Series A* **1** (1949) 87–92.
Murphy, M. C. and Branch, G. D. *JISI* **206** (1969) 1347–1364.
Murphy, M. C. and Branch, G. D. *JISI* **209** (1971) 546–561.
Mutiu, T. A., Kinderman, A. J. and Bernstein, I. M. *The Hot Deformation of Austenite*, ed. J. B. Ballance, T.M.S.–A.I.M.E., New York, USA (1977) 410–427.
Mutton, P. J. M. AS. Thesis, University of Melbourne (1985) Referred to by Sawley *et al*. (1987).
Myers, E. J. *Proc. First Int. Cong. in Stereology*, Vienna Medical Academy (1953) 15/1, 15/7.
Myers, J., Willoughy, G. and Ham, R. K. *Central Electricity Research Laboratories Report RD/L/R 1514*, Leatherhead, Surrey, England (1968).
Nabarro, F. R. N. *Proc. Roy. Soc.* **A381** (1982) 285.
Nagakura, S., Suzuki, T. and Kusunoki, M. *Trans. JIM* **22** (1981) 699–709.
Nagakura, S., Hirotsu, Y., Kusunoki, M., Suzuki, T. and Nakamura, Y. *Metall. Trans.* **14** (1983) 1025–1031.
Nakamura, T., Mikami, T. and Nagakura, S. *Trans. JIM* **26** (1985) 876–885.
Nakamura, T. and Nagakura, S. *International Conference on Martensitic Transformations* – ICOMAT–86, Japan Institute of Metals (1986) 386–391.
Nakasugi, H., Matsuda, H. and Tamehiro, H. *Alloys for the 1980's*, Climax Molybdenum, Ann Arbor, Michigan, USA (1980) 213.
Nakasugi, H., Matsuda, H. and Tamehiro, H. *Steels for Line Pipe and Pipeline Fittings*, Metals Society, London (1983) 90.
Nam, W. J. *ISIJ International* **39** (1999) 1181–1187.
Nath, B. *Int. Conf. on Welding Technology of Energy Applications*, eds. S. A. David and G. M. Slaughter, Oak Ridge National Labs. TN, USA (1982) 1–25.
Nath, B. *2nd Int. Conf. on Creep and Fracture of Engineering Materials and Structures*, Pineridge Press Ltd., Swansea, UK (1984) 827–838.
Naylor, J. P. *Metall. Trans. A* **10** (1979) 861.
Naylor, J. P. and Krahe, P. R. *Metall. Trans.* **5** (1974) 1699–1701.
Naylor, J. P. and Krahe, P. R. *Metall. Trans.* **6A** (1975) 594–598.
Nehrenberg, A. E. *J. of Metals* **188** (1950) 162–180.
Nemoto, M. *High Voltage Electron Microscopy*, Academic Press, New York, NY (1974) 230–234.
Nilan, T. G. *Trans. Met Soc. AIME* **239** (1967) 898–909.
Nishiyama, Z. *Sci. Rep. Tohoku Univ.* **23** (1934) 325.
Nishioka, K. and Tamehiro, H. *Microalloying '88: International Symposium on Applications of HSLA Steel*, Chicago, Illinois (September 1988) 1–9.
Norström, L.-A. *Scandinavian Journal of Metallurgy* **23** (1976) 159–165.
North, T. H., Mao, X. and Nakagawa, H. *The Metallurgy, Welding and Qualification of Microalloyed (HSLA) Steel Weldments*, American Welding Society (1990) 219–248.

Nutting, J. *Advanced Heat Resistant Steels for Power Generation*, IOM Communications, London, eds. R. Viswanathan and J. Nutting (1998) 12–30.
Oblak, J. M., Goodenow, R. H. and Hehemann, R. F. *Trans. AIME* **230** (1964) 258–259.
Oblak, J. M. and Hehemann, R. F. *Transformations and Hardenability in Steels*, Climax Moly., Ann Arbor, USA (1967) 15–30.
Ochi, T., Takahashi, T. and Takada, H. *Proc. of 30th Mechanical Working and Steel Processing Conference*, Iron and Steel Society, Warrendale, PA (Oct. 1988).
Ohmori, Y. *Trans. ISIJ* **11** (1971a) 95–101.
Ohmori, Y. *Trans. ISIJ* **11** (1971b) 249.
Ohmori, Y. *Proc. Int. Conf. on Martensitic Transformations*, ICOMAT '86, Japan Institute of Metals (1986) 587–594.
Ohmori, Y. *Materials Transactions (Japan Institute for Metals)* **30** (1989) 487–497.
Ohmori, Y. and Honeycombe, R. W. K. *Proc. ICSTIS, Suppl. Trans. ISIJ* **11** (1971) 1160–1164.
Ohmori, Y., Ohtani, H. and Kunitake, T. *Trans. ISIJ* **11** (1971) 250–259.
Ohmori, Y., Ohtani, H. and Kunitake, T. *Metal Science* **8** (1974) 357–366.
Ohtsuka, K., Xu, Y., Okamoto, H. *Unpublished research*, National Research Institute for Metals in Japan and Tottori University (2000).
Oka, M. and Okamoto, H. *Proc. Int. Conf. on Martensitic Transformations*, ICOMAT '86, Japan Institute of Metals (1986) 271–275.
Oka, M. and Okamoto, H. *Metall. Trans. A* **19A** (1988) 447.
Okabe, R., Koshizuka, N., Tanaka, M., Katamine, A. and San–Nomiya, Y. *Trans. ISIJ* **23** (1983) 390.
Okamoto, H. and Oka, M. *Metall. Trans. A* **17A** (1986) 1113–1120.
Oldland, R. B. *Australian Welding Research* (1985) 31.
Olefjord, I. *Int. Metals. Rev.* **23** (1978) 149–163.
Olson, G. B. Unpublished research, Northwestern University, Chicago, USA (1984).
Olson, G. B. *Scripta Metall.* **21** (1987) 1023–1028.
Olson, G. B. and Cohen, M. *Metall. Trans.* **7A** (1976a) 1897–1904.
Olson, G. B. and Cohen, M. *Metall. Trans.* **7A** (1976b) 1905–1914.
Olson, G. B. and Cohen, M. *Metall. Trans.* **7A** (1976c) 1915–1923.
Olson, G. B. and Owen, W. S. *New Aspects of Martensitic Transformations*, Tokyo, Japan, Institute of Metals (1976) 105–110.
Olson, G. B. and Cohen, M. *Scripta Metall.* **11** (1977) 345–347.
Olson, G. B. and Cohen, M. *Acta Metall.* **27** (1979) 1907–1918.
Olson, G. B. and Cohen, M. *Ann. Rev. Mater. Sci.*, eds. R. A. Huggins, R. H. Bube and D. A. Vermilyea, Annual Reviews Inc., California, USA (1981) 1–30.
Olson, G. B. and Cohen, M. *Solid–Solid Phase Transformations*, eds. H. I. Aaronson *et al.*, TMS-AIME, Warrendale, Pennsylvania, USA (1981) 1209–1213.
Olson, G. B. and Cohen, M. *Metall. Trans. A* **14A** (1983) 1057–1065.
Olson, G. B. and Cohen, M. *Dislocations in Solids*, ed. F. R. N. Nabarro, **7** (1986) 297.
Olson, G. B., Bhadeshia, H. K. D. H. and Cohen, M. *Proc. Int. Conf. Solid → Solid Phase Transformations*, ed. G. W. Lorimer, Institute of Metals, London (1988) 322–325.
Olson, G. B., Bhadeshia, H. K. D. H. and Cohen, M. *Acta Metall.* **37** (1989) 381–389.
Olson, G. B., Bhadeshia, H. K. D. H. and Cohen, M. *Metall. Trans. A* **21A** (1990) 805–809.

Oriani, R. A. and Josephic, P. H. *Acta Metall.* **22** (1974) 1065–1074.
Orlová, A. Tabolová, Z. and Čadek, J. *PhilosophicalMagazine* **26** (1972) 1263–1274.
Owen, W. S. *Trans. ASM* **46** (1954) 812–829.
Owen, W. S. *Metals Technology* **14** (1980) 1–13.
Owen, W. S., Wilson, E. A. and Bell, T. *High Strength Materials*, ed. V. F. Zackay, Wiley, New York (1964) 167–212.
Oriani, R. A. and Josephic, P. H. *Acta Metall.* **22** (1974) 1065–1074.
Padmanabhan, R. and Wood, W. E. *Materials Science and Engng.* **66** (1984) 1–11.
Pan, Y.-T. and Lee, J-Y. *Materials Science and Engineering A* **A136** (1991a) 109–119.
Pan, Y.-T. and Lee, J-Y. *Metallurgical Transactions A* **A136** (1991b) 2818–2822.
Pan, Y.-T. and Lee, J-Y. *Proc. Conf. Processing, Microstructure and Properties of Microalloyed and Other Modern High Strength Low Alloy Steels*, ed. A. J. DeArdo, ISS/AIME, Warrendale, PA, USA (1992) 487–496.
Pan, Y.-T. and Lee, J-Y. *Materials and Design* **15** (1994) 331–338.
Papadimitriou, G. and Fourlaris, G. *J. de Physique IV* **7** (1997) C5 131–136.
Parker, E. R. and Zackay, V. F. *Engineering Fracture Mechanics* **7** (1975) 371–375.
Parker, E. R. *Metall. Trans.* **8A** (1977) 1025–1042.
Parker, E. R., Ritchie, R. O., Todd, J. A. and Spencer, P. N. *Research on Chrome–Moly Steels*, MPC–21, American Society of Mechanical Engineers, New York (1984) 109–116.
Patel, J. R. and Cohen, M. *Acta Metall.* **1** (1953) 531.
Pati, S. R. and Cohen, M. *Acta Metall.* **19** (1971) 1327–1332.
Paxton, H. W. *Metall. Trans.* **1** (1970) 3479–3500.
Paxton, H. W. *Metall. Trans.* **3** (1972) 1035–1042.
Perovic, P., Purdy, G. R. and Brown, L. *Scripta Metall.* **15** (1981) 217–221.
Petch, N. J. *Advances in Physical Metallurgy*, eds. J. A. Charles and G. C. Smith, The Institute of Metals, London (1990) 11–25.
Pfeil, L. B. *Proc. Roy. Soc.* **112** (1926) 182–195.
Pichl, W. and Krystian, M. *Materials Science and Engineering A* **A273–275** (1999) 209–212.
Pickering, F. B. *Int. Conf. on Electron Microscopy*, Springer Verlag OHG, Berlin (1958) 628–637.
Pickering, F. B. *Transformations and Hardenability in Steels*, Climax Molybdenum, Ann Arbor, USA (1967) 109–132.
Pickering, F. B. *Physical Metallurgy and the Design of Steels*, Applied Science Publishers, Essex, UK (1978) 104.
Pickering, F. B. *Phase Transformations*, Institution of Metallurgists, London, series 3, No. 11, **2** (1979) VI 7–13.
Pickering, F. B. *Constitution and Properties of Steels*, VCH publishers, eds .R. W. Cahn, P. Haasen and E. J. Kramer, Germany (1992) 339–399.
Pilling, J. and Ridley, N. *Metall. Trans. A* **13A** (1982) 557–563.
Pippard, A. B. *Classical Thermodynamics*, Cambridge University Press (1981).
Pitsch, W. *Acta Metall.* **10** (1962) 897.
Pokhodnya, I. K. and Shvachko, V. I. *International Journal of Hydrogen Energy* **22** (1997) 285–289.
Pomey, J. *Mem. Sci. Rev. Metall.* **63** (1966) 507–532.

Porter, L. E. and Rosenthal, P. C. *Acta Metall.* **7** (1959) 504–514.
Portevin, A. and Chevenard, P. *Compt. Rend.* **204** (1937) 772.
Portevin, A. and Jolivet, H. *Annales de l'Academie des Sciences Techniques á Varsorie* **4** (1937) 177.
Portevin, A. and Jolivet, H. *Compt. Rend.* **207** (1938) 1412.
Prado, J. *Journal of Materials Science Lett.* **5** (1986) 1075–1076.
Prado, J., Catalan, J. J. and Marsal, M. *Journal of Materials Science* **25** (1990) 1939–1946.
Purdy, G. R. and Hillert, M. *Acta Metall.* **32** (1984) 823–828.
Purdy, G. R., Weichert, D. H. and Kirkaldy, J. S. *TMS–AIME* **230** (1964) 1025–1034.
Putatunda, S. K. and Gadicherla, P. K. *Materials Science and Engineering A* **A268** (1999) 15–31.
Race, J. Private communication, University of Cambridge (1990).
Radcliffe, S. V. and Rollason, E. C. *JISI* **191** (1959) 56–65.
Radcliffe, S. V., Schatz, M. and Kulin, S. A. *JISI* **201** (1963) 143–153.
Raghavan, V. and Entwistle, A. R. *Physical Properties of Martensite and Bainite*, Special Rep. 93, ISI, London (1965) 30–37.
Raghavan, V. and Cohen, M. *Metall. Trans.* **2** (1971) 2409.
Rao, B. V. N. and Thomas, G. *Metall. Trans. A* **11A** (1980) 441–457.
Rao, M. M. and Winchell, P. G. *Trans. Met Soc. AIME* **239** (1967) 956–960.
Rauch, G. C. and Leslie, W. C. *Metall. Trans.* **3** (1972) 373.
Ray, R. K. and Jonas, J. J. *International Materials Reviews* **35** (1990) 1–36.
Reed, R. and Bhadeshia, H. K. D. H. *Recent Trends in Welding Science and Technology*, eds. S. A. David and J. Vitek, ASM International, Ohio, U.S.A. (1989) 205–210.
Rees, G. PhD Thesis, University of Cambridge (1991).
Rees, G. and Bhadeshia, H. K. D. H. *Materials Science and Technology* **8** (1992) 985–996.
Rees, G. and Bhadeshia, H. K. D. H. *Materials Science and Technology* **10** (1994) 353–358.
Reisdorf, B. G. *TMS–AIME* **227** (1963) 1334.
Ricks, R. A., Howell, P. R. and Barritte, G. S. *International Conference on Solid → Solid Phase Transformations*, eds. H. I. Aaronson *et al.*, TMS–AIME, Warrendale, PA, USA (1981b) 463–468.
Ricks, R. A., Howell, P. R. and Barritte, G. S. *Journal of Materials Science* **17** (1982) 732–740.
Ridal, K. A. and Quarell, A. G. *JISI* **200** (1962) 366–373.
Ridal, K. A. and McCann, J. *Physical Properties of Martensite and Bainite*, Special Report 93, Iron and Steel Institute (London) (1965) 147–148.
Ridley, N. *Phase Transformations in Ferrous Alloys*, TMS–AIME, Warrendale, PA (1984) 210–236.
Rigsbee, J. M. and Aaronson, H. I. *Acta Metall.* **27** (1979) 351.
Rigsbee, J. M. and Aaronson, H. I. *Acta Metall.* **27** (1979) 365.
Ringer, S. R. Barbaro, F., Krauklis, P. and Easterling, K. E. *Microstructure Control to Achieve Properties In Modern Steels*, Inst. of Metals and Materials Australasia, Melbourne, Australia (1990) 1–6.
Ritchie, R. O. *J. Engng. Materials Technology (Trans. ASME, H)* **99** (1977a) 195–204.
Ritchie, R. O. *Metal Science* **11** (1977b) 368–381.
Ritchie, R. O., Castro, M. H. C., Zackay, V. F. and Parker, E. R. *Metall. Trans. A* **9A**

(1978) 35–40.
Ritchie, R. O. *International Metals Reviews* **4** (1979) 205–230.
Ritchie, R. O., Knott, J. F. and Rice, J. R. *J. Mech. Phys. Sol.* **21** (1973) 395–400.
Ritchie, R. O., Moss, C. M. and Suresh, S. *J. Engng. Materials Technology (Trans. ASME, H)* **102** (1980) 293.
Ritchie, R. O., Parker, E. R., Spencer, P. N. and Todd, J. A. *J. Materials for Energy Systems* **6** (1984) 151–162.
Roberts, C. S., Averbach, B. L. and Cohen, M. *Trans. ASM* **45** (1957) 576.
Roberts, M. J. *Metall. Trans.* **1** (1970) 3287–3294.
Robertson, J. M. *Journal of the Iron and Steel Institute* **119** (1929) 391–426.
Robson, J. D. and Bhadeshia, H. K. D. H. *Materials Science and Technology* **13** (1997) 631–644.
Rodriguez-Ibabe, J. M. *Materials Science Forum* **284–286** (1998) 51–62.
Rouns, T. N. and Rundman, K. B. *AFS Transactions* **95** (1987) 851–874.
Rudberg, E. *Jernkontorets Ann.* **136** (1952) 91.
Rundman, K. B., Moore, D. J., Hayrynen, K. L., Dubensky, W. J. and Rouns, T. N. *J. Heat Treating* **5** (1988) 79.
Russell, K. C. *Metall. Trans.* **2** (1971) 5–12.
Sachs, K., Ralph, B. and Salter, J. *Heat Treatment '79*, Metals Society, London (1980) 141–146.
Sadovskii, V. D. *Probl Mettaloverskie Term Obrab* (1956) 31–52, Central Electricity Generating Board Translation 7648.
Saeki, M., Kurosawa, F. and Matsuo, M. *Trans. ISIJ* **26** (1986) 1017–1035.
Samajdar, I., Girault, E., Verlinden, B., Aernoudt, E. and Van Humbeeck, J. *ISIJ International* **38** (1998) 998–1006.
Sandvik, B. P. J. and Nevalainen, H. P. *Metals Tech.* **15** (1981) 213–220.
Sandvik, B. P. J. *Metall. Trans. A* **13** (1982a) 777–787.
Sandvik, B. P. J. *Metall. Trans. A* **13** (1982b) 789–800.
Sandvik, B. P. J. and Wayman, C. M. *Metall. Trans. A* **14A** (1983) 809–822.
Sarikaya, M., Tokushige, H. and Thomas, G. *International Conference on Martensitic Transformations* ICOMAT 86, Japan Inst. of Metals, Tokyo, Japan (1986) 613–618.
Sawley, K. J., Preston, R. R. and Pendleton, R. *Abstracts of the conference on Bainite*, Institute of Metals, London (25 April 1985).
Sawley, K. J., Bolton, P. J. and Pell, G. M. *Wear of Materials*, ed. K. C. Ludema, Amer. Soc. of Mech. Engineers, New York (1987) 133–143.
Sawley, K. J., Benyon, J. A. and Jones, E. G. *9th International Wheelset Congress*, Quebec, Canada, Paper 2–6 (September 1988) 1–12.
Schaaber, O. *J. Metals* **7** (1955) 559–560.
Schanck, J. L. *Industrial Heating* (September 1969) 1664.
Scheil, E. *Arch. Eisenhuttenwesen* **12** (1935) 565.
Scheil, E. *Hart.–Tech. Mitt.* **7** (1955) 9.
Schissler, J. M., Arnould, J. and Metauer, G. *Mem. Sci. Rev. Metallurgie* **6** (1975) 779–793.
Schmatz, D. J. and Zackay, V. F. *Trans. ASM* **51** (1959) 476.
Schrader, A. and Wever, F. *Arch. Eisenhuttenwesen* **23** (1952) 489–495.
Self, P., Bhadeshia, H. K. D. H. and Stobbs, W. M. *Ultramicroscopy* **6** (1981) 29.

Senior, B. A. *The Effects of Retempering on the Microstructure of Ferritic Steels*, Central Electricity Generating Board Report TPRD/L/3220/R87 (1988).
Shackleton, D. N. and Kelly, P. M. *Acta Metall.* **15** (1967) 979–992.
Shackleton, D. N. and Kelly, P. M. *I.S.I. Special Rep. 93*, London (1965) 126–134.
Shea, M. M. and Ryntz, E. F. *Trans. Am. Foundrymen's Soc.* **94** (1986) 683.
Shepperson, S. and Allen, C. *Wear of Materials*, ed. K. C. Ludema, Amer. Soc. of Mech. Engineers, New York (1987) 572–583.
Shewmon, P. *Metall. Trans. A* **7A** (1976) 279.
Shewmon, P. *Materials Science and Technology* **1** (1985) 2.
Shieh, C. S., Din, T. A., Lui, T. S. and Chen, L. H. *AFS Transactions* **133** (1993) 365–371.
Shieh, C. S., Lui, T. S. and Chen, L. H. *Materials Transactions of the Japan Institute of Metals* **36** (1995) 620–625.
Shiga, C., Amano, K., Enami, T., Tanaka, M., Tarui, R. and Kusuhara, Y. *Technology and Applications of High Strength Low Alloy (HSLA) Steels*, ASM International (1983) 643–654.
Shih, C. H., Averbach, B. L. and Cohen, M. *Trans. AIME* **203** (1955) 183–187.
Shimizu, K. and Nishiyama, Z. *Mem. Inst. Sci. Ind. Res.*, Osaka University, (1963) 42.
Shimizu, K., Ko, T. and Nishiyama, Z. *Trans. JIM* **5** (1964) 223–228.
Shiokawa, T. Unpublished research quoted in Moore (1985).
Shim, J. H., Byun, J. S., Cho, Y. W., Oh, Y. J., Shim, J. D. and Lee, D. N. *ISIJ International* **40** (2000) 819–823.
Shipway, P. and Bhadeshia, H. K. D. H. *Materials Science and Technology* **11** (1995) 1116–1128.
Shipway, P. and Bhadeshia, H. K. D. H. *Materials Science and Engineering A* **A223** (1997) 179–185.
Shively, J. H., Hehemann, R. F. and Troiano, A. R. *Corrosion* **22** (1966) 253–256.
Singh, S. B. and Bhadeshia, H. K. D. H. *Materials Science and Technology* **12** (1996) 610–612.
Singh, S. B. and Bhadeshia, H. K. D. H. *Materials Science and Engineering A* **A245** (1998) 72–79.
Singh, S. B. PhD Thesis, University of Cambridge (1998).
Siriwardene, P. P. L. G. PhD Thesis, University of Cambridge (1955).
Smirenskaya, N. A., Kogan, L. I. and Entin, R. I. *Fiz. Metal. Metalloved.* **41** (1976) 1019–1028.
Smith, C. S. *A History of Metallography*, University of Chicago Press (1960) 225.
Smith, E. *Physical Basis of Yield and Fracture*, Inst. of Phys. and Phys. Soc., Oxford (1966) 36.
Smith, G. M. PhD Thesis on 'The Microstructure and Yielding behaviour of some Ti Steels', University of Cambridge (1984).
Smith, G. V. and Mehl, R. F. *Trans. AIMME* **150** (1942) 211–226.
Smith, M. F., Speich, G. R. and Cohen, M. *Trans. Met Soc. AIME* **215** (1959) 528–530.
Smith, Y. E. and Siebert, C. A. *American Society for Testing and Materials*, Special Technical Publication 480 (1970) 131–151.
Smith, J. F. *Acta Metall.* **28** (1980) 1555–1564.
Snieder, G. and Kerr, H. W. *Canadian Metallurgical Quarterly* **23** (1984) 315–325.

Solana, F., Takamadate, C., Bernstein, I. M. and Thompson, A. W. *Metall. Trans. A* **18A** (1987) 1023–1028.
Speich, G. R. *Decomposition of Austenite by Diffusional Processes*, Interscience, New York (1962) 353–369.
Speich, G. R. *Trans. AIME* **245** (1969) 2553–2564.
Speich, G. R. *Innovations in Ultrahigh–Strength Steel Technology*, eds. G. B. Olson, M. Azrin and E. S. Wright, 34th Sagamore Army Materials Conference, Watertown, Massachusetts, USA (1987) 89–112.
Speich, G. R. and Cohen, M. *Trans. Met Soc. AIME* **218** (1960) 1050–1059.
Speich, G. R. and Warlimont, H. *JISI* **206** (1968) 385–392.
Speich, G. R., Cuddy, L. J., Gordon, C. R. and DeArdo, A. K. *Int. Conf. on Phase Transformations in Ferrous Alloys*, eds. Marder, A. R. and Goldstein, J. I., ASM, Cleveland, Ohio, USA (1984) 341–392.
Spencer, P. N., Dauskardt, R. H., Parker, E. R. and Ritchie, R. O. *High Temperature Technology* **7** (1989) 17–26.
Spielfeld, J. *Materials Science and Engineering A* **A273–275** (1999) 639–643.
Srinivasan, G. R. and Wayman, C. M. *Trans. Met Soc. AIME* **242** (1968a) 79–81.
Srinivasan, G. R. and Wayman, C. M. *Acta Metall.* **16** (1968b) 609–620.
Srinivasan, G. R. and Wayman, C. M. *Acta Metall.* **16** (1968c) 621–636.
Stark, I. and Smith, G. D. W. *Journal de Physique* **48** (C) 6 (1987) 447–452.
Stark, I., Smith, G. D. W. and Bhadeshia, H. K. D. H. *Solid → Solid Phase Transformations*, Institute of Metals, London (1988) 211–215.
Stark, I., Smith, G. D. W. and Bhadeshia, H. K. D. H. *Metall. Trans. A* **21A** (1990) 847–845.
Steven, W. and Haynes, A. J. *JISI* **183** (1956) 349–359.
Stewart, J., Thomson, R. C. and Bhadeshia, H. K. D. H. *Journal of Materials Science* **29** (1994) 6079–6084.
Stickels, C. A. *Metall. Trans.* **5** (1974) 865–874.
Strang, A., Beech, S. M. and Gooch, D. J. *Materials for Advanced Power Engineering*, ed. D. Coutsouradis, Netherlands (1994) 549–560.
Strang, A., Vodarek, V. and Bhadeshia, H. K. D. H. *Modelling of Microstructural Evolution in Creep Resistant Materials*, eds. A. Strang and M. McLean, IOM Communications London (1999) 129–150.
Strangwood, M. PhD Thesis, University of Cambridge (1987).
Strangwood, M. and Bhadeshia, H. K. D. H. *Advances in Welding Science and Technology*, ed. S. A. David, ASM, Metals Park, Ohio, USA (1987) 209–213.
Strangwood, M. and Bhadeshia, H. K. D. H. *Solid → Solid Phase Transformations*, Institute of Metals, ed. G. W. Lorimer, London (1988) 466–470.
Sudo, M., Higashi, M., Hori, H., Iwai, T., Kambe, S. and Shibata, Z. *Trans. Iron and Steel Institute of Japan* **21** (1981) 820–827.
Sudo, M., Tsukatani, I. and Shibata, Z. *Metallurgy of Continuously Annealed Sheet Steel*, eds. B. L. Bramfitt and P. L. Mangonon Jr., TMS–AIME, Warrendale, Pennsylvania (1982) 301–319.
Sudo, M. and Iwai, T. *Trans. Iron and Steel Institute of Japan* **23** (1983) 294.
Sugden, A. A. B. and Bhadeshia, H. K. D. H. *Metall. Trans. A* **19A** (1988) 669–674.

Sugden, A. A. B. and Bhadeshia, H. K. D. H. *Metall. Trans. A* **20A** (1989a) 1597–1602.
Sugden, A. A. B. and Bhadeshia, H. K. D. H. *Metall. Trans. A* **20A** (1989b) 1811–1818.
Suresh, S., Zamiski, G. F. and Ritchie, R. O. *Metall. Trans. A* **12A** (1981) 1435.
Svensson, L.–E and Bhadeshia, H. K. D. H. *J. Materials Science* **24** (1989) 3180–3188.
Swallow, E. and Bhadeshia, H. K. D. H. *Materials Science and Technology* **12** (1996) 121–125.
Takahashi, M. and Bhadeshia, H. K. D. H. *J. of Materials Science Letters* **8** (1989) 477–478.
Takahashi, M. and Bhadeshia, H. K. D. H. *Materials Science and Technology* **6** (1990) 592–603.
Takahashi, M. and Bhadeshia, H. K. D. H. *Transactions of The Japan Institute for Metals* **32** (1991) 689–696.
Tamehiro, H., Habu, R., Yamada, N., Matsuda, H. and Nagumo, M. *Accelerated Cooling of Steel*, Ed. P. D. Southwick, TMS–AIME (1985a) 401–414.
Tamehiro, H., Yamada, N. and Matsuda, H. *Trans. ISIJ* **25** (1985b) 55–61.
Tamehiro, H., Takeda, T., Matsuda, S., Yamamoto, K. and Okumura, N. *Trans. ISIJ* **25** (1985c) 982–988.
Tamehiro, H., Murata, M., Habu, R. and Nagumo, M. *Trans. ISIJ* **27** (1987a) 120–129.
Tamehiro, H., Murata, M., Habu, R. and Nagumo, M. *Trans. ISIJ* **27** (1987b) 130–138.
Tamehiro, H., Nishioka, K., Murata, M., Habu, R. and Kawada, Y. *International Symposium on Accelerated Cooling of Rolled Steel*, Winnepeg, Canada, August (1987) 1–8.
Tamukai, S., Onoe, Y., Nakajima, H., Umeno, M., Iwanaga, K. and Sasaji, S. *Tetsu-tó-Hagane* **67** (1981) 1334.
Tanaka, T. *Int. Metals Reviews* **4** (1981) 185–212.
Tanaka, T. *Accelerated Cooling of Rolled Steel*, eds. G. E. Ruddle and A. F. Crawley, Pergamon Press, Oxford, UK (1988) 187–208.
Taylor, K. A., Olson, G. B., Cohen, M. and Vander Sande, J. B. *Metall. Trans. A* **20A** (1989) 2717–2736.
Taylor, K. A., Chang. L., Olson, G. B., Smith,G. D. W., Cohen, M. and Vander Sande, J. B. *Metall. Trans. A* **20A** (1989b) 2749–2765.
Terada, Y., Chijiiwa, R., Tamehiro, H., Kikuma, T. and Kazuo, F. *First International Conference on New Manufacturing Technology (World Techno–Fair in Chiba '90)* Chiba, Japan (1990) Preprint available from the Nippon Steel Corporation, Japan.
Thelning, K.-A. *Scand. J. Metall.* **7** (1978) 252.
Thewlis, G. *Joining and Materials* (January 1989a) 25–32.
Thewlis, G. *Joining and Materials* (March 1989b) 125–129.
Thewlis, G. *Transformation Kinetics of Submerged Arc Weld Metal*, British Steel internal report IXJ–165–90 (May 1990) 1–11.
Thewlis, G., Whiteman, J. A. and Senogles, D. J., *Materials Science and Technology* **13** (1997) 257–274.
Thielen, P. N., Fine, M. E. and Fournelle, R. A. *Acta Metall.* **24** (1976) 1–10.
Thomas, G., Schmatz, D. and Gerberich, W. *High Strength Materials*, ed. V. F. Zackay, 263 J. Wiley and Sons, NY (1965) 263.
Tom, T. D. Eng. Thesis, University of California, Berkely (1973) quoted in Zackay and Parker (1975).
Tomita, Y. and Okabayashi, K. *Metall. Trans. A* **14A** (1983a) 485–492.

Tomita, Y. and Okabayashi, K. *Metall. Trans. A* **14A** (1983b) 2387–2393.
Tomita, Y. and Okabayashi, K. *Metall. Trans. A* **16A** (1985a) 73–82.
Tomita, Y. and Okabayashi, K. *Metall. Trans. A* **16A** (1985b) 83–91.
Tomita, Y. *Metall. Trans. A* **18A** (1987) 1495–1501.
Tomita, Y. *Metall. Trans. A* **18A** (1988) 2513–2521.
Tomita, Y. *Materials Science and Technology* **7** (1991) 481–489.
Tomita, Y. *International Materials Reviews* **45** (2000), 23–37.
Thompson, M. W. *Defects and Radiation Damage in Metals*, Cambridge University Press, UK (1969) 356.
Thomson, R. Private Communication, University of Cambridge (1990).
Thomson, R. C. and Bhadeshia, H. K. D. H. *Materials Science and Technology* **10** (1994) 193–208.
Thomson, R. and Miller, M. K. *Applied Surface Science* **87/88** (1995) 185–193.
Thompson, S. W., Colvin, D. J. and Krauss, G. *Scripta Metall.* **22** (1988) 1069–1074.
Tomota, Y., Kuroki, K., Mori, T. and Tamura, I. *Mater. Sci. Eng.* **24** (1976) 85.
Trivedi, R. *Metall. Trans.* **1** (1970) 921–927.
Troiano, A. R. *Trans. ASM* **52** (1960) 54–80.
Troiano, A. R. and Greninger, A. B. *Metal Prog.* **50** (1946) 303.
Troiano, A. R. and Klinger, L. J. *Trans. ASM* **44** (1952) 775–802.
Tsay, L. W. and Lin, Z. W. *Fatigue and Fracture of Engineering Materials and Structures* **21** (1998) 1549–1558.
Tsivinsky, S. V., Kogan, L. I. and Entin, R. I. *Problems of Metallography and the Physics of Metals*, ed. B. Ya Lybubov, State Scientific Press, Moscow, 1955. Translation published by the Consultants Bureau Inc., New York (1959) 185–199.
Tsubakino, H. and Harada, H. *Tetsu-tó-Hagane Journal of The Iron and Steel Institute of Japan* **83** (1997) 587–592.
Tsuji, N., Ayada, M., Takashima, T. and Saito, Y. *Tetsu tó Hagane Journal of The Iron and Steel Institute of Japan* **85** (1999) 419–426.
Tsukatani, I., Hashimoto, S. and Inoue, T. *ISIJ International* **2** (1991) 992–1000.
Tsuya, K. *J. Mech. Lab. Japan* **2** (1956) 20.
Tsuzaki, K., Yamaguchi, K., Maki, T. and Tamura, I. *Tetsu tó Hagane Journal of The Iron and Steel Institute of Japan* **74** (1988) 234–241.
Tsuzaki, K., Ueda, T., Fujiwara, K. and Maki, T. *New Materials and Processes for the Future*, Proc. 1st Japan International SAMPE Symposium and Exhibition, Society for the Advancement of Materials and Process Engng., Chiba, Japan (1989) 699–704.
Tsuzaki, K., Nakao, C. and Maki, T. *Materials Transactions, JIM* **32** (1991) 658-666.
Turnbull, D. *Metallurgical Transactions A* **12A** (1981) 695.
Tweed, J. T. H. and Knott, J. F. *Metal Science* **17** (1983) 45.
Tzeng, T. C., *Materials Science and Engineering*, **A293** (2000) 2145–2153.
Ueda, S., Ishikawa, M. and Ohashi, N. *Boron in Steels*, eds. S. K. Banerji and J. E. Morral, TMS–AIME, Warrendale, PA (1980) 1–18.
Ueda, Y. and Takita, M. *Proc. 2nd Int. Conf. on Austempered Ductile Iron*, American Soc. for Metals, Metals Park, Ohio (1986) 141.
Ueshima, Y., Isobe, H., Mizoguchi, S, Maeda, H. and Kajioka, H. *Tetsu tó Hagane* **75** (1989) 501–508.

Umemoto, M., Horiuchi, K. and Tamura, I. *Trans. Iron Steel Inst. of Japan* **22** (1982) 854.
Umemoto, M., Bando, S. and Tamura, I. *Proc. Int. Conf. on Martensitic Transformations* (ICOMAT '86), Japan Institute of Metals (1986a) 595–600.
Umemoto, M., Furuhara, T. and Tamura, I. *Acta Metall.* **34** (1986b) 2235–2245.
Umemoto, M., Horiuchi, K. and Tamura, I. *Tetsu-tó-Hagane* **66** (1980) 400.
Vagarali, S. S. and Odette, G. R. *Metall. Trans. A* **12A** (1981) 2071.
Vasudevan, P., Graham, L. W. and Axon, H. J. *JISI* **190** (1958) 386–391.
Venugopalan, D. and Kirkaldy, J. S. *Hardenability Concepts with Applications to Steels*, eds. Doane, D. V. and J. S. Kirkaldy, TMS of AIME (1977) 249–268.
Vilella, J. R., Guellich, G. E. and Bain, E. C. *Trans. ASM* **24** (1936) 225–261.
Vilella, J. R. *Trans. AIME* **140** (1940) 332.
Vitek, J. M., Packan, N. H. and David, S. A. *Advances in Welding Science and Technology* Proc. of an Int. Conf. on Trends in Welding Research, ed. S. A. David, ASM International, Ohio, USA (1986) 203–208.
Vyhnal, R. F. and Radcliffe, S. V. *Acta Metall.* **15** (1967) 1475–1488.
Viswanathan, R. *Metals Technology* **8** (1974) 284–294.
Wada, T. and Eldis, G. T. *Transformation characteristics of 2.25Cr–1Mo Steel*, Application of 2.25Cr–1Mo Steel for Thick-Wall Pressure Vessels, ASTM STP 755, American Society for Testing Materials (1982) 343–362.
Wada, T. and Cox, T. B. *Advanced Materials for Pressure Vessel Service with Hydrogen at High Temperatures and Pressures*, ed. M. Semchyshen, MPC-18, American Society of Mechanical Engineers, New York (1982) 111–121.
Wada, T. and Cox, T. B. *Research on Chrome-Moly Steels*, MPC-21, American Society of Mechanical Engineers, New York (1984) 77–93.
Wagner, C. *Zeit fur Electrochem* **65** (1961) 581.
Wakasa, K. and Wayman, C. M. *Acta Metall.* **29** (1981) 991–1011.
Watanabe, J. and Murakami, Y. *American Petroleum Institute, preprint no. 28–81* (1981) 216–224, quoted by Bodnar *et al.*, 1989.
Watson, J. D. and McDougall, P. G. *Acta Metall.* **21** (1973) 961.
Wayman, C. M. *Introduction to the Crystallography of Martensitic Transformations*, MacMillan, New York (1964) 168.
Wechsler, M. S., Lieberman, D. S. and Reed, T. A. *Trans. AIMME* **197** (1953) 1503–1515.
Weidig, U., Kaspar, R., Pawelski, O. and Rasp, W. *Steel Research* **70** (1999) 172–177.
Wenyan, L., Jingzin, Q. and Hesheng, S. *Journal of Materials Science* **32** (1997) 427.
Wever, F. *Z. Metallkunde* **24** (1932) 270.
Wever, F. and Jellinghaus, W. *Mitt. Kaiser-Wilhelm-Inst. Eisenforsch.* **14** (1932) 85.
Wever, F. and Lange, H. *Mitt. Kaiser-Wilhelm-Inst. Eisenforsch.* **14** (1932) 71.
Wever, F. and Hensel, H. *Mitt. Kaiser-Wilhelm-Inst. Eisenforsch.* **19** (1937) 47.
Wever, F. and Mathieu, K. *Mitt. Kaiser-Wilhelm-Inst. Eisenforsch.* **22** (1940) 9.
Wenyan, L., Jingixin, Q. and Hesheng, S. *Journal of Materials Science* **32** (1997) 427–430.
White, J. S. and Owen, W. *JISI* **197** (1961) 241–243.
Wiester, H. J. *Z. Metallkunde* **24** (1932) 276.
Williams, W. F. *World Steel Review* **1** (1991) 18–22.
Wilson, A. D. *Microalloyed HSLA Steels*, ASM, Metals Park, Ohio, USA (1988) 259–275.
Wilson, D. V., and Oates, G. *Acta Metall.* **12** (1964) 21.

Wilson, E. A. *Scripta Metall.* **12** (1978) 961.
Wilson, E. A., Allen, S. P. and Butler, J. *Metal Sci.* **16** (1982) 539.
Wilson, A. D., Hamburg, E. G., Colvin, D. J., Thompson, S. W. and Krauss, G. *Microalloyed HSLA Steels*, ASM International (1988) 259–275.
Wilson, P. W. PhD Thesis, University of Cambridge (1991).
Winchell, P. G. and Cohen, M. *Trans. ASM* **55** (1962) 347.
Winterton, K. *JISI* **151** (1945) 79.
Woodhead, J. H. and Quarell, A. G. *JISI* **203** (1965) 605–620.
Wright, P. H., Harrington, T. L., Szilva, W. A. and White, T. R. *Fundamentals of Microalloying Forging Steels*, eds. G. Krauss and S. K. Banerji, The Metallurgical Society of the AIME, Warrendale, Pennsylvania, USA (1987) 541–566.
Yakel, H. C. *Int. Met. Rev.* **30** (1985) 17–40.
Yalki, H. K. and Edmonds, D. V. *Journal of Materials Science* **34** (1999) 711–717.
Yamamoto, K., Hasegawa, T. and Takamura, J–I. *ISIJ International* **36** (1996) 80–86.
Yamamoto, K., Matsuda, S., Haze, T., Chijiiwa, R. and Mimura, H. *Residual and Unspecified Elements in Steel*, ASM Int., Ohio, USA (November 1987) 1–24.
Yang, J. R. and Bhadeshia, H. K. D. H. *Advances in Welding Science and Technology* ed. S. A. David, ASM, Metals Park, Ohio, USA(1986) 187–191.
Yang, J. R. and Bhadeshia, H. K. D. H. *Proc. of Int. Conf. on Welding Metallurgy of Structural Steels*, TMS AIME, Warrendale, Pennsylvania (1987) 549–563.
Yang, J. R. and Bhadeshia, H. K. D. H. *Proc. of Int. Conf. Phase Transformations '87*, ed. G. W. Lorimer, Institute of Metals, London (1988) 203–206.
Yang, J. R. and Bhadeshia, H. K. D. H. *Materials Science and Technology* **5** (1989a) 93–97.
Yang, J. R. and Bhadeshia, H. K. D. H. *Materials Science and Engineering* **A118** (1989b) 155–170.
Yang, J. R. and Bhadeshia, H. K. D. H. *American Welding Journal* **69** (1990) 305s–309s.
Yang, J. R., Huang, C. Y., Huang, C. F. and Aoh, J. H. *Journal of Materials Science* **30** (1995)) 5036–5041.
Yang, J. R., Huang, C. Y., Hsieh, W. H. and Chiou, C. S. *Materials Transactions JIM* **37** (1996) 579–585.
Yang, J. R. and Chang, L. C. *Materials Science and Engineering A* **A223** (1997) 158–167.
Yates, J. K. *Science in Parliament* (July/August 1996).
Yescas-Gonsalez, M. CPGS Thesis, University of Cambridge (1999).
Yoshizawa, H., Morishima, K., Nakashiro, M., Kihara, S. and Umaki, H. *Creep Resistant Metallic Materials*, Vitkovice, Czech Republic (1996) 164–173.
Yu, J. *Metall. Trans. A* **20A** (1989) 1561–1564.
Yutori, T. and Ogawa, R. *Tetsu-tó-Hagane* **61** (1979) 991–1011.
Zener, C. *Trans. AIME* **167** (1946) 550–595.
Zener, C. *Journal of Applied Physics* **20** (1949) 950.
Zhang, M.-X. and Kelly, P. M. *Materials Characterization* **40** (1998a) 159–168.
Zhang, M.-X. and Kelly, P. M. *Acta Materialia* **46** (1998b) 4081–4091.
Zheng, T. C. *Materials Science and Engineering* **A293** (2000) 185–190.

Author Index

Subject Index